Oil families and petroleum geochemistry of the western part of the Sirt Basin Libya

Moftah Ahmed Dieb

A thesis submitted for the degree of Doctor of Philosophy (Ph.D.) at Newcastle University

School of Civil Engineering and Geosciences, Faculty of Science, Agriculture and Engineering

Newcastle upon Tyne

NE1 7RU

UK

March 2015

Declaration

I hereby certify that this work is my own, except where otherwise acknowledged, and that it has been submitted previously for a degree at this, or any other university.

Moftah Ahmed Dieb

Acknowledgements

All praise is due to Allah the designer of the universe and all that lies within and beyond it. I would like to thank the Libyan petroleum Institute for financial support throughout the duration of this study, National Libyan Oil Corporation and Libyan Oil Company in Libya for providing samples and data.

I would like to extend my thanks to supervisor Dr. Martin Jones for his advice, guidance and encouragement of the research and also for valuable contributions towards the success of my PhD research, and also for his constructive criticism and correction of my manuscript. I would like also to thank Professor Andrew Aplin for his suggestions and discussion during my PhD study.

I am also expressing my appreciation for the assistance received from all staff at Ceg School who has provided their time and expertise whenever I have needed it, namely, Mr Bernie Bowler, Mr Paul Donohoe and Phil Green. I would like also to thank Mrs Yvonne Hall for her help.

Thanks are extended to all staff members of the Libyan petroleum Institute, especially to the exploration department for their helps. Thanks go to Dr. Mahmoud Benissa in particular for his help and advice.

A special thanks to my loving spouse Aisha, for all her encouragement, support and patience throughout the last four years, My Sons Ahmed and Mohamed, My daughters Heba, Hanin, Mouda, Nour and Yousra, to whom I owe a lot. My brother and sisters also deserve special thanks for their support and encouragements. May Allah the most high reward them abundantly.

Finally, I would like to dedicate this research to the spirit of my parents, and particularly to my father who hoped and predicted for me get this degree from 35 years ago.

Abstract

This thesis describes a detailed geochemical evaluation of the hydrocarbon potential of source rocks and the origins of the crude oils in the western and central parts of the Sirt Basin in Libya. The Sirt Basin is one of North Africa's richest and most prolific oil-bearing basins, with most of the oil being considered to be derived from the Campanian Sirte Shale and other local source rocks such as Rachmat, Etel and Hagfa Shale formations. The primary aims of this research were to determine the main source rocks that generated petroleum, determine the number of genetically distinct oil families in the basin and compare them with their parent source rocks, and to assess the regional migration and the filling directions of the reservoirs, since this information can exert a profound influence on current and future exploration activities across the study area.

A study was undertaken on these source rocks and crude oils using 269 rock cuttings and 51 crude oil samples from several boreholes and oilfields in the Sirt Basin. Routine geochemical analysis in addition to biomarker analysis by gas chromatography-mass spectrometry, compound specific carbon isotopic analysis on *n*-alkanes and diamondoid analyse were carried out on selected source rock samples and on all of the crude oil samples.

The geochemical results demonstrated the presence of various organic-rich zones within the Upper Cretaceous Sirte Shale and Rachmat source rocks. The Sirte Shale Formation is considered to have variable fair, good to very good source potential, and has good hydrocarbon generation in the study area. The Rachmat Formation shale is considered as the second potential source rock in the basin. Vitrinite reflectance, Spore Colour Index, and pyrolysis Tmax data indicate that the Upper Cretaceous shale samples are early to mid-mature in the west of the basin, and middle to late mature in the north central of the basin. Optical analysis of palynofacies slides showed that structureless, amorphous organic matter is dominant, along with the presence of some phytoclasts and reveals moderate to well preserved, fluorescent Type II marine kerogen and Type II-III kerogen.

A number of biomarker and other organic facies and maturity indicating molecular marker parameters, as well as isotopic data, show that the crude oils in the western and

central parts of the Sirt Basin are genetically related and only minor variations are present between them, likely due to minor organic facies variations in the Sirt Shale and Rachmat source rocks. The biomarker parameters show dissimilarities between the crude oils in eastern part relative to the western and central part of the basin, due to variations in the organic facies and depositional environments setting of the source rocks or due to higher maturity. Based on molecular marker characteristics, oil-oil correlation identified nine oil families, plus two subfamilies in the study area: Oils from families 1A, 1B, 2, 3 and 4 are situated in the western and central parts of the Sirt Basin, while oil families 5, 6, 7, 8 and 9 are located in the eastern part of the basin. Crude oils of families 1A, 1B, 2, and 3 were interpreted as having been generated from a suboxic to anoxic marine, clay-rich and early to middle maturity source rock. Molecular and other compositional variation between oil families were attributed to organic facies and subtle maturation variations. Age-related biomarker parameters in the oils suggested that their source was Upper Cretaceous.

Migration of the generated and expelled oil and gas from the Sirte Shale and Rachmat source rocks to the reservoirs of the Upper Cretaceous-Tertiary petroleum system was interpreted to have occurred along both vertical and lateral pathways along the faults, in the Oligocene to Miocene, while oil carbazole data indicated that this migration was generally likely to have been over relatively short distances.

Preface

This thesis describes a detailed geochemical evaluation of the petroleum fluids in the Sirt Basin located in the central of Libya. These crude oils were found in the Mesozoic and Tertiary carbonate and clastics reservoirs rocks, which are sealed by evaporite and shale strata. The PhD thesis consists of nine chapters, including the introduction and general geology of the Sirt Basin (chapter 1), the molecular and biomarker identifications (chapter 2), the methodology (chapter 3), the Upper Cretaceous source rock evaluation (chapter 4), the oil-oil correlation (chapter 5), oil to source correlation (chapter 6), Sirt Basin Petroleum system (chapter 7), and the conclusion and future work (chapter 8).

Chapter one provides a detailed review of the geological setting of the Sirt Basin in the central of Libya. This chapter provides tectonic structure feature of the North Africa and Arabia, Sea level changes and black shale deposition in the North Africa and Arabia. It provides an introduction to the Sirt Basin, geographic location of the basin, origins and tectonic evolution of the Sirt Basin. It also provides a detailed summary of the general stratigraphy of the sediments, lithology units as well as detailed descriptions of the stratigraphic and depositional setting of the source rock, reservoirs, traps and seals bed units. The chapter also includes the reservoir quality of the reservoir rocks. It thus presents a detailed review of the petroleum history of the Sirt Basin.

Chapter two presents summary review of the origin of petroleum and petroleum geochemistry literature for molecular marker identification applied in this thesis.

Chapter three presents a detailed description of the methods and technique used in this project. This chapter also describes the statistical data analysis using the principal component analysis method.

Chapter four provides a characterization of the Upper Cretaceous source rock using total organic carbon (TOC) content, Rock-Eval analysis data, molecular, biomarkers and aromatic hydrocarbons, compound specific carbon isotope analysis and statistical evaluations of these data.

Chapter five presents the characterization of the crude oils for identifying the similar or different features of oils for use in an oil correlation study in the Sirt Basin.

Chapter six presents a characterization of the Upper Cretaceous Sirte Shale and Rachmat potential source rocks and a comparison to the crude oils that have been generated from the source rocks in the Sirt Basin, using an oil to source correlation approach.

Chapter seven gives a detailed description of the petroleum system by using kinetic and 1D basin modelling analysis of the main potential source rock in the Sirt Basin. The main aim of this chapter is to determine the burial and the hydrocarbon generation history of source rocks in the Sirt Basin through the modelling of subsidence history and thermal maturity, and to predict the migration pathways for the source rock and reservoirs.

Chapter eight includes the conclusions and ideas for future work.

Table of Contents

List of Figures

List of Tables

Chapter 1. General Introduction

The Sirt Basin in north central Libya is one of the youngest sedimentary basins of the African Craton, with an onshore area of approximately 375,000 Km^2 and an estimated sedimentary volume of 1.3 million km^3 (Abadi *et al.*, 2008). It is considered to be one of the richest and prolific oil-bearing basins in the world, containing more than 100 oil and gas fields, including several giants. It is considered to be the largest petroleum province so far discovered in Libya (Hallett, 2002).

More than 1600 wildcat wells were drilled in the Sirt Basin, resulting in 250 discoveries with recoverable reserves of 45 billion barrels (bbl.) of oil and 33 trillion cubic feet (tcf) of gas (Hallett, 2002). Nearly 80% of the total recoverable oil and gas were discovered in shallow plays before 1970 (Hallett, 2002). After that time the exploration activity was retarded due to lack of technologies such as advanced seismic acquisition and processing, advanced geochemical studies, computer related geoscience technology, limited understanding and application of petroleum system analysis and ineffective use of sequences stratigraphic concepts (Hallett, 2002). Therefore, achievement the aims and objectives of this geochemical study may assist exploration for oil and gas in the study area.

1.1 Background and Research Objectives

The distribution of petroleum (oil and gas) in any sedimentary basin is controlled by combination of a number of processes and elements that may have changed through the geological history of the basins. The essential elements and processes that make up a petroleum system include a petroleum source rock, thermal maturation, a migration pathway, reservoir rock, trap and seal (Magoon and Dow, 1994).

Petroleum Geochemistry continues to play a critical role to find the remaining resource that is becoming more difficult to locate, discover and produce, and it is clear that geochemical analysis is increasingly becoming a vital tool for minimizing exploration risk (Peters, 2005b).

Despite the considerable amount of basic geochemical analyses that has been done in the Sirt Basin, the geochemical knowledge of this basin is still incomplete and not well

understood, because this wealth of data has not yet been incorporated with information from modern geochemical analytical techniques, such as biomarker data from Gas Chromatography–Mass Spectrometry (GC-MS), specific carbon isotope analysis (GC-IRMS) data and basin modelling analyses using these data.

These techniques, which are now becoming widely applied in geochemical investigations, have the possibility of resolving questions regarding the timing of oil generation, thermal history and subsequently, secondary migration distance and pathways of the oil from source rock to trap within the Sirt Basin. Due to the exploration and production complexities that encountered by most of the operations oil companies working for exploring on the oil and gas in the Sirt Basin, particularly in the central and southwest region, therefore it becomes necessary to perform this geochemical research study that may help to solve such kinds of problems.

Secondary migration distance and pathway information is not achievable using seismic surveys but (Larter and Aplin, 1995) illustrated that the organic geochemistry can be used to resolve petroleum migration history, to determine the volume of petroleum migration and volumes of water interacted with it and to distinguish between oils which have migrated throughout the pore system in fine grained rocks and those have migrated via fractures and faults (Larter *et al.*, 1996).

In general, organic compounds that have different molecular weights, polarities and stereochemistries should behave differently during the various adsorptive processes which may take place during the migration of petroleum in the subsurface. Seifert and Moldowan (1978) used biomarker alkanes to describe regional petroleum migration pathway but (Yamamoto *et al.*, 1991) showed that parameters derived from biomarker alkanes are affected by other factors such as variation in source organic matter input, depositional environments and thermal maturity. Peters and Moldowan (1993) also noted limitations of biomarker alkanes for petroleum migration assessment in the subsurface.

Subsequently, several geochemical studies were carried out in both field and laboratory have shown potential indicators of petroleum migration distance in more polar compound in petroleum; such as aromatic nitrogen compounds including carbazoles

and benzocarbazoles (Yamamoto *et al.*, 1991; Li *et al.*, 1992; Li and Larter, 1993; Li *et al.*, 1994; Larter and Aplin, 1995; Li *et al.*, 1995b; Larter *et al.*, 1996; Li *et al.*, 1997; Taylor *et al.*, 1998).

1.1.1 Aims and Objectives

This study concentrates on molecular marker signatures for identifying those phenomena mentioned above in order to better understand these processes and thus the whole petroleum system of the Sirt Basin.

A number of objectives were planned in order to achieve this broad aim.

- To determine the number of genetically distinct oil families in the basin,
- Utilize geochemical characteristics of the oil families to infer their source facies,
- Determine thermal maturity level and degree of preservation,
- Determine the most likely source unit in each part of the study area by comparing the distribution of oil families and their inferred source facies with regional stratigraphic and available source rock data,
- Attempt to correlate each oil family to the specific source stratigraphic unit,
- Attempt to predict oil properties at different maturity levels,
- Estimate migration directions by comparing oil family distributions with the location of known oil kitchens source rock within the study area,
- Determine the timing of hydrocarbon generation within each source rock.

In order to realise these objectives, routine and advanced geochemical techniques were carried out including gas chromatography-mass spectrometry (GC-MS) for biomarker analyses, compound specific carbon isotope analyses (GC-IRMS) and basin modelling analysis. Achievement of these aims and objectives will reduce the risks that associated with the exploration activity within the study area in the following ways.

1. Assessment of the maturity-levels of effective source rocks and improve the understanding of the vertical and lateral distributions of the major oil kitchens.
2. Establishing the source rocks and kerogen types responsible for generating and expelling these petroleum fluids (i.e. likelihood of oil or gas).

3. Inputs to determine the filling history and timing of charging of the reservoirs in the study area (basin modelling).
4. Estimation of the volumes of oil and gas generated and expelled from effective source rocks.
5. Determine the relationship between effective source rock(s) and oil(s) as well as oil family with each other (i.e. oil to source and oil-to-oil correlations).
6. To suggest the migration pathways and filling directions of the fields across the study area.
7. Improving the overall understanding of possible prospective areas.

1.2 Tectonic structure features of the North Africa and Arabia

During the Late Jurassic and Early Cretaceous times an accelerated rifting system affected much of the Africa-Arabia Craton as evidenced by the development of rifts in Yemen and Somalia and the multidirectional central African rift system (Guiraud *et al.*, 1992; Guiraud, 1995). In the Early Cretaceous Barremian and Albian periods, the south and equatorial Atlantic was opened. In the south-eastern part of the Sirt Basin, the Sarir and Hameimat Troughs were developed with an E-W trend during Late Jurassic-Early Cretaceous rifting. In the same period, other E-W trend basins subsided, with marked subsidence in North Africa (Algeria, Tunisia and Egypt) as well as along the western part of the west and central African rift system (Niger Trough, South Chad, Benue and the North Cameroon Troughs) (Guiaud, 1987; Bayoumi, 1989). During the Neocomain and Early Aptian times, the subsidence in the basins mentioned above was an N-S extension in the African Plate, which was controlled by the stretching of the crust due to the rotation of Africa around a pole as shown in Figure 1.1 (Fairhead, 1988). This rotation around the pole was related to the opening of the south Atlantic and the relative movement of the Austral block, as shown in Figure 1.1 (Fairhead, 1988; Guiraud *et al.*, 1992). However, the direction of extensions observed in the central African basins and also the Sirt Basin were notably parallel to small circles centred on the rotation pole. During Neocomain and Early Aptian times, the opening of the central Atlantic continued between North America and North West Africa and this was accompanied by left-lateral movements between Eurasia and Africa (Ziegler, 2001). The rifting was had an E-W trend at the Sarir and Hameimat Troughs in the Sirt Basin,

which may be related to the opening of the central Atlantic Ocean and was probably influenced by the left-lateral opening of the Tethys Ocean (Ziegler, 2001) In the Early Aptian, the trend of the opening of the south Atlantic changed and the rotational pole defined the relative movement of Africa and South America (Klitgord, 1986), as shown in Figure 1.5b. In this period, the maximum tensional stresses in North and Central Africa changed from N-S to NE-SW (Guiraud *et al.*, 1992) and the changes in the motion of Africa to the northeast caused the development of the major NW-SE horsts and grabens of the Sirt Basin.

The NW-SW extension caused by the northeastern movement of the Arabian block in response to slip vectors described by the pole of rotation (Guiraud *et al.*, 1992; Guiraud, 1992) was imposed by the collision of Africa and Europe and the opening of the western Mediterranean Sea (Gealey, 1988; Anketell, 1996). These directions of extension were observed in the Sirt Basin, in east Niger and Sudan. Meanwhile, the main pattern of movement between Africa and Europe was left-lateral at the same time (Anketell, 1996). In the Early Aptian, unconformities on the surface were observed in almost all African basins, with some exceptions such as the Sudan rift and Abu Gharadig Basin (Janssen *et al.*, 1995). In addition, in the late Jurassic, the earliest rifting occurred with rhyolitic and basaltic volcanism (Hallett and El Ghoul, 1996). During late Jurassic-Early Cretaceous times, granite intrusion and basic volcanic rocks were observed in the Sirt Basin (Cahen *et al.*, 1984). In the Late Cretaceous, faulting was predominantly extensional and largely expressed as NW-SE trending rifts situated to the northwest of the Neocomain troughs in the south and east of the Sirt Basin. At the same time subsidence continued in many basins of the central and west African rift system due to the thermal relaxation of the Early Cretaceous rifts; for example in the Bangor, Anza, Abu Gharadig, Senegal, and Doba Doseo-Salamt Basins (Guiraud *et al.*, 1992; Guiraud, 1992). Rapid subsidence occurred during the Cenomanian-Turonian ages which was caused by tectonic drive (Janssen *et al.*, 1995).

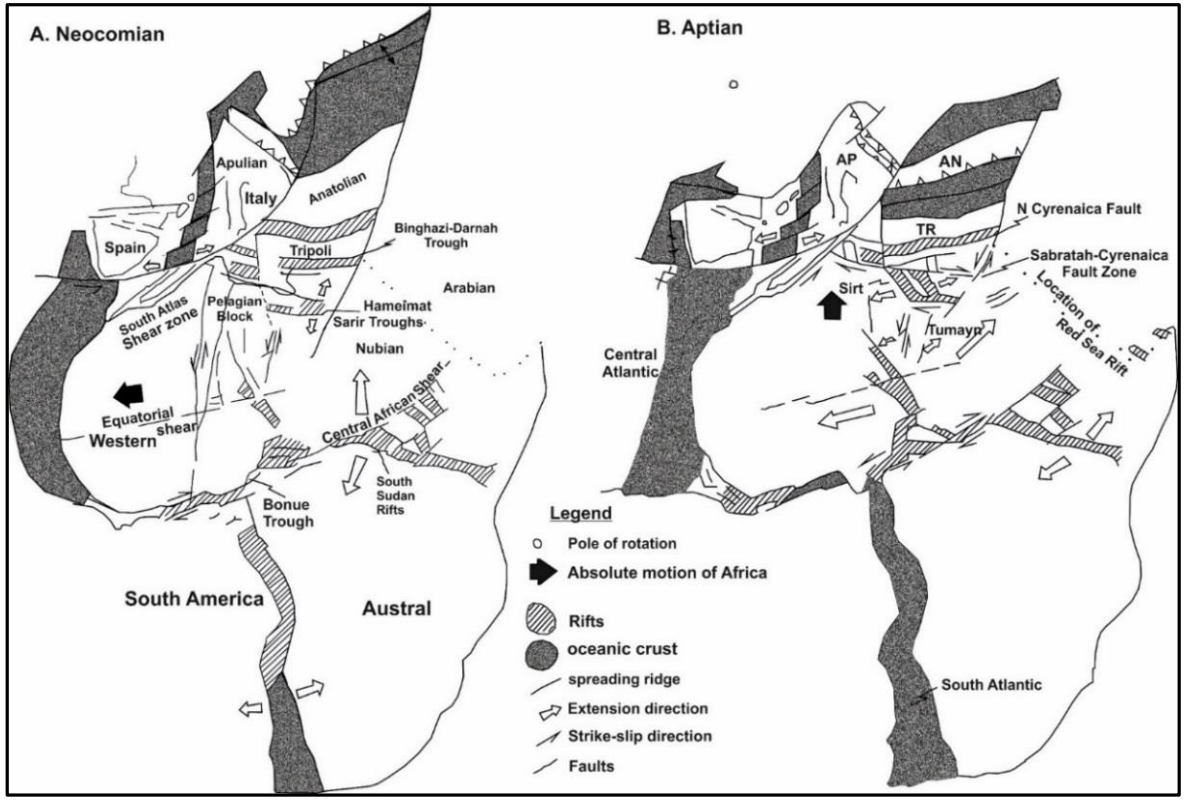

Figure 1.1: Development of African rift system and closure of the Tethys during: (A) Neocomain; (B) Mid-Aptian (Gealey, 1988; Anketell, 1996; Wilson et al., 1998), modified after Abadi, 2002.

In Santonian times, the most important change in relative motion occurred between Africa and Eurasia. During this time a change from left-lateral to right-lateral movement occurred (Savostin *et al.*, 1986; Le Pichon *et al.*, 1988). The counter-clockwise movement of Africa resulted in the onset of the Alpine collision between Africa and Eurasia (Ziegler, 1988; Ziegler, 2001). This collision was marked by a compressional event reflected in a period of strong tectonic activity in North Africa and Europe (Ziegler, 1990) and then ending with rapid subsidence in most African basins (Janssen *et al.*, 1995). The Santonian was also marked by erosional unconformity in the Gabon Coastal and Senegal basins (Janssen *et al.*, 1995).

During Paleocene-Early Eocene times, the rifting in the Sirt Basin resulted in rapid subsidence, particularly in the trough areas. Also during this phase subsidence along the continental margins of the Somalia and Kenya basins increased (Janssen *et al.*, 1995), while along the west and central African rift subsidence continued.

In the Middle Eocene-Miocene times, major subsidence occurred in the eastern part of the Sirt Basin due to thermal relaxation and resultant basin fill, whereas in other places in the basin the onset of continental sedimentation commenced. The Oligocene-Miocene times were marked by the rifting and opening of the Red Sea, the Gulf of Aden and the east African rift system. The Lumu embayment and Mozambique and Rovuma Basins were affected by the development of the East Africa rift system and subsidence was renewed (Janssen *et al.*, 1995).

Volcanic activity occurred in this phase in the west of the Sirt Basin and produced the As Sawada, Al Haruj and Gharyan volcanoes as a result of the intersection of differently oriented fracture zones. In addition, magmatic activity became widespread in Africa on a regional scale and an extensive basaltic volcanic field formed in the North Africa and Arabia regions. The magmatic activity within African Plate was widespread in the Late Oligocene to recent times, and the major phase of volcanism

occurred in the Early and Late Miocene (Wilson *et al.*, 1998). This reflects change in the plate tectonic regime induced by the Alpine collision.

In the Sirt Basin, high rift-type subsidence rates are clearly restricted to the central troughs, while platform regions show very little subsidence. Sediment accumulation is concentrated in the rift grabens, and the subsidence rates vary greatly between grabens and adjacent platforms. The depositional environment deepened progressively during the Late Cretaceous transgressive cycle, which was the combined result of tectonic subsidence and a eustatic sea level rise in the Sirt Basin (Schröter, 1996). The Middle-Late Cretaceous was characterized by offshore shelf carbonate deposition over much of North Africa (Carr, 2003). Offshore mudstone was deposited on the Saharan Platform and in the Sirt Basin (Carr, 2003). There was also marginal marine deposition in Eastern Algeria and marginal marine to shallow marine deposition in Egypt. During Cenomanian-Turonian times, widespread marine deposition took place interbedded with the non-marine sandstone facies of the Nubian Formation (Carr, 2003). Deposition was accompanied by intensive basement block-faulting, which dominated depositional trends in the Sirt Basin. In the Late Cretaceous, regional subsidence took place with progressive marine onlap onto high areas (Belazi, 1989). Distinct variations in the stratigraphic thickness of offshore marine shale are recognized, with thick shale deposited in trough areas and thinning onto highs where shallow marine sandstone was deposited. Marine deposition occurred within the Sirt Troughs characterized by sandy paralic to the non-marine fringe (El-Bakai, 1996). Clastic sediments passed transgressively up into Late Cretaceous shallow water limestone, which passed laterally basin wards into interbedded open-marine limestone and shale (Belazi, 1989). This limestone passed gradually into shale with thin interbedded limestone and sandstone. The Sirt Basin was an open marine area in the latest Cretaceous times (Belazi, 1989).

1.3 Campanian-Maastrichtian Organic Rich Strat in North Africa

In North Africa, the Campanian-Maastrichtian organic-rich strata have TOC values reaching up to 16 wt% occurring in the Moroccan Tarfaya Basin and the Atlas Gulf area, the Sirt Basin in Libya, and the Southern Western Desert, Red Sea Coast and Gulf of Suez in Egypt (Luening *et al.*, 1998; Luning, 2003) as shown in Figure 1.2. However, during this period, the sediments in Algeria, west Libya and Tunisia are characterized by poor organic contents. During the Campanian-Maastrichtian, the black shale deposits were accompanied by a major eustatic transgression occurring in the early Campanian that led to high sea levels until late Campanian times. Deposition of the black shale is thought to have resulted from a rise in sea levels and the highstand system tract in combination with restricted water circulation in the Atlas Gulf and Sirt Basin grabens and elevated high surface water productivity in the Tarfaya Basin and Egypt basins (Luening *et al.*, 1998). Furthermore, in the Sirt Basin, Libya and Gulf of Suez, Egypt, the black shale of the Campanian-Maastrichtian formed the main hydrocarbon source rocks. However, in North Africa the distribution of the Campanian-Maastrichtian black shales seems to be less extensive than that of the Cenomanian-Turonian, but the Campanian-Maastrichtian organic-rich shales are considered more important due to them representing the main hydrocarbon source rocks in the Sirt Basin and Gulf of Suez basins (Luning, 2003). Cenomanian-Turonian marine deposits are considered source rocks in the southern Sirt Basin, Libya. The Campanian-Maastrichtian (Late Cretaceous) shales are source rocks in the western, central and eastern Sirt Basin, Libya, the Western Desert Basin, Egypt, and the Saharan Atlas and Rharb Basin, in Algeria and Morocco. In the Gulf of Gabes, Tunisia, the source rocks are Late Cretaceous carbonates (Carr, 2003).

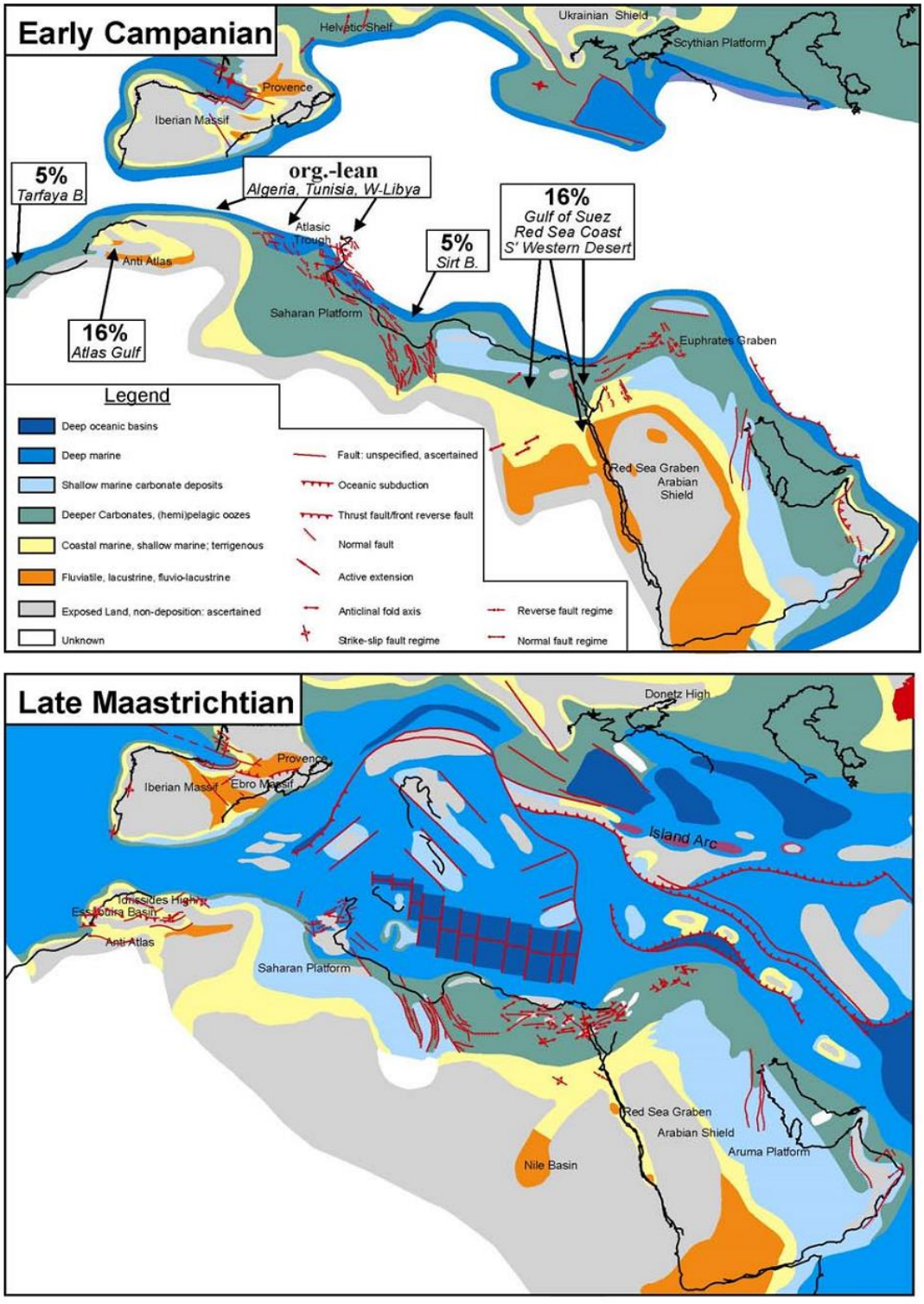

Figure 1.2 Early Campanian/Late Maastrichtian palaeogeography of North Gondwana, simplified after (Philip, 2000a; Philip, 2000b) and (Luning, 2003). Boxed percentage values indicate maximum TOC reported for specific areas.

1.4 Sea Level Changes

Suess (1904) reported that the apparently synchronous episodes of deposition and non-deposition of marine strata in several parts of the world was as a result of changes in sea level where rises and falls might be eustatic (global) in origin. Since then, other researchers have suggested that the sea level histories of different parts of the world show an apparent synchronicity of these events to episodes of global tectonics (Sloss, 1993).

There are coincidence between a major transgression and ocean anoxic events. Hays and Pitman (1973) observed that the high global sea level during the Cretaceous is highly related to high rates of sea floor spreading and concomitant increase in the volume of mid-Cretaceous ridge, also to thermal uplift of the sea floor associated with massive submarine volcanisms (Schlanger *et al.*, 1981) and the emplacement of large igneous provenances. During the Cretaceous time a maximum sea level probably reach-up to 255 m high (Haq *et al.*, 1987). Furthermore, high level of Co2 in the atmosphere resulted in comparatively temperate Polar Regions and extremely warm sea-surface temperature (Wilson and Norris, 2001). This temperature is estimated for Cretaceous time and rerecorded their peak between 32 and 33±3 °C (Wilson and Norris, 2001). The cool oxygenated bottom water is not occurred during Cretaceous time, and may was replaced by salinity-driven deep water formation. This led to develop density stratification of the Cretaceous oceans and basins wide oxygen deficient with the most intense anoxia occurring in the deepest parts of the tectonically isolated basin such as the Cretaceous North and South Atlantic Ocean.

Haq *et al.* (1987) reported that sea level fluctuations have significant implications for the organic productivity of the ocean and sediment distribution patterns along continental margins and in interior basins. Therefore studying and understanding sea level changes is important and of interest for hydrocarbon exploration. Haq *et al.* (1987) illustrated that there are two eustatic curve scales, which are short and long term, and these represent the best estimate of sea level rises and falls compared with present day mean sea levels.

For the long term scale, the Late Palaeozoic (Pennsylvanian and Permian) generally show low sea levels, reaching the lowest point in the Tatarian, and this was continued into the Triassic and Early Jurassic, where the sea level remained low throughout the Middle Jurassic and rose in the Bajocian, but fell again in the Late Bathonian in the Middle Jurassic. In the Callovian, this trend was reversed, where a long-term sea level rise continued through the Oxfordian, reaching a highest Jurassic peak in the Kimmeridgian (Haq *et al.*, 1987). After a transient but marked decline in the Cretaceous Early Valanginian, the sea level began to rise rapidly, remaining high throughout Cretaceous times. In the Upper Cretaceous Early Turonian, the sea level reached its highest levels through the Mesozoic and Cenozoic periods. In the Upper Cretaceous and during the Coniacian, Santonian, Campanian, Maastrichtian and Danian times, the sea levels stayed high. In this phase the main study samples, containing major hydrocarbon source rocks of the Sirt Basin, were deposited within the graben areas. After that the sea level gradually declined and this was noted in the latest Cretaceous and continued through Cenozoic times (Haq et al., 1987).

In the short term scale, the major sea level falls were at the base of the Portlandian in the Upper Jurassic, Early Aptian in the Lower Cretaceous, Middle Cenomanian, Late Turonian, Late Maastrichtian in the Upper Cretaceous, Early Thanetian in the Upper Paleocene, at the Latest Ypresian in the Lower Eocene, Bartonian in the Middle Eocene, near the Rupelian-Chattian boundary in the Oligocene, Burdigalian-Langhian in the Lower-Middle Miocene, Late Serravallian in the Middle Miocene, and throughout the Late Pliocene-Pleistocene times, while in Oligocene times the sea level dropped in large part as a result of the increasing influence of glaciation (Haq *et al.*, 1987). These sea level falls are strongly associated with major unconformities which occurred worldwide (Haq *et al.*, 1987).

In general, during the Triassic, the sea level was relatively low across North Africa, and continental deposition and erosion therefore occurred. In the Triassic the Hercynian unconformity was progressively onlapped, during which there was a gradual rise in the relative sea level, with minor accelerations in the increase leading to a brief intercalation of marginal and shallow marine deposition within the generally continental successions (Carr, 2003). At the end of the Triassic, a rapid increase in the

sea level covered the continental regions, leading to the deposition of carbonates and evaporites. During the Early Jurassic, the sea level continued rising, producing generally eastwards-backstepping sedimentary facies, and the transgression reached a maximum in the Bathonian time. After that, the sea level fell, and shallow marine and continental deposits became progressively dominant (Carr, 2003). During Aptian times the sea level fell, until the maximum regression occurred at the end of the Albian. Generally, during the late Cretaceous, the relative sea level rose in North Africa and progressively deeper water sediments were deposited . However, in North Africa, the gradual fall in relative sea level during the Early-Middle Cretaceous was not recognized in global sea level curves, and this may reflect an uplift associated with the Austrian compressional phase, a precursor to the Alpine Orogeny. The Upper Cretaceous transgression event in the North African Plate started in the Early Cenomanian and progressively advanced across the continent with only minor regression cycles occurring during the Turonian and Santonian, and reached its maximum extent during the Late Maastrichtian, as shown in Figure 1.2 (Haq *et al.*, 1987). In addition, the major second order eustatic sea level rise commenced in the Early Campanian (Haq *et al.*, 1987; Lüning *et al.*, 1998; Luning, 2003) and during this time the sea reached its highest level, while falling somewhat during Cenomanian-Turonian times (Haq *et al.*, 1987). The sea level gradually fell during the Late Campanian to Late Maastrichtian (Schandelmeier, 1997), as shown in Figure 1.3. The sea level was development in the different third order cycles where no Tethyan wide correlation exist so far (Cf. Hardenbol, 1998). However, the marine sediments were generally deposited at restricted levels to the outer edge areas in the North African continent, apart from some embayment and seaway related to former rifts (Lüning *et al.*, 1998).

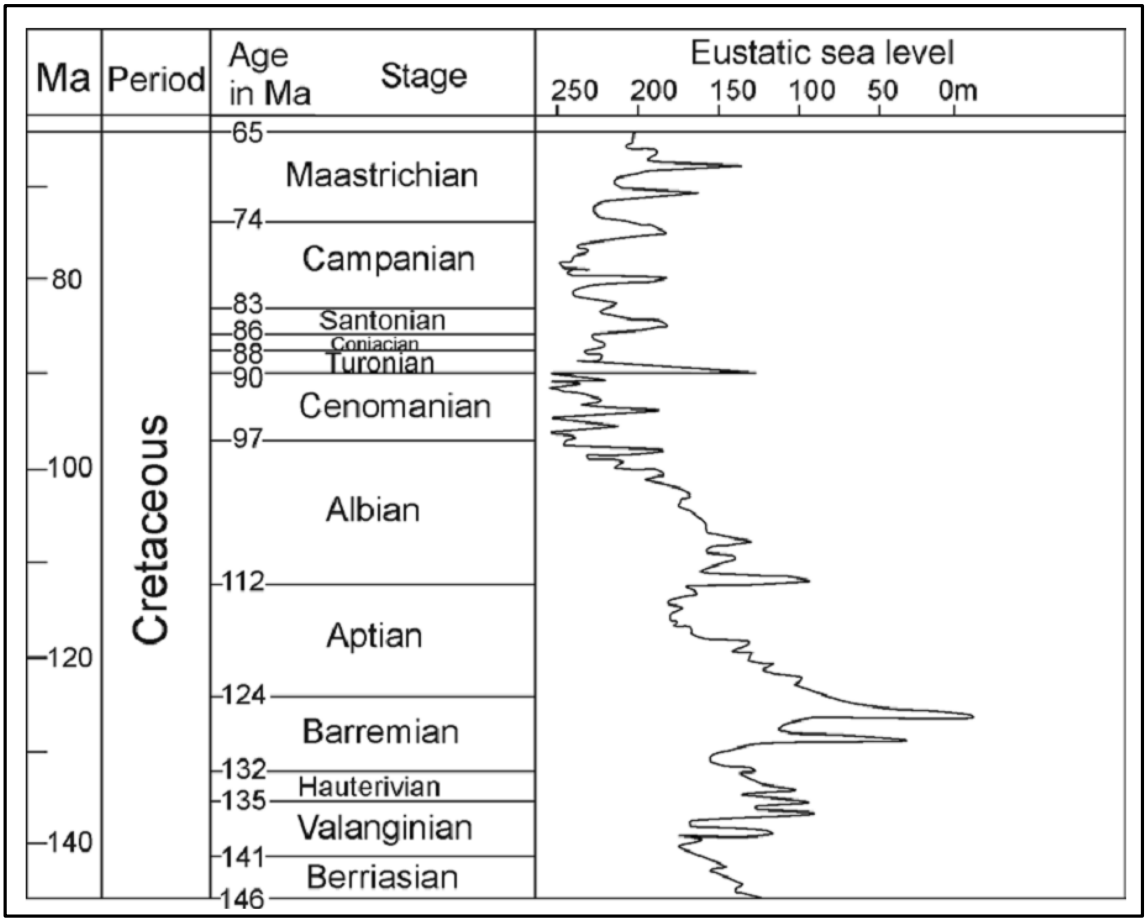

Figure 1.3: Eustatic sea-level curve for NE and NW Africa, after Schandelmeier and Reynolds, 1997 (time scale after Harland et al. 1990). Major flooding occurred during the early Campanian with gradual sea-level fall from the late Campanian to the end Maastrichtian, modified after Lüning, 2003.

According to Tyson (1995), transgression cycles are strongly related to the increased acceleration in sea level rises and are marked by increases and diversity in the abundance of marine palynomorphs, and also by a progressive decrease in the abundance of phytoclast particles. This system tract generally leads to the deposition of condensed sections of sediments. Usually at the maximum flooding surface, the highest diversity of marine palynomorphs (especially dinocyts) is recorded (Tyson, 1995). The abundance of amorphous organic matter in sediments often depends on the nature of the condensed section. In a condensed section deposited under oxic conditions, the amorphous material is at minimum abundance, whereas in anoxic conditions it reaches high abundance (Tyson, 1995).

1.5 Geographic and Tectonic Setting of the Sirt Basin

In the late Early Cretaceous times, the Sirt Basin was rifting and opened wide with a northwest-southeast trend. Marine transgression started to slowly fill the trough areas in Cenomanian times (Thomas, 1995). The sedimentary sections contain thick heterogeneous clastics, thin bedded evaporates and shallow marine carbonates. In the Cenomanian to Santonian times, the subsidence was slow and increased appreciably during the Campanian, with the rapid thick deposition of organic-rich marine shale in the trough regions. Figure 1.4 shows a location map for the wells and oilfields studied in the Sirt Basin. The Sirt Basin in northern, central Libya is one of the youngest sedimentary rifting basins of the African Craton. It is bounded to the south by Tibisti Massif and to the west by Al Gargaf Uplift and the Ghadamis and Murzuq Basins. To the North, it is bounded by the Gulf of Sirt, to the east of the Cyrenaica Platform and Al Bottnan Basin. The tectonic features of the Sirt Basin were formed by large scale subsidence and block faulting in response to Late Jurassic to Early Cretaceous rifting (Goudarzi, 1980; Guiraud, 1998) that controlled the sedimentary deposition pattern during the Late Cretaceous and Early Tertiary (Gumati and Kanes, 1985). The Mesozoic-Tertiary tectonic evolution of the African Plate is directly linked to the opening history of the Atlantic Ocean and the dynamics of Africa-Eurasia convergence (Guiraud *et al.*, 1992). The Sirt Basin represents a major intracratonic rift system on the north central African Plate and comprises a complex of horsts and grabens that began to develop in the Late Jurassic. The tectonic evolution of the Sirt Basin includes thermal arching and repeated phases of rifting that ended in the Late Cretaceous and Palaeocene to Early Eocene, and were followed from Late Eocene onward by thermal subsidence (Abadi *et al.*, 2008). In the Sirt Basin, the tectonic structure was built during the Jurassic where the basement and Cambrian-Ordovician rocks were exposed at the Hercynian surface unconformity in most of the basin area this phenomena remained until the late Jurassic, but there were exceptions in discrete marginal areas, where Triassic deposited sediments occurred. Between the Late Jurassic to Early Cretaceous, a variable thickness of continental siliciclastics in the south and marginally marine siliciclastics in the north was deposited on the Hercynian surface. Extensional and possibly transtensional faulting, followed by uplift and erosions deformed the Sirt-Tibesti arch during Albian or Early Cenomanian time; this activity phenomena were an

overture to the subsequent collapse of the arch (El-Alami, 1996; Hallett and El Ghoul, 1996). Hallett (2002) and others (reference therein) observed that on the Sirt Arch rifting and volcanic activity were continued through the Jurassic and into Early Cretaceous accompanied by the accumulation of extensive areas of continental deposited of sands. It has been suggested that at this time the Sirt Arch was situated over a fixed-mantle hotspot which thinned and weakened the overlying crust (El Ghoul, 1996). The structural alignment created trends, which is most obvious in the S and SE, and for the most part E-W, E-S-E-W-NW, and NE, W-SW (Goudarzi, 1980; Gumati and Kanes, 1985; Gumati and Schamel, 1988; Guiraud *et al.*, 1992; Guiraud and Bosworth, 1997; Guiraud, 1998).

Subsequently, on the structural highs at the Sirt unconformity, the subsurface sediments are composed of a mixture of Jurassic to Early Cretaceous siliciclastics sediments that were deposited within grabens or semi grabens on the Cambrian-Ordovician rocks or basement (Goudarzi, 1980; Gumati and Kanes, 1985; Guiraud, 1998; Hallett, 2002; Abadi et al., 2008).

In the early of Cenomanian, the main Sirt Basin rift phase was formed and produced a distinctive configuration of the basin with the collapse of the Sirt-Tibesti arch. It is represented from east to west by the Maragh, Agedabia, Hameimat, Sarir, Hagfa (Maradah) troughs, Kotla grabens, Zellah and Dor El Abida troughs and finally the Hun Graben. They are separated by the Amal Platform, Rakb high, Zelten, Beda and Dahra Platforms and Waddan uplift as shown in Figure 1.3. These structural features have great significance for the hydrocarbon generation, migration and accumulation from the troughs along the block basement faults to the platforms where most of the oil fields are situated (Gumati and Kanes, 1985; Gumati and Schamel, 1988; El-Alami et al., 1989; Gumati et al., 1996; Hallett and El Ghoul, 1996; Hallett, 2002; Abadi et al., 2008).

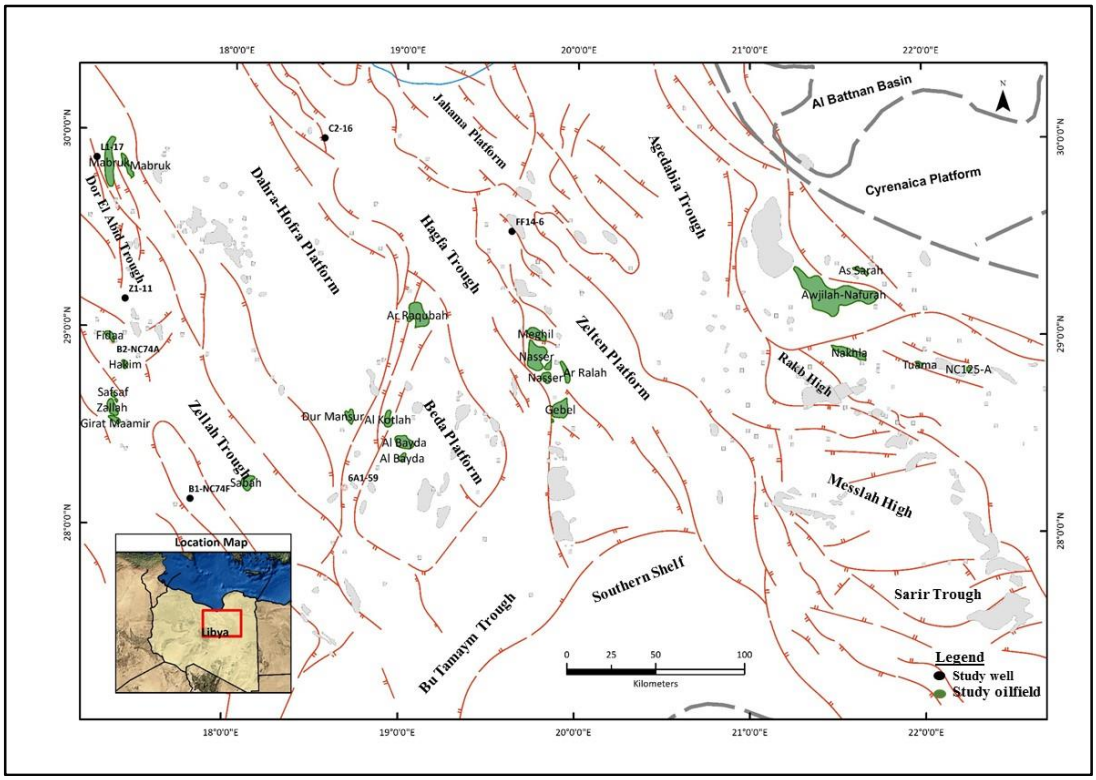

Figure 1.4: Tectonic structural feature map of the Sirt Basin Libya, showing location of the study wells and oilfields (after Abid, 2008).

Several researchers established that the main orientation of the Sirt Basin structural features was N-NW-S-SE, this was continued throughout the regular incidents of faulting during the Late Cretaceous and Palaeocene. A huge thickness of shale, carbonate and evaporite sediments were deposited in troughs, which represent the main source rocks, reservoir and seal rocks in the basin, whereas a considerably reduced thickness of dominantly shallow marine carbonates and siliciclastics was deposited on the platforms and those characterize the reservoirs unit and traps (Barr and Weeger, 1972; Gumati and Kanes, 1985; Baird et al., 1996; Roohi, 1996b; Hallett, 2002; Abadi et al., 2008)

The tectonic evolution of the Sirt Basin has been studied by many authors who confirmed different phases of uplifting and subsidence within the basin. Abadi et al. (2008) observed that this Sirt Basin history is comprised of four tectonic phases as shown in Figure 1.6.

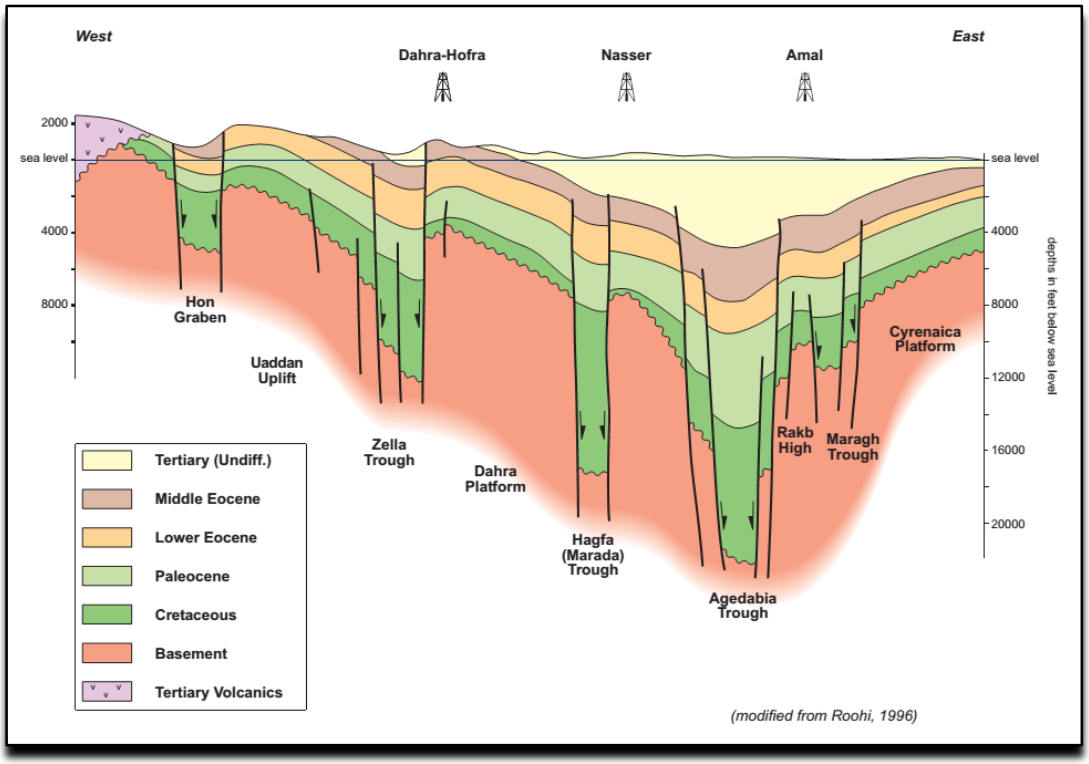

Figure 1.5: East-west regional structural cross section of the Sirt Basin (modified from Roohi, 1996).

The first, (Phase I**)** is related to the Late Jurassic to Early Cretaceous and is represented by subsidence in the southeast of the basin along an E-W structural trend. Secondly, Phase II is related to the Late Cretaceous, which includes five time intervals (Cenomanian, Turonian, Coniacian and Santonian, Campanian and Maastrichtian). This phase represents the major and rapid subsidence within the basin along the NW-SE structural trend as well as the main important petroleum source rock collection of sediments. Thirdly, Phase III is related to the Palaeocene to Early Eocene, and this phase contains most of the oil reservoir in the basin. Finally, Phase IV is related to the Middle Eocene until the present day. However, these tectonic phases had a significant effect on the main stratigraphic units within the basin. The subsidence phases I, II and III were produced as a result of fault activity connected to renewed rifting stages during the development of these phases. Phase IV was caused by sediment load and thermal reduction within the Sirt Basin (Abadi *et al.*, 2008).

In the southern part of the Sirt Basin a marginal marine system was developed and this continued until Coniacian times. In addition, and during Palaeocene times a shallow

marine environment was developed with active subsidence affecting most of the Sirt Basin troughs (Guiraud and Bosworth, 1997).

Subsequently, and during the Early Eocene the Sirt Basin was affected by subsidence in most of the grabens and this was associated with regressions causing the deposition of evaporite sediments (Hun evaporite and Gir Formations) in the western and southern sides of the basin. The Late Eocene was recognized by marine deposits due to a transgression event that was developed throughout the Early Oligocene. At this period in the Agedabia trough, subsidence was active along NW structural trend (Guiraud and Bosworth, 1997).

In the Post-Middle Miocene period, a regression event occurred as a result of the rapid fall in the sea level as continental sediments entered and were deposited in the basin. A rise in subsidence could be connected to compression events due to the collision between Europe and Africa (Van Der Meer and Cloetingh, 1993).

1.6 Stratigraphic Framework of the Sirt Basin

The nature of sediments deposited in the Sirt Basin is typical of a rift complex configuration (Figure 1.4). Therefore, the stratigraphic units within the Sirt Basin were controlled by of the basement structure, which separated the basin into discrete structural features (Figure 1.5). Abadi *et al.* (2008) recognized five sedimentary sequences that comprised the Sirt rift Basin: Pre-rift sediments, which consists of Palaeozoic and Triassic strata; Syn-rift basin in the Sirt Basin are comprised of three cycles sedimentary fills, which are Syn-rift fill I represented by Late Jurassic-Early Cretaceous marine siliciclastics rocks; Syn-rift basin fill II represented by the Late Cretaceous marine siliciclastics and carbonate rocks; and Syn-rift basin fill III represented by the Palaeogene sediments (Palaeocene to Early Eocene) and characterized by carbonate and evaporite strata; Post-rift basin fill by Neogene continental siliciclastic strata. In general, the syn-rift fill II that represented by the Late Cretaceous stratum contains most of the source rocks, whereas the Syn-rift fill III that represented by the Palaeocene strata contain most of the reservoir, traps and seal rocks within the Sirt Basin.

The Palaeozoic sequences are poorly developed due to non-deposition in the Late Palaeozoic and also to Hercynian and Early Mesozoic erosion (Abadi *et al.*, 2008). Following the non-deposition and erosion times, the Cretaceous strata was deposited directly above the Precambrian and Cambro-Ordovician rocks (Figure. 1.6). The Precambrian rocks were penetrated on the basement highs at several locations in the Sirt basin such as Dahra, Beda and Zelten Platforms and the Messlah and Rakb Highs and they were found to consist of granites and other volcanic rocks (Abadi *et al.*, 2008). The oil-bearing fractures and the weathered zone of the granitic basement of the giant Nafoora Augila oilfield in Rakb High are primary examples of the potential of the basement fracture rocks as reservoirs (Williams, 1972; Mansour and Magairyah, 1996). The basement rocks in the Sirt Basin comprise of granites, volcanic and metamorphic rocks of Precambrian and Early Cambrian age. These kinds of rocks are exposed only in the central Gargaf Arch, Jabal Awaynat and Tibesti mountains.

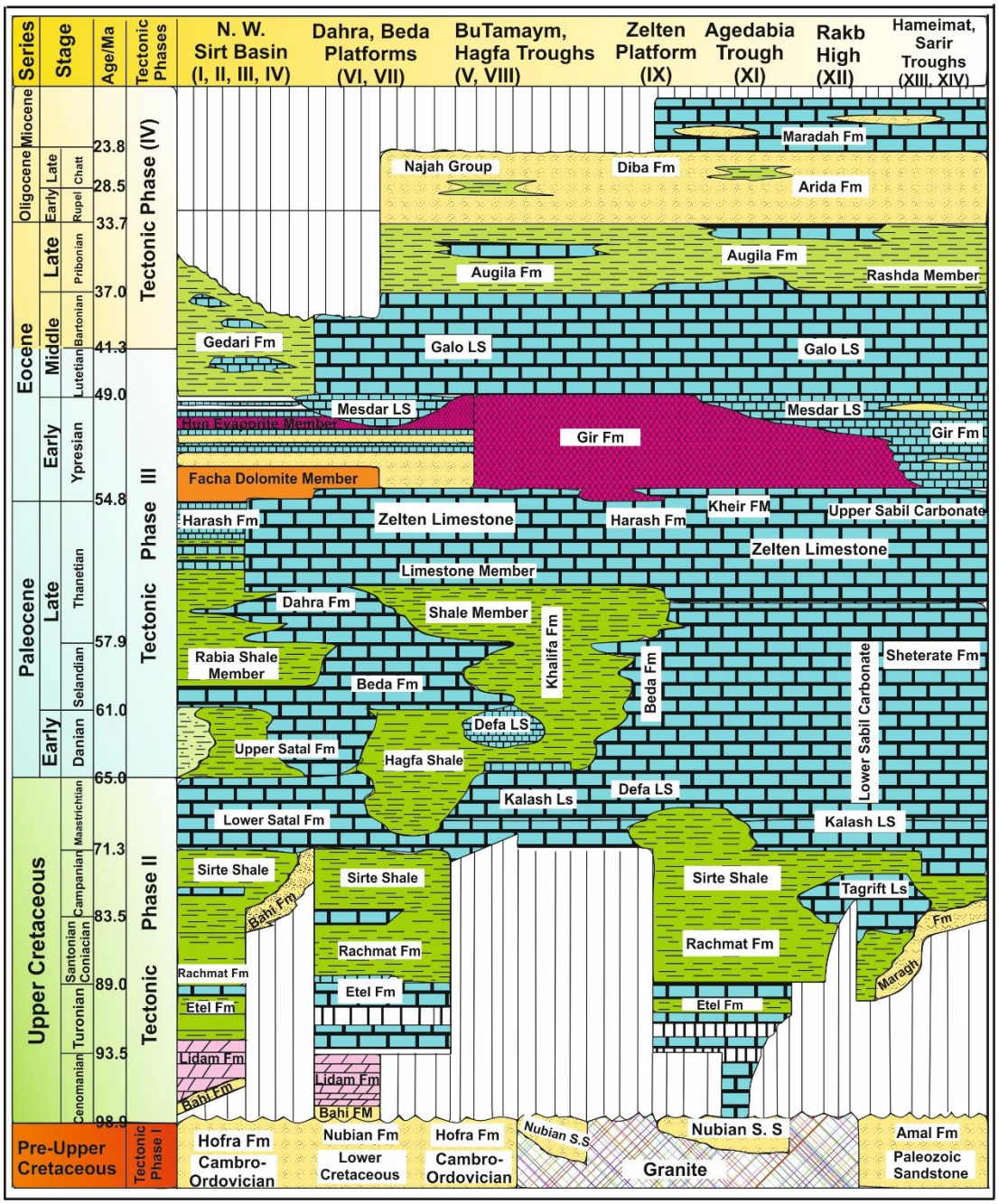

Figure 1.6: Stratigraphic–lithologic correlation chart of the Upper Cretaceous and Tertiary sequences of the Sirt Basin, After Abid, 2002.

1.7 Sirte Shale and Rachmat Black Shales Deposition

Demaison (1980) reported that there are several biological, physical and physico-chemical factors can influence the accumulation of organic matter in aquatic environments. Biological factors include primary biological productivity and biochemical degradation. Physical factors include the modes of transit of organic

matter to depositional sites, sediment particle size, and sedimentation rate and physico-chemical factors include the redox conditions under which the sediments were deposited. These factors interact to determine the qualitative and quantitative preservation of organic matter in sediment (Demaison, 1980).

Bordovskiy (1965) demonstrated that the main source of aquatic organic matter is phytoplankton, which are mostly comprised of single-cell microscopic algae residing in the uppermost layers of water illuminated by sunlight, or the euphotic zone. Also, the availability of mineral nutrients, and particularly nitrates and phosphate, is considered to be another principal limiting factor in addition to light in the euphotic zone. The other source of organic matter in the aquatic environment is terrestrial material transported from rivers and streams. Land plant productivity is largely dependent on the amount of rainfall on the supporting landmass (Demaison, 1980). Tissot and Welte (1984) reported that the biological productivity of the marine aquatic environment represents the most important factor in the potential for source beds, despite the abundance of organic matter in non-marine aquatic environments varying in subaerial environments as a result of the widespread occurrence of land plants. The chances of the preservation of organic matter in subaquatic environments is far greater.

In the past few decades, the frequent association of source rocks with the early part of transgressive sedimentary cycles has remained a major stratigraphic enigma (Wignall and Hallam, 1991). In this context, several of the world's best hydrocarbon source rocks belong to the category of transgressive black shale deposits, with organic facies AB being typical (Huc, 1988; Creaney and Passey, 1993). However, marine rather than terrestrial organic matter tends to be abundant in organic matter detritus, while amorphous organic matter is the typical maceral (Pasley *et al.*, 1991; Gregory and Hart, 1992).

Black shales were deposited over large regions of the ocean floor several times during the Phanerozoic period. These strata have attracted interest from geologist, petroleum geologist and petroleum geochemist for many reasons, not least of which is their great economic important as represent the source of more than 90% of global recoverable oil and gas reserves. There is more than one factor has been put forward to control the genesis of the black shales, which are including, plate tectonic configuration of

continents and the opening and closure of marine seaways; sea level rise and the flooding of shelves; the structure of the basins in which deposition occurred; and the evolution of marine and terrestrial biota and thus climate changes. In general, during the Cretaceous times, several tectonic and climatic factors favoured the development of anoxic conditions in the ocean. For the cretaceous a total of six ocean anoxia events have been recognized representing episode of globally widespread black shales deposition in marine environments that correlate closely with transgression.

Deposition of black shales strata in most of the area was restricted to a short period envelope termed the Campanian-Maastrichtian oceanic anoxia event. During this periods, a favourable combination of factors existed which led to the development of exceptionally strong oxygen-depletion in the North African Tethys. The Campanian-Maastrichtian black shales in North Africa are laterally discontinuous and their distribution and thickness were controlled by the palaeorelief. The thickest and regionally most extensive Campanian-Maastrichtian organic-rich shale in North Africa occur in Libya, namely in the Sirt Basin. Between 1 and 6% of the organic carbon burial during the Campanian-Maastrichtian was deposited in the relatively small restricted troughs in the Sirt Basin.

Many black shales are deposited on erosive or hiatal surfaces where they mark the initial stages of transgression. More commonly, black shales occur at the peak of transgression at the time the maximum shoreline retreated (Wignall, 1994). In this situation they represent the condensed section associated with the maximum flood surface (Creaney and Passey, 1993).

In fact it has only recently been appreciated that two distinct types of transgression black shales may be present in the stratigraphic record (Wignall and Maynard, 1993; Wignall, 1994). These are basal transgressive (BT) black shales and maximum flooding (MF) black shales.

The Sirt Basin is considered to be basal transgressive (BT) black shales since the Sirt Basin is silled basin. The presence of local topographic depressions during the initial stages of transgression appears to be the crucial factor in the formation of basal transgressive black shale. Hallam and Bradshaw (1979) have recognized the

irregularities of the bottom topography for black shale formation that would have locally inhibited bottom water circulation and allowed isolated pockets of stagnant water to persist, as shown in the model in Figure 1.7. Hallam's irregular bottom topography model was renamed as the puddle model for BT black shales. Huc (1988) also illustrated that, rather than merely restricting bottom water circulation, hollows would also have served as traps for fine-grained sediments and organic detritus. Tyson and Pearson (1991) suggested that the bottom water oxygen demand may have been high, further enhancing oxygen restriction. Hence, the low sediment influx may have caused the most rapidly subsiding depocentre to become emphasised. Sliter (1989) reported that the black shales actually accumulated during a series of relatively brief events commonly associated with intervals of sea level rise, for instance throughout Cenomanian-Turonian and Campanian-Maastrichtian times, which are termed oceanic anoxic events (OAEs). These phenomena are discussed with reference to the Sirt Basin below.

The Cretaceous period is characterized by a serious of marine anoxic phases (Schlanger, 1976); associated with wide speared organic matter burial and black shales deposition. During the Cenomanian-Turonian and Campanian-Maastrichtian oceanic anoxia events, organic-rich strata was deposited in the rift shelf basin and slope across North African. High sea level during the ocean anoxia events enhanced increased surface water productivity on a global scale throughout increased sea-surface area availability for marine phytoplankton colonization, large scale nutrient supply leaching of flooded lowlands probably have caused anoxic and maybe even euxinic conditions in water column. The grabens within the Sirt Basin may have been separated from the open sea by sills (Hallett, 2002). The Sirt Basin was a basin with unique geometry with an opening into the Mediterranean Sea during Campanian times, when marine transgression occurred from the north side. The presence of planktonic and benthonic foraminifera throughout the formation in the northern Sirt Basin, are indicative of an open marine and outer neritic environment (Barr and Weeger, 1972). Longitudal trough areas, however, gave rise to restricted marine environments further into the interior of the Basin (El-Alami *et al.*, 1989). These carried tracts of inactive mixing of water masses with a tendency to the development of stagnant waters. The lower part of the Sirte Shale barring the northern part of the basin contains bulimines (Foraminifera)

(Barr and Weeger, 1972), while the upper part of the section contain both planktonic and benthonic foraminifera. The presence of the bulimines indicates the prevalence of a restricted marine environment. Such kinds of environments lead to the depletion of oxygen. This indicates the tendency towards the development of stagnant waters as it becomes a zone of insufficient mixing of the water mass (Demaison, 1984). Furthermore, the bulimines are recognized to tolerate such stressed environments in stagnant conditions with low oxygen levels (Haynes, 1981). Subsequently, bulimines develop small, smooth and thin skeletons in the marine environment. At the upper formation, a tendency towards the amelioration of the marine reducing environment occurs as indicated by the presence of both planktonic and benthonic foraminifera (Cushman, 1974). Furthermore, based on benthonic foraminiferal analysis, the lowest Sirte Shale is thought to represent a middle neritic setting, while the middle and upper Sirte Shale mark a further deepening and an increase in oxygen-deficiency (El-Alami *et al.*, 1989). At the same time, oxygenated water dominated over the platform areas where deposition of carbonate sediments took place. Generally, during the deposition of the Sirte Shale rocks there was continuity in the growth of the tectonic structure into a horst-grabens fabric in a shallow marine basin. Therefore, a huge amount of subsidence and transgression may have occurred alongside the tectonic development (El-Alami *et al.*, 1989). The flow current of the surface was persistently towards the basin, which may have caused a continual supply and concentration of nutrients (El Alami, 1989). A fluvial drainage system may have curried and deposited the plant nutrients in the graben areas (El-Alami *et al.*, 1989). These systems transported solutes leached from soil in the horsts to grabens. However, mineral nutrients with the presence of light may lead to prolific primary biological productivity, resulting in the depletion of oxygen, and also in the graben areas, the semi-enclosed confined seas may have promoted water stratification to increase the oxygen depletion (El-Alami *et al.*, 1989). In the Sirte Shale there is good evidence of the presence of anoxic conditions associated with the continual supply of nutrients, which are in the form of laminations, the attainment of brownish-black colours, the presence of phosphate nodules and pyritic concentration, non-bioturbated sequences and the absence of macrofossils (El-Alami *et al.*, 1989).

The Sirte Shale Formation was deposited during a major sea level rise during Campanian times. This transgression also caused local anoxity in the rapidly subsiding and/or partially restricted areas. The anoxic sea bottom conditions and consequent preservation of organic matter makes it an excellent source rock in the Sirt Basin. However, mineral nutrients with the presence of light may lead to prolific primary biological productivity resulting in the depletion of oxygen. Also in the graben areas such as the Hameimat and Agedabia Troughs, the confined semi-enclosed seas may have promoted water stratification to increase oxygen depletion, primarily created by a sluggish deep basin circulation in restricted basins. In the Sirte Shale Formation there is good evidence of the presence of anoxic conditions associated with a continual supply of nutrients, in the form of laminations, the attainment of a brownish-black colour, the presence of phosphate nodules and pyritic concentrations, non-bioturbated sequences and the absence of macrofossils (El-Alami *et al.*, 1989). It is therefore probable that anoxia rather than organic productivity exerted the major control on the accumulation of organic-rich marine sediments and the development of organic-rich petroleum source rocks in the Sirte Shale Formation.

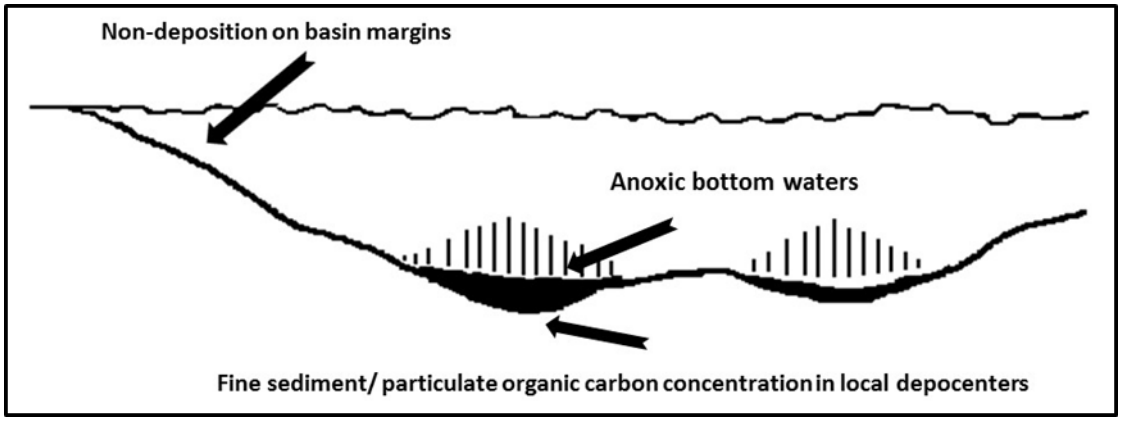

Figure 1.7: Puddle model for basal transgressive (BT) black shales for Sirte Shale, after Hallam and Bradshaw (1979) and Wignall (1994).

1.8 Campanian-Maastrichtian Organic Shales deposits in North Africa and Arabia

1.8.1 Libya Sirt Basin

In the Sirt Basin, Campanian-Maastrichtian organic shales occur in the graben areas and include the Sirte Shale Formation. The deposition of the Sirte Shale Formation mainly took place in the protected environment of sediment-starved rift grabens. This protected environment prevented the oxidation of the organic matter content through restricted circulation and prevented the dilution of the organic content due to low sediment influx, which led to the development and preservation of source rock quality shales (Schröter, 1996). The Sirte Shale represents the deepest facies consisting of a transgressive succession (Barbieri, 1994) and reflects deeper marine, slow deposition in grabens under anaerobic conditions (Tawadros and Tawadros, 2001). The Sirte Shale Formation is overlain by the upper Maastrichtian Kalash Formation and underlain by Lower Campanian Tagrifet Limestone (Barr and Weeger, 1972). There is a gradual transition in the lower part of the Sirte Shale Formation that passes laterally into the dark-brown, argillaceous micritic limestone with planktonic foraminifer assemblages, rare benthic fauna and the pyrite Tagrifet Formation. Similar to the Sirte Shale Formation, the Tagrifet Formation is characterized by a low oxygen, low energy conditions, with a supposed water depth at approximately 40 metres (El-Alami et al., 1989). The lithology of the Sirte Shale Formation is characterized by laminated, non-bioturbated, grey to dark grey to brown, calcareous silty shale in the lower part of the section. This represents the deepest facies that contains transgressive sequences which reflect deeper marine sediments and which showed slow deposition in trough areas under anaerobic conditions (Lüning, 2003). According to benthonic foraminiferal analysis, the lowest Sirte Shale Formation is believed to represent a middle neritic setting, as in Figure 1.2 (Lüning, 2003), while the middle and upper parts of the Sirte Shale Formation mark a further deepening and an increase in oxygen-deficiency (Lüning, 2003). At the same time, where oxygen was available within the water column, carbonate sedimentation took place leading to deposition over platform areas. The thickness of the Sirte Shale Formation varies and ranges from a few hundred metres to 900 metres in the graben areas. The Sirte Shale sedimentary section is

characterized by high gamma-ray values associated with maximum organic richness in the section type situated in well O2-59 on the edge of the Al Beda Platform (Hallett, 2002).

1.8.2 Tunisia and Algeria

Generally, the Algeria and Tunisia structures encompass the Atlas Fold and Thrust belt to the north and the Saharan Platform to the south, separated by the South Atlas Fault. Over the Saharan Platform, Cretaceous deposition is relatively thin and weak affected by tectonic movements, with the exception of local strike-slip movement (Bishop, 1988; Busson, 1998). In general, the sediments in the Atlas belt are highly influenced by sedimentary extensional and compressional phases (Bishop, 1988; Busson, 1998).

Eastern Algeria and Tunisia were covered by a large shelfal sea in Campanian-Maastrichtian times; see Figure 1.2. Most of the sediments mainly consist of marls and carbonates, but in Algeria and Tunisia the Campanian-Maastrichtian organic-rich strata have not been recorded, due to a low water depth that did not allow the deposition of the black shale formation (Askri, 1995). The Cenomanian-Turonian Bahloul Formation represents the main organic-rich zone in the Cretaceous/Tertiary boundary, and also The Eocene Bou Dabbos Formation (e.g. Gaaya and Ghenima, 1998).

1.8.3 Egypt

Structurally, the subsequent late Triassic/early Jurassic break-up of the Turkish-Apulian terrane from Egypt, where the northern part of Egypt was subjected to extensional stress, resulted in the formation of half-grabens (e.g. Moustafa and Khalil, 1990; Hirsch *et al.*, 1995; Guiraud and Bosworth, 1999). In Egypt, the half-grabens became inverted during the Turonian-Coniacian periods onwards (e.g. Luening *et al.*, 1998). This intra-plate deformation was important in the beginning of the collision of Afroarabia and Eurasia along the Cyprus subduction zone and the Bilits-Zagros suture zone. During Oligocene times from about 30 Ma, the rifting and separation of Arabia from Africa in the southern Red Sea started, and in the early Miocene at about 20 Ma

in the northern Red Sea and Suez Gulf rifting and separation also commenced (e.g. Baldridge *et al.*, 1991).

The Campanian-Maastrichtian Brown Limestone is organically rich in the Gulf of Suez area (Alsharhan, 2003). In addition, the Campanian-Maastrichtian interval is organically enriched in other places, such as the Duwi and Sudr formations in the Red Sea at the surface exposures in the Safaga and Quseir areas. In Egypt, in some places, the Campanian-Maastrichtian stratum was removed by Tertiary uplift and erosion (Dolson *et al.*, 2001). The Brown Limestone, consisting of limestones with interbeds of highly calcareous laminated shales and marls, represents marine outer sublittoral facies. In the Gulf of Suez region, the Brown Limestone has thicknesses ranging from 25-70 metres. It is also characterized by abundant phosphorite and glauconite. This formation was deposited during a strong Campanian sea level rise (Haq *et al.*, 1987) because of widespread flooding of the Northeast African and Northwest Arabian shelf (Figure 1.2).

The Duwi Formation consists of marl interbedded with phosphate beds. It is conformably overlain by the Dakhla Formation (Said, 1962). The lower Dakhla is similar to the Duwi Formation, characterized as organic-rich but lacking the development of the phosphorite beds, which may be due to raised water depth (Robison, 1995; Alsharhan, 2003). Robison (1995) reported that the Brown Limestone, Duwi and Dakhla Formations are organically enriched in the Red Sea region, in the southern Western Desert, and in the Gulf of Suez. Their total organic carbon values reach up to 8 wt%, and locally to 20 wt%. The Brown Limestone contain the highest average TOC of all potential source rocks in the Gulf of Suez, with Type II oil-prone kerogen, and also Type I is present (Alsharhan, 2003). The, organically rich laminated shale of the Brown Limestone was deposited under dysoxic to anoxic marine conditions (Robison, 1995). It has a low abundance of pyrite, suggesting that little iron was available, resulting in the formation of sulphur-enriched organic matter (Robison, 1995). The Brown Limestone Formation is thought to be the main candidate source

rock in the Gulf of Suez (Robison, 1995; Alsharhan, 2003). The black shale of the Campanian-Maastrichtian Brown Limestone Formation is mature in large parts of the Gulf of Suez and represents the oil kitchen source rock (Robison, 1995).

1.9 Source Rocks in the Sirt Basin

The Upper Cretaceous shales of the Sirte Shale, and Rachmat Formations are indicated in several studies (see below) as being the principal petroleum source rock units, in addition to other local source rocks such as the Etel and Hagfa Shale Formations, in the Sirt Basin.

1.9.1 Rachmat Formation

The Upper Cretaceous Coniacian-Santonian Rachmat Formation represents typically consists of shale with minor interbeds of limestone, sandstone and dolomite (Barr and Weeger, 1972). The Formation occurs widely in the Sirt Basin, but is absent on regional highs such as in the Amal and Dahra-Hofra Platforms and Waha area. The shale units are characterized by grey to dark grey fissile to slightly blocky, non-calcareous, and glauconitic and pyritic, while the lower units are more frequently limestone. In the Sirt Basin, the formation has thicknesses ranging from 150m to nearly 500m (Barr and Weeger, 1972). The Rachmat Formation was deposited under marine conditions and is considered a source rock for hydrocarbon generation (Hamyani *et al.*, 1984; El-Alami *et al.*, 1989; Gumati *et al.*, 1996; Hallett, 2002). The Rachmat Formation has total organic carbon (TOC) contents ranging from 0.5 to 4.65 wt% (Hamyani *et al.*, 1984; El-Alami *et al.*, 1989). The Rachmat Formation contains predominantly amorphous kerogen comprising a mixture of mainly marine derived sapropel and degraded, terrestrially derived organic matter and varies in composition between Type II and III (El-Alami *et al.*, 1989).

1.9.2 Sirte Shale Formation

The Upper Cretaceous black shales of the Campanian Sirte Shale Formation are considered as the main candidate source rock in the Sirt Basin (Hamyani *et al.*, 1984; Gumati and Schamel, 1988; El-Alami *et al.*, 1989; Gumati *et al.*, 1996; Hallett and El Ghoul, 1996; Ben Ashour, 2000; Hallett, 2002). The formation is widely distributed

throughout the graben of the basin and has a variable thickness and richness. The thickness of the formation is varied and ranges from 500m in the west part of the basin at Zellah Trough to over 700m in the east part of the basin at Agedabia Trough (Barr and Weeger, 1972; Hamyani *et al.*, 1984; El-Alami *et al.*, 1989; El-Alami, 1996; Gumati *et al.*, 1996; Ben Ashour, 2000). The Sirte Shale Formation is dominated by shale sections with thin limestone interbedded. It consists mainly of dark grey, brown to black shale, which is calcareous and carbonaceous for the most part and grades into shaly limestone, while the base of formation is usually silty and sandy and characterized by glauconite and pyrite (Barr and Weeger, 1972). It contains a total organic carbon (TOC) contents ranging from 0.5 wt% to more than 6 wt%, predominantly as an amorphous organic matter (OM) with some contribution of terrestrial and algal OM and contains Type II to Type II-III kerogen, which was deposited under marine conditions (El-Alami *et al.*, 1989).

1.9.3 Kalash Formation

The Upper Cretaceous Maastrichtian Kalash Formation is widespread over most of the Sirt Basin and are up to 600m thick in the Agedabia Trough (Barr and Weeger, 1972). The Formation consists mainly of limestone with dolomite, lime marls and shales interbedded. The limey marl with shale units of the Kalash Formation are characterized by being lean to moderately organic matter, and have TOC contents ranging from 0.34 wt% to 1.25 wt%, predominantly of amorphous, oil prone Type II Kerogen, which was deposited under suboxic to slightly anoxic marine environments (Baric *et al.*, 1996).

1.10 Reservoir Rocks

Generally, in the Sirt Basin, petroleum is produced from several reservoir units that extend from Precambrian to Oligocene in age. The hydrocarbon distribution in the Sirt Basin has been highly controlled by major tectonic events (Goudarzi, 1980; El-Alami *et al.*, 1989; Gumati *et al.*, 1996; Ben Ashour, 2000; Hallett, 2002; Abadi *et al.*, 2008). These oil reservoirs are mostly composed of Mesozoic clastic rocks, and Tertiary carbonate rocks. Gumati *et al.* (1996) showed that the major reservoir units in the Sirt Basin are situated in the fractured Precambrian basement rocks and also in Cambro-Ordovician sandstones of the Gargaf Group in the Amal, and Nafoora Augila oilfields.

Whereas, at the Sarir, Amal, and Abutfill oilfields, the lower Cretaceous Nubian Sandstone Formation is considered as the main reservoir unit producing hydrocarbons in the eastern Sirt Basin (El-Alami, 1996; Gumati *et al.*, 1996). The carbonate rocks of the Upper Cretaceous, Palaeocene, Eocene and Oligocene ages create the main reservoir beds at the Bahi, Beda, Dahra, Defa, Gialo, Hakim, Mabruk, Nasser, Raguba, Safsaf, Sabah and Zelten oilfields in the centre and western Sirt Basin (El-Alami *et al.*, 1989; El-Alami, 1996; Gumati *et al.*, 1996).

1.10.1 Hofra Sandstone Formation: Cambro – Ordovician

The Cambro-Ordovician Hofra Sandstone Formation comprises of clean quartz sandstones with trace amounts of shale, siltstone, conglomerate and thin interbedded volcanic rocks (Barr and Weeger, 1972). It has thickness of 1105m, increasing to around 1369m towards northwest and is unconformably underlain by igneous metamorphic basement rocks, while the upper contact shows a major Hercynian unconformity. It is characterized by the presence of secondary fracture porosity and produces oil in the Balat, Belhedan, Ora, Raguba and Samah oilfields. It could be equivalent to Amal Formation in the eastern part of the Sirt Basin (Barr and Weeger, 1972).

1.10.2 Bahi Sandstone Formation: Late Cretaceous

The Upper Cretaceous Cenomanian Bahi Sandstone Formation consists of interbedded sandstone, siltstone, conglomerate and shale, but is predominantly sandstone. It has a thickness ranging from a few meters to a maximum of about 122m (Barr and Weeger, 1972). The upper contact is conformable with the Cenomanian Lidam Formation or other Upper Cretaceous formations, while the lower boundary is unconformable with the Palaeozoic rocks. It has varying porosity between 12 to 28% associated with a permeability of about 150 md. The Bahi Formation was deposited in very shallow marine environment in the first transgressive cycle of the Upper Cretaceous (Sghair and El-Almi, 1996).

1.10.3 Lidam Formation: Late Cretaceous

The Upper Cretaceous Cenomanian Lidam Formation is comprised of grey to light brown coloured dolomite with sandstone and glauconite particularly in the lower part, and represents the first distinctive marine deposit overlying the basement rocks, which are Palaeozoic strata, Nubian Formation or Amal Formation, depending on location (Barr and Weeger, 1972; Roohi, 1996). It has a thickness of about 600m in the troughs but less in the flanks and platform areas. It was deposited in shallow marine environments, lagoonal in part and intertidal depending on their location in the basin. Baird *et al.* (1996) showed maps illustrating that the Lidam Formation is existent in the Zellah, Abu Tumayam, Marada, Agedabia, and Hameimat Troughs, but absent or non-deposited over major platform areas for instance the Al Dahra-Hofra, Zelten, and Amal Platforms. The Lidam Formation is an important oil reservoir unit in the western Sirt Basin, and, Mansour and Magairyah (1996) also showed that the Lidam Formation forms a significant oil reservoir unit in the eastern Sirt Basin.

1.10.4 Satal Carbonate Formation: Late Cretaceous-Early Paleocene

The Satal Formation carbonate rocks of the Maastrichtian-Danian age occur in the subsurface of the western Sirt Basin, but has restricted areal distribution on the Al Beda and Al Dahra-Hofra Platforms. The Satal Formation has thickness of 130m with excellent porosity and permeability. The Satal Formation was subdivided into two members (Barr and Weeger, 1972). The Upper Cretaceous lower member consists mainly of argillaceous calcilutite and calcarenite limestone with thin dolomite and shale. The Palaeocene upper member consists of light grey to white calcarenite and calcilutite dolomite, anhydrite and shale beds. The contact with the underlain Sirt Shale Formation is conformable, but unconformable with the Hofra Formation. The upper contact is sharp, but seems to be conformable with the Thalith Member of the Beda Formation of the Middle Palaeocene age (Barr and Weeger, 1972). The Satal Formation is considered one of the principal oil reservoir units in the western Sirt Basin. It has produced oils only in Al Dahra Platform, Ali and Almas oilfields (El-Alami *et al.*, 1989; Roohi, 1996; Roohi, 1996b; Hallett, 2002).

1.10.5 **Beda Formation: Late Palaeocene**

The Palaeocene Seladndian Beda Formation is widespread in the western Sirt Basin. The formation consists of various interbedded limestones with calcareous shales and dolomites. However, the Beda Formation becomes more shaly in the northwest of the basin. It is subdivided into two members, upper Rabia Shale Member and lower Thalith Member (Barr and Weeger, 1972). The Thalith member is dominated by argillaceous limestone with traces of pyrite and glauconite, and minor shale or chalky marl and has about 35m thick. The lower contact is conformable with the Hagfa Shale or Satal Formation, where upper contact is conformable with the Rabia Shale Member. The Rabia Shale Member is predominantly shale and mudstone with minor limestone interbedded. It has a thickness of about 70m and is conformable with both the underlying Thalith Member and overlying Dahra Formation (Barr and Weeger, 1972).

In the Zellah Trough the Beda Formation reaches a maximum thickness of 500m with an average of 180m in the platforms (Bezan *et al.*, 1996).

Bezan *et al.* (1996) subdivided the Beda Formation into two members, the lower Beda, Farrud Member and the upper Beda, Ora Member in the Dahra field, and Zellah Trough in the western Sirt Basin. The Farrud Member is consists of skeletal, oolitic calcarenite limestone transient to dolomite, with excellent reservoir characteristics, which is an oil producing in several oilfields such as the Ghani oilfield. It has a thickness of about 45m. The Farrud Member was deposited in shallow marine environments. Porosity in the Farrud member ranges as high as 35% (Bezan *et al.*, 1996).

The Ora Member of the Upper Beda Formation comprises mainly of dolomite. The member has various thicknesses ranging from 12 to 100m in Beda Platform and Kotla Graben, respectively. This member is an oil producing for several oilfields in Beda Platform. At the Wadi oilfield the Lower Beda carbonate Formation is found restricted between two deeper shale sections contains oil at the Wadi and Zaqqut oilfields (Bezan *et al.*, 1996; Roohi, 1996; Hallett, 2002).

1.10.6 Dahra Formation: Late Palaeocene

The Palaeocene Thanetian Dahra Formation is widespread in the western Sirt Basin and is composed of up to 100m of chalky, calcarenite, calcilutite argillaceous or pyritic limestone and dolomite with thin dark grey shale interbedded (Barr and Weeger, 1972). However, in the southwestern part of the Sirt Basin, the lower part changes to shale. The lower boundary is conformable with the Rabia Shale Member of the Beda Formation and upper contact conformable with Khalifa Formation. The Dahra Formation forms the main reservoir unit in the Al Dahra-Hofra oilfields. The formation is highly porous and represents good to very good reservoir and is often termed by oil operating companies as Mabruk Limestone Formation since it forms the principal reservoir rocks on the Mabruk oilfield in the north-western part of the Sirt basin (Roohi, 1996; Roohi, 1996b; Hallett, 2002).

1.10.7 Zelten Formation: Late Palaeocene

The Late Palaeocene Thanetian Zelten Formation is distributed in the central and western parts of the Sirt Basin and consists of argillaceous to shaly, chalky fossiliferous calcilutite to calcarenite limestone with subordinate dolomite (Barr and Weeger, 1972). In the east of the Sirt Basin, the formation becomes bioherms. It conformable overlies the Khalifa Formation or Lower Sabil Carbonate, and is conformable overlain by the Harash Formation (Barr and Weeger, 1972). The formation has various thickness variations recorded; in Zellah and Marada Troughs, it is about 140m, and over 150m in the Agedabia Trough. It has porosity reached up to 40% in the Nasser oilfield and the formation, forms the reservoir rock unit for the Nasser oilfield on the Zelten Platform (Hamyani *et al.*, 1984; Roohi, 1996; Hallett, 2002).

1.10.8 Facha Dolomite Member: Early Eocene

The Eocene Facha Member of the Gir Formation is confined to the western Sirt Basin and consists mainly of massive dolomites with minor amounts of anhydrite (Barr and Weeger, 1972). It was deposited in the open marine environment and is conformable with the overlying Hun Evaporite Member. It has a thickness of about 104m which is fairly constant in the area of its occurrence (Barr and Weeger, 1972). It forms the principal reservoir in western part of the basin, especially for those oilfields Aswad,

Sabah, and Zellah (Hamyani *et al.*, 1984; El-Alami *et al.*, 1989; Elag, 1996; Gumati *et al.*, 1996; Hallett, 2002). In addition, the Facha Dolomite Member is important to the other area located in the Dahra and Beda Platforms and Zellah Trough, where the Hun Evaporite Member is representing the cap rock for the Facha reservoir. Elag (1996) studied the porous Facha dolomite member from several wells and observed that the upper part of the member is considered the best reservoir unit in Zellah Trough. Therefore the Facha Dolomite Member is one of the significant targets for the hydrocarbon exploration in the Sirt Basin.

1.11 Petroleum History of the Sirt Basin Libya

The Sirt Basin is largest petroleum province discovered in Libya so far (Hamyani *et al.*, 1984; El-Alami *et al.*, 1989; El-Alami, 1996; Gumati *et al.*, 1996; Hallett and El Ghoul, 1996; Mansour and Magairyah, 1996; Roohi, 1996; Hallett, 2002; Abadi *et al.*, 2008). Active search operations for hydrocarbons in Libya began in 1956 and first well (A1-18) was drilled in the large anticline structure in the northern Cyrenaica Platform by the Libyan American Company, but was dry (Hallett, 2002). In 1958 the first commercial oil was discovered in the Bahi oilfield which has oil in the Palaeocene carbonate rocks on the western margin of the Dahra Platform in well A1-32 by the Oasis Oil Operation Company (Hallett, 2002). Subsequently, Oasis discovered oil on drilling the B1-32 well on the Dahra Platform, the Dahra oilfield was named (Hallett, 2002). On a nearby concession (11), the Mobil oil company drilled the A1-11 well, which proved another major discovery (Hallett, 2002). Esso started drilling operations in the central of the Sirt Basin and made a small discovery in Eocene carbonate rocks at concession 5, then after drilling the C1-6 well on the Palaeocene carbonate rocks in the Zelten Platform, discovered a giant field with reserves of 2.2 billion barrels, named the Zelten oilfield (Hallett, 2002). This discovery changed and improved the economic face of the Libyan oil industry. The Libyan economic sector was developed due to the discovery of several giant oilfields during the period of 1959 to 1961. At that time the Oasis Operation Oil Company discovered two giant oilfields, the Al Waha field (A1-59 well) south of Zelten Platform, when they drilled into a Late Cretaceous nearshore carbonate reservoir, and the Defa field (B1-59) when they drilled into the Palaeocene carbonate in the Zelten Platform at concession 59 (Hallett, 2002). Since that time, many

oilfields, including giants were found such as Augila, As Sarir, Intisar, Intisar D, Tuamma, Hamid and Abutiffel oilfields with other small discovery (Hallett, 2002). During 1999 to 2002 Libya was under sanctions from the USA and European, which led to reduce the exploration activity. At that time Libya had an estimated total reserve between 40 to 50 billion barrels of recoverable oil (Hallett, 2002). In 2005 the Libyan government opened areas through bids (EPSA IV) for encouraging foreign companies to undertake new exploration for oil and gas in Libya (Hallett, 2002). Most of these areas require the application of advanced new technologies to discover the remaining oil and gas fields.

In the last three decay most of the exploration activity in the Sirt basin has been concentrated on the high structural areas and platforms, but nowadays in Libya, the search for deep plays is taking priority as results of the availability of new technologies. This exploration activity has been successful and new discoveries have been found in the troughs areas.

Chapter 2. Molecular marker and biomarker Identification

2.1 Petroleum Origin and Compositions

This section describes the different molecular petroleum markers used in this study. Petroleum is composed primarily of hydrocarbon, existing in the gaseous or liquid phases in natural reservoirs (Hunt, 1995). Petroleum is defined by the American Petroleum Institute (API) as a mixture of hydrocarbons that exists in the liquid phase in natural subsurface reservoirs and which remains liquid at atmospheric pressure after passing through surface separating facilities (Waples, 1985; Hunt, 1995). Petroleum mainly consists of only the two elements hydrogen and carbon, but may often also contain minor elements such as nitrogen, sulphur and oxygen, while traces of heavy metals, for instance, nickel and vanadium may also be present (Hunt, 1995).

2.2 Normal-Alkanes and Isoprenoids

Hydrocarbon molecules, usually occur in the structural forms, alkanes, cycloalkanes, alkenes and arenes (Hunt, 1995). Alkanes are open-chain molecules with single bonds between the carbon atoms; cycloalkanes are alkane rings; alkenes have one or more double bonds between the carbon atoms; and arenes are hydrocarbons with one or more benzene rings.

The *n*-alkanes or paraffins are aliphatic saturated hydrocarbon fractions. In recent sediments they can be derived from cuticular waxes of land plants, from marine and lacustrine plankton and from bacteria, but in thermally mature sediments they can also be derived from the thermal breakdown of kerogen (Waples, 1985; Hunt, 1995; Peters *et al.*, 2005b).

Cycloparaffins or naphthenes are formed by the carbon atoms being joined in a ring structure, and are considered the most common molecular structures in petroleum. Generally, naphthenes rings have five or six carbon atoms. The quantity of naphthenes usually increases in heavier fractions and decreases in light fractions (Hunt, 1995).

The hydrocarbon fractions of both land plants and marine usually contain traces of isoprenoid hydrocarbons (Hunt, 1995). Pristane and phytane are the best known, and most common isoprenoids are present in recent and ancient organic sediments and in

crude oils. Chlorophyll is considered to be the main source of pristane and phytane, which are mainly derived from the phytoll side chain of chlorophyll. Variations in pristane or phytane abundance are then based on the redox potential of the depositional environment. Oxygenated environments result in pristane, and reducing environments phytane (Tissot and Welte, 1984). The pristane to phytane (Pr/Ph) ratio can thus be utilised to determine the depositional environment as well as being a maturity indicator (Waples, 1985). A Pr/Ph ratio of less than 1.0 indicates that the organic sediment or crude oil was deposited under anoxic conditions, whereas more than 2.0 indicate an oxic environment. It is clear however, that Pr/Ph ratios are affected factors other than the degradation of phytoll in certain environments, and therefore these ratios should also be used with caution when interpreting oil source environment data (Peters, 2005b).

Other ratios or parameters can be determined from *n*-alkane and acyclic isoprenoid alkane compounds and used to evaluate thermal maturity, organic matter type and to estimate depositional environments such as the isoprenoid/*n*-alkane ratio (Pr/*n*-C_{17} and Ph/*n*-C_{18}); the terrigenous-alkanes/aquatic *n*-alkane ratio (TAR) (*n*-C_{27}/*n*-C_{17} or *n*-C_{25}/*n*-C_{17}) and the carbon preference index (CPI) (Hunt, 1995; Peters *et al.*, 2005a; Peters, 2005b). As well as thermal maturity and depositional environment, the Pr/*n*-C_{17} and Ph/*n*-C_{18} ratios are used to determine level of biodegradation in crude oils (Hunt, 1995) and reference there in.

The carbon preference index (CPI) that is derived from *n*-alkanes distribution can be used to evaluate the thermal maturity of the source rock and crude oil, but caution must be exercised since a high CPI indicates low maturity and land plant input, while values of approximately 1.0 suggest, but do not prove, that an oil or rock extract is either thermally mature and/or may have arisen from a predominance of marine input(Peters, 2005b).

2.3 Tricyclic and Tetracyclic Terpanes

Many terpanes in petroleum originate from prokaryotic bacterial membrane lipids (Ourisson *et al.*, 1982). These bacterial terpanes include several homologous series, including acyclic, bicyclic, tricyclic, tetracyclic, and pentacyclic compounds. Tricyclic

terpanes are commonly distributed in petroleum and source rocks of lacustrine and marine origin (Hunt, 1995). Moldowan *et al.* (1983) identified the tricyclic terpanes homologous extending out to C_{45} in many source rocks and crude oils. The tricyclic terpane compounds are commonly recognized up to C_{29}, and above that are often hidden by hopanes in m/z 191 mass chromatograms.

Concentrations of tricyclic terpanes seem to increase with increasing maturity in crude oils due to their breaking off from asphaltenes and kerogens (Kruge, 1986). The ratio of tricyclic terpanes to hopanes has been reported to increase with increasing maturity, which is believed to be as a result of the greater relative generation of tricyclic terpanes from kerogen at higher maturity (Peters and Moldowan, 1993). Levels of tricyclic terpanes have also been used as molecular maturity parameters due to their resistance to biodegraded (Neto *et al.*, 1986).

The tetracyclic terpane series ranges from C_{24} to $C_{27,}$ although there is some evidence for extension homologous up to C_{35} (Aquino Neto *et al.*, 1983). They are believed to be derived by the thermal or microbial breakage of five membered E-rings in hopanes or precursor hopanoids, or may be from bacteria through the biosynthetic route or from terrigenous precursors (Peters, 2005b).

2.4 Pentacyclic Triterpenoids

The pentacyclic terpane compounds are classified into two groups, hopanoids and non-hopanoids. The hopanoids are the most common biomarkers in the biosphere and geosphere. They occur in the membranes of prokaryotes, and most have been isolated from organisms and organic-rich sediments. The hopanoids are widespread distribution among bacteria and cyanobacteria (blue-green algae) as well as other primitive organisms. Although, bacteria are considered to be the major source of hopanoids, they are also found in ferns, lichens, and a few higher plants (Ourisson *et al.*, 1982). Hopanoids are thermodynamically unstable when occurring in natural 17β(H), 21β(H) stereochemistry inherited from their biosynthetic origin, such as found in immature sediments, but once the sedimentary organic matter is buried deeper and where diagenesis and catagenesis processes (maturation) have occurred, more stable

hopanoids with 17α(H), 21β(H) stereochemistry are formed. The distribution of hopanes is monitored by m/z 191 fragment ions by GC-MS.

Many hopane ratios can be used to assess the thermal maturity of crude oils and source rocks as well as to identify origin and depositional environment, such as the C_{27} Ts/(Ts+Tm) (Seifert and Moldowan, 1978), C_{29}Ts/C_{30} 17α(H)-hopane (Volkman *et al.*, 1983); C_{29} Ts/(C_{29} hopane + C_{29} Ts) (Moldowan *et al.*, 1991); C_{30} 17β, 21α(H)-mortane/C_{30} 17α, 21β(H)-hopane (Seifert and Moldowan, 1980); and the 22S/(22S+22R) homohopane isomerization ratios (Seifert and Moldowan, 1980).

The distributions of the extended C_{31} to C_{35} hopanes (homohopane) can be used to deduce redox conditions during deposition of the source rocks. The C_{35} homohopane index (C_{35}/(C_{31} to C_{35})) usually expressed as a percentage. It has been used as an indicator for redox marine sediments during diagenesis, with a high ratio indicating anoxia conditions; although this ratio is also affected by thermal maturity. High values of C_{35} homohopane are usually associated with marine carbonate or evaporite sediments (Boon *et al.*, 1983; Connan *et al.*, 1986; Mello *et al.*, 1988a; Ten Haven *et al.*, 1988; Clark and Philp, 1989).

The non-hopanoid pentacyclic triterpanes include gammacerane, friedelane, oleananes and lupanes. Gammacerane is found in many oils and source rocks, particularly in hypersaline environment, and is characterized by a high resistance to biodegradation (Seifert *et al.*, 1984). The oleanane pentacyclic triterpanes are derived from higher plants and angiosperms of the Upper Cretaceous Age and younger. 18αH-oleanane can be used in petroleum geochemistry for oil to source rock correlation in several basins particular with Upper Cretaceous to Tertiary sediments that contain high terrestrial material input.

2.5 Steranes and diasteranes

Steranes are very common constituents of sedimentary organic matter and crude oils. They are thought to be derived from sterol in the cell walls of eukaryotes and may be carrying out a similar function as that of bacteriohpanetetrol in prokaryotes (Peters and Moldowan, 1993; Peters, 2005b). Sterols are abundant in the biosphere; they vary widely in distribution, size and structure. The early alteration products of sterols may

be formed by microbial activity with low temperature chemical reactions associated with specific sources or depositional environments. This makes them useful in correlation studies of crude oils and related bitumen. Two major series have been recognized, regular steranes and diasteranes. The steranes observed often contain 19 to 30 carbon atoms, with C_{27} to C_{29} the most common. Steranes derived from marine origin extend from C_{26} to C_{30}. The degree of isomerisation at C-14, C-17 and C-20 of regular steranes series has been extensively used to evaluate the maturity of crude oils and source rocks (Mackenzie *et al.*, 1980; Seifert and J. M. Moldowan., 1981; Mackenzie, 1984).

Sterane distributions are apparent in GC-MS m/z 217 or 218 mass fragmentograms. Because of the complexity of steranes and hopanoids, they have become widely used as biomarkers for evaluating the source, maturity, migration, biodegradation and correlation of crude oils with parent source rocks (Hunt, 1995). The occurrence of C_{30} 4-desmethylsterane in crude oil is the most powerful means to identify the input of marine organic matter to the source rock (Moldowan *et al.*, 1985; Peters *et al.*, 2005a; Peters, 2005b).

Diasteranes, which have also termed rearranged steranes, appear in significant quantities in petroleum at the moderate mature zone. The amount of diasteranes compared to regular steranes depends on maturity, lithology type and the depositional redox conditions of the source rocks. Diasteranes are often used to differentiate between clastics rocks with high diasterane concentrations from carbonate rocks that have low diasterane concentrations (Mello *et al.*, 1988b). Diasteranes appear to be more stable than regular steranes, which leads them to be more dominant with increasing maturity.

Because biomarkers are derived from biological precursor molecules exist in specific organisms that live only under certain conditions, it is logical to attempt to use biomarkers as indicators of those life conditions (Waples and Machihara, 1990). However, biomarker data should always be fully integrated with all other available geochemical and geological information in order to make the most reasonable interpretation possible for basin studied.

2.6 Diamondoids

Diamondoids are compounds which naturally occur in all oils, condensates and source rocks in different amounts (Wingert, 1992; Dahl *et al.*, 1999). Diamondoids are saturated polycyclic hydrocarbon compounds with a diamond-like structure comprised of rigid fused carbon structures similar to tiny pieces of diamond (Wingert, 1992). Diamondoids in petroleum are thought to be formed from enzymatically-created lipids with subsequent structural rearrangement during the process of source rock maturation and oil generation(Peters, 2005b). Because of this, the diamondoid content of petroleum has been used to distinguish source rock facies and evaluate the thermal maturity(Peters, 2005b). Diamondoids are thermally more stable and more resistant to biological degradation than most other hydrocarbon compounds (Dahl *et al.*, 1999). Based on that, two diamondoid maturity parameters have been used to determine the thermal maturity of source rocks and crude oils (Chen *et al.*, 1996). These are the methyladamantane index (MAI) and the methydiamantane index (MDI).

2.7 Monoaromatic, Diaromatic and Triaromatic Steroids

Aromatic markers are important components in crude oils and ancient organic sediments, and can provide valuable geochemical knowledge about the organic matter input, depositional environments, thermal maturity and oil-oil, and oil-source rock correlation (Radke, 1987; Peters, 2005b). The aromatic markers contain a complex mixture of compounds such as mono-, dia- and triaromatic components. As the aromatic steroids have high resistance to biodegradation, they can be used for the purposes of correlations in degraded oils (Larter *et al.*, 2012). Hussler *et al.* (1981) noted that the occurrence of monoaromatic steroids in immature sediments indicates the early diagenetic phase, whereas the triaromatic steroids are believed to have originated from aromatization and the loss of methyl groups from aromatic steroids with increasing thermal maturity.

2.8 Polycyclic Aromatic Hydrocarbons (PAHs)

Aromatic hydrocarbons are abundant in crude oils and source rocks and have the potential to provide significant information on sedimentary environments, source input, thermal maturity, migration, and oil-oil and/or oil-source rock correlation (Garrigues

and Ewald, 1983; Radke, 1987; Radke *et al.*, 1994; Peters *et al.*, 2005b). Polycyclic aromatic hydrocarbons (PAHs) are not produced in living organisms and are almost never present in organic matter (Hase and Hites, 1976). Most PAHs in crude oils are the products of complex chemical transformations of naphthenic and/or olefinic biological ancestors during thermal stress in catagenesis phases, because living organism cannot produce aromatic hydrocarbons in significant quantities (Radke, 1987). They are thought to be derived from the modification of biological source compounds, for instance, steroids and terpenoids (Bendoraitis, 1974; Laflamme and Hites, 1979). Phenanthrene compounds seem to be produced from steroids, and alkylnaphthalenes compounds appear to be derived from terpenoids (Breger, 1960; Ishiwatari and Fukushima, 1979). Ourisson *et al.* (1979) observed that the most abundant and widely distributed alkylnaphthalene compounds in the sedimentary environment are bacterially derived hopanoids. Several series of aromatic hydrocarbons have been described, including naphthalenes, alkylnaphthalenes, and phenanthrene and alkylphenanthrenes components. Radke (1987) observed that aromatic hydrocarbons are useful tools in evaluating the maturity of crude oils and organic maturation in high maturity level.

2.9 Heterocyclic Aromatic Compounds

Heteroatomic aromatic hydrocarbons compounds include dibenzothiophene (DBTs), dibenzofurans (DBFs), carbazoles (Cs) and fluorenes (Fs). Those components are significant constituents in sedimentary organic matter, and it is clear that all of these compounds have the same structural features apart from the heteroatoms. Therefore, it is assumed that heterocyclic compounds may have the same source precursors within organic in sediments. The abundance of heterocyclics aromatic hydrocarbons in petroleum and organic sediments has been shown to be related to the sedimentary depositional environment. For instance, sulphur-containing heterocyclic components are more common in marine water depositional environments, whereas oxygen-containing heterocyclic components are abundant in freshwater depositional environments.

The dibenzothiophene and alkyldibenzothiophenes sulphur heterocyclics aromatic hydrocarbons have been used to evaluate the thermal maturity of crude oils, organic

sediments and coal (Radke, 1987; Radke and Willsch, 1991; Chakhmakhchev *et al.*, 1997). In addition, the pyrrolic nitrogen compound has also been shown to depend on thermal maturity and organic facies changes (Clegg *et al.*, 1997; Zhang *et al.*, 2008). Some studies on crude oils and source rocks lead to the conclusion that concentrations of carbazoles are usually not influenced by changes in thermal maturity and depositional environments (Li *et al.*, 1999). Therefore, carbazole and benzocarbazole compounds are thought to be able to be indicators of migration (Larter *et al.*, 1996).

2.10 Stable Carbon Isotopic Compositions

The stable carbon isotope composition of crude oils is principally controlled by the isotopic composition of their precursor sedimentary organic matter. The stable isotope composition of carbon, sulphur, nitrogen, and hydrogen are often used with biomarkers to determine the genetic relationship between oils and bitumens and their source rocks (Sofer *et al.*, 1986; Hoefs, 1987; Schoell *et al.*, 1994; Peters *et al.*, 2005a). The present study focused only on carbon isotopes because, this is the dominant element in petroleum. Stable isotope composition data in combination with biomarker data can be used extremely successfully as tools for oil-oil and oil-source rock correlation studies compared to the use of biomarkers alone (Bjorøy *et al.*, 1991; Schwab and Spangenberg, 2007).

In general, the stable isotope measurements were performed on whole oils and bulk saturated and aromatic fractions of hydrocarbons, but stable isotope measurements can now be accurately carried out on individual abundant compounds. This analytical technique is termed compound specific isotope analysis (CSIA), (Matthews and Hayes, 1978; Hayes *et al.*, 1987; Freeman *et al.*, 1990; Hayes *et al.*, 1990). CSIA or gas chromatography-isotope mass spectrometer (GC-IRMS) allows the stable carbon isotopic analysis of individual *n*-alkanes and other compounds eluted from gas chromatography. CSIA has become a powerful tool for reconstructing geochemical pathways for organic carbon based on the idea that compounds with common biological origins have similar isotopic compositions (Hayes *et al.*, 1987; Freeman *et al.*, 1990).

2.11 Light Hydrocarbons

The light hydrocarbons (C_4-C_9) are not biomarkers because their carbon skeletons are too small to maintain evidence of specific biological origin(Peters *et al.*, 2005b). Most of the light hydrocarbons have been formed by the catagenetic breakdown of bigger molecular precursors. The smallest group of hydrocarbons, which can be considered as biomarkers, is the C_{10} monoterpenoids. Light hydrocarbons can; however, provide significant information concerning their source, thermal maturity and post-expulsion history. Previous geochemical studies have observed that several secondary processes can alter and remove light hydrocarbons in crude oils, including biodegradation, water washing and evaporation, whereas many other processes can increase the abundance of light hydrocarbons, such as during the late stage of generation, reservoir cracking and different migration processes involving phase separation, evaporative fractionation, and admixtures of condensates.

This study focuses on the phenomena related to evaporative fractionation, which involves complex processes, including the separation of gas from oil in the subsurface. Evaporative fractionation may result from pressure reduction due to fault movement or erosion, or from the entry of additional gas into reservoir rocks. This could cause the transfer of low and intermediate molecular weight material into the vapour phase. In general, the light hydrocarbon (C_6-C_7) parameters can be used to determine thermal maturity, correlate oil and condensates, and indicate several reservoir alteration processes.

Chapter 3. Analytical Methods

3.1 Introduction

A total of 51 crude oils and 269 ditches cutting rock samples from the Sirt Basin, Libya, were investigated using petroleum geochemical methods. Figure 3.1 shows a flow chart and list of the analyses performed in this study. The rock samples were selected from eight different boreholes distributed throughout the western and central parts of the Sirt Basin and the crude oil samples were from 24 oilfields in the Sirt Basin.

In this chapter, explanations of the experimental techniques applied and descriptions given of the rock and crude oil samples used in the study.

3.2 Sample Preparation

The ditch cutting rock samples from the Sirt Basin were collected from the Upper Cretaceous Sirt Shale, Rachmat and Kalash Formations. All rock samples were carefully washed with water and/or DCM solvent to remove any mud or drilling oil based muds. They were then placed in an oven at 30-40 °C and left overnight to dry. After that, the dark, dark grey, dark brown and black shale fragments were manually picked and 3-10 g was ground into powder using a mortar grinder before being transferred to labelled vials for further geochemical analysis.

3.3 Total Organic Carbon (TOC) Analysis

The total organic carbon content of the sediments was determined using a LECO CS-244 Carbon Analyser instrument. Approximately 0.1g of each rock sample was weighed into a porous crucible and then treated with 1ml of 20% hydrochloric acid (HCl) to remove all inorganic carbonate carbon ($CaCO_3$). The crucibles were left to dry for about 4-6 hours and then transferred into an oven at 30-60 ºC to dry overnight prior to TOC measurement. Before sample analysis, the apparatus was calibrated using a steel standard of known carbon content from 3 to 5 standards before each run and recalibrated, if necessary, after every tenth sample. In addition, duplicate samples were analysed to confirm the results. Once the samples were dried, iron chips were added in order to facilitate combustion at >1500ºC. The carbon in each sample was then oxidized in an oxygen stream and converted to CO_2 with the carbon dioxide concentration then

measured using an infra-red. The total quantity of carbon (then purely organic carbon) was calculated and reported as a percentage of the mass of the sample.

3.4 Rock Eval Pyrolysis Analysis

To assess the hydrocarbon potential of the source rocks, a Rock-Eval II (Oil Show Analyser) instrument was used for bulk geochemical screening analysis in the Petroleum Geochemistry Laboratory at Newcastle University. Rock-Eval pyrolysis has become a common analytical method for obtaining quantitative information on the quantity, quality, type and thermal maturity of sedimentary organic matter, and a number of parameters derived from it are used for characterizing hydrocarbon source rocks (Peters, 1986). The parameters measured included, S_0, S1, S2 (as mg HC/g rock), and T*max* (ºC). In addition, two other parameters were calculated: Hydrogen Index (HI: S2/TOC*100), and Production Index (PI: S1/ (S1+S2)). The PI parameter is used to determine the extent of petroleum generation based on the fact that S1 will increase and S2 will decrease when petroleum is generated from organic matter (kerogen). However, the Oxygen Index (OI: S3/TOC*100) was not measured because the instrument used was as old model unable to measure S3 values (mg CO_2/TOC*100). The pyrolysis temperature (Tmax) is the temperature corresponding to the maximum hydrocarbon yield (S2) during pyrolysis, and this reflects the thermal maturity of the sample as well as its kerogen type. More mature samples need higher temperatures in order to crack the heavy hydrocarbon compounds and remaining kerogen. The accuracy of the system was assessed using a standard shale sample (352/123) that has a known TOC of 5.15 wt%, S1 0.27 mg HC/ gm rock, S2 13.59 mg HC/ gm rock, and a Tmax value of 430 ºC. Duplicate samples were also analysed.

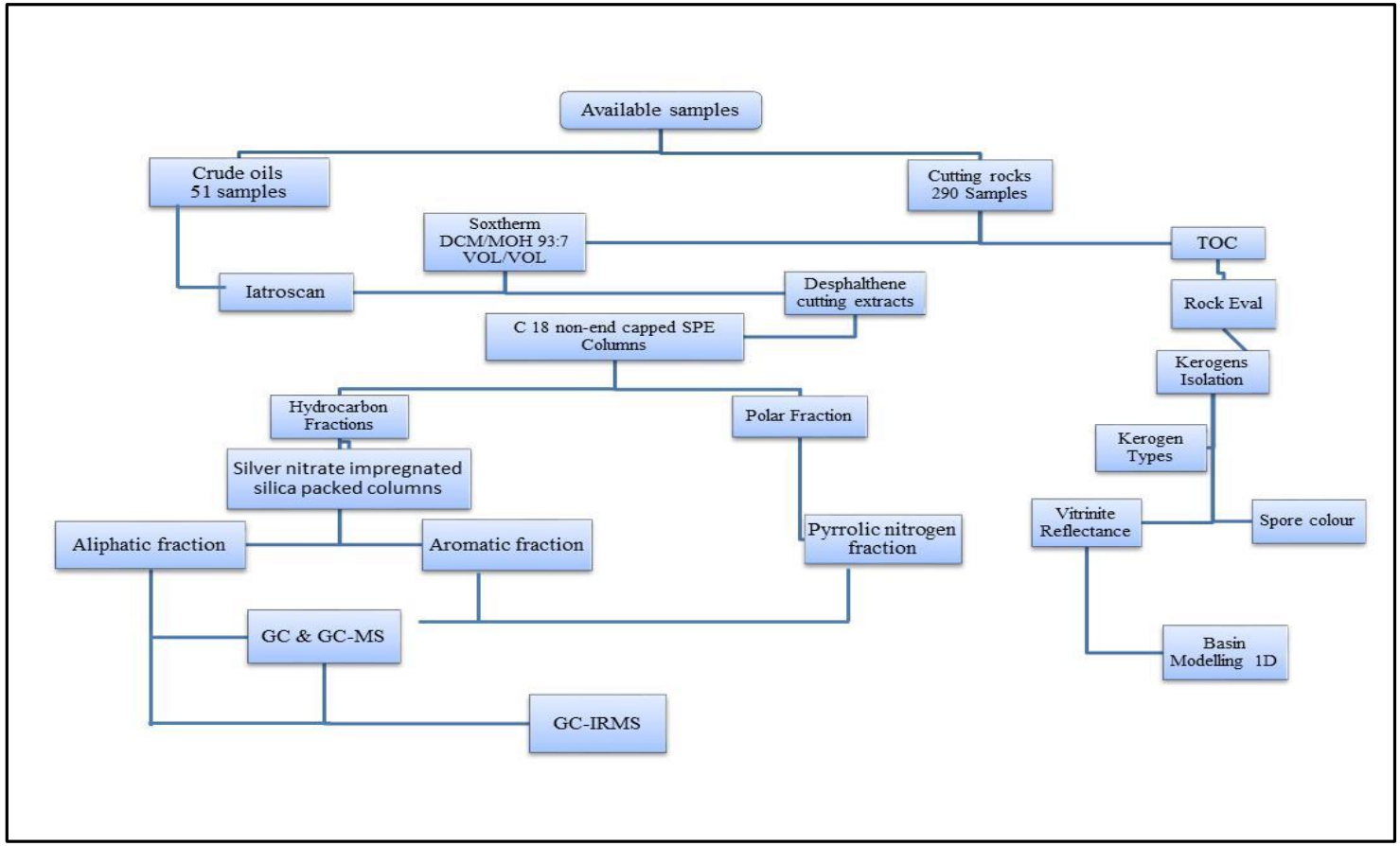

Figure 3.1: Flow chart of all analyses performed on samples for this study.

Approximately 100 mg aliquots of the powdered shale samples were progressively heated under a controlled temperature programme in an inert atmosphere. The temperature programme of the instrument involved three heating phases and extending up to 20 minutes. Firstly, the sample was heated at 100ºC for a period of three minutes, during which free hydrocarbon gases were released (S_0). This was followed by a rise in furnace temperature at a rate of 25ºC/min to 300ºC where it was held for a period of three minutes to allow for liquid and semi-solid hydrocarbons to be released (S1). Thirdly, the furnace temperature was increased from 300ºC to 550ºC at a rate of 25ºC/min, where it was held at 550ºC for two minutes. At this phase of heating, the kerogen within the sediments was pyrolysed to generate hydrocarbons (S2). The S1 peak is an indication of the light indigenous hydrocarbons present within a source rock. The S2 peak is a measure of the quantity of hydrocarbons produced by thermal conversion (pyrolysis) of the kerogen and therefore indicative of the genetic potential. The temperature at which maximum hydrocarbon generation occurs (which corresponds to the temperature of the S2 peak maximum) is the T*max* value, which is used as an indication of the thermal maturity for the kerogen (Espitalie *et al.*, 1977). An S2 peak of greater than 0.2 mg HC/g rock is used as the threshold for reliability of Tmax data (Peters, 1986; Peters and Cassa, 1994). The total organic carbon content (TOC) and Rock-Eval data for all measurements are shown in Table 4.1, Appendix I.

More details of the analytical procedure and Rock-Eval parameters are available at Peters (1986) and Hunt (1995). In addition, summaries of the interpretive guidelines for Rock-Eval results are available at Peters (1986) and Peters and Cassa (1994).

3.5 Kerogen isolation and slide preparation

Fifty nine ditches cutting rock samples from eight wells in the Sirt Basin were selected for kerogen isolation and visual kerogen assessment. The selected samples were characterized by TOC contents of more than 0.5%, and more than 100 mg HC/ g TOC values for HI. They covered both the immature and mature sections and concentrated on the shale components of the source rocks. The sample intervals throughout the sedimentary sections was about 30 feet.

Standard palynological procedures were used to prepare the kerogen slides for transmitting white light microscopy. The shale cuttings samples were crushed with a pestle and mortar to pieces of about 5mm in diameter, and approximately 3 g of each were placed in a 500 ml PTFE beaker. 50 ml of 20% concentrated hydrochloric acid (HCl) was then added steadily to remove carbonate minerals, and the samples were then allowed to stand for an hour or more until any visible reaction ceased. After that the samples were washed three times with distilled water to remove the HCl. Subsequently, 100 ml aliquots of 40% hydrofluoric acid (HF) were progressively added to dissolve and remove clay minerals and silicates, and the samples, then were allowed to stand for at least 24 hours before again being washed three times with distilled water. 20% concentrated HCl was then added to remove any new formed calcium fluoride crystals and the samples were washed a further three times with distilled water to remove the HCl. The organic residues were sieved in distilled water using 20 µm nylon mesh sieves, and each residue was transferred to a labelled vial. The organic residues were well mixed prior to the pipetting of a portion onto a circular glass coverslip. After being left to dry, the coverslip was then mounted onto a standard slide using Elvacite (2204) mounting medium, which is an acrylic resin with weak fluorescence.

3.6 Spore Colour Index (SCI)

Spore colours were determined from strew mounts of kerogen observed in transmitted light using the Spore Colour Index scale (SCI). Spore colour data are presented in term of the Robertson Spore Colour Index (SCI), which was determined by comparison of the colour of palynomorphs in the isolated kerogen with standard reference slides of single mounted palynomorphs. These palynomorphs are assigned values from 1–10 in order of increasing colour, from transparent to pale yellow, orange, brown and finally black. Such colour changes develop during the maturation of sporomorphs. During colour determination, care was taken to ensure the consistency of the measured grain, with pigmented, thick-walled and caved spores being excluded from the database (Collins, 1990). On the spore colour index scale a value of 1.0-3.0 indicates immature; 3.5–5.0 indicates the beginning of the oil window; a value of 5.5-7.5 represents the stage of peak oil generation; a value of 8.0 represents the start of the wet gas zone and a value of 9.0 the beginning of the dry gas zone.

3.7 Fluorescence

Most of the organic slides in the present study were examined under white light transmitted and blue light fluorescence microscopy using an Olympus BH2-RFCA microscope with x20 magnification or a x40 objective for more detailed examination of particular particles. Organic matter often shows natural fluorescence when excited with ultraviolet or blue light from a mercury (HGO) lamp. Fluorescence is "essential for assessing the proportion of higher oil-prone constitute and the preservation state (and hence hydrocarbon potential) of amorphous and palynomorphs organic matter" (Tyson, 1995). As blue UV radiation has little penetrative power, the emitted fluorescent light comes primarily from the surface of particles. Blue light excitation was used for a visual assessment. Elvacite ™ 2044 (ICI) acrylic mounting resin displayed good properties for fluorescence assessment, as it gives a dark green background. As fluorescence intensity increases with the power of the objective used, comparative observation must use a standard magnification, and here a x20 objective was used. Fluorescence properties are affected by preservation state as well as organic matter source (Tyson, 1995). Non-fluorescent amorphous organic matter was not assumed to be of terrestrial origin, since in most marine sediments it usually represents degraded plankton-derived amorphous material (Tyson, 1995). The quantitative preservation scale or fluorescence scale used by (Tyson, 1995), which was used, was designed for unoxidised immature kerogen, and it should not be used for samples of high maturity. This scale was designed with 6 points, FS1-6 for the evaluation of immature kerogen in rock samples

FS1: Kerogen is all non-fluorescent (except perhaps for rare fluorescing palynomorphs, especially telalginite algae, or cuticle).

1a) Amorphous (AMO) very rare (< 5%) or absent (*i.e.* at contamination levels).

1b) Amorphous (AMO) presents (common to abundant).

FS2: Most palynomorphs fluoresce, and amorphous (AMO) material remains predominantly non-fluorescent. These groups are subdivided into parts.

2a) most palynomorphs show dull orange-yellow fluorescence.

2b) most palynomorphs show yellow-orange fluorescence.

FS3: Most palynomorphs fluoresce and the matrix of autochthonous amorphous (AMO) matter shows dull fluorescence just visible above the background.

FS4: The amorphous (AMO) matrix shows moderate and heterogeneous fluorescence.

FS5: The amorphous (AMO) matrix shows stronger but heterogeneous fluorescence.

FS6: The matrix of autochthonous amorphous (AMO) material shows rather homogeneous and very strong fluorescence, bright yellow, like telalginite (such as prasinophyte). This rarely occurs in marine sediments.

3.8 Vitrinite Reflectance

Vitrinite reflectivity determination was made primarily on mounted whole rock samples. Vitrinite reflectance (%*Ro*) is a maturation parameter based on the change in the reflectance of polished vitrinite particles and zooclast materials with increasing time and temperature. Vitrinite reflectance represents a major indicator of thermal maturity in oil and gas exploration. Detailed discussions of vitrinite reflectance measurement can be found in Van Krevelen (1993) and Taylor *et al.* (1998).

3.8.1 Sample Preparation

Crushed samples were mounted in resin blocks by placing them in small plastic pill-boxes and then adding a viscous solution of five parts of resin mixed with one part of epoxy hardener, then leaving them for six hours to dry and set hard. Polishing these blocks involved grinding them on a diamond lap to remove surface irregularities. The blocks were then polished on a Meta Service machine using 600 and 1200 grade corundum paper, with isopropyl alcohol used as a lubricant. Then a series of progressively finer alumina powders (5/20 grade followed by 3/50 grade and finally gamma grade) for about one minute per grade were utilized with a Selvyt cloth to provide the final polish.

3.8.2 **Vitrinite Reflectance Measurements**

Petrological observation and random vitrinite reflectance measurements were carried out using a Leica POL-II reflected light microscope with MPV Compact 2 (linked with Geoform software for data acquisition) and an x50/0.85 oil objective. The immersion oil used had a refractive index of 1.518 at 23ºC in sodium light (589.3nm). The light source was a 12 volt, 100 watt tungsten filament lamp, light from which travelled through a polarizer and a field iris diaphragm until it reached a glass plate reflector which acted as the vertical illuminator. This reflected light onto the sample through the objective, which was then reflected back through the objective and passed either through the eyepiece or to the photomultiplier. Then, light traveling to the photomultiplier passed through an aperture diaphragm and a Schott interference filter with a narrow band pass peaking at 546 nm. The equipment was left to warm up for 20 to 30 minutes prior to measurements.

The resin blocks were plasticine mounted on glass slides using a press to ensure that the surface of the block was parallel to the stage of the microscope. Vitrinite reflectance was determined by comparing the intensity of light reflected back from the surface of the sample with that reflected from a surface of known reflectance. The photomultiplier generated an electric signal whose strength was proportional to the light intensity entering it. The microscopy was set up so that the measuring aperture of the photomultiplier was centred on the same point as the cross line seen through the eyepieces.

Vitrinite reflectance data were gathered by measuring the reflectance of up to 50 individual particles of vitrinite macerals at a specific wavelength of λ=546 nm with the appropriate filter fitted in front of the photomultiplier. The number of measurements was reduced for low particle concentrations. Whilst determining the reflectance of each sample, the stability of the microscope system was checked regularly by re-measuring the reflectance of certified standards made of glass or specific minerals (for example 0.88 % and 1.633 %) after each sample or every 20 minutes. Ideally, two or more standards should be used to establish the linearity of the measurement. The same spot 0.16 µm and diaphragm sizes were used for measuring both the standards and samples. However, bimodal or overlapping populations are common when measuring vitrinite

particles. The sampling of caved vitrinite particles may result in anomalously low reflectance populations, whereas recycled or oxidized vitrinite and semifusinite may contribute to anomalously high reflecting population.

3.9 Organic Geochemical Analysis

3.9.1 Sample Preparation of Rock Samples

34 ditches cutting rock samples were washed and ground as described in Section 3.2

3.9.2 Soxhlet Extraction of Source Rock Cutting Samples

Cleaned and crushed shale samples were extracted using a Soxhlet extractor using pre-extracted cellulose extraction thimbles and cotton wool for 6 hours using an azeotropic solvent mixture of dichloromethane and methanol with the ratio DCM:MeOH of 93:7. In order to remove any elemental sulphur from the extracts, activated copper turnings were added to each extraction beaker that contained 100 ml of the solvent mixture and a few anti-pumping granules. After the extraction processes were completed, the solvent was removed from the extracts by evaporation using a Heidolph rotary evaporator at a water bath temperature of 30-40ºC for several minutes. Then the extracts were collected and concentrated to 2-3 ml. An aliquot of the concentrated extract was transferred to a pre-weighed vial and the solvent was reduced to dryness in a stream of dry nitrogen in order to quantify the amount of total extractable material. However, the process of removal of solvents may lead to loss of the lighter hydrocarbons which have similar evaporation rates to that of the solvent. In practice, only hydrocarbons heavier that about *n*-C15 are retained for further analysis.

3.9.3 Iatroscan Thin Layer Chromatography-Flame Ionisation Detection (TLC-FID)

Iatroscan analysis offers a relatively fast screening method for quantifying aliphatic and aromatic hydrocarbons and non-hydrocarbons in crude oil and rock extracts (Karlsen and Larter, 1991). Separation of the rock extracts and crude oil samples into their main components of saturated hydrocarbons, aromatic hydrocarbons, resin and asphaltenes (SARA) was performed using Chromarod-S III silica rods and an Iatroscan MK-5 analyser equipped with a flame ionisation detector (FID). The Iatroscan analysis

was carried out for the geochemical screening of 34 ditches cutting shale samples and 51 crude oil samples from the oil fields and exploration wells of the Sirt Basin. This technique involved the application of a small volume of a sample of a solution of oil or rock extract to the chromatography rods and the development of the rods in a series of solvents to separate the various compound classes. Prior to the sample being applied to the rods, the rods were cleaned in the Iatroscan MK-5 FID analyser to remove any contamination by passing them through the hydrogen flame of the FID. A 3 µl aliquot of the crude oil or rock extract in a solvent solution (of about 5 mg/ml in DCM) was carefully applied dropwise onto the chromarods using a 10 µl syringe. A 3 µl aliquot of a standard (Crude oil from the Veslefrikk Field, Norwegian Sector of the North Sea) solution with a known SARA fraction percentage was always spotted onto the first two rods in each batch as shown in Table 3.2. The rods were then developed using three types of solvents, i.e. hexane, toluene, and finally a mixture of dichloromethane and methanol (93:7 v:v). The rods were first eluted in *n*-hexane up to 100% of rod length for about 25 minutes, and after that left to dry in the air for 3 minutes. The rods were then eluted in toluene to 60% of rod length for about 15 minutes, and left to dry in air for 6 minutes. Finally, the rods were eluted in a mixture of dichloromethane and methanol (93:7 v:v) up to 30% of the rod length before been dried in an oven at 60ºC for 90 seconds to remove any residual solvent. Then the rods were analysed using the Iatroscan MK-5 apparatus and the data were collected and processed using Lab Systems Atlas software. The Iatroscan chromatograms contained four peaks, which corresponded to the four separated fractions: saturated hydrocarbons, aromatic hydrocarbons, resins and asphaltenes (see Figure 3.2). To validate the results, each sample was run in duplicate and the average of the two results was recorded.

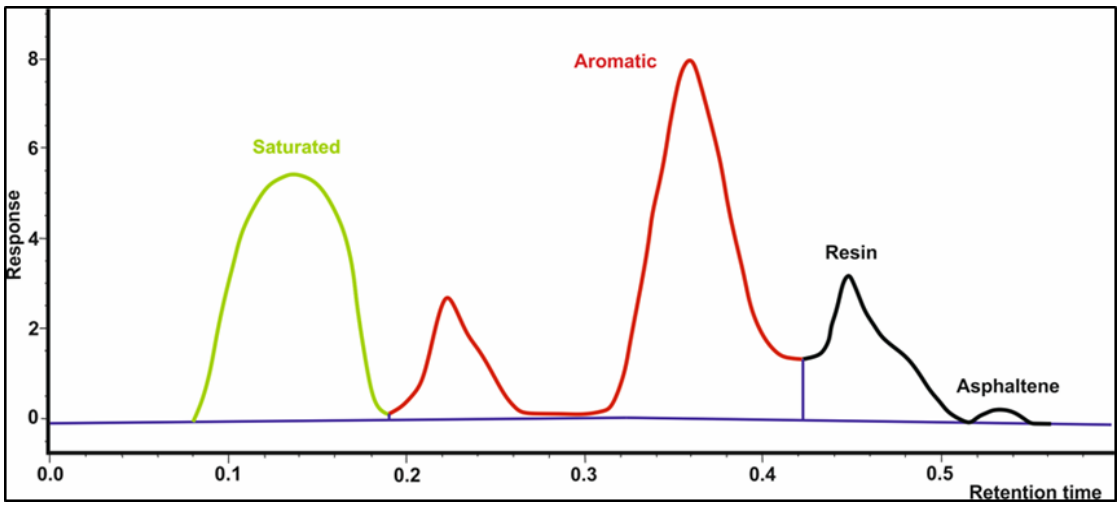

Figure 3.2: Iatroscan TLC-FID chromatogram showing the distribution of saturated and aromatic hydrocarbon, resin and asphaltene fractions in crude oil from Sirt Basin.

The standard oil sample (VFO) was analysed along with every set of analysed samples to calculate the response factors for the distinct oil SARA fractions.

Equation 3.1

$$\text{Response Factors} = \frac{\text{Area of standard}}{\text{Standard conc. X volume standard solution applied onto rod (3 µl)}}$$

where:

Standard conc. = % of individual fractions of the standard oil (VFO) X concentration of oil (VFO) X vol. of oil loaded (3 µl).

The concentration of each fraction in the source rock extract and crude oil samples were quantified and calculated using the following equation:

Equation 3.2

$$\text{F \% (mg/g)} = \frac{\text{Area F}}{\text{Sum of areas of all fractions x RF Std}}$$

where: F = fraction normalised to the total identified area; RF Std = response factor of the fraction F

Table 3-1: A composition based on the weight of fractions of crude oil from the Veslefrikk Field at Norwegian Sector of the North Sea used as standard for quantification of the Sirt Basin source rock extracts and crude oils.

Hydrocarbon Fraction	Percentage (%)
Aliphatic	57
Aromatic	36
Resin	6
Asphaltene	2

3.9.4 Asphaltene Precipitation (Deasphaltening)

Crude oil or source rock extract samples, which have asphaltene contents of approximately 2% or more generally require deasphaltening prior to analysis using solid phase extraction (SPE) fractionation. This is to avoid the precipitation of asphaltenes, which can result in the blocking of the SPE column when hexane is used as either a diluent when diluting viscous oils or an eluent when eluting a hydrocarbon fraction from a C_{18} non-end caped SPE column. This may lead to restricted solvent flow, trapping of the aliphatic and aromatic hydrocarbon fractions on the column and thus leading to poor separation. For this reason, the 35 crude oil and 16 source rock samples from the Sirt Basin, which contained >2% asphaltenes were deasphaltene prior to their SPE separation. Aliquots (about 40–50 mg) of the crude oil or source rock extract samples were accurately weighed, and then 9ml cold *n*-hexane was added to each sample, which were then shaken and sonicate in a sonic bath for 3-4 minutes, then left overnight in a fridge at ~4°C. The next day the samples were centrifuged three times at 3000 rpm for about 5 minutes and the supernatant containing the fraction carefully transferred into a labelled flask using a Pasteur pipette. These steps were repeated 5-6 times until the supernatant was almost colourless. After that, the hexane solvent was evaporated using nitrogen to about 1ml and the fraction, and then transferred to a clean 3ml vial using only *n*-hexane solvent ready for the subsequent analysis.

3.9.5 Solid Phase Extraction (SPE) Separation

In this study 3ml non-end caped C_{18} solid phase extraction (SPE) columns were used for the separation of hydrocarbon and non-hydrocarbon compounds from crude oil and source rock extracts according to the technique developed at Newcastle University and described by (Bennett and Larter, 2000).

Prior to starting solid phase extraction, mixtures of internal standards were prepared for the quantification of aliphatic and aromatic hydrocarbons, carbazoles and phenols. Squalane and 1,1-binaphthyl were used as internal standards to quantify saturated and aromatic hydrocarbon fractions, respectively. The squalane standard was prepared at a concentration of 205.512mg/100 ml of n-hexane for the crude oil samples and 99.56mg/50 ml of n-hexane for source rock extracts. For the aromatic hydrocarbon fractions 1,1-binaphthyl (1,1 BN) standard was prepared at a concentration of 39.853 mg/100 ml of DCM for the crude oil samples and 9.96 mg/50 ml for organic extract samples.

The D8-carbazole internal standard was used to quantify carbazoles in crude oils and source rock extracts, and was prepared by adding 0.5mg and 0.73mg, respectively, of D8-carbazole to 25ml of a mixture of hexane and toluene (9:1 v:v). The standard was added to each sample before isolating non-hydrocarbon compounds, while the squalane and 1,1 BN internal standards were added to each sample before separating the aliphatic and aromatic hydrocarbon fractions.

For the isolation of hydrocarbon and non-hydrocarbon compounds from crude oil and source rock extracts, the 3ml non-end capped C_{18} columns were pre-cleaned with 6ml of DCM, and then the DCM was removed from each column using gentle air flush, after which the columns were left overnight to dry on top of an oven set at 60ºC. Subsequently, 3ml of hexane was added prior to sample loading to each column for pre-conditioning. After that, the residual solvents were removed with a gentle air flush. Approximately 30 to 70mg samples of crude oil or source rock extracts were carefully loaded on the top frit of the cartridges using a Pasteur pipette. In cases where the sample was not readily absorbed into the sorbent, a gentle, positive pressure was needed to force the sample into the frit. Then about 0.5ml of hexane was loaded to wash the

column sides from any oil or organic extracts residues. After allowing the solvent height to fall to the level of the frit, another 0.5ml of hexane was carefully added to allow continued elution until the solvent reached the frit. The remaining 4ml of hexane was added to elute the hydrocarbon fractions. Finally, a very gentle air flush was applied to each column to displace residual hexane from the sorbent bed, and the lower tip of the cartridge was cleaned with 0.5ml of hexane. The hydrocarbon fractions were kept in 10ml vials in a fridge for further separation into aliphatic and aromatic hydrocarbon fractions.

The polar compounds were eluted from the SPE column with 5ml of DCM. Approximately 0.5ml of DCM was used to wash the column sides and lower walls of the cartridge and the remaining DCM was added to elute the entire polar fraction. A very gentle air flush was applied to each column to displace residual DCM from the sorbent bed, and also the lower tip of the cartridge was cleaned with about 0.5ml of DCM. The DCM elutes containing polar compounds, including carbazoles and phenols, were kept in 10ml vials. The polar fractions were concentrated to 0.5ml by evaporating under a stream of nitrogen before further geochemical analysis were conducted. However, the samples were not evaporated to dryness in order to avoid loss of more volatile compounds such as phenol. Approximately 0.25ml of the polar fractions containing the carbazoles was further reduced to 100µl and transferred to 150µl tapered inserts in auto-sample vials and sealed before carbazole analysis by GC-MS.

3.9.6 Separation of Saturated and Aromatic Hydrocarbons using Silver Nitrate Impregnated Silica (SPE Ag^+ silica)

3.9.6.1 Column Preparation

The saturated and aromatic hydrocarbons were separated using the silver nitrate Ag+ silica method developed at Newcastle University by Bennett and Larter (2000). The packed columns are not available commercially and therefore they needed to be prepared in the laboratory. Exactly 30g of Kiesel 60G silica gel (Merck) was weighed into a 500ml conical flask containing 60ml of distilled water plus 3g of silver nitrate in order to make about 40 solid phase extraction columns. The mixture was carefully

shaken until a homogenous creamy liquid is formed, with no lumps of silica visible. The sides and bottom of the flask was covered completely with aluminium foil to prevent photochemical degradation of the silver nitrate. To allow water vapour to escape from the mixture, small holes were made in the aluminium foil cap on the top of the flask, and then the flask placed in an oven at 80ºC to dry for up to 1 week. After the mixture was completely dry, the columns were prepared by adding approximately 550mg of the silica to each empty SPE cartridge column, which was then carefully compacted using a glass rod. The prepared columns were used immediately for optimum efficiency; otherwise light may affect the silver nitrate within the silica.

3.9.6.2 Sample Addition

The prepared columns were carefully cleaned with 5ml of hexane, using a positive air pressure to flush the solvent through the columns. This was performed using a plastic syringe installed in each individual column via a PTFE adaptor and manual pressure. The hydrocarbon fractions obtained from the crude oil and source rock extracts using the C_{18} non-end capped SPE method, were evaporated down close to 1ml (1000 µl). 10µl of an internal standard with a mixture of 822.048µg squalane and 1.19559µg 1,1-binaphtyl were added to the hydrocarbons fraction to quantify the *n*-alkane, aliphatic, and aromatic hydrocarbons, respectively. For source rock extract samples 10µl aliquots of the internal standard containing a mixture of 59.736µg squalane and 0.996µg 1,1-binaphthyl were also added to each hydrocarbon sample. A 100µl aliquot of the solution containing the internal standards and hydrocarbon fraction was then loaded into the Ag+ impregnated silica column. The aliquot was loaded directly into the top frit of the column. The frit and column wall were cleaned and washed with 0.5ml taken from 2ml of hexane. A slightly positive air pressure was carefully forced into the aliquot to pass the sample into the Ag+ impregnated silica. After that, the remaining 1.5ml hexane was slowly added to the column to elute the saturated hydrocarbon fraction. Then gentle air pressure was applied to displace the residual solvent and sample retained in the silica, and also the bottom tip of the column was then cleaned with 0.5ml of hexane. At the end of the procedure, the saturated hydrocarbon fractions for each sample were collected in 10ml vials. Subsequently, and by applying a similar process that is used for isolation the saturated hydrocarbon fractions, the aromatic

fractions were eluted from the Ag+ impregnated silica column using 4ml of DCM and were collected in separate 10ml vials.

The saturated and aromatic hydrocarbon fractions were reduced in volume to 1ml and transferred to auto sampler vials for analysis using GC and GC-MS.

3.10 Gas Chromatography (GC) of Aliphatic Hydrocarbon Fractions of the Crude Oil and Source Rock Samples

Gas chromatography was used to analyse the hydrocarbon fractions of the 51 crude oil and 34 source rock samples from the Sirt Basin. The hydrocarbon fractions obtained from the silver nitrate Ag+ silica solid phase extraction of the crude oil and source rock samples were analysed using an HP 5890 series II instrument equipped with automatic injection. The GC analysis was performed using a capillary column (HP, 30m x 0.25mm id x 0.25 µm film thickness) with hydrogen as carrier gas with a flow rate of ~1 ml/min at 50KPa column head pressure. A flame ionization detector (FID) was used and the GC temperature program started at an initial temperature 50°C for two minutes, which was ramped up to 300°C at the rate of 5°C/min. Acquisition of data, was controlled by Thermo Atlas software. In order to identify the *n*-alkane peaks a VFO oil standard was analysed with each set to check the reproducibility of the *n*-alkane data.

The quantification of the *n*-alkanes and isoprenoid alkanes was achieved using squalane as the internal standard. The concentration of each individual compound is determined by the following equation:

Equation 3.3

$$\boldsymbol{X}\ (\mu \boldsymbol{g/g\ oil, extract}) = \left(\frac{\mathbf{1000}}{\mathbf{WT.}}\right)\boldsymbol{x}\ \mathbf{CIS}(\mu\ \boldsymbol{g})\boldsymbol{x}\ \left(\frac{\mathbf{A}\boldsymbol{x}}{\mathbf{A}\boldsymbol{is}}\right)$$

Where,

X = concentration of individual *n*-alkane (µg/g of oil or extract);

Wt. = weight of oil or extract sample in mg that was added to the original SPE column;

C_{IS} = concentration (µg) of the internal standard (squalane in hexane) added to the sample;

A*x* = peak area of the *n*-alkane in the chromatogram;

A*is* = peak area of the internal standard (squalane) in the chromatogram.

3.11 Gas Chromatography-Mass Spectrometry of the Aliphatic and Aromatic Hydrocarbon fractions

All saturated and aromatic hydrocarbon fractions obtained from the different sample sets of crude oil and source rock extracts were analysed using an Agilent 7890A GC split/splitless injector (280°C) linked to an Agilent 5975C MSD (mass selective detector) with an ionisation energy of 70 eV, inlet temperature 230°C, quadruple temperature 150°C, multiplier voltage 1800, and GC/MSD interface temperature 310°C. The chromatographic separation of components was achieved using an Agilent HP-5 fused silica capillary column, which was 30m long, with an internal diameter of 0.25mm, and 0.25µm film thickness. The mass spectrometer was operated in selected ion monitoring (SIM) mode for both fractions and also in full scan mode for a small number of saturated and aromatic hydrocarbon fractions.

For saturated hydrocarbon biomarker analysis a 1µl aliquot of the hydrocarbon fraction in hexane was injected using an Agilent 7683B auto-sampler, and the split was opened after 1 minute. After the solvent peak had passed, data acquisition commenced, and the GC oven temperature increased from 50°C to 310°C at a rate of 5°C/min, where it was held isothermally at 310°C for 10 minutes. Helium was used as a carrier gas at a flow rate of 1 ml/min, with an initial pressure of 50KPa, split at 30 ml/min.

For aromatic compound analysis, the oven temperature was first held at 50°C for 5 minutes and then rose from 50°C to 300°C with a 5°C /min temperature ramp, where it was held isothermally at 300°C for 20 minutes. Identification of various components in the mass chromatograms was based on the combination of their mass spectra, retention times, and comparison with VFO standard data and published data.

Concentrations of individual steranes, tricyclic terpanes and hopanes were measured semi-quantitatively by comparing their peak areas in the appropriate mass

chromatograms relative to that of the squalane internal standard. The aromatic hydrocarbons were semi-quantified using 1,1-binaphthyl (m/z 253) as a standard. The reference standard oil (VFO) was run at the beginning of each batch to check the reproducibility of the biomarker data.

The concentrations of the measured compounds were calculated as follows:

Equation 3.4

$$Xb(a)\ (\mu g/g\ oil, extract)\ = (\frac{1000}{Wt})\ x\ CIS(\mu\ g) x\ (\frac{\mathrm{Ab(a)}}{AIS})$$

Where:

$X_{b(a)}$ = concentration (µg/g of oil or extract) of the compound to be quantified (biomarker or aromatic hydrocarbon);

Wt. = weight of oil or extract sample in mg, that was added into the original SPE column;

C_{IS} = concentration (µg) of the surrogate standard (squalane in hexane or 1,1-binaphthyl in DCM) added to the sample;

$A_{b(a)}$ = area of biomarker or aromatic hydrocarbon;

A_{IS}= area of squalane or 1,1-binaphthyl internal standard.

Note that quantitative values were not corrected for differences in mass spectral response between the various compounds and the corresponding standards. The concentrations reported in this study are therefore semi-quantitative, assuming relative response factors of one between target analyses and standards.

3.12 Gas Chromatography-Mass Spectrometer for Alkylcarbazoles Compounds

Prior to analysing the alkylcarbazole and benzocarbazole fractions by GC-MS, the DCM solvent was reduced to approximately 100µl and transferred to 150µl tapered glass inserts, which were then placed in regular 2ml auto-sampler vials and sealed. The GC-MS analysis of the carbazole fractions were performed on an Agilent 7890A GC

split/splitless injector (310°C) linked to an Agilent 5975C MSD with an electronic voltage of 70eV, source temperature 230°C, quadruple temperature 150°C, multiplier voltage 1800V, and interface temperature 310°C. Data acquisition was controlled using Chemstation software in ion mode (23 ions 0.7cps 50ms dwell) for greater sensitivity. A 1µl aliquot of the fraction in DCM was injected using an Agilent 7683B auto-sampler and the split opened after 1 minute. After the solvent peak had passed, the GC temperature program and data acquisition commenced. Separation was performed on an Agilent fused silica capillary column (30m x 0.25mm i.d) coated with 0.25µm dimethyl polysiloxane (HP-5) phase. The GC temperature was programmed to rise from 40°C to 200°C at the 10°C/ min and then to 310°C at a rate of 4°C/min and held at 310°C for 15 minutes. Helium was used as the carrier gas with a flow rate of 1ml/min, an initial pressure of 50kPa, with the split at 30 ml/min.

The alkylcarbazole C_0-C_3 and benzocarbazole isomers were identified based on Bowler *et al.* (1997) and also by comparison of retention characteristics with the VFO standard. The reference standard oil (VFO) was run at the beginning of each batch to check the reproducibility of the carbazole data.

The concentrations of individual compounds were calculated using the following equation, assuming a response factor of one, thus this analysis is only semi-quantitative.

Equation 3.5

$$C\ (\mu g/\ g\ oil/extract)\ = \frac{1000}{\text{Wt. S.}} \text{x}\ IS\ (\mu\text{g}) \text{x} \frac{Ac}{\text{AIS}}$$

Where:

C = compound to be quantified;

Wt S = weight in grams of the sample (oil or extract) applied to the SPE;

IS (µg) = weight of D8 carbazole added to the pyrrolic nitrogen fractions;

Ac = peak area of the alkylcarbazole isomer;

A_{IS} = the peak area of the D8 carbazole.

3.13 Gas Chromatography Isotope Ratio Mass Spectrometry (GC-IRMS)

A total of 23 saturated hydrocarbon fractions were selected from the crude oil and source rock samples from the Sirt Basin for analysis using gas chromatography isotope ratio mass spectrometry (GC-IRMS). The $\delta^{13}C$ isotope ratio measurements were performed on individual *n*-alkanes in the aliphatic hydrocarbon fractions (e.g. Bjorøy *et al.* (1994) and Sofer *et al.* (1991)). Before analysing the saturated hydrocarbon fraction samples, the Schimmelman A4 Standard, containing a mixture of *n*-C16 to *n*-C30 *n*-alkanes of known $\delta^{13}C$ isotope values, was analysed. This test was performed at the start of each day in order to assess if any, systematic errors occurred and to account for any instrument drift. The standards were prepared in Indiana University, USA in the laboratory of Dr. Arndt Schimmelman. An acceptable deviation level of ± 0.5 per mil was set for each *n*-alkane peak. In the standards, the isotopic value variation was found to be below ± 0.2 per mile in most cases. The specific carbon isotope compound (GC-IR-MS) analysis of the alkane fraction was performed on a Thermo Trace Ultra GC using a split-less injector at 280°C linked to a Thermo Delta V+ IR-MS (HT voltage 3-5KV, trap current 0.75mA, box current 0.7mA) via a Combustion III Interface. The data acquisition was controlled using Thermo Isodat software in carbon mode monitoring the CO_2 $^{44/45/46}$ and thus the $^{\delta}C$ $^{12/13}$ ratio. A 1µl aliquot of the sample in hexane was injected by a CTC auto-sampler and the split opened after 1 minute. The GC was temperature programmed from 50 to 300°C at the 5°C/min and held at the final temperature for 6 minutes with helium gas used as the carrier gas at a flow of 1ml/min, initial pressure of 50kPa, and split at 20 ml/min. The solvent peak was diverted to the FID and CO_2 reference gas was pulsed into the mass spectrometer. After 7 minutes the back flush valve directed the split sample via the combustion furnace at 940°C containing copper, nickel, and platinum as catalysts. The eluting compounds were then oxidized and the gases generated pass through to the reduction furnace at 650°C where any nitrous oxides were reduced to N_2 and surplus oxygen removed from the analyte. Then the CO_2 gas and water passes into the capillary interface where the water is removed in a nafion tube and then passed to an open split narrow bore capillary interface. After that, the gas was transferred to the IRMS through a micro-capillary

isolation valve, where the gas was ionized and resulting ions separated by a magnetic field to 3 cup detectors for masses 44, 45, 46. An isotope ratio value was determined from a pulsed CO_2 reference gas calibrated from reference *n*-alkanes in the A4 standard. The CO_2 generated from the combustion of individual *n*-alkanes compounds in the reactor were transferred with helium gas through a capillary joined to the isotope ratio mass spectrometer, where δC^{13} isotope ratios were determined for the CO_2 representative of each *n*-alkane peak. Chromatographic separation was performed on a fused silica capillary column (30m x 0.25mm i.d) coated with 0.25µm phenylmethylpolysiloxane (DB-5) phase. The acquired data were processed using the Isodat dynamic background integration workspace software to give the peak retention times and isotope ratios as $\delta^{13}C$ values. All samples were analysed in duplicate to check data quality.

The ideal sample peak intensity of the instrument was around 4V (4000mv). However, even though many of the samples were concentrated to approximately 50µl in hexane, some peaks only gave weak signals up to 1-2V. Since the chromatographic resolution of the GC-IRMS instrument is lower than that of GC-MS (due to the presence of the oxidation furnace and many connections in the chromatographic system of the GC-IRMS), closely eluting peaks such as of nC_{17}/pristane and nC_{18}/phytane often do not give a baseline separation, and so the values of the co-eluting C_{17} and C_{18} peaks are actually C_{17}+Pr and C_{18}+Ph. Thus, the integrated $\delta^{13}C$ isotope values may be incorrect. Also, if the sample peak intensities were above 5V, then the values have been usually more negative (lighter) than the true values. Another problem was that, after a more concentrated peak eluted, sometimes the following peaks give more negative (lighter) values, which was evident in several samples and especially after a strong squalane peak.

3.14 Headspace Gas Light Hydrocarbon Analysis

The analysis of light hydrocarbons from the selected crude oil samples were determined by gas chromatography of the whole oil without any pre-treatment, which provides a useful and rapid tool for correlation studies. Seven crude oil samples with high aromatic hydrocarbon contents were included in this study. All of the crude oil samples were from the Sirt Basin, including the 4J2-6 Well at West Meghil oilfield, B1-47 well at

the Beda oilfield, A28-NC74B well at the Zellah oilfield, B2—NC74A well at the Fidda oilfield, A1-NC125 well at the Concision 125, and A15-17 and A46-17 wells at the West Mabruk oilfield. These samples were weighed into vials which were then sealed and left overnight to allow the equilibration of the phase. Analyses were performed on an Agilent 5975C MSD gas chromatography mass spectrometer fitted with a HPIMS capillary column (60m x 0.25mm id, and 0.25µm film thickness), with helium gas used as the carrier gas with a flow rate of 1ml/min at 105.2 KPa column head pressure and split at 52 ml/min. The GC-MS oven temperature program started at 30 ^{0}C for 5 minutes, and was then ramped to 80 ^{0}C at the rate of 5 ^{0}C/min with a hold time of 1 min, then ramped to 320 ^{0}C at 25 ^{0}C/min, where held for 5 minutes. The total isotherm time was 30.6 minutes. Acquisition of data was controlled by Agilent Chemstation software. The sample of approximately 0.2µl was injected manually in split mode with a split ratio of 50:1. Samples were analysed in full scan mode in the range 10-235 auto mass units.

3.15 Kinetic Modelling of Source Rocks

KinEx is a kinetic modelling software suite developed by ZetaWare Interactive Petroleum System Tool used to determine the generation, preservation and primary expulsion of oil and gas. The expelled petroleum and gas oil ratio (GOR) can be predicted from a source rock with inter-bedded organic facies using KinEx. This model uses simple distributions of different organic facies and kerogen types. A set of organic facies (A, B, C, D/E and F) (Pepper and Corvi, 1995) and temperature rate program have been used for calibration and calculation for the kitchen of the source rocks (Magoon and Dow, 1994; Pepper and Corvi, 1995). A thermal history that is imported from Genesis modelling software can be used to assess the volume per area of petroleum expelled from the kitchens in the source rock. This kinetic modelling was applied to samples from eight wells in the Sirt Basin, 6A1-59, B1-NC74F, B2-NC74A, C2-16, FF14-6, L1-16, L1-17, and Z1-11. The geochemical characteristics of the Sirte Shale and Rachmat source rocks formations, such as initial organic carbon (TOC°), initial hydrogen index (HI°), and thickness, with selected appropriate thermal heating rates, were used in the model, allowing volumes of generating and expelled hydrocarbons to be calculated and the timing of these processes to be estimated.

3.16 Basin Modelling Analysis (1D)

Basin modelling is defined as the numerical modelling of any physical process which takes place in a sedimentary basin, including basin formation, sediment transport and predictive stratigraphy (Hermanrud, 1993). The main aim of this basin modelling, analysis was to quantify hydrocarbon generation and accumulation. The modelling of processes such as heat flow, fluid flows, compaction, and hydrocarbon generation, expulsion and secondary migration considered the most important elements of basin modelling (Magoon and Dow, 1994).

The basin modelling software Genesis, which was developed by ZetaWare as part of its Interactive Petroleum System Tool, was used to analyse the burial history, estimate the time of the hydrocarbon generation and expulsion in the Sirt Basin. The software suite, covered the entire 1D model with an element solver for temperature and pressure coupled, amongst other variables with hydrocarbon generation. A 1-D simulation can be performed in a matter of minutes, depending on the computing parameters involved.

The subsidence and thermal modelling of the 6A1-59, B1-NC74F, B2-NC74A, C2-16, FF14-6, L1-16, L1-17 and Z1-11 wells was carried out in order to compare calculated maturity values with measured values. This may help in evaluating the structural history of the sedimentary sections and the analysis, including the kinetic modelling of the maturation of the source rocks, can be used to evaluate the timing of hydrocarbon generation (Pepper and Corvi, 1995).

The temperature boundary conditions imposed on subsidence history are the heat flux at the base of the modelled section and the temperature at the sediment seawater interface. The input temperature boundary conditions are used to calculate the temperature at regularly and closely-spaced time and depth intervals. In this way the thermal history of the section is modelled, providing a basis for calculations of subsequent maturity and hydrocarbon generation (Waples, 1980). Different heat flow values and sediments seawater interface temperatures may be applied for each defined event.

To construct the burial history, the basic input data included formation tops of the stratigraphic unit, absolute time of deposition in a million years (Ma), lithological

composition, hiatus age, thickness and age eroded intervals and heat flow data calculated from the previously determined vitrinite reflectance. In the current study, the lithological composition of the stratigraphic sequences for each well was obtained from the final and composite log. Absolute age in all different stratigraphic units was defined using the time stratigraphic chart in Libya.

The 1-D present day heat flow values for the modelled wells are shown in Table 7.1. The Rachmat and Sirt Shale source rocks consist of Type II and Type II-III kerogens, according to the Rock-Eval results and petrographic analyses. For all modelled wells, the average of the original hydrogen index values with TOC are given in Table 4.4 for the Type II kerogen for the Sirt Shale Formation and the Type II-III kerogen for Rachmat Formation.

The rate of the kerogen breakdown depends on the type of organic matter concerned and the thermal maturity from exposure burial (Pepper and Corvi, 1995). Maximum thermal maturity is often determined from several maturity measurements; for instance, vitrinite reflectance, T_{max}, and spore colour index (Waples, 1980; Tissot and Welte, 1984; Waples, 1985; Hunt, 1995). Nevertheless, whereas thermal maturity is certainly related to hydrocarbon generation, the timing and rate of hydrocarbon generation vary widely depending on the organic matter that is present in the source rock. For example, marine or lacustrine source rocks that contain oxygen and are sulphur-rich will generate hydrocarbons under lower thermal stress than marine shale or lacustrine source with lower sulphur levels (Waples, 1980; Lewan *et al.*, 1985; Waples, 1985; Orr, 1986; Hunt, 1995). Gas generation is variable at different source rock types. The principal gas generation plays a part in generating induced fracturing for primary migration of hydrocarbons (Waples, 1980; Waples, 1985; Issler and Snowdon, 1990; Magoon and Dow, 1994). Temperature is the primary factor which controls, organic maturation and hydrocarbon generation, and therefore the analysis of vitrinite reflectance data is an important component of basin modelling studies (Espitalie *et al.*, 1977; Waples, 1980; Tissot and Welte, 1984; Hunt, 1995). Vitrinite reflectance profiles, measured from 78 samples representing eight wells, were built for each well. The vitrinite reflectance measurements were used to calibrate the burial history models. The vitrinite reflectance data calibrations are plotted in Figures 7.1 to 7.8, and the burial history models of the

analysed wells are shown in Figures 7.9 to 7.16. Other information such as well names, depth in metres, formation, age, and averages of vitrinite reflectance data, TOC and HI are shown in Appendices I and II.

3.17 Statistical data analysis: Principal component analysis

Little variation was observed in the wells studied, and therefore statistical assessment was required in order to illustrate any approach pattern in these variations. Principal component analysis was used for this purpose. Principal component analysis is a method of identifying patterns in data, and expressing these patterns in such a way as to highlight similarities and differences (Jolliffe, 2002) and reference therein. Since patterns can be hard to find in data of high dimensionality, where graphical representation is not available, principal component analysis (PCA) is considered one of the most powerful tools for analysis of such data. It is a multivariate statistical technique which distinguishes relationships between samples and variables in complex data sets, and summarizes the main sources of variance which are termed the principal components (Jolliffe, 2002). Principal component analysis usually explains the bulk of data variability in just a few principal components, allowing for the data set to be plotted graphically in two dimensions (Jolliffe, 2002).

In this study principal component analysis was used to help determine which source organic facies or depositional environment parameters, and molecular biomarker maturity were important controlling variables. Principal component analysis can show the loadings plots of extract biomarker variables that related to thermal maturity, source facies and/or depositional environment. Consequently, the principal component analysis (PCA) can be used as a data reduction tool to manage huge volumes of data, and it can extract subtle but significant distinctions between samples.

The output data of the principal component analysis are represented by scores and loadings. Scores are numbers that express the influence of an eigenvector on a specific sample, or the contribution of each principal component to each data point (Jolliffe, 2002). Loading on the other hand expresses the influence of the original variable within the principal component. The distribution of principal component scores and loadings can help in identifying the sources of variability in the data set. Therefore, the influence

of each individual component is controlled by a number of variables (loadings) or compound (Jolliffe, 2002). Often most of the variation can be explained by the first, second or third principal components; and applying the cross-plots of the first and second principal components can might reveal the various groups of oils within any sedimentary basin.

Many researchers have used principal component techniques for analysing geochemical data to correlate between oil-source and oil-oil studies. These include Bigge and Farrimond (1998) and Parfitt and Farrimond (1998) who used this statistical technique to determine the amount of biodegradation in a suite of oil seep along the Dorset coast and Mupe Bay in the Wessex Basin, using the PCA statistical program XL-STAT software.

The geochemical data sets used in the present study include 32 variables (TOC, S2, biomarker concentrations, and maturity parameters, carbazole and benzocarbazole data) for the crude oil and source rock extract samples selected from the Sirt Basin. These variables were analysed using principal component analysis to illustrate the major variations within the main components, steranes, hopanes, tricyclic terpanes, aromatic ratios, carbazoles and benzocarbazoles distributions. The variables used in the analysis are listed in Table 4.2.

Chapter 4. Petroleum geochemistry of the Sirt Basin

4.1 Introduction

This chapter presents a regional geochemical outline of the study area, which includes information about the organic matter contents, source facies, and variations in hydrocarbon maturity of the Upper Cretaceous potential source rocks within the centre and western part of the Sirt Basin. This chapter also assesses the main source rocks responsible for the generation of all the hydrocarbons so far discovered in the study area, in order to characterize the Sirt Basin petroleum system. The hydrocarbon source potential of the Sirte Shale, Rachmat and Kalash formations in the Sirt Basin were investigated using total organic carbon (TOC) and Rock-Eval pyrolysis measurements, and most of these samples have been subjected to the optical analysis of kerogen in order to determine the organic facies and the level of thermal maturity. Maturity has been evaluated using T*max*, spore colour index (SCI) and the reflectance of macerals. The analysis of molecular biomarkers and specific carbon isotope compounds are also used to identify the source rock characterization, thermal maturity and depositional environments in the Sirt Basin. It is generally well documented that the Upper Cretaceous, Sirte Shale and Rachmat formations are responsible for generation of most of the oil and gas within the central and western part of the Sirt Basin (El-Alami *et al.*, 1989; Ben Ashour, 2000).

4.2 Source Rock Evaluation

A petroleum source rock is defined as any unit of rock that has generated and expelled oil and/or gas in sufficient quantities to form commercially viable accumulations (Dow, 1977; Tissot and Welte, 1984; Hunt, 1995). The petroleum source rock potential of sedimentary rocks often depends to a considerable degree on the quantity (TOC), quality, and thermal maturity of organic matter as well as bed thickness (Peters, 1986; Hunt, 1995). Therefore the significant attributes of a good source rock are that it has enough organic matter of sufficient quality to generate significant hydrocarbons, and that the level of maturity must have been high enough for this to occur (Marshall *et al.*, 1985).

The abundance of organic matter in sediments is usually evaluated as the relative percentage of organic carbon on a dry weight basis. Most organic rich sediments deposited in the dysoxic to anoxic conditions of black shale facies usually have TOC values ranging between 3% and 20% (Tyson, 1995). However, although this technique is a readily available and simple measure of the organic matter content of sediments, difficulties may arise when interpreting TOC values. The main difficulty concerns dilution, because the TOC is considered to be a relative percentage and therefore depends not only on the supply and preservation of organic matter but also for the supply and preservation of siliciclastics and biogenic materials (Tyson, 1995). Another problem is related to the great changes in organic facies, particularly in a phytoclast dominated setting and such changes might not be reflected in changes in TOC measurements (Tyson, 1995). In spite of these problems, however, the TOC percentage is widely used in geochemical studies, because it is simple, fast to analyse and can provide a good overview for further geochemical analysis.

In the present study, total organic carbon content values below 0.5% are termed poor for the purposes of interpretation and thus considered to be indicative of no significant source potential. Values between 0.5% and 1.0% are considered to be indicative of fair source potential; values between 1.0% and 2.0% represent good source potential, whilst values above 2.0% are indicative of possible source potential depending on maturity and kerogen type (Tissot and Welte, 1984; Waples, 1985; Langford and Blanc-Valleron, 1990)

The source rock evaluation in this study is based on the ditch-cutting rock samples from the Kalash, Sirte Shale, and Rachmat formations from eight wells (6A1-59, B1-NC74F, B2-NC74A, C2-16, FF14-6, L1-16, L1-17, and Z1-11) in the central and western part of the Sirt Basin. The bulk geochemical parameters determined during screening analyses are given in Tables 4.1 in the Appendix I. A description of the sample preparation method and rationale behind the use of this type of analysis can be found in, sections 3.2 and 3.3.

4.2.1 Source Rock Richness of the Well Sections of the Sirt Basin

Mesozoic marine siliciclastic sedimentary rocks of the central and western part of the Sirt Basin include substantial sections of organic-rich shale from the Upper Cretaceous sedimentary section, which is thought to be the principal source of petroleum in the oil and gas fields of that province (e.g. Hamyani *et al.*, 1984; El-Alami *et al.*, 1989; Hallett and El Ghoul, 1996; Ben Ashour, 2000; Hallett, 2002; Burwood *et al.*, 2003; Aboglila, 2011). These shale sections include the Kalash, Sirte Shale, and Rachmat formations. They have been described and their petroleum source parameters characterized from 269 cutting rock samples of eight boreholes. Therefore, to determine whether or not these sediments contain sufficient organic matter to generate hydrocarbons, rock cutting samples from geographically scattered study wells were analysed using TOC and Rock-Eval pyrolysis. Samples were taken from a range depths and stratigraphic intervals from the Kalash, Sirte Shale and Rachmat formations in the central and western part of the Sirt Basin. Most of the wells analysed in the central and western part of the Sirt Basin are cutting samples spaced between 30 and 50 feet intervals.

In the present study, the Sirt Shale Formation is penetrated in all eight wells, but with various thicknesses based on their geographical location in the basin. Sirte Shale occurs predominantly as a laminated, carbonaceous, non-bioturbated sequence of dark grey to mainly dark brown to black shales grading into shaly limestone at the lower part (El-Alami *et al.*, 1989).

Total organic carbon contents of the 269 samples vary between 0.46% and 6.73% by weight according to variations in the lithology of the Kalash, Sirte Shale and Rachmat formations. High TOC values of about 6.73% occur in the lower Sirt Shale Formation samples in the B1-NC74F well at the eastern Zellah Trough. Meanwhile, the lowest TOC values are encountered in the samples from well FF14-6 (12410 feet) at 0.35 wt%, and well B1-NC74F (7000 feet) at 0.51 wt% as shown in Tables 4.1 in Appendix I. The bulk geochemical parameters determined during screening analyses, total organic carbon contents (TOC) and Rock-Eval pyrolysis data (S1, S2, HI, PI and *Tmax*) for the Upper Cretaceous section are presented in Tables 4.1 in the Appendix I and plotted against depth in Figures 4.1 to 4.8.

4.2.2 Geochemical Characteristics of the Kalash Formation Source Rock

Among the study wells, the Kalash Formation is only penetrated in the 6A1-59 well. This borehole is situated in an area where the Kotla Graben and Zellah Troughs (SE Zellah Trough and SW Kotla Graben) merge together, creating an integrated fault system. The Kalash Formation is characterized by limestone interbedded with shaly limestone, and is subdivided into upper and lower parts based on their organic carbon content and lithology. The upper part extends from 7130 to 7170 feet with a thickness of around 40 feet. The shale unit of the Kalash Formation has organic carbon content ranging between 3.04 to 3.81%, with an average of 3.42%. This shale unit has a potential yield ranging between 17.27 and 23.97 mg HC/g rock with a mean value of 20.66 mg HC/g rock as shown in Figures 4.1 and 4.9. Combined with organic carbon, all samples displayed an above average hydrocarbon potential yield, indicating that the upper unit of the Kalash Formation is considered to be a hydrocarbon source rock. The HI values range from 524 to 596 mg HC/g TOC, with an average of 564 mg HC/g TOC, suggesting that organic sediments are dominated by amorphous organic matter, with Type II kerogen, and they have been preserved in an anoxic environment (Espitalie *et al.*, 1977; Tissot and Welte, 1984; Marshall *et al.*, 1985; Waples, 1985; Langford and Blanc-Valleron, 1990; Hunt, 1995; Tyson, 1995). This type of kerogen may generate significant amounts of hydrocarbons, and is particularly oil-prone if it reaches a sufficient level of thermal maturity (Dow, 1977; Espitalie *et al.*, 1977; Tissot and Welte, 1984; Marshall *et al.*, 1985; Hunt, 1995).

The lower unit of the Kalash Formation is characterized by limestone with shale. The lower part extends from 7180 to 7210 feet with a thickness of around 30 feet. The shale unit of the Kalash Formation has an organic carbon content of between 0.82 to 1.22% with an average of 0.94%, and a hydrocarbon yield range of 0.75 to 2.89 mg HC/g rock with a mean value of 1.45 mg HC/g rock as shown in Figures 4.1 and 4.9. This suggests that the organic sediment in the lower unit has fair potential as a hydrocarbon source. It has HI values ranging between 83 to 224 mg HC/g TOC, with an average of 137 mg HC/g TOC, suggesting that this organic sediment is composed of Type II-III kerogens.

4.2.3 Geochemical Characteristics of the Sirte Shale Formation Source Rock

The 6A1-59 well is located in an area where the Kotla Graben and Zellah Troughs (SE Zellah Trough and SW Kotla Graben) are merging together to create an integrated fault system. The Sirte Shale Formation (7220-7280 feet) is 60 feet thick and characterized by dark grey to black shale. It is clear from the bulk screen data that Rock-Eval pyrolysis data agree with the distribution of total organic content (TOC) values in most of the samples analysed. The Sirte Shale Formation has a total organic carbon content ranging from 1.98% to 3.88% with an average of 2.71%, and potential yield ranges from 7.22 to 23.87 mg HC/g rock with an average 13.42 mg HC/g rock (Tables 4.1 in the Appendix I, Figures 4.1 and 4.9). , suggesting a very good source rock potential (Langford and Blanc-Valleron, 1990; Hunt, 1995).

Thus, it can be seen that the majority of the samples contain above average levels of organic enrichment, of TOC more than 1.0 wt% (e.g. Bissada, 1982). The HI values range from 338 to 569 mg HC/g TOC, with an average of 448 mg HC/g TOC (Table 4.1 in the Appendix I, Figure 4.9), suggesting a hydrocarbon oil-prone Type II kerogen.

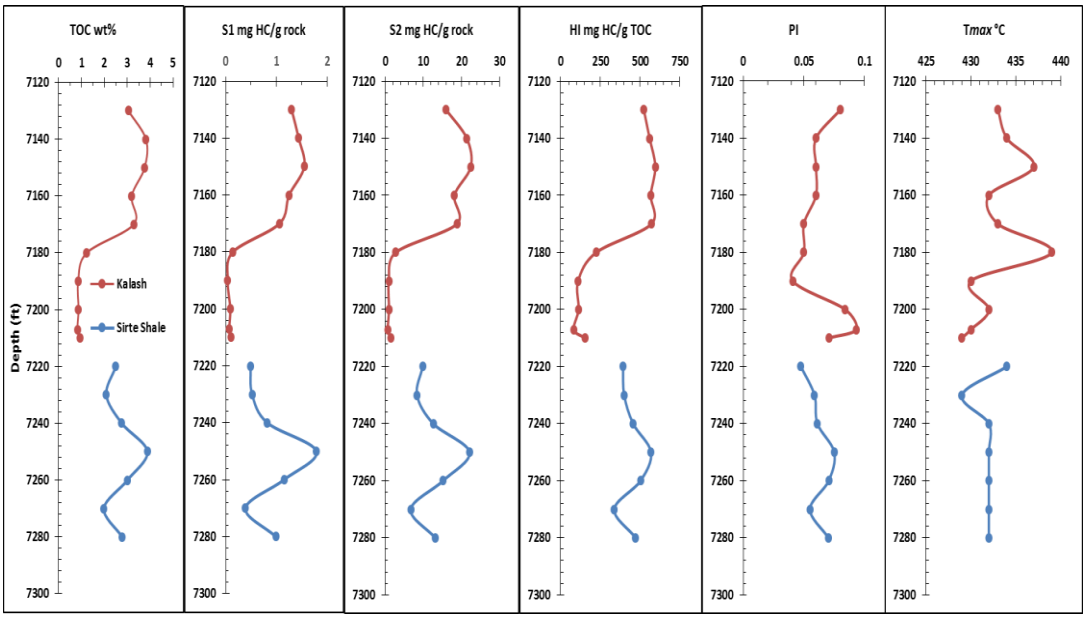

Figure 4.1: Geochemical logs for the Upper Cretaceous, Sirte Shale and Kalash source rocks of the well 6A1-59 in the Sirte Basin.

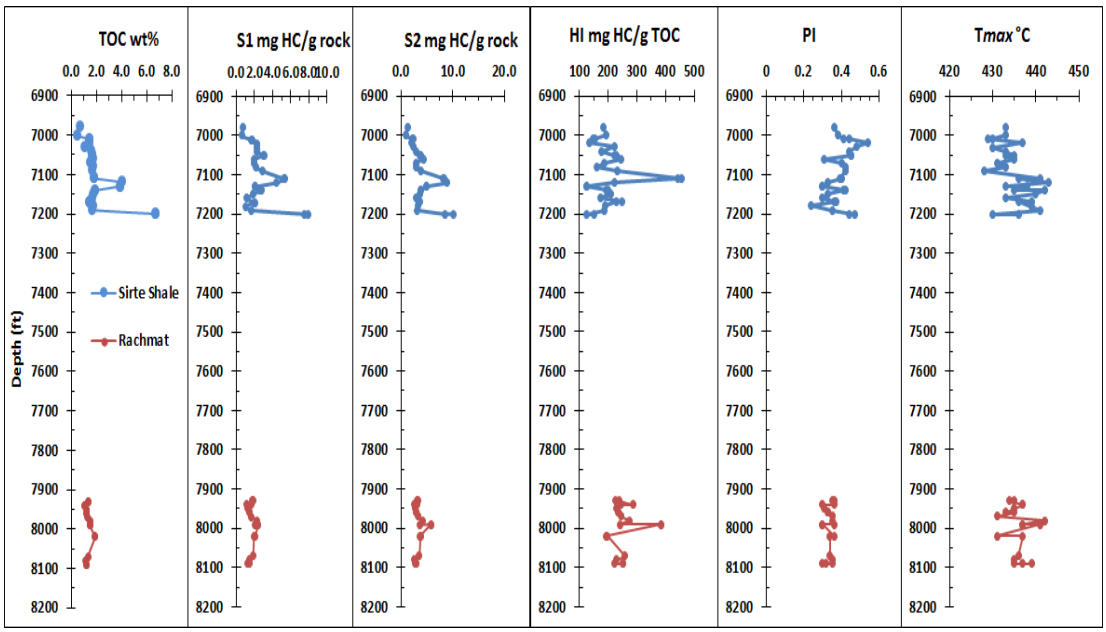

Figure 4.2: Geochemical logs for the Upper Cretaceous, Sirte Shale and Rachmat source rocks of the well B1-NC74F in the Sirte Basin.

The B1-NC74F well is located in the southeast of Zellah Trough (west Sabah oilfield) of the Sirt Basin. All of the data for it were obtained from the analysis of cuttings samples taken usually over 30 feet depth intervals. Unfortunately, there has been no coring of the Sirte Shale Formation in any of the wells analysed in the Sirt Basin. Particularly in this well there is a problem when evaluating the source rock potential, because it was drilled using oil-based muds. Therefore, caution must be exercised during geochemical evaluation. The Sirte Shale Formation extends from 7010 to 7200 feet with an average thickness of about 190 feet, and consists of dark grey, very dark to olive black shales with limestone content. The Sirte Shale Formation has good, very good to excellent TOC values, ranging from 1.11% to 6.73% with a mean value of 2.31% (Tables 4.1 in the Appendix I, Figures 4.2 and 4.9). This enrichment may reflect the improvement in the quality of the organic matter in the Sirte Shale Formation, which is comprised mainly of amorphous marine organic matter with a minor contribution of terrestrial organic matter. It has been found to have moderate to excellent generating potential, with potential yield between 3.96 and 17.98 mg HC/g rock with an average of 7.31 mg HC/g rock (Tables 4.1 in the Appendix I, Figure 4.2 and 4.9). In fact, most of the analysed samples show yields consistent with good or excellent hydrocarbon source rocks, where the potential yield (S1+S2) is greater than 6 mg HC/g rock (Tissot and Welte, 1984). It has HI values ranging from 125 to 455

mg HC/g TOC, which suggests organic sediments of Type II to Type II-III kerogens, and a significant amount of oil and oil-gas could be generated.

The B2-NC74A well is located in the south-easterly extent of the Fidda oilfield in the Zellah Trough at the western edge of the Sirt Basin. In this well the Sirt Shale Formation is penetrated only at 240 feet thick. It is subdivided into two parts based on their organic-richness (TOC %) and potential yield (S1+S2). The upper Sirte Shale Formation (9500-9570 feet) is represented by 70 feet thick and characterized by grey to dark grey shale interbedded with sandstone. The total organic carbon content of the Upper Sirte Shale Formation was 0.58 to 0.81%, with a mean value of 0.71%. Consequently, all the samples analysed contained below the average level of organic enrichment. Rock-Eval pyrolysis shows that the total generation yield (S1+S2) of the upper section ranges from 1.40 to 1.73 mg HC/g rock, with a mean of 1.56 mg HC/g rock (Tables 4.1 in the Appendix I, Figure 4.3 and 4.9). For organic carbon, all of these samples appear to have below average hydrocarbon potential yields (S1+S2) were less than 2.5 mg HC/g rock) and may, therefore, be considered as having poor hydrocarbon source rock potential. This section gives HI values ranging from 141 to 175 mg HC/g TOC (Tables 4.1 in the Appendix I, Figures 4.3 and 4.9), suggesting that this organic sediment is Type II-III Kerogen.

The lower part of the Sirte Shale Formation consists of very dark grey to black shale, and has a total organic carbon content ranging from 0.79 to 1.72 wt% with an average of 1.34 wt%. The Lower Sirt Shale Formation is shown to have low, moderate to slightly good generating potential with potential yields between 1.50 and 4.79 mg HC/g rock at an average of 3.14 mg HC/g rock (Tables 4.1 in the Appendix I, Figures 4.3 and 4.9). The majority of the samples analysed appeared to promise above average hydrocarbon yields, and may therefore be classified as hydrocarbon source rock. The HI values range from 79 to 188 mg HC/g TOC, suggesting moderate hydrocarbon potential and this organic sediment is Type II-III Kerogen.

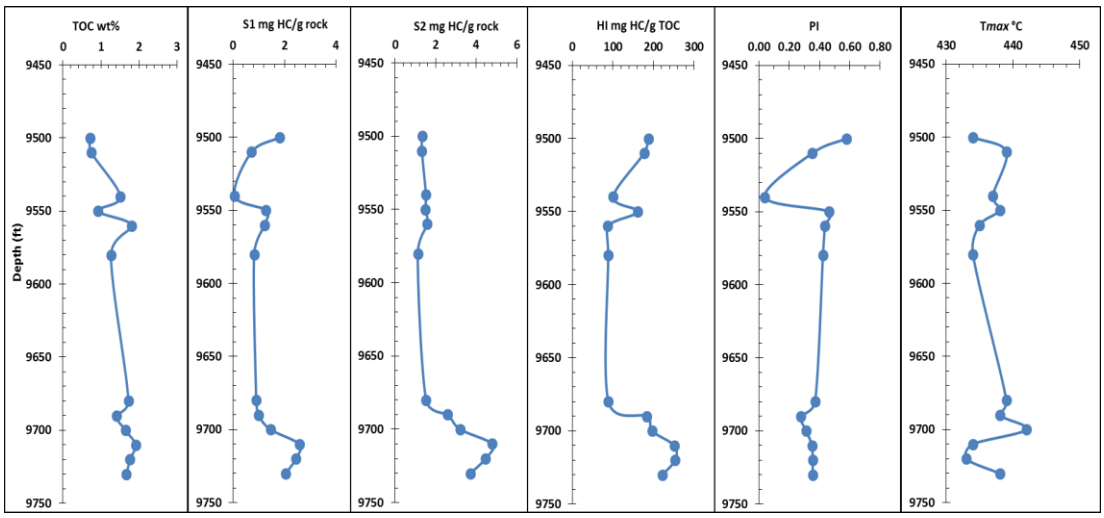

Figure 4.3: Geochemical logs for the Upper Cretaceous, Sirte Shale source rock of the well B2-NC74A in the Sirte Basin.

The C2-16 well is located in the south-easterly extent of the Bazuzi oilfield in the Marada Trough in the central part of the Sirt Basin. The Sirte Shale Formation has a thickness of around 1240 feet, and it extends from 9780 to 11020 feet. The formation consists of dark grey, very dark to slight black shales with minor of sandstone and limestone. It has fair to good TOC values, which range from 0.78 to 1.66 wt% with a mean value of 1.16 wt%. It has low generating potential with potential yields between 0.50 and 3.14 mg HC/g rock, with an average of 1.33 mg HC/g rock (Tables 4.1 in the Appendix I, Figure 4.4 and 4.9). As for organic carbon, most of these samples appeared to have below average hydrocarbon yields, and may rate only as poor to fair source rock potential. HI values ranged between 34 to 159 mg HC/g TOC, suggesting that the organic sediments are Type III or III-II kerogens. The moderate to slightly high TOC levels that are associated with low hydrocarbon yields and hydrogen index values, which may be as a result of the effects of mineral matrix or higher maturity on organic sediments (e.g. Tyson, 1995).

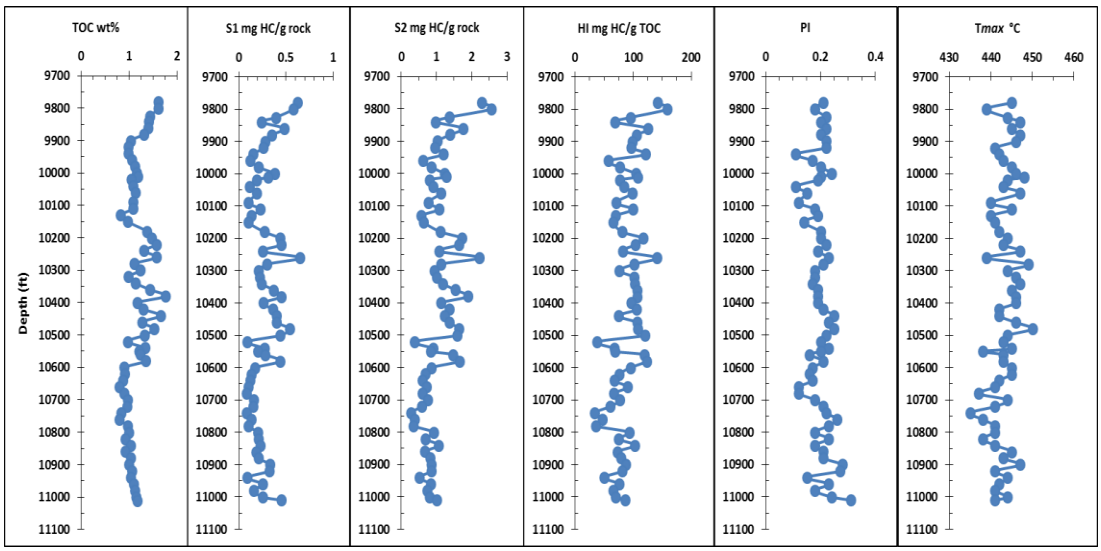

Figure 4.4: Geochemical logs for the Upper Cretaceous, Sirte Shale source rock of the well C2-16 in the Sirte Basin.

The FF14-6 well is located in the southwestern extent of the Attahadi oilfield in the Wadayat Trough in the central part of the Sirt Basin. The Sirte Shale Formation here has a thickness of around 1817 feet, and it extends from 11270 to 13087 feet. The formation is characterized by dark grey shale interbedded with limestone and sandstone. It has TOC contents in the samples ranging between 0.39 wt% and 3.43 wt% with an average of 0.88 wt%, and potential yield ranges from 0.02 to 2.32 mg HC/g rock with an average of 0.48 mg HC/g rock (Tables 4.1 in the Appendix I, Figures 4.5 and 4.9), indicating that the organic sediments have poor to slightly fair potential as source rock. The hydrogen index (HI) values range from 3 to 134 mg HC/g TOC, indicating that organic sediment is comprised of Type III to III-IV kerogen. The low to moderate TOC values, low hydrocarbon potential, and associated with low HI values, may due to high maturity, which led to deplete in hydrogen from the expulsion of the hydrocarbons, mostly as gas. The Sirte Shale source rock in this well showed vitrinite reflectance (*%Ro*) values between 1.0% and 1.50 %*Ro* (See Table 4.1 in the Appendix I, Figures 4.5 and 4.9). However, the Sirte Shale and Rachmat source rocks in the other study wells show values less than 1.0 %*Ro* (Hamyani *et al.*, 1984; El-Alami *et al.*, 1989; Ben Ashour, 2000). This is consistent with the Tmax values, and spore colour indices (See Table 4.1 in the Appendix I, Figures 4.5 and 4.9).

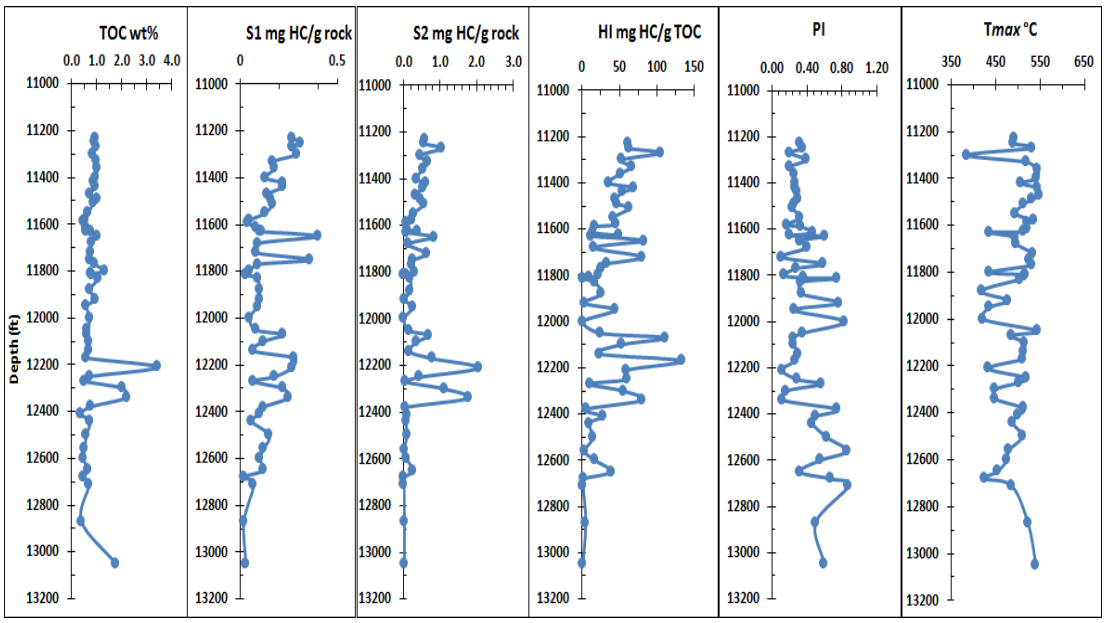

Figure 4.5: Geochemical logs for the Upper Cretaceous, Sirte Shale source rock of the well FF14-6 in the Sirte Basin.

The L1-16 well is located in the Nuflian High at the centre of the Sirt Basin. The Sirte Shale Formation here has a thickness of around about 960 feet, which extends from 7400 to 8360 feet. Based on lithology and total organic carbon, the Sirt Shale Formation is subdivided into upper and lower units. The upper unit extends from 7400 to 7680 feet (at 270 feet thick) and is represented by medium dark grey to dark grey and black shale. It has TOC values ranging from 0.95 to 1.34 wt% with a mean value of 1.15 wt%, and the hydrocarbon yield ranges between 1.39 and 3.15 mg HC/g rock with an average of 2.28 mg HC/g rock (Tables 4.1 in the Appendix I, Figure 4.6 and 4.9), indicating that the organic sediments represent fair to good potential as source rock. The HI values range from 133 to 270 mg HC/g TOC, with an average of 180 mg HC/g TOC, suggesting that the organic sediments are almost entirely amorphous with some contribution from terrestrial organic matter, with Type II-III kerogens, and preserved in a suboxic environment. This type of kerogen may have generated a moderate amount of hydrocarbons. Meanwhile, the lower unit extends from 7700 to 8360 feet, with a thickness of about 660 feet. It is characterized by medium dark grey shale interbedded with limestone and sandstone. The total organic carbon of the lower Sirte Shale Formation range from 0.50 to 1.08 wt.%, with a mean value of 0.78 wt.%, and the total generation yield (S1+S2) of the lower section ranges from 0.68 to 2.14 mg HC/g rock with a mean of 1.23 mg HC/g rock. As with organic carbon, all of these samples appear

to have below the average hydrocarbon potential yields (S1+S2) less than 2.5 mg HC/g rock) and may, therefore, be considered as having poor hydrocarbon source rock potential. This section has HI values ranging from 90 to 255 mg HC/g TOC, suggesting that the organic sediments is composed of Type II-III kerogens.

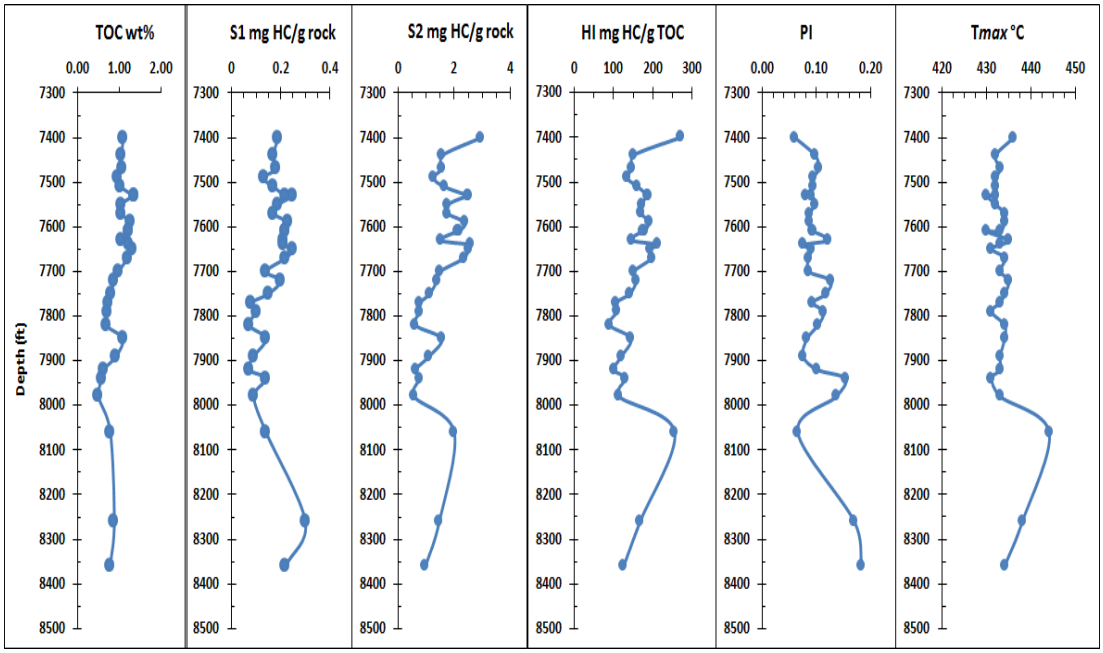

Figure 4.6: Geochemical logs for the Upper Cretaceous, Sirte Shale source rock of the well L1-16 in the Sirte Basin.

The L1-17 well is situated in the western extent of the Mabruk oilfield in the Dor Al Abid Trough in the north-western part of the Sirt Basin. In this study well, the Sirte Shale Formation extends from 6060 to 7030 feet, and has a thickness of about 970 feet. Based on the total organic carbon and lithology, the formation was again subdivided into upper and lower units. The upper unit extends from 6060 to 6608 feet, with a thickness of around 550 feet, but the lower unit extends from 6640 to 7030 feet with a thickness of about 380 feet. The upper section consists of dark grey to black shale interbedded with limestone and has TOC values ranging between 0.99 to 2.41 wt% with a mean value of 1.62 wt%. The hydrocarbon yield ranges from 1.12 to 7.26 mg HC/g rock, with an average of 4.38 mg HC/g rock (Tables 4.1 in the Appendix I, Figures 4.7 and 4.9). From the organic carbon, the majority of these samples displayed above average hydrocarbon yield of 2.5 mg HC/g rock, and may be classified as having good hydrocarbon potential as a source rock. The HI values range between about 105 to 359 mg HC/g TOC, with an average of 245 mg HC/g TOC, suggesting that the

organic sediment comprises Type II to II-III kerogens, preserved in a suboxic to anoxic marine environment. This type of kerogen may also have generated significant amounts of hydrocarbons. On the other hand, the lower Sirte Shale Formation consists of dark grey to medium dark grey shale interbedded with limestone. This lower unit has TOC values ranging from 0.50 to 0.87 wt%, with a mean value of 0.71 wt%, and a hydrocarbon yield range of 0.28 to 1.29 mg HC/g rock with an average of 0.84 mg HC/g rock (Table 4.1 in the Appendix I, Figures 4.7 and 4.9), indicating poor to fair potential as source rocks. The HI values range between 54 to 154 mg HC/g TOC with a mean value of 108 mg HC/g rock, suggesting that the organic sediment is a mixture of Type II-III kerogen.

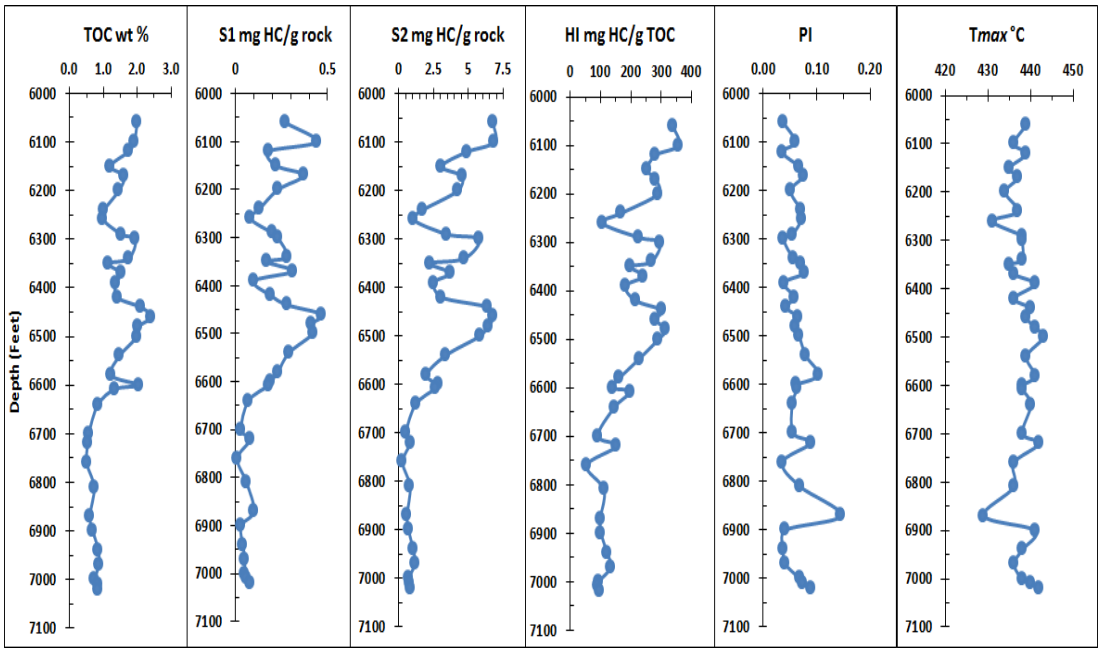

Figure 4.7: Geochemical logs for the Upper Cretaceous, Sirte Shale source rock of the well L1-17 in the Sirte Basin.

The Z1-11 well is located in the northern extent of the Ghani-Zenad oilfield in the Tagrifet Trough at the western part of the Sirt Basin. The Sirte Shale Formation here extends from 8050 to 8243 feet with a thickness of around 193 feet. It consists of dark grey, dark brown to olive black shale, and has TOC values that range from 1.34 to 1.97 wt% with a mean value 1.65 wt% (Tables 4.1 in the Appendix I, Figures 4.8 and 4.9). It has moderate to good generating potential, with a potential yield between 3.01 and

6.54 mg HC/ g rock at an average of 4.70 mg HC/g rock (Tables 4.1 in the Appendix I, Figures 4.8 and 4.9). It is thus rated as a good potential source rock, with HI values ranging between 201 to 308 mg HC/g TOC and an average of 255 mg HC/g rock, suggesting that the organic sediment is comprised of Type II kerogen.

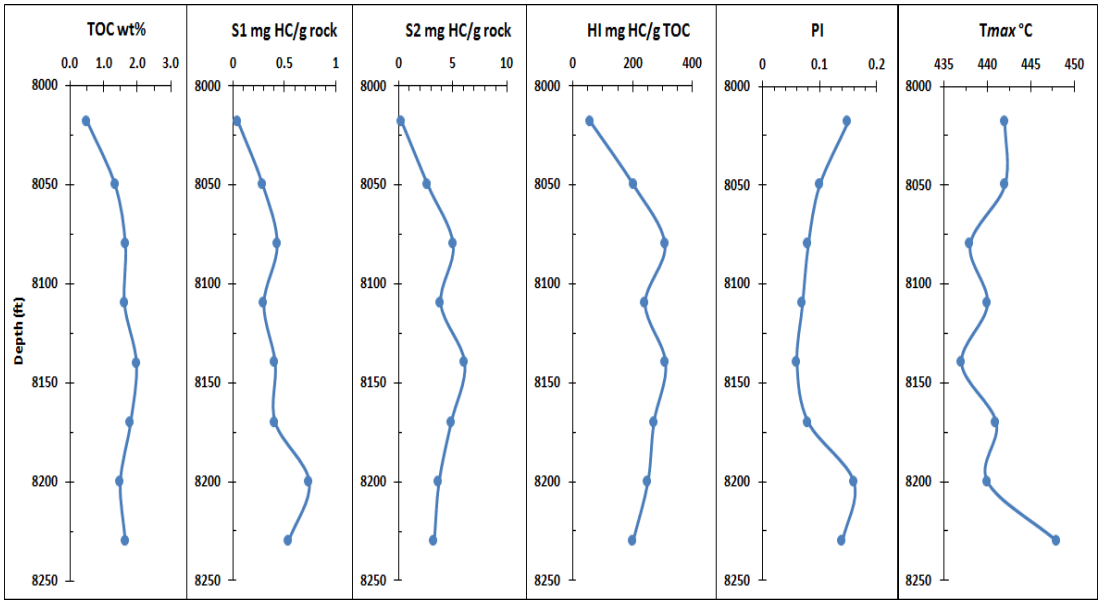

Figure 4.8: Geochemical logs for the Upper Cretaceous, Sirte Shale source rock of the well Z1-11 in the Sirte Basin.

4.2.4 Geochemical Characteristics of the Rachmat Formation Source Rock

The Rachmat Formation is only penetrated in the B1-NC74F well in the southeast of Zellah Trough (west Sabah oilfield) of the Sirt Basin. The Rachmat Formation here extends from 7930 to 8090 feet with a thickness of around 160 feet. It is characterized by medium dark grey, dark grey to black shale interbedded with sandstone and limestone. The total organic carbon content of the Rachmat shales ranges from 1.05 to 1.90 wt% with an average of 1.36 wt% (Tables 4.1 in the Appendix I, Figures 4.2 and 4.9). It has a generation potential ranging between 3.68 to 8.17 mg HC/g rock with a mean value of 5.16 mg HC/g rock, indicating that the formation has good source rock potential for hydrocarbon generation. Its HI values range from 194 to 385 mg HC/g TOC, with an average of 254 mg HC/g rock, suggesting a Type II kerogen.

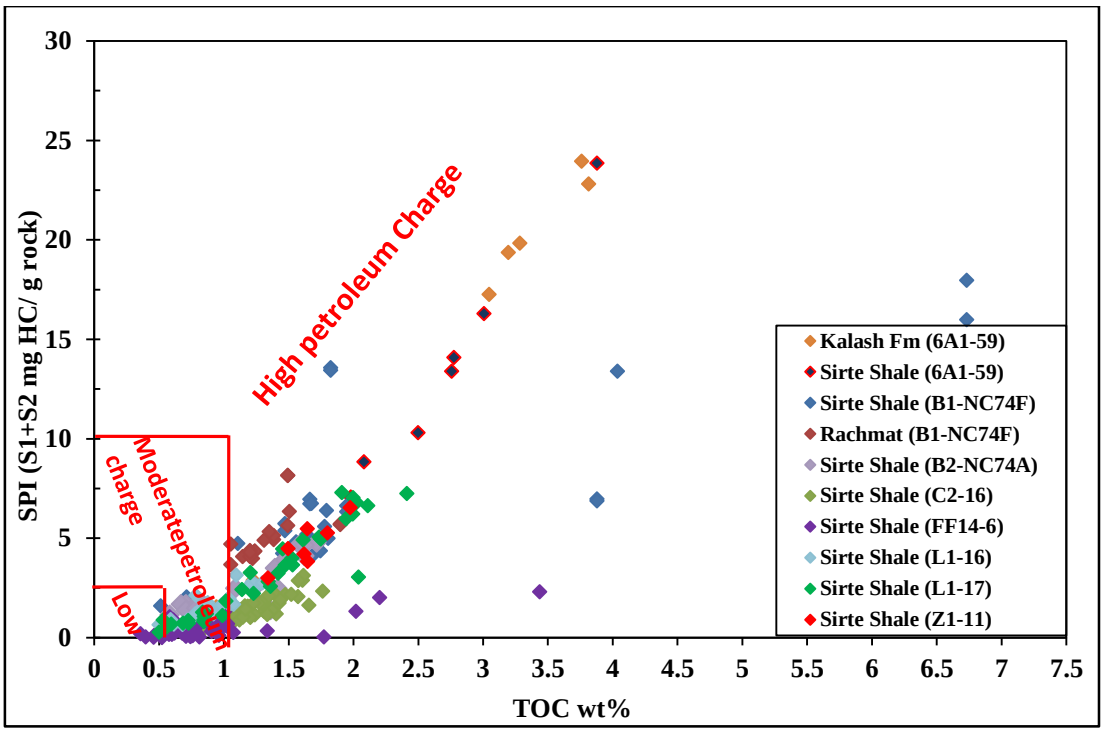

Figure 4.9: Cross plot between hydrocarbon potential yield (S1+S2) and TOC wt.% of the Upper Cretaceous source rocks in the western Sirt Basin.

The Sirte Shale Formation in the L1-17 well in the Dor Al Abid Trough, and in the Z1-11 well in the Tagrifet Trough, and the Rachmat Formation in well B1-NC74F in the south east of the Zellah Trough have mean hydrogen indices from regression slope lines of 249, 258, and 252, respectively (Table 4.1 in Appendix, Figure 4.10), indicating moderately oil-prone Type II kerogens.

For the Upper Kalash and Sirte Shale formations in the 6A1-59 well in the Kotla Graben and Zellah Trough, the regression slopes yield means hydrogen indices of 567 and 478 respectively, indicating Type II kerogen and good oil-prone source rock.

4.2.5 S2 versus TOC

The application of a linear regression of the TOC vs. S2 data is argued to be the best tool for calculating the average HI (Langford and Blanc-Valleron, 1990). The resulting diagram can be used to indicate the petroleum potential and the type of kerogen present depending on maturity (Langford and Blanc-Valleron, 1990). The HI calculated from the slope of the S2 vs. TOC is generally higher than the mean of measured HI values by a factor of about 100 (Cornford *et al.*, 1998). Figure 4.10 shows the S2 versus a

TOC diagram for the Kalash, Sirte Shale, and Rachmat formations of the Upper Cretaceous Sequence in the eight wells (6A1-59, B1-NC74F, B2-NC74A, C2-16, FF14-6, L1-16, L1-17, and Z1-11) in the Sirt Basin. The regression slope of the lines for the Upper Sirte Shale samples in the B2-NC74A well at the Zellah Trough, the Lower Sirte Shale in well L1-16 at Nuflian High, the Sirte Shale samples in the C2-16 well at Marada Trough, and the Sirte Shale samples in the FF14-6 well at the Wadayat Trough, have yield mean hydrogen indices of 147, 141, 94, and 47 mg HC/g TOC respectively. These lines indicate Type III kerogen, and may be these wells able to generate moderate to high amounts of gas. The variation in these hydrogen indices may be due to organic facies changes, low preservation or increasing maturity, particularly in the Nuflian High and Wadayat Trough sites. This also suggests that the Sirte Shale Formation is currently Type III kerogen, but that this is a result of high maturity and genetically it was almost certainly Type II kerogen. Furthermore, microscopy (See section 4.4) shows that the rocks are dominantly of amorphous organic matter and generally Type II kerogen. These Sirte Shale source rocks have already generated oil and gas and the original TOC and HI values, prior to generation, would have been significantly higher.

The upper Sirte Shale samples in well L1-16 in the Nuflian High, and from Zellah Trough in the B1-NC74F well, the lower Kalash samples in the well 6A1-59, and the lower Sirte Shale samples in well B2-NC74A contain Type II-III kerogen, with mean yield hydrogen indices 181, 169, 158, and 152, respectively (Table 4.1 in Appendix, Figure 4.10). The samples of the Sirte Shale and Kalash formations have a moderate richness with the amorphous marine organic matter with some contribution of terrestrial organic matter. Variations in the hydrogen indices may again be due to organic facies changes or reflect the poorer preservation of organic matter.

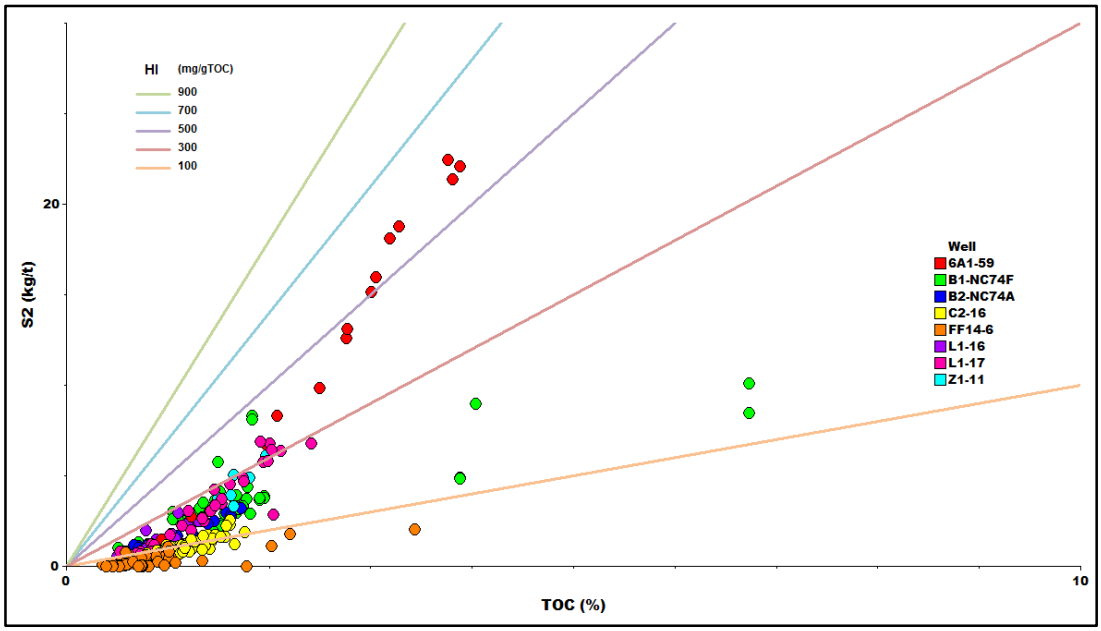

Figure 4.10: Cross plot of the hydrocarbon potential (S2) versus % TOC for the Upper Cretaceous succession in eight selected wells in the Sirt Basin.

4.3 Organic Facies and Thickness Map of the Sirte Shale Formation

The distribution of the organic facies and thickness of the Sirt Shale Formation is highly influenced by the Campanian-Maastrichtian paleogeography (Hallett, 2002). The maximum thickness of Sirt Shale with high TOC values more than 1 wt% occur in the central parts of the graben regions, as shown in Figure 4.7. El-Alami et al. (1989) have illustrated the main depocentres of the Sirt Shale Formation in the Sirt Basin, including the Agedabia Trough (750 m thick, > 1% TOC), Zellah and Maradah Troughs (300 m), and Kotla graben (300 m). The main thickness of the Sirte Shale Formation present in the trough areas is contains Type II kerogen, while thinner Sirt Shale existing towards the horst platform areas often contain lean organic matter consisting of Type III kerogen (El-Arnauti and Shelmani, 1988; Hallett, 2002). Figure 4.7 shows an isopach organic-richness map of the Sirte Shale Formation, showing source richness at the top of the Sirte Shale source rock. The richness map for the given horizons were integrated with the net cumulative thickness maps for the Sirte Shale source rocks. The map shows that the maximum thickness of the formation occurs in the central parts of the trough regions. In the Agedabia Trough, the Sirte Shale has a thickness of 5000 feet and contains more than 1% TOC. Meanwhile, in the Zellah and Marada Troughs the Sirte Shale has a thickness of about 1250 feet, and in the Kotla graben the thickness is over 1000 feet. The organic

carbon content in these troughs have values more than 5% within some intervals of the Sirte Shale Formation.

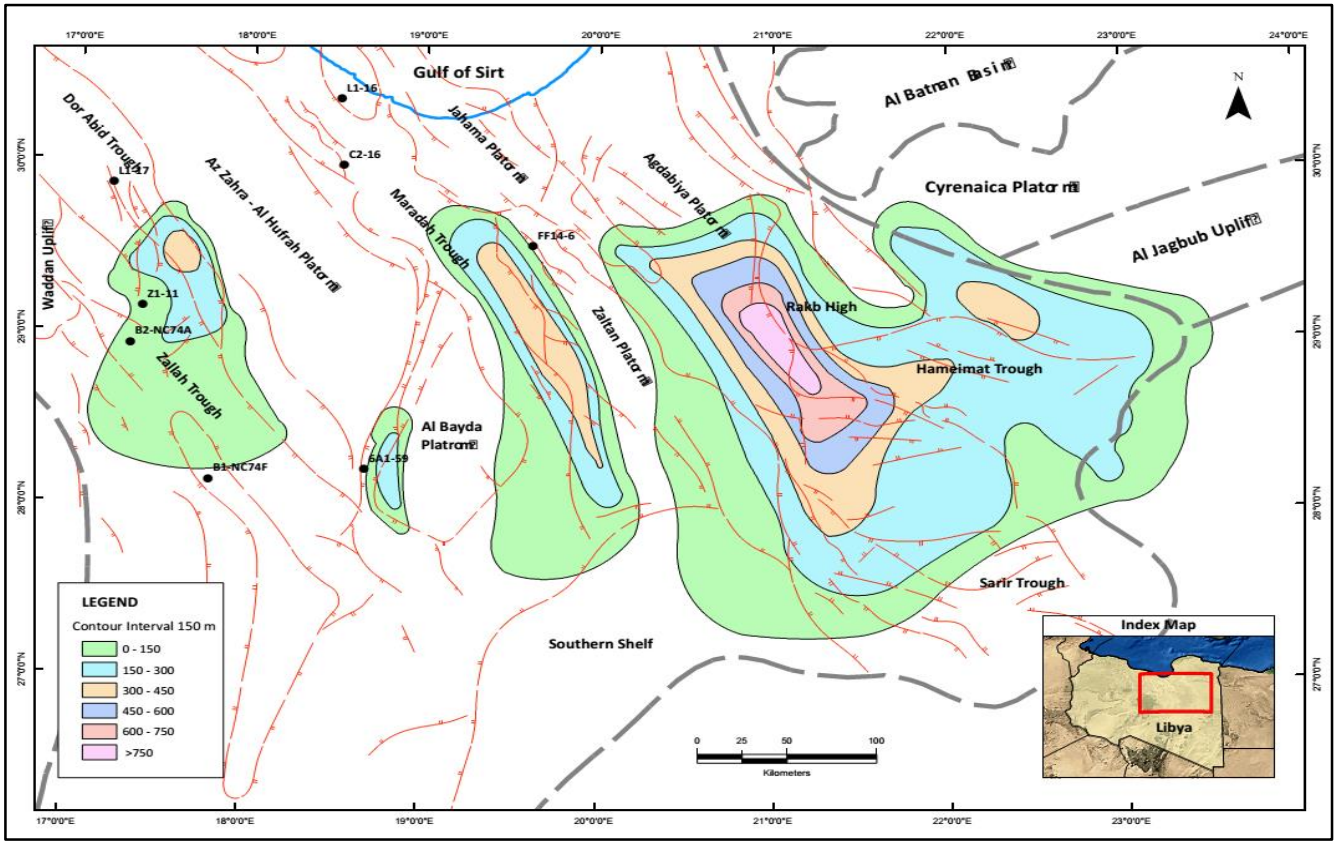

Figure 4.11: Cumulative source rock (> 1% TOC) thickness of the Campanian-Maastrichtian Sirte Shale in the Sirt Basin, controlled by Cretaceous graben/horst relief, modified after El-Alami et al. (1989).

4.4 Maturity Evaluation

4.4.1 Bulk Geochemical Maturity Parameters

In the present study, 269 cutting samples from the Upper Cretaceous sequence were analysed using Rock-Eval pyrolysis. These samples were collected from eight boreholes distributed in the western part of the Sirt Basin and represent the Kalash, Sirte Shale and Rachmat formations source rocks. The results are listed in the Tables 4.1 and 4.2 in Appendix I.

4.4.1.1 Pyrolysis Temperature Index (T*max*)

Generally, Tmax values increase with increasing depth but they vary with kerogen type as well as maturity. In the Sirt Basin, thermal maturity increases eastward and north toward the deep basin troughs. Samples analysed in this study yield estimate of present-day thermal maturity, ranging from near the top, middle and lower oil window to gas window based on pyrolysis T*max* values, and also confirmed by SCI, and vitrinite reflectance measurements. Of well 6A1-59 in the Zellah Trough in the western part of the basin, Tmax values range from 429 to 439 ºC for the Kalash section and from 429 to 432 ºC for the Sirte Shale section. In well B1-NC74F in the southeast Zellah Trough, T*max* values range from about 428 to 443 ºC through the Sirte Shale section, and from 431 to 442 ºC in the Rachmat section. In well B2-NC74A in the west Zellah Trough, T*max* values are low for the Sirte Shale section was ranging from 425 to 436 ºC. For wells 6A1-59, B1-NC74F, and B2-NC74A, the data shows that the Kalash, Sirte Shale and Rachmat formations have average Tmax values of 433, 436, and 432 ºC respectively, indicating that these sedimentary sections are in the immature to early mature zone for hydrocarbon generation. Meanwhile, in well L1-16 in the Nuflian High, the Tmax ranges between 430 to 444 ºC through the Sirte Shale section. Of well L1-17 in the Dor Al Abid Trough, the T*max* values range between 429 to 442 ºC in the Sirte Shale sections. In the well Z1-11 in the Tagrifet Trough in north-west Sirt Basin, the T*max* values range from 438 to 448 ºC. For the wells L1-16, L1-17, and Z1-11, the Tmax maturity data illustrate that the Sirte Shale Formation has an average values of 433, 438, and 441 ºC respectively, indicating that they are within the early to middle mature zone. In well C2-16 in the Marada Trough in the central Sirt Basin, the T*max*

values are slightly higher and ranging about 435 to 450 ºC through the Sirte Shale section. For well FF14-6 in the Wadayat Trough in the centre of the Sirte Basin, the T*max* values are high and range from 436 to 541 ºC through the Sirte Shale section. The T*max* maturity data in wells C2-16 and FF14-6 show that the Sirte Shale Formation has average T*max* values of 444 and 499 ºC respectively, indicating that the samples analysed are within the middle, late mature to post mature zone. Therefore, from the source rock samples from the northeast of the basin in the Wadayat Trough where well FF14-6 is located, the Sirte Shale Formation has probably reached the onset of the condensate window.

Figure 4.12 shows a plot of the hydrogen indices versus pyrolysis temperature T*max* values. This diagram shows considerable lateral and vertical variations in hydrogen indices due to kerogen facies changes and maturity. Most of the Sirte Shale samples are in the early to middle mature petroleum generating range (435 to 460 ºC), and most of the kerogens are Type II-III, but several are immature and post mature. However, the Upper Kalash and Sirte Shale formations in well 6A1-59 give relatively high hydrogen indices considering their level of maturity (432-434 ºC), and they are classified as early mature and contain Type II kerogen. Meanwhile, in wells C2-16, and FF14-6, most of the kerogen is Type III or III-II in the Sirte Shale Formation. A general decrease in the hydrogen indices in the Sirte Shale Formation reflects increasing maturity, whereas in the L1-16 well the reduction in hydrogen indices may be related to organic facies change as well as increasing maturity. In general, T*max* values tend to increase gradually with increasing depth of burial towards the depocenter of the basin. Towards the northeast part of the basin at wells C2-16 and FF14-6, the T*max* is relatively higher than those located in the west and southwest at wells 6A1-69, L1-16, L1-17, B1-NC74F, and B2-NC74A. Furthermore, increasing T*max* values was noted from southwest to the northeast and southeast of the basin. This may reflect changes and an increase in the geothermal gradient in the Sirt Basin (c.f. Gumati and Schamel, 1988)

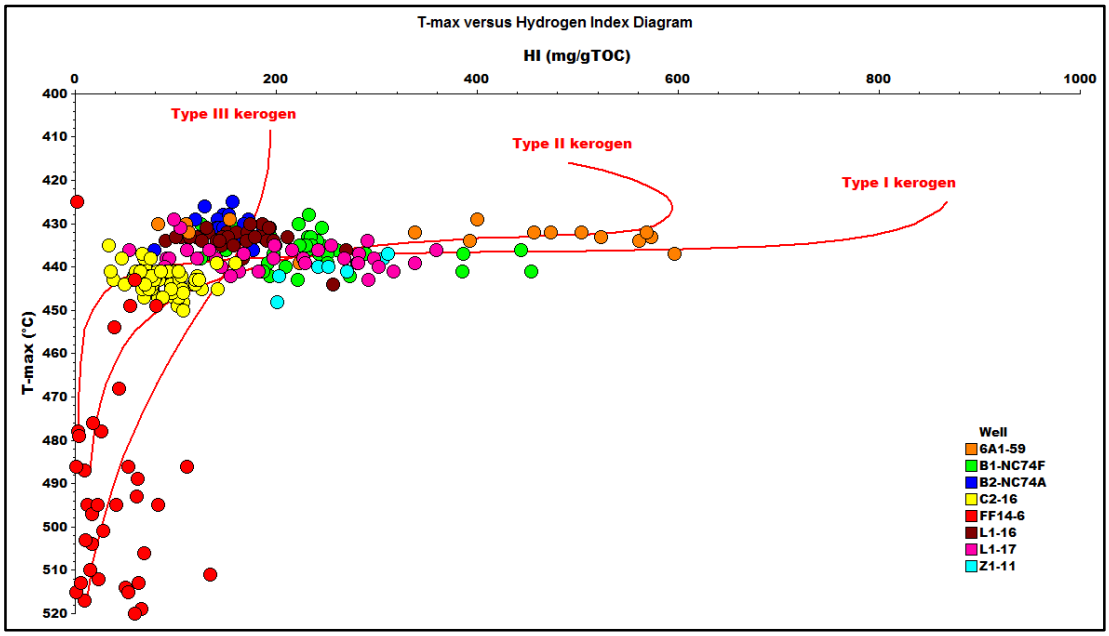

Figure 4.12: Cross plot of T*max* versus hydrogen index of the Kalash, Sirte Shale and Rachmat formation of the Upper Cretaceous Sequences.

4.4.1.2 Production Index (PI)

The Production Index (PI) is calculated using Rock-Eval free hydrocarbon (S1) and potential hydrocarbons (S2) from the equation: S1/(S1+S2). Production index values less than 0.1 indicate an immature zone of oil generation, values from 0.1 to 0.4 suggest the oil window, though values less than 0.4 can indicate wet gas zone, whereas values more than 0.4 may suggest migrated hydrocarbons (Peters, 1986). Figure 4.13 shows cross plots of the Tmax versus production indices for wells 6A1-59, B1-NC74F, B2-NC74A, C2-16, FF14-6, L1-16, L1-17, and Z1-11.

This plot shows increasing maturity with depth, and there also are clear variations between the Kalash, Rachmat and Sirte Shale sections. These are probably due to burial depths and perhaps also changes in geothermal gradients within the Sirt Basin. The plot also shows differences in production indices between the Kalash Formation and Sirte Shale Formation in wells 6A1-59 and L1-17, which are immature to early mature. The data for the Sirte Shale and Rachmat formations at the wells B1-NC74F, B2-NC74A, C2-16, L1-16 and in some samples of FF14-6, which are located between 0.1-0.4 PI, suggests that the samples are within the margin mature to middle mature zone for hydrocarbon generation. Some samples from well B1-NC74F have PI values higher than 0.4, and this may indicate samples saturated with hydrocarbons in an accumulation

zone and/or contamination from drilling base mud. The majority of the Sirte Shale samples in well FF14-6 had high T*max* values above 470 ºC with high PI values greater than 0.4 PI, indicating that the samples analysed are within the post mature zone. This may indicate that the Sirte Shale has already generated substantial amounts of hydrocarbon oil and gas and now produces only gas.

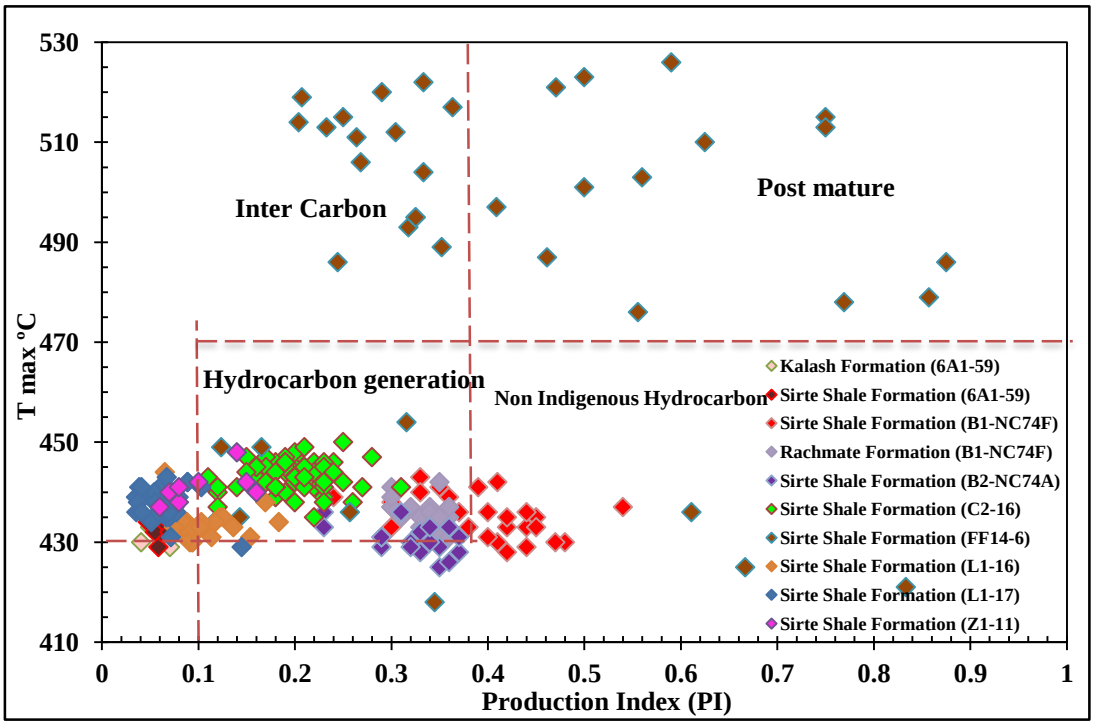

Figure 4.13: Cross plot of T*max* versus production Index of the Kalash, Sirte Shale, and Rachmat Formation, Upper Cretaceous sequences.

4.4.2 **Spore Colour Index (SCI)**

In the present study, 53 cutting samples from six wells have been analysed for spore colour index. The spore colour index data for wells 6A1-59, C2-16, FF14-6, L1-16, L1-17, and Z1-11 are given in Table 4.2 in the Appendix I and plotted against depth in Figure 4.22. The data excluded the wells B1-NC74F and B2-NC74A due to the absence of cutting rock samples. In the Upper Cretaceous marine sequences, where land plant spores are absent, colour measurements were made of the dinoflagellates and amorphous organic matter. Calibration studies have shown that the major colour changes in dinocyts occur in the late mature zone (Collins, 1990).

In the southeast Zellah Trough and southwest Kotla Graben in well 6A1-59, SCI determinations were made on 10 samples from the interval between 7140 to 7280 feet for both Kalash and Sirte Shale formations. The SCI for the Kalash Formation shows a slight gradual increase with depth from 3.5 to 4.5 at depths of 7140–7210 feet. The amorphous organic matter exhibits a yellow to yellow-orange colour under blue florescence see Plate 4.1 in Figure 4.14. The dinoflagellate colour index data were obtained at the same time as the amorphous colour. The data shows a slight increase with depth from 2.0 to 3.0. Both measurements indicate that the Kalash Formation is within the immature to marginally mature stage. The SCI for the Sirte Shale Formation at this interval of 7220 to 7280 feet displays a slight increase from 4.5 to 5.5. The amorphous fluorescence data agree well with the SCI, showing changes with increasing depth from yellow orange to orange to dull orange. The dinoflagellate colour index data also show a slight increase with depth from 3.0 to 4.0. The SCI determinations indicate that the Sirte Shale Formation is within the early mature stage.

For well L1-16 in the Nuflian High at the centre of the Sirt Basin, SCI determinations were made on 11 samples from the interval 7400 to 8260 feet. Spores were absent in whole sections, and therefore most measurements were made on the amorphous organic matter and dinocyts. The data show an increase from 4.0 to 6.0 with increasing depth. These measurements agree with that of amorphous fluorescence, which changes from yellow to yellow orange, then orange to dull orange and some samples have brown fluorescence see Plates 4.2 and 4.3 in Figures 4.15 and 4.16. The dinocyts colour data also show an increase from 3.5 to 4.5, (5.0), and changes in colour under blue light fluorescence from yellow to yellow orange, to orange. The SCI determinations suggest that the Sirte Shale Formation samples are within the early mature to middle mature stage.

SCI determinations were then made of 14 samples from the 6120 to 7020 feet interval of well L1-17 in the Dor Al Abid Trough. The spore colour index and dinocyts colour gradient show a gradual increase with depth, from 3.5 to 5.5 and 2.5 to 4.0, respectively, within the Sirte Shale Formation. The amorphous fluorescence changes from yellow to yellow orange and to orange throughout the sections analysed, see Plates 4.4 and 4.5

in Figures 4.17 and 4.18. Both measurements indicate that the Sirte Shale Formation samples are within the early mature to the beginning of the middle mature stages.

For well Z1-11 in the Tagrifet Trough in the western part of the Sirt Basin, the SCI measurements were made of 3 samples from the interval 8050 to 8170 feet within the Sirte Shale Formation. The SCI data show a slight increase with depth from 5.0 to 6.0, and from 3.5 to 4.5 for dinocyts colour. The amorphous fluorescence changes from yellow orange, orange to dull orange, and to brown, while the dinocyts fluorescence changes from orange to dull orange see Plate 4.6 in Figure 4.19. The SCI data show that the Sirte Shale Formation is within the middle mature stage.

For well C2-16 in the Marada Trough at the centre of the Sirt Basin, spore colour index determinations were made of 17 samples from the interval of 9780 to 11000 feet. Spores and pollen were absent in most of the sections, and therefore most of the spore colour measurements were based on amorphous organic matter and dinocyts. The spore colours for both show an increase from 6.5 to 7.5 and 4.5 to 6.0, respectively at a depth from 9780 to 10240 feet, and from 7.5 to 8.5 for amorphous organic matter and from 6.5 to 7.0 for dinocyts below 10380 feet. The amorphous fluorescence agrees well with the SCI data and changes from orange to dull orange, and from brown to dull brown to no fluorescence, while the dinocyts fluorescence changes from orange to dull orange, and from dull orange to brown as shown in Plate 4.7 in Figure 4.20. The SCI determinations indicate that the Sirte Shale Formation is within the middle mature to late mature stage.

SCI determinations were made on 12 samples from the 11250 to 12870 feet intervals of well FF-14-6 in the Wadayat Trough at the centre of the Sirt Basin. The spore colour index and dinocyts gradient show a gradual increase of SCI with depth from 7.5 to 9.0 and 6.0 to 7.0, respectively, within the Sirte Shale Formation. The amorphous fluorescence agrees well with the SCI data and changes from dull orange to dull brown, and from dull brown to non-fluorescent, while the dinocyts fluorescence changes from very dull orange to brown, and dull brown to non-fluorescent as shown in Plate 4.8 in Figure 4.21. The SCI determinations indicate that the Sirte Shale Formation is within the late mature to post mature stage.

Figure 4.14: Including **Plate 4.1,** transmitted light and fluorescent blue light microphotographs of the amorphous organic matter, palynomorphs (spore and dinocyts), and phytoclasts. Microphotography from 1 to 8 for well 6A1-59

Plate 4.1

1-2) Amorphous in transmitted and blue light fluorescent (x25), Kalash Formation. Depth 7170 feet, spore colour indices (SCI) ≈ 3.5-4.0.

3-4) Dinocyts in transmitted and blue light fluorescent (x25), Kalash Formation. Depth 7180 feet, spore colour indices (SCI) ≈ 4.0.

5-6) Dinocyts in transmitted and blue light fluorescent (x40), Kalash Formation. Depth 7180 feet, spore colour indices (SCI) ≈ 4.0.

7-8) Algal organic matter in transmitted and blue light fluorescent (x40), Kalash Formation. Depth 7180 feet.

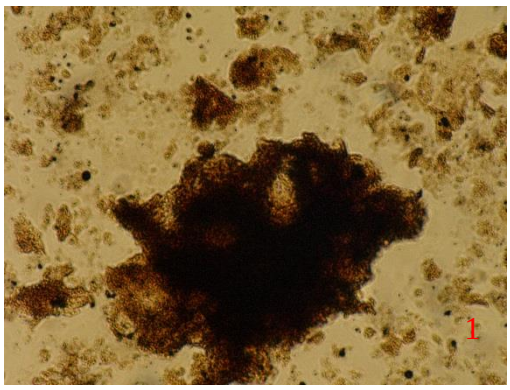
1


2

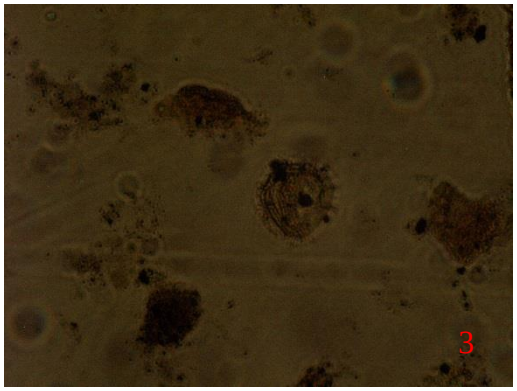
3

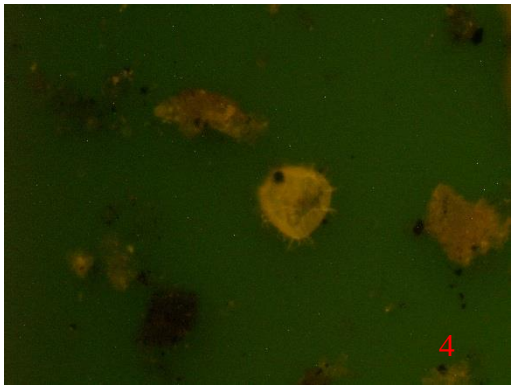
4

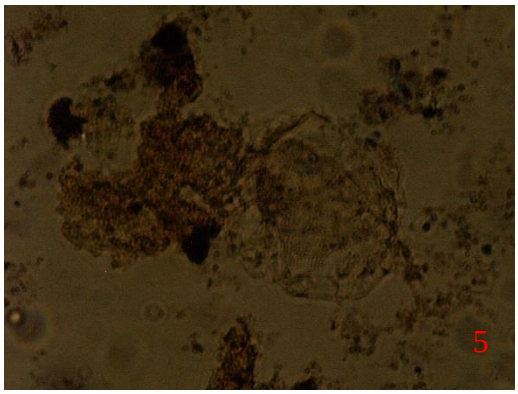
5

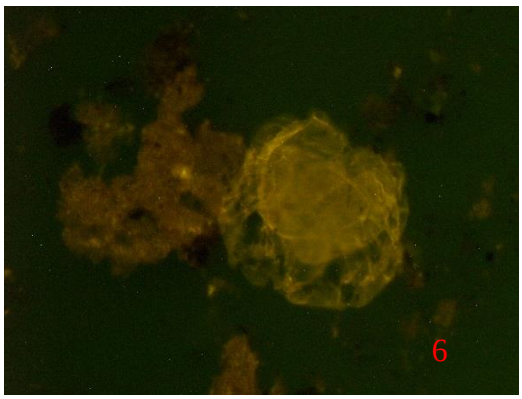
6

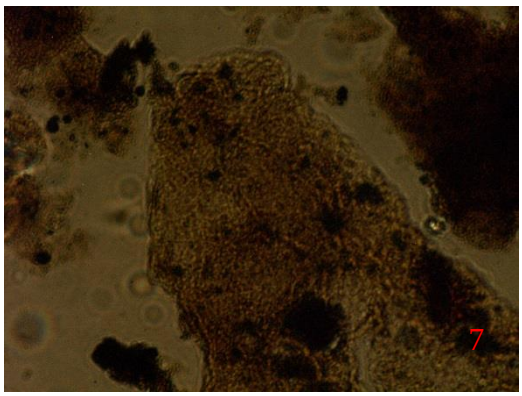
7

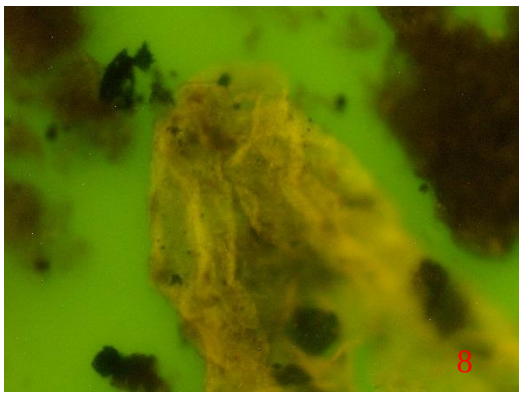
8

Figure 4.15: Including **Plate 4.2,** transmitted light and fluorescent blue light microphotographs of the amorphous organic matter, palynomorphs (spore and dinocyts), and phytoclasts. Microphotography from 9 to 16 for well L1-16.

Plate 4.2

9-10) Amorphous and dinocyts in transmitted and blue light fluorescent (x25), Sirte Shale Formation. Depth 7400 feet, spore colour indices (SCI) ≈ 4.0-4.5.

11-12) Amorphous in transmitted and blue light fluorescent (x25), Sirte Shale Formation. Depth 7700 feet, spore colour indices (SCI) ≈ 5.0-5.5.

13-14) Amorphous in transmitted and blue light fluorescent (x25), Sirte Shale Formation. Depth 7700 feet, spore colour indices (SCI) ≈ 5.0-5.5.

15-16) Amorphous and phytoclasts organic matter in transmitted and blue light fluorescent (x25), Sirte Shale Formation. Depth 8260 feet, spore colour indices (SCI) ≈ 6.0-6.5.

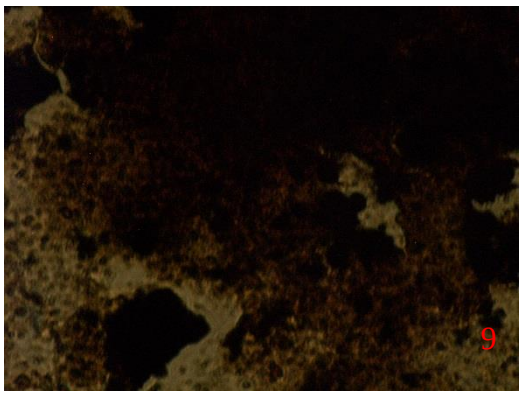
9

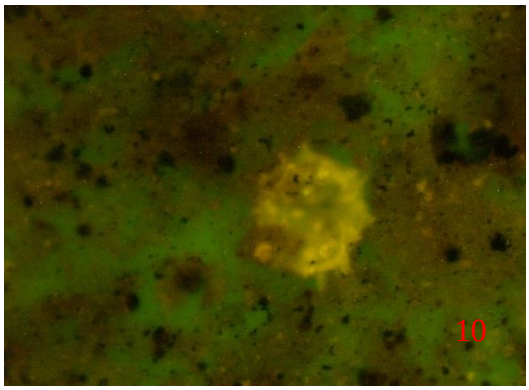
10

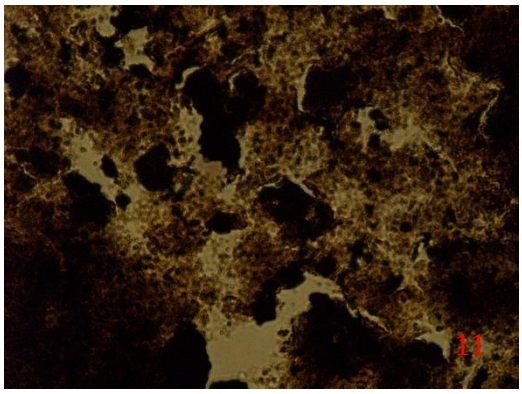
11

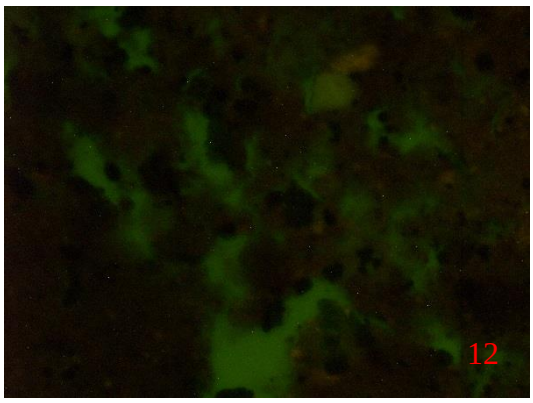
12

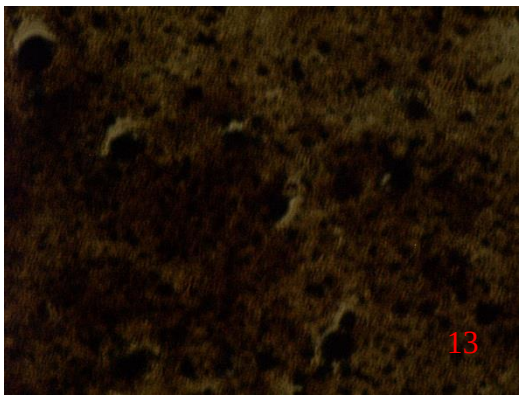
13

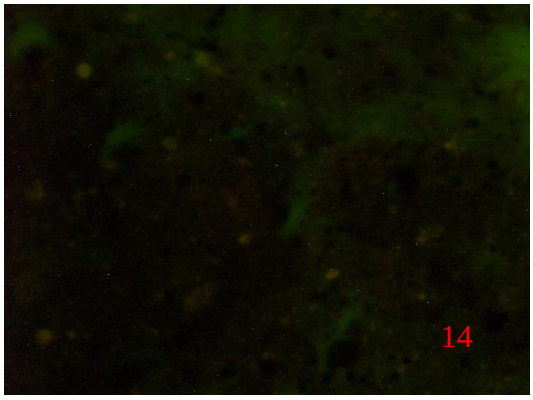
14

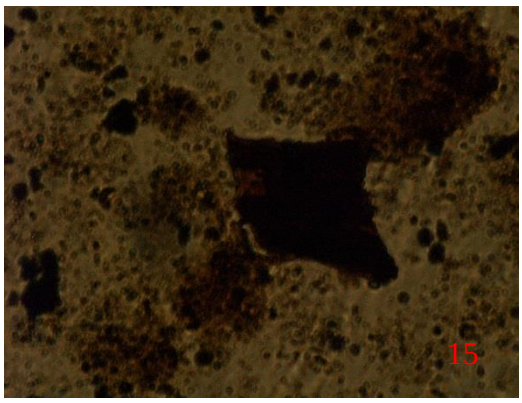
15

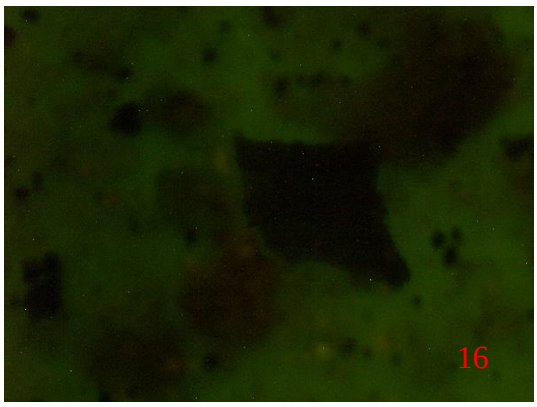
16

Figure 4.16: Including **Plate 4.3**, transmitted light and fluorescent blue light microphotographs of the amorphous organic matter, palynomorphs (spore and dinocyts), and phytoclasts. Microphotography from 17 to 24 for well L1-16.

Plate 4.3

17-18) Amorphous and dinocyts in transmitted and blue light fluorescent (x25), Sirte Shale Formation. Depth 7940 feet, spore colour indices (SCI) ≈ 5.5-6.0.

19-20) Amorphous and dinocyts in transmitted and blue light fluorescent (x25), Sirte Shale Formation. Depth 8060 feet, spore colour indices (SCI) ≈ 5.5-6.0.

21-22) Amorphous and dinocyts in transmitted and blue light fluorescent (x25), Sirte Shale Formation. Depth 8260 feet, spore colour indices (SCI) ≈ 6.0-6.5.

23-24) phytoclasts (vitrinite maceral) in transmitted (x25), Sirte Shale Formation. Depth 8260 feet, spore colour indices (SCI) ≈ 6.0-6.5.

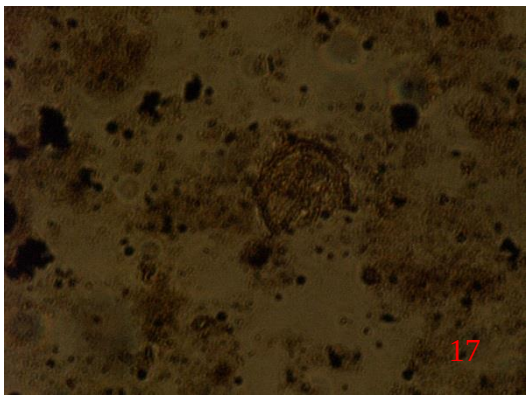
17

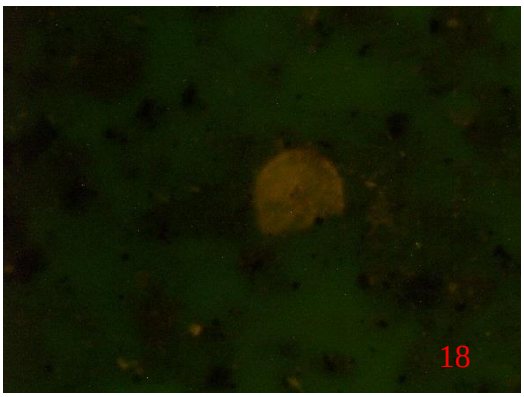
18

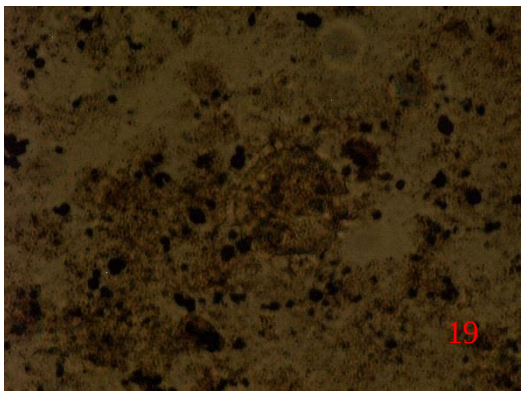
19

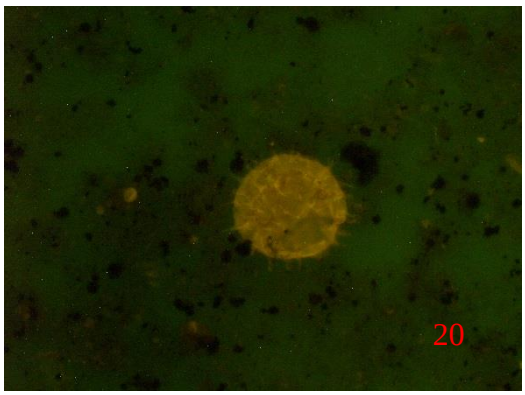
20

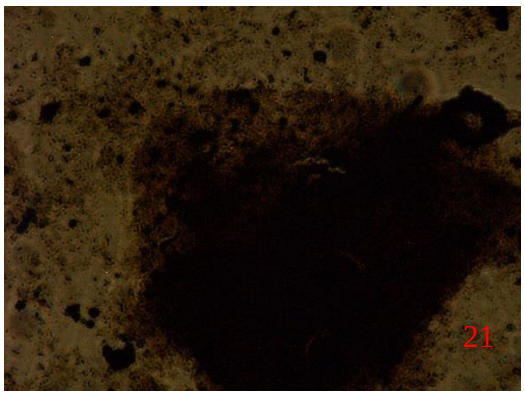
21

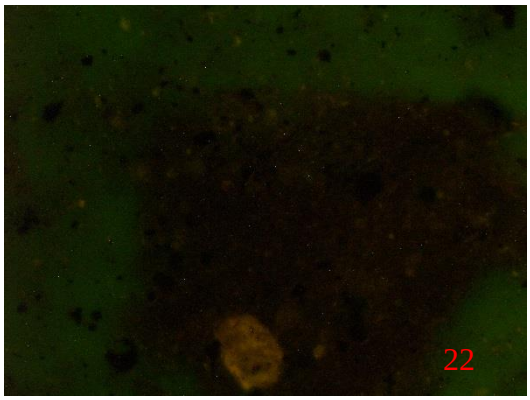
22


23

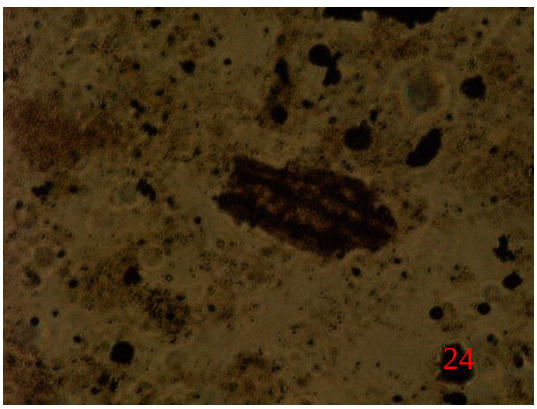
24

Figure 4.17: Including **Plate 4.4**, transmitted light and fluorescent blue light microphotographs of the amorphous organic matter, palynomorphs (spore and dinocyts), and phytoclasts. Microphotography from 25 to 32 for well L1-17.

Plate 4.4

25-26) Amorphous and dinocyts in transmitted and blue light fluorescent (x25), Sirte Shale Formation. Depth 6120 feet, spore colour indices (SCI) ≈ 3.5-4.0.

27-28) Amorphous and dinocyts in transmitted and blue light fluorescent (x25), Sirte Shale Formation. Depth 6120 feet, spore colour indices (SCI) ≈ 3.5-4.0.

29-30) Amorphous in transmitted and blue light fluorescent (x25), Sirte Shale Formation. Depth 6170 feet, spore colour indices (SCI) ≈ 3.5-4.0.

31-32) Dinocyts and algal organic matter in transmitted and blue light fluorescent (x25), Sirte Shale Formation. Depth 6260 feet, spore colour indices (SCI) ≈ 3.5-4.0.

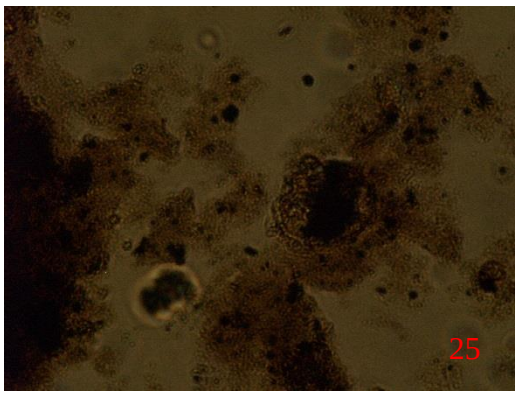
25

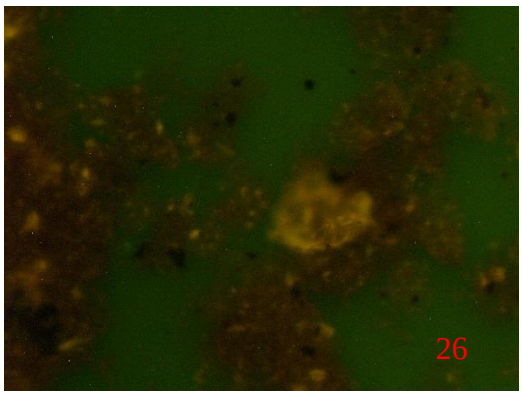
26

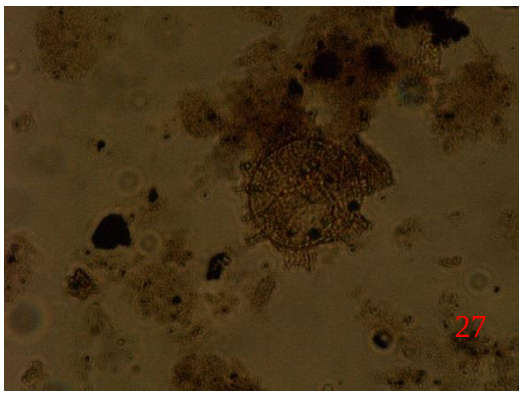
27

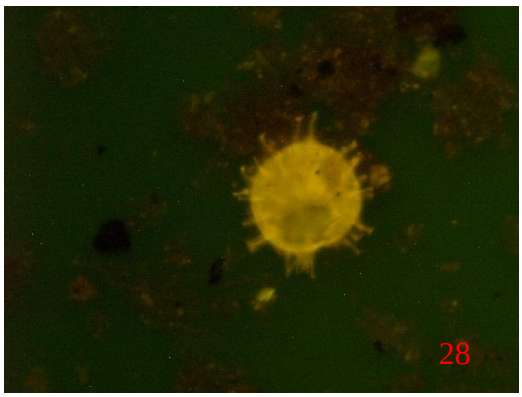
28

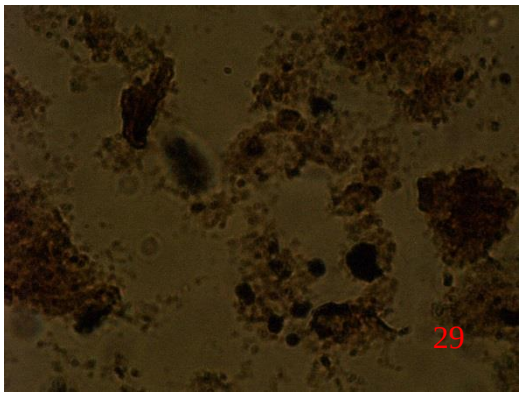
29

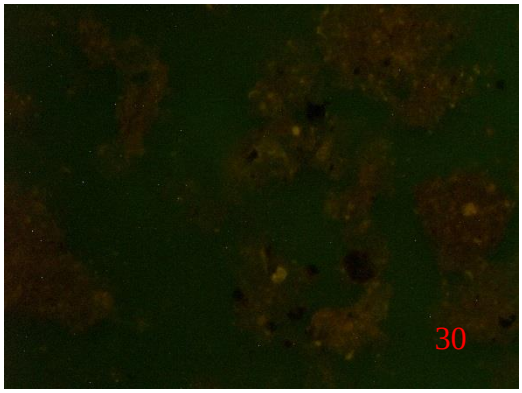
30

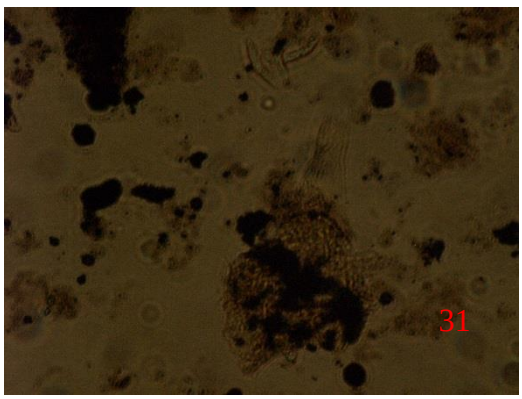
31

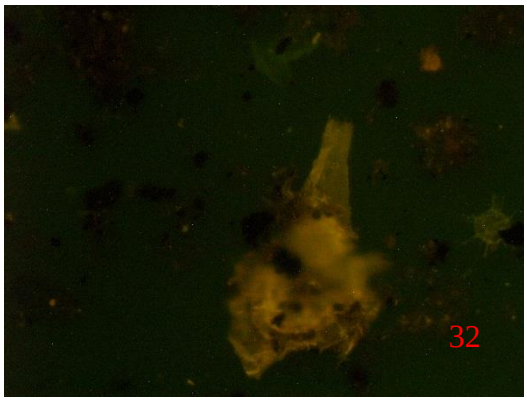
32

Figure 4.18: Including **Plate 4.5**, transmitted light and fluorescent blue light microphotographs of the amorphous organic matter, palynomorphs (spore and dinocyts), phytoclasts and Zooclasts (foraminifer). Microphotography from 33 to 40 for well L1-17.

Plate 4.5

33-34) Amorphous and dinocyts in transmitted and blue light fluorescent (x25), Sirte Shale Formation. Depth 6260 feet, spore colour indices (SCI) ≈ 3.5-4.0.

35-36) Amorphous and dinocyts in transmitted and blue light fluorescent (x25), Sirte Shale Formation. Depth 7000 feet, spore colour indices (SCI) ≈ 4.5.

37) Zooclasts (foraminifer) in transmitted (x25), Sirte Shale Formation. Depth 6810 feet.

38) Phytoclasts (vitrinite macerals) in transmitted (x25), Sirte Shale Formation. Depth 7000 feet.

39-40) Dinocyts in transmitted and blue light fluorescent (x25), Sirte Shale Formation. Depth 7020 feet, spore colour indices (SCI) ≈ 5.0.

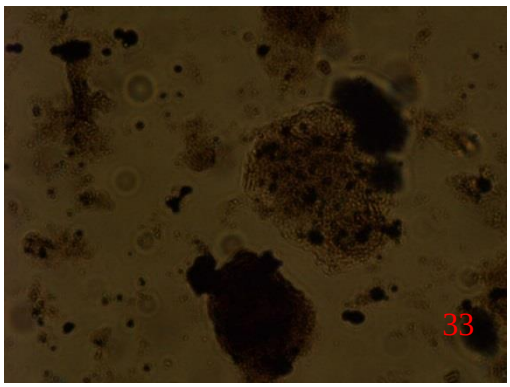
33

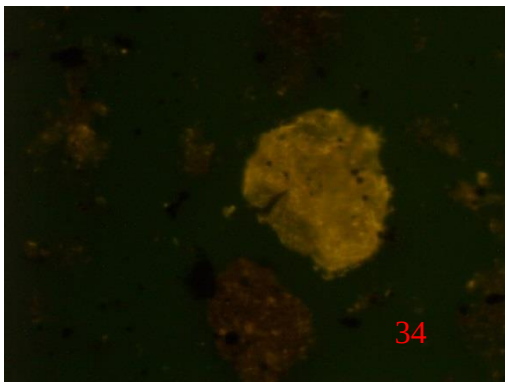
34

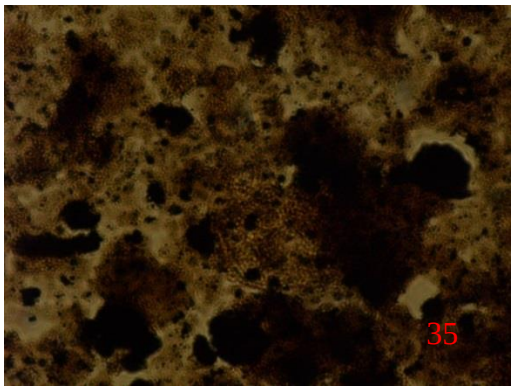
35

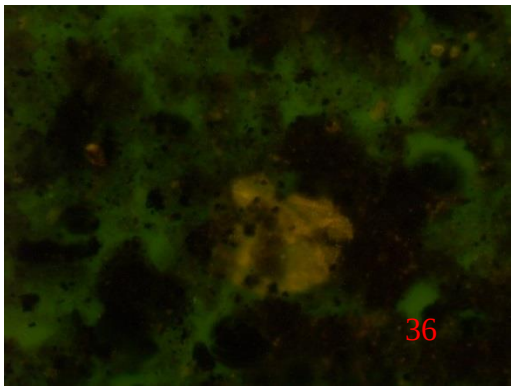
36

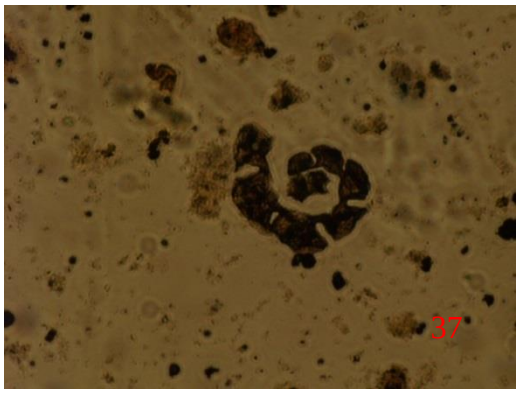
37

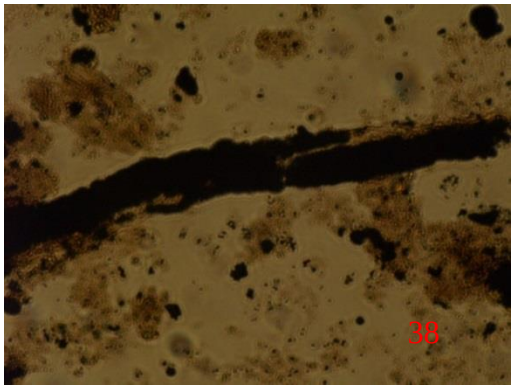
38

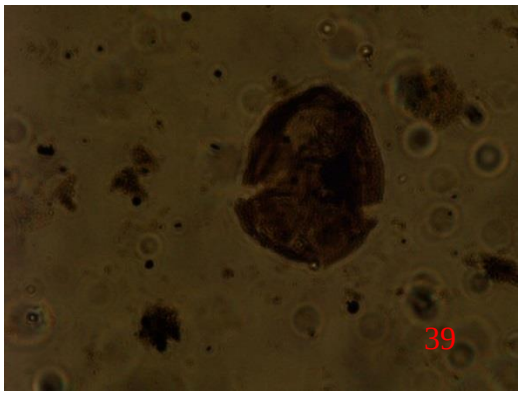
39

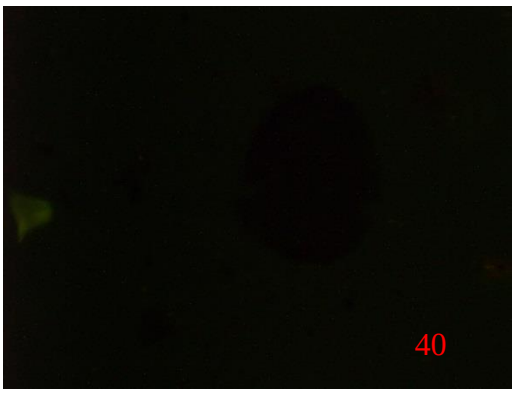
40

Figure 4.19: Including **Plate 4.6**, transmitted light and fluorescent blue light microphotographs of the amorphous organic matter, palynomorphs (spore and dinocyts), and phytoclasts. Microphotography from 41 to 48 for well Z1-11.

Plate 4.6

41-42) Dinocyts in transmitted and blue light fluorescent (x40), Sirte Shale Formation. Depth 8050 feet, spore colour indices (SCI) ≈ 5.0-5.5.

43) Amorphous and dinocyts in transmitted (x25), Sirte Shale Formation. Depth 8170 feet, spore colour indices (SCI) ≈ 6.0.

44) Amorphous and phytoclasts (vitrinite maceral) in transmitted (x25), Sirte Shale Formation. Depth 8170 feet, spore colour indices (SCI) ≈ 6.0.

45-46) Palynomorphs (spore) in transmitted and blue light fluorescent (x40), Sirte Shale Formation. Depth 8170 feet, spore colour indices (SCI) ≈ 6.0.

47-48) Amorphous and dinocyts in transmitted and blue light fluorescent (x25), Sirte Shale Formation. Depth 8170 feet, spore colour indices (SCI) ≈ 6.0.

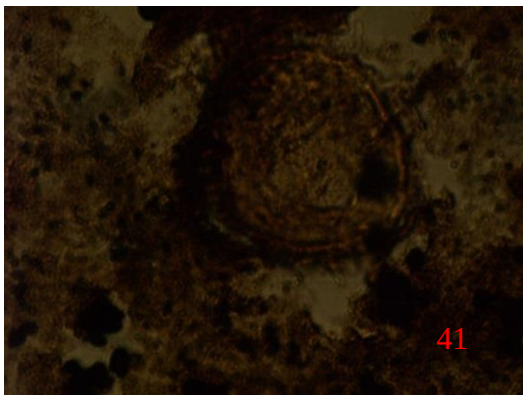
41

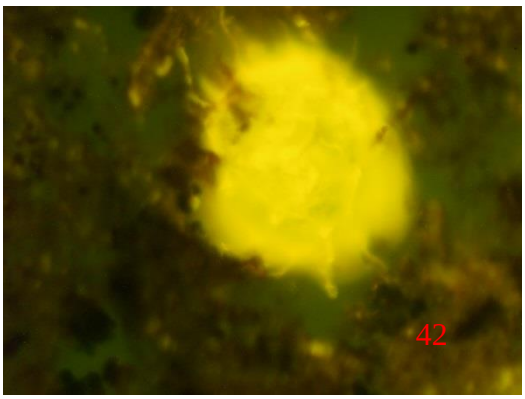
42

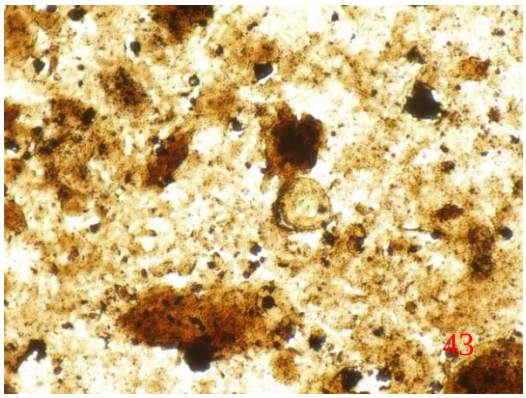
43

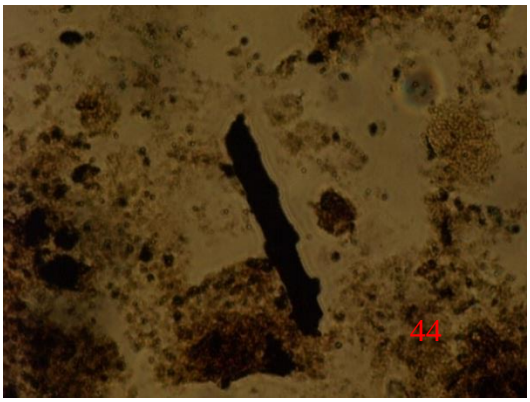
44

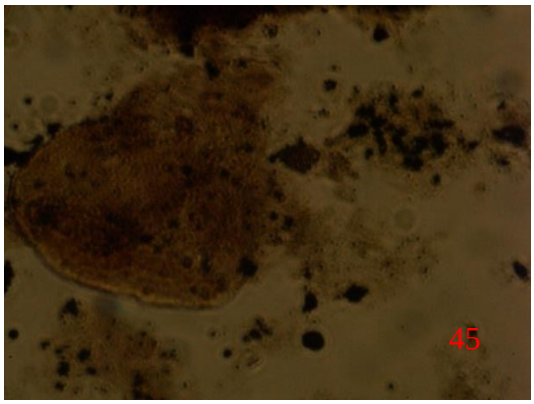
45

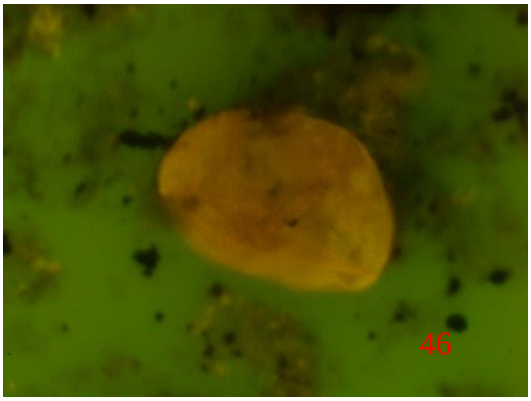
46

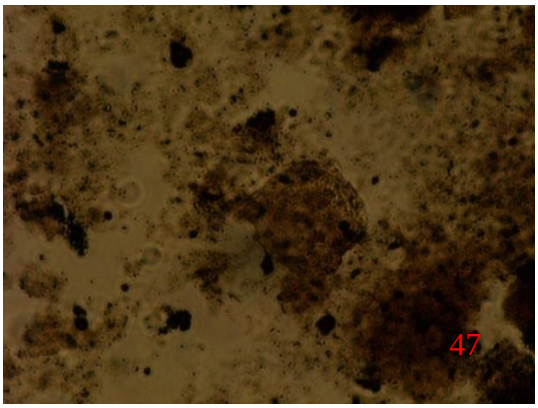
47

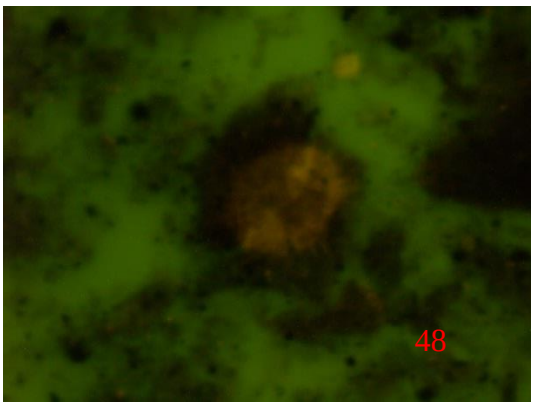
48

Figure 4.20: Including **Plate 4.7**, transmitted light and fluorescent blue light microphotographs of the amorphous organic matter, palynomorphs (spore and dinocyts), and phytoclasts. Microphotography from 49 to 56 for well C2-16.

Plate 4.7

49-50) Amorphous in transmitted and blue light fluorescent (x25), Sirte Shale Formation. Depth 9780 feet, spore colour indices (SCI) ≈ 6.5-7.0.

51-52) Amorphous in transmitted and blue light fluorescent (x25), Sirte Shale Formation. Depth 9840 feet, spore colour indices (SCI) ≈ 7.0.

53-54) Dinocyts and amorphous in transmitted and blue light fluorescent (x25), Sirte Shale Formation. Depth 10010 feet, spore colour indices (SCI) ≈ 7.5.

55-56) Dinocyts and amorphous in transmitted and blue light fluorescent (x25), Sirte Shale Formation. Depth 10600 feet, spore colour indices (SCI) ≈ 8.0.

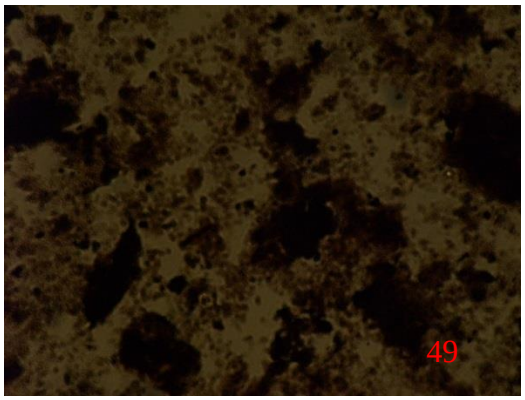
49

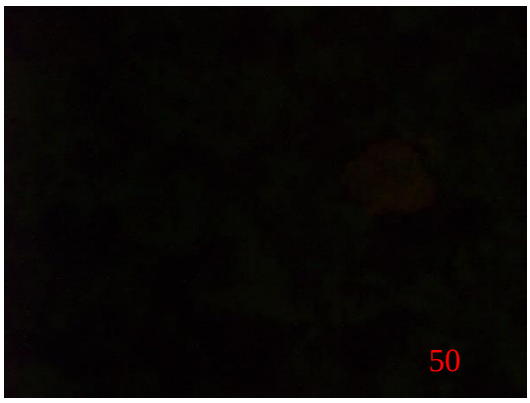
50

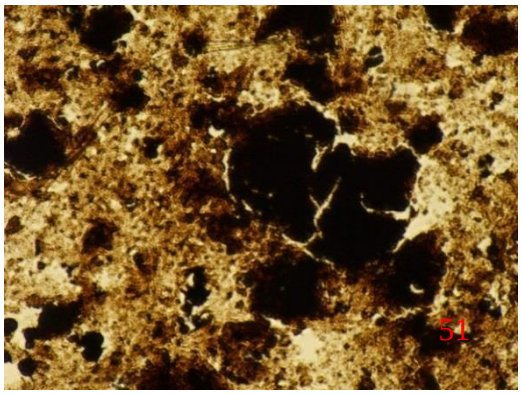
51


52

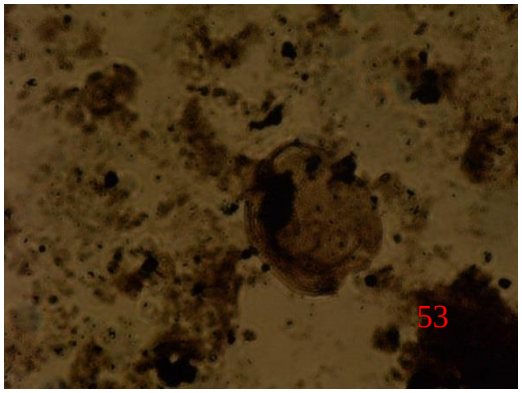
53

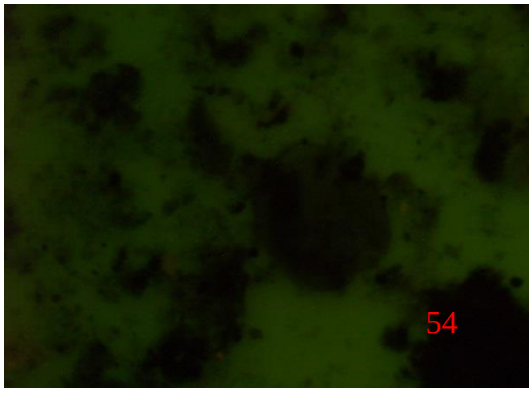
54

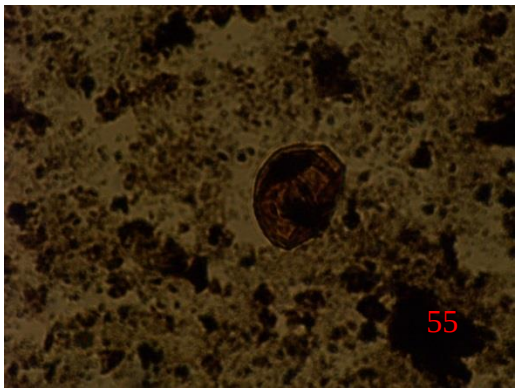
55

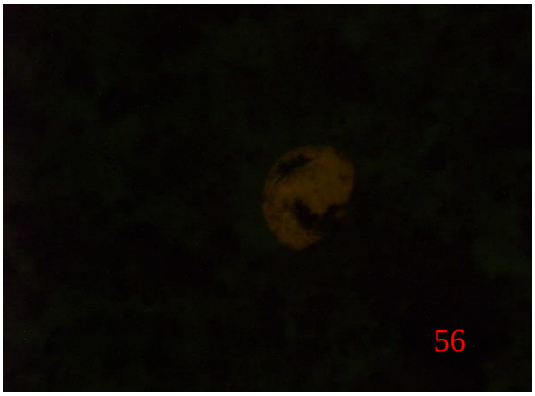
56

Figure 4.21: Including **Plate 4.8**, transmitted light and fluorescent blue light microphotographs of the amorphous organic matter, palynomorphs (spore and dinocyts), and phytoclasts. Microphotography from 57 to 64 for well FF14-6.

Plate 4.8

57-58) Amorphous in transmitted and blue light fluorescent (x25), Sirte Shale Formation. Depth 11510 feet, spore colour indices (SCI) ≈ 8.0.

59-60) Amorphous in transmitted and blue light fluorescent (x25), Sirte Shale Formation. Depth 11650 feet, spore colour indices (SCI) ≈ 7.5-8.0.

61-62) Phytoclasts (vitrinite macerals) in transmitted (x25), Sirte Shale Formation. Depth 12270 feet.

63-64) Amorphous and Phytoclasts (vitrinite macerals) in transmitted (x25), Sirte Shale Formation. Depth 12870 feet, spore colour indices (SCI) ≈ 8.5-9.0.

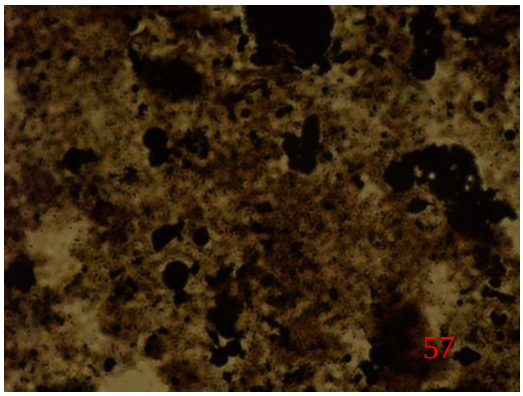
57

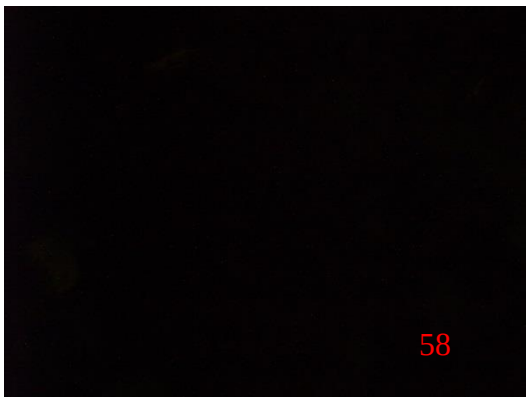
58

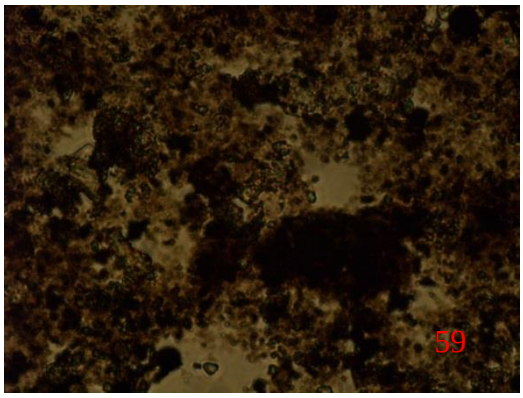
59


60

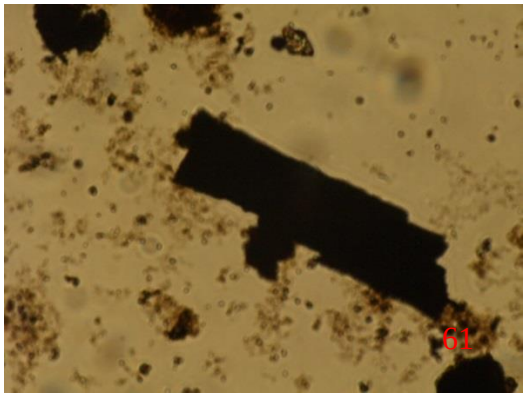
61

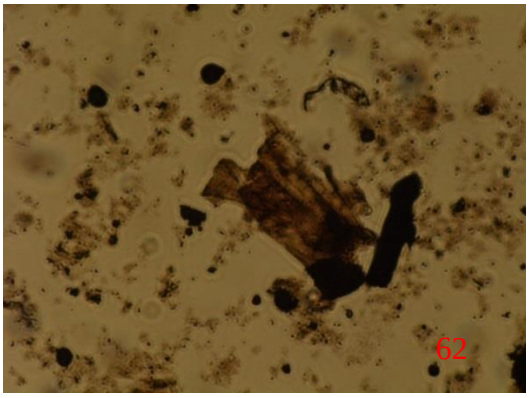
62

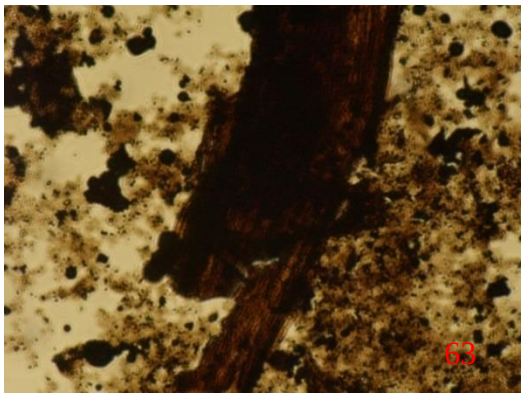
63

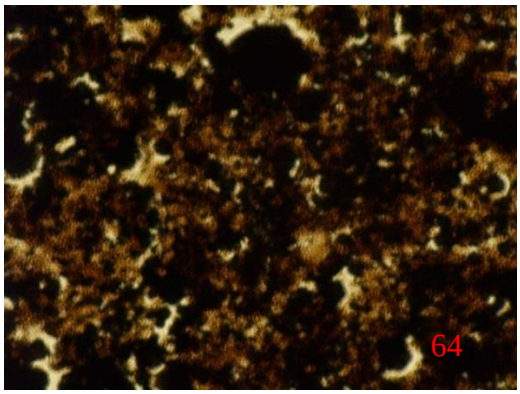
64

4.4.3 Vitrinite Reflectance

The vitrinite reflectance data was measured on 75 samples from eight wells as given in Table 4.2 in Appendix I and plotted against depth in Figure 4.22, which show mean reflectance values, standard deviations and histogram data for the upper Cretaceous section of the Kalash, Sirte Shale, and Rachmat Formations as given in figures in Appendix I. For all parts of the study area vitrinite reflectance measurements throughout the Upper Cretaceous section ranges from 0.51 to 1.50 *%Ro*. Figure 4.22 shows the variations in spore colour indices and vitrinite reflectance measurements with depth for the Sirte Shale and Rachmat of the Upper Cretaceous source rock samples in the Sirt Basin.

For well 6A1-59 located in an integrated fault system between the Kotla Graben and Zellah Troughs, the mean vitrinite reflectance values for both Kalash and Sirte Shale formations are between 0.51 %*Ro* and 0.55 %*Ro*, indicating the early mature zone. Meanwhile, for wells B1-NC74F and B2-NC74A in the Zellah Trough; L1-16 in the Nuflian High; L1-17 in the Dor Al Abid Trough; and Z1-11 in the Tagrifet Trough, the mean random reflectance values for both Sirte Shale and Rachmat formations are in the range 0.50 %*Ro* to 0.70 %*Ro*, indicating the early to middle mature zone. These results are in agreement with other maturity parameters such as T*max*, PI, and SCI. While in the wells C2-16 in the Marada Trough and FF14-6 in the Wadayat Trough toward the northeast centre of the Sirt Basin, the measured vitrinite reflectance values for the Sirte Shale Formation range from 0.74 %*Ro* to 1.50 %*Ro*, suggesting that the Sirte Shale Formation is within the middle to late mature stage in terms of hydrocarbon generation. These results are also in agreement with other maturity parameters such as T*max* and SCI (See Figures 4.22 and 4.23, Tables 4.1 and 4.2 in Appendix I). However, some results show slight disagreement with those for other maturity parameters, which may be due to caved or reworked organic matter from younger or old rocks, or the measurement of semifusinite instead of vitrinite. Figures 4.24 and 4.25 shows Plates of a reflected light photograph of vitrinite macerals in the studied wells.

It is clear that the maturity of the Upper Cretaceous succession in the Marada Trough and in the Wadayat Trough at the centre of the Sirt Basin is higher than in the Dor Al

Abid Trough, Zellah Trough, the Nuflian High, and the Tagrifet Trough at the western part of the basin.

This trend of maturity agrees well with the Rock-Eval maturity data of T*max* pyrolysis temperature, production index and SCI. This may be related to present day overburdening, to tectonic activity during the Late Cretaceous, and to higher geothermal gradients in the Wadayat Trough and Marada Trough (e.g. Gumati and Schamel, 1988).

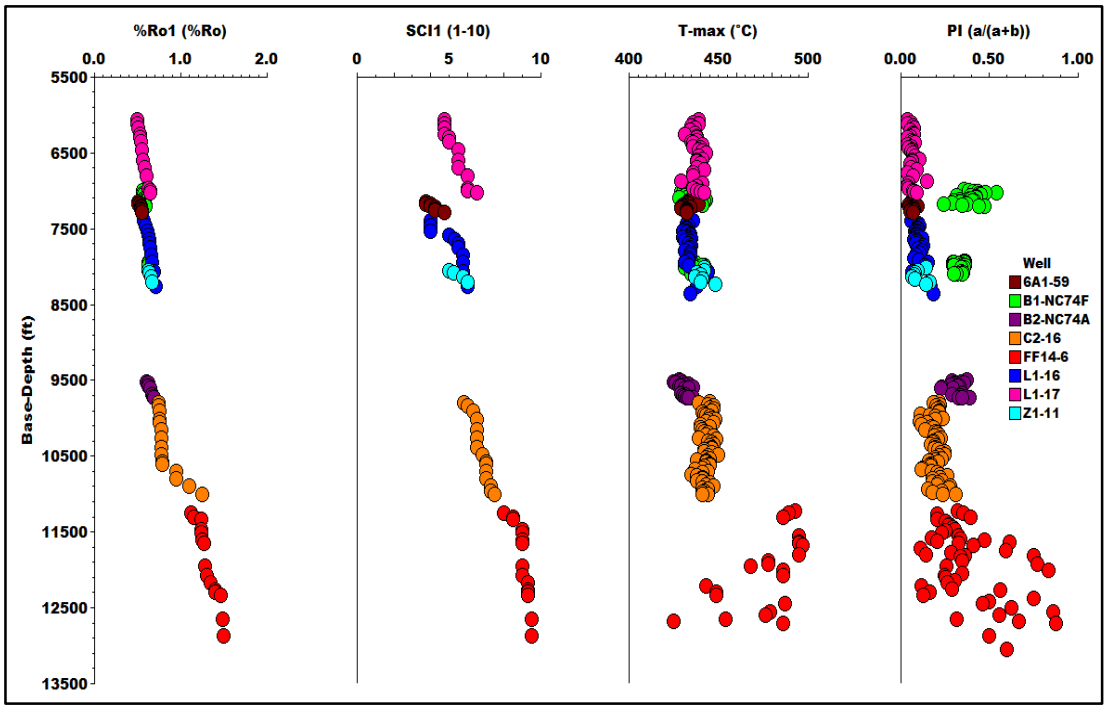

Figure 4.22: Geochemical maturity logs for the Upper Cretaceous source rocks in the Sirt Basin.

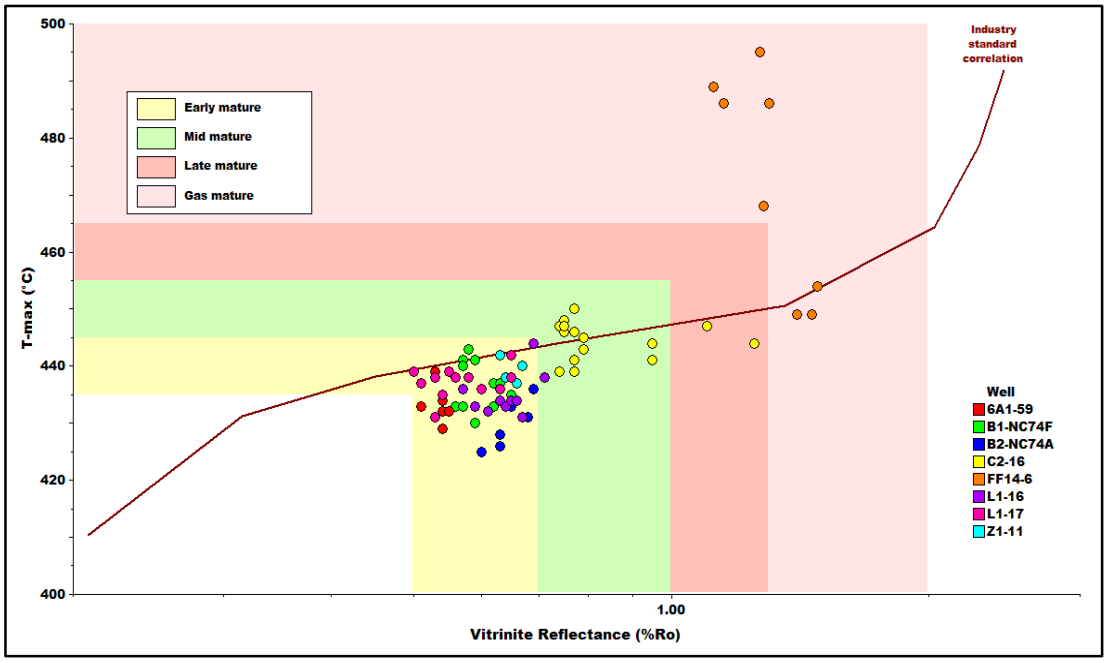

Figure 4.23: Cross plot of the T*max* °C versus vitrinite reflectance measurements (%Ro) for the Upper Cretaceous source rock in the Sirt Basin.

The low maturity in the Zellah Trough may have resulted from uplift and erosion during rifting in the Miocene to Eocene. The missing stratigraphic section of the Zellah Trough was estimated to be from 3000 to 4000 feet, and that will have affected the present day geothermal gradient (e.g. Gumati and Schamel, 1988; Ben Ashour, 2000). Therefore, the Upper Cretaceous source rocks from the Zellah Trough and Dor Al Abid Trough in the western part of the Sirt Basin are in the early to middle mature stages, whereas further northeast at wells C2-16 in the Marada Trough and FF14-6 in the Wadayat Trough, they are in the main oil window or are over-mature.

Figure 4.24: Including **Plate 4.9 and 4.10,** incident light photomicrographs of vitrinite macerals, x50 oil immersion objective.

1) Vitrinite (0.54 *%Ro*), Kalash Formation, depth 7210 feet, well 6A1-59.
2) Vitrinite (0.54 *%Ro*), Kalash Formation, depth 7210 feet, well 6A1-59.
3) Vitrinite (0.54 *%Ro*), Kalash Formation, depth 7210 feet, well 6A1-59.
4) Vitrinite (0.62 *%Ro*), Sirte Shale Formation, depth 7930 feet, well B1-NC74F.
5) Vitrinite (0.65 *%Ro*), Sirte Shale Formation, depth 8060 feet, well B1-NC74F.
6) Vitrinite (0.67 *%Ro*), Sirte Shale Formation, depth 9690 feet, well B2-NC74A.
7) Vitrinite (0.64 *%Ro*), Sirte Shale Formation, depth 7640 feet, well L1-16.
8) Vitrinite (0.70 *%Ro*), Sirte Shale Formation, depth 8260 feet, well L1-16.
9) Vitrinite (0.65 *%Ro*), Sirte Shale Formation, depth 8260 feet, well L1-17.
10) Vitrinite (1.10 *%Ro*), Sirte Shale Formation, depth 11950 feet, well FF14-6.
11) Vitrinite (1.15 *%Ro*), Sirte Shale Formation, depth 12070 feet, well FF14-6.
12) Vitrinite (1.15 *%Ro*), Sirte Shale Formation, depth 12070 feet, well FF14-6.
13) Vitrinite (1.20 *%Ro*), Sirte Shale Formation, depth 12270 feet, well FF14-6.
14) Vitrinite (1.25 *%Ro*), Sirte Shale Formation, depth 12270 feet, well FF14-6.
15) Vitrinite (1.5 *%Ro*) and semifusinite macerals, Sirte Shale Formation, depth 12870 feet, well FF14-6.
16) Vitrinite (1.5 *%Ro*), Sirte Shale Formation, depth 12870 feet, well FF14-6.

Figure 4.24: Plate 9

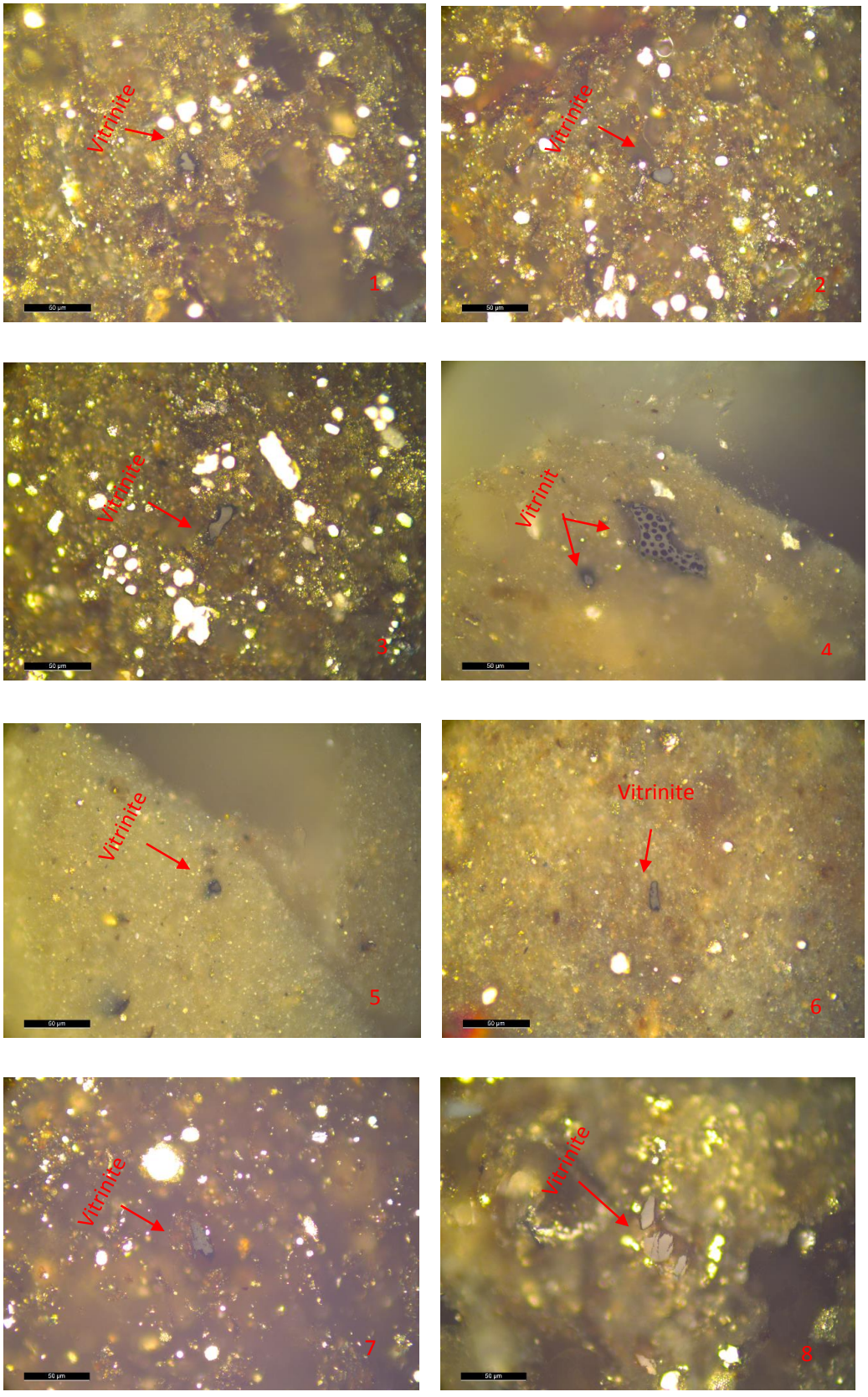

Figure 4.24: Plate 10

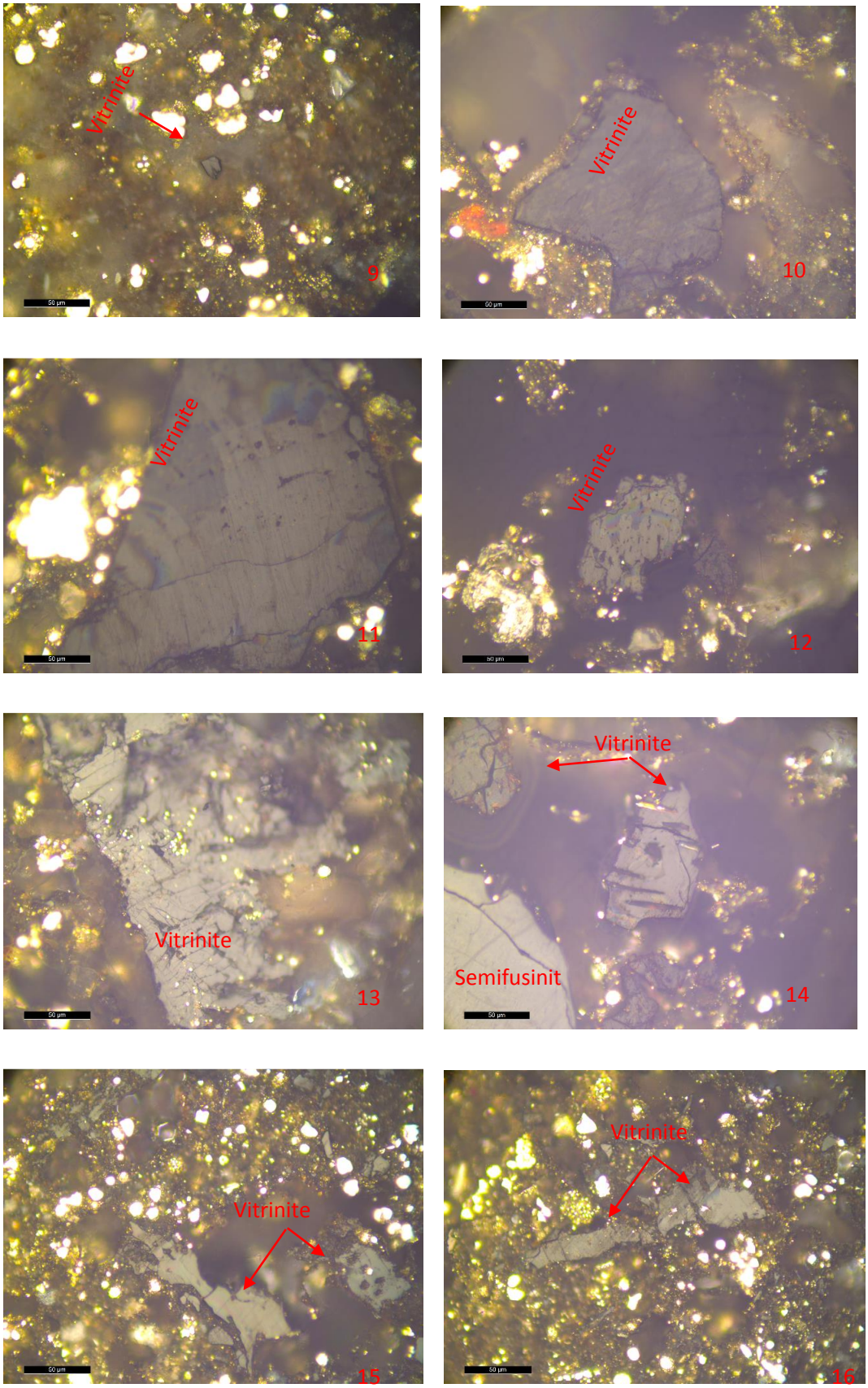

4.5 Kerogen Composition

Optical studies provides information concerning the characteristics of organic matter, and the relative abundance of different kerogen constituents within the Upper Cretaceous sequence (see Table 4.2 in Appendix I and Figures 4.6 to 4.13). In well 6A1-59, the dominant kerogen in the Kalash Formation is yellow to yellow-orange disseminated, to slightly more dense structureless amorphous organic matter, with small amounts of dinocyts and phytoclasts (vitrinite and inertinite). Meanwhile, the Sirt Shale has yellow-orange to orange structureless amorphous organic matter, with few algal and dinocyts, and woody material. The fluorescence scale (FS) reported by Tyson (1995) shows that the Kalash and Sirte Shale formations have yellow to yellow-orange amorphous and yellow dinocyts fluorescence, suggesting suboxic to anoxic facies, as they have better preservation of amorphous material. Figure 4.17 shows the average hydrogen indices for each point on Tyson's fluorescence scale. The plot shows hydrogen indices increasing with amorphous fluorescence from 3 to 5 FS. For wells L1-16 and L1-17, the dominant kerogen in the Sirte Shale is yellow-orange to orange, and orange to brown disseminated to slightly dense to more highly dense structureless amorphous material with yellow to yelloworange dinocyts and phytoclasts. The fluorescence scale shows that the Sirte Shale Formation has yellow-orange to dull orange and brown fluorescence, and dinocyts have yellow-orange to slight orange fluorescence, indicating suboxic to anoxic facies.

The Sirte Shale Formation samples show better preservation of amorphous organic matter compared with other stratigraphic unit in the well-studied, but the hydrogen indices remain less than 300 mg HC/g TOC, perhaps reflecting maturity effects. Common pyrite framboid are observed in most kerogen slides of the Sirte Shale Formation, indicating sulphate-reducing anaerobic depositional conditions. In the well Z1-11, the dominant kerogen in the Sirte Shale is yelloworange to orange to brown dense structureless amorphous organic matter with minor yellow to yelloworange dinocyts and woody material, mainly vitrinite. The fluorescence scale shows that the Sirte Shale Formation has orange to dull orange and brown fluorescence, and the dinocyts have yelloworange to slight orange fluorescence, indicating suboxic to anoxic facies.

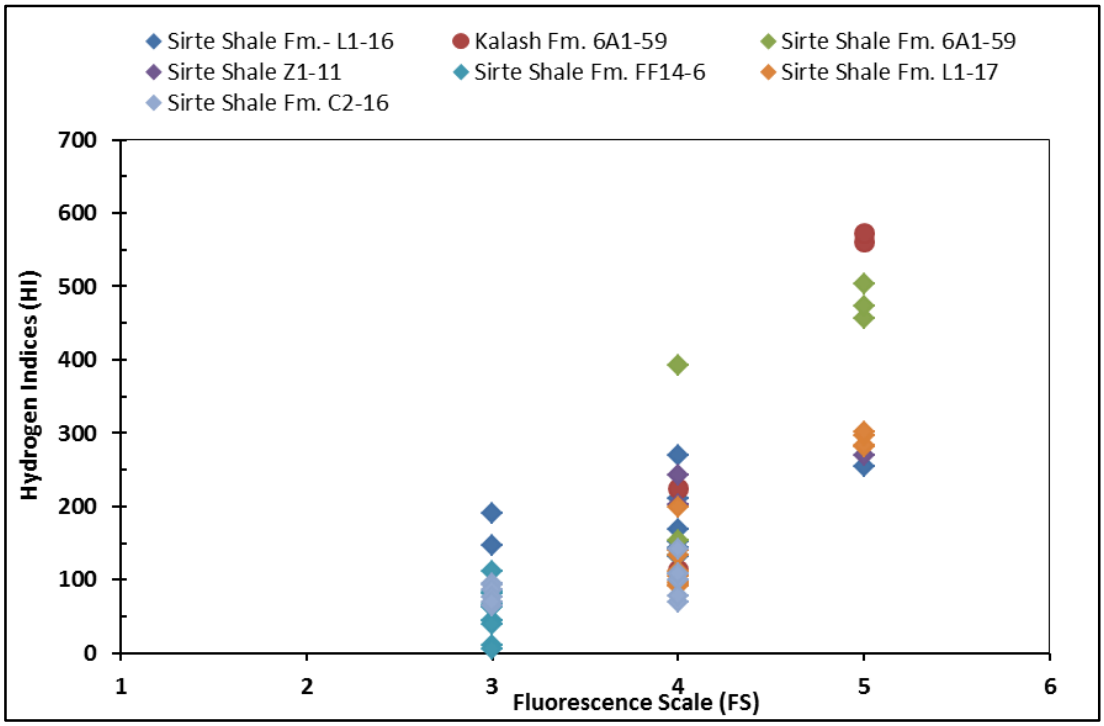

Figure 4.25: Cross plot of the hydrogen indices and fluorescence scale for the Upper Cretaceous succession in the Sirt Basin.

For wells C2-16 and FF14-6, the dominant kerogen in the Sirte Shale is orange, dark orange to brown and black disseminated to dense structureless amorphous organic matter with minor amounts of dinocyts and woody materials (vitrinite and inertinite). The fluorescence scale shows that the samples generally have dull orange to brown fluorescence and some samples at the deepest intervals exhibit no fluorescence, and the dinocyts have orange to dull orange fluorescence, indicating suboxic to anoxic facies. The common framboid pyrite is again observed.

4.5.1 Organic Facies Map for the Sirte Shale Formation

A regional map of the distribution kerogen types in the present day Sirte Shale (Figure 4.26) shows non-source facies (Type IV kerogen) prevalent in areas close to the horsts. This kerogen facies is inferred to have been deposited in oxic conditions, which existed in the shelf flanks and in the northern part of the basin. This phenomenon is also characteristic of areas of the western part of the Zellah Trough. The oxic conditions may have resulted from the replenishment of oxygen in open marine environments. The map clearly shows that facies seems to grade from gas-prone (Type III kerogen)

to oil-prone (Type II kerogen) towards the central parts of the graben regions, while the Type I kerogen facies that is strongly oil-prone has not been found in the Sirte Shale Formation within the Sirt Basin. Therefore, the possible prevalence of suboxic followed by anoxic conditions that obtained may be because of increasing water depth. The Sirte Shale Formation in the Sirt Basin is considerably more organically rich than the Campanian-Maastrichtian sediments in Algeria and Tunisia, but less organic-rich relative to the Brown Limestone, Duwi and Dakhla Formations in the Red Sea region, in the southern Western Desert, and in the Gulf of Suez, Egypt (Luning, 2003) .

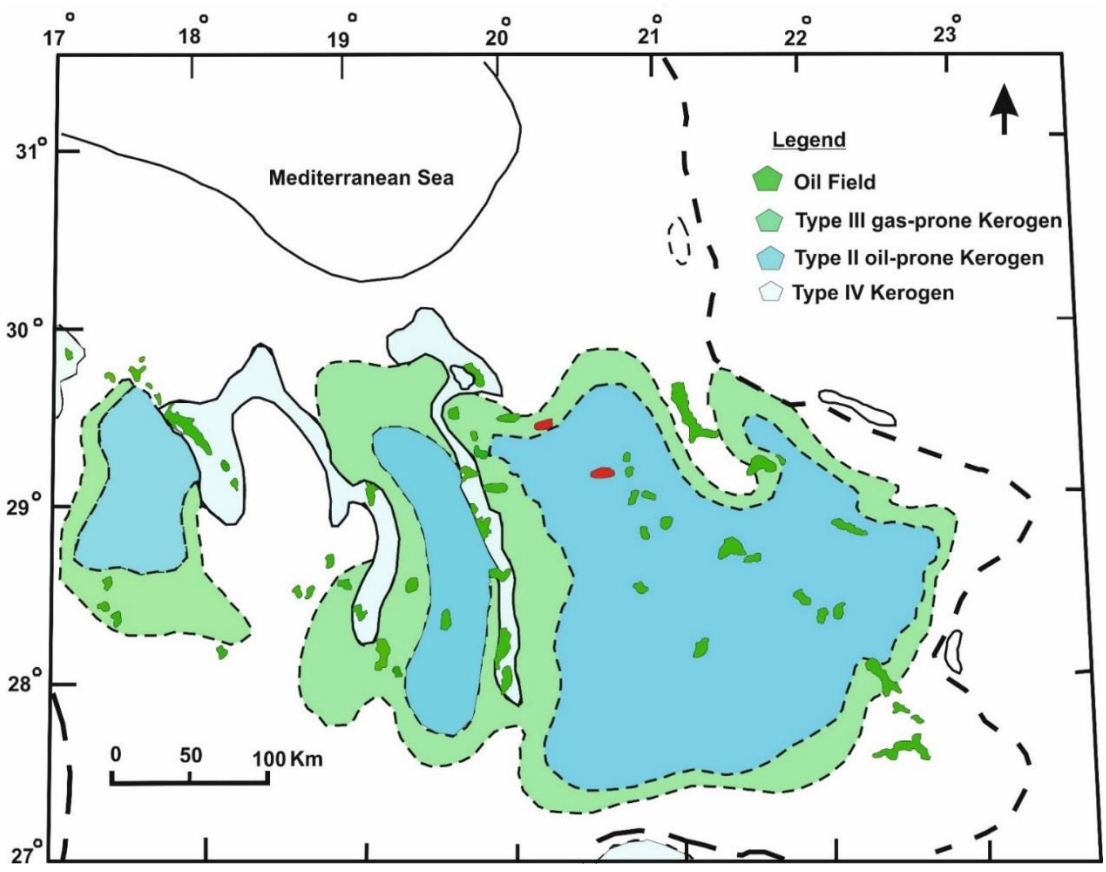

Figure 4.26: Distribution of the organic facies (Kerogen), Sirte Shale Formation, Sirt Basin, modified after El-Alami *et al.* (1989).

4.6 Molecular Characteristics of Source Rocks

This section describes the organic molecular geochemistry of the set of Upper Cretaceous source rock samples collected from eight wells in the Sirt Basin. The source facies and the level of thermal maturity of the source rock samples are evaluated in terms of the distribution of saturated and aromatic hydrocarbon compounds. A total of 34 cutting rock samples from the Upper Cretaceous source rocks were extracted, fractionated and separated into the main components which were saturated and aromatic hydrocarbons, resins and asphaltene compounds. The saturated, aromatic, resin and asphaltene (SARA) data for most of the sample solvent extracts showed that they were predominantly saturated in nature, with varying amounts of aromatic hydrocarbons and moderate to high amounts of resins and asphaltenes. The results are listed in Table 4.3 in Appendix I.

4.6.1 *n*-Alkanes and Isoprenoid Alkanes

Overall the hydrocarbon chromatograms profile was dominated by alkanes in the *n*-C_{12} to *n*-C_{35} range for most source rock samples, as shown in Figure 4.27. The characteristics and distribution of normal alkanes in crude oils and source rocks can be used to indicate the organic matter source input, maturity, depositional environments and level of biodegradation (Peters and Moldowan, 1993; Hunt, 1995; Peters, 2005b). The distributions of most analysed samples contain *n*-alkanes in the C_{10} to C_{35} range, typically maximising at *n*-C_{17}, *n*-C_{18} or *n*-C_{19} as shown in Figure 4.27, which suggests marine organic matter with some contribution to the biomass from algae and plankton. The gas chromatograms of most of the samples are dominated by saturated rather than aromatic hydrocarbons, but in some samples the gas chromatograms show slightly high aromatic hydrocarbons (see Table 4.3 in Appendix I), which represent more than 15% of the wells 6A1-59 and L1-17 in the Zellah Trough.

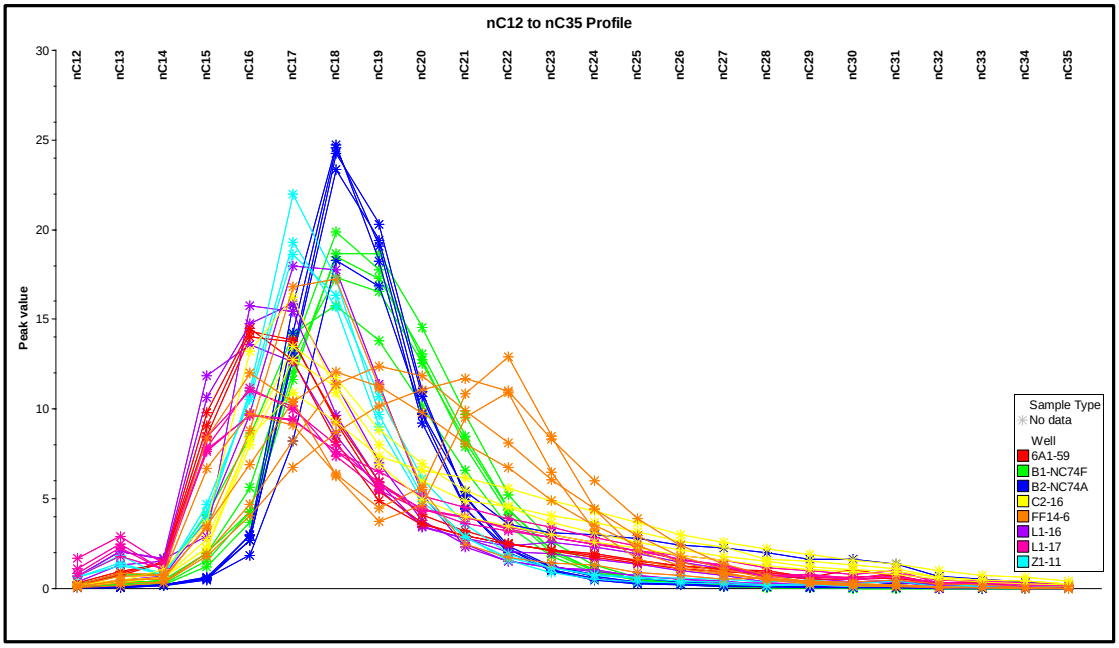

Figure 4.27: *n*-alkane distribution patterns for samples from eight wells in the Sirt Basin.

Meanwhile, the samples from well FF14-6 at the 12290 and 12330 feet interval appear to be bimodal. The first mode is predominantly in the *n*-C_{14} to *n*-$C_{19\ range}$, and the second in the *n*-C_{20} to *n*-C_{24} range. This second mode in these samples suggests that there was more than one type of organic matter input. The predominance of *n*-C_{17} over *n*-C_{25} in all source rock sample extracts analysed may reflect a high input of marine derived organic matter, but this may also be due to the influence of maturation(Peters and Moldowan, 1993; Peters, 2005b). Zhang *et al.* (2000) reported that the absence of the second mode in the oils is because the organic matter that could generate it was not present, or that the second mode may have been removed due to the high thermal maturity of the oils. Low molecular weight hydrocarbons less than *n*-C_{12} were not observed, perhaps because of evaporative loss during sample processing. Most of the Sirte Shale and Rachmat Upper Cretaceous source rock extract samples were found to contain extremely low amounts of pristane and phytane compared to *n*-alkanes. Nevertheless, for the study wells 6A1-59, C2-16, FF14-6, L1-16, L1-17 and Z1-11, the Pr/Ph ratios were greater than 1.0, ranging between 1.05 and 2.06 (2.39). This may be due to variations in the depositional environments of organic matter (Peters and Moldowan, 1993). The variation in Pr/Ph ratios ranging from 0.69 to 2.39 may suggest that the source rock samples were deposited under mixed dysoxic to anoxic conditions,

as shown in Figure 4.28. For the well FF14-6 at the interval below 12290 feet and well 6A1-59 at the interval between 7150 to 7170 feet, the Pr/Ph ratios ranged between 2.06 and 2.39, and 1.85 to 2.02 respectively, suggesting that the high Pr/Ph ratios may be due to the influence of maturity on Pr/Ph or the presence of strongly clay rich source rock.

On the other hand, for wells B1-NC74F and B2-NC74A, the Pr/Ph values range from 0.69 to 0.95, suggesting anoxic conditions and there are minor changes occurred in the Sirte Shale and Rachmat formations organic facies.

Using the *n*-alkane terrestrial aquatic ratio ($C_{27}+C_{29}+C_{31}/C_{15}+C_{17}+C_{19}$) (TAR), Silliman *et al.* (2002) observed that *n*-alkanes with a ratio below 1.0 are from marine source inputs, while those above 1.0 are from land plant source input. Philp (1985) illustrated that the ratio C_{17}/C_{25} can be used to determine the origin of organic matter inputs, where ratios less than 1.0 indicate the terrestrial input, whereas those greater than 1.0 are marine inputs. However, a cross plot of both ratios showed that the source rock sample extracts appeared in the region of marine origin, but in different depositional conditions as shown in Figure 4.29.

The carbon preference index (CPI) of the cutting sample extracts range between 0.92 to 1.17, however, generally these values do not show any predominance of odd or even carbon atoms, suggesting that most of the samples are early mature to mature, as shown in the Table 4.4 in Appendix I.

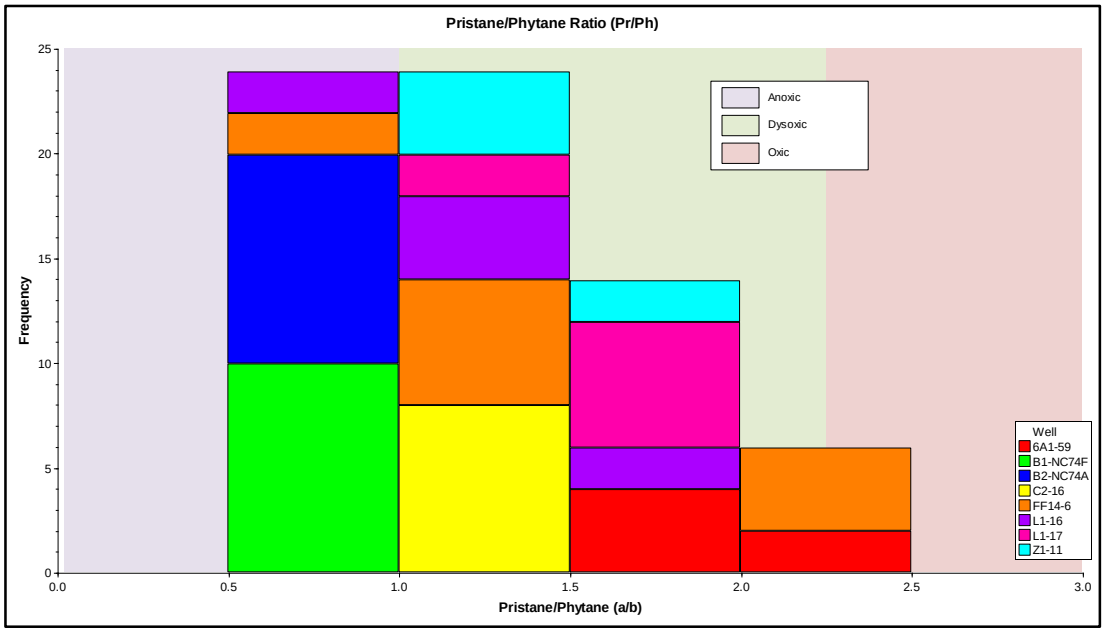

Figure 4.28: Pristane/Phytane ratios in the rock extract samples measured (interpretation fields from pIGI software).

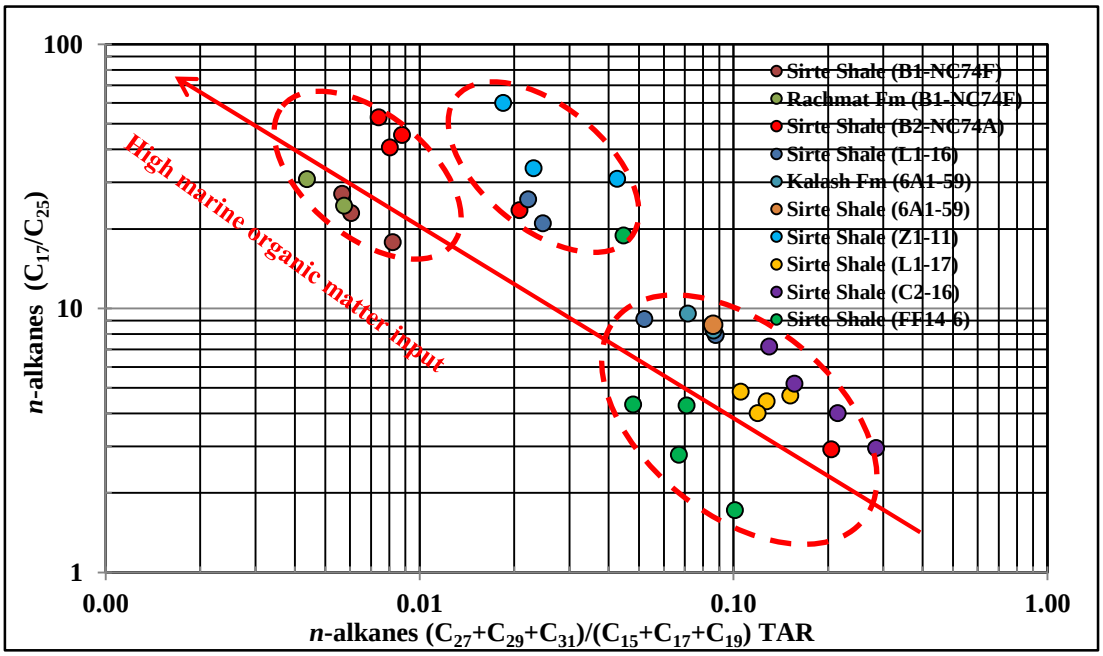

Figure 4.29: Cross plot of C_{17}/C_{25} versus $(C_{27}+C_{29}+C_{31})/(C_{15}+C_{17}+C_{19})$ n-alkanes for the rock extract samples measured.

The extract samples analysed showed Pr/*n*-C_{17} ratios in the range 0.30 to 0.88, and Ph/*n*-C_{18} ratios in the range 0.23 to 1.18, as shown in the Table 4.4 in Appendix I. According to Didyk *et al.* (1978), this indicates that the organic matter had a marine origin. Figure 4.30 shows a crossplot of Pr/*n*-C_{17} versus Ph/*n*-C_{18} for the source rock extracts from the Kalash, Sirte Shale, and Rachmat formations and the full data can be

found in Table 4.4 in Appendix I. The diagram suggests that these source rock samples originated from Type II mixed marine and terrestrial to marine organic matter deposited in reducing environments.

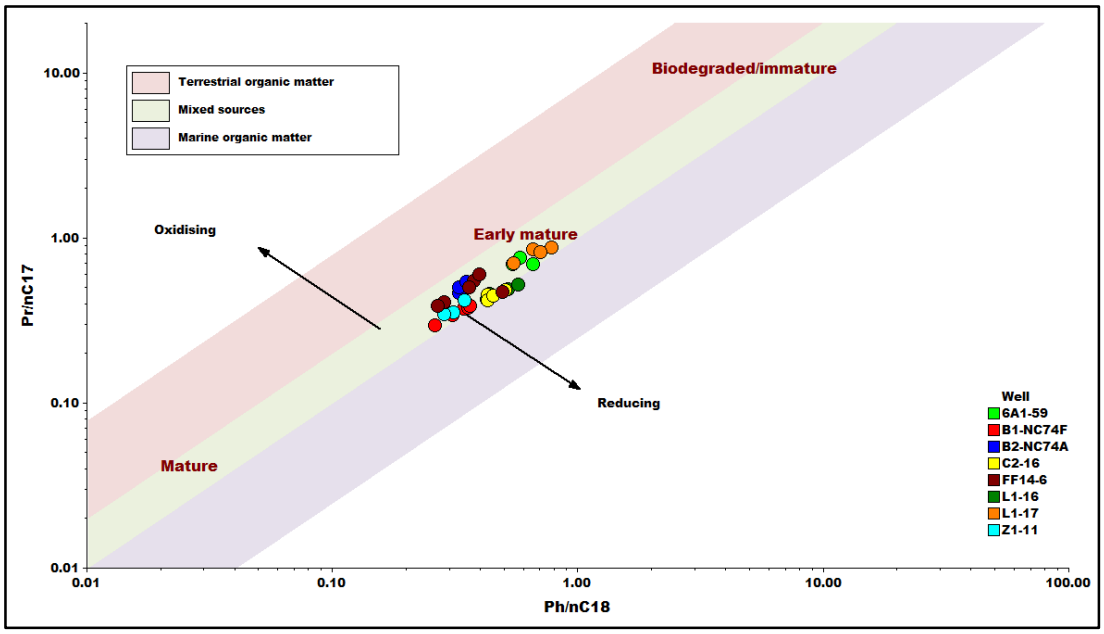

Figure 4.30: Cross plot of Phytane Ph/n-C18 versus Pristane Pr/n-C17 for rock sample (interpretation fields from pIGI software).

4.6.2 Sterane and Triterpanes

4.6.2.1 Source Facies Characterisation

The sterane and terpane distributions of the extracted shale samples from the Kalash, Sirte Shale and Rachmat Formations are shown in Figure 4.31, 4.34, 4.35 and 4.36. Biomarker data obtained from m/z 217 mass chromatograms are given in Table 4.5 in Appendix I with peak identification in Table 4.1. Biomarker geochemical ratios based on the steranes and triterpanes applied in this study are shown in Table 4.6 and 4.7 in Appendix I. According to the distributions of steranes and triterpanes, the Upper Cretaceous source rock samples analysed appear heterogeneous in composition.

The distribution of C_{27}, C_{28}, and C_{29} steranes and C_{27}, C_{28}, and C_{29} iso-steranes for the Upper Cretaceous source rocks analysed are shown in Figures 4.32 and 4.33. The plot for the Upper Cretaceous source rocks samples is in a close area of the ternary diagram showing a slightly higher relative abundance of C_{27} and C_{29} steranes and iso-steranes

compared to the C_{28} forms, indicating marine shale (Moldowan *et al.*, 1985), while in wells 6A1-59, L1-16, and L1-17 the abundance of C_{27} was similar to that of C_{28} sterane, which also indicate marine origins. In addition, some samples from well FF14-6 contained C_{27} steranes that were more abundant than C_{28} and C_{29} steranes, suggesting a high proportion of marine source input.

Moldowan *et al.* (1985) reported that the C_{28}/C_{29} αββ sterane ratio can be used as a reliable age-related parameter for marine settings since it increases from the Precambrian to Tertiary Ages as a result of an increase in C_{28} steranes and a decrease in C_{29} sterane content over geological time. This ratio ranges from 0.49 to 1.58 with an average of 0.95 in the samples analysed (See Table 4.5 in Appendix I), which might be an indication of Cretaceous source rocks.

The biomarker data (Table 4.5 in Appendix I, Figure 4.31) showed that most of the extracted source rock samples had moderate to high diasterane contents, suggesting clay-rich catalysis source rocks.

The biomarker data for terpanes (Table 4.6 in Appendix I, Figure 4.34) shows that C_{30} 17α(H), 21β(H) regular hopanes were the most abundant series members, followed by C_{29}αβ norhopane. The ratios of C_{29}/C_{30} hopane were between 0.35 and 0.97, whereas for well C2-16 the 18α(H) trisnorneohopane (Ts) was dominant over C_{30} αβ hopane and C_{29} αβ norhopane. However, in wells 6A1-59, B1-NC74F and L1-16, the 17α(H) trisnorhopane (Tm) was predominant over the 18α(H) trisnorneohopane (Ts), with Tm/Ts ratios ranging from 1.06 to 1.78. For wells B2-NC74A, C2-16, FF14-6, L1-17 and Z1-11, the Ts were more abundant than Tm, with Tm/Ts ratios between 0.40 and 1.0. The C_{30} βα(H) mortane and oleanane were present in varying abundance, but gammacerane was absent in all extracted source rock samples.

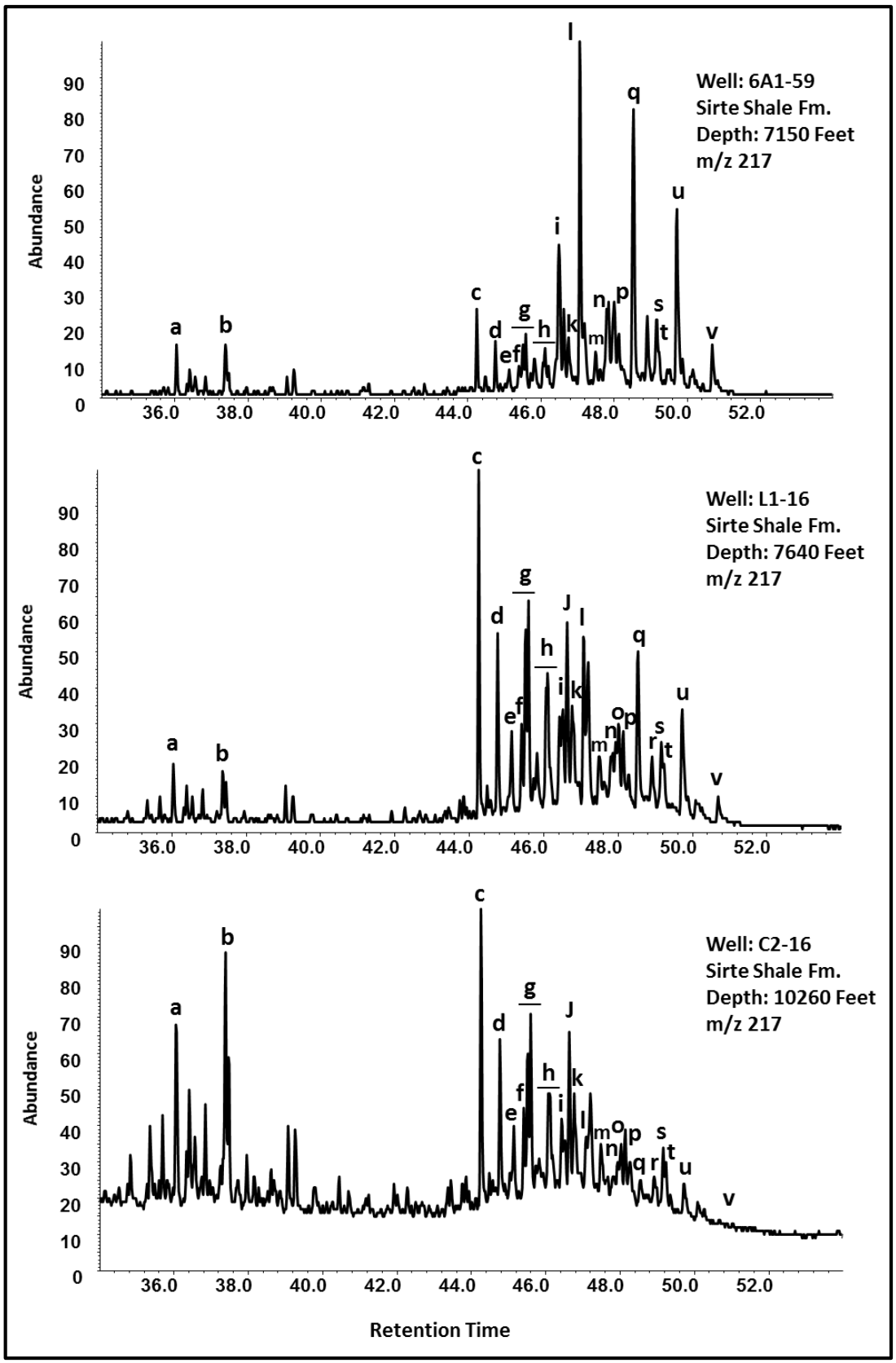

Figure 4.31: m/z 217 mass chromatograms showing the distribution of steranes in the Kalash and Sirte Shale formations.

Table 4-1: Identification of sterane peaks in the m/z 217 mass chromatograms.

Steranes (m/z 217) Compound Name	Peaks
C_{21}	a
C_{22}	b
$C_{27}\beta\alpha$ diasterane (20S)	c
$C_{27}\beta\alpha$ diasterane (20R)	d
$C_{27}\alpha\beta$ diasterane (20S)	e
$C_{27}\alpha\beta$ diasterane (20R)	f
$C_{28}\beta\alpha$ diasterane (20S) + (24S+R)	g
$C_{28}\beta\alpha$ diasterane (20R) + (24S+R)	h
$C_{27}\alpha\alpha\alpha$ sterane (20S) + C28ab diasterane (20S)	i
$C_{27}\alpha\beta\beta$ sterane (20R) + C29ba diasterane (20S)	j
C_{27} $\alpha\beta\beta$ sterane (20S) + (C28ab diasterane (20R)	k
$C_{27}\alpha\alpha\alpha$ sterane (20R)	l
$C_{29}\beta\alpha$ diasterane (20R)	m
$C_{30}\alpha\beta$ diasterane (20S)	n
$C_{28}\alpha\beta\beta$ sterane (20R) + C29 ab diasterane (20S)	o
C_{28} $\alpha\beta\beta$ sterane (20S)	p
$C_{28}\alpha\alpha\alpha$ sterane (20R)	q
$C_{29}\alpha\alpha\alpha$ sterane (20S)	r
$C_{29}\alpha\beta\beta$ sterane (20R)	s
$C_{29}\alpha\beta\beta$ sterane (20S)	t
$C_{29}\alpha\alpha\alpha$ sterane (20R)	u
$C_{30}\alpha\alpha\alpha$ sterane (20R)	v

The Upper Cretaceous source rock samples can be separated into two main groups with regard to sterane and triterpane distribution. The group I contain samples from wells 6A1-59, L1-16 and L1-17 and most of these samples have moderate to high organic carbon contents and petroleum yield (S1+S2). This group is characterised by the occurrence of a low abundance of hopanes relative to regular steranes and also by

regular sterane C_{27} to C_{29} ααα (S+R)+C_{27} to C_{29} αββ (S+R)/ C_{29}+C_{30} 17α(H)-hopane+C_{31} to C_{33} αβ homohopane (S+R)) ratios greater than 0.90 (Table 4.6 in Appendix I). This suggests higher input from eukaryotic versus prokaryotic organisms, which may be due to the better preservation of steroid compounds in a highly anoxic depositional environment (e.g. Moldowan *et al.*, 1985; Connan *et al.*, 1986). Also, there is relatively a low abundance of extended tricyclic terpanes from C_{29} to C_{30}, and no easily detectable occurrence of the extended C_{32} to C_{35} tricyclic terpanes (See Figure 4.34, Table 4.7 in Appendix I). The C_{24} tetracyclic/C_{26} tricyclic (S+R) ratio was in the range 0.38 to 1.80, showing moderate to the high abundance of the C_{24} tetracyclic terpanes compared to the C_{26} tricyclic terpanes, and with high C_{29} αβ relative to C_{29} Ts and C_{30} α(H) diahopane and also showing high C_{30} α(H) hopane relative to C_{30} α(H) diahopane as shown in Table 4.6 in Appendix I. In addition, high relative abundances of pentacyclic relative to tricyclic terpanes were found, as shown in Figure 4.34. The abundance of diasteranes relative to regular steranes in the Upper Cretaceous source rock samples has been evaluated for the C_{29} isomers using the ratio: C_{29} 13β(H),17α(H)-diasterane 20R/[C_{29} 13β(H),17α(H)-diasterane 20R+C_{29} 5α(H),14α(H),17α (H)-sterane 20R]. This ratio appears to be lower in the group I Sirte Shale source rock samples than in the group II Sirte Shale and Rachmat source rock samples.

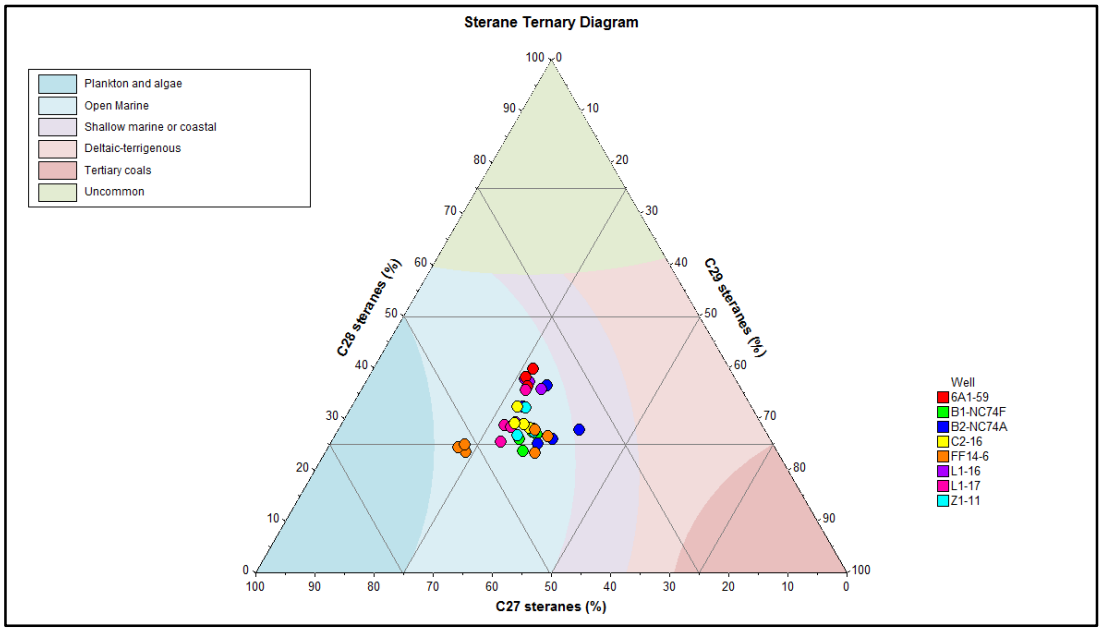

Figure 4.32: C_{27}, C_{28}, and C_{29} sterane ternary diagram showing the depositional environment of the shales from the Kalash, Sirte Shale and Rachmat formations in the Sirt Basin (interpretational fields from pIGI software).

Group II consists of the wells B1-NC74F, B2-NC74A, C2-16, FF14-6, and Z1-11. Most of these samples have variable low to moderate, to slightly high organic carbon content and petroleum potential, and are characterized by relatively high abundances of tricyclic terpanes relative to pentacyclic terpanes. This group is also characterised by the occurrence of low to moderate abundances of hopane relative to regular steranes, and has regular sterane C_{27} to C_{29} ααα (S+R)+C_{27} to C_{29} αββ (S+R)/ C_{29}+C_{30} 17α(H)-hopane+C_{31} to C_{33} αβ homohopane (S+R) ratios in the range of 0.30 to 2.59. This may suggest moderate to high input from eukaryotic compared to prokaryotic organisms, though it may also be due to moderate to better preservation of steroidal compounds in suboxic to anoxic depositional environment (Moldowan *et al.*, 1985; Connan *et al.*, 1986). There is a relatively low abundance of extended tricyclic terpanes from C_{29} to C_{30}, and no detectable extended C_{32} to C_{35} tricyclic terpanes. The C_{24} tetracyclic/C_{26} tricyclic ratios are in the range of 0.30 to 2.79, showing moderate to high abundances of the C_{24} tetracyclic terpanes compared with the C_{26} tricyclic terpanes, with high C_{29} αβ relative to C_{29} Ts and C_{30} α(H) diahopane. There are also high levels of C_{30} α(H) hopane relative to C_{30} α(H) diaphone, as shown in Table 4.6 in Appendix I. In addition, group II has a similar slightly higher relative abundance of Ts over Tm, moderate to high abundances of diasteranes relative to regular steranes. Within the steranes, C_{27} βα diasteranes (S+R) and C_{29} βα S are more abundant, as shown in Figure 4.35.

The C_{35}α/C_{34}α homohopane ratios showed that all of the extract samples had ratios below 0.80, suggesting that the organic matter was derived from a marine shale source. The C_{31} to C_{35} homohopanes showed a predominance of C_{31} over other homologous, and this may suggest a moderately to highly reducing marine clastic facies. For well B1-NC74F, the chromatogram (See Figure 4.36) showed a slightly elevated abundance of C_{34} homohopane and this may reflect different type of bacterial input in marine carbonate(Peters and Moldowan, 1993; Peters, 2005b).

For most of the wells studied, the C_{31} 22R homohopane/C_{30} α(H)-hopane ratios varied between 0.17 and 0.88, as shown in Table 4.6 in Appendix I. This may suggest a mixture of marine shale and carbonate source rocks. Most of the wells had very low homohopane indices ranging from 0.02 to 0.10. These values suggest suboxic to anoxic depositional environments for shale source material. In addition, the homohopane

distribution found affected by decrease and increase of thermal maturity (Peter and Moldowan, 1991). But also the homohopane distribution was observed that affected by decrease and increase of thermal maturity (Peters and Moldowan, 1991).

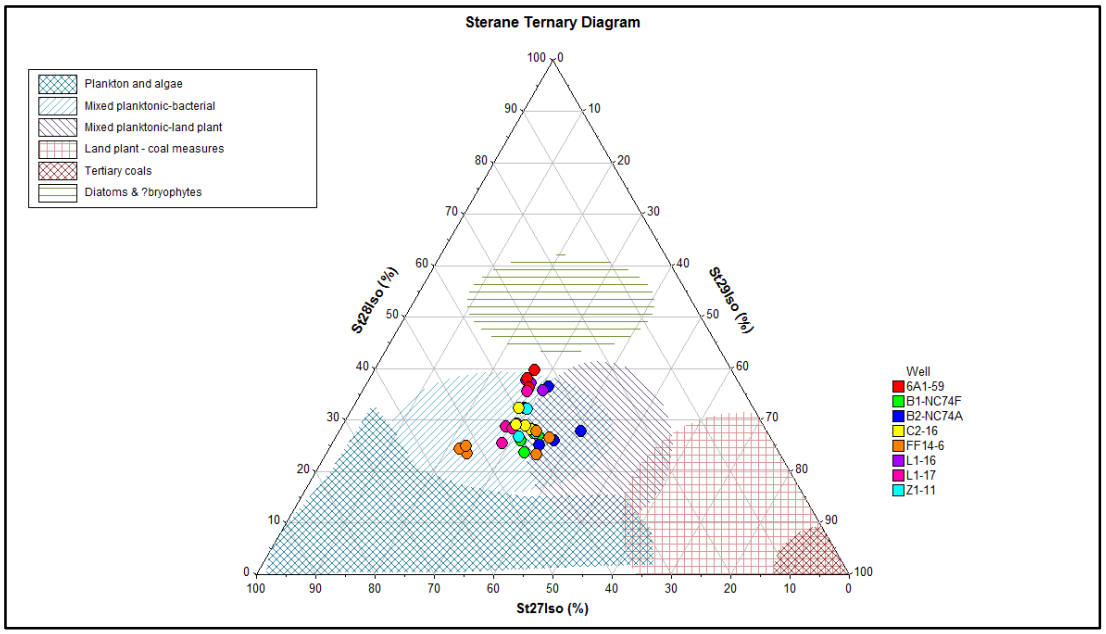

Figure 4.33: Ternary diagram of C_{27}, C_{28}, and C_{29} isosteranes showing sedimentary depositional environments of the Kalash, Sirte Shale and Rachmat formation samples (interpretational fields from pIGI software).

In most of the Upper Cretaceous source rock samples analysed the biomarker alkanes are dominated by steranes, ranging from 0.0026 to 1.256µg/g, with a mean value of 0.176µg/g extracts. The hopane concentrations in the same source rock samples were varied between 0.00468µg/g and 0.5456µg/g extracts with an average of 0.1361µg/g extracts. The tricyclic terpane concentrations of the same samples are ranging from 0.0070 to 0.2881µg/g extracts, with a mean value of 0.1113µg/g extracts. The source rock samples of the Sirte Shale Formation in well 6A1-59 at the 7150 feet interval exhibit the highest concentration of steranes, hopanes and tricyclic terpanes, whereas the lowest concentrations were recorded in well Z1-11 at 8200 feet intervals. Figures 4.38-4.40 compare the sterane, hopane, and tricyclic terpane concentrations for the main source rocks in the Sirt Basin. The triterpane distributions of the 6A1-59, B2-NC74A, L1-16, and L1-17 wells are typical of early to middle mature marine source rocks and the major compounds in the chromatograms are C_{30} and C_{29} 17α(H)-hopanes. Hopanes are in higher relative abundance compare to the tricyclic terpanes and this

feature differentiates the sediments in the 6A1-59, B2-NC74A, L1-16, and L1-17 wells from other study wells. The representative m/z 191 mass chromatograms for B1-NC74F, C2-16, FF14-6, and Z1-11 wells (Figure 4.35) show higher abundances of tricyclic terpanes relative to pentacyclic terpanes, with the C_{23} tricyclic terpane the most abundant compound. This feature of these wells differentiates them from first four wells. The high abundance of tricyclics in the study wells may be associated with some particular bacterial or algal source inputs, with markers that arise from different prokaryotic membranes or due to higher thermal maturity. However, the higher total sterane/hopane ratio of more than 0.6 for the 6A1-59, B1-NC74F, C2-16, FF14-6, L1-16, and L1-17 wells may reflect relatively high eukaryotic organism inputs, while the low ratio in the B2-NC74A and Z1-11 wells indicate more contribution from prokaryotic membranes lipids inputs.

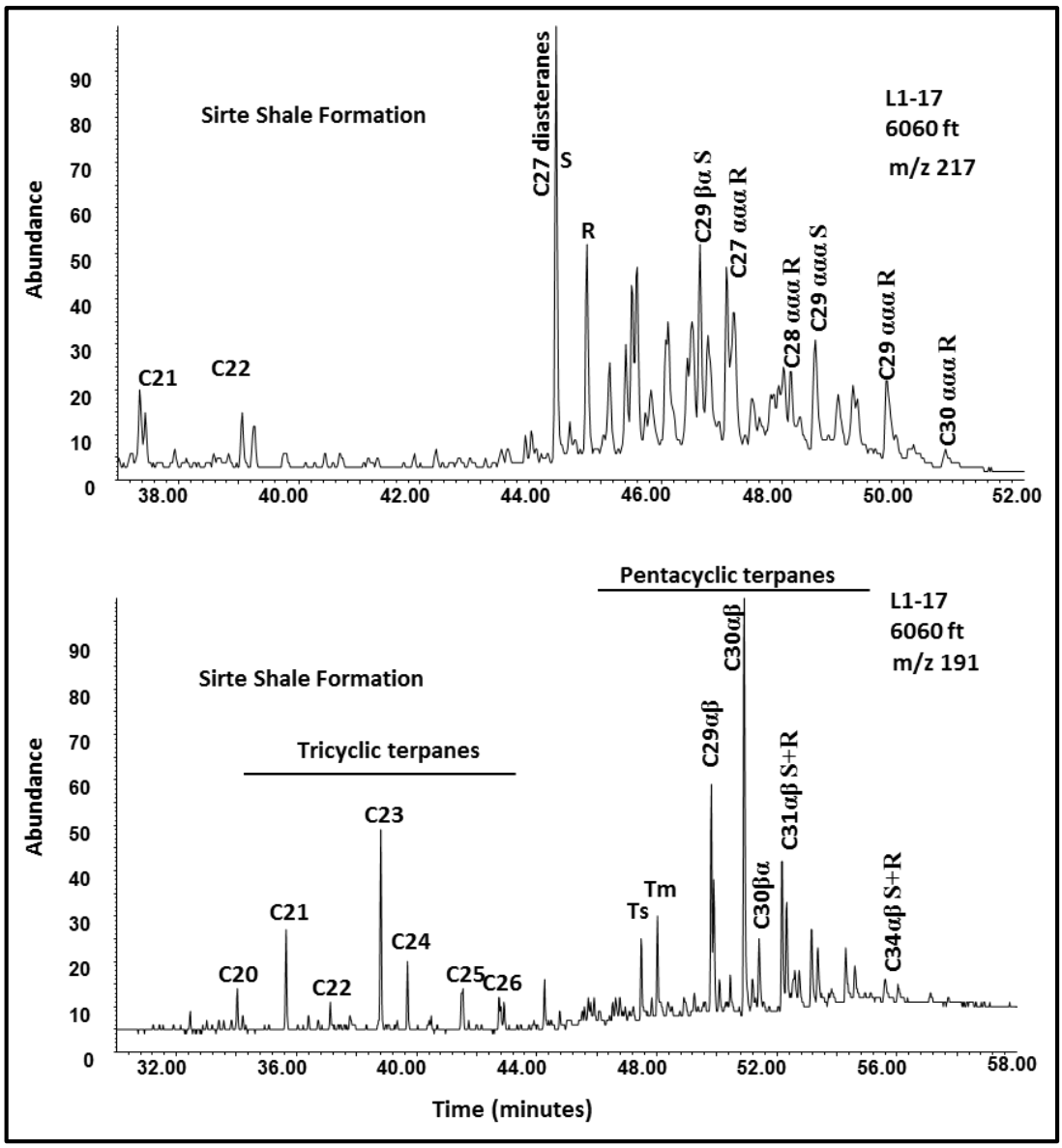

Figure 4.34: m/z 191and 217 mass chromatograms showing the distribution of triterpanes and steranes of the Sirte Shale Formation in the Dor Al Abid Trough.

The major tricyclic terpanes appear to be more abundant than the tetracyclic terpanes in rocks and crude oils (Aquino Neto *et al.*, 1983) in most of the wells in this study. The C_{23} tricyclic terpane was predominant, followed by C_{19}, C_{20}, and C_{24} homologous, suggesting a marine source depositional environments (Ekweozor and Strausz, 1981; Neto *et al.*, 1986; Peters and Moldowan, 1993; Peters, 2005b). The C_{22}/C_{21} tricyclic terpane ratios ranged from 0.22 to 0.41, and the C_{24}/C_{23} tricyclic ratios between 0.33 and 0.68, indicating marine shale to carbonate source rocks, as shown in Figure 4.37.

The low C_{24}tet/C_{23}tri ratio of less than 0.41 and the absence of the C_{25} to C_{27} tetracyclic terpanes, suggests that the organic matter was derived from a marine clastic source associated with low terrestrial organic matter input (Aquino Neto *et al.*, 1983; Peters and Moldowan, 1993; Peters, 2005b).

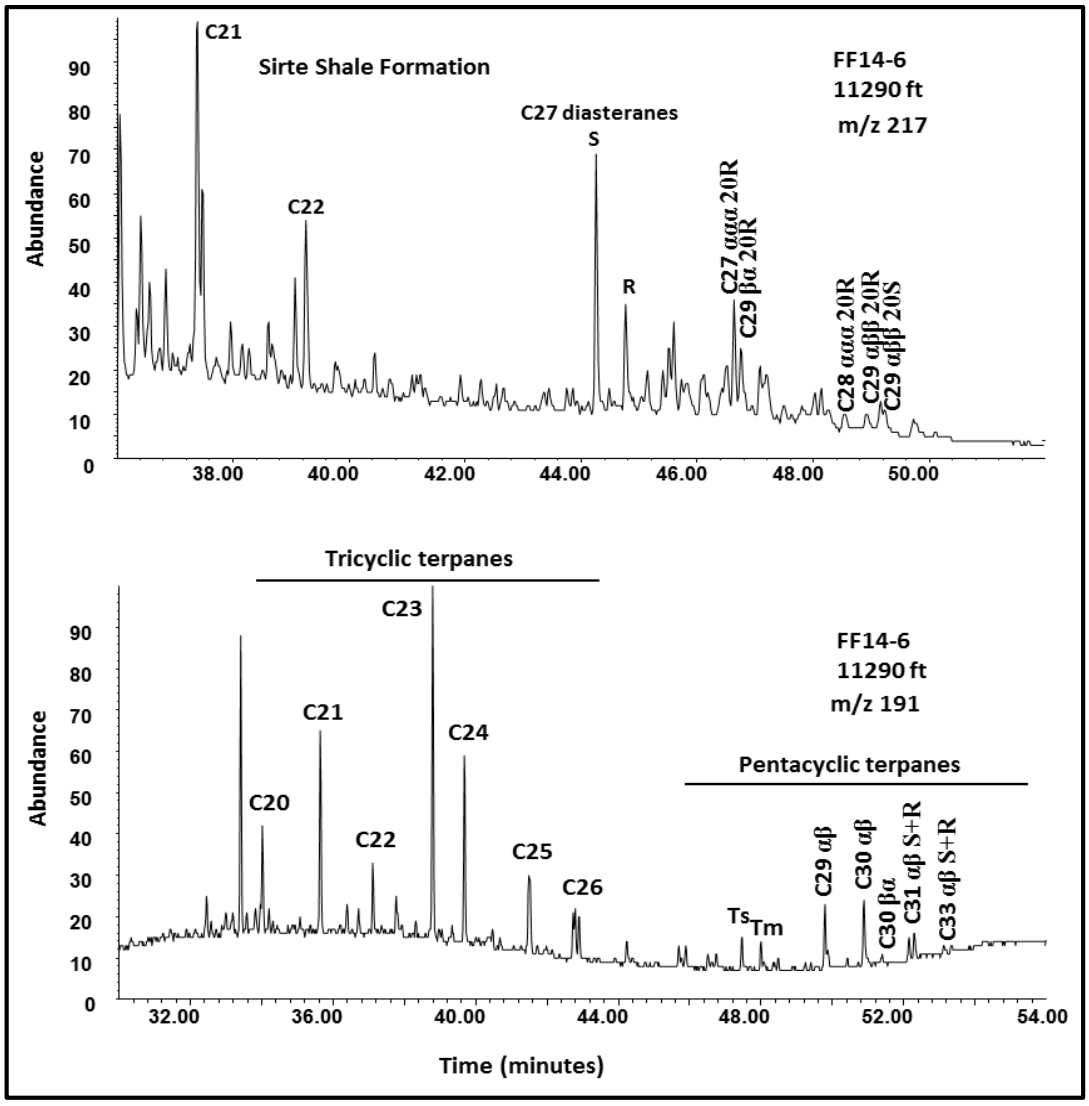

Figure 4.35: m/z 191 and 217 mass chromatograms showing the distribution of triterpanes and steranes of the Sirte Shale Formation samples from the Wadayat Trough in the central of the Sirt Basin.

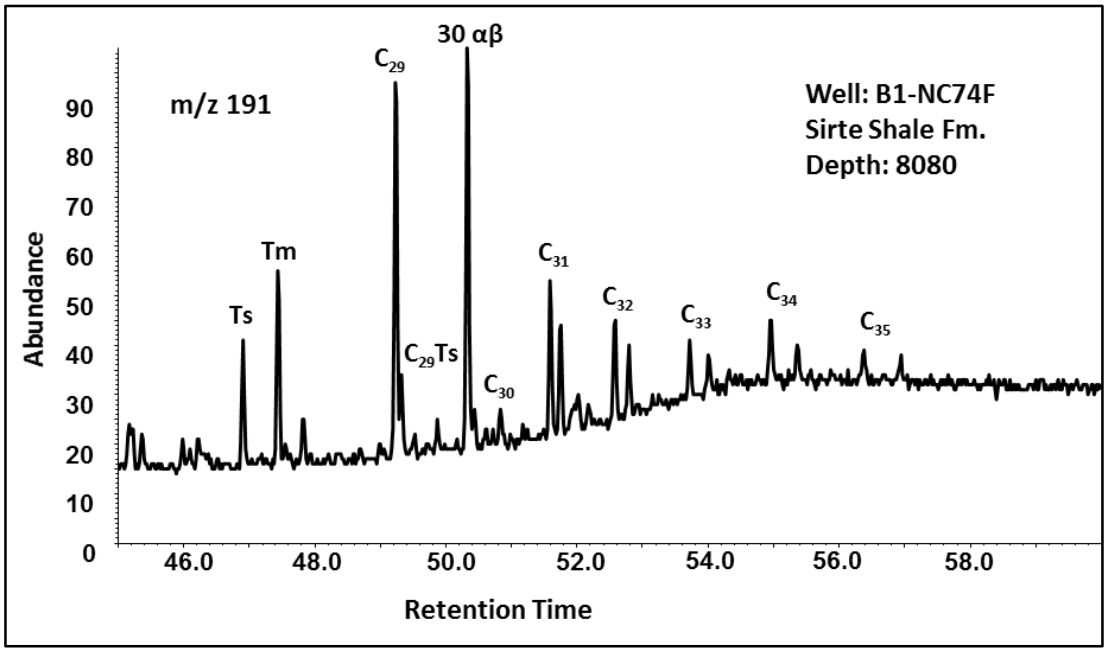

Figure 4.36: m/z 191 mass chromatogram showing slightly elevated abundance of the C_{34} homohopane of the Sirte Shale Formation in the Zellah Trough.

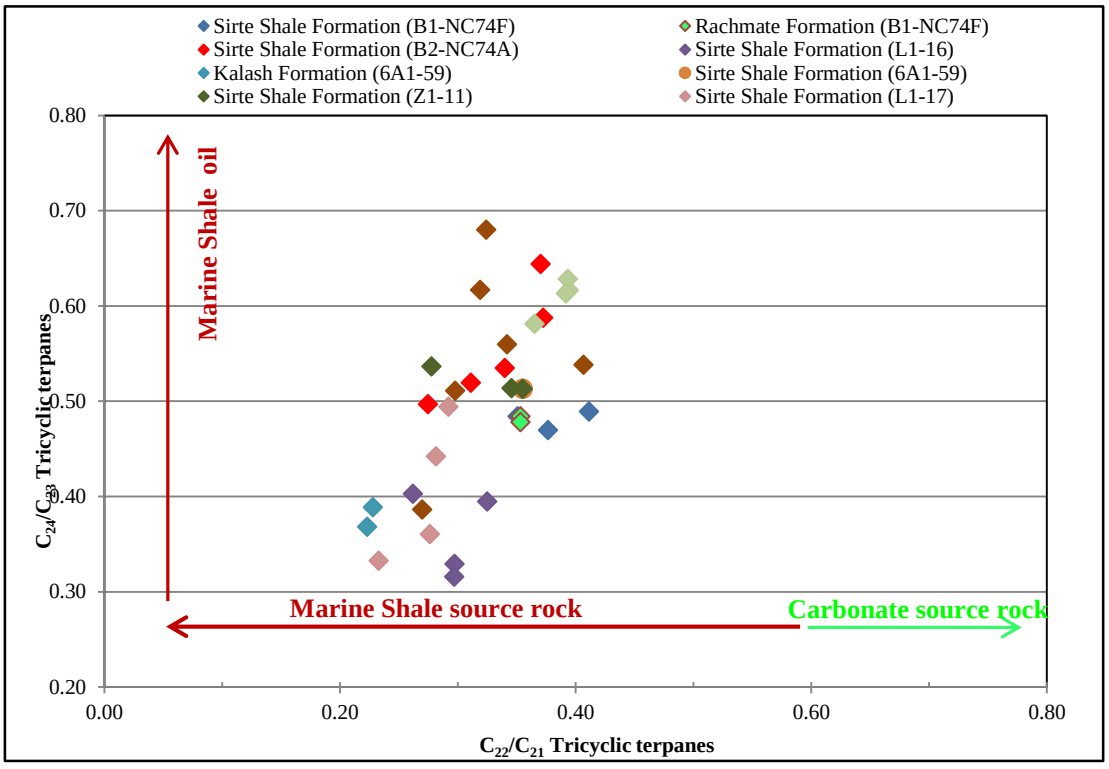

Figure 4.37: Cross plot of the C_{22}/C_{21} Tricyclic terpanes versus C_{24}/C_{23} Tricyclic terpanes from the Upper Cretaceous source rocks in the Sirt Basin. Interpretations fields after (Peters, 2005b).

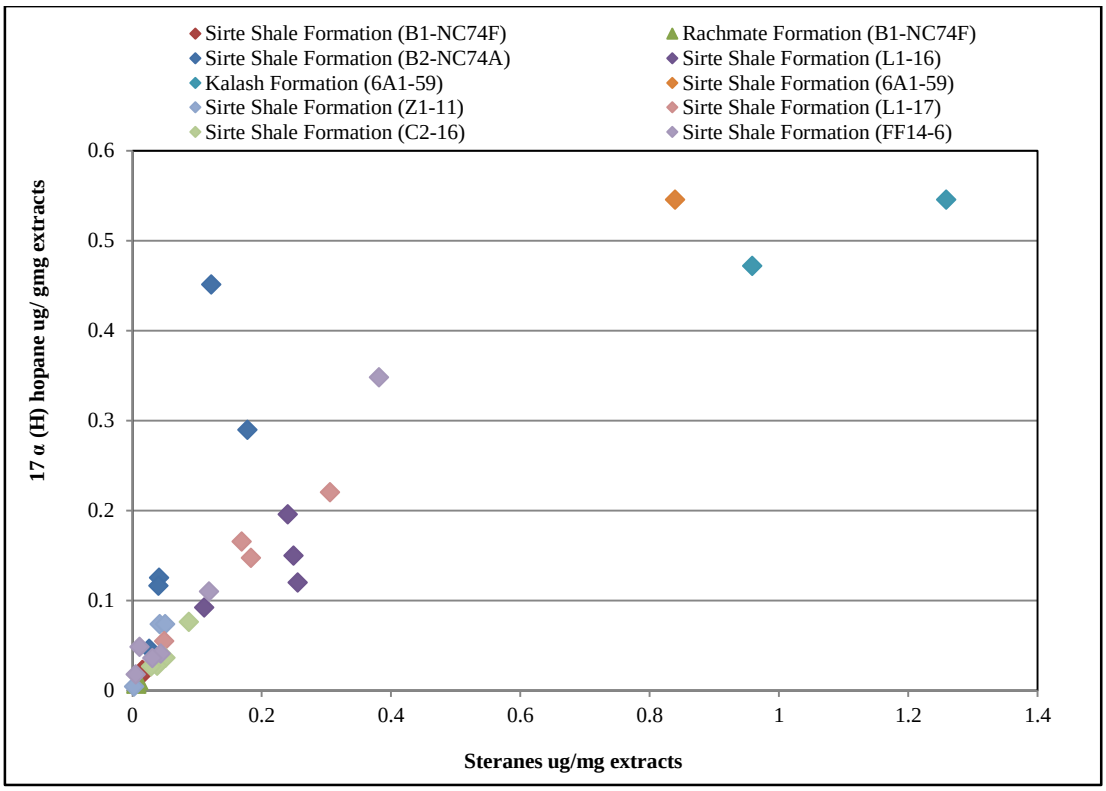

Figure 4.38: Cross plot of the concentrations of steranes versus 17α (H)-hopanes (µg/mg extracts) in the main source rocks from the Sirt Basin.

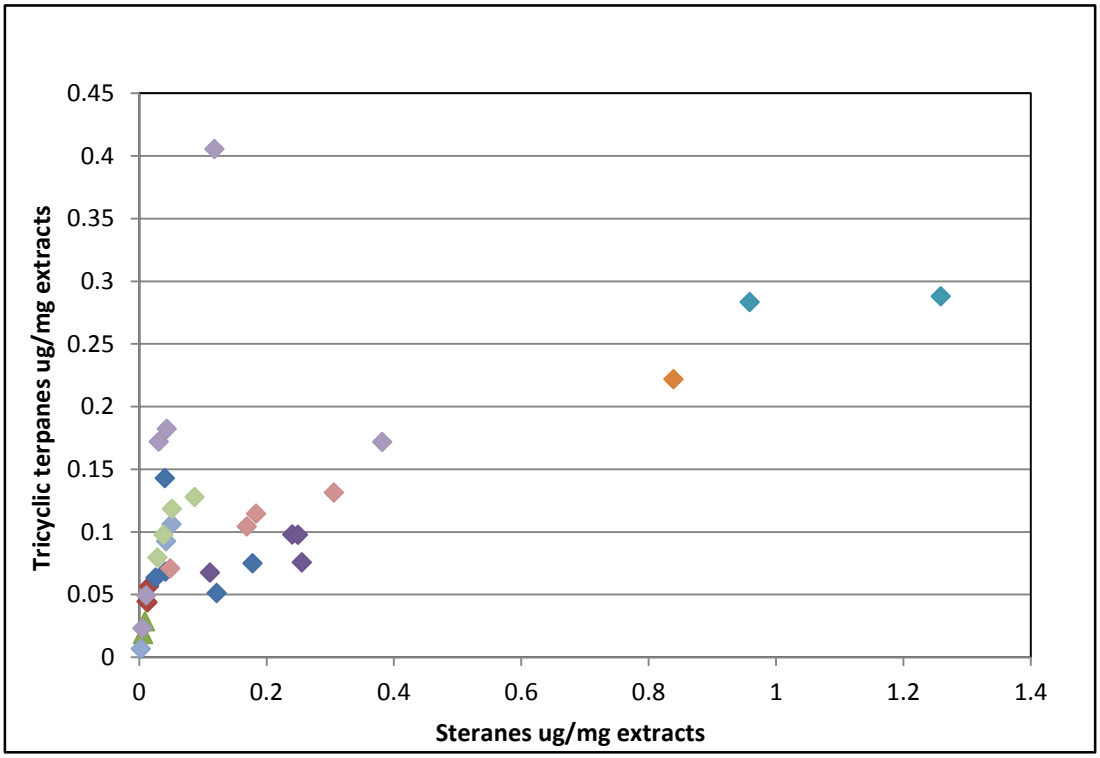

Figure 4.39: Cross plot of the concentrations of steranes versus tricyclic terpanes (µg/mg extracts) in the main source rocks from the Sirt Basin.

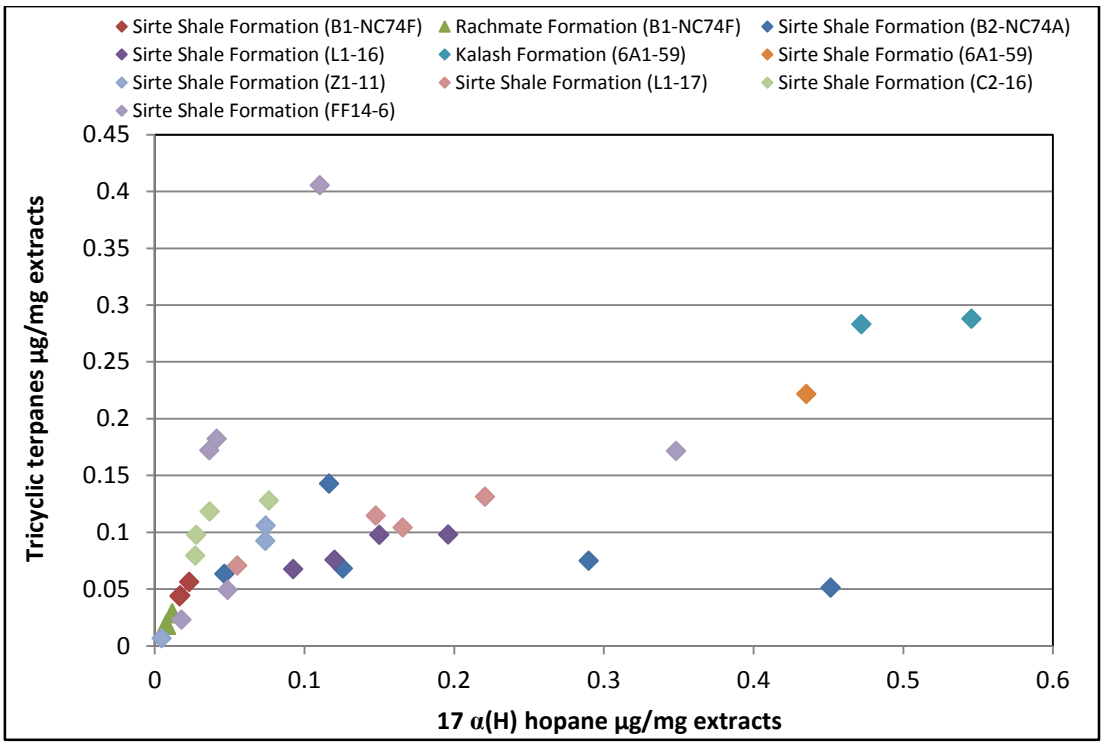

Figure 4.40: The cross plot of the concentrations of 17α (H) hopanes versus tricyclic terpanes (µg/mg extracts) in the main source rocks from the Sirt Basin.

4.7 Principal Component Analysis (PCA)

Principal component analysis (PCA) is a multivariate statistical method which recognises the relationships between samples and variables in complex data sets, and summarises the main sources of variance as principal components (Meglen, 1992; Jolliffe, 2002). PCA has been widely used as a data reduction technique capable of handling large volumes of data and able to extract subtle but significant differences in the sample set (Meglen, 1992; Kline, 1994; Jolliffe, 2002).

The data are composed of 32 variables, which include TOC, S2, molecular marker concentrations and two maturity ratios, for the 34 source rock samples from the Sirte Shale and Rachmat formations. The source sample data were analysed by PCA to determine the major sources of variation within the sterane, hopane and tricyclic terpane distributions, and the variables used in this analysis are listed in Table 4.2. The first three principal components obtained represent 61.6%, 13.2%, and 9.2%, respectively, of the variance within the data set. This type of variance analysis allows the relationships between samples to be studied in simple two-dimensional score plots: PC1 versus PC2 and PC1 versus PC3. This includes the effects of all the original

variables, which are sourced facies, molecular biomarker concentrations, and maturity, which together represent the bulk of the variability in data of 74.8%. Figure 4.41 and 4.42 shows the PC1 versus PC2 and PC1 versus PC3 plots for the Sirte shale and Rachmat source rock samples. The cross plots separate the source rock samples into three groups. Group A consists of all samples of well 6A1-59; group B samples from wells B2-NC74A (9570 and 9610 feet), FF14-6 (11320 feet), L1-16 (7400, 7590, and 7640 feet), and L1-17 (6060, 6300, and 6460 feet); and group C comprises samples from wells B1-NC74A (7050, 7110, 7190, and 8080 feet), B2-NC74F (9520, 9540, and 9580 feet), C2-16 (9800, 10260, 10380, 10580 feet), FF14-6 (11290, 11650, 12290, and 12330 feet), L1-16 (7850 feet), L1-17 (6600 feet), and Z1-11 (8080, 8140, and 8200 feet). However, the sample from well FF14-6 at depth 11615 feet is located away from the rest of the Sirte Shale source rock samples, and shows a lower abundance of sterane, diasterane, hopane, and tetracyclic terpanes C_{24}, but higher abundance in tricyclic terpane relative to other samples from the Sirte Shale source rock.

Figure 4.43 presents an interpretation of the three principal components using loading plots. These charts present the loadings of the different variables at the three principle components; large loadings are either negative or positive, and indicate a significant influence of each variable on that principle component. It is generally agreed that loadings can be considered high when values are more than 0.6, either negative or positive, moderately high when above 0.3, and low when less than 0.3 (Kline, 1994; Jolliffe, 2002). A low loading suggests that there is little or no correlation between the variables and the PCs.

The first principal component PC1 explains 61.6% of the total variance in the data analysis, and high loadings (>0.6) are found in the parameters C_{23}-C_{30} tricyclic terpane, C_{24} tetracyclic terpane, sterane, diasterane, hopane, total organic carbons (TOC), hydrocarbon petroleum potential (S2), and C_{20}TAS/(C_{20}TAS+ C_{28} (S+R)) triaromatic steroid maturity. Moderately high loadings (>0.3) are obtained for C_{22}, C_{24} tricyclic terpanes, C_{30} diahopane, and calculated vitrinite reflectance (%*Rc*). In interpreting this data analysis, it is clear that organic facies, represented by total organic carbon and hydrocarbon potential with maturity, have a major effect on the concentrations of biomarkers in the Sirte Shale and Rachmat source rocks. Maturity parameters appear

to control the concentrations and distributions of biomarkers, but with less significance than organic facies.

The second principal component PC2 explains 13.2% of the total variance in the data analysis. High loadings are observed for C_{22}, C_{24}, and C_{25} tricyclic terpanes and the maturity ratio C_{20}TAS/(C_{20}TAS+C_{28} (S+R)) for triaromatic steroids. In addition the loadings for C_{21}, C_{23}, C_{26}, C_{28}, and C_{29} used tricyclic terpanes, C_{30} diahopane, and calculated vitrinite reflectance (%*Rc*) are considered to be moderately high loadings (>0.3). Consequently, it could be considered that maturity appears to have more effect on PC2 than organic facies, and this may influence the distributions of biomarkers in the Sirte Shale and Rachmat source rocks.

The third principal component is less significant than the first and second PCs, representing 9.2% of the total variance in the data set. No high loadings are recorded for this component. Moderate loadings are found for total organic carbon, potential hydrocarbon potential, C_{30} tricyclic terpane, C_{29} Tm hopane, C_{30} diahopane, C_{27} βα (20S+20R) diasterane, and C_{27} ααα (20S+20R) sterane. Therefore, it could be considered that source facies and maturity have some impact on the PC3. It is clear that from the analysis of the data set that PC3 is controlled by changes in organic facies and maturity in the Sirte Shale and Rachmat source rocks.

The combination of PC1 and PC2 and PC1 with PC3 account for 74.2% and 70.8%, respectively, of the total data set, showing similar effects of the source organic facies and maturity on the concentration and distribution of biomarkers in the Sirte Shale and Rachmat source rocks.

It is obvious from the analysis that the Sirte Shale source rock samples in groups A and B are dominated by the abundance of total organic carbon, hydrocarbon potential, steranes, diasteranes, and hopanes while they have relatively lower abundances of tricyclic terpanes, suggesting that both groups have a moderate to high input of eukaryotes relative to prokaryotic organisms and this also reflects the lower thermal maturity effects (Ourisson *et al.*, 1982; Moldowan *et al.*, 1985; Moldowan *et al.*, 1986; Peters and Moldowan, 1993; Peters, 2005b). This may be as a result of a better preservation of steroid and hopanoid compounds in suboxic to anoxic marine

environments. The abundance of diasterane compounds may be due to clay-rich lithology. Both groups appear less impacted by maturity than group C.

The Sirte Shale and Rachmat source rocks from group C showed moderate total organic carbon values and petroleum potential compared with the other two groups. Group C samples had less tricyclic terpanes, tetracyclic terpanes, steranes, diasteranes, hopanes, and diahopane relative to groups A and B. The difference in biomarker distributions in the Sirte Shale and Rachmat source rocks in group C may be due to effects of dilution during deposition, which appears to lead to slightly higher mineral carbon contents relative to total organic carbon. Alternatively, changes in depositional environments may have led to moderate preservation in organic matter within suboxic conditions, or it might be that the organic matter exhibited to higher thermal maturity due to overburden sediments, which maybe led to low biomarker concentration.

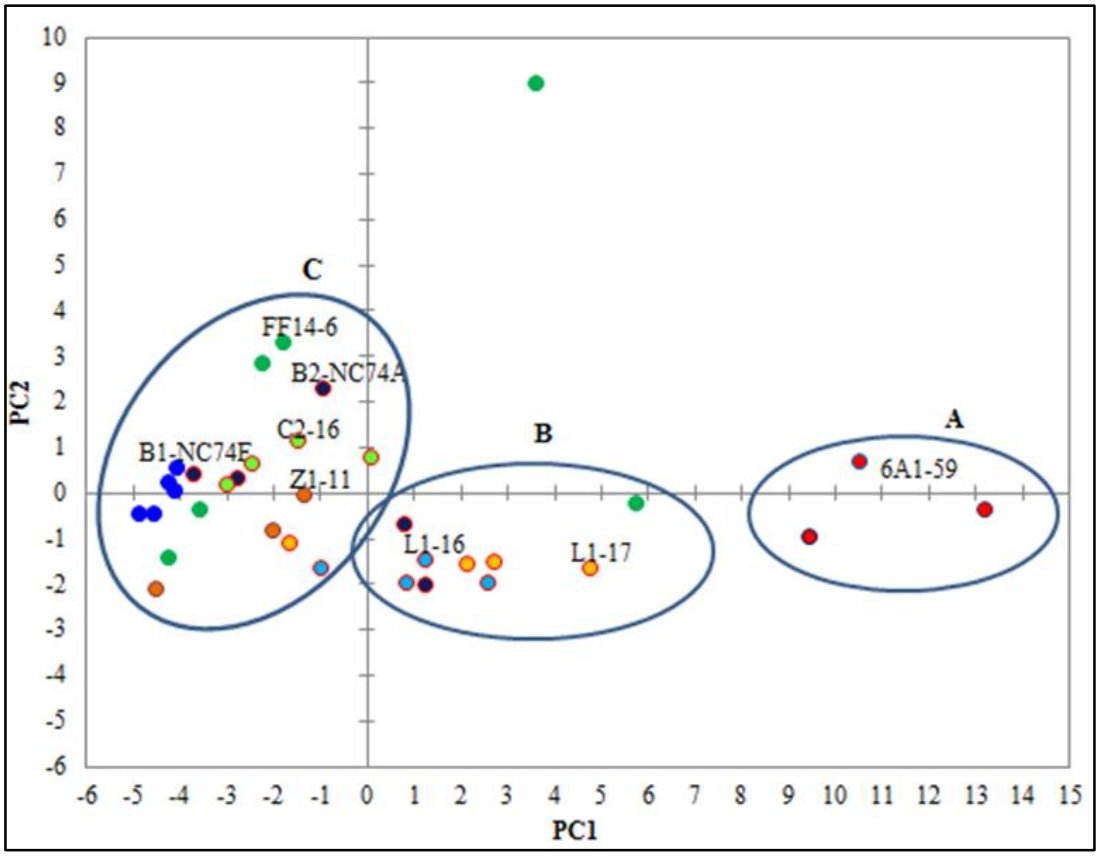

Figure 4.41: Cross plot of the PC1 versus PC2 for the Sirte Shale and Rachmat source rocks. Sample groups A, B and C are shown.

Table 4-2: Bulk geochemical data and biomarker compounds used in the principle component analysis.

Source Facies	
1	**TOC (wt %)**
2	**S2 (mg HC/ g rock)**
Tricyclic terpanes and hopanes (m/z 191)	
3	**C_{21} Tricyclic terpane**
4	**C_{22} Tricyclic terpane**
5	**C_{23} Tricyclic terpane**
6	**C_{24} Tricyclic terpane**
7	**C_{25} Tricyclic terpane**
8	**C_{24} Tetracyclic terpane**
9	**C_{26} Tricyclic terpanes (22S+22R)**
10	**C_{28} Tricyclic terpanes (22S+22R)**
11	**C_{29} Tricyclic terpanes (22S+22R)**
12	**C_{30} Tricyclic terpanes (22S+22R)**
13	**22,29,30-Trisnorneohopane (Ts)**
14	**22,29,30-Trisnorhopane (Tm)**
15	**C_{29} 17α(H), 21β(H)-30-norhopane**
16	**18α(H)-30-norneohopane(C29 Ts)**
17	**C_{30} diahopane**
18	**C_{30} 17α (H), 21β (H) hopane**
Steranes (m/z 217)	
19	**C_{21} (ααα+αββ) prgnanes**
20	**C_{22} (ααα+αββ) homopregnanes**
21	**C_{27} 13β (H), 17α (H) diasterane 20S**
22	**C_{27} 13β (H), 17α (H) diasterane 20R**
23	**C_{29} 13β (H), 17α (H) diasterane 20S**
24	**C_{27} 5α (H), 14α (H), 17α (H) sterane 20R**
25	**C_{29} 13β (H), 17α (H) diasterane 20R**
26	**C_{29} 5α (H), 14α (H), 17α (H) sterane 20S**
27	**C_{29} 5α (H), 14α (H), 17α (H) sterane 20R**
αββ Steranes (m/z 218)	
28	**C_{27} 5α (H), 14β (H), 17β (H) sterane (20S+20R)**
29	**C_{28} 5α (H), 14β (H), 17β (H) sterane (20S+20R)**
30	**C_{29} 5α (H), 14β (H), 17β (H) sterane (20S+20R)**
Maturity parameters	
31	**% Rc= 0.4+ (0.60*MPI-1)**
32	**C_{20} TAS/ [(C20 TAS + C28 5 α(H) (S+R) TAS]**

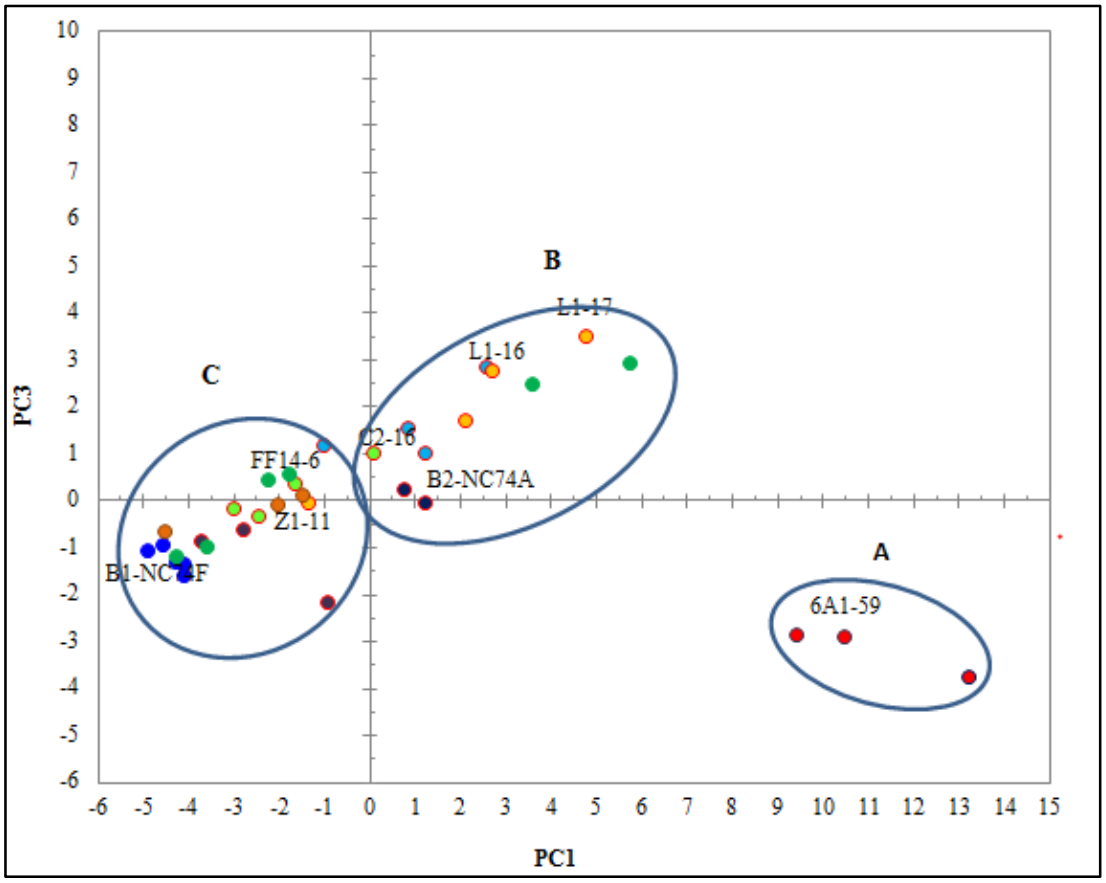

Figure 4.42: Cross plot of the PC1 versus PC3 of the Sirte Shale and Rachmat source rocks. Sample groups A, B and C are shown.

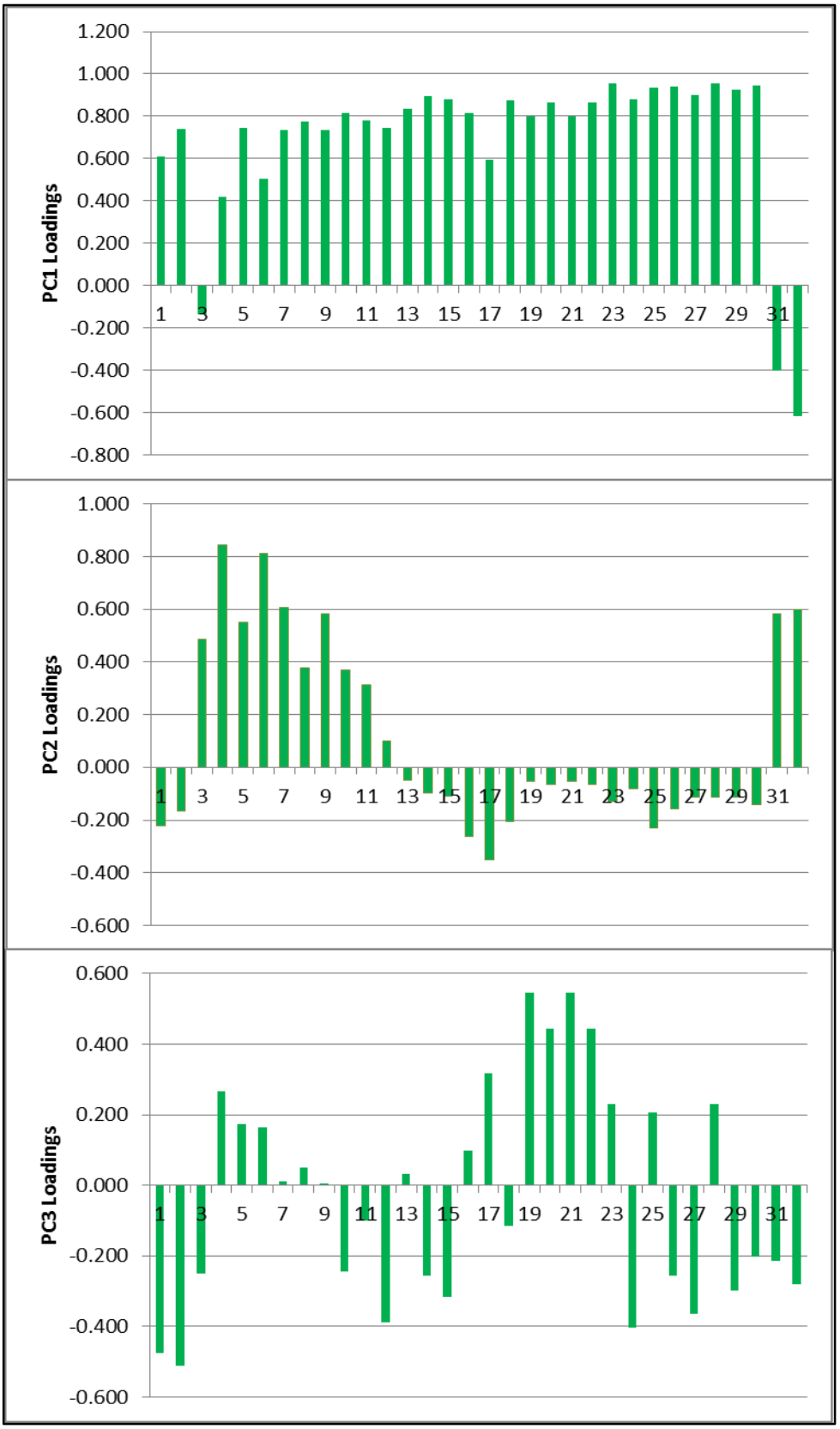

Figure 4.43: Loadings plots showing the composition of the first three PCs, which scored 61.6%, 13.2% and 9.2% of total variance in the data analysis set, respectively.

4.8 Aromatic Compounds

4.8.1 Monoaromatic and Triaromatic Steroidal hydrocarbons

The distribution of monoaromatic steroids (MAS) was monitored using m/z 253 from the aromatic fractions of the source rock samples of the Sirte Shale Formation in the Sirt Basin as shown in Figure 4.44. For most of the study wells, the short chain C_{21} and C_{22} compounds are present in greater abundance than the long chain C_{27} to C_{29} compounds. This may reflect the fact that the short chain molecules are more resistant to the effects of maturity. Most of the samples analysed were characterized by the predominance of the C_{21} MAS. The distributions of long chain C_{27} to C_{29} monoaromatic steroids appear to show moderate to high abundance in the wells 6A1-59, B1-NC74F, B2-NC74A, L1-16 and L1-17, relative to the other wells C2-16, FF14-6, and Z1-11. This may be due to the effects of maturity of long chain monoaromatic compounds or to changes in organic facies. The vitrinite reflectance and biomarker maturity data show that the rock samples from the C2-16, FF14-6, and Z1-11 wells are higher maturity than those from other wells. Most of the samples are dominated by $C_{27}\alpha R$, $C_{29}\beta$ and $C_{28}\alpha$ (S and R), and $C_{28}\beta$ S monoaromatic steroid hydrocarbons, as shown in Figure 4.45. The predominance C_{27}, C_{29} and C_{28} monoaromatic steroid hydrocarbons can be attributed to marine sourced organic matter inputs (Peters, 2005b).

The distributions of triaromatic steroids (TAS) were monitored using m/z 231 from the aromatic fractions, as shown in Figure 4.46. The short (C_{20} and C_{21}) and long chain ($C_{26}S$ to $C_{28}R$) TAS were present with different distributions in the source rock samples. Short chain C_{20} and C_{21} TAS were observed in all samples and in relatively greater abundance than the long chain $C_{26}S$ to $C_{28}R$ TAS in the wells B1-NC74F, B2-NC74A, Z1-11, and C2-16, for FF14-6 at the intervals 11615, 11290, 11650, and 12290 feet, and L1-17 at depth of 6600 feet. However, in wells 6A1-59, L1-16, and L1-17, and in FF14-6 at the depths 11320 and 12330 feet, the long chains were relatively more abundant than short chains. The TAS hydrocarbons from C_{26} to C_{28} are thought to originate from the demethylation and aromatization of monoaromatic steroids. But, short chain compounds are supposedly produced from the homolytic scission of long chain TAS with increased thermal maturity (Seifert and Moldowan, 1978; Mackenzie *et al.*, 1981). The long chain TAS C_{26} to C_{28} seem to be in very low in abundance in

well B1-NC74F compared with the other wells. Most of the source rock samples show a predominance of $C_{26}R+C_{27}S$, and $C_{27}R$ TAS, as shown in Figure 4.47. This may reflect the fact that all of the source rock samples have originated from similar organic matter input, but with different depositional environments and levels of thermal maturity.

Figure 4.48 shows the cross plot of the $C_{26}S/C_{28}S$ triaromatic steroids versus $C_{27}R/C_{28}R$ triaromatic steroids ratios for the Sirte Shale and Rachmat source rock extracts. The diagram shows the low abundance of the $C_{26}S$ TAS relative to the $C_{28}S$ TAS and $C_{27}R$ TAS relative to $C_{28}R$ TAS in wells B1-NC74F and B2-NC74A, suggesting differences in the source organic matter inputs and depositional environments, which may be high anoxic marine to lacustrine environments compared to the other study wells. For wells 6A1-59, C2-16, FF14-6, L1-16, L1-17 and Z1-11 the ratios were higher, indicating similar organic matter inputs that were deposited under dysoxic to anoxic marine conditions (e.g. Peters and Moldowan, 1993; El-Gayar, 2005; Peters, 2005b). Whereas two source rock samples from well FF14-6 at depths 12290 and 12330 show higher abundance in $C_{26}S$ relative to $C_{28}S$ TAS and low abundance in $C_{27}R$ relative to $C_{28}R$ TAS, when compared to the other source rock extracts samples. This indicates that there are differences in organic matter inputs and depositional environments, which may have contained marine and terrestrial organic matter inputs and were deposited in dysoxic marine environments. The reason of this higher $C_{26}S$ relative to $C_{28}S$ TAS and low abundance in $C_{27}R$ relative to $C_{28}R$ TAS is thought to be the highest degree of thermal maturity, since those samples are the deepest and this result are agree with other biomarker maturity results (see section 4.8.1) (e.g. Seifert *et al.*, 1984; Riolo *et al.*, 1986; Peters and Moldowan, 1993; Peters, 2005b).

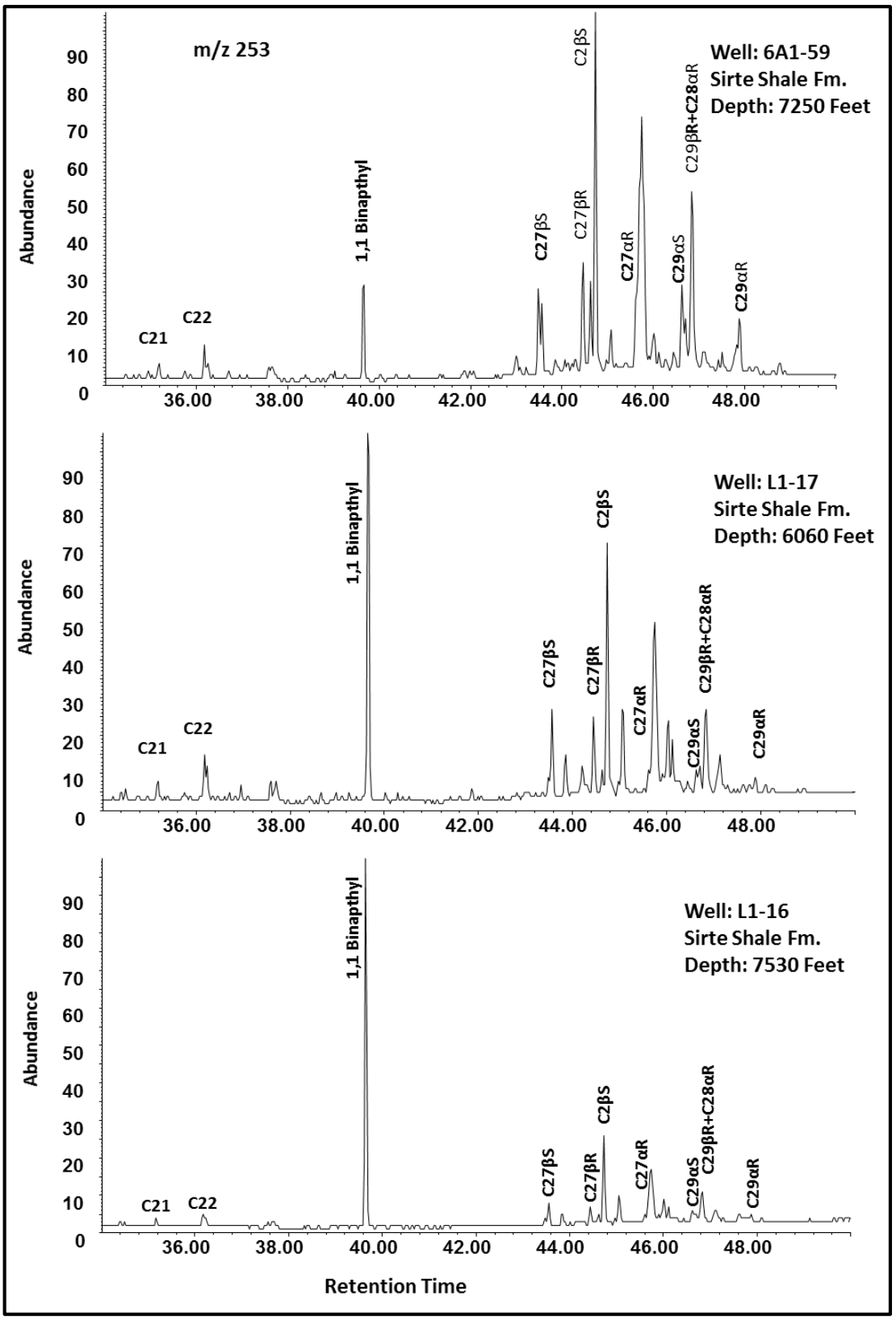

Figure 4.44: Example m/z 253 mass chromatograms showing the distributions of the monoaromatic steroidal hydrocarbons in the Sirte Shale source rock samples.

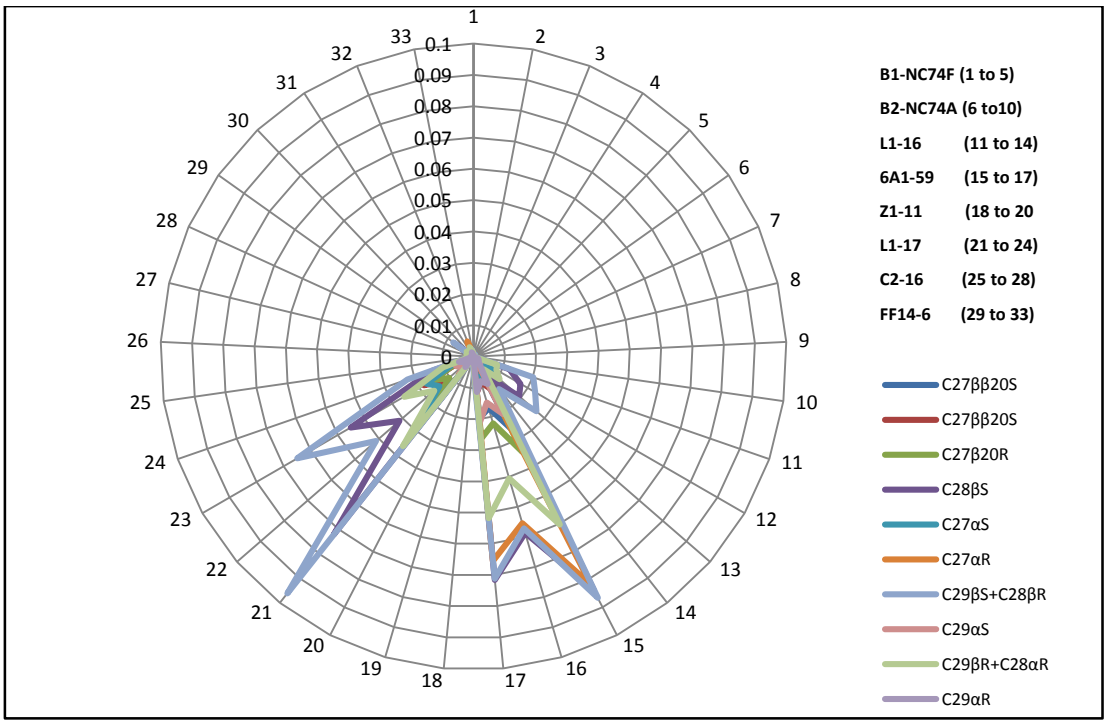

Figure 4.45: Rose diagram shows presence and abundance of the monoaromatic steroidal hydrocarbons in the Upper Cretaceous source rocks of the Sirt Basin. Sample codes are given in Table 4.6 in Appendix I.

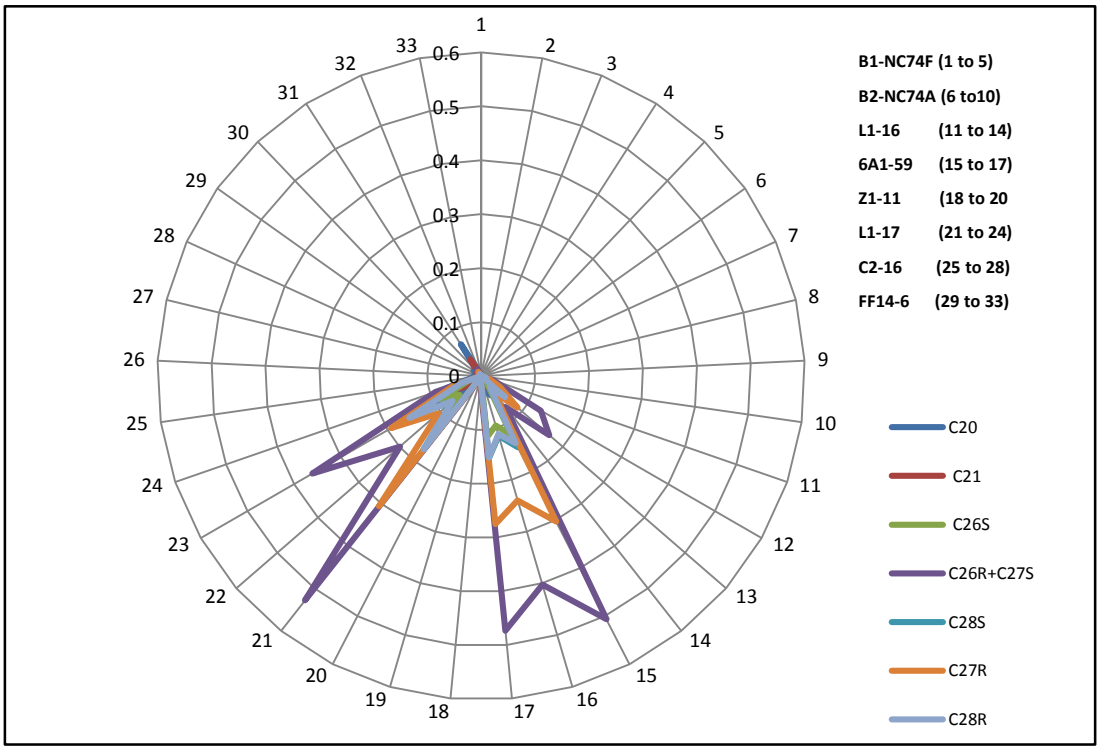

Figure 4.46: Rose diagram shows presence and abundance of the triaromatic steroidal hydrocarbons in the Upper Cretaceous source rocks of the Sirt Basin.

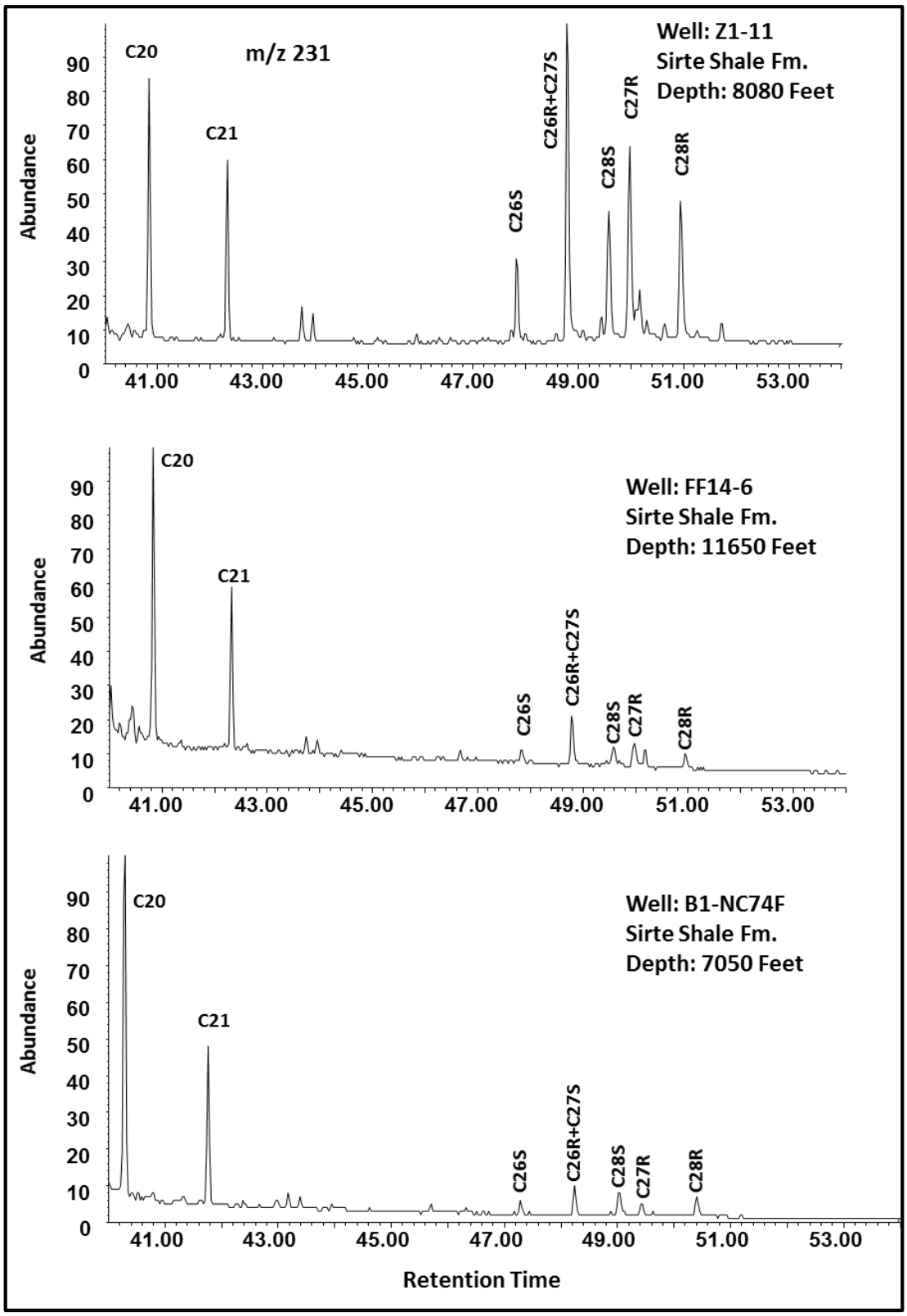

Figure 4.47: Example m/z 231 mass chromatograms showing the distributions of the triaromatic steroidal hydrocarbons in the Sirte Shale source rock samples.

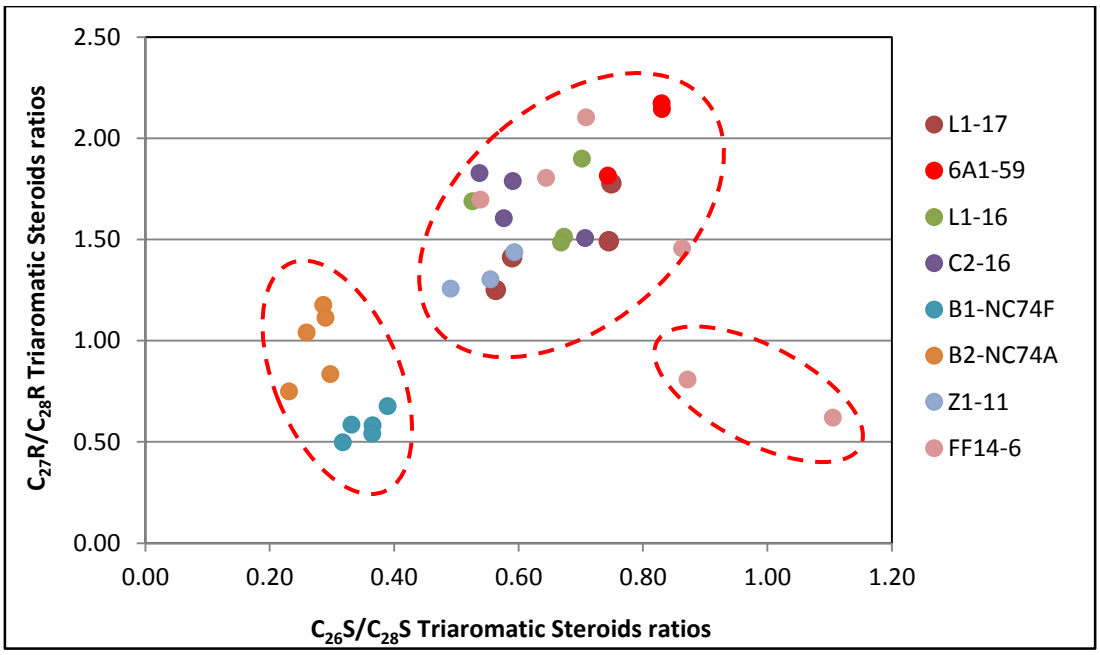

Figure 4.48: Cross plot of the $C_{26}S/C_{28}S$ triaromatic steroids versus $C_{27}R/C_{28}R$ triaromatic ratios for the Sirte Shale and Rachmat source rock extracts in the Sirt Basin. Sample codes are given in Table 4.8 in Appendix I.

4.8.2 **Alkylnaphthalenes**

In the extracted rock samples the distributions of aromatic hydrocarbons that were monitored showed a high relative abundance of phenanthrene (48-80%), followed by dibenzothiophene (5-16%), naphthalene (0.53-9.61%), and biphenyl (0.48-16.31%), with only low levels of fluorene (0.54-3.93%) and triaromatic steroids (0.02-6.14%). This may indicate that the organic sediments were derived from depositional environments of clastic marine source rocks with some land plant inputs (e.g. Garrigues and Ewald, 1983; Strachan *et al.*, 1986; Püttmann and Villar, 1987; Strachan *et al.*, 1988; Forster *et al.*, 1989; Budzinski *et al.*, 1995; Requejo *et al.*, 1996; Bastow *et al.*, 1998).

The concentrations of the naphthalene (N), methylnaphthalenes (MN), dimethylnaphthalenes (DMN), trimethylnaphthalenes (TMN), and tetramethylnaphthalenes (TeMN) are very low in the Sirte Shale and Rachmat formation source rocks from the wells B1-NC74F and B2-NC74A, relative to other wells studied, with a predominance of tetramethylnaphthalene compounds, as shown in Figure 4.49. However, the aromatic hydrocarbon concentrations (µg/g extractable organic matter) in the Sirte Shale source rock for the wells 6A1-59, C2-16, FF14-6, L1-

16, L1-17, and Z1-11 are considered to be moderate to high, with greater abundance of the trimethylnaphthalene compounds. Trimethylnaphthalenes are therefore the most abundant alkylnaphthalene compounds (as shown in Figures 4.49 and 4.50), whose relative abundances decrease in the order TMN>DMN>TeMN>MN>N for the wells 6A1-59, C2-16, FF14-6, L1-16, L1-17, and Z1-11. The most abundant naphthalene compounds in wells B1-NC74F and B2-NC74A are the tetramethylnaphthalenes, where their relative abundances decrease in the order TeMN>TMN > DMN >MN>N, but they are less dominant when compared with other study wells. The total concentrations of DMN were low of less than 2.35 µg/mg extracts in the 6A1-59, B1-NC74F, B2-NC74A, C2-16, L1-16, L1-17, and Z1-11 wells, and at the depths of 11290,11615, and 11650 feet for well FF14-6, showing reduced DMN contributions in the organic sediments. This may reflect marine origin, because terrestrial organic matter contains relatively higher amounts of DMN. Whereas in well FF14-6 at the depths 11320, 12290, and 12330 feet, the total DMN concentrations are between 4.31 and 4.86 µg/mg extracts, suggesting either some contribution of terrestrial organic matter or that these organic sediments were affected by higher thermal maturity.

The presence of the 1,2,7-TMN isomer has been used as a marker of angiosperm input, and TDE-1 and TDE-2 ratios are used to distinguish marine from coal swamp, lacustrine, and deltaic depositional environments (Strachan *et al.*, 1986). The TDE-1 ratio represents 1,2,5-TMN/1,2,4-TMN, and the TDE-2 ratio represents 1,2,7-TMN/1,2,6-TMN. Also the 1,2,7-/1,3,7-TMN ratio can be used to differentiate between marine oils and source rocks from the higher plant material (Strachan *et al.*, 1986; Strachan *et al.*, 1988). For the wells studied, the extract samples of the Upper Cretaceous source rock give TDE-1 and TDE-2 ratios in the ranges of 2.50 to 5.21 and 0.39 to 2.15 respectively. This suggests marine depositional environments with some contribution of angiosperm land plants, as shown in Figure 4.51. The high abundances of the 1,2,5-TMN relative to 1,2,4-TMN and high abundance of the 1,2,7-TMN relative to the 1,2,6-TMN in some analysed samples may be due to a arise of methyl rearrangement of other trimethylnaphthalene isomer that derived from other precursors (Strachan et al., 1988). The results obtained for the relative abundance of the trimethylnaphthalenes in all sediment samples are listed in Table 4.8 in Appendix I. Furthermore, the 1,2,7-/1,3,7-trimethylnaphthalene ratios for the Sirte Shale and

Rachmat source rocks for all wells were low and ranged from 0.20 to 0.52. This may indicate that the Sirte Shale and Rachmat formations were deposited within an anoxic marine environment with less of a contribution from land plants.

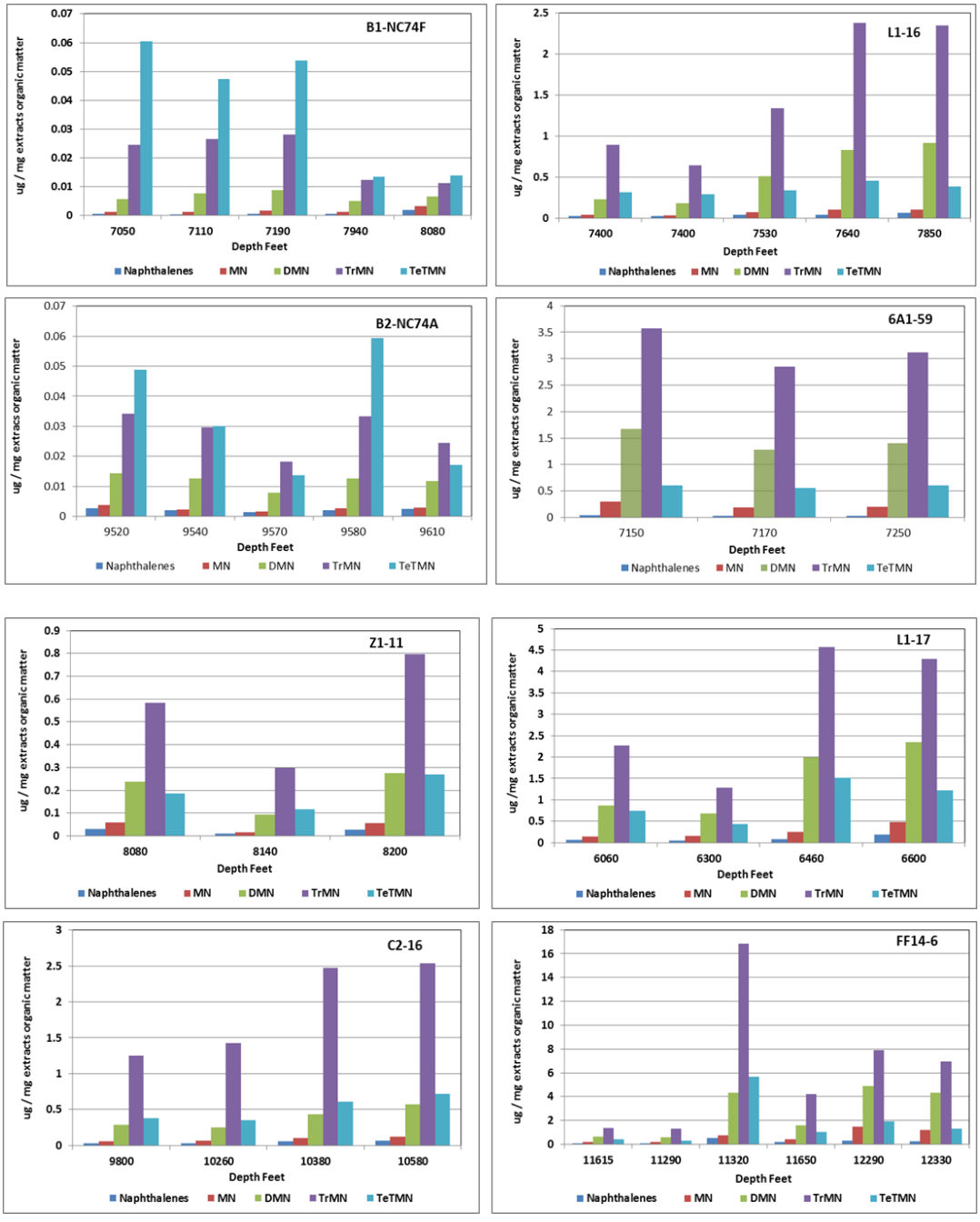

Figure 4.49: Aromatic hydrocarbon concentrations of the main Upper Cretaceous source rocks from eight wells in the Sirt Basin, Naphthalenes (N), Methylnaphthalenes (MN), Trimethylnaphthalenes (TMN), Tetramethylnaphthalenes (TeMN).

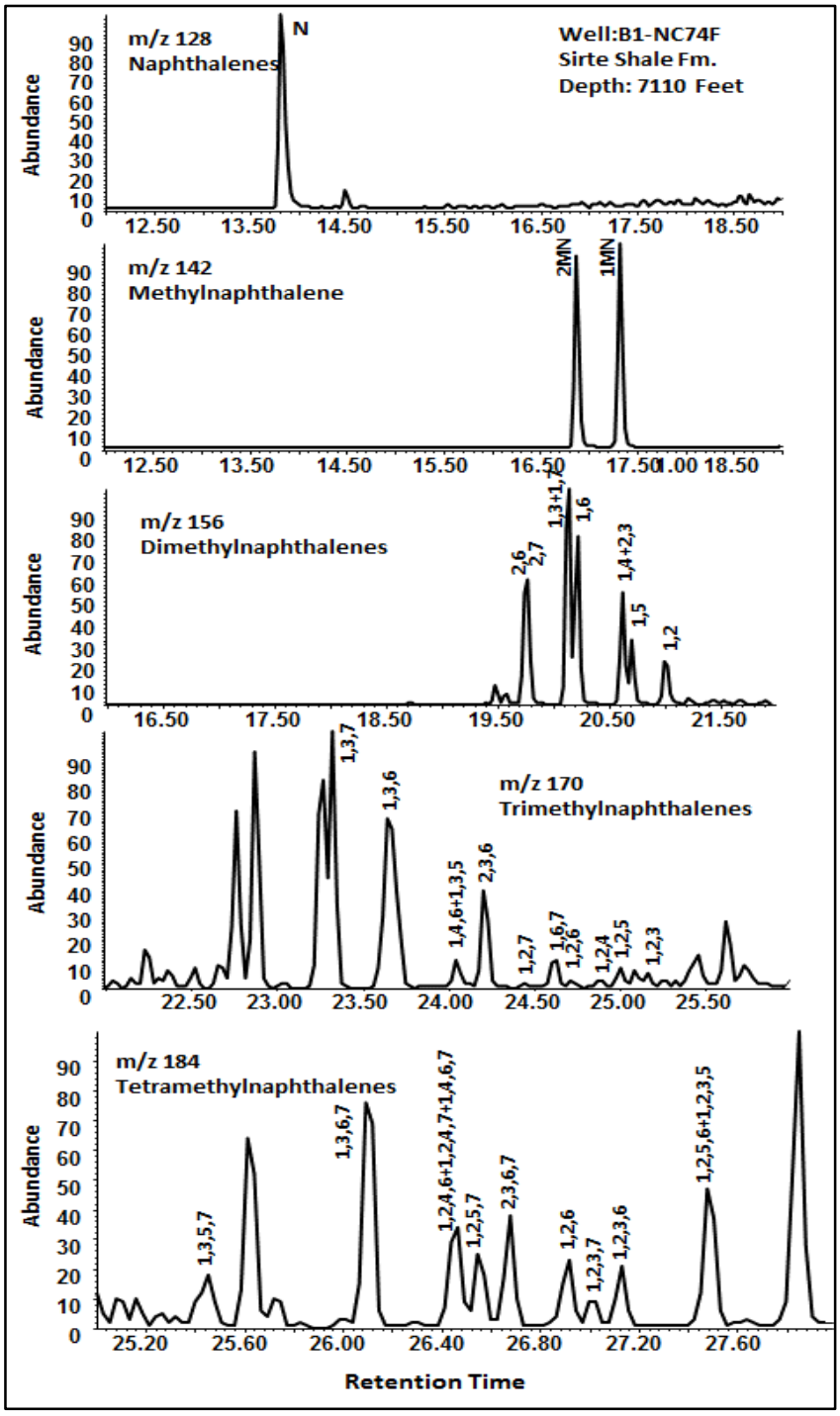

Figure 4.50: Mass chromatogram of the aromatic fractions of the Sirte Shale source rocks from well B1-NC74F (7110 Feet) showing the distribution of naphthalene, methylnaphthalenes, dimethylnaphthalenes, trimethylnaphthalenes, and tetramethylnaphthalenes (m/z: 128, 142, 156, 170 and 184, respectively).

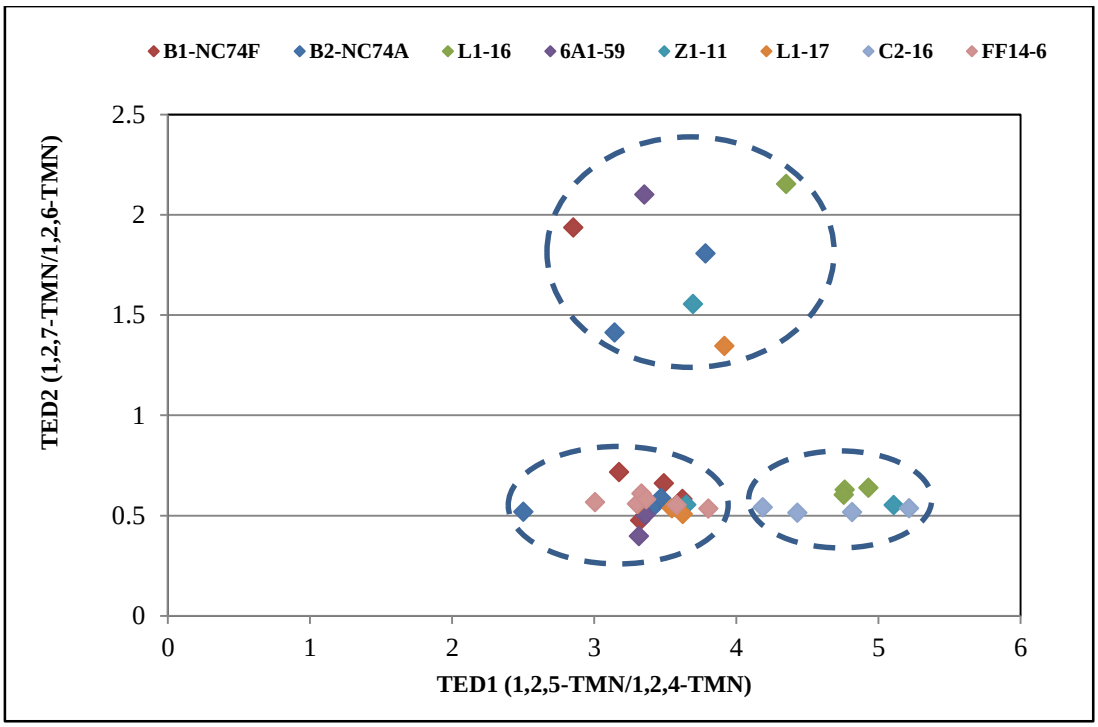

Figure 4.51: Cross plot of the TDE-1 (1,2,5-/1,2,4-trimethynaphathalene) versus TDE-2 (1,2,7-/1,2,6-trimethylnaphathalene for the Upper Cretaceous source rocks in the Sirt Basin. Sample codes are given in Table 4.8 in Appendix I).

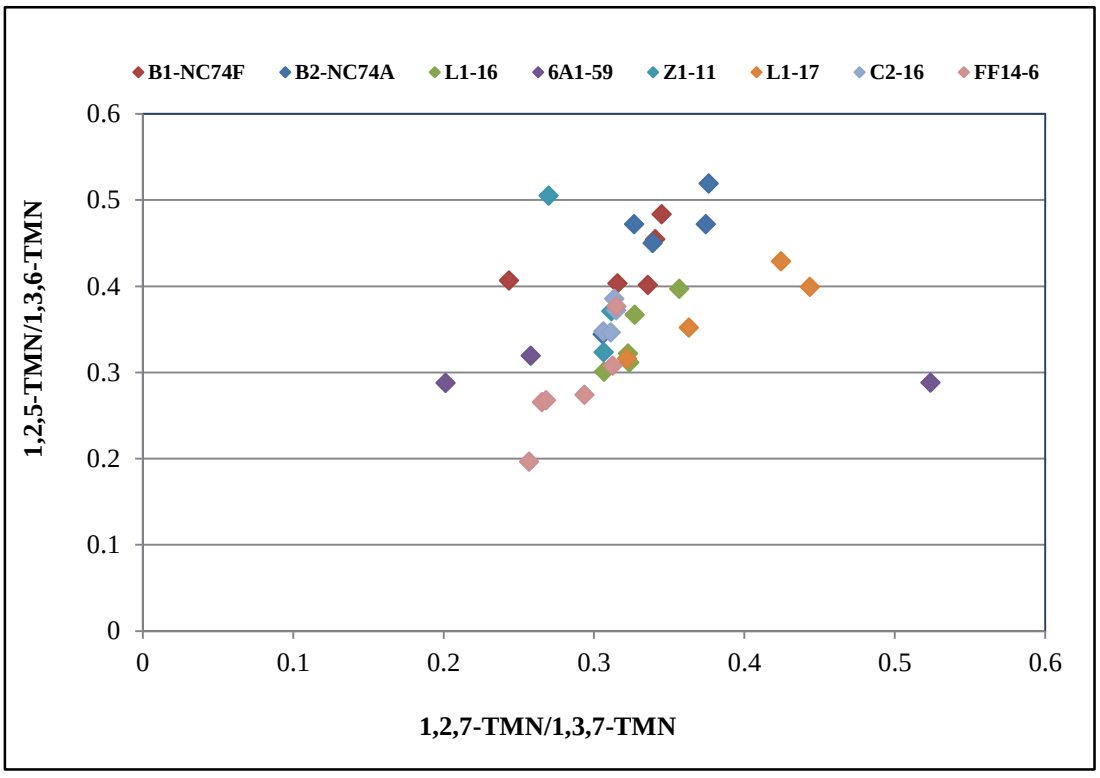

Figure 4.52: Cross plot of the 1,2,7-/1,3,7-Trimethynaphathalanes versus 1,2,5-/1,3,6-Trimethylnaphathalanes for the Upper Cretaceous source rocks in the Sirt Basin. Sample codes are given in Table 4.8 in Appendix I.

The very low relative abundance of 1,2,5-TMN, which less than 0.52 in the Sirte Shale and Rachmat source rock samples, indicating that they were derived from a marine origin and may be attributed to the absence of land plant terpenoids in the source organic matter of the source, or it may be that its formation via the aromatization of other hydrocarbon compounds such as C_{15} bicyclic alkanes did not occur (Noble *et al.*, 1986; Strachan *et al.*, 1986; Strachan *et al.*, 1988).

The crossplot of the 1,2,7-TMN/1,3,7-TMN versus 1,2,5-TMN/1,3,6-TMN ratios for the marine Upper Cretaceous source rocks in Figure 4.52 shows that they are consistent with the fact that these rocks consist mainly of siliciclastic marine shales with low contribution of higher plants, showing low values of both ratios with means of 0.37 and 0.32, respectively (Strachan *et al.*, 1986; Strachan *et al.*, 1988). The position of a sample in such a plot is dependent primarily upon type of organic matter in the source rock and maybe modified by the secondary maturity effect (Strachan *et al.*, 1988). However, these extracts samples apparently originated from source material which was initially even more depleted in 1,2,5-TMN and 1,2,7-TMN and their precursors. Therefore, these organic samples were sourced from organic matter deposited under conditions, which did not favour high aromatisation processes. These were probably typical marine environment. The data concerning sterane distribution and kerogen type suggests that the samples from these wells are typical of marine shale (Strachan et al., 1986; Strachan et al., 1988).

4.8.3 **Alkylphenanthrenes**

The source rock samples of the Upper Cretaceous sequences from the eight selected wells in the Sirt Basin showed a predominance of the phenanthrene aromatic hydrocarbon compounds and the distributions of these in the Sirte Shale source rock are displayed in Figure 4.53. Strachan *et al.* (1986) reported that phenanthrenes appear to be produced from steroids and that difference in the relative abundance of various alkylphenanthrenes can be attributed to source origins. The high abundance of 9-methylphenanthrene (9-MP) has been attributed to the marine character of organic matter, whereas the dominance of 1-methylphenanthrene (1-MP) is due to terrestrial organic matter (Budzinski *et al.*, 1995). The 1-MP/9-MP ratios determined from the Upper Cretaceous source rocks analysed signed in the range of 0.28 to 0.92 with an

average of 0.60, except for one sample in well Z1-11 at a depth of 8140 feet where it was found to be 1.52, and this higher 9-MP to 1-MP abundance reflects the marine source precursors of these compounds.

The 1-MP/9-MP versus 1,7-DMP/(1,3-, 3,9, 2,10, 3,10-DMP) ratios have been used to characterise the sources of organic matter from different ages (Alexander *et al.*, 1992b). Figure 4.54 shows a cross plot of the 1-MP/9-MP versus 1,7-DMP/(1,3-, 3,9, 2,10, 3,10-DMP) ratios. Most of the source rock samples data are scattered and concentrated in the middle of the chart. The high abundance of 9-MP and 1,3-, 3,9-, 2,10-, 3,10-DMP indicates marine origins for these isomers, whereas the slightly higher abundance of 1-MP and 1,7-DMP for the samples from well Z1-11 at a depth of 8140 feet indicates some terrestrial contributions.

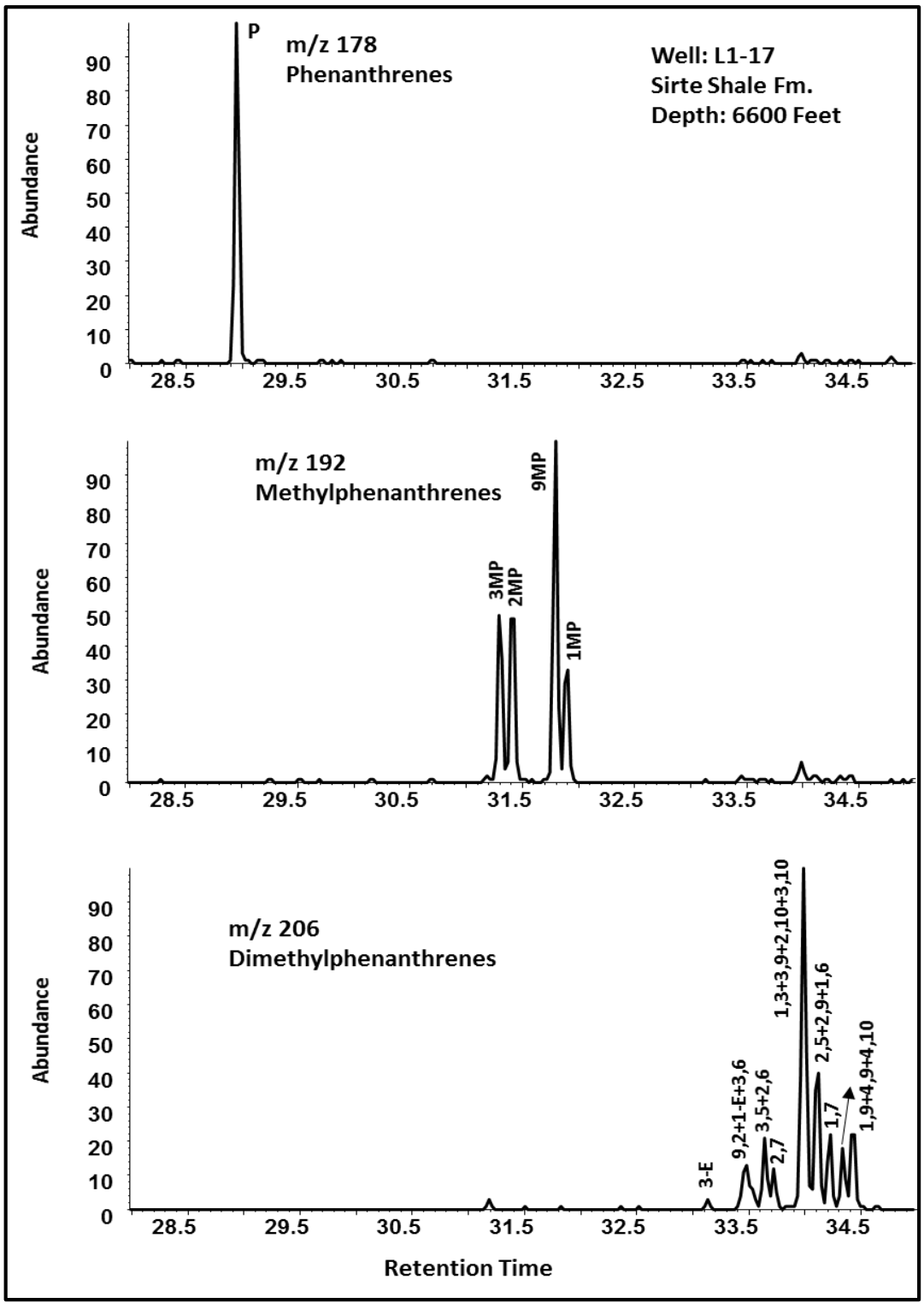

Figure 4.53: Mass chromatograms of the aromatic fraction of the Sirte Shale source rock from well L1-17 (6600 Feet) showing the distribution of phenanthrene, methylphenanthrenes, and dimethylphenanthrenes, (m/z: 178, 192 156, and 206, respectively).

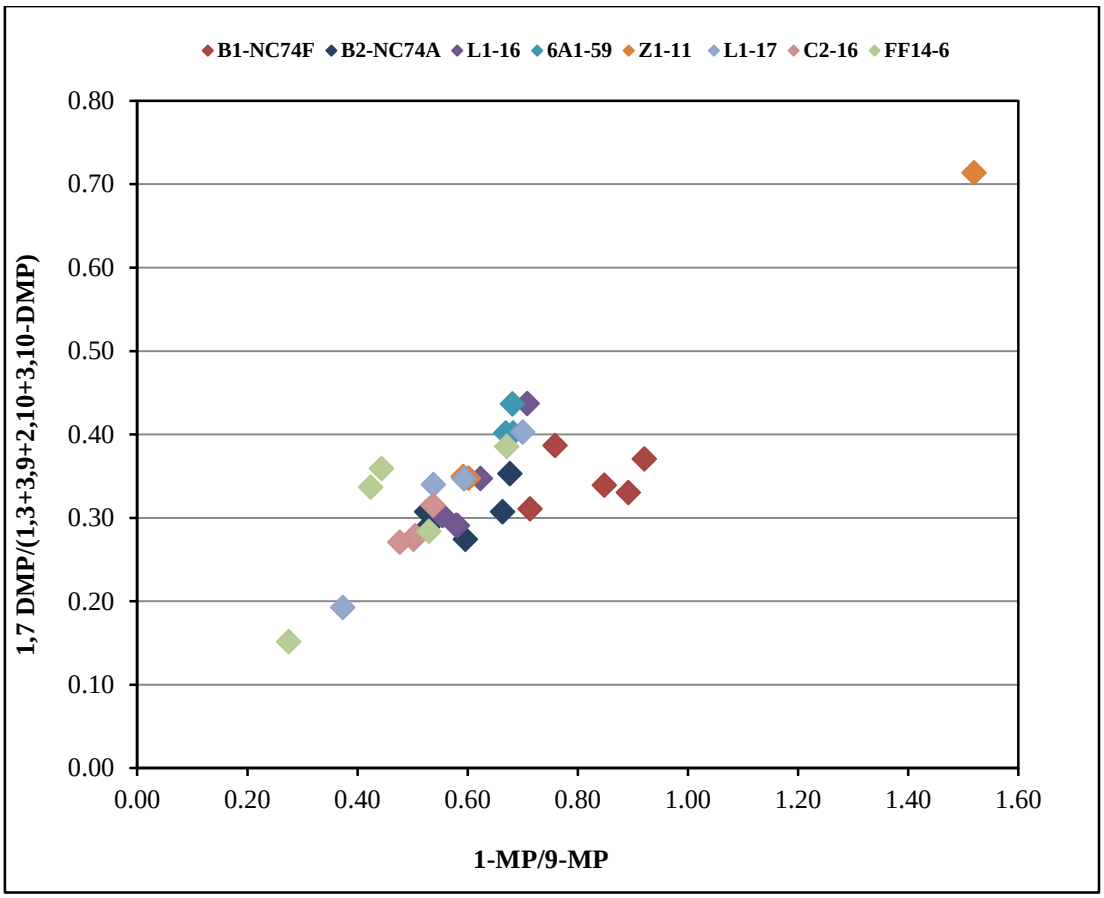

Figure 4.54: Cross plot of the 1-MP/9-MP versus 1,7-DMP/(1,3-, 3,9, 2,10, 3,10-DMP) for the analysed Upper Cretaceous source rocks in the Sirt Basin.

4.8.4 **Alkyldibenzothiophenes**

The relative amounts of alkyldibenzothiophenes and their alkylated analogues with pristane and phytane ratios can be used as indicators of depositional environment (Hughes *et al.*, 1995; Jinggui *et al.*, 2005). The dibenzothiophene to phenanthrene ratio (DBT/P) in oils can be used as an indicator of source rock lithology, with a DBT/P ratio less than 1.0 indicating shale type facies, whereas values more than 1.0 indicates carbonate lithology, when sulphur is incorporated with organic matter means that its DBT content will be higher (Hughes et al., 1995). Figure 4.55 shows the crossplot of the DBT/P against Pr/Ph ratios, which indicates that most of the source rocks from the Sirte Shale and Rachmat Formations are from marine to lacustrine shales and their Pr/Ph ratios signed within the range from 0.73 to 2.39, supporting the notion of marine suboxic to anoxic depositional environments.

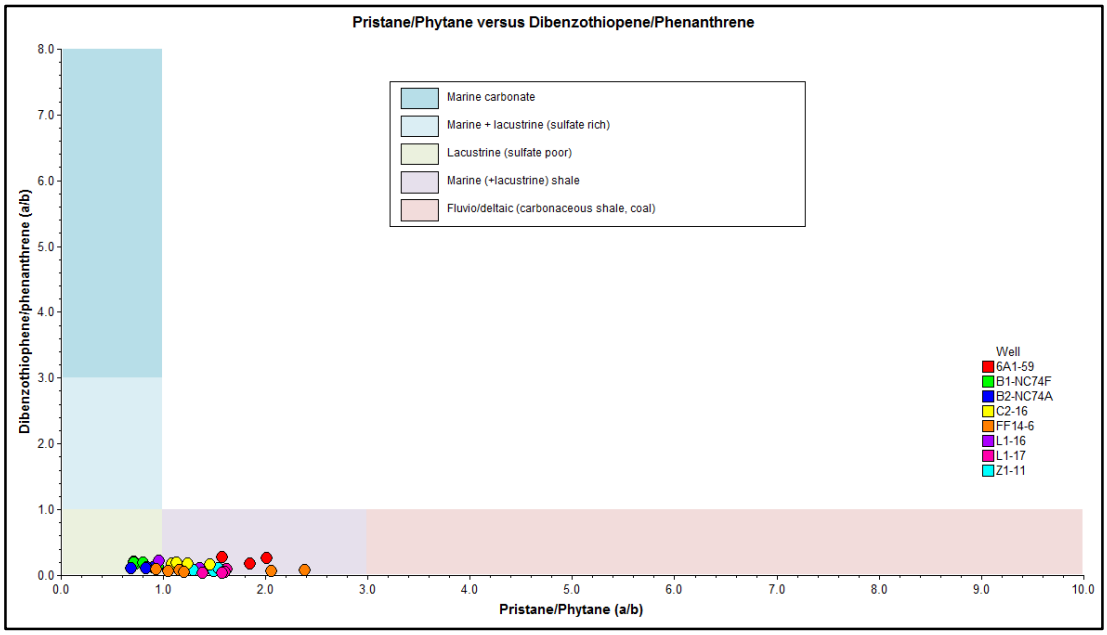

Figure 4.55: Cross plot of the DBT/P versus Pr/Ph of the Upper Cretaceous source rocks analysed. Interpretation fields are from pIGI software using values from Hughes et al. (1995).

4.9 Maturity Assessment Using Molecular Organic Compounds

4.9.1 Steranes and Triterpanes

The values of all of the biomarker maturity parameters measured based on these compounds are shown in Table 4.5 in Appendix I. The maturity-sensitive sterane stereoisomer ratios of the Upper Cretaceous, Sirte Shale and Rachmat source rock samples based on the percentage of C_{29} ααα 20S/(20S+20R) steranes suggest that not all of the samples have reached the values corresponding to the beginning of petroleum generation, which are %20S values of approximately 40% as reported by Mackenzie *et al.* (1980). For the Sirte Shale source rock samples in the wells 6A1-59 and L1-16, the ratios of C_{29} sterane 20S/(20S+20R) and C_{29} sterane αββ/(αββ+ααβ) ranged from 0.26 to 0.32 and 0.27 and 0.36, respectively, indicating immaturity to early mature. In the wells B1-NC74F, B2-NC74A, C2-16, FF14-6, L1-17, and Z1-11, these ratios range from 0.31 to 0.70 and 0.32 to 0.59, respectively, indicating the early to middle maturity. Although most of the source rock samples analysed had reached the equilibrium stage (of 0.50-0.55) for the C_{29} sterane 20S/(20S+20R) ratio. Whereas are not reached the equilibrium stage (of 0.67-0.71) for the αββ/(αββ+ααβ) sterane ratios, which may be due to the latter ratio being somewhat slower to reach equilibrium than 20S/(20S+20R)

ratio (Seifert and Moldowan, 1986), as shown in Figure 4.56. In addition to, the αββ/(αββ+ααβ) sterane ratios appears to be independent of source organic matter input (Peters, 2005b). The variations between both ratios may also be attributed to the different heating rates in the subsurface within source rocks, (e.g Mackenzie and McKenzie, 1983) or different levels of clay catalysis (e.g. Huang *et al.*, 1990).

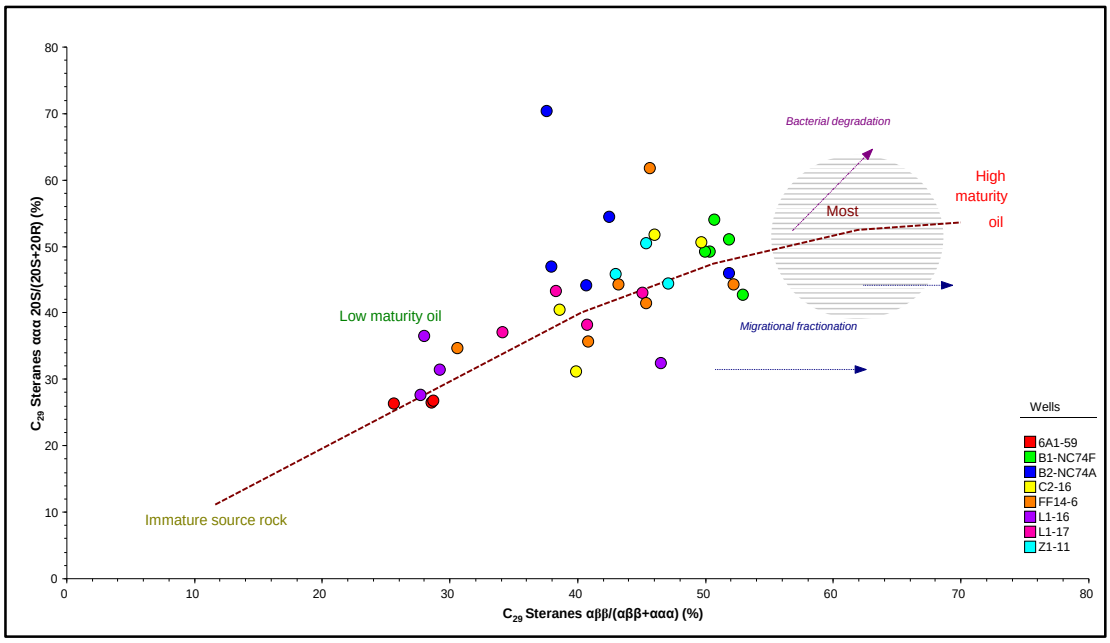

Figure 4.56: Cross plot of the C_{29} ααα 20S/(20S+20R) versus C29 ββ/(ββ+αα) steranes from the Upper Cretaceous source rocks in the Sirt Basin. Interpretation fields are from pIGI software.

In the Sirte Shale and Rachmat source rock samples, the triterpane T_S/(Ts+Tm) ratios ranged from 0.36 to 0.45 for wells B1-NC74F and 6A1-59, between 0.47 and 0.71 in wells B2-NC74, FF14-6, L1-16 and Z1-1, and from 0.73 to 0.83 at the C2-16 well (Table 4.6 in Appendix I), indicating that most of the samples are within early to middle mature zone (e.g. Moldowan *et al.*, 1986; Peters and Moldowan, 1993; Peters, 2005b). The C_{29}Ts/(C_{29}Ts+C_{29} Tm αβ) hopane ratio ranged from 0.17 to 0.42 for the wells 6A1-59, B1-NC74F, B2-NC74A and L1-16, suggesting an immature to early mature stage of hydrocarbon generation, but in the wells C2-16 and L1-17, the ratios increased in the range 0.33 to 0.61, indicating the early to middle mature stage (e.g. Moldowan *et al.*, 1986; Peters and Moldowan, 1993; Peters, 2005b). In well FF14-6 these ratios were lower (in the range of 0.19 to 0.34), suggesting they were immature zone, but this does not reflect the actual thermal maturity for this well, because it is situated in a higher

thermal maturity part of the basin as shown by vitrinite reflectance data 1.50 Ro% and SCI data 8.5 (Table 4.2 in Appendix I). Therefore, these samples may have been affected by facies changes, or had lower biomarker concentrations with anomalous distributions due to exposure to a high level of thermal maturity as shown in Figure 4.57. This suggests that this ratio cannot be used to accurately assess maturity for these samples.

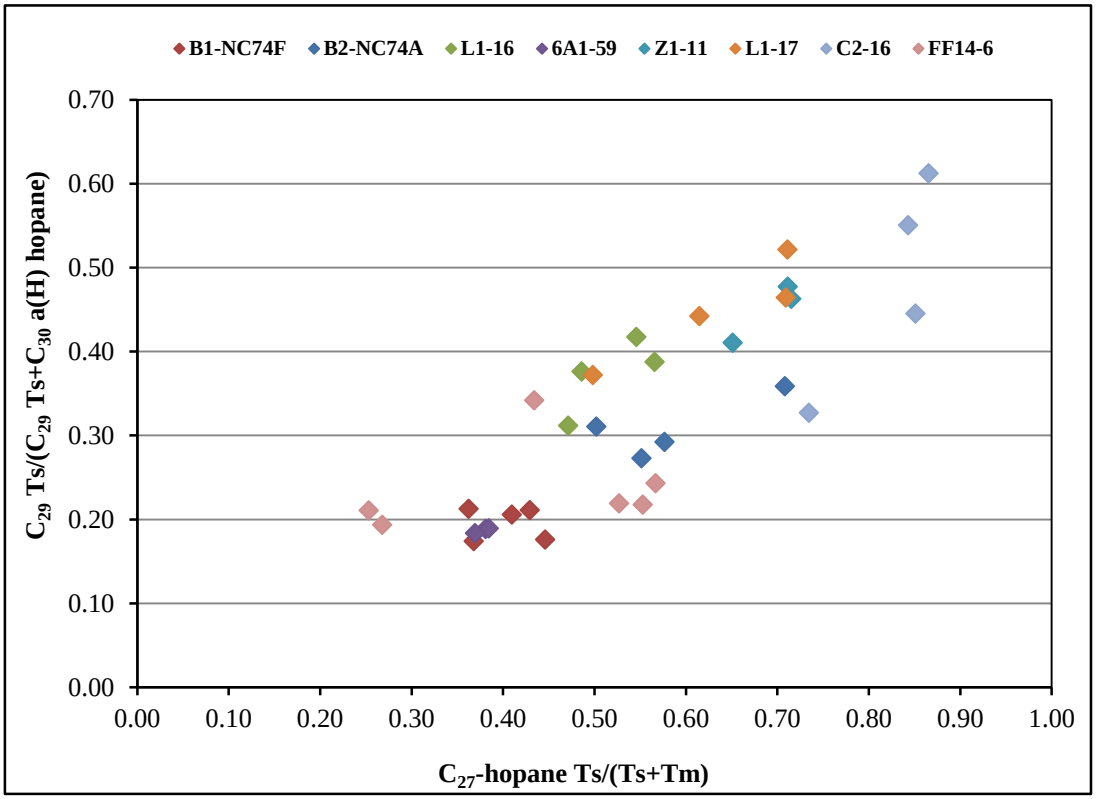

Figure 4.57: Cross plot of C_{27} Ts/(Ts+Tm) hopane versus C_{29} Ts/(C_{29} TS+C_{29} αβ Tm) for the Upper Cretaceous source rocks analysed.

The Sirte Shale and Rachmat formations have C_{30} 17α(H) diahopane/(C_{30} 17α(H) diahopane+C_{30} 17α(H) hopane) ratios in the range of 0.03 to 0.13 for the wells 6A1-59, B1-NC74F, B2-NC74A, and L1-16, suggesting an immature to early mature zone for petroleum generation (e.g. Cornford *et al.*, 1988). The ratios are slightly higher from 0.13 to 0.49, for the wells C2-16, L1-17, Z1-11, indicating an early to middle mature zone, whereas the ratio decreases in the range of 0.04 to 0.12 at the well FF14-6, suggesting an immature stage for hydrocarbon generation; but again this does not appear to reflect its real thermal maturity, as discussed above. The Upper Cretaceous source rocks showed moderate to high values of the mortane/hopane ratio (0.07 to 0.15)

with some between 0.17 and 0.25, indicating an early to middle mature zone for the FF14-6 (12290 and 12330 feet) samples (e.g. Mackenzie *et al.*, 1980; Seifert and Moldowan, 1980). The higher ratios at wells C2-16 may have been affected by organic facies changes or much higher maturity. The ratio of [C_{32} 17α,21β homohopane (22S)]/[C_{32} 17α,21β homohopane (22S)+ C_{32} 17α,21β homohopane (22R)] increases from 0 to 0.60 during maturation, and equilibrium occurs between 0.57 and 0.62 (e.g. Seifert and Moldowan, 1978; Mackenzie *et al.*, 1981; Mackenzie, 1984; Peters and Cassa, 1994; Zhang *et al.*, 2000; Peters, 2005b). Most of the Upper Cretaceous source rock samples analysed had reached this equilibrium stage, showing values between 0.57 and 0.68, indicating that the early phase of oil generation had been reached.

4.9.2 Aromatic Compounds

4.9.2.1 Aromatic Steroids Hydrocarbons

The distribution of C-ring monoaromatic steroid (MAS) and ABC-ring triaromatic steroid (TAS) hydrocarbons in the Upper Cretaceous source rock samples were monitored using the m/z 253 and 231 fragmentations as shown in Figures 4.45 and 4.46, respectively. The abundance ratios of the short-chain to long-chain components have generally been used as maturity indicators. The mass chromatograms in Figures 4.44 and 4.47 show clear differences in the distribution patterns of monoaromatic and triaromatic steroid hydrocarbons for the wells studied. In wells C2-16, FF14-6 and Z1-11 the chromatogram noise level is high and the concentrations of monoaromatic steroids are very low, which indicates a high level of maturity and that any monoaromatic steroids have been cracked. The monoaromatic steroid hydrocarbon components are difficult to identify in some source rock sample extracts from the wells C2-16 and FF14-6 due to the high level of maturation indicating that the complete aromatization of C-ring monoaromatic to ABC-ring triaromatic steroid hydrocarbons had occurred, but this was not noticed in other studied wells.

Figure 4.58 shows the cross plot of the MA(I)/MA (I+II) versus TA(I)/TA(I+II) ratios. From this it is clear that the complete aromatization of C-ring monoaromatic to ABC-ring triaromatic steroids in the Sirte Shale Formation has not occurred in the wells 6A1-59, L1-16, and L1-17, suggesting an immature to early mature stage of petroleum

generation (e.g. Seifert and Moldowan, 1978; Seifert and Moldowan, 1986; Peters, 2005b). However, in the wells B1-NC74F, B2-NC74A, C2-16, FF14-6, and Z1-11, aromatization had occurred in the Sirte Shale and Rachmat formations, suggesting a middle to late mature stage of hydrocarbon generation. These maturity observations confirm that the Sirte Shale and Rachmat source rock strata situated towards the northeast of the Sirt Basin are in the middle to late mature stage compared to the Sirte Shale source rocks located towards the southwest of the Sirt Basin. This is in agreement with the T*max*, measured vitrinite reflectance, and spore colour indices discussed earlier in this chapter.

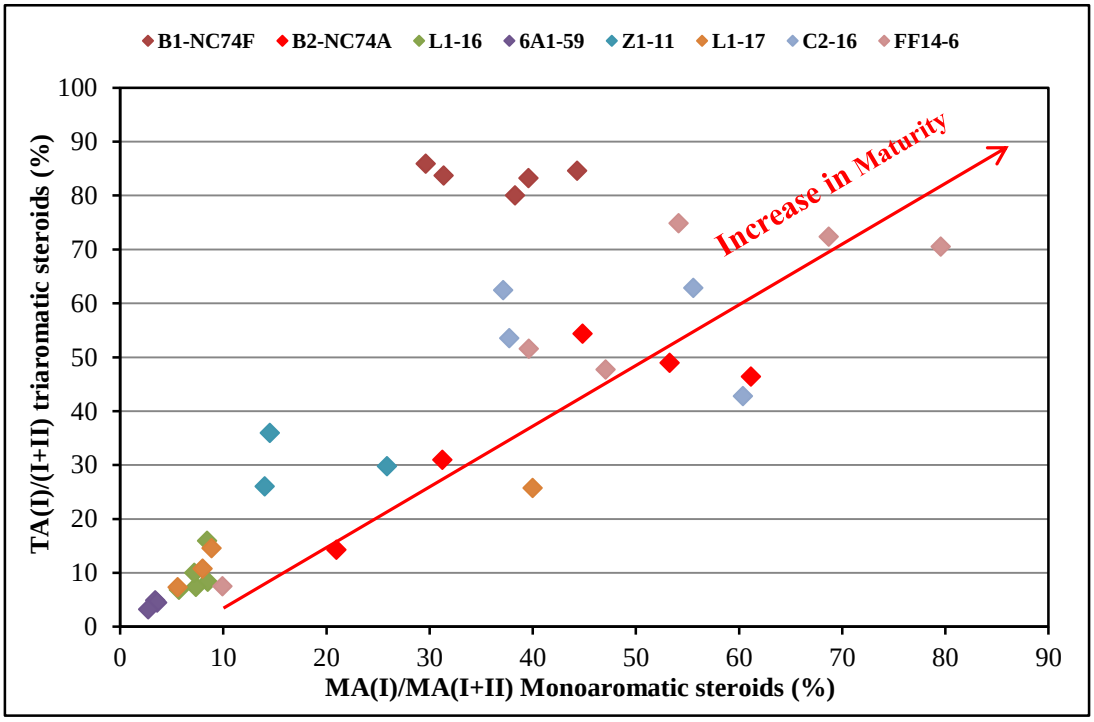

Figure 4.58: Cross plot of the monoaromatic steroids MA(I)/(I+II) versus triaromatic steroids TA(I)/TA(I+II) for the analysed Upper Cretaceous source rocks.

4.9.2.2 Alkylnaphthalenes

Assessment of the thermal maturity of the Upper Cretaceous source rock samples was conducted using many of the alkylnaphthalene maturity ratios listed in Table 4.3.

The relative distributions of C_0-C_4 alkylnaphthalenes in the Upper Cretaceous source rocks are displayed in Figure 4.50, while differences in the concentrations of the alkylnaphthalenes are shown in Figure 4.49. The concentrations and maturity-

indicating ratios of the alkylnaphthalene compounds for all samples analysed are listed in Table 4.7 in Appendix I. Figure 4.59 shows the 2-MN/1-MN versus (2,6-DMN+2,7-DMN)/(1,5-DMN) cross plot for the Sirte Shale and Rachmat source rock samples, where both ratios increase with increasing thermal maturity, and it is clear from the chart that the Sirt Shale source rocks at the wells B1-NC74F, FF14-6 and C2-16 are more mature. This is reflected in the high concentrations of varying alkylnaphthalene components relative to the Sirte Shale source rock samples from other wells studied.

Table 4-3: Maturity parameters based on alkylnaphthalene components.

Abbreviati	Defination	Substiution patttern	Reference
MNR	2-MN/1-MN	β/α	Radke et al., (1982b)
DNR-1	(2,6-DMN + 2,7-DMN)/1,5-DMN	(ββ + αα)/αα	Radke et al., (1982b)
TNR-1	2,3,6-TMN(1,4,6-TMN + 1,3,5-TMN)	(βββ/ααβ+αβα)	Alexander et al., (1985)
TNR-2	(1,3,7-TMN + 2,3,6-TMN)/(1,3,5-TMN + 1,3,6-TMN + 1,4,6-TMN)	(αββ+βββ)/(αββ+αα)	Radke et al., (1986)
TMNR	1,3,7-TMN/(1,3,7-TMN + 1,2,5-TMN)	αββ/(αββ+αβα)	van Arsen et al., (1999)
TeNR	2,3,6-TMN/1,2,3,6-TeMN	ββββ/αβββ	van Arsen et al., (1999)
TeMNR	1,3,6,7-TeMN/(1,2,5,6-TeMN + 1,2,3,5-TeMN)	αβββ/(αβαβ+αββα)	van Arsen et al., (1999)

MNR = methylnaphthalene ratio

DNR = dimethylnaphthalene ratio

TNR = trimethylnaphthalene rtio

TMNR = trimethylnaphthalene ratio

TeMNR = tetramethylnaphthalene ratio

4.9.2.3 Alkylphenanthrenes

The values of the methylphenanthrene index MPI-1 of the Upper Cretaceous source rock samples analysed ranged from 0.40 to 0.81, and the values of calculated vitrinite reflectance (%*Rc*) ranged between 0.64 to 0.89%, indicating that the Sirte Shale and Rachmat source rocks are in the early to middle mature zone for hydrocarbon generation (c.f. Radke, 1987). This is in agreement with the results from other maturity parameters.

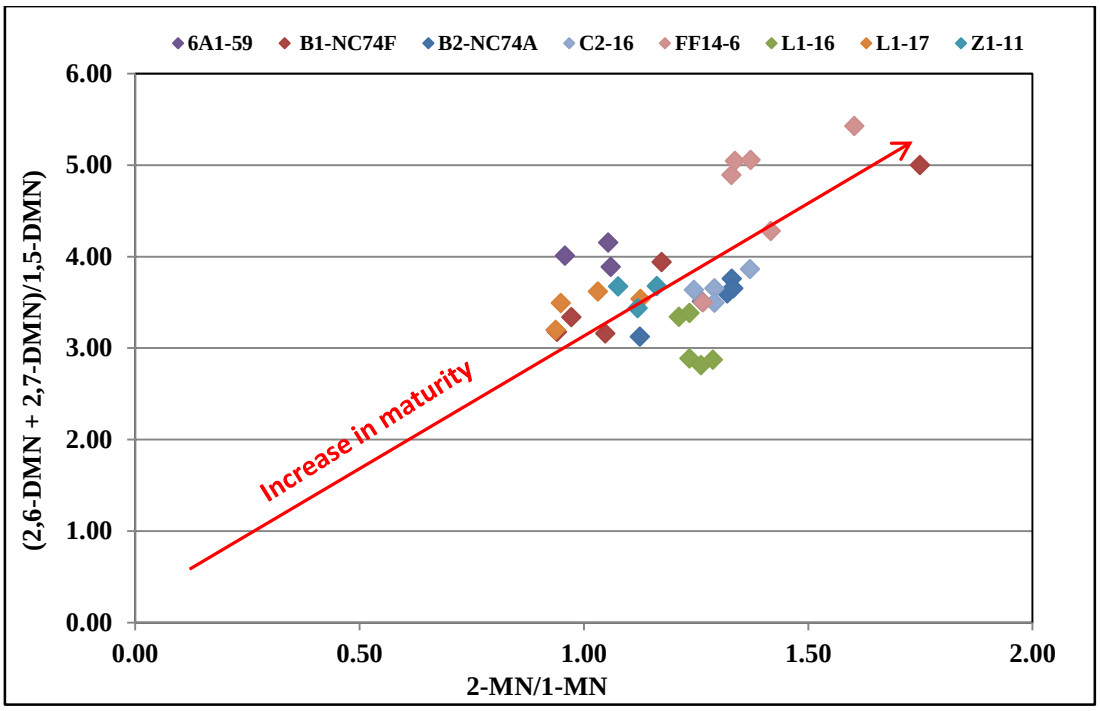

Figure 4.59: Cross plot of the 2-MN/1-MN versus 2,6-DMN+2,7-DMN)/(1,5-DMN) for the Sirte Shale and Rachmat source rocks.

4.10 *n*-Alkane Carbon Isotopic Composition of the Source Rock

The stable carbon isotopic compositions of *n*-alkanes (*n*-C_{14} to *n*-C_{31}) were measured using GC-MS-IRMS for 10 source rock samples. The $\delta^{13}C$ values are plotted in Figure 4.60, which clearly shows that the values from the Sirte Shale and Rachmat source rocks cover a broad range between -38.3 and -26.5‰. The profile of $\delta^{13}C$ values of *n*-alkanes from the source rocks samples studied show similar trends for most of the samples analysed, except for well L1-16 where variations are observed in the $\delta^{13}C$ isotope values in *n*-C_{18}, while their values after the *n*-C_{19} are more similar. This anomalous *n*-C_{18} $\delta^{13}C$ value may be due to the co-elution of phytane with *n*-C_{18}. However, for other studied wells, the profile show that *n*-C_{17} and *n*-C_{18} partially coelute with other compounds (probably pristane and phytane, respectively). From the characteristics of the carbon isotope versus carbon number slope profile, most of the source rock samples analysed appear with a nearly flat profile that is generally associated with the characteristics of $\delta^{13}C$ expelled from sources rich in marine organic matter input with some algae contribution (Murray *et al.*, 1994). This flat profile may be produced by homogeneity in the *n*-alkanes $\delta^{13}C$ distribution that is thought to be as a result of the derivation of organic carbon from a closely uniform carbon pool. Under

such circumstances there is typically few an isotopic difference between long and short chain alkanes (Murray *et al.*, 1994). This similarity in the isotope profiles of most of the Sirte Shale and Rachmat source rock samples analysed may reflect the origin of organic source facies rich in marine organic matter, which has been inferred from the molecular biomarker analyses. The profile of $\delta^{13}C$ values of *n*-alkanes from the wells 6A1-59 and C2-16 shows depletion in the $\delta\ ^{13}C$ isotope from *n*-C_{27} to *n*-C_{32}, which may due to production of isotopically lighter compounds from the source rock. This data for the Sirte Shale and Rachmat source rock sample extracts are presented in Table 4.4. For the well C2-16, the Sirte Shale source rock extracts show a trend toward isotopically lighter values with increasing *n*-alkanes chain length (negative slope) with an isotopic range being typically 3-4‰. This feature may indicate some contribution of the terrestrial organic matter (Bjorøy *et al.*, 1991; Clayton, 1991; Hayes, 1993; Clayton and Bjorøy, 1994; Dawson *et al.*, 2007). The similarity in the isotope profiles of source rock extract samples analysed from the wells 6A1-59, B1-NC74F, C2-16 and FF14-6 may reflect an origin of organic source facies rich in marine organic matter, which has been inferred from the molecular biomarker analyses, as shown in Figure 4.61. The Sirte Shale source rock samples from L1-16 seem to be completely different isotopically compared with the other source rock samples, and they contain the lightest (most negative $\delta^{13}C$) isotope values (as shown in Figure 4.62), which may be consistent with the marine source content, with moderate to high contributions of terrestrial organic matter input. The Sirte Shale source rock from the well B2-NC74A showed higher (isotopically heavier) values of $\delta^{13}C$, suggests marine sources with high contribution of algal organic matter input. But this interpretation is opposite of what Aboglila (2011) have reported that the more negative ^{13}C values are consistent with marine source, whereas the more positive values are indicative of a terrestrial contribution in the eastern Sirt Basin. From *n*-C_{19} to *n*-C_{24} a slight trend toward isotopically lighter values was found with increasing *n*-alkanes carbon chain length, with $\delta^{13}C$ values varying from 0.80‰ to 2.5‰, and also showing a slight negative slope in this range, suggesting that terrestrial organic matter input is predominant in these extracts organic matter samples. Isotope values with *n*-C_{14} to *n*-C_{18} being isotopically heavier than *n*-C_{19} + *n*-alkanes are maybe due to the maturity influence of the source rock. The less mature organic extracts tend to have isotopically lighter *n*-C_{14} to *n*-C_{18}, for instance L1-16 well compare to other studied wells or that has been sourced

differently. It is clear from the slight difference in the isotopic composition of the *n*-alkanes in the wells studied can be attributed to slight variations in the organic facies and depositional environment, as well as maturity effects. This is also indicated by the previous analyses such as *n*-alkanes and isoprenoid distributions and saturated and aromatic hydrocarbon distributions.

Table 4-4: Compound specific isotopic analyses $\delta^{13}C$ values for n-alkanes of the Sirte Shale and Rachmat source rocks.

Well Name	**6A1-59**	**B1-NC74F**	**B1-NC74F**	**B1-NC74F**	**B2-NC74A**	**C2-16**	**FF14-6**	**FF14-6**	**FF14-6**	**L1-16**
Depth Feet	**7250**	**7050**	**7190**	**7940**	**9570**	**9800**	**11290**	**11320**	**11650**	**7530**
Source Rock		**Sirte Shale**		**Rachmale**			**Sirte Shale**			
n-C_{14}								-30.7		-28.8
n-C_{15}	-30.2	-29.6		-29.1		-29.8	-28.5	-28.2		-31.8
n-C_{16}	-30.1	-29.4	-29.2	-29.2		-28.9	-29.5	-28.8	-29.1	-32.3
n-C_{17}	-31.4	-29.2	-29.8	-30	-30.3	-30.4	-30.9	-30.9	-30.1	-33.5
n-C_{18}	-29.4	-30	-29.7	-26.2	-25.9	-31.4	-26.9	-29.7	-30.3	-38.3
n-C_{19}	-30.8	-32.6	-34.2	-31.6	-29.2	-34.2	-33	-33.9	-31	-35.5
n-C_{20}	-31.7	-33.2	-35.3	-31.9	-29.1	-32.9	-32.7	-33.9	-32.1	-33.9
n-C_{21}	-30.8	-34.1	-35.4	-31.4	-28.3	-32.4	-33.1	-32.1	-32.8	-31.9
n-C_{22}	-30.9	-33.4	-34.1	-29.9		-32.6	-32.7	-32.1	-33.5	-34
n-C_{23}	-31.3	-32.9	-33			-32.6	-32	-32.4	-33.1	-32.8
n-C_{24}	-30.9	-30.1				-32.6	-32	-32	-32.7	-33.1
n-C_{25}	-30					-32.3	-30.9		-30.8	-32.7
n-C_{26}	-30.3					-31.8	-30.4		-30.2	
n-C_{27}	-29.4					-31.9	-31.9		-30.6	
n-C_{28}	-31.8					-33.3				
n-C_{29}						-33.4				
n-C_{30}						-34.3				
n-C_{31}						-35.2				

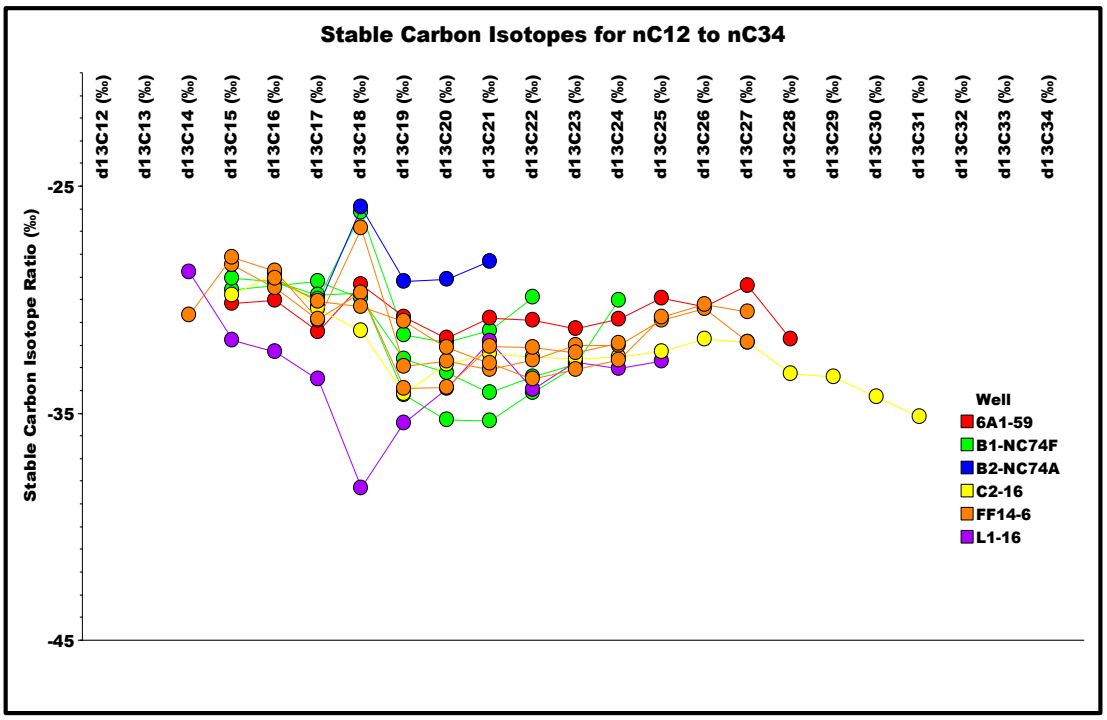

Figure 4.60: *n*-Alkane stable carbon isotope plot for the Sirte Shale and Rachmat samples.

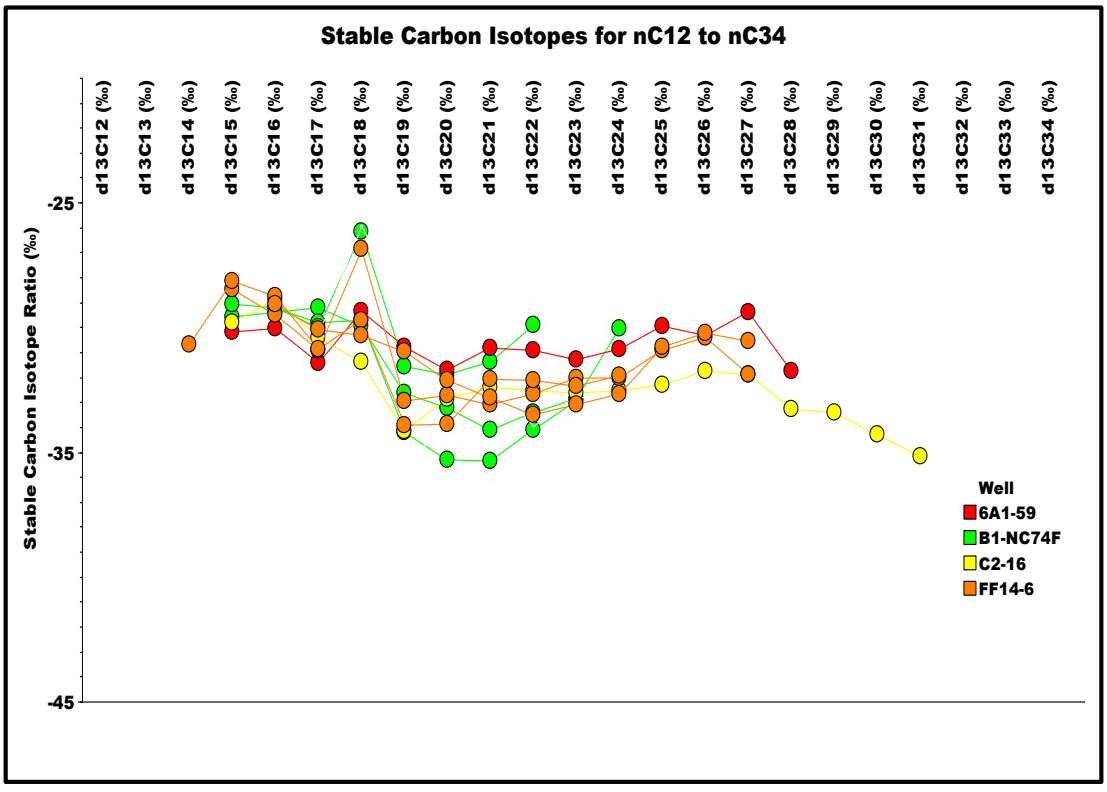

Figure 4.61: *n*-alkane stable carbon isotope plot for the Sirte Shale and Rachmat samples.

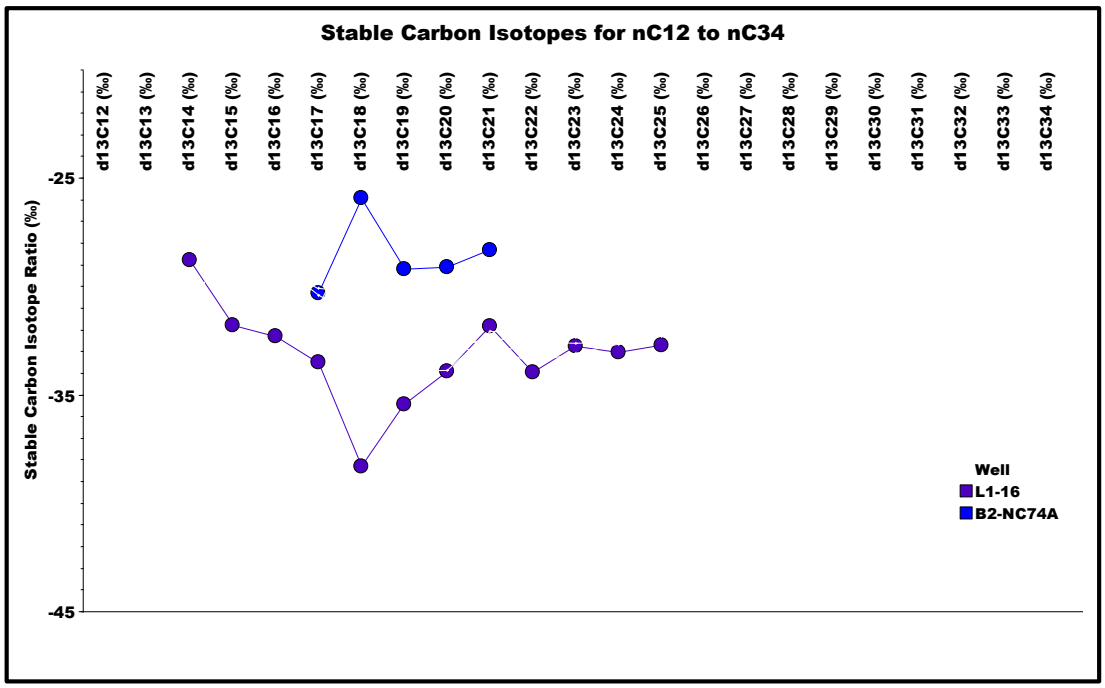

Figure 4.62: *n*-alkane stable carbon isotope plot for the Sirte Shale and Rachmat samples.

4.11 Summary

The Sirte Shale and Rachmat formations are considered to be the major petroleum source rocks in the Sirt Basin (Hamyani *et al.*, 1984; El-Alami *et al.*, 1989; Baird *et al.*, 1996; Gumati *et al.*, 1996; Ben Ashour, 2000; Hallett, 2002; Burwood *et al.*, 2003). Several organic geochemical analyses have been conducted on a set of cuttings rock samples from the central and western part of the Sirt Basin. The palaeoenvironment of deposition has been determined using total organic carbon (TOC) analyses, Rock-Eval pyrolysis, organic petrography, molecular biomarker ratios, and compound specific carbon isotope analyses of *n*-alkanes from the primary source rocks in the basin.

The dark grey, brown, and black shales of the Kalash Formation are in the early mature stage and have TOC values in the range of 3.04 to 3.81% with an average of 3.42%, which represent good source rock potential. Their Type II kerogen is dominated by yellow to orange fluorescent amorphous marine organic matter. In spite of the high TOC and good kerogen preservation, no significant hydrocarbon generation can be anticipated from this formation at the current low level of thermal maturity in the wells studied.

The Sirte Shale source rock samples of the Upper Cretaceous sequence are found to vary in their organic carbon richness due to changes in the organic facies and/or diluted by a clay mineral matrix. The Sirte Shale source rock samples exhibited fair, good to extremely rich organic matter contents, represented by TOC values in the range of 0.50 to 6.73% with a mean value of 1.41%. The medium dark grey, dark grey to brown and black shale of the Sirte Shale Formation samples are in the early or middle to late mature stages, and have fair to excellent source rock potential. Their Type II to II-III kerogen is dominated by yellow-orange, dull orange to brown fluorescent amorphous organic matter, which is sometimes non-fluorescent at higher maturity levels, and with minor contributions of phytoclast material. It has produced a significant amount of hydrocarbons, particularly oil and with some gas.

The dark grey to black shale of the Rachmat Formation is in the middle mature stage, and has a TOC content ranging between 1.05 to 1.90% with an average of 1.36%, which is rated as having good source rock potential. Their Type II kerogen is dominated by yellow-orange to dull orange fluorescent amorphous organic matter with a minor contribution of terrestrial organic matter. This is in agreement with the results of earlier studies (e.g. El-Alami *et al.*, 1989; El-Alami, 1996; Ben Ashour, 2000), that stated that the Sirte Shale and Rachmat formations are the principal source for most of the oil discovered so far in the Sirt Basin. This has probably produced significant amounts of both oil and gas based on their richness as well as maturity.

The maturity assessment of source rock samples based on the T*max*, production indices, spore colour index, and vitrinite reflectance measurement values for the Upper Cretaceous sedimentary section show that the samples analysed are in the early mature, middle to late mature stage. Vitrinite reflectance measurements show that the Kalash Formation is marginally mature for hydrocarbon generation, while the Sirte Shale and Rachmat formations are of varying thermal maturity throughout the basin depending on their situation. Towards the west part of the basin, they are in the early to middle mature stage, while in the middle to late mature toward in the northeast and central parts of the basin. Furthermore, both formations are in the main oil window, but at higher levels of maturity, they are in the gas to condensate windows.

Maturity evaluation of the source rock samples using biomarkers and aromatic hydrocarbon distributions shows a range of maturity levels in the Kalash, Sirte Shale and Rachmat source rock samples. These ratios for the Kalash, Sirte Shale and Rachmat source rock samples show estimated vitrinite reflectance (%*Rc*) values ranging from 0.64 to 0.89%, suggesting that these source rock samples are in the early to middle mature zone for hydrocarbon generation. This is an agreement with the values of other maturity parameters such as the Rock-Eval pyrolysis T*max*, spore colour indices and vitrinite reflectance measurements at lower to middle maturity levels, but at higher maturity levels these ratios are not in agreement with other parameters, particularly at the Wadayat Trough and Marada Trough in the northeast and central part of the Sirt Basin.

Normal alkanes of most of the extracts from the source rock samples show a predominance of short-chain hydrocarbons over long-chain hydrocarbons, corresponding to the early to middle mature stage generally seen with a Type II to Type II-III kerogen of marine origin (Didyk *et al.*, 1978; Tissot and Welte, 1984; Hunt, 1995; Peters, 2005b; Killops and Killops, 2009). The pristane to phytane ratio is low to moderate in most source rock samples, suggesting that the sediments were deposited in mixed dysoxic to anoxic conditions. The higher values of Pr/Ph measured in some samples may be due to the influence of maturity on the ratio or might indicate a more clay rich rock. The Pr/*n*-C_{17} and Ph/*n*-C_{18} ratios, suggest that source rock samples originated from Type II mixed marine and terrestrial to marine organic matter deposited in reducing environments.

Most of the Upper Cretaceous source rock samples show a predominance of C_{27} over C_{29} steranes, suggesting a mainly marine source input. The source rock samples had moderate to high contents of diasteranes consistent with clay-rich source rocks. The Upper Cretaceous source rock samples can be separated into two main groups with regard to sterane and triterpane distributions. Group I contain samples from wells 6A1-59, L1-16 and L1-17 and is characterised by the occurrence of low to moderately abundant hopanes relative to regular steranes, suggesting higher input from eukaryotic versus prokaryotic organisms, and this may be due to the better preservation of steroid compounds in a highly anoxic depositional environment. There is also a relatively low

abundance of extended tricyclic terpanes from C_{29} to C_{30}, with no occurrence of the extended C_{32} to C_{35} tricyclic terpanes, and a moderate to high abundance of the C_{24} tetracyclic terpanes compared with the C_{26} tricyclic terpanes. In addition, they have high C_{29} αβ relative to C_{29} Ts and C_{30} α(H) diahopane, and also high C_{30} α(H) hopane relative to C_{30} α(H) diahopane, as well as high pentacyclic terpanes relative to tricyclic terpanes.

Group II consists of samples from wells B1-NC74F; B2-NC74A; C2-16; FF14-6; L1-17; and Z1-11. Most of these samples have low to moderate TOC contents and Rock Eval petroleum yields. They are characterized by high tricyclic terpanes relative to pentacyclic terpane, and by the occurrence of low to moderately abundant hopanes relative to regular sterane, suggesting moderate input from eukaryotic versus prokaryotic organisms, and this may be due to the moderate to better preservation of steroid compounds in a suboxic to anoxic depositional environment. There is also a low abundance of extended tricyclic terpanes from C_{29} to C_{30}, and no occurrence of the extended C_{32} to C_{35} tricyclic terpanes. There is a moderate to high abundance of the C_{24} tetracyclic terpanes compared with the C_{26} tricyclic terpanes, with high C_{29} αβ relative to C_{29} Ts and C_{30} α(H) diahopane, and also high C_{30} α(H) hopane relative to C_{30} α(H) diahopane. In addition, this group has a similar to slightly higher relative abundance of Ts over Tm, moderate to high abundance of diasteranes relative to regular steranes, and within the steranes C_{27} βα diasterane S+R and C_{29} βα S are more abundant.

Facies characterisation of the source rock samples using principal component analysis and biomarker ratios were used to separate the Upper Cretaceous source rock samples into three groups. Group A contains three samples from well 6A1-59, and group B contains two samples from well B2-NC74A, three from well L1-16, and three from well L1-17. Group C contains three samples from well B2-NC74A, one from well L1-16, one from well L1-17, four from well C2-16, four from well FF14-6, and four more from well Z1-11.

The similarity in the isotope profiles of most of the Sirte Shale and Rachmat source rock samples analysed may reflect the origin of organic source facies rich in marine organic matter, which has been inferred from the molecular biomarker analyses. In

addition, the Sirte source rock samples from L1-16 seem to be different isotopically from the other source rock samples, and contain the lightest $\delta^{13}C$ isotope values, which may due to a marine source consists of higher terrestrial contributions. The Sirte Shale samples from well B2-NC74A showed heavier of $\delta^{13}C$, suggests marine sources with high contribution of algal organic matter.

Chapter 5. Oil to oil correlation

5.1 Introduction

In the present study, 51 crude oil samples were obtained from 24 oilfields across the central, western and eastern parts of the Sirt Basin (Figure 5.1). The oil samples are from various carbonate and clastic reservoir rocks ranging in age from Cretaceous to Eocene at different depths, with clastic reservoirs more common from the Cretaceous and carbonate rock reservoirs dominated by those from Tertiary times (Hamyani *et al.*, 1984; Gumati and Kanes, 1985; Gumati and Schamel, 1988; El-Alami *et al.*, 1989; Ben Ashour, 2000; Burwood *et al.*, 2003; Aboglila, 2011). Detailed organic geochemical characterizations of the samples were conducted in order to enable oil-oil correlations, the classification of oils into genetic families, definition of their thermal maturity and identification of secondary modifications. This investigation was also done to reveal information on the migration pathways of the petroleums, which in turn may lead to more effective exploration activity in the basin studied. Saturated hydrocarbon biomarker, aromatic hydrocarbon analyses and compound specific carbon isotopic analysis for *n*-alkanes were carried out using gas chromatography (GC), gas chromatography-mass spectrometry (GC-MS), and gas chromatography-isotope ratio mass spectrometry (GC-IRMS). The biomarkers in crude oil samples can be used to estimate source rock age, lithology, and depositional and redox environments during sedimentation, along with the organic matter type, quality and maturity (Dahl *et al.*, 1994). observed that the estimation of the source characteristics depends on the assumption that some compositional parameters in crude oils do not differ significantly from those in the bitumen remaining in the source rock at the time of oil expulsion. Gürgey (2003) also reported that no significant variations in oil composition occurred during migration and accumulation in the reservoir rocks.

5.2 Oil-Oil Correlation

Oil-oil or oil-source rock correlations are comparisons of chemical and physical properties of two or more oil samples or extracts source rock in order to determine whether there is a genetic relationship between those samples (Waples and Machihara, 1990). Oils and their mature source rocks often contain nearly identical biomarker

signatures (Seifert and J. M. Moldowan., 1981; Moldowan *et al.*, 1989; Fan *et al.*, 1991; Moldowan *et al.*, 1992; Peters and Moldowan, 1993; Curiale, 1994; Hunt, 1995; Baird *et al.*, 1996; Peters, 2005b; Killops and Killops, 2009) . However, because most biomarker distributions change with increasing maturity, correlations should be based on biomarker parameters that are independent of maturity (Waples and Machihara, 1990). Alternatively, any variation resulting from maturity must be excluded while making the correlations. Oil-to-oil correlations require geochemical parameters, which are mostly not altered by common geochemical processes such as biodegradation, maturation, and secondary migration (Peters and Moldowan, 1993). Correlations which depend on molecular ratios may be better because these ratios are often more resistant to secondary alteration processes (Peters, 2005b). Therefore, *n*-alkane compositions can give significant evidence about source type, depositional environment and maturity. Also the isoprenoids pristane and phytane, which are relatively resistant to the above mentioned processes, have been frequently used in oil to oil correlation (Waples, 1985; Peters and Moldowan, 1993; Hunt, 1995). In addition, saturated hydrocarbon biomarkers, aromatic hydrocarbon parameters and specific carbon isotope analysis have been widely used in oil-oil and oil-source correlations.

The oil-oil correlation method assumes that the same source rock and depositional environment will generate oils with similar geochemical characteristics. If this assumption holds, these genetically related oils can be differentiated from unrelated oils (Hunt, 1995).

In the current study, oil-oil correlations were based on the following parameters: Pr/Ph; *n*-C_{17}/Pr; *n*-C_{18}/Ph; (*n*-C_{13}+*n*-C_{14}+*n*-C_{15})/(*n*-C_{25}+*n*-C_{26}+*n*-C_{27}) and *n*-C_{17}/*n*-C_{27}. Various biomarkers and biomarker parameters were also used such as: C_{27} trisnorhopane, C_{30} hopane, C_{30} diahopane, C_{31} and C_{32} R homohopanes, C_{34} and C_{35} 22S extended hopanes, homohopane index, C_{19}-C_{26} tricyclic and C_{24} tetracyclic terpanes, C_{27}, C_{28} and C_{29} steranes, and C_{27} diasteranes, various aromatic hydrocarbon ratios, together with specific carbon isotopic compositions of the individual *n*-alkane components in the oils.

In the present study, the oils analysed are non-biodegraded based on a higher relative abundance of *n*-alkanes, pristane, phytane and the absence of 25-norhopanes and an obvious unresolved complex mixture (UCM).

5.2.1 Source Facies Characterisation and Comparison

The distribution of active oilfields in the Sirt Basin study area is shown in Figure 5.1. The western Sirt Basin oilfield includes Aswad, Fidda, Hakim, Mabruk, Sabah, Safsaf, and Zellah. Meanwhile, the central Sirt Basin oilfields include Beda, Dor Mansour, Kotla, Meghil, Nasser, Raiah, Raguba, South Jebel, and Zelten. Crude oil samples from the central and western Sirt Basin are characterized by moderate to high API gravities ranging from 38 to 42º, relatively high saturated hydrocarbon contents (38-69%), moderate to high aromatic hydrocarbons (24-55%), low to moderate resins (5-23%) and low asphaltene (0.42-6%) contents, and with varying saturated hydrocarbon to aromatic hydrocarbon ratios (0.70-2.97) as shown in Table 5.1. In contrast, the crude oil samples from the eastern Sirt Basin include the As Sarah, Augila Nafoora, Nakhla, Tuamma oilfields, and two wells from concession NC125 at the nearby Bu-Attifel oilfield, in the east Sirt Basin, oils display moderate to high API gravities ranging from of 34 to 44º, relatively higher saturated hydrocarbons (39-73%), moderate aromatic hydrocarbons (23-35%), and low resins and asphaltenes (2-18% and 1-3%, respectively).

5.2.1.1 *n*-Alkanes and Isoprenoid Alkanes

Gas chromatography data for the saturated hydrocarbon fractions from the samples analysed show almost identical smooth *n*-alkane distributions, with no indication of biodegradation being present in any of the oils as shown in Figures 5.2 and 5.3. The *n*-alkane distributions for each oilfield are characteristic with respect to their peak carbon number and percentage distributions are listed in Table 5.1. In the western and central Sirt Basin, the oil samples collected from the Mabruk, Beda, Dor Mansour, Kotla, Meghil, Nasser, Raiah, Raguba, South Jebel and Zelten oilfields display similar *n*-alkane envelopes dominated by *n*-C_{11}-*n*-C_{18} and very low amounts of *n*-C_8-*n*-C_{11} as shown in Figure 5.2. However, the oil samples from the Aswad, Hakim, Fidda, Safsaf, and Zellah oilfields show similar *n*-alkane envelopes dominated by *n*-C_8-*n*-C_{16} with a

relatively low abundance of heavier *n*-alkanes (*n*-C_{23}+). The oil samples in the east Sirt Basin show considerable differences in their compound class composition, but they show consistently similar *n*-alkane distributions. The oil samples collected from the Nakhla, NC125, and Tuamma oilfields differ from those of the Augila Nafoora and As Sarah oilfields on the basis of their carbon number distributions. The oil samples from the former three show identical *n*-alkane envelopes dominated by *n*-C_{11}-*n*-C_{21} and very low amounts of *n*-C_8-*n*-C_{10}, but contain relatively more abundant heavier *n*-alkanes (*n*-C_{23}+) than the Augila Nafoora and As Sarah oilfields. The latter oilfields also show similar *n*-alkane envelopes dominated by *n*-C_{13}-*n*-C_{21} and very low amounts of *n*-C_8-*n*-C_{11} as shown in Figure 5.2. The *n*-alkane envelopes also illustrate that the oil samples collected from the eastern Sirt Basin contain relatively more abundant heavier *n*-alkanes (*n*-C_{23}+) than those from the central and western Sirt Basin. Most of the crude oil samples show little odd over even predominance of long-chain *n*-alkanes indicated by carbon preference indices between 0.91 and 1.12. The crude oil samples from the Aswad, Beda, Dor Mansour, Hakim, Fidda, Safsaf, Sabah oilfields and the three wells in the Mabruk oilfield in the central and western Sirt Basin are considered to be lighter oils than the other oils in the study area.

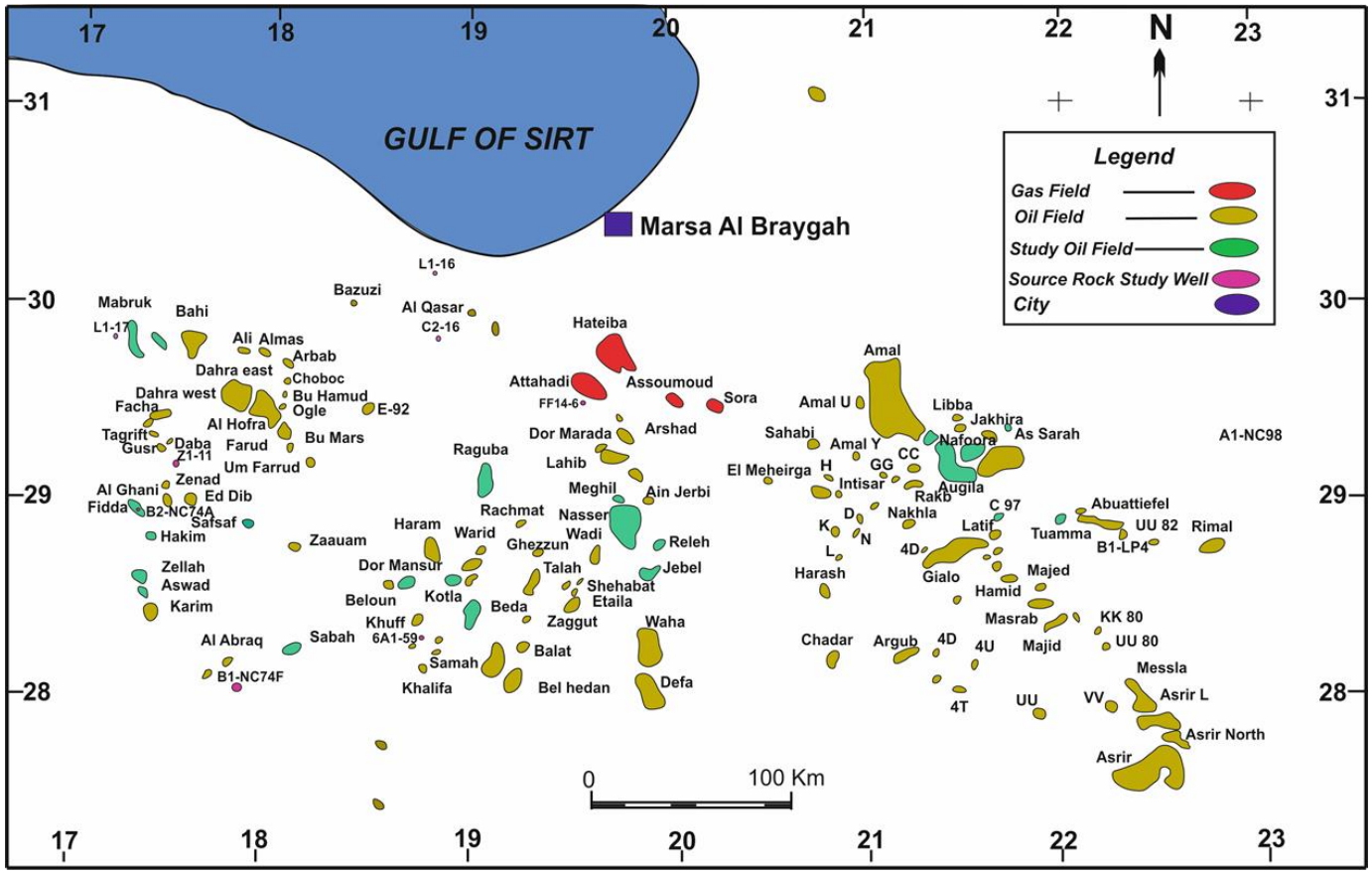

Figure 5.1: Location of the oil and gas fields in the Sirt Basin, Libya, after Weenekers et al. (1996).

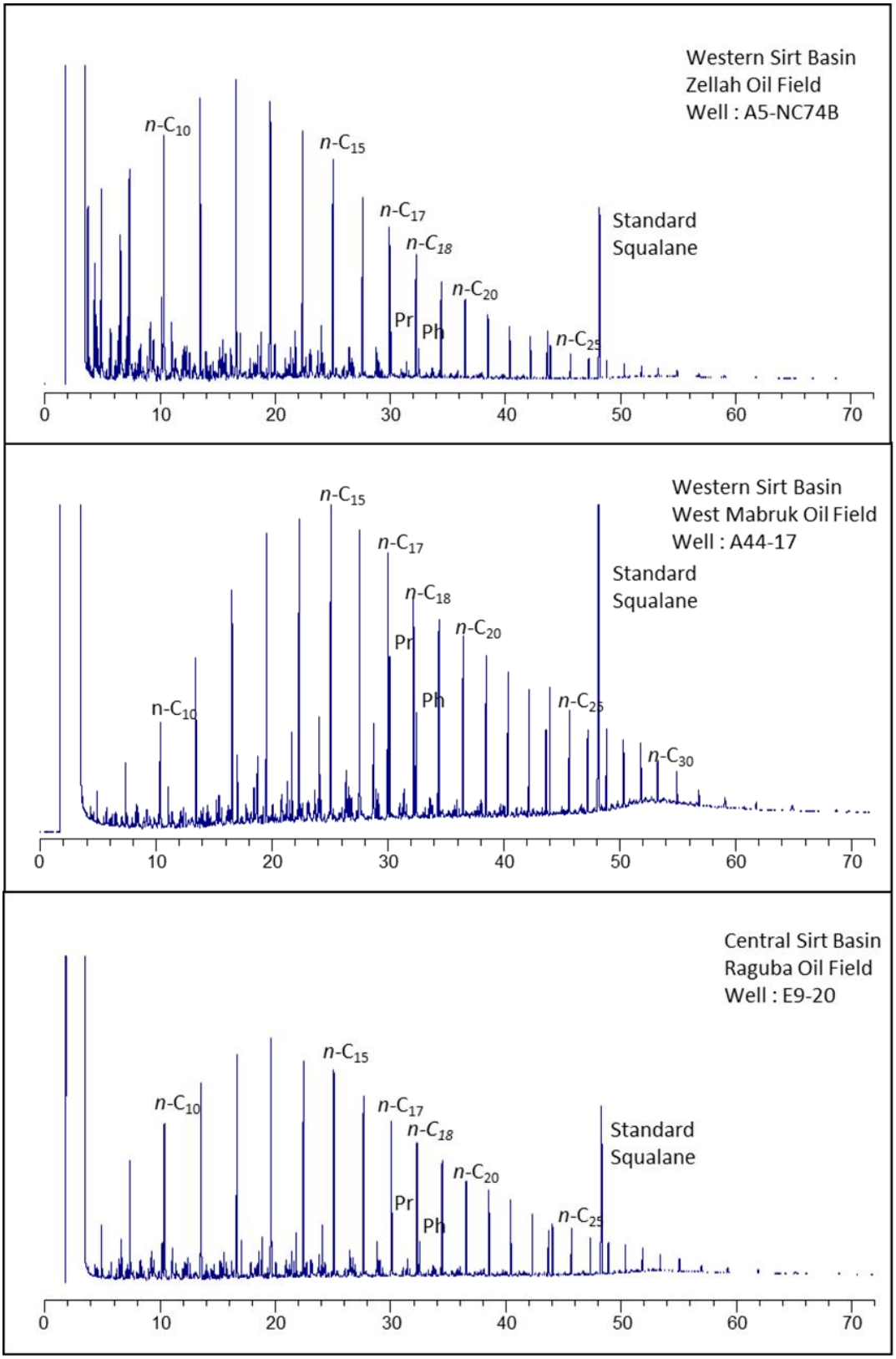

Figure 5.2: Gas chromatograms showing *n*-alkane distributions of selected oil samples representing the Raguba, West Mabruk, and Zellah oilfields in the central and western Sirt Basin.

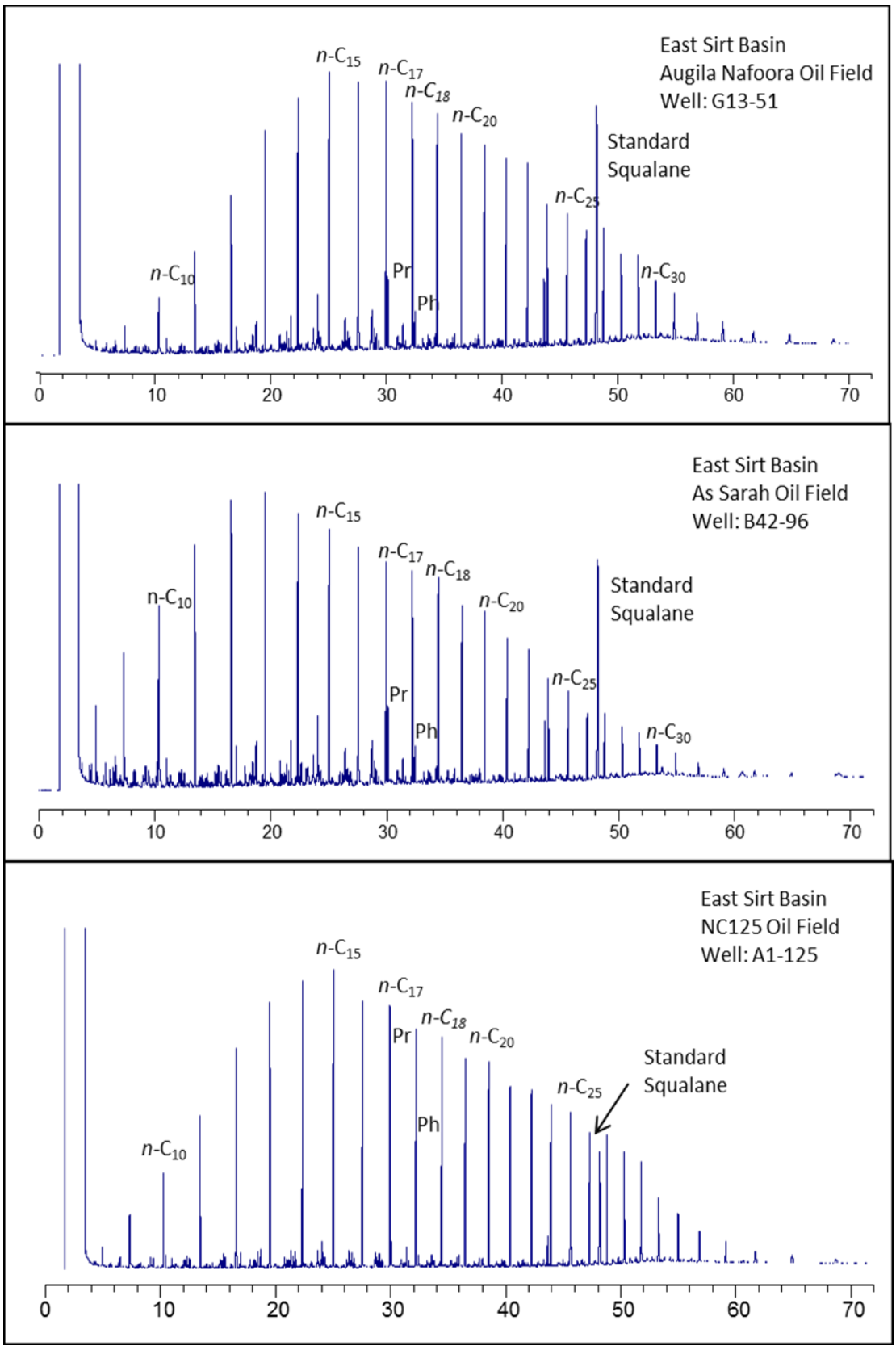

Figure 5.3: Gas Chromatograms showing *n*-alkane distributions of selected oil samples representing the Augila Nafoora, As Sarah, and NC125 oil fields in the East Sirt Basin.

This feature is expressed by the values of the *n*-C_{17}/*n*-C_{27} *n*-alkane index ratios, which have relatively high values for those oilfields ranging from 4.61 to 9.34 compared to the remaining oilfield samples that have values ranging between 1.53 and 4.60. This may be due to the higher maturity of the oil samples from these oilfields. In fact, the oil samples from Augila Nafoora, As Sarah, Nakhla, NC125 and Tuamma in the east Sirt Basin are revealed to have lower *n*-alkane index ratios as a result of a higher abundance of the heavier *n*-alkanes in the Sirte Shale, Rachmat and Middle Nubian Shale source rocks compared to the Sirte Shale in the west and centre of the Sirt Basin (e.g. Figure 5.5, Table 5.1).

Slightly higher relative abundances of long-chain *n*-alkanes in the eastern part of the Sirt Basin are indicated by the crossplot of relative proportions of *n*-C_{15}-*n*-C_{19} versus *n*-C_{27}-*n*-C_{31} *n*-alkanes as shown in Figure 5.4, suggesting slightly higher contributions of terrigenous organic matter to the source rock composition. Consistent with this interpretation, the Pr/Ph ratios display high values in the eastern part of the basin.

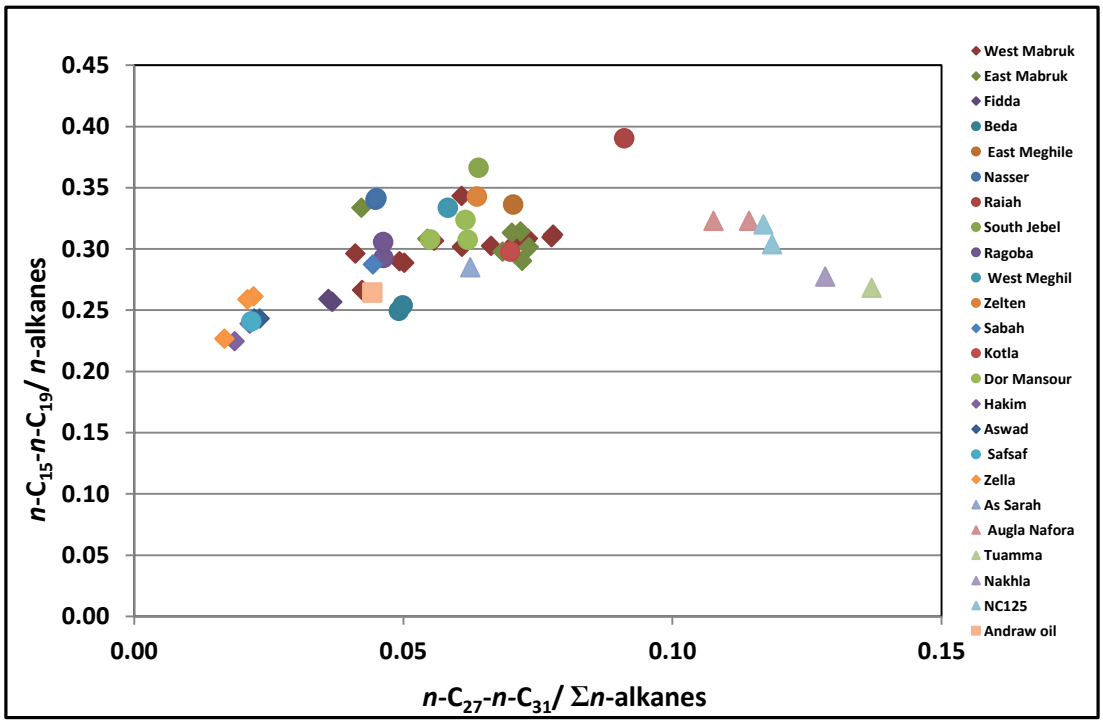

Figure 5.4: Cross plot of the *n*-C_{27}-C_{31} versus *n*-C_{15}-C_{19} *n*-alkane concentrations of the crude oils in the Sirt Basin: squares represent oils from west basin, circles oils from a centre and triangles oils from east basin.

Figure 5.5 shows the *n*-C_{17}/*n*-C_{27} ratios against the concentrations of *n*-alkanes in oils from the study area. The crude oil samples can be clearly separated into five groups: Group I contain oils from the Aswad, Hakim, Safsaf and Zellah oilfields; Group II oils from Beda, Dor Mansour, Fidda, Mabruk, Meghil, Nasser, Raiah, Raguba, Sabah, South Jebel and Zelten oilfields; Group III two wells from the west Mabruk and As Sarah oilfields; Group IV crude oils from the Augila Nafoora oilfield; and Group V including crude oil samples from the Nakhla, NC125 and Tuamma oilfields. The cross plot shows that groups I, II, III and IV have higher contributions from marine organic matter relative to groups V, but the latter has higher *n*-alkane concentrations compared to the other groups, suggesting differences in the source organic matter inputs and depositional environments as well as exposure to a higher level of maturity.

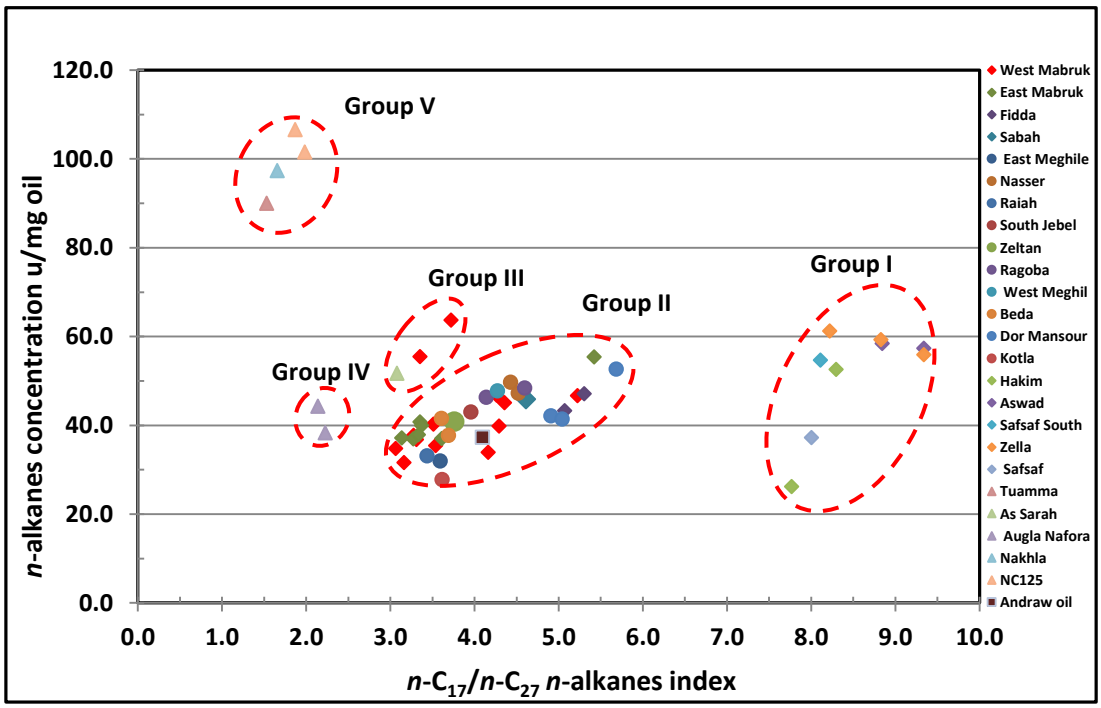

Figure 5.5: Cross plot of the *n*-alkanes index ratios versus concentrations of *n*-alkanes for the crude oils in the Sirt Basin: squares represent oils from west basin, circles oils from a centre and triangles oils from east basin.

The Pr/Ph ratios show that the crude oil samples from the Aswad, Hakim and Zellah oilfields in the Zellah Trough and Dor Mansour oilfield in the Kotla Graben have relatively similar and lower Pr/Ph ratios ranging from 1.26 to 1.46. Meanwhile, crude oils from the Mabruk and Sabah oilfields in the Zellah Trough and the Beda, Meghil, Nasser, Raiah, Raguba, South Jebel, Safsaf and Zelten oilfields in the central part of

the Sirt Basin have quite similar and have slightly higher Pr/Ph ratios ranging from 1.49 to 1.80. Whereas crude oils from the Augila Nafoora, As Sarah, Nakhla, NC125, and Tuamma oilfields in the east part of the Sirt Basin have relatively similar and even higher Pr/Ph ratios ranging from 1.85 to 2.05. The Pr/Ph ratios for all oilfields indicates that the crude oils were generated from source rocks that have nearly similar depositional environments, which were suboxic to anoxic conditions.

The Pr/*n*-C_{17} versus Ph/*n*-C_{18} diagram shown in Figure 5.6 indicates that all of the oils contain mixtures of marine and terrigenous organic matter deposited under suboxic to anoxic conditions (e.g. Peters and Moldowan, 1993; Hunt, 1995; Peters, 2005b). The mixed organic matter source input, suboxic depositional conditions and higher maturity of the source rocks of the Nakhla, NC125 and Tuamma oilfields are further supported by their relatively high Pr/Ph ratios of 1.85 to 2.05, respectively. Whereas the remaining oilfields have moderate Pr/Ph ratios ranging from 1.26 to 1.80, which may show suboxic to anoxic conditions in their source rock, depositional environments and lower levels of maturity. However, and also according to the Pr/*n*-C_{17} and Ph/*n*-C_{18} ratios, the crude oil samples can be separated into nine oil families and two subfamilies as shown in Figure 5.6 and listed in Table 5.1. Family 1A includes the Beda, Fidda, Hakim, East Meghil and Mabruk oilfields showing moderate Pr/*n*-C_{17} and Ph/*n*-C_{18} ratios ranging from 0.56 to 0.85 and 0.53 to 0.65, respectively. Family 1B contains the oils from the Nasser, Raiah, Raguba, Sabah, South Jebel, West Meghil and Zelten oilfields, showing Pr/*n*-C_{17} and Ph/*n*-C_{18} ratios ranging from 0.49 to 0.57 and 0.32 to 0.44, respectively. Family 2 includes only the oil from Kotla oilfield, which is displaying slightly higher Pr/*n*-C_{17} and Ph/*n*-C_{18} ratios of around 0.84 and 0.78, respectively. Family 3 comprises the oil from the Dor Mansour oilfield showing moderate ratios ranging from 0.27 to 0.40 and 0.31 to 0.48, respectively. Family 4 includes the oils from the Aswad, Safsaf and Zellah oilfields showing lower to moderate Pr/*n*-C_{17} and Ph/*n*-C_{18} ratios ranging from 0.29 to 0.42 and 0.30 to 0.38. Family 5 comprises oil from the As Sarah oilfield showing moderate Pr/*n*-C_{17} and Ph/*n*-C_{18} ratios of 0.42 and 0.22. Family 6 contains oil from Augila Nafoora oilfield, having ratios of 0.33 and 0.19. Oil families 7, 8 and 9 contain the oils from the NC125, Tuamma and Nakhla oilfields showing very low Pr/*n*-C_{17} and Ph/*n*-C_{18} ratios ranging from 0.09 to 0.11 and 0.05 to 0.06. These very low

ratios may indicate that the oil samples have been exposed to higher levels of thermal maturity.

Figure 5.7 displays the *n*-C_{17}/*n*-C_{27} versus Pr/Ph ratios, clearly separating the oil samples into 9 oil families and two subfamilies which agree well with the results obtained using Pr/*n*-C_{17} and Ph/*n*-C_{18} ratios, where all the oil samples are plotted in the normal oil region.

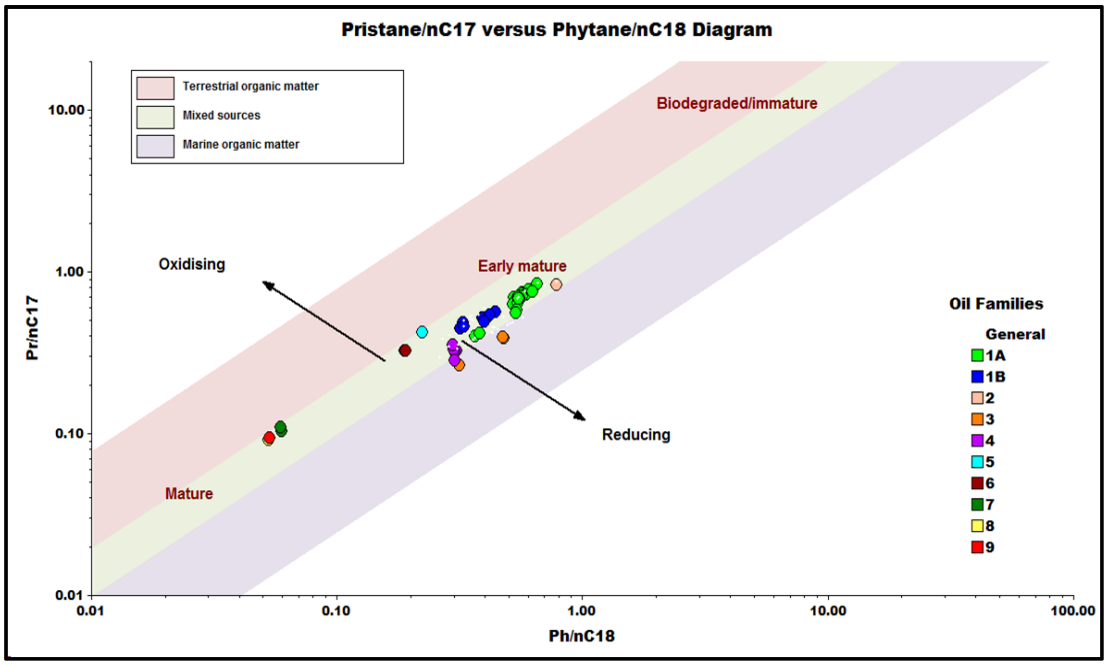

Figure 5.6: Cross plot of Pr/*n*-C_{17} versus Ph/*n*-C_{18} ratios for the crude oil samples. Interpretation fields from pIGI software.

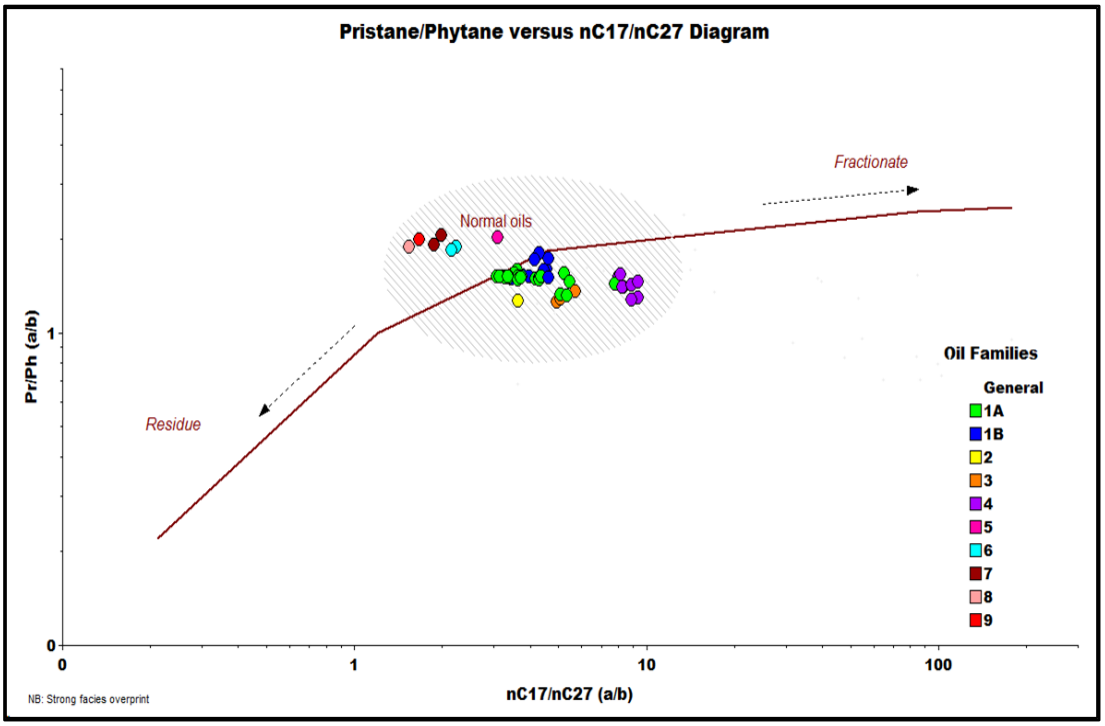

Figure 5.7: Diagram of the *n*-C_{17}/*n*-C_{27} versus Pr/Ph ratio of the oil samples from the Sirt Basin Interpretation field from pIGI software.

Table 5-1 *n*-alkane and isoprenoid data for the oil fields in the western, central and eastern Sirt Basin.

Location	Group	Oil Filed	Well Name	Pr/Ph	Pr/nC17	Ph/n-C18	nC17/nC27	Σ n-alkanes ug/mg	$C_{13}+C_{14}+C_{15}$/ $C_{25}+C_{26}+C_{27}$	Hydrocarbon percantage (%)					CPI	OER
										Sats.	Arom.	NSO	Asphlt	Sat./Arom.		
West Sirt Basin	1A	West Mabruk	A31-17	1.51	0.73	0.57	3.16	31.58	3.09	43.82	45.69	8.89	1.61	0.96	1.05	1.02
			A29-17	1.52	0.75	0.58	3.35	55.44	3.45	50.96	38.72	8.86	1.46	1.32	1.03	1.00
			A86-17	1.52	0.74	0.57	3.31	36.77	3.34	47.95	29.32	19.73	3.01	1.64	1.03	0.98
			A44-17	1.52	0.74	0.57	3.06	34.80	2.98	56.75	33.98	8.82	0.45	1.67	1.02	0.92
			A66-17	1.51	0.72	0.57	3.54	35.43	3.52	45.82	32.65	18.78	2.75	1.40	1.04	0.95
			A15-17	1.52	0.74	0.57	3.28	37.77	3.39	60.25	29.54	9.30	0.91	2.04	1.02	0.94
			M1-17	1.50	0.85	0.65	4.16	33.90	3.24	54.35	35.56	8.67	1.41	1.53	0.99	1.00
			A46-17	1.55	0.79	0.60	3.51	40.24	3.27	42.60	47.47	8.25	1.68	0.90	1.00	0.95
			A82-17	1.55	0.63	0.52	5.22	46.69	5.71	38.87	55.70	5.17	0.26	0.70	0.99	0.96
			A94-17	1.50	0.73	0.59	4.27	46.78	4.58	53.01	36.94	7.47	2.57	1.44	1.00	0.93
			A39-17	1.52	0.69	0.55	3.72	63.71	4.16	54.67	37.38	7.30	0.65	1.46	1.04	1.01
			A27-17	1.49	0.76	0.63	4.29	39.85	4.12	54.87	37.83	6.83	0.48	1.45	0.99	0.93
			A38-17	1.52	0.71	0.57	4.36	45.11	4.47	58.30	32.81	7.80	1.09	1.78	0.98	0.95
		East Mabruk	A84-17	1.52	0.71	0.55	3.61	37.02	3.79	52.78	24.51	20.13	2.57	2.15	1.07	1.40
			A101-17	1.51	0.71	0.56	3.27	36.92	3.40	51.71	22.55	23.23	2.51	2.29	1.00	1.58
			A103-17	1.52	0.71	0.55	3.13	37.16	3.44	44.21	30.28	21.53	3.98	1.46	1.07	1.00
			A58-17	1.52	0.70	0.54	3.35	40.73	3.64	43.39	39.22	15.02	2.36	1.11	1.04	0.95
			A3-17	1.50	0.70	0.54	3.37	39.99	3.50	44.42	32.48	21.26	1.84	1.37	1.03	0.97
			A7-17	1.52	0.71	0.55	3.33	37.88	3.61	47.29	32.49	18.26	1.97	1.46	1.04	0.98
			A97-17	1.46	0.64	0.54	5.42	55.37	5.44	59.01	28.62	10.02	2.35	2.06	1.03	0.98
		Fidda	B1-NC74A	1.33	0.59	0.54	5.07	43.27	5.93	56.06	38.07	5.87	0.00	1.47	1.03	0.93
			B2-NC74A	1.32	0.56	0.54	5.30	47.13	6.55	45.57	45.55	7.11	1.77	1.00	1.01	0.96
		Beda	B1-47	1.49	0.69	0.55	3.66	41.56	4.56	39.05	48.34	12.19	0.42	0.81	1.04	0.97
			B1-47	1.51	0.69	0.55	3.61	37.72	4.03	39.05	48.34	12.19	0.42	0.81	1.00	1.01
Centre Sirt Basin		East Meghile	J3-6	1.59	0.70	0.53	3.59	31.96	3.40	42.04	35.84	21.27	0.85	1.17	1.03	0.98

Cont. Table 5.1 *n*-alkane and isoprenoid data for the oil fields in the western, central and eastern Sirt Basin.

Location	Group	Oil Filed	Well Name	Pr/Ph	Pr/nC17	Ph/n-C18	nC17/nC27	Σ n-alkanes ug/mg	$C_{13}+C_{14}+C_{15}$/ $C_{25}+C_{26}+C_{27}$	Hydrocarbon percantage (%)					CPI	OER
										Sats.	Arom.	NSO	Asphlt	Sat./Arom.		
Centre Sirt Basin	1B	Nasser	C98-6	1.60	0.52	0.39	4.52	47.22	4.65	51.09	39.23	7.96	1.71	1.30	1.02	0.93
			C98-6	1.59	0.53	0.39	4.43	49.70	4.50	51.09	39.23	7.96	1.71	1.30	1.01	0.93
		Raiah	DD12-6	1.50	0.52	0.41	3.44	33.15	2.44	40.36	39.72	17.68	2.25	1.02	1.02	0.97
		South Jebel	4B1-6	1.52	0.55	0.42	3.96	43.00	3.98	42.30	44.91	11.87	0.92	0.94	1.00	0.99
		Ragoba	E9-20	1.73	0.45	0.32	4.60	48.42	5.53	55.24	35.01	5.67	4.09	1.58	1.01	0.95
			E82-20	1.71	0.46	0.33	4.14	46.31	5.50	54.09	35.84	5.61	4.46	1.51	1.17	0.96
		West Meghil	4J2-6	1.80	0.49	0.32	4.27	47.78	4.65	58.10	28.44	9.92	3.54	2.04	1.03	1.32
		Zelten	4G1-6	1.53	0.57	0.44	3.76	40.81	3.92	45.60	40.81	10.53	3.06	1.12	1.06	1.00
West Sirt Basin		Sabah	G3-NC74F	1.50	0.50	0.40	4.61	45.87	5.70	57.75	35.11	6.11	1.03	1.64	1.03	1.00
Centre Sirt Basin	2	Kotla	C46-47	1.27	0.84	0.78	3.61	27.76	3.11	44.07	37.73	13.25	4.96	1.17	1.00	0.96
Centre Sirt Basin	3	Dor Mansour	Z3-47	1.26	0.39	0.48	4.91	42.17	3.91	45.82	39.72	8.43	6.03	1.15	1.04	0.97
			Z5-47	1.28	0.40	0.47	5.04	41.40	3.94	49.99	41.58	5.18	3.25	1.20	1.02	0.97
			GG1-47	1.36	0.27	0.31	5.69	52.64	4.24	56.28	34.58	7.29	1.85	1.63	1.03	0.98
West Sirt Basin	4	Hakim	A1-NC74A	1.41	0.40	0.37	8.30	52.56	12.41	69.16	23.32	6.74	0.78	2.97	1.00	0.91
			A2-NC74A	1.43	0.42	0.38	7.77	26.22	10.31	55.06	39.14	4.75	1.04	1.41	1.04	1.00
		Aswad	B18-NC74B	1.30	0.29	0.30	9.34	57.36	11.23	64.10	31.11	4.61	0.18	2.06	0.92	1.04
			B18-NC74B	1.28	0.29	0.30	8.85	58.41	10.64	64.10	31.11	4.61	0.18	2.06	0.91	0.87
		Safsaf	C1-NC74B	1.52	0.34	0.30	8.01	37.21	11.83	64.72	26.09	7.96	1.23	2.48	0.98	0.93
		Safsaf South	D6-NC74B	1.54	0.36	0.30	8.11	54.67	12.21	59.23	29.26	8.20	3.30	2.02	1.06	0.96
		Zella	A5-NC74B	1.41	0.33	0.31	8.22	61.22	11.21	57.80	36.68	5.02	0.50	1.58	1.06	0.94
			A5-NC74B	1.43	0.32	0.30	8.83	59.30	12.19	57.80	36.68	5.02	0.50	1.58	1.03	0.94
			A28-NC74B	1.46	0.33	0.30	9.34	55.91	12.43	63.09	32.45	4.28	0.19	1.94	1.02	0.90
East Sirt Basin	5	As Sarah	B42-96	2.03	0.42	0.22	3.08	51.70	3.32	50.68	32.45	14.84	2.03	1.56	1.10	1.06
	6	Augla Nafora	G31-51	1.88	0.33	0.19	2.23	38.29	1.87	41.55	31.73	18.01	8.71	1.31	1.12	1.07
			G274-51	1.85	0.33	0.19	2.14	44.33	1.68	39.20	35.25	16.41	9.14	1.11	1.09	1.05
	7	NC125	N1-125	1.92	0.10	0.06	1.87	106.57	1.77	64.65	26.56	8.24	0.55	2.43	1.07	1.07
			A1-125	2.05	0.11	0.06	1.98	101.54	1.73	73.41	23.70	2.06	0.84	3.10	1.07	1.02
	8	Tuamma	C7-97	1.89	0.09	0.05	1.53	89.98	1.56	59.07	25.27	12.33	3.33	2.34	1.06	1.03
	9	Nakhla	G7-97	2.00	0.09	0.05	1.66	97.35	1.75	61.51	29.02	4.88	4.59	2.12	1.07	0.56

5.2.1.2 Steranes and Terpanes

The partial m/z 191 and 217 mass chromatograms of oils selected from several oilfields in the Sirt Basin showing the distribution of triterpanes (tricyclic and hopane) and steranes, respectively, are displayed in Figure 5.8 and 5.9. The values of biomarker parameters and concentrations of biomarker are listed in Table 5.1 in Appendix II.

Generally, the m/z 191 mass chromatograms reveal that the crude oil samples in this project contain very low to moderate abundances of the extended tricyclic terpanes relative to the 17α(H) hopanes, low to moderate C_{27} Ts compare to Tm, and lower C_{29} Ts and C_{30} diahopane than C_{29} 17α(H) hopane peaks. However, the oils analysed from the east part of the basin show high C_{29} Ts and C_{30} diahopane relative to C_{29} 17α(H) hopane. On the other hand, the m/z 217 mass chromatograms reveal that the oils are characterized by a predominance of C_{27} and C_{29} diasteranes relative to regular steranes, reflecting the shale-rich nature of the source rocks.

The crude oil samples can also be separated into nine oil families and two subfamilies with respect to triterpane and sterane distributions, consistent with those from the *n*-alkane and isoprenoid alkane distributions. Family 1A includes the Beda, Fidda, East Meghil, Hakim and Mabruk oilfields. The oils in this family contain low C_{28}-C_{29}-(S+R) extended tricyclics/C_{28}-C_{29}-(S+R) extended tricyclics+C_{29}-C_{30} 17α(H) hopanes, moderate to high C_{29} ααα+αββ (S+R) regular steranes/C_{29} ααα+αββ (S+R) regular steranes + C_{29}-C_{30} 17α(H) hopanes ratios. Family 1B contains oil samples collected from the Nasser, Raiah, Raguba, Sabah, South Jebel, West Meghil, and Zelten oilfields, Family 2 includes oil from the Kotla oilfield, and Family 3 comprises the oils from the Dor Mansour oilfield, all showing similar ratios of the parameters mentioned above as shown in Figure 5.10. Family 4 includes the oils from the Aswad, Safsaf and Zellah oilfields and Family 6 contains oil from Augila Nafoora oilfield showing the lowest ratios of these parameters. Family 5 comprises oil from the As Sarah oilfield and Family 7 oils from NC125, and Family 9 oil from the Nakhla oilfields that show the highest ratios of the C_{28}-C_{29}-(S+R) extended tricyclics/C_{28}-C_{29}-(S+R) extended tricyclics+C_{29}-C_{30} 17α(H) hopanes, consistent with low C_{29} ααα+αββ (S+R) regular steranes/ C_{29} ααα+αββ (S+R) regular steranes+C_{29}-C_{30} 17α(H) hopanes ratios. Family 8, containing oil from the Tuamma oilfield, have the highest ratios of the C_{28}-C_{29}-(S+R)

extended tricyclics/C_{28}-C_{29}-(S+R) extended tricyclics+C_{29}-C_{30} 17α(H) hopanes, and lowest ratios of the C_{29} ααα+αββ (S+R) regular steranes/ C_{29} ααα+αββ (S+R) regular steranes+C_{29}-C_{30} 17α(H) hopanes ratios.

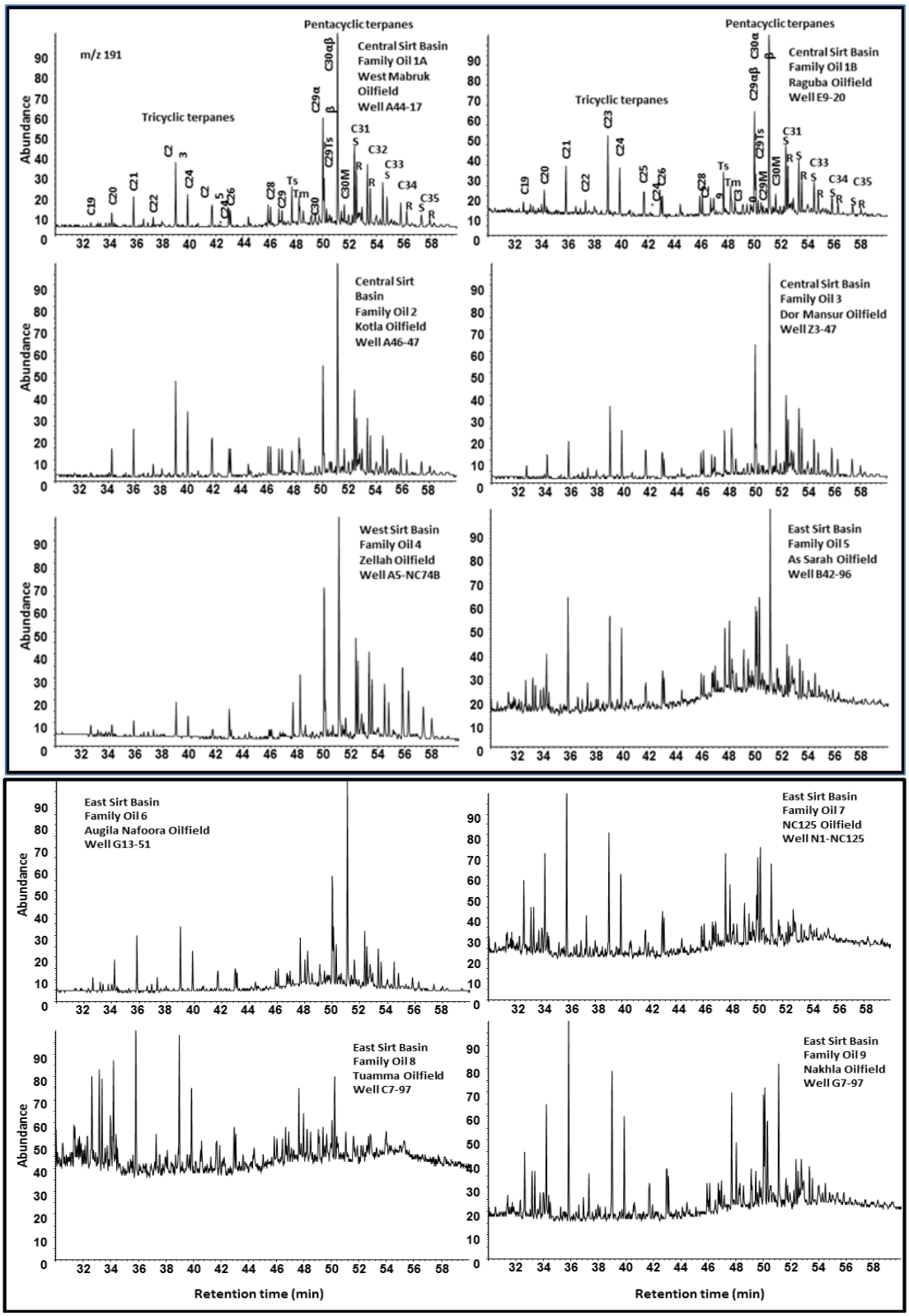

Figure 5.8: The distributions of tricyclic and pentacyclic terpanes (m/z 191) for representatives of the oil families in the Sirt Basin.

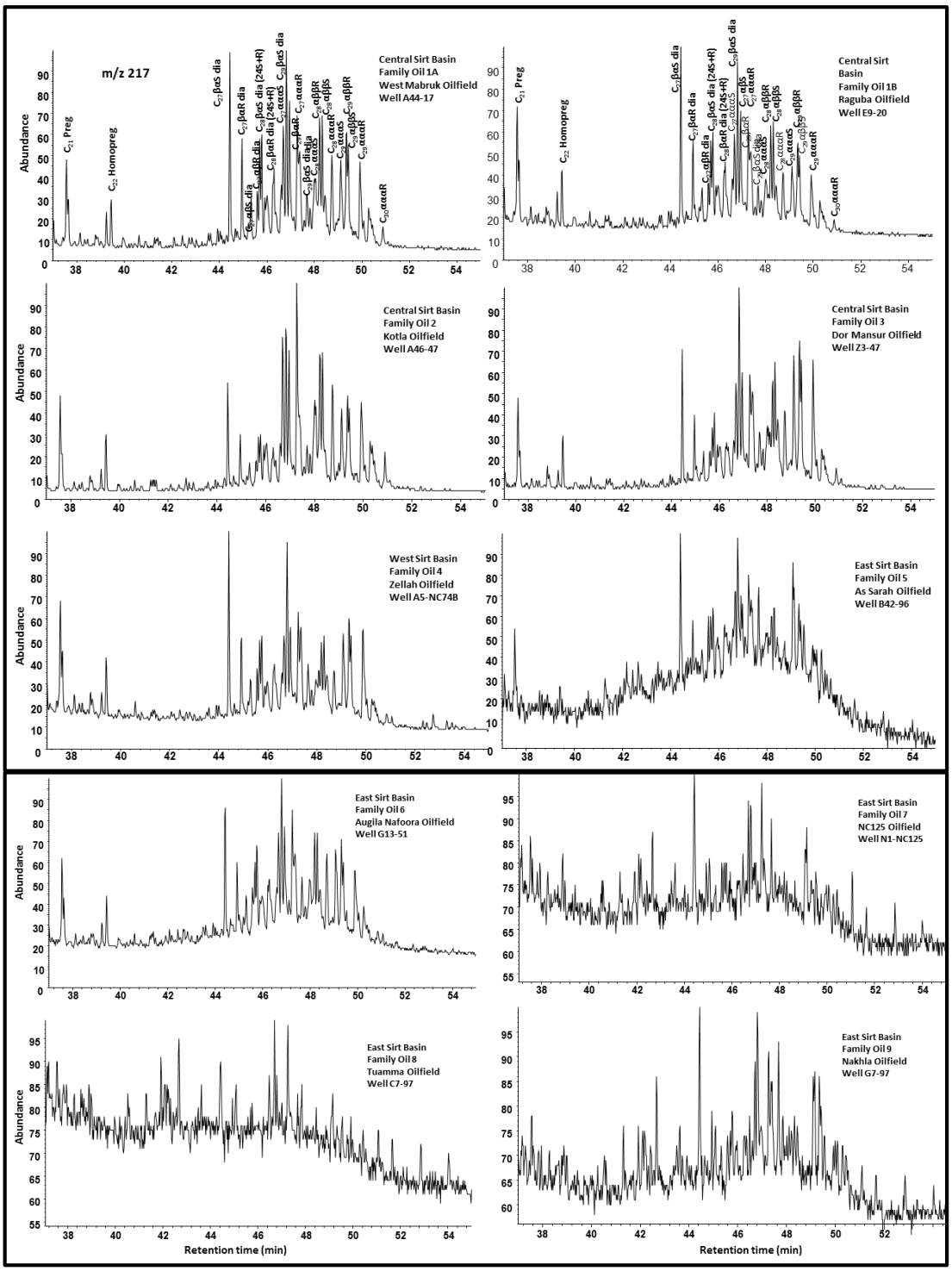

Figure 5.9: The distribution of steranes (m/z 217) for representatives of the oil families in the Sirt Basin.

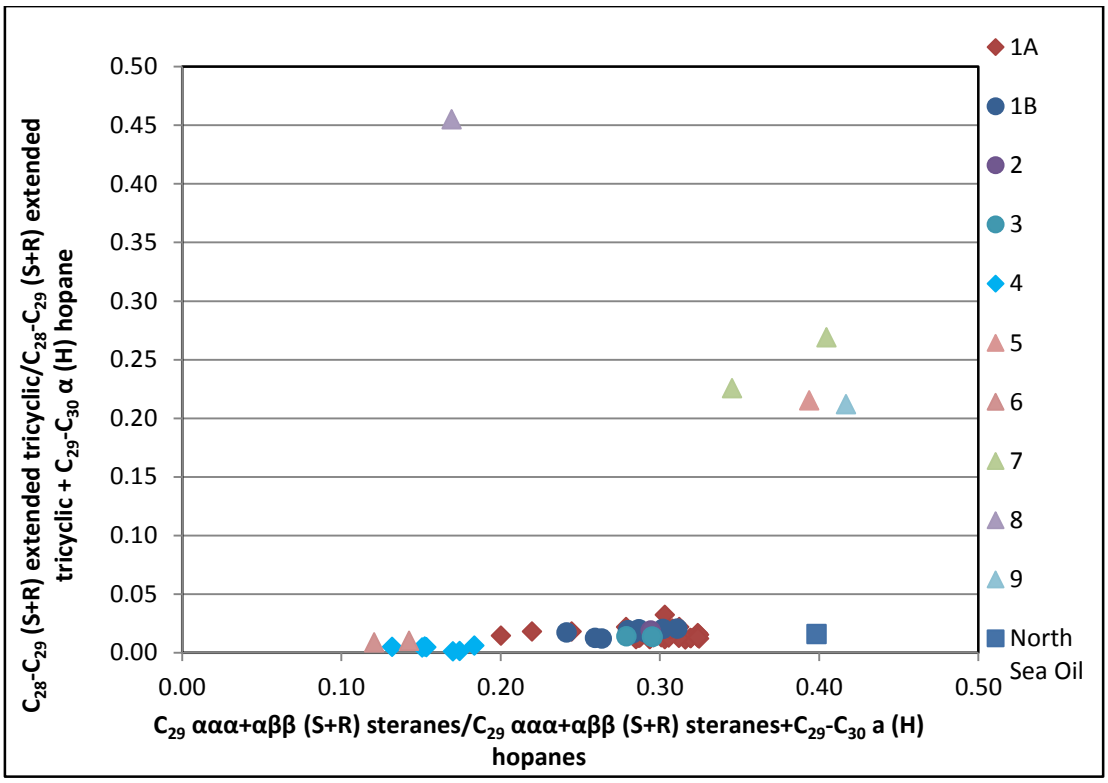

Figure 5.10: Cross plot of the C_{29} ααα+αββ (S+R) steranes/C_{29} ααα+αββ sterane (S+R) + C_{29}-C_{30} α (H) hopanes versus C_{28}-C_{29} (S+R) extended tricyclic/C_{28}-C_{29} (S+R) extended tricyclic + C_{29}-C_{30} α (H) hopane ratios for oil families in the Sirt Basin. Squares represent oils from west, circles oils from a centre and triangles oils from east basin.

On the basis of the relative amounts of extended tricyclic terpanes and regular steranes compared to hopanes, the oil samples collected from Aswad, Safsaf, south Safsaf and Zellah in oil families 4 at the west part of the Sirt Basin and As Sarah, Augila Nafoora, NC125, Tuamma and Nakhla in oil families 5-9 in the east part of the basin were generated from marine organic matter with major contributions of prokaryotic organisms versus eukaryotic organisms (c.f. Moldowan *et al.* (1985) and Connan *et al.* (1986)). Whereas for the oil samples from the remaining oil families 1A, 1B, 2 and 3, which show moderate to high amounts of steranes versus hopanes, it is suggested that these oils were generated from source rock with organic matter having moderate to higher input from eukaryotic organisms (algal) versus prokaryotic organisms (e.g. Tissot and Welte, 1984).

Seifert and Moldowan (1978) observed a systematic increase in the tricyclic terpane/17α(H) hopane ratios with increasing thermal maturity, and this was as a result of high amounts of tricyclics compare to hopanes being released from kerogen at higher

levels of maturity (Aquino Neto *et al.*, 1983). In this study, both ratios illustrate good correlations with maturity, showing an increase in regular steranes and tricyclic terpanes relative to the 17αβ(H) hopanes, as is shown below.

Figure 5.11 shows the relationship between sterane/hopane ratios versus C_{29} ααα*R* ethylcholestane percentage for all oil families. It is clear from the diagram that oil families 4 and 6 plot in the top left corner, having low sterane/hopane ratios and high C_{29} ααα*R* sterane concentrations, suggesting that these oils are characterized by relatively high inputs of land plants, and/or microbially reworked or algal organic matter and were deposited in marine to lacustrine environments. However, C_{29} steranes can be derived from brown and green algae (Moldowan *et al.*, 1985) and diatoms (Volkman *et al.*, 1981) as well as cyanobacteria (Fowler and Douglas, 1984). Oil families 1A, 1B, 2 and 3 have moderate to high sterane/hopane ratios and C_{29} ααα*R* concentrations, and plot in the middle of the diagram, suggesting that these oils are derived from marine organic matter with low contributions of terrestrial organic matter and deposited in marine conditions. However, oil families 5, 8 and 9 have low sterane/hopane ratios and this is associated with low C_{29} ααα*R* ethylcholestane, indicating that oils were generated from marine algal organic matter with low to moderate contributions of land plants and deposited in marine environments. Also, family 7 oils show low concentrations of the C_{29} ααα*R* and sterane/hopane ratios, suggesting that the oil was generated from marine organic matter with a low to moderate contribution of terrestrial material and was deposited in marine environments. In oil families 5, 7, 8 and 9, the low sterane/hopane ratios are due to the exposure to a higher level of thermal maturity.

The relationship between the C_{30}/C_{29} ααα*R* sterane ratio and C_{29} ααα*R* ethylcohleastene percentage is shown in Figure 5.12. This shows that oil families 3 and 4 have the lowest C_{30}/C_{29} sterane ratios and the highest concentrations of C_{29} ααα*R* steranes, suggesting the presence of non-marine and/or higher contribution from algal organic matter or land plant (e.g. Peters and Moldowan, 1993). Oil families 1A, 1B and 6 have moderate C_{30}/C_{29} sterane ratios and C_{29} ααα*R* concentrations, perhaps indicating shallow marine depositional environments. In contrast, oil families 5, 7, 8 and 9 have higher C_{30}/C_{29} ratios and lower C_{29} ααα*R* concentrations, indicating that these oils were generated

from clastic source rocks deposited under deeper marine dysoxic conditions. This might suggest that the oils studied were derived from three different sources, with different depositional environments and organic matter inputs. These variances in depositional environments may reflect the geographical distributions of the source rock within the Sirt Basin. Family 4 is located on the flanks of the western part of the basin and may originate from pre-Upper Cretaceous source rock or from the Sirt Shale Formation, whereas oil families 1A, 1B, 2 and 3 in the western and central parts of the basin may have been derived from the Sirte Shale and Rachmat formations. Family 6 in the eastern part of the basin seems to have generated oil from the Sirte Shale Formation, because it plotted within the same region as oil families 1A, 1B, 2 and 3 (Figure 5.12). Whereas oil families 5, 7, 8 and 9 in the eastern part of the basin may have originated from the Sirte Shale and/or Pre-Upper Cretaceous Middle Nubian Shale Formation, since they are suggested to be derived from deeper marine clastic source rocks.

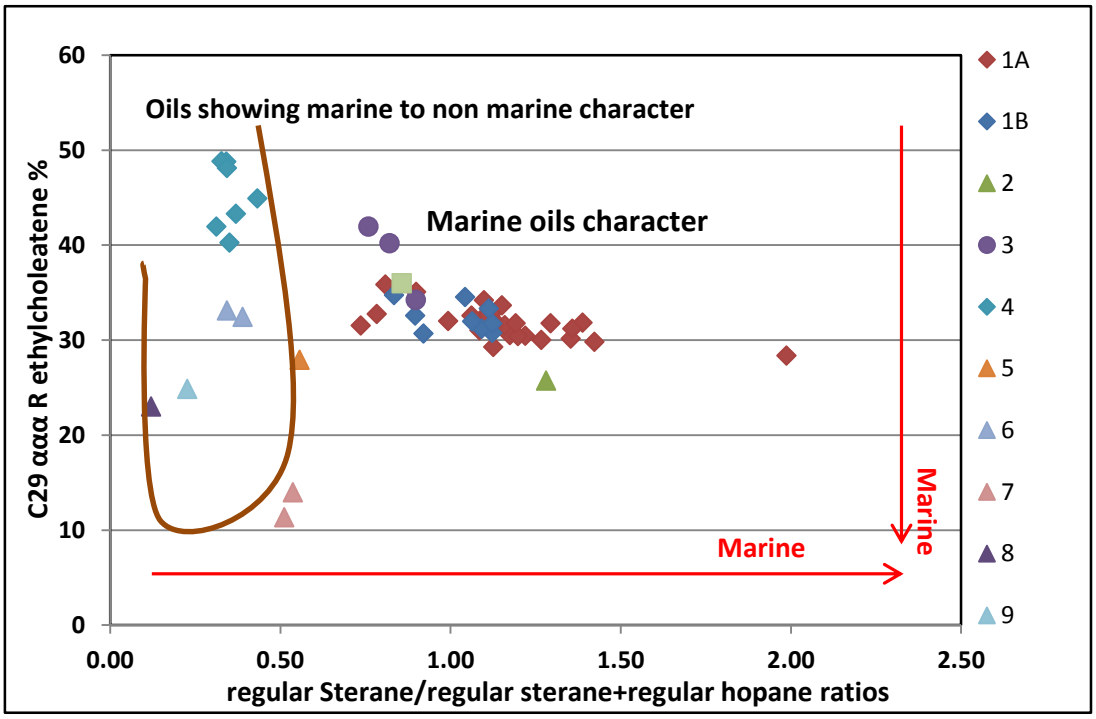

Figure 5.11: Cross plot of the sterane/hopane ratios versus C_{29} ααα 20R ethylcholestane (%) for oil families in the Sirt Basin, squares represent oils from west, circles oils from a centre and triangle soils from east basin.

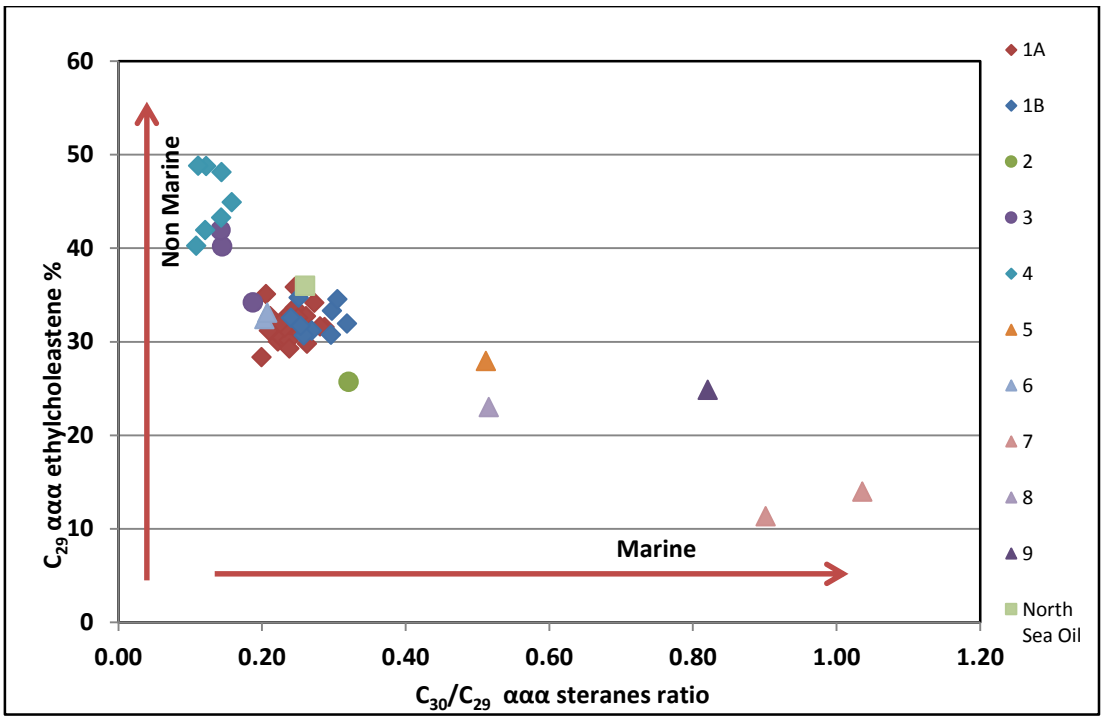

Figure 5.12: Cross plot of the C_{30}/C_{29} sterane ratio versus C_{29} ααα 20R ethylcholestane (%) for oil families in the Sirt Basin, squares represent oils from west, circles oils from a centre and triangles oils from east basin.

In addition, the same oil families of oils can be recognized using other facies biomarker parameters, for instance C_{29} diasterane R/C_{29} diasterane R+C_{29} ααα R sterane (Curiale, 1992), C_{29} 17α(H) hopane/C_{30} 17α(H) hopane (Subroto *et al.*, 1991) and C_{24} tetracyclic terpane/C_{26} tricyclic terpanes (S+R) ratios and extended tricyclics C_{28}+C_{29} (S+R)/Ts (Holba *et al.*, 2000). In this study, the moderate diasterane/sterane ratios (0.20 to 0.58) for all oil families, low to moderate abundance (0.35 to 0.86) of C_{29} 17α(H) hopane compared to C_{30} 17α(H) hopane, low abundance (0.02 to 0.25) of the tetracyclic terpanes relative to C_{26} tricyclics, and relatively moderate to high abundance (0.48 to 4.40) of the extended C_{28}-C_{29} tricyclic terpanes compared to Ts, indicate that the oils originated from a clay-rich source rock, and deposited under suboxic to anoxic conditions. While clay minerals play a role in the presence of diasteranes in sedimentary basins, C_{24} tetracyclic terpanes are more abundant in oils sourced from carbonate and evaporite source rocks or from terrigenous organic matter (Connan and Dessort, 1987). Also, the proportion of diasteranes compared to regular steranes has been shown to be dependent upon maturity, because the original steranes are converted gradually to mixtures of diasteranes and steranes with increased thermal maturity (Hughes *et al.*, 1985). Moldowan *et al.* (1986) reported that diasterane abundance was

also controlled by the redox conditions during the deposition of organic matter. The higher extended tricyclic C_{28}+C_{29} (S+R)/Ts ratios and lower C_{24} tetracyclic/C_{26} tricyclic ratios in oil families 1A, 1B, 2 and 3, may suggest that these oils are derived from similar clay-rich source rocks, which may be the Sirte Shale Formation. Family 4 oil shows the lowest values of the parameters mentioned above, suggesting that the oils are derived from different source rocks and depositional environments compared to all of the other oil families. Oil families 5, 6 and 7 show lower to moderate of C_{28}+C_{29} (S+R)/Ts, lower C_{24} tetracyclic/C_{26} tricyclics, lower C_{29} 17α(H) hopane/C_{30} 17α(H) hopane, and lower C_{29} diasterane R/C_{29} diasterane R+C_{29} ααα sterane ratios, suggesting that these oil families were generated from different source rocks compared to those from oil families 1A, 1B, 2, and 3; or from the same sources but which were deposited under different deposition conditions. Family 8 oil in the east part of the basin shows slight differences in the measured parameters relative to oil families 5 to 7, with higher C_{24} tetracyclic/C_{26} tricyclics relative to other oil families (0.25), and lower C_{29} 17α(H) hopane/C_{30} 17α(H) hopane, and C_{29} diasterane R/C_{29} diasterane R+C_{29} ααα sterane ratios, suggesting that the oil was generated from a source rock that had different characteristics to those of other oil family, or it was deposited in different depositional environments, as shown in Figure 5.13.

The depositional environment settings for all oil families can be deduced from the diagram of Pr/Ph versus C_{29} ααα+αββ (R+S) steranes/C_{30} 17α(H) hopane, as shown in Figure 5.14. The oils can be grouped into ten families based on their depositional environments. Oil families 1A, 1B, 2, and 3 were deposited in shallow dysoxic marine environments, oil families 4 and 6 plot in the dysoxic marine to the more lacustrine environment area of Figure 5.14, while oil families 5 to 9 were deposited in dysoxic to slightly oxic marine conditions. The diagram shows that oils produced in the west and central part of the basin are very different from the oils produced in the east part of the basin. This may be due to variations in organic matter inputs, changes in the source depositional environments and also to the differences in the level of thermal maturity.

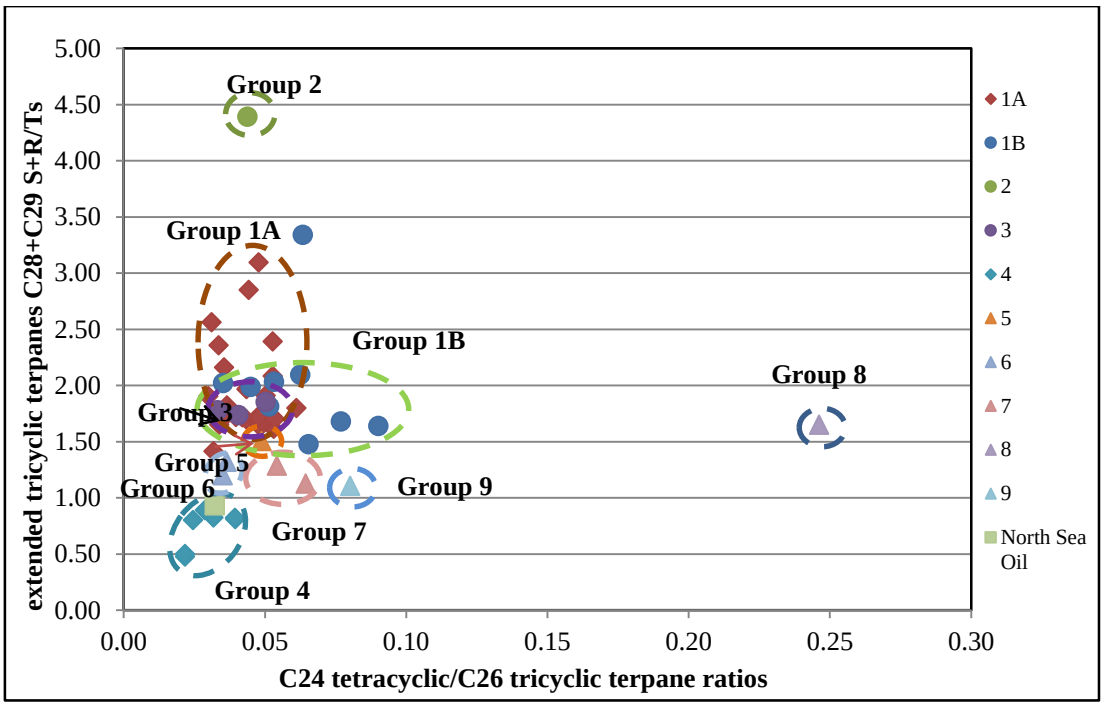

Figure 5.13: Cross plot of the C_{24} tetracyclic/C_{26} tricyclic terpane versus extended tricyclic terpane C_{28}+C_{29} (S+R)/ TS for oil Families in the Sirt Basin, squares represents oils from west, circles oils from a centre and triangles oils from east basin.

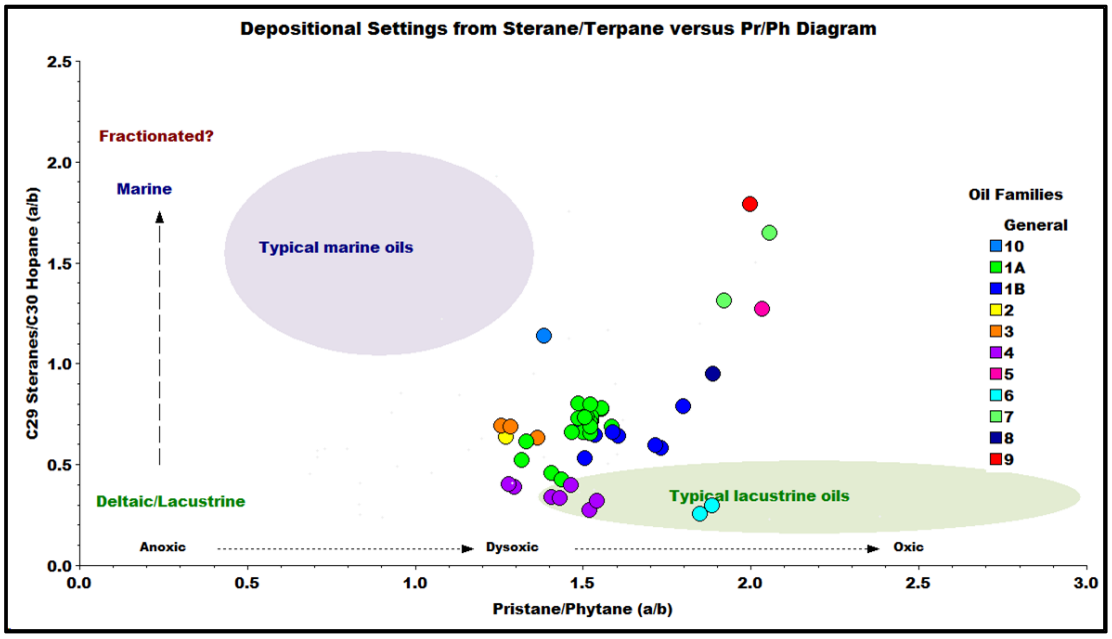

Figure 5.14: Cross plot of the Pristane/Phytane versus C_{29} sterane/C_{30} hopane ratios for oil families in the Sirt Basin.

A predominantly marine organic matter contribution to most of the crude oil analysed can be inferred from a relatively high abundance of the C_{27} compared to C_{29} regular steranes, and the presence of C_{30} regular steranes. Most crude oil in families 1A, 1B, 2,

5, 6, 7, 8 and 9 display a linear or anti-linear shape of the C_{27}, C_{28} and C_{29} regular sterane relative abundance curve as shown in Figure 5.15. Whereas crude oils from oil families 3 and 4 shows a V shape for regular steranes. Sterane distributions are dominated by regular steranes with $C_{27} \geq C_{28} > C_{29}$ with relatively high diasterane distributions. These families of oils usually display other features, such as the absence of 18 α (H)-oleanane, a high abundance of steranes rather than hopanes and almost as high an abundance of pentacyclic terpanes compare to tricyclic terpanes, except for oil families 7, 8 and 9, and this may be due to exposures to high maturity.

These biomarker data indicate that the sources of the crude oils were clay-rich clastics deposited in dysoxic to anoxic environments, and with relatively high inputs of algal and/or bacteria and this consistent also with some contributions of land plants.

Most of the oil in the sample set shows relatively high abundances of terpanes, which are derived from bacterial membrane lipids (Ourisson *et al.*, 1982). The distributions of terpanes (Figure 5.8) in most of the samples from oil families 1A to 6 are very similar, showing an abundance of the pentacyclic terpanes (hopanes) relative to tricyclic terpanes. The samples from oil families 7 to 9 are also similar, but they have much larger proportions of tricyclic terpanes relative to pentacyclic terpanes (Figure 5.8). This may reflect differences in source organic facies, depositional environments, and thermal maturity. The majority of the oil samples show a predominance of the C_{29} αβ and C_{30} αβ hopanes, with the former being more abundant in oil families 1A to 6. This may indicate differences in origin and depositional environment as well as thermal maturity for the oil samples from oil families 1A to 6 in the central and western part of the basin compared to oil families 7 to 9 in the east part of the Sirt Basin. The abundance of 18 α(H)-22,29,30-trisnorneohopane (Ts) is high in the crude oils from oil families 1A, 1B, 5, 6,7, 8 and 9, whereas that of the regular 22,29,30-trisnorhopane (Tm) is low. Meanwhile, in oil families 2, 3 and 4, Tm is more abundant than Ts, and the most likely reasons for high Ts is that most of the oils in the study area were generated from clay-rich clastic source facies, since this facies is believed to play an important role in converting Tm to Ts during the diagenesis zone (McKirdy and Aldridge, 1981). The high abundance of Tm and low Ts in oil families 2 to 4 may suggest that these oils are

derived from more carbonate-rich sediments or that the oils are less mature than those in other oil families.

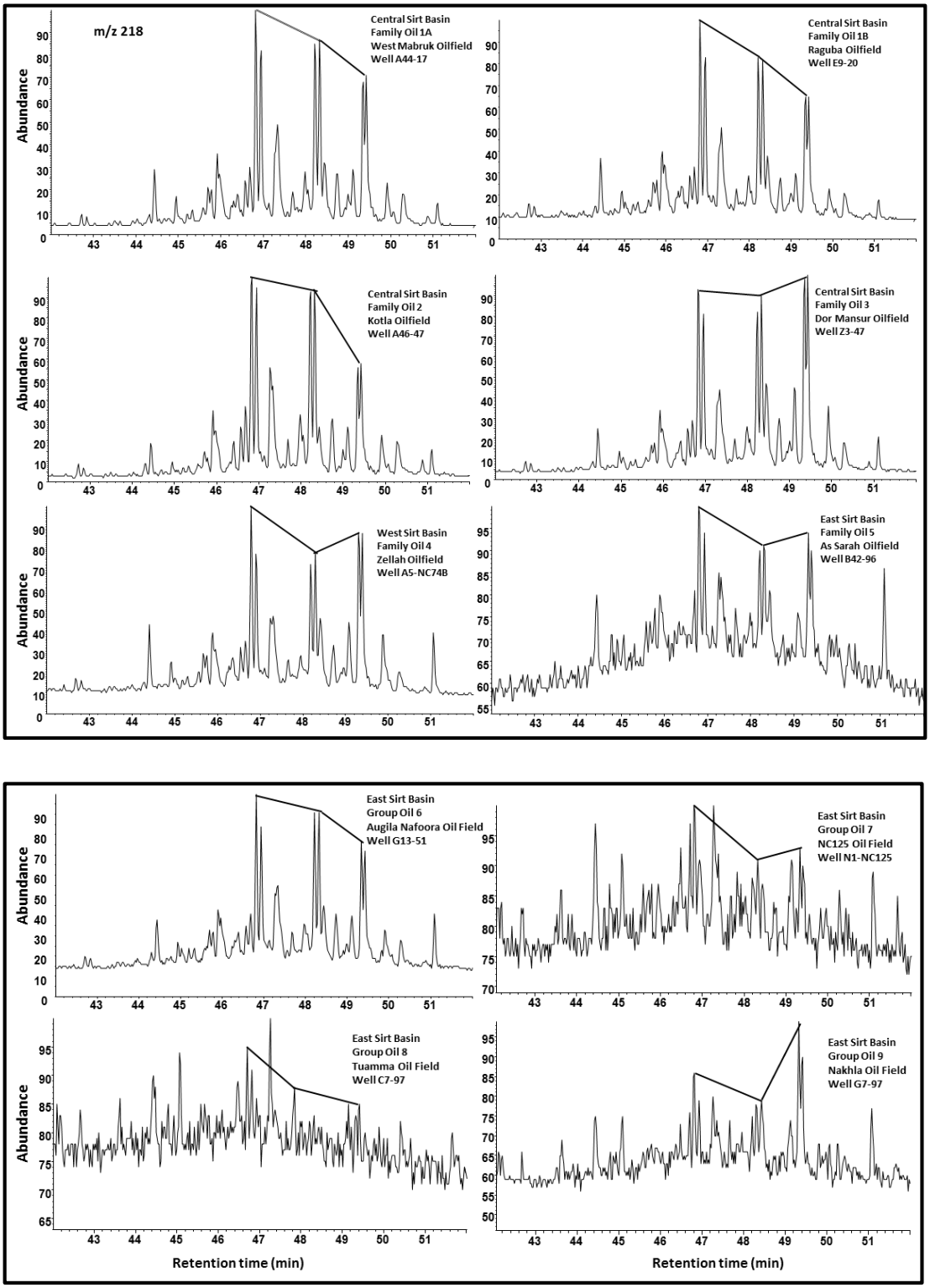

Figure 5.15: m/z 218 mass chromatograms showing the distributions of steranes of representative samples from oil families in the Sirt Basin.

The relative distributions of C_{31}-C_{35} 17α(H),21β(H), 22S and 22R homohopanes in marine petroleums is used as an indicator of the redox conditions during and immediately after deposition of the source sediments. The $C_{35}/(C_{31}$-$C_{35})$ ratio, or homohopane index, provides an indication of depositional settings and the maturity of related oils or source rocks (Peters, 2005b) . Crude oils from oil families 3 and 4 have significantly higher homohopane index values than the other families, indicating a more reducing depositional environment for their source rock (e.g. Peters and Moldowan, 1991), and this is also reflected by the Pr/Ph ratios, as shown in Table 5.1. The C_{31} 22R/C_{30} 17α(H)-hopane ratios in these oils are low (0.25 to 0.35), suggesting that they originated from lacustrine to marine source rock (Peters, 2005b). Meanwhile the other oil family display, low to moderate homohopane index values, suggesting less reducing depositional environments (suboxic) for the source rocks, and this conclusion is also supported by the Pr/Ph ratios. The C_{29} 17α(H) hopane/C_{30} 17α(H) hopane ratios in Table 5.1 in Appendix II show that all of the oil families have ratios lower than 0.8, indicating that the oils originated from clastic marine source rocks.

Abundant C_{19} to C_{29} tricyclic terpanes are present in most of the oil samples. The distribution of the tricyclics, with βα isomers and low molecular weight tricyclics being predominant, indicates the moderate to high maturity characteristics of the oil (Seifert and J. M. Moldowan., 1981; Aquino Neto *et al.*, 1983; Peters and Moldowan, 1993; Farrimond *et al.*, 1999; Peters, 2005b). The C_{23} βα isomer is the most prominent tricyclic terpane in the crude oil samples from oil families 1 to 6; while those from oil families 7 to 9 shows the C_{21} βα isomer in more abundance. The C_{24} tetracyclic terpanes show relatively low abundances and this may be suggest marine clastic facies, since this compound is reported in oils believed to be sourced from terrigenous organic matter and it is also common in marine oils sourced from mudstone to carbonate source rock (Peters, 2005b). C_{26}/C_{25} tricyclic terpane along with C_{31} R hopane/C_{30} αβ(H)-hopane ratios are useful as supporting parameters to distinguish lacustrine from marine oils (Peters, 2005b). The high C_{26}/C_{25} tricyclic terpane and C_{31} R hopane /C_{30} αβ hopane ratios for family 4 indicate that this oil family originated from lacustrine source rocks, while the low ratios for the rest of the oil family, suggest that oil they were generated from marine or marine to lacustrine source rocks, as shown in Figure 5.16.

The C_{28}/C_{29} steranes ratio is considered as a consistent age-related parameter for a marine depositional setting since it increases from Precambrian to Tertiary as a result of the relative increase of C_{28} sterane and the decrease of C_{29} sterane content over geological time (Moldowan *et al.*, 1985). The increase in C_{28} steranes is thought to be due to the increased difference in phytoplankton assemblages such as diatoms (Moldowan *et al.*, 1985). Grantham and Wakefield (1988) reported that the C_{28}/C_{29} sterane ratio is < 0.5 for lower Palaeozoic and older oils, 0.4-0.7 for Upper Palaeozoic to Lower Jurassic oils, and greater than 0.7 for Upper Jurassic to Miocene oils. However, this ratio should apply only to samples from marine source rock (Peters and Moldowan, 1993). In this study, the crude oils analysed have C_{28}/C_{29} sterane ratios ranging between 0.36 and 1.04 with the majority of the oil samples having ratios greater than 0.7, suggesting Upper Cretaceous oils, in the Mesozoic time; while the oils from the Aswad, Safsaf and Zellah oilfields in oil family 4, oil family 8 (Tuamma oilfield) and oil family 9 (Nakhla oilfield) having ratios in the range of 0.36 to 0.60, suggesting that these oils may have been generated in the Upper Palaeozoic to Lower Jurassic ages (c.f. Moldowan et al., 1985; Peters and Moldowan, 1993).

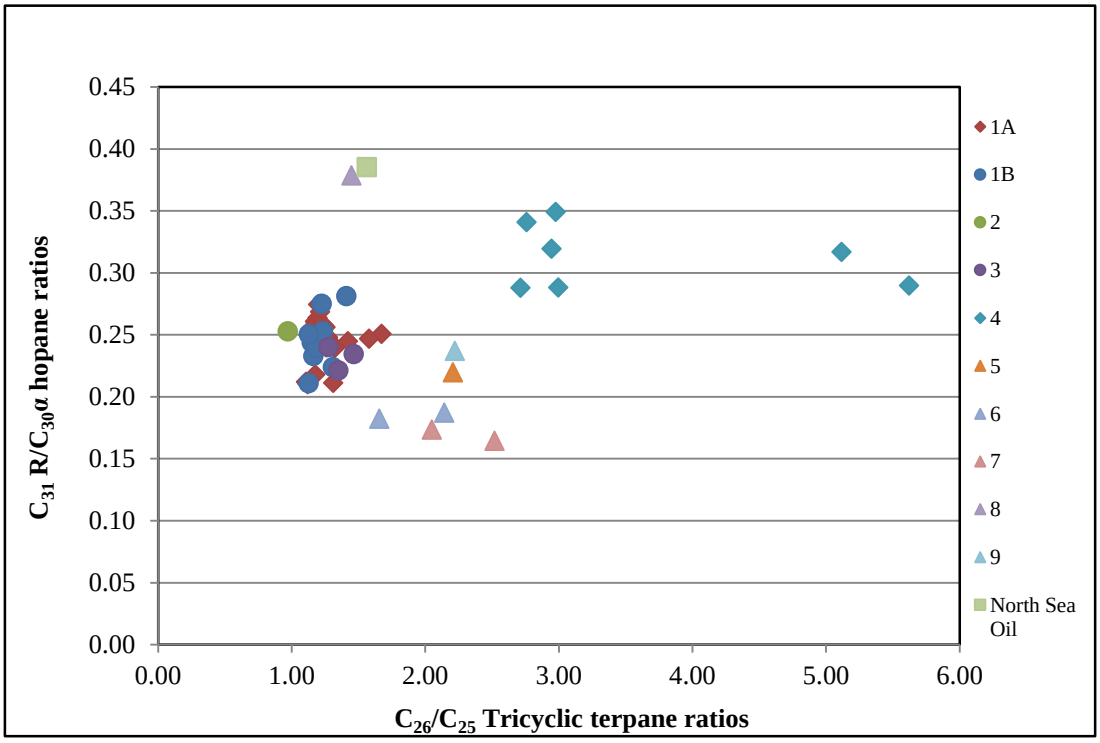

Figure 5.16: Cross plot of the C_{26} /C_{25} tricyclic terpane versus C_{31}R/ C_{30} α hopane for oil families in the Sirt Basin, squares represent oils from west, circles oils from a centre and triangles oils from east basin.

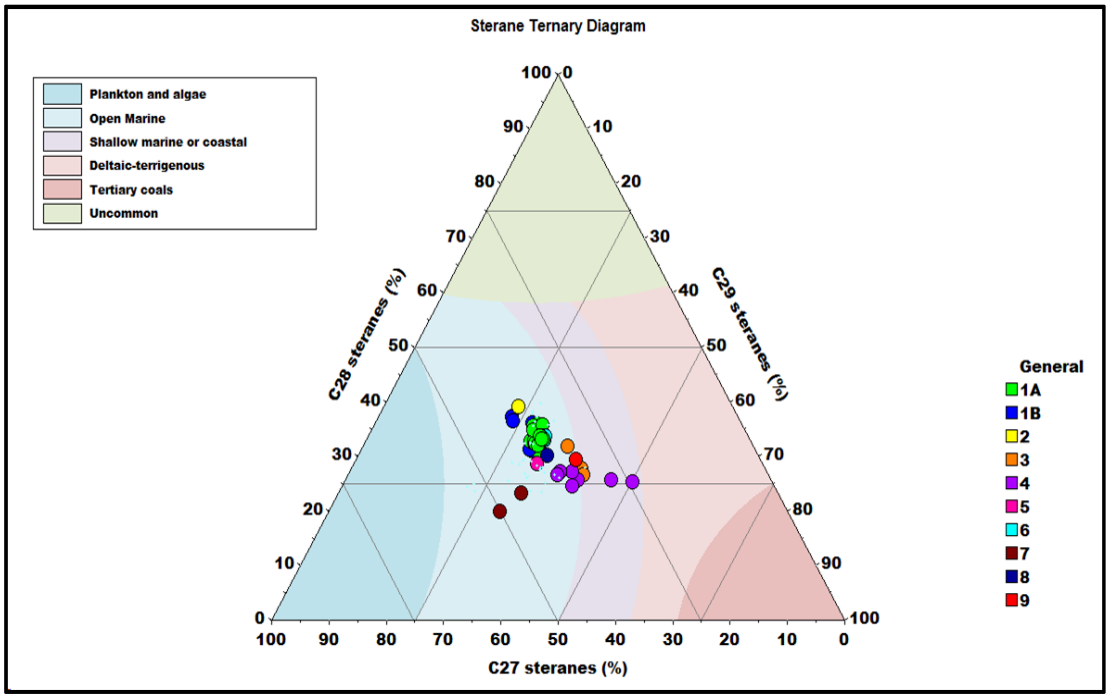

Figure 5.17: Ternary diagram of C_{27}, C_{28}, and C_{29} steranes showing depositional environments of the oil families from the Sirt Basin. Interpretational overlays from pIGI software.

The distributions of the C_{27}, C_{28} and C_{29} ααα 20R steranes in the ternary diagram shown in Figure 5.17 suggest that most of the crude oil samples can be separated into several oil families. It is possible to distinguish oil families 1A, 1B, 2, 5, 7, 8 and 9, which are slightly more dominated by C_{27} and C_{28} compare to C_{29} and are plotted in the open marine region. Whereas oil families 3 and 4 are rather more dominated by C_{27} and C_{29} rather than C_{28} and are plotted in between open marine and shallow marine environments. In contrast, oil families 7, 8 and 9 are more dominated by C_{27} than both C_{28} and C_{29} and is plotted within the marine region. The overlapping between the different oil families may suggest that most of the crude oil was generated from the same or similar source rocks (c.f. Moldowan *et al.*, 1985; Peters and Moldowan, 1993).

On the other hand, the distributions of C_{27}, C_{28} and C_{29} αββ sterane obtained from the m/z 218 mass chromatograms can also be used to distinguish between different families of oils from different source rock or different organic facies in the same source rock, as shown in Figure 5.18. It is clear from the diagram that oil families 1A, 1B, 2, 5 and 6 are plotted in the area characterised by higher inputs of mixed plankton and bacteria. Oil families 3, 4, 8 and 9 are plotted in the area characterised by higher contributions

of mixed plankton, bacteria and land plants, whereas oils from family 7 are characterised by higher contributions of the mixed plankton and bacteria (c.f. Moldowan *et al.*, 1985; Peters and Moldowan, 1993).

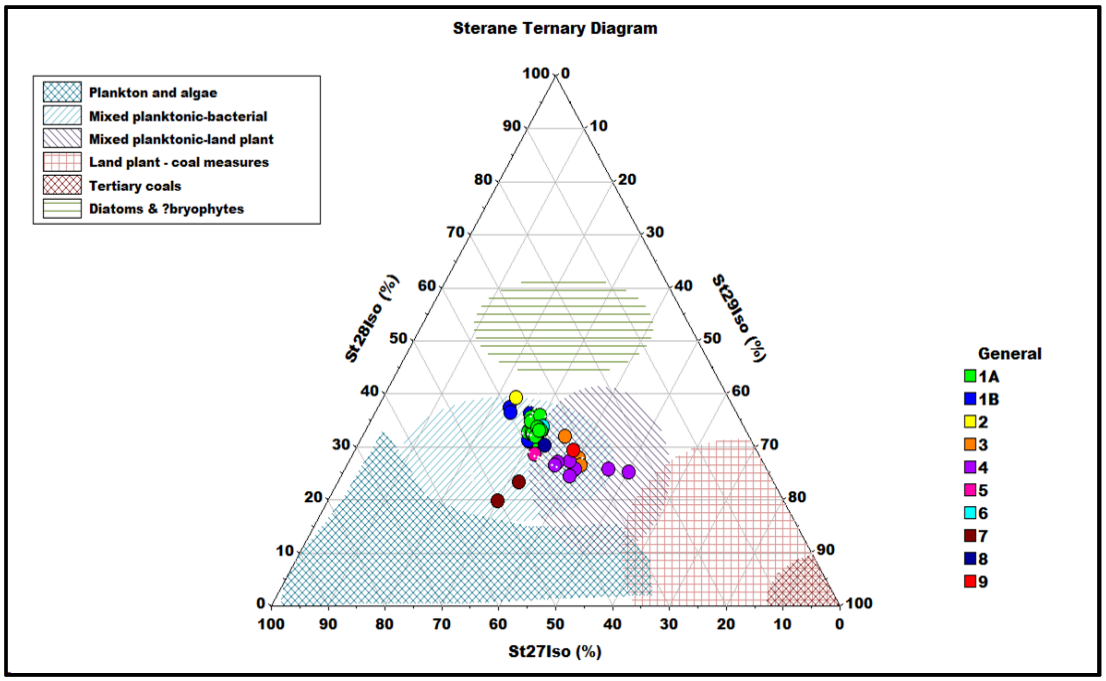

Figure 5.18: Ternary diagram of C_{27}, C_{28}, and C_{29} αββ steranes showing depositional environment of the oil families in the Sirt Basin. Interpretational overlays from pIGI software.

5.2.1.3 Aromatic Compounds

The distributions of monoaromatic steroids (MAS) were monitored using m/z 253 from the aromatic fractions of the crude oil samples in the study area, as shown in Figure 5.19. For most of the crude oil samples in all of the oil families, short chain C_{21} and C_{22} compounds are present in greater abundance than long chain C_{27} to C_{29} compounds. This may reflect the fact that short chain components are more resistant to maturity (Peters, 2005b). In addition, most of the samples analysed were characterized by a predominance of the C_{21} MAS. The levels of long chain C_{27} to C_{29} monoaromatic steroids appear to be high in oil families 1A, 1B, 2, 3, 4 and 6, while low in oil families 5, 7, 8 and 9. This may be due to the effects of maturity of long chain monoaromatic compounds or to changes in organic facies in these oil families. Most of the crude oil samples from oil families 1A, 1B, and 2 are dominated by C_{28}β S and C_{29}β and C_{28}α (S

and R) MAS respectively, while oil families 3 and 4 are dominated by $C_{29}\beta$ and $C_{28}\alpha$ (S and R) and $C_{28}\beta$ S compounds, respectively, as shown in Figure 5.19.

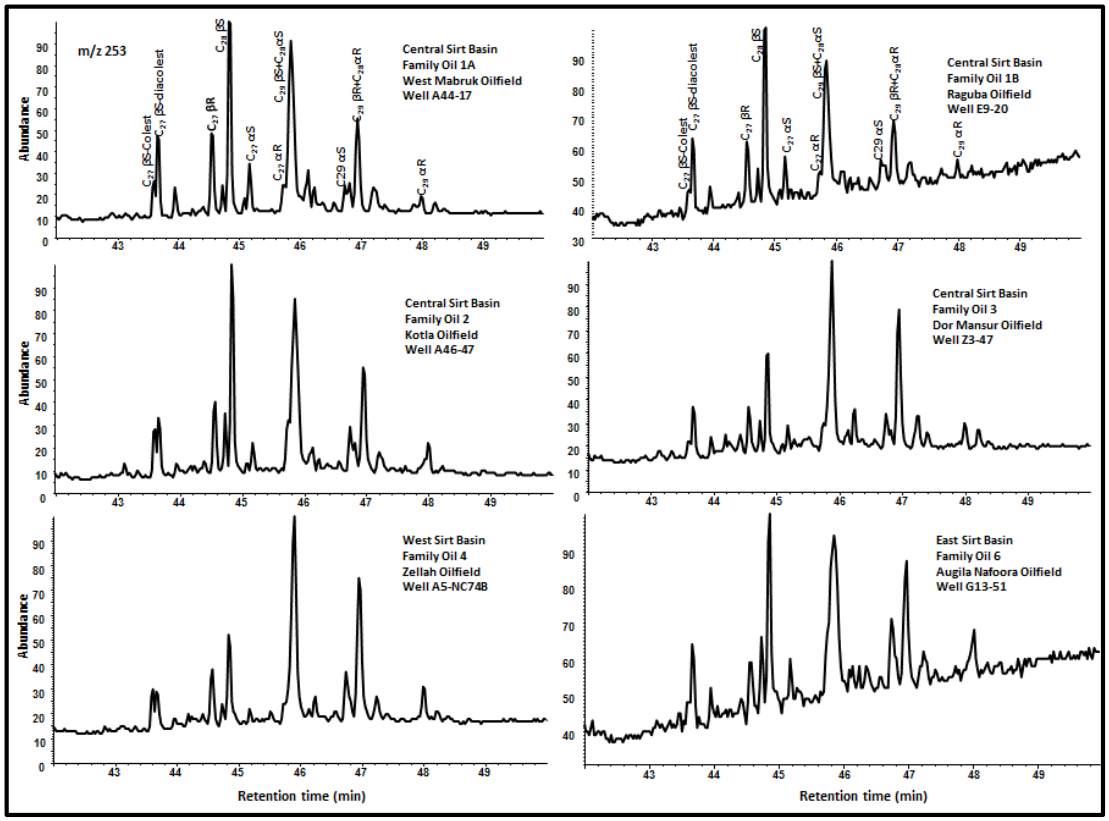

Figure 5.19: m/z 253 mass chromatograms showing the distribution of monoaromatic steroids in representative samples from oil families in the Sirt Basin.

The predominance of C_{27} and C_{28} MAS can be attributed to organic matter derived from marine sources, while oil derived from non-marine source rocks contain high C_{29} monoaromatic steroids (Peters, 2005b). On the other hand, non-marine algae may contain relatively higher amounts of C_{29} sterols which could form C_{29} MAS, while terrestrial organic matter often is poor in C_{27} and C_{28} MAS (Moldowan *et al.*, 1985; Volkman *et al.*, 1986).

MAS data from the oil samples analysed plot on the C_{27}-C_{28}-C_{29} ternary diagram in areas associated with terrigenous, marine, or lacustrine input, as shown in Figure 5.20. The main applications of such diagrams are to help with oil-to-oil and oil-to-source rock correlations and to help describe the depositional environments of source rocks for the oils. This diagram can provide supporting evidence for correlations between oils in the Sirt Basin, and can be used in distinguishing oils derived from marine shale

source from those derived from non-marine shale source (Moldowan *et al.*, 1985). The distribution of the C_{27}, C_{28} and C_{29} MAS for oil families 1A, 1B, 2, 3, and 6 plot in a close area of the diagram, showing relatively higher abundances of C_{27} and C_{28} relative to C_{29} components, suggesting marine source inputs. Family 5, showing relatively higher abundances of C_{27} relative to C_{28} and C_{29}, suggests a high contribution of marine organic matter (algae) with little contribution of terrestrial inputs, deposited in a marine environment. The slightly higher abundance of C_{29} MAS in oil families 4, 7, 8 and 9 may reflect some contribution of algal and/or terrestrial organic inputs deposited in marine settings. The diagram also shows differences in the concentrations of the C_{28} MAS relative to C_{27} and C_{29} MAS, and this may be partly due to variations in the organic matter source input and/or depositional environments (Peters, 2005b). However, most marine oils contain a higher proportion of C_{28} MAS than non-marine oils (e.g. Moldowan *et al.*, 1985). Oil families 1A, 1B, 2, 3, 4 and 6 that have higher concentrations of the C_{28} MAS, suggesting marine source input when compare with the oil families 5, 7, 8 and 9 that have lower concentration, which is also marine consistent but with some contribution from terrigenous organic matter. The latter oil families may have exposure to a higher series of aromatization process due to high levels of thermal maturity, and this is well agreement with C_{27}, C_{28} and C_{29}-sterane diagram. The $C_{28}/(C_{28}+C_{29})$ MAS ratios (Table 5.2 in Appendix II) show that oil families 1A, 1B, 2, 3, and 6 have relatively high values ranging from 0.61 to 0.85, indicating that oils were generated from marine organic matter input, whereas samples from the Aswad and Zellah oilfields in family 4, the As Sarah oilfield in family 5, and families 7 to 9 have ratios less than 0.5 which may indicate marine shale origins consistent with some terrigenous and bacteria inputs. However, the relatively slightly higher abundance of the C_{29} MAS may reflect some contribution of algal and/or terrestrial organic matter inputs deposited in marine settings for those oil families (e.g. Moldowan *et al.*, 1985; Volkman *et al.*, 1986; Peters *et al.*, 1989).

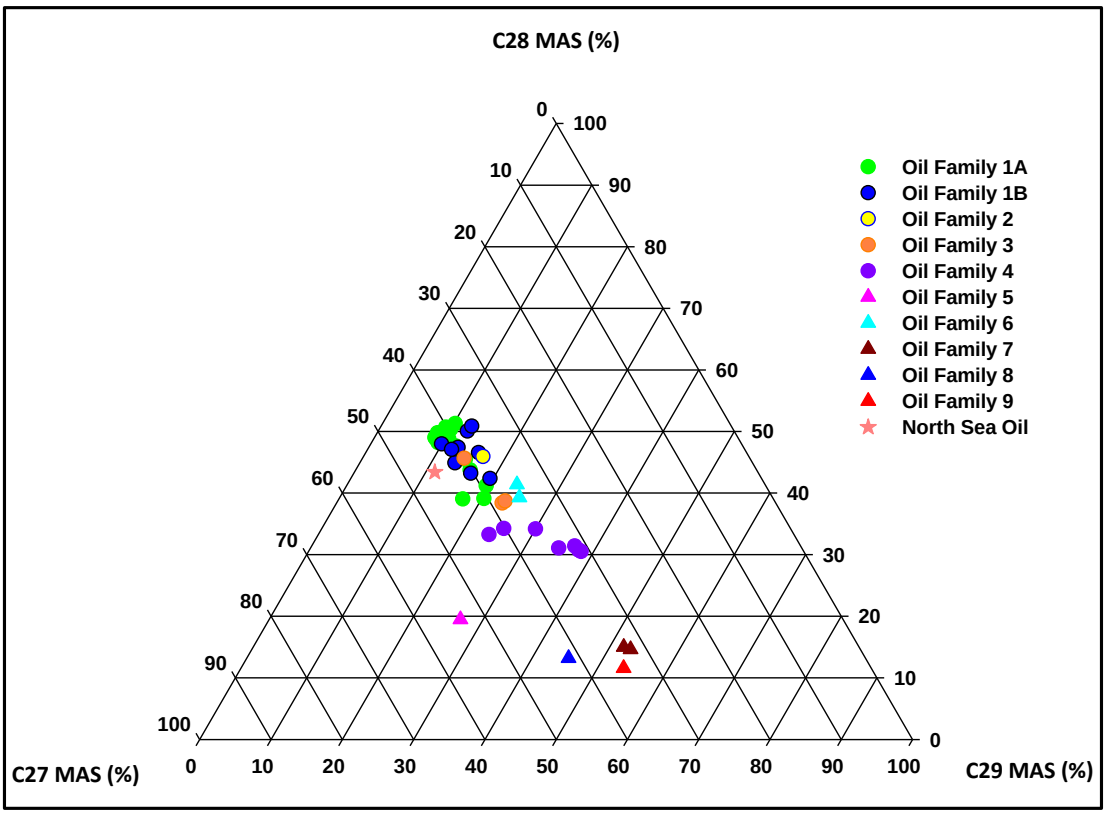

Figure 5.20: Ternary diagram with C_{27}, C_{28}, and C_{29} monoaromatic steroid relative abundances showing marine depositional settings of the sources of the oil families in the Sirt Basin.

The distributions of triaromatic steroids (TAS) were monitored using m/z 231 mass chromatograms of the aromatic fractions of the family oil samples, and examples of them are shown in Figure 5.21. The long chain TAS hydrocarbons C_{26} to C_{28} are thought to originate from the demethylation and aromatization of monoaromatic steroids. But short chain compounds are supposedly produced from the homolytic scission of long chain TAS with increased thermal maturity (Seifert and Moldowan, 1978; Mackenzie *et al.*, 1981). In the oil samples analysed the short chain C_{20} and C_{21} and long chain $C_{26}S$ to $C_{28}R$ TAS are present with different distributions. The presents of short chain C_{20} and C_{21} TAS are observed in all samples and in relatively greater abundance than the long chain $C_{26}S$ to $C_{28}R$ TAS in oil families 1B, 4 and 5. In oil families 1A, 2, 3, and 6 the long chains are relatively more abundant than short chains. The long chain TAS C_{26} to C_{28} seems to be very low in abundance in oil families 4, 5, 7, 8 and 9 compared with the other oil families, which may due to the higher maturity in those oil families. Most of the oil samples show a predominance of $C_{26}R+C_{27}S$, and $C_{27}R$ TAS in oil families 1A, 1B, 2, 5 and 6, as shown in Figure 5.21. This may reflect

the fact that all of the oil samples in these families originated from similar organic matter input, but with different levels of thermal maturity. Whereas oil samples from oil families 3, 4, 5, 7, 8 and 9 show nearly similar levels of abundance of $C_{26}R+C_{27}S$, and $C_{27}R$ TAS as shown in Figure 5.21, which may suggest that these oil families were derived from mixtures of marine and non-marine organic matter input.

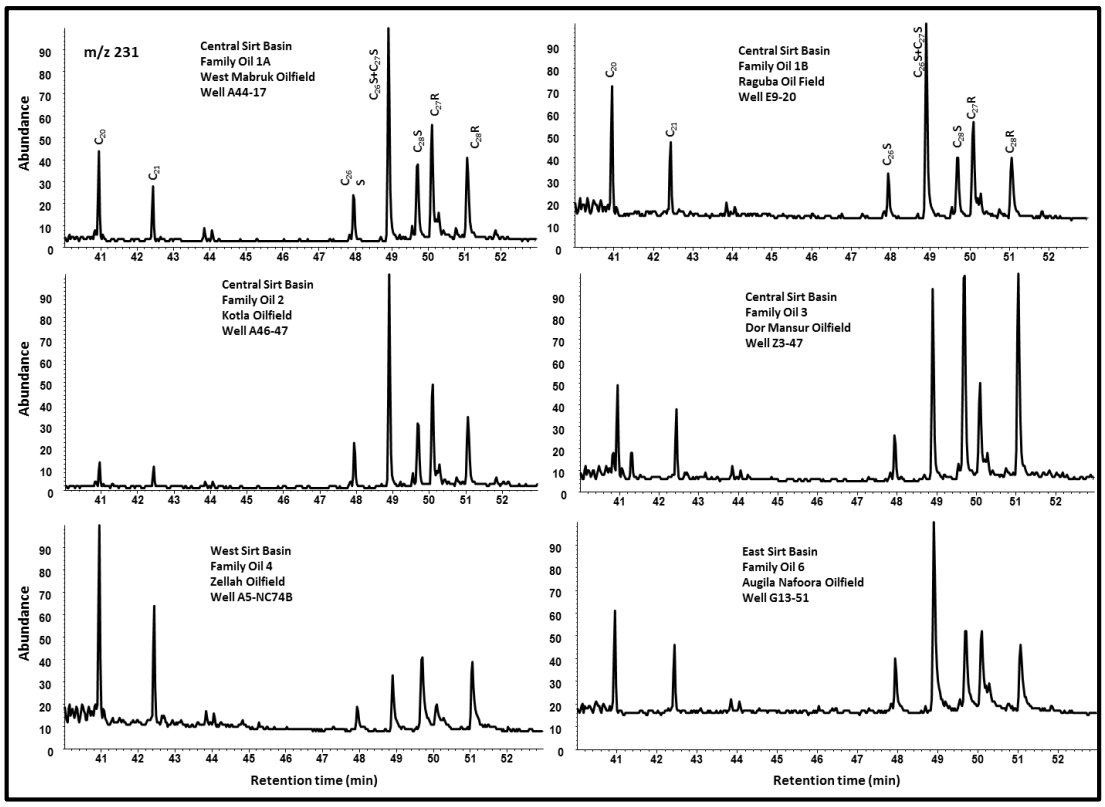

Figure 5.21: Distribution of triaromatic steroids (m/z 231) for oil families in the Sirt Basin.

Figure 5.22 shows a crossplot of the $C_{26}S/C_{28}S$ triaromatic steroids versus $C_{27}R/C_{28}R$ triaromatic ratios for the crude oil samples in the Sirt Basin. The diagram shows a low abundance of the $C_{26}S$ TAS relative to the $C_{28}S$ TAS and $C_{27}R$ TAS relative to $C_{28}R$ TAS for the family 4 oils and family 3 oils at the wells Z3-47 and Z5-47 in the Dor Mansur oilfield in the central part of the basin, suggesting differences in source organic matter inputs with high contribution of bacteria and were deposited in lacustrine to marine environments, compared to the other oil families. For the oil families 1A, 1B, 2, 6 and the well GG1-47 in the Dor Mansur oilfield in family 4, the chart shows a low abundance of the $C_{26}S$ TAS relative to the $C_{28}S$ TAS and higher abundance of the $C_{27}R$ TAS relative to $C_{28}R$ TAS, indicating similar marine organic matter inputs with some

contribution of terrigenous organic matter for these oil families which were deposited in marine conditions (Peters, 2005b). Oil families 5, 7 and 9 have values of both ratios greater than 1.0, indicating that these oil families have similar marine to terrestrial organic matter inputs and may also have similar deposition environments. Family 8 shows a higher abundance of $C_{26}S$ relative to $C_{28}S$ TAS and low abundance of $C_{27}R$ relative to $C_{28}R$ TAS when compared to the other oil families, indicating source marine depositional environments, which may have contained marine and terrestrial organic matter inputs. The diagram assists in distinguishing between five potential petroleum families (the circled red lines) in the Sirt Basin: two in the central and western part of the basin and three in the eastern part.

The distributions of aromatic hydrocarbons (Figure 5.23, Table 5.3 in Appendix II) showed an abundance of naphthalene (20-75%) with relatively high amounts in oil families 2, 3 and 4 (58, 64 and 75%, respectively), followed by phenanthrene (8-55%) with the highest percentage recorded in oil families 1B, 5, 6 and 7 (44, 51, 48 and 55%, respectively), dibenzothiophene (0.39-14%), fluorene (1.62-11.92%) and biphenyl (2.20-36.43%), with the highest percentage registered in oil families 7 and 9 (19.54 and 36.43%, respectively), but with only low levels of monoaromatic and triaromatic steroids (0.02-8%). The data show that the oil samples are characterised by a relatively high abundance of diaromatic and triaromatic hydrocarbons, including naphthalene, phenanthrene and dibenzothiophene, with low levels of biphenyl, fluorene, and monoaromatic and triaromatic steroids. This may indicate that the crude oils originated from clastic marine depositional environments with relatively high contributions of land plants and/or bacteria. The relatively higher abundances of the alkylnaphthalene compounds in the oil samples may be related to their production from terpenoids precursors derived from microbacteria and land plants (Alexander *et al.*, 1992b).

The aromatic hydrocarbon concentrations of naphthalene, methylnaphthalenes, dimethylnaphthalenes, trimethylnaphthalenes, and tetramethylnaphthalenes are very low in oil families 2, 5, 6, 7, 8 and 9, relative to the other oil families 1A, 1B, 3 and 4 (Table 5.3 in Appendix II, Figure 5.23). In general, the concentrations of dimethylnaphthalene compounds were low at less than 0.07 µg/g oil in all oil families. Oil families 2, 5, 6, 7, 8 and 9 have the lowest concentrations of dimethylnaphthalenes

of less than 0.01 µg/gm oil as shown in Figures 5.23 and 5.24. This may reflect the oils marine origin, because terrestrially derived organic matter contains relatively higher amounts of dimethylnaphthalenes (Radke *et al.*, 1986; Radke *et al.*, 1994). Some oil samples from oil families 1A, 1B, 3 and 4 have also low concentrations of dimethylnaphthalenes ranging from 0.03 to 0.068 µg/gm oil, which may indicate some contribution of terrestrial organic matter inputs in marine environments.

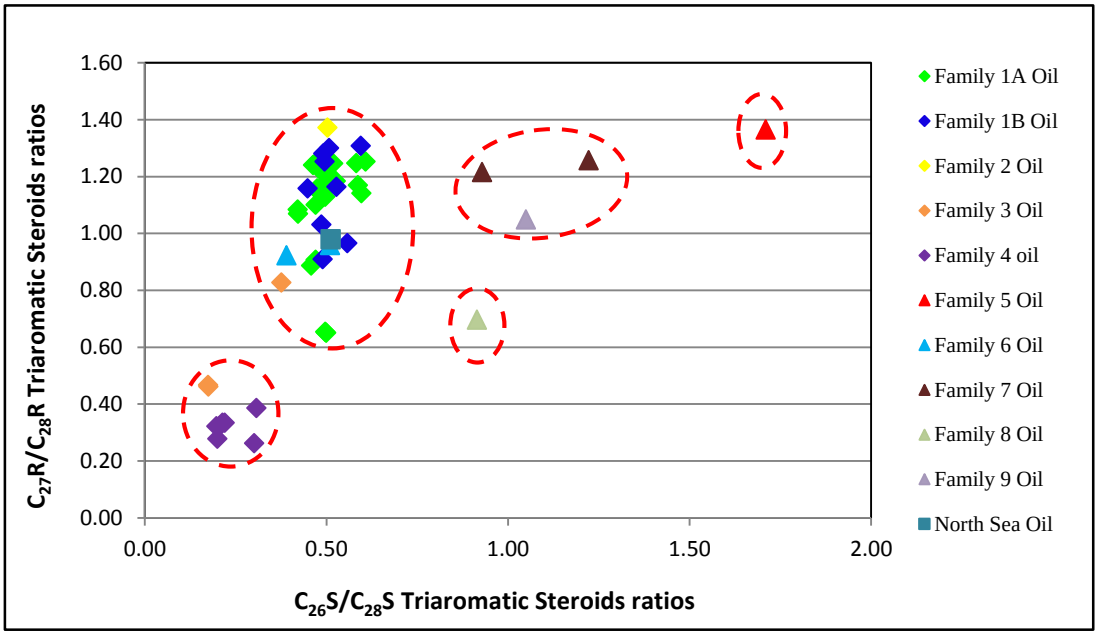

Figure 5.22: Cross plot of the $C_{26}S/C_{28}S$ triaromatic steroids versus $C_{27}R/C_{28}R$ triaromatic ratios for oil families in the Sirt Basin.

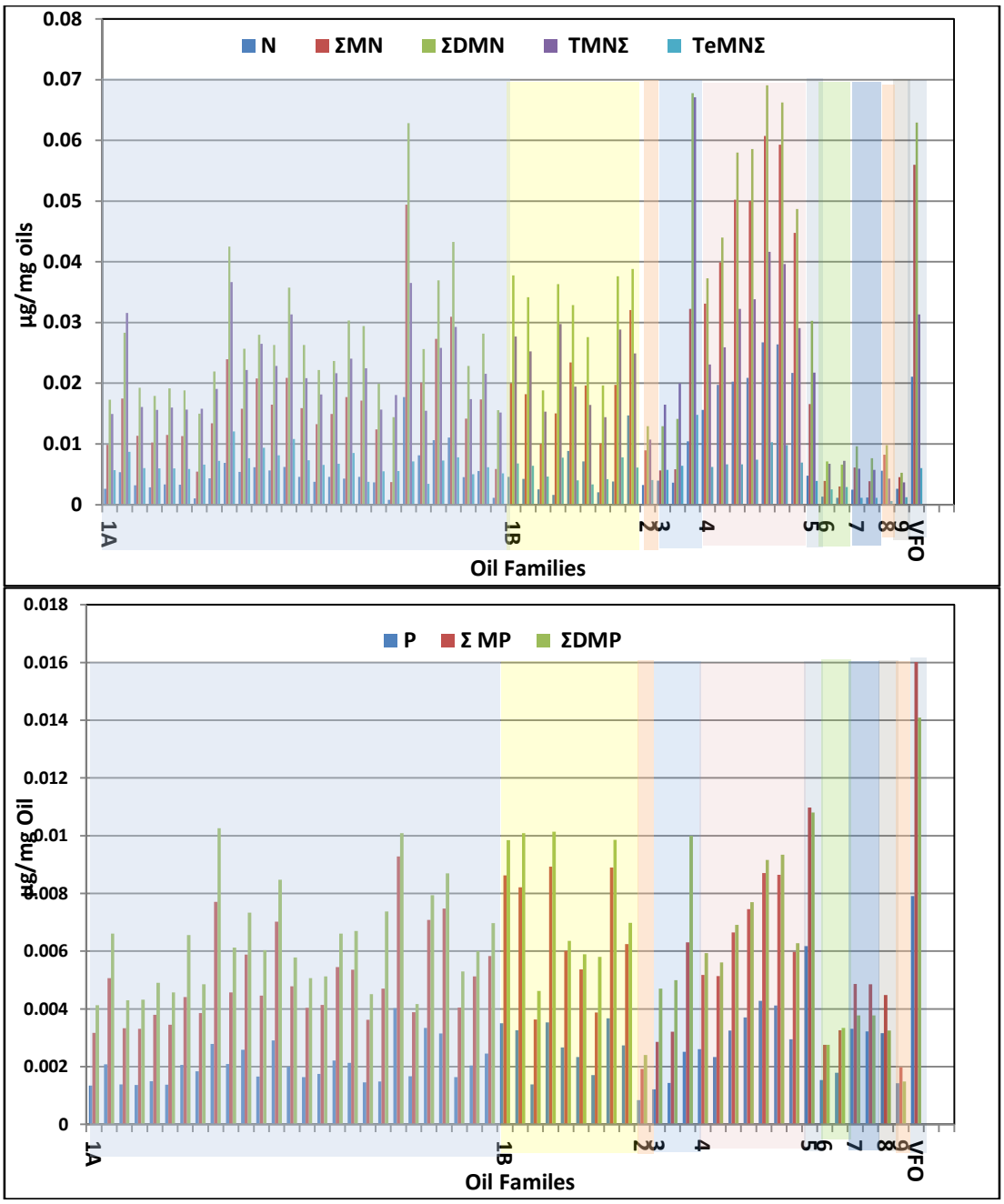

Figure 5.23: Aromatic hydrocarbon concentrations of the oil families in the Sirt Basin (and a reference North Sea oil). Abbreviations: Naphthalene (N), Methylnaphthalenes (MN), Dimethylnaphthalenes (DMN), Trimethylnaphthalenes (TMN), Tetramethylnaphthalenes (TeMN), Phenanthrene (P), Methylphenanthrene (MP) and Dimethylphenanthrene (DMP) compounds.

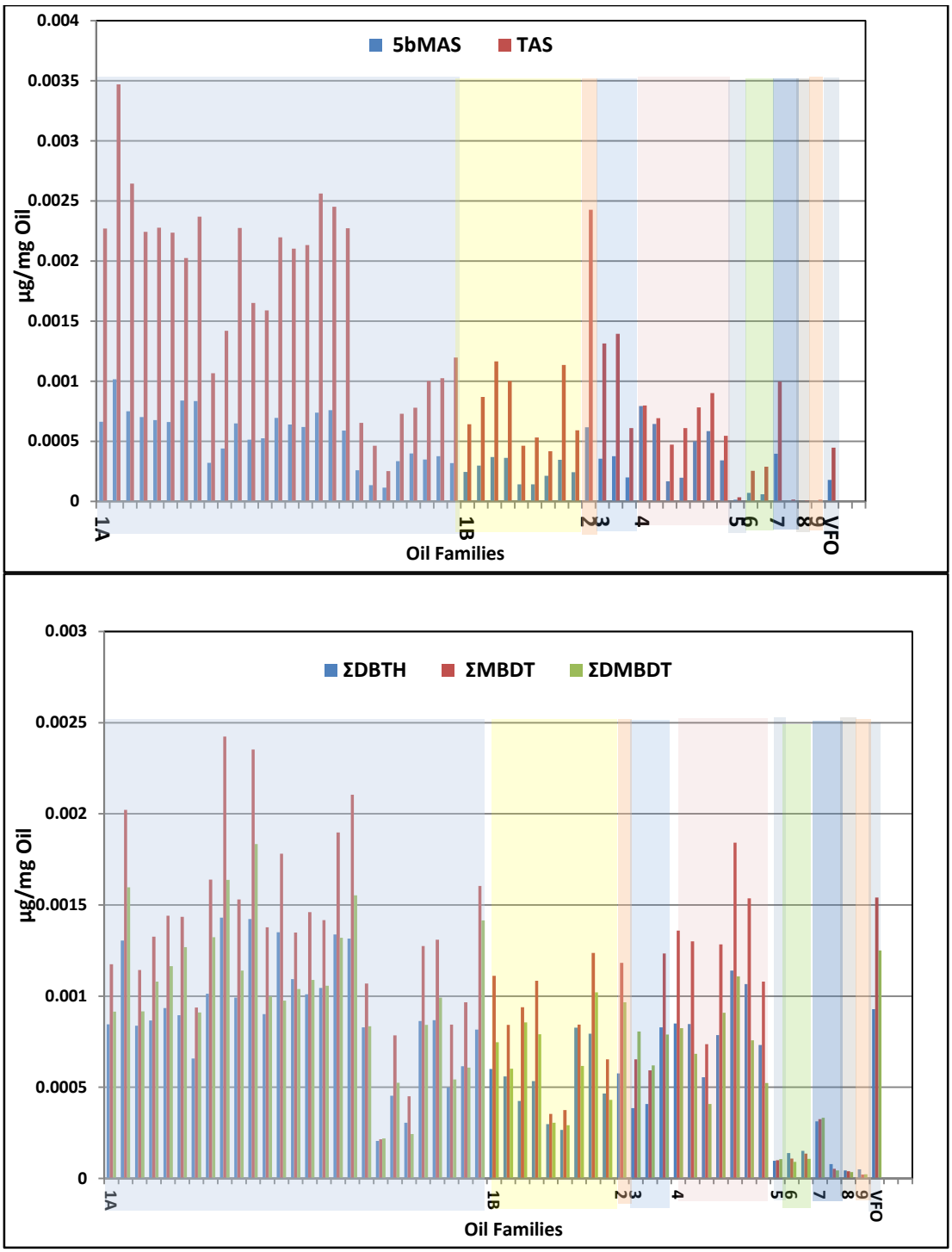

Figure 5.24: Aromatic hydrocarbon concentrations of the oil families in the Sirt Basin (and reference North Sea oil). Monoaromatic Steroids (MAS) and Triaromatic Steroids (TAS) dibenzothiophene (DBT), Methyldibenzothiophenes (MDBT), Dimethyldebenzotiophenes (DMBDT).

The TDE1 ratio (1,2,5-TMN/1,2,4-TMN), and the TDE2 ratio (1,2,7-TMN/1,2,6-TMN) and also the 1,2,7-/1,3,7-trimethylnaphthalene ratio can be used to differentiate between marine oils and source rocks from higher plant material (Strachan *et al.*, 1986;

Strachan *et al.*, 1988). The oil families 1A, 1B, 2, 4 and 6 are characterised by lower TDE1 and TDE2 ratios, ranging from 1.87 to 4.99 and 0.21 to 0.40, respectively (Table 5.4 in Appendix II, Figure 5.25). This may suggest marine depositional environments with some contributions of angiosperm land plants, as shown in Figure 5.25. Family 3 is characterised by the highest TDE1 ratios (20.67-29.44) and low TDE2 ratios (0.23-0.46), while the high abundance of 1,2,5-TMN in this family may suggest that this component originated from a cyanobacteria hopanoid precursor . Oil families 5, 7, 8 and 9 are also characterised by relatively high TDE2 ratios compared with the other oil families, ranging from 0.52 to 0.87 and this is associated with low TDE1 ratios ranging from 3.31 to 5.41, suggesting marine organic matter with slightly higher contributions of angiosperm land plant input. Furthermore, the 1,2,7-/1,3,7-trimethylnaphthalene ratios for all oil families were low, ranging from 0.09 to 0.40. This may indicate that the crude oils were derived from marine organic matter in dysoxic to anoxic settings, with some contribution of land plants in the marine depositional environment. The 1,2,5/1,3,6- trimethylnaphthalene ratios showed high values (2.94-4.11) in the family 3 compared with other oil families which had values of less than 0.67, suggesting that family 3 oils may have higher angiosperm land plant inputs and that the source rock was deposited in marine suboxic to anoxic conditions, as shown in Figure 5.26. The results obtained for the relative abundance of the trimethylnaphthalenes in all crude oil samples are listed in Table 5.4 in Appendix II.

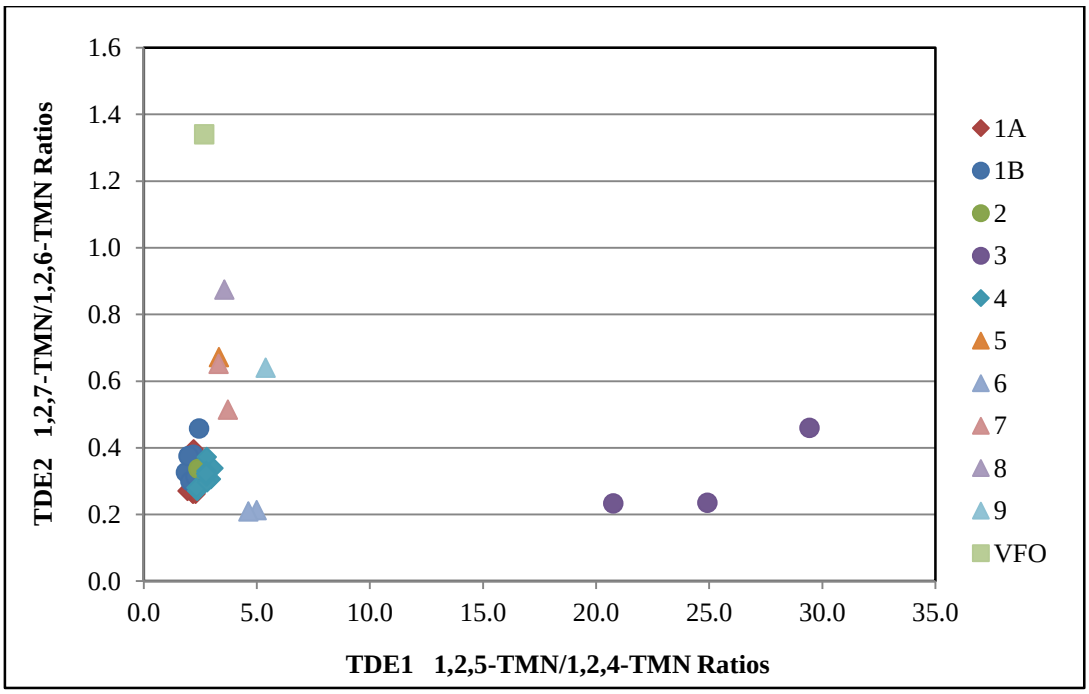

Figure 5.25: Cross plot of the TDE1 (1,2,5-/1,2,4-Trimethylnaphthalene) versus TDE2 (1,2,7-/1,2,6-Trimethylnaphthalenes for the oil families in the Sirt Basin, squares represent oils from the west, circles oils from a centre and triangles oils from east basin.

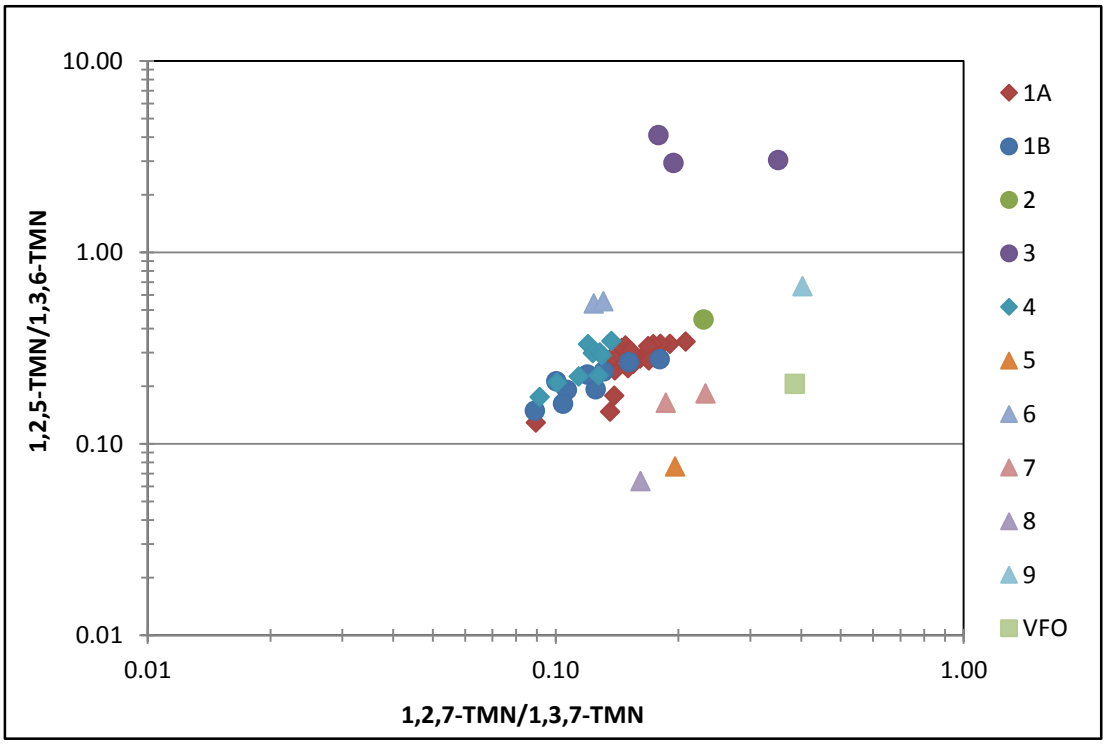

Figure 5.26: Cross plot of the 1,2,7-/1,3,7-Trimethylnaphthalene versus 1,2,5-/1,6,6-Trimethylnaphthalene for the oil families in the Sirt Basin, squares represent oils from the west, circles oils from a centre and triangles oils from east basin.

The 1-MP/9-MP ratios determined from the crude oil samples in oil families 1A, 1B, 2, 4, 5, 6, 7, 8 and 9 lie in the range of 0.54 to 0.73 with an average of 0.68, where for family 3 it was found to range between 0.79 and 0.85 with an average of 0.81 (Figure 5.27, Table 5.4 in Appendix II). This higher 9-MP abundance than 1-MP, may reflect the marine source precursors of these compounds, though with some isomers from land plant origins, particularly in Family 3 (c.f. Budzinski *et al.*, 1995).

Figure 5.27 shows a cross-plot of the 1-MP/9-MP versus 1,7-DMP/(1,3+3,9+2,10+3,10-DMP) ratios, which have been used to characterise the different sources of organic matter from different geological ages (Alexander *et al.*, 1992b). Some of the oil sample data are scattered, but most are concentrated largely in the right bottom corner of the plot. The high abundance of 9-MP and 1,3-, 3,9, 2,10 and 3,10-DMP indicate marine origins for these isomers, whereas the slightly higher abundance of 1-MP and 1,3,7-DMP for the sample from Family 3 indicates some isomers with terrigenous origins.

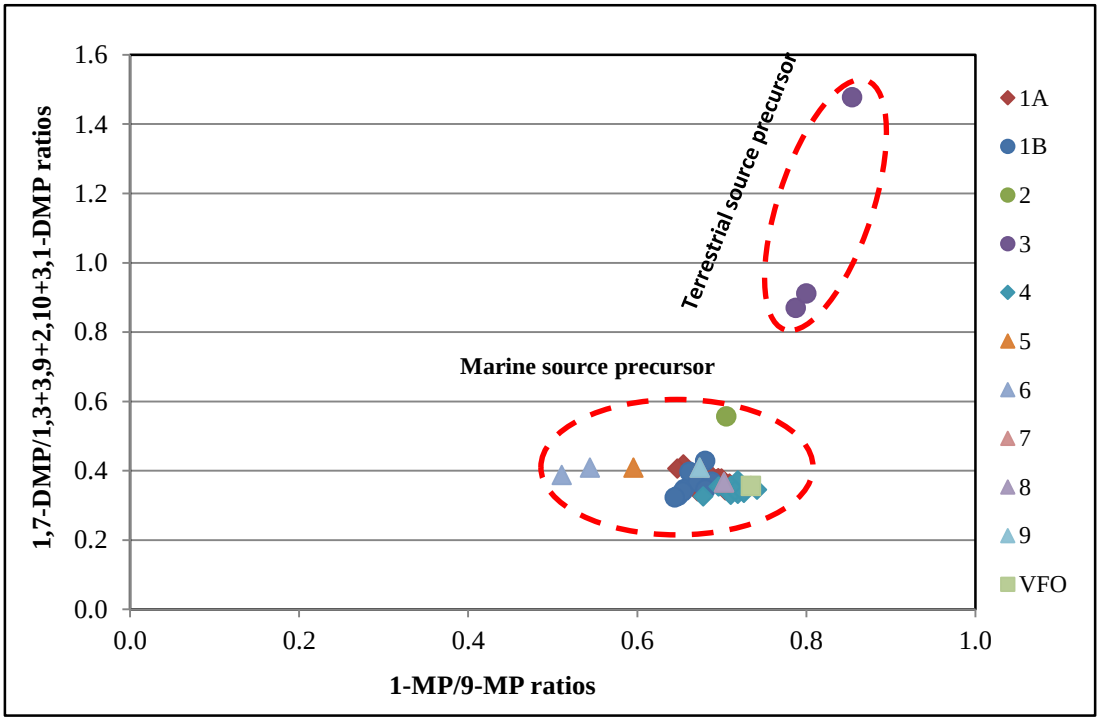

Figure 5.27: Cross plot of the 1-MP/9-MP versus 1,7-DMP/(1,3-, 3,9, 2,10, 3,10-DMP) for the oil families in the Sirt Basin, squares represent oils from the west, circles oils from a centre and triangles oils from east basin.

The relative abundances of alkyldibenzothiophenes and their alkylated analogues, with pristane to phytane ratios can be used as indicators of source depositional environments (Hughes *et al.*, 1995; Jinggui *et al.*, 2005). In particular, the dibenzothiophene to phenanthrene (DBT/P) and pristane/phytane ratios can be used as indicators of source rock depositional environment and lithology. The Pr/Ph ratio (Table 5.2) of the Sirt Basin oils is less than 2.05, indicating suboxic to anoxic source depositional conditions. The concentrations of dibenzothiophene in crude oil samples of all oil families are very low and increase towards the central and western parts of the basin, where Family 1A contains the highest concentrations, Oil Families 1B, 2, 3 and 4 have moderate concentrations, while oil families 5 to 9 in the east part of the basin contain very low concentrations. This may be due to the presence of low salinity waters or high levels of transition metals during a deposition in the central and western part of the basin, whereas in the eastern part of the basin in oil families 5 to 9 the organic matter was deposited in relatively more saline water (Hughes *et al.*, 1995). The DBT/P ratio of the Sirt Basin oils ranges from 0.01 to 0.68 (Table 5.4 in Appendix II), indicating that these oils have originated from clastic marine source input. The DBT/P versus Pr/Ph measurement suggested by Hughes *et al.* (1995) has been widely used for distinguishing source lithology and depositional environments. Figure 5.27 shows the cross plot of the DBT/P versus Pr/Ph ratios, where the values fall into a typical pattern. The diagram shows that most of the oil samples fall in the zone proposed for oils from marine plus lacustrine shales. Generally, oil families 5 to 9 show lower ratios than the other families, but there is an overlap between the oil samples from oil families 1A, 1B and oil families 2 to 4. Geographically, the overlapping of oil families 1A to 4 is distinctive from the rest of the oil family, because they are located in central and western parts of the Sirt Basin. The diagram also shows lower abundances of dibenzothiophene relative to phenanthrene, and therefore it was probably sourced from siliciclastic rich marine source rocks, according to Hughes *et al.* (1995). This may be taken as an indication that the crude oils have low sulphur contents. The cross plot also indicates that Sirt Basin oils are derived from marine and possibly lacustrine shales, and their Pr/Ph ratios lie within the range 1.32 to 2.05, which supports the notion of their marine source suboxic to anoxic depositional environments.

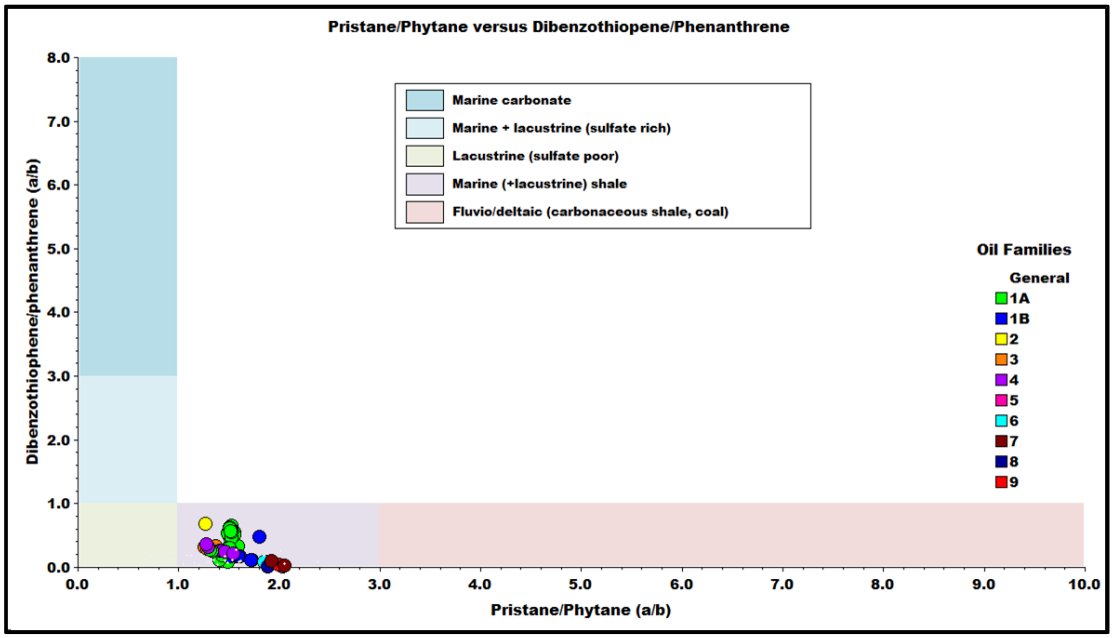

Figure 5.28: Cross plot of the DBT/P versus Pr/Ph of the oil families in the Sirt Basin. Interpretational field is from pIGI software.

5.3 Principal Component Analysis (PCA)

A multivariate statistical Principal Component Analysis (PCA) of selected biomarker ratio results for the 51 crude oil samples analysed from Sirt Basin, was used to determine the differences or similarities between the samples.

The data are composed of 10 variables, which include biomarker ratios and two maturity ratios, for the crude oil samples. Data were analysed using PCA to determine the major sources of variation within the sterane, diasterane, hopane and diahopane distributions, and the variables used in this analysis are listed in Table 5.2. The first three principal components (PC1, PC2 and PC3) obtained represent 63.7%, 17.8%, and 7.2%, respectively, of the variance within the data set. This type of variance analysis allows the relationships between samples to be studied in simple two-dimensional score plots of PC1 versus PC2. This includes the effects of all the original variables, which are source facies, molecular biomarker ratios, and maturity, which together represent the bulk of the variability in data at 81.5%. PC1 is characterised by a high loading of the maturity parameters. This may indicate that thermal maturity is the most significant factor controlling the composition and distribution of biomarkers in the Sirt Basin oils. PC2 is characterised by high loadings of biomarker parameters influenced by source

rock type and depositional environment. PC3 is characterised by high loadings for the sterane and hopane source parameters and is therefore considered to be primarily dependent on source organic matter type. Figure 5.29 shows the PC1 versus PC2 plots for the crude oil samples. The cross plot separates the crude oil samples into eight groups. Group 1 consists of all samples from the Mabruk and Kotla oilfields; group 2 samples from the Beda, Nasser, South Jebel, West Meghil and Zelten oilfields; group 3 the Dor Mansour, East Meghil, Fidda, Hakim, Augila Nafoora and Raguba oilfields; group 4 the Aswad, Safsaf and Zellah oilfields; group 5 the As Sarah oilfield; group 6 the Tuamma oilfield; group 7 the NC125 oilfield; and group 8 represent the Nakhla oilfield.

Figure 5.30 presents an interpretation of the three principal components using loading plots. These charts present the loadings of the different variables at the three principal components, where large loadings are either negative or positive and indicate a significant influence of each variable on that principal component. It is generally agreed that loadings can be considered high when values are more than 0.6, either negative or positive, moderately high when above 0.3, and low when less than 0.3 (e.g. Kline, 1994; Jolliffe, 2002). A low loading suggests that there is little or no correlation between the variables and the PCs.

In the first principal component, PC1, moderately high loadings (>0.3-0.6) are found for the C_{30} diahopane/C_{30} 17α hopane, C_{29} Ts/C_{29} hopane, C_{29} αααS/αααS+αααR sterane, C_{29} αββ/αββ+ααα sterane, and %C_{27} sterane parameters. In interpreting this, it is clear that organic facies, which is represented by the C_{30} diahopane/C_{30} α hopane, C_{29}Ts/C_{29} hopane ratios and %C_{27} sterane, plus the C_{29} αααS/αααS+αααR sterane, and C_{29} αββ/αββ+ααα sterane maturity parameters, that have a major effect on the concentration of biomarkers in the crude oils as shown in Table 5.2. Maturity parameters also appear to control the distributions of biomarkers and hence are more significant than organic facies effects.

For the second principal component, PC2, moderately high loadings are observed for Ts/Tm, ΣC_{27} diasterane/Σ C_{27} sterane, C_{29}% and sterane/hopane ratios. Consequently, it could be considered that organic facies appears to have more effect on PC2 than

maturity, and that this may have impacted on the distributions of biomarkers in the crude oils from the Sirt Basin.

The third principal component is less significant than the first and second PCs, (representing 7.2% of the total variance in the data set) and no high loadings are recorded for this component. Moderate loadings are found for the Ts/Tm, ΣC_{27} diasterane/Σ C_{27} sterane, and C_{28}% parameters. Therefore, it could be considered that source facies has the most impact on the distribution of the biomarker in the Sirt Basin crude oils.

The combinations of PC1 and PC2 and PC1 with PC3 account for 81.5% and 70.9% respectively of the total data set, showing nearly similar effects of source organic facies and maturity on the concentration and distribution of biomarkers in the crude oils from the Sirt Basin.

It is clear from the analysis that the crude oil samples in groups 1 and 2 are dominated by the high ΣC_{27} diasteranes/ΣC_{27} steranes ratio and C_{28}%, while they have low to moderate levels of C_{27}% and C_{29}% sterane, suggesting that both groups have a moderate input of eukaryotes and prokaryotic organisms as well as indicating that they originate from source rocks with high clay content deposited in predominantly reducing marine environments. The crude oils from group 3 showed moderate to high abundance of %C_{29} steranes and low ratios of C_{29}Ts/C_{29} hopane, Ts/Tm and sterane/hopane, indicating moderate eukaryote algae input and/or land plant organic matter and this also consistent with moderate contributions from prokaryotic organisms (e.g. bacteria) (Volkman, 2003), suggesting deposition in a suboxic marine environment. Group 4 samples had high C_{29}% and low sterane/hopane, Ts/Tm and C_{29}Ts/C_{29} hopane ratios relative to the other oil families. This indicates that this group has high contributions of prokaryotic organisms, (e.g. cyanobacterial algal organic matter and bacteria) relative to eukaryotes and the oil was deposited in lacustrine to marine environment. Groups 5 to 8 oils are dominated by C_{27}%, C_{30} diahopane/C_{30} hopane, C_{29} αααS/αααS+αααR sterane, and C_{29} αββ/αββ+ααα sterane ratios, while low in C_{29}% and C_{28}%, and with a low ΣC_{27} diasteranes/ΣC_{27} steranes ratio. This indicates moderate to high contributions of algal and prokaryotic organisms to the source rock deposited in suboxic marine environments. Alternatively, changes in depositional environments

may have led to moderate preservation in organic matter within suboxic conditions, or it might be that the organic matter exhibited higher thermal maturity due to overburden sediments (e.g. Gürgey, 2003).

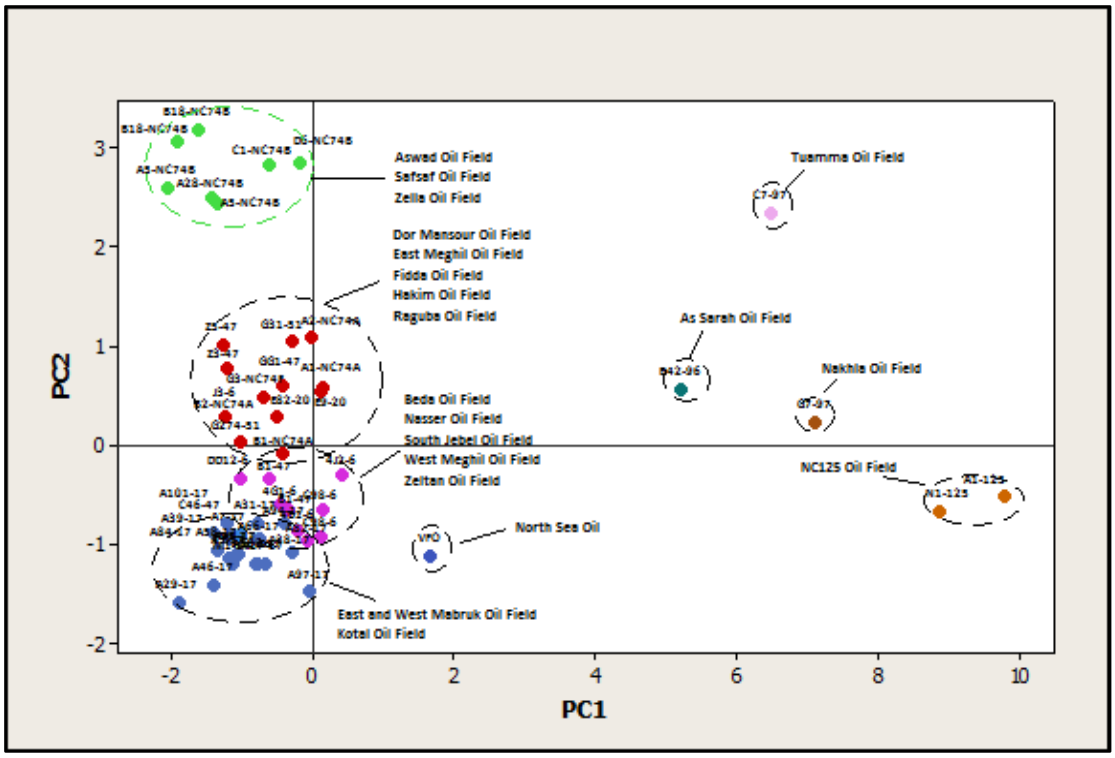

Figure 5.29: Cross plot of PC1 versus PC2 for the biomarker data of the crude oil samples from the Sirt Basin.

Table 5-2: The correlation matrix of the bulk geochemical data and biomarker parameters used in the principle component analysis (PC1, PC2 and PC3) for crude oils in Sirt Basin.

Variable Number	Variables Parameters	C_{27} Ts/Tm	C_{30}dia/C_{30} H	C_{29}Ts/C_{29} H	C_{29} S/(S+R)	C_{29} αββ/(αββ+ααα)	Σ C27 dia/ Σ C_{27} Sterane	C_{27}%	C_{28}%	C_{29}%	Sterane/ hopane	Percentage of variance explained (%)
1	C_{27} Ts/Tm	1.000										
2	C_{30}dia/C_{30} H	0.866	1.000									
3	C_{29}Ts/C_{29} H	0.832	0.872	1.000								
4	C_{29} S/(S+R)	0.019	0.698	0.799	1.000							
5	C_{29} αββ/(αββ+ααα)	0.513	0.782	0.816	0.885	1.000						
6	Σ C_{27} dia/Σ C_{27} Sterane	-0.147	-0.539	-0.472	-0.753	-0.756	1.000					
7	C_{27}%	0.425	0.878	0.880	0.864	0.839	-0.650	1.000				
8	C_{28}%	-0.168	-0.723	-0.581	-0.590	-0.584	0.499	-0.768	1.000			
9	C_{29}%	-0.535	-0.499	-0.681	-0.364	-0.343	-0.166	-0.558	0.147	1.000		
10	Sterane/hopane	0.612	0.465	0.768	0.619	0.577	-0.152	0.657	-0.328	-0.770	1.000	
	PC1	0.234	0.351	0.379	0.353	0.361	-0.248	0.381	-0.276	-0.233	0.295	63.70
	PC2	-0.369	0.077	-0.133	0.174	0.154	-0.507	0.078	-0.278	0.548	-0.382	17.80
	PC3	-0.494	0.294	0.011	-0.163	-0.280	0.386	0.195	-0.557	-0.246	-0.075	7.20

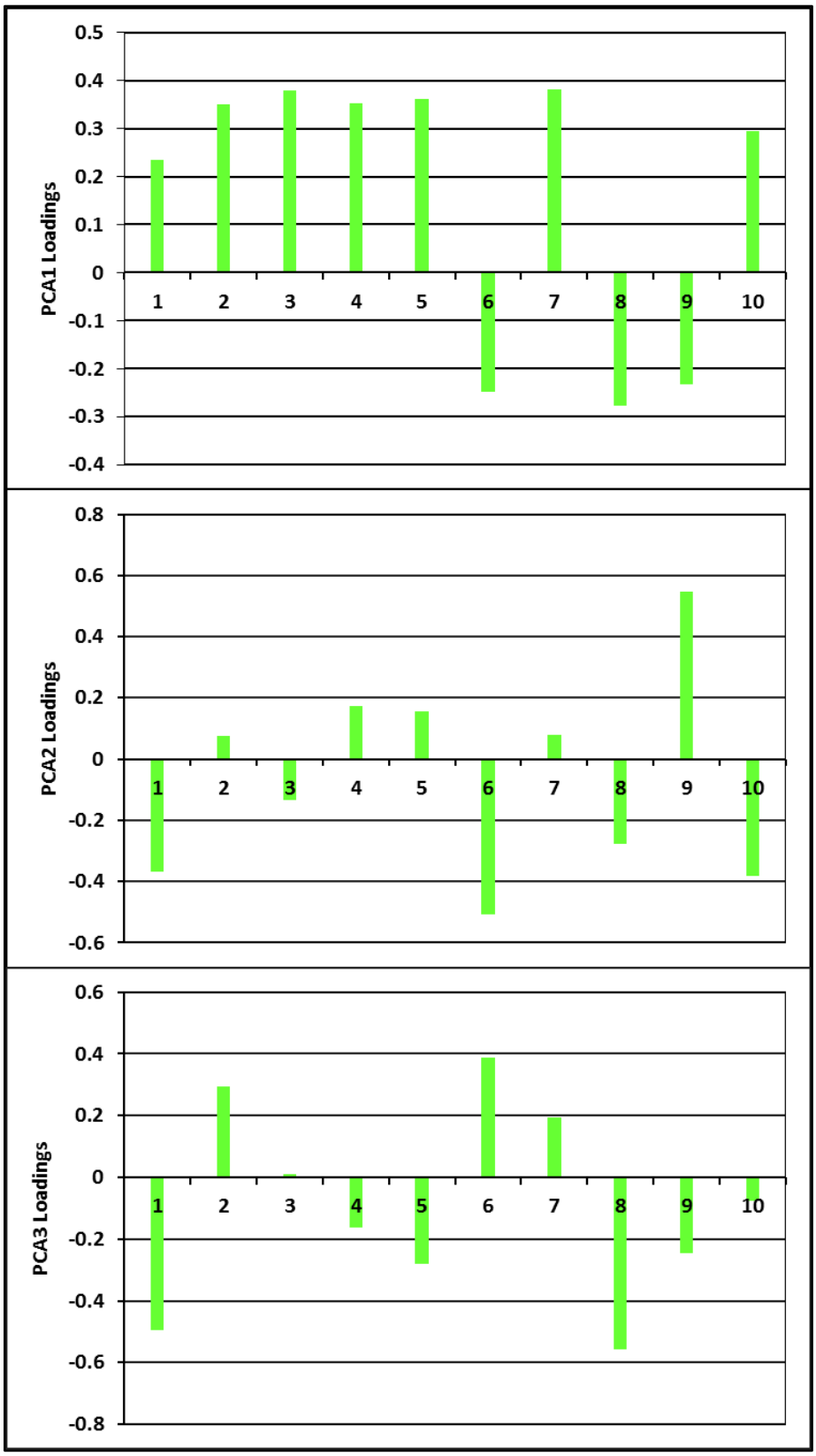

Figure 5.30: Loadings plots showing the composition of the first three PCs, PC1, PC2 and PC3, which scored 63.7%, 17.8% and 7.2% of total variance in the data analysis set, respectively.

5.4 Carbon Isotopic Composition of Compounds

In this study, compound-specific isotope analysis (CSIA) has been performed to determine the stable carbon composition of the *n*-alkanes from the crude oils. The stable carbon isotopic composition of the *n*-C_{10} to *n*-C_{32} alkanes was measured using GC- IRMS for 13 crude oil samples. The $\delta^{13}C$ values of these *n*-alkanes are plotted in Figure 5.31, which shows that the values of the crude oil samples cover a broad range between -22.5 to -40.3‰. The profile of $\delta^{13}C$ values of the *n*-alkanes from the crude oil samples studied showed a similar trend for most of the samples analysed, except for oil families 1A and 6 where variations are observed in the $\delta^{13}C$ isotope values in *n*-$C_{18,}$ but their $\delta^{13}C$ isotope values after *n*-C_{19} are more similar. The high *n*-C_{18} $\delta^{13}C$ values may be due to the partial co-elution of phytane with *n*-C_{18}. Also, the profile of $\delta^{13}C$ values of *n*-alkanes from oil families 1A, 1B, 3, 4 and 5 shows depletion in the $\delta^{13}C$ isotope from *n*-C_{27} to *n*-C_{32}, which may be due to their production from lighter carbon compounds in the kerogen source rock. Most of the crude oil samples analysed appear with a nearly flat isotopic profile which is generally associated with the characteristics of those expelled from sources rich in marine organic matter input (Murray *et al.*, 1994). This flat profile may be produced by homogeneity in the *n*-alkane $\delta^{13}C$ distribution that is thought to be a result of the derivation of organic carbon from a closely uniform carbon pool. This similarity in the isotope profiles of the crude oil samples analysed from oil families 1A, 1B, 3, and 4 may reflect an origin of organic source facies rich in marine organic matter, which has also been inferred from the molecular biomarker analyses, as shown in Figure 5.32. Family 6 seems to be similar isotopically with oil families 1A, 1B, 3 and 4, as it shows lighter $\delta^{13}C$ isotopic values in the short chained components below *n*-C_{21}, while with increasing *n*-alkane chain length, the $\delta^{13}C$ isotope compositions show trends toward isotopically heavier values (positive slope), with isotopic range being typically 5-9‰ throughout oil families 5 to 9, as shown in Figure 5.33. This may be due to production of *n*-alkanes from source rocks characterised by marine organic matter with high contributions from algal organic matter in oil families 6 and 9. Meanwhile oil families 5 appear to be characterised by marine organic matter with high contributions of terrestrial organic matter. In oil family 7 the $\delta^{13}C$ isotope values of the short chain *n*-C_{11} to *n*-C_{16} alkanes show trends toward isotopically heaviest values, while within the *n*-C_{17} to *n*-C_{26} the

$\delta^{13}C$ isotope trend show a trend toward lighter $\delta^{13}C$ isotope values. However, with increasing *n*-alkanes chain length after *n*-C_{27} the $\delta^{13}C$ isotope measurements show a trend toward isotopically heavier (positive) values. This phenomenon may indicate that the source rocks that generated these oils are characterised by mixed of marine organic matter with moderate to high contributions from Algal organic matter (e.g. Bjorøy *et al.*, 1991; Bjorøy *et al.*, 1992). The crude oil from the Nakhla field (Family 9) showed isotopically heavier values of $\delta^{13}C$, suggesting a marine source with a high contribution of algal material or that this oil was generated at a higher level of thermal maturity. Family 5, represented by the As Sarah oilfield had the isotopically lightest (more negative $\delta^{13}C$ isotope values) components, which may be consistent with a marine source containing higher terrigenous organic matter inputs or exhibited to lower levels of thermal maturity. In general, the negative values are predicted if terrigenous productivity prevails in the sedimentary record, while more positive $\delta^{13}C$ isotope values can be indicative of input from predominantly algal, with *n*-alkanes derived from algae being richer in $\delta^{13}C$ isotope values. It is clear that the isotopic composition of crude oils within each oil family is probably controlled by source organic matter and depositional environment, as well as maturity, which is indicated by previous analyses such as those of *n*-alkane, isoprenoid and other saturated and aromatic hydrocarbon distributions. The crude oils could be separated into a set of ten similar oil families, which hence provided additional evidence for the existence of at least ten oil families of petroleum in the study area. The variance in *n*-alkane carbon isotopic compositions of the saturated fractions is consistent with different sources. The data for the compound-specific isotopic analyses showing the $\delta^{13}C$ values of the *n*-alkanes of the different oil families are presented in Table 5.3.

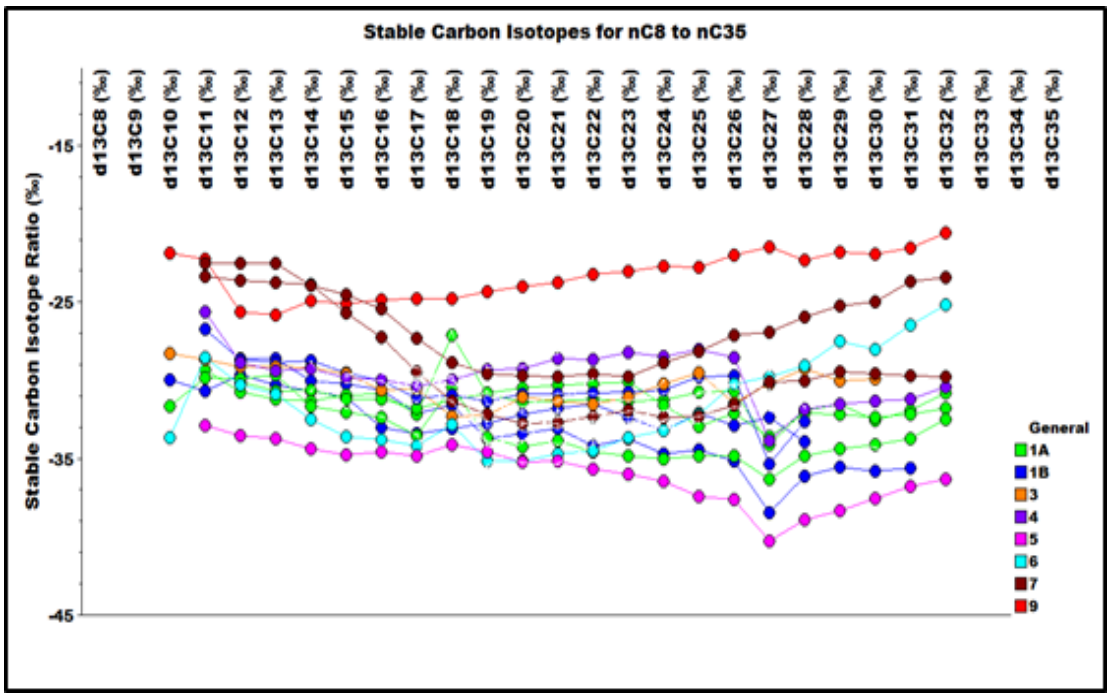

Figure 5.31: *n*-alkane stable carbon isotope plots for the all Sirt Basin oil families analysed.

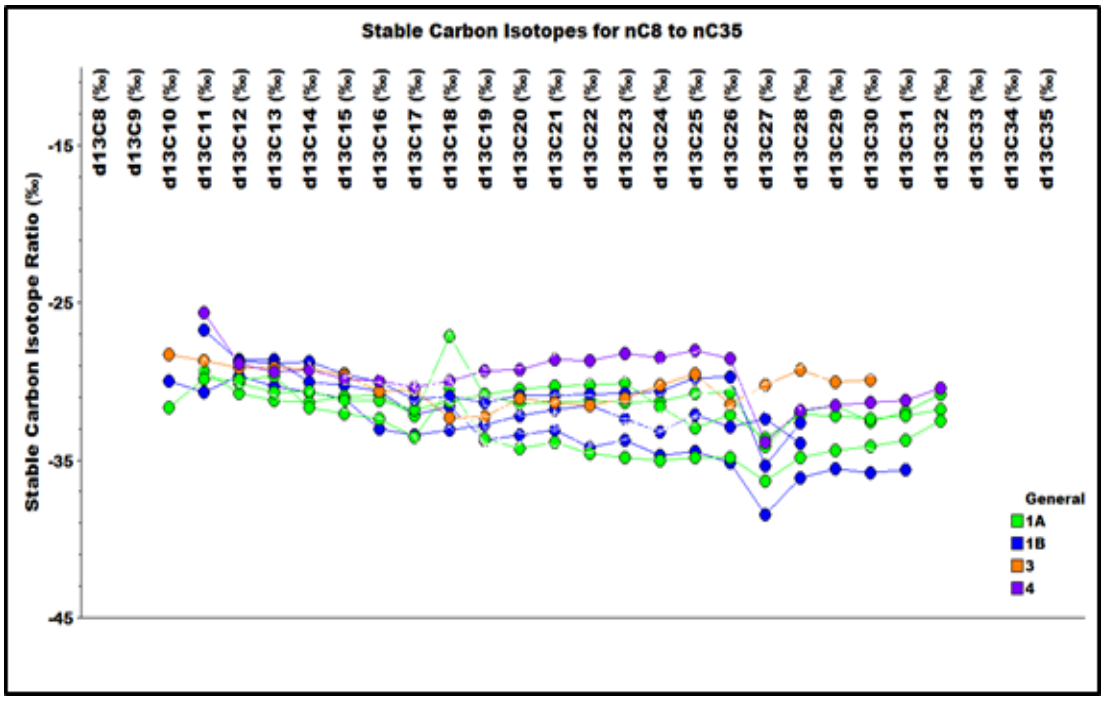

Figure 5.32: *n*-alkane stable carbon isotope plot for the western and central Sirt Basin oil families 1A, 1B, 3 and 4.

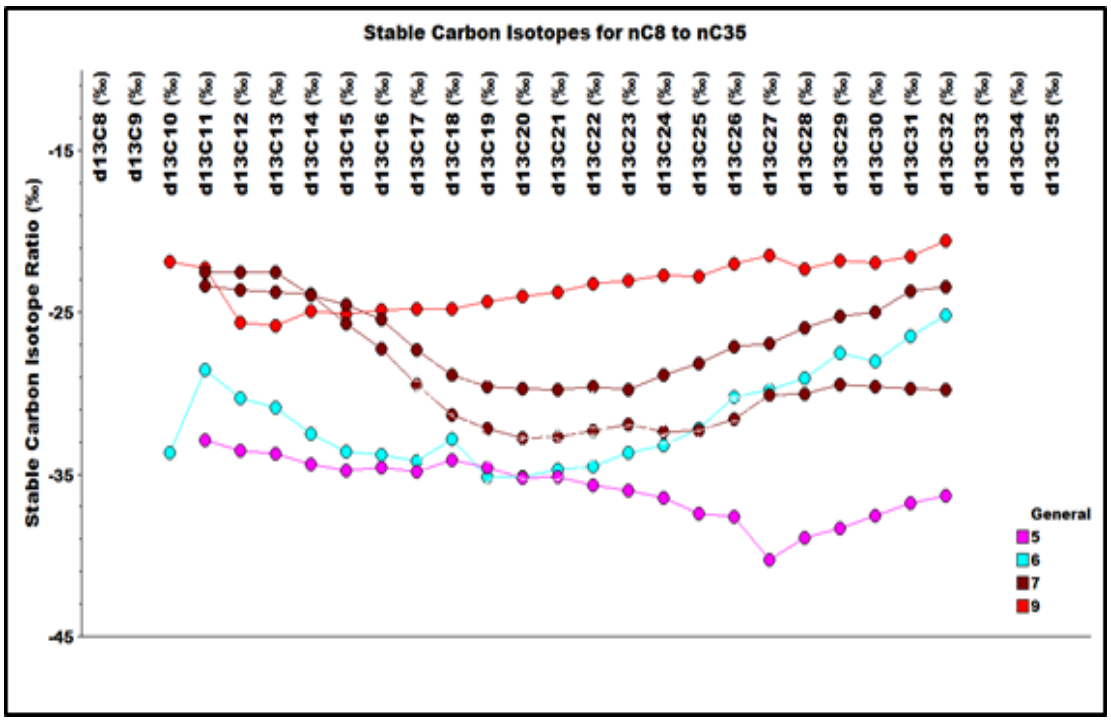

Figure 5.33: *n*-alkane stable carbon isotope plot for the eastern Sirt Basin oil families 5, 6, 7 and 9 oils.

Table 5-3: Compound specific isotopic $\delta^{13}C$ values for n-alkanes of the oil families in the Sirt Basin.

Oil Field	West Mabruk		East Mabruk	Safsaf	South Jebel	West Meghil	Ragoba	Dor Mansour	As Sarah	Augla Nafora	Tuamma	NC 125	
Well	A31-17	A38-17	A58-17	C1-NC74B	4B1-6	4J2-6	E82-20	Z5-47	B42-96	G13-51	C7-97	A1-NC125	N1-NC125
Location	West Sirt Basin					Central Sirt Basin				East Sirt Basin			
Groups	1A			4		1B		3	5	6		7	
n-C_{10}			-31.7			-30.0		-28.3		-33.7	-21.9		
n-C_{11}	-29.3		-29.9	-25.7		-30.7	-26.7	-28.7	-32.9	-28.6	-22.3	-22.5	-23.4
n-C_{12}	-30.8	-30.1	-29.9	-28.9	-28.6	-29.7	-28.7	-29.2	-33.6	-30.3	-25.6	-22.5	-23.7
n-C_{13}	-31.2	-30.7	-29.7	-29.4	-28.6	-30.3	-28.9	-29.2	-33.7	-30.9	-25.8	-22.5	-23.8
n-C_{14}	-31.4	-30.6	-31.7	-29.3	-30.1	-30.7	-28.8	-29.2	-34.4	-32.5	-24.9	-24.0	-23.9
n-C_{15}	-31.0	-31.2	-32.1	-29.9	-30.2	-31.1	-29.5	-29.6	-34.8	-33.6	-25.1	-24.5	-25.7
n-C_{16}	-30.9	-31.2	-32.4	-30.0	-30.6	-33.0	-30.1	-30.6	-34.6	-33.8	-24.9	-25.5	-27.3
n-C_{17}	-32.2	-31.8	-33.6	-30.4	-32.1	-33.4	-31.2	-30.6	-34.8	-34.2	-24.8	-27.3	-29.5
n-C_{18}	-27.1	-31.3	-30.4	-30.0	-31.6	-33.1	-31.0	-32.3	-34.1	-32.9	-24.8	-28.9	-31.4
n-C_{19}	-30.9	-30.8	-33.7	-29.4	-33.7	-32.8	-31.3	-32.3	-34.6	-35.2	-24.4	-29.6	-32.2
n-C_{20}	-31.4	-30.5	-34.3	-29.3	-33.4	-32.2	-30.9	-31.1	-35.3	-35.2	-24.0	-29.7	-32.8
n-C_{21}	-31.4	-30.3	-33.9	-28.6	-33.1	-31.8	-30.9	-31.3	-35.2	-34.7	-23.8	-29.8	-32.7
n-C_{22}	-31.2	-30.3	-34.6	-28.7	-34.2	-31.5	-30.8	-31.5	-35.7	-34.5	-23.2	-29.6	-32.3
n-C_{23}	-31.4	-30.1	-34.8	-28.2	-33.8	-32.4	-30.8	-31.1	-36.0	-33.7	-23.1	-29.8	-31.9
n-C_{24}	-31.3	-31.6	-35.1	-28.5	-34.7	-33.2	-30.6	-30.3	-36.5	-33.2	-22.7	-28.9	-32.4
n-C_{25}	-30.8	-33.0	-34.8	-28.0	-34.5	-32.1	-29.8	-29.5	-37.4	-32.2	-22.8	-28.2	-32.3
n-C_{26}	-30.7	-32.1	-34.8	-28.6	-35.2	-32.9	-29.7	-31.5	-37.6	-30.2	-22.0	-27.2	-31.6
n-C_{27}	-34.2	-33.6	-36.4	-33.9	-38.5	-32.4	-35.4	-30.3	-40.3	-29.8	-21.5	-27.0	-30.1
n-C_{28}	-31.9	-32.1	-34.9	-31.9	-36.2	-33.9	-32.7	-29.3	-38.9	-29.1	-22.4	-26.0	-30.1
n-C_{29}	-31.6	-32.2	-34.4	-31.5	-35.6			-30.1	-38.3	-27.5	-21.8	-25.3	-29.5
n-C_{30}	-32.6	-32.4	-34.1	-31.4	-35.8			-29.9	-37.6	-28.0	-22.0	-25.0	-29.6
n-C_{31}	-31.9	-32.2	-33.7	-31.2	-35.6				-36.8	-26.5	-21.6	-23.7	-29.7
n-C_{32}	-30.8	-31.8	-32.5	-30.5					-36.3	-25.2	-20.6	-23.4	-29.8

5.5 Thermal Maturity

Saturated and aromatic molecular marker compounds have been extensively used to determine the thermal maturity of oils and source rocks (Peters, 2005b). However, it has also been observed that biomarker and aromatic compound ratios can sometimes be influenced by changes in organic facies and depositional environment (Peters, 2005b). The maturity of crude oils can be evaluated based on sterane and terpane biomarker ratios and diamondoid compounds, as well as aromatic hydrocarbon compounds, which include aromatic steroids, alkylnaphthalenes, alkylphenanthrenes, and alkyldibenzothiophenes (e.g. Alexander *et al.*, 1985; Radke, 1987; Radke, 1988; Alexander *et al.*, 1992b). Therefore, a combination of saturated and aromatic hydrocarbon molecular markers was used to determine the thermal maturity of these Sirt Basin crude oils. In the present study, the assessment of the thermal maturity of the crude oil samples was achieved using the following biomarker parameters: [20S/(20S+20R)]- 5α(H),14α(H),17α(H) C_{29} steranes; 5α(H),14β(H),17β(H)/[5α(H),14β(H),17β(H)+5α(H),14α(H),17α(H)][αββ/(αββ+ααα)]-C_{29} steranes (Mackenzie *et al.*, 1980); C_{27} hopane Ts/(Ts+Tm) (Seifert and Moldowan, 1978); C_{30} diahopane/(C_{30} diahopane+C_{30} αβ hopane, C_{30} βα Moretane/(C_{30} βα Moretane+C_{30} 17αβ hopane), and [C_{32} 17α,21β homohopane (22S)]/[C_{32} 17α,21β homohopane (22S)+ C_{32} 17α,21β homohopane (22R)] (Seifert and Moldowan, 1978; Mackenzie and McKenzie, 1983; Peters and Cassa, 1994; Zhang *et al.*, 2000; Peters, 2005b). The values of all of these maturity parameters are listed in Table 5.5 in Appendix II.

5.5.1 Steranes and Terpanes

The values of the sterane based thermal maturity parameters, C_{29} ααα 20S/(20S+20R) and ββ/(ββ+αα) ratios for oil families 1A, 1B, 2, 3, 4 and 6 are ranged closely between 0.42-0.57 and 0.42-0.60, respectively (Table 5.5 in Appendix II), suggesting a similar thermal maturity for these oil families, whereas the equilibrium stages occur between 0.52-0.55 and 0.67-0.71, respectively. These maturity values indicate that most of the oils have not reached full maturity with respect to the equilibrium values suggested by Seifert and Moldowan (1986). Meanwhile, oil families 5, 7, 8 and 9 of oils from wells

located in the eastern part of the basin have C_{29} ααα sterane 20S/(20S+20R) and αββ/(αββ+ααα) maturity ratios ranging between 0.74-0.88 and 0.66-0.69, respectively, indicating a similar level of thermal maturity for these oil families and that the oils have reached their equilibrium phase as shown in Figure 5.34. This maturity data may indicate that oils generated from source rocks in the eastern part of the basin are more mature than those from source rocks in the central and western parts of the basin. This also suggests that the maturity of oils is related to the maturity of the source rock, which is deeper in the east of the basin than in the centre and west, or to the extent of reservoir maturation. In addition, the slight difference in the αββ/(αββ+ααα) C_{29} sterane ratios between oil families that have not reached equilibrium and those have may be a result of the effects of source and deposition variations in these ratios.

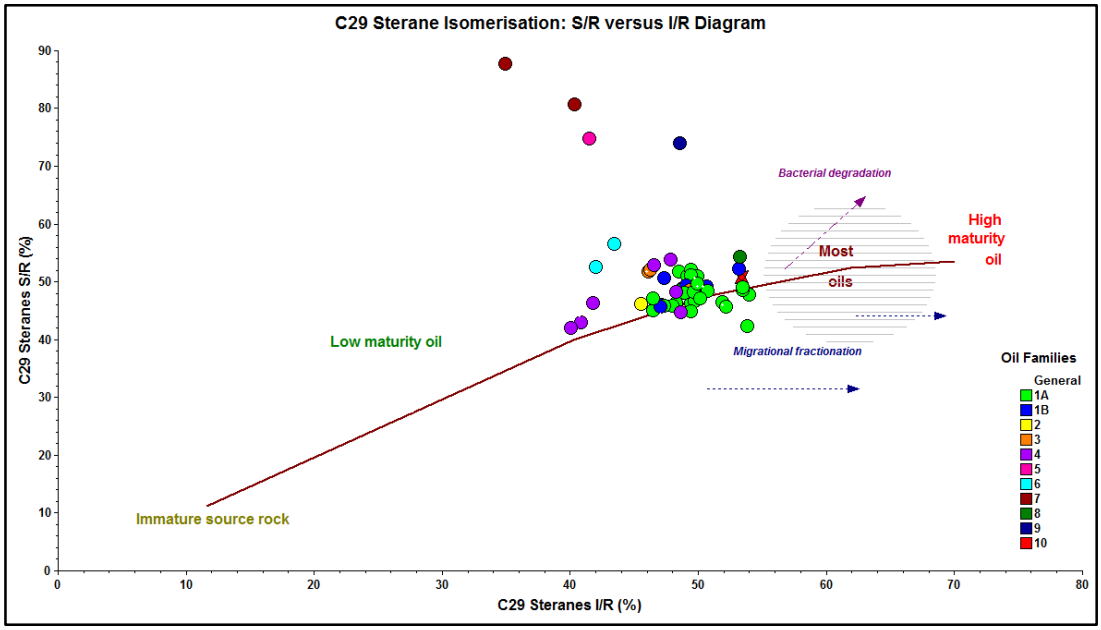

Figure 5.34: Cross plot of C_{29} sterane I/R (C_{29} αββ 20R+20S)/C_{29} ααα (20S+20R) versus C_{29} ααα 20S/C_{29}ααα 20R sterane percentage of the crude oils in the Sirt Basin.

The values for C_{27} Ts/(Ts+Tm) ratios range from 0.39 to 0.68 (Table 5.5 in Appendix II) for the oil families 1A, 1B and 6, indicating that the Tm is less abundant than Ts and that most of the oil samples are within the early mature to mature stages of thermal maturity. One oil sample in family 1A collected from the East Mabruk oilfield (well A97-17) in western Sirt Basin showed a higher value of Ts/(Ts+Tm), 0.73, which may indicate the significant effect of source organic matter and depositional environment variation. For oil families 2 and 3, the ratios ranged from 0.37 to 0.41, indicating an

immaturity to early thermal maturity. Family 4 oils contain the lowest ratios, ranging of 0.19 to 0.37, indicating an immature to early mature stage. This perhaps also reflects that these oils originated from carbonate source rocks (e.g. McKirdy and Aldridge, 1981; McKirdy *et al.*, 1984; Rullkötter *et al.*, 1985). Oil families 5, 7, 8 and 9 show relatively high values of the ratio in the range of 0.64 to 0.74, (Table 5.5 in Appendix II) indicating a middle mature stage. Variations in the Ts/(Ts+Tm) ratios in each family of oils indicate that the ratio is not only controlled by thermal maturity, but other factors such as organic matter source and depositional environment may also have significant effects (e.g. Moldowan *et al.*, 1986).

The [C_{32} 17α,21β homohopane (22S)]/[C_{32} 17α,21β homohopane (22S)+C_{32} 17α,21β homohopane (22R)] ratio increases from 0 to 0.60 during maturation (Table 5.5 in Appendix II), and the equilibrium phase occurs between 0.57 and 0.62. Most of the crude oil samples analysed had values varying between 0.57 and 0.63, indicating equilibrium values for this ratio and that the early phases of oil generation had been reached (e.g. Seifert and Moldowan, 1980).

The values of the C_{30} 17α(H) diahopane/(C_{30} 17 α(H) diahopane+C_{30} 17α(H) hopane) ratios of the crude oil samples are in the range of 0.04 to 0.14 (Table 5.5 in Appendix II) for the oil families 1A, 1B, 2, 3, and 4, suggesting immaturity to early maturity for petroleum generation. The ratios are relatively higher (from 0.16 to 0.64) for oil families 5, 6, 7, 8 and 9, indicating the middle mature zone (e.g. Moldowan *et al.*, 1986; Peters and Moldowan, 1993; Peters, 2005b) .

The C_{30} βα Moretane/(C_{30} βα Moretane+C_{30} 17αβ hopane) ratio decreases with thermal maturity from 0.80 in immature bitumen to < 0.15 in mature source rock (Mackenzie *et al.*, 1980; Seifert and Moldowan, 1980). The crude oil samples analysed showed moderate values of the moretane/hopane ratio (0.08 to 0.11) for oil families 1A, 1B, 2, 3, and 4, indicating the early to middle mature zone; oil families 5, 6, 7, 8 and 9 had the highest ratios, ranging from 0.15 to 0.51, and suggesting the middle to highly mature stages. The higher values may be due to them having been affected by other factors such as organic facies changes and/or the depositional environment of the source rock (e.g. Mackenzie *et al.*, 1980).

The tricyclic C_{20}-C_{30} tricyclic terpanes/(C_{20}-C_{30} tricyclic terpanes+C_{27}-C_{35} αβ hopanes) parameter has been proposed to measure maturity when vitrinite reflectance (*Ro%)* values reach up to 1.4% (Peters and Moldowan, 1993). In addition, the C_{23} tricyclic terpane/C_{23} tricyclic terpane+C_{30} αβ hopane parameter is found to increase with increasing thermal maturity, but both parameters are influenced by differences in the sources of the compound classes (De Grande *et al.*, 1993). Greenwood and George (1999) also reported that the tricyclic/hopane ratios should be applied within sample groups of similar organic facies in order to avoid variations among the oil groups not related to thermal maturity. Figure 5.35 displays clear variations in degree of thermal maturity for both ratios. Oil Family 4 shows the lowest values, while oil families 5, 7, 8 and 9 show the highest values, indicating that these oil families, located in the eastern part of the basin, have higher levels of thermal maturity compared to the other oil families located in the central and western parts of the basin (Table 5.5 in Appendix II). This variation may also be attributed to difference in organic facies, and/or that the oils are derived from deeper sedimentary sections of the source rock in the east, relative to the central and western parts of the basin, which may have been generated from shallower source rocks.

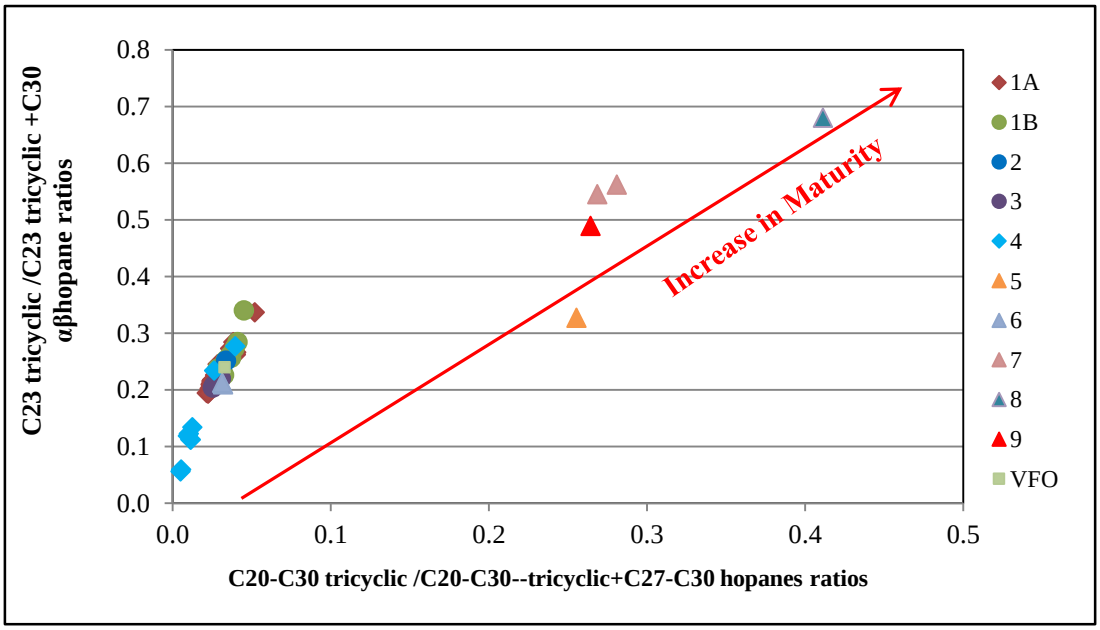

Figure 5.35: Cross plot of C_{20}-C_{30} tricyclic/C_{20}-C_{30} tricyclic+C_{27}-C_{30} hopanes versus C_{23} tricyclic/C23 tricyclic+ C_{30} αβ hopane ratios for the oil families in the Sirt Basin. Squares represent oils from the west, circles oils from a centre and triangles oils from east of the basin.

5.6 Aromatic Compounds

5.6.1 Aromatic Steroidal Hydrocarbons

The TA (I)/TA(I+II) ratio is calculated from the sum of the C_{20} and C_{21} triaromatic steroids TA(I) and the C_{26} to C_{28} (20S+20R) triaromatic steroids TA(II) (Peters, 2005b). For both monoaromatic steroids and triaromatic steroids, scission ratios were used as a summation of carbon numbers C_{20} and C_{21} short chain TA and C_{26} to C_{28} (20S+20R) long chain TA to reduce complications caused by the effects of source organic matter input (Peters, 2005b). In addition, both parameters are useful in the late oil-generative window. These triaromatic steroid hydrocarbon components are difficult to identify in some crude oil samples of the oil families 5, 7, 8 and 9, due to the low abundance of the triaromatic steroids probably related to high maturity and source effects. This phenomenon suggests that the complete aromatization of C-ring monoaromatic to ABC-ring triaromatic steroid hydrocarbons may have occurred, but this was not noticed in the other oil families studied.

The MA(I)/MA (I+II) versus TA(I)/TA(I+II) ratios increase from 0 to 100% during the thermal maturation of source rock or crude oils (e.g. Moldowan and Fago, 1986). Oil families 1A, 1B, 3 and 6 may have source rocks with similar characteristics and have values of MA(I)/(MA (I+II) ratios ranging from 12 to 34% and TA(I)/TA(I+II) ratios ranges from 12 to 43% (Table 5.6 in Appendix II). Family 2 oil has the lowest values (6%) for both ratios; while some oils from oil family 4, such as the Safsaf, and oil families 5, 7, 8 and 9 have the highest values for both ratios compared to other oil families, ranging from 45 to 69% and 60 to 85%, respectively (Table 5.6 in Appendix II).

Figure 5.36 shows the cross-plot of the MA(I)/(MA (I+II) versus TA(I)/TA(I+II) ratios. From this diagram, it is clear that the complete aromatization of C-ring monoaromatic to ABC-ring triaromatic steroids have not occurred in oil families 1A, 1B, 2, 3 and 6, situated towards the central and western parts of the Sirt Basin, as well as from samples from some oil fields in family 4. This suggests an early to middle mature zone for these oils, but in family 4 in the Safsaf fields, and oil families 5, 7, 8 and 9, located towards the east of the Sirt Basin, aromatization has occurred, suggesting middle to late mature

stages for these oils. This is in agreement with the results from other sterane and triterpane biomarker maturity parameters discussed earlier in this chapter.

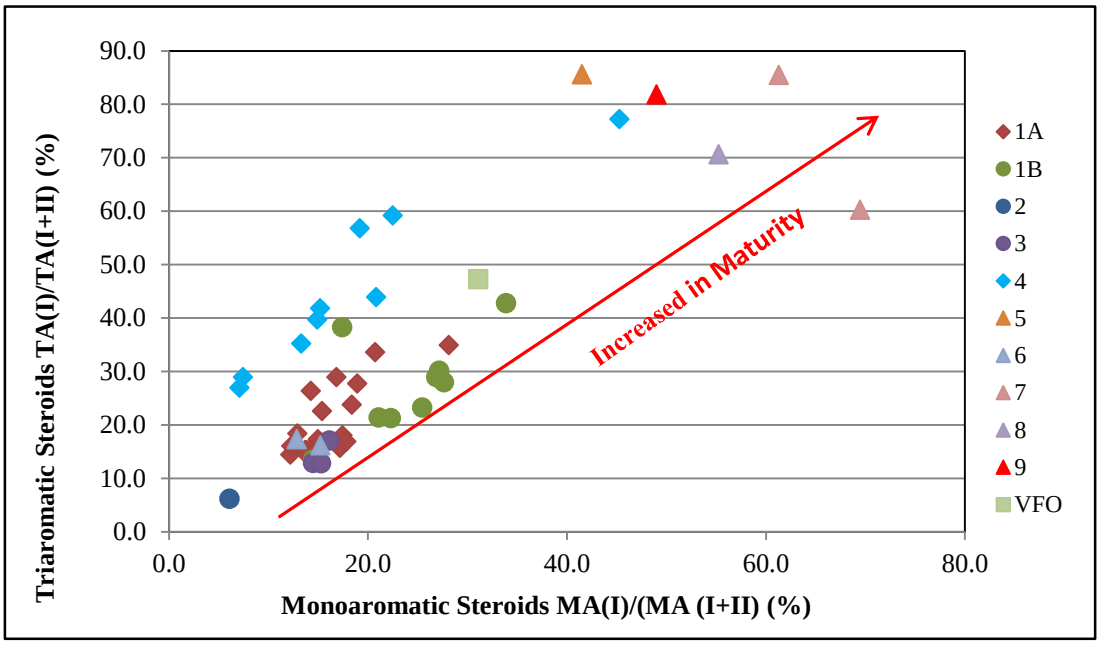

Figure 5.36: Cross plot of the MA(I)/MA(I+II) monoaromatic steroids versus TA(I)/Ta(I+II) triaromatic steroids for the oil families in the Sirt Basin. Squares represent oils from the west, circles oils from a centre and triangles oils from east basin.

5.6.2 **Alkylphenanthrenes**

In the present study the alkylphenanthrene and alkylnaphthalene maturity parameters used and their values are listed in Table 5.6 in Appendix II. Alkylaromatic isomers which are substituted at the β-position have been observed to become increasingly dominant at higher maturity levels compared to related isomers with α-substitution (Radke, 1987). Radke (1988) reported that the methylphenanthrene index (MPI-1) can be as useful for maturity assessment since MPI-1 shows a good positive linear correlation with vitrinite reflectance in the oil window zone (0.65-1.35 %*Ro*), and also good negative correlations at higher levels of maturity (1.35-2.0 %*Ro*). However, MPI-1 can be influenced by source lithology and organic matter type as well as the possible effects of migration (Radke *et al.*, 1982a; Cassani *et al.*, 1988). The values of MPI-1 and vitrinite reflectance calculated from it (%*Rc*) for crude oils in the present study are in the range of 0.41 to 0.77 and 0.56 to 1.04%, respectively, showing moderate to high maturity for the source rocks generating these oils. The MPI-1 values for oil families 1A, 1B, 2, 3, 4 and 5 range from 0.54 to 0.77, and the values of calculated vitrinite

reflectance (%*Rc*) range between 0.72 to 1.04%, indicating that these oil families are in the middle mature zone. For oil families 6, 7, 8 and 9, the MPI-1 and calculated vitrinite reflectance (%*Rc*) values range from 0.41 to 0.65 and 0.56 to 0.79, respectively, suggesting early to middle mature zones. In these oil families, the low MPI-1 and *%Rc* values may be due to the variations in the types of organic matter input or lithology as well as the lower concentrations of these compounds in the source rocks that have generated these oils in the eastern part of the basin. Radke *et al.* (1986) observed experimentally that alkylnaphthalenes are a better maturity indicator than alkylphenanthrenes because the latter is more affected by organic facies changes.

5.6.3 **Alkylnaphthalenes**

The assessment of the thermal maturity of the present crude oil samples was conducted using many of the alkylnaphthalene maturity ratios listed in Table 4.2 in chapter 4. The dimethylnaphthalene ratio (DMNR-1= (2,6-DMN+2,7-DMN)/(1,5-DMN) is another useful aromatic hydrocarbon maturity parameters for samples having a mean vitrinite reflectance (%*Ro*) equal to or higher than 1.0%, showing a linear increase in the ratio from 2 to 12 with increasing thermal maturity (Radke *et al.*, 1984; Radke, 1987). The DMNR-1 ratios for oil families 1A, 1B, 4, 6, 7, 8 and 9 are in the range of 4 to 16.1, clearly showing that the thermal maturity of the crude oils had reached the middle to late oil generating window, particularly in oil families 1A, 4, 5, 6, 7, 8 and 9, while oil families 2 and 3 oils were in the range of 2.20 to 3.32, indicating early maturity.

The 2-MN/1-MN versus (2,6-DMN+2,7-DMN)/(1,5-DMN) cross-plot for the oil families is shown in Figure 5.37, where both ratios increase with increasing thermal maturity, and this indicates that the crude oils in families 5 and 8 are more mature than the other oil families. Oil families 1A, 1B, 2, and 6 contain moderate values for both ratios, indicating middle maturity, while Family 3 oils have the lowest values, indicating early maturity. The low ratios in oil families 7 and 9, may be related to the low concentrations of methyl and dimethylnaphthalenes in these crude oil samples.

The trimethylnaphthalene ratio (TNR-1) was calibrated with the sterane isomerization ratio (20S/20R) which reaches an equilibrium value when the TRN-1 ratio exceeds 1.0 (Radke *et al.*, 1986). TRN-1 values for the Mabruk oilfield samples in family 1A and

oil families 4, 5, 7, 8 and 9 range from 0.80 to 1.40, indicating that the source rocks generating these oils had reached the middle to high maturity. Higher values of family 1A may be because this oil was generated from the deeper part of the source rock in the north Zellah Trough at the Gedari depression, or that these oils may have been thermally cracked during secondary oil migration from the Marada Trough in the centre of the Sirt Basin. In contrast, the oil families 1B, 2, 3 and 6 have TRN-1 values of less than 0.80, indicating that the source rock generating these oils had reached the early to middle mature zone.

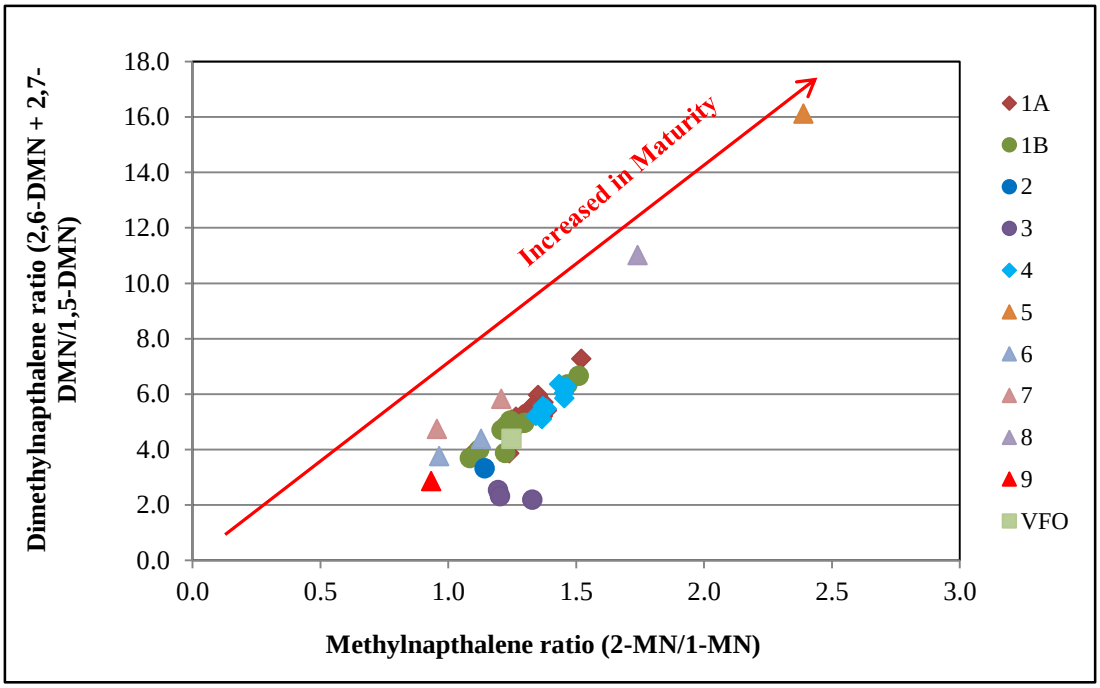

Figure 5.37: Cross plot of the methylnaphthalene versus dimethylnaphthalene ratios for the oil families in the Sirt Basin. Squares represent oils from the west, circles oils from a centre and triangles oils from east basin.

5.6.4 **Diamondoids**

In the present study, the methyl diamantane index (MDI) for the Mabruk oilfield in oil Family 1A, the Raiah oilfield in family 1B, oil families 2 (Kotla oilfield) and 3 (Dor Mansour oilfield) have relatively high values ranging from 52 to 59% (Table 5.6 in Appendix II), which indicates the same range of thermal maturity for these crude oils as shown in Figure 5.38, but these estimates do not reflect the maturity levels measured using other biomarker maturity parameters for shallower reservoirs. Therefore, the presence of high maturity oils in reservoirs of shallow depth, particularly in these oil

families, may be from moderate to long-distance secondary oil migration. The MDI values for the Beda, East Meghil and Fidda oilfields in an oil family 1A and oil family 4 indicate moderate maturity with values ranging from 45 to 50%. This suggests that these crude oils have similar degrees of thermal maturity. The moderate MDI values may suggest a moderate distance of oil migration for these oil families. Oil family 1B and 5 to 9 have MDI values between 33 and 46%, indicated the presence of low maturity oils and may suggest a short distance of oil migration.

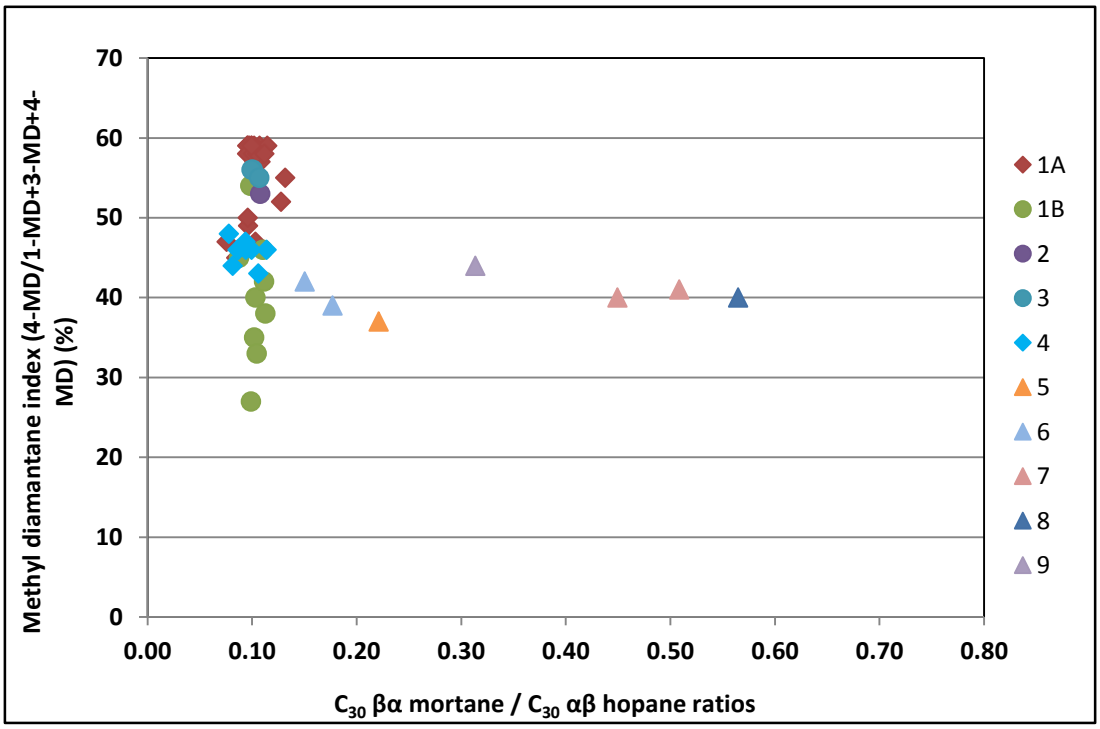

Figure 5.38: Cross plot of the C_{30} βα moretane/ C_{30} αβ hopane versus methydiamantane index for the oil families in the Sirt Basin. Squares represent oils from the west, circles oils from a centre and triangles oils from east basin.

5.7 Occurrence of carbazole and benzocarbazole pyrrolic nitrogen compounds in oils as migration indicators.

The pyrrolic nitrogen distributions of the Sirt Basin oils showed that the alkylcarbazole concentrations are higher than the benzocarbazoles (Figure 5.39). Oil families 1B and 1A contain high abundances of both alkylcarbazoles and benzocarbazoles relative to the other oil families. In most of the oils the relative abundance of dimethylcarbazoles is high in comparison to the methylcarbazoles, with oil family 3 the highest (Table 5.4a and b). The benzocarbazole [a]/[a]+[c] ratio of studying oils, covers a range from 0.41

to 0.76., (Table 5.4a and b) and this ratio does not appear to be affected by maturity or source organic facies for the studied oils, as shown in Figure 5.40. Therefore, the decrease in benzocarbazole concentrations with decreasing benzocarbazole ratios, as shown in Figure 5.41, is thought to be due to fractionation during secondary migration and thus roughly reflect the distance that an oil migrated (e.g. Larter *et al.*, 1996).

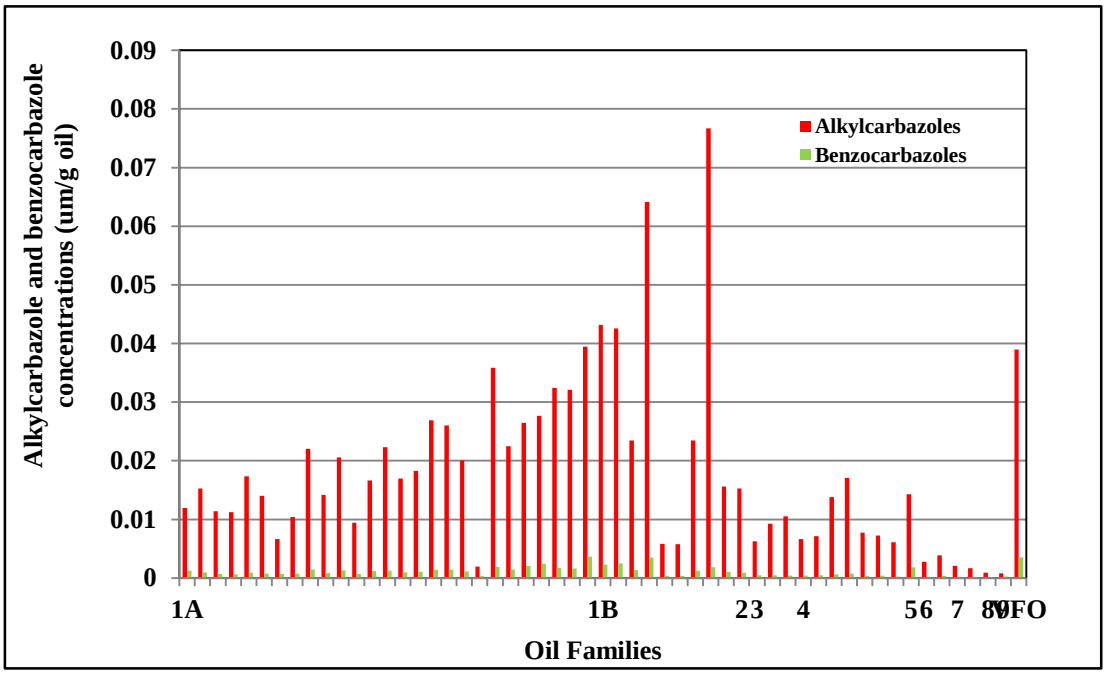

Figure 5.39: Concentrations of alkylcarbazoles and benzocarbazoles in the oil families in the Sirt Basin.

It appears from Figure 5.41, that oil families 1A and 4 represent oils derived from the Sirte Shale source rock and maybe older source rock (Family 4 oil) in the Sirt Basin have moderate to slightly long distance migration paths, compared to the other oil families. Oil families 1B, 2, 3, 9 and well G13-51 (Augila Nafoora oilfield) in oil family 6 represent oils originating from the Sirte Shale Formation that show short to moderate distance migration.

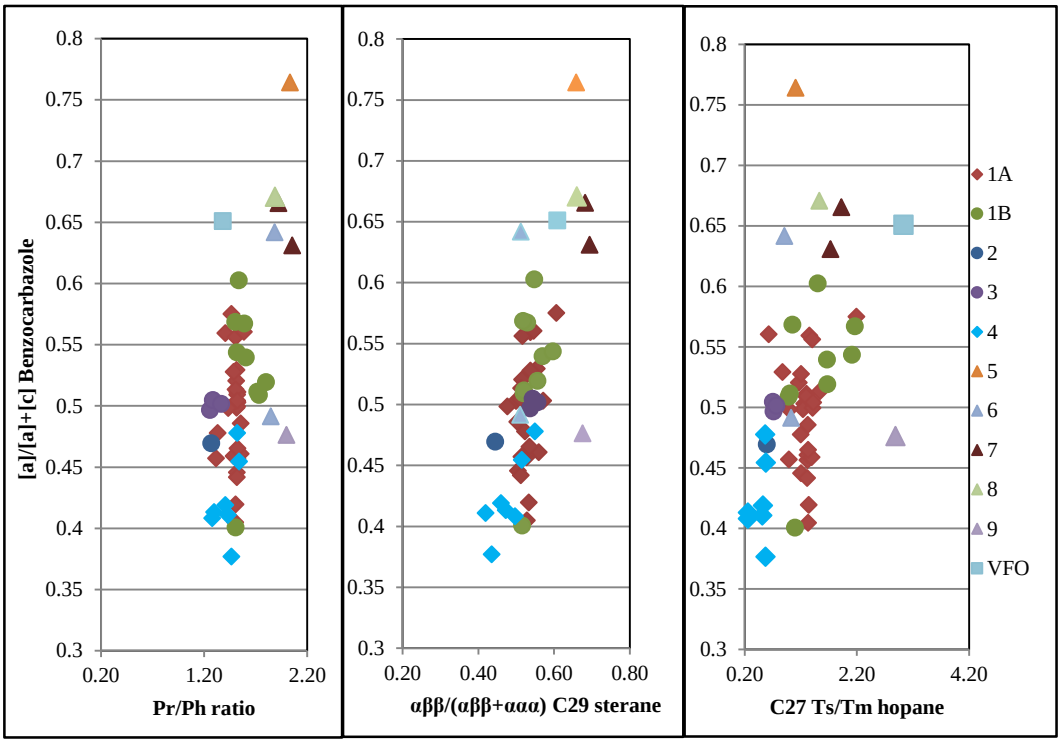

Figure 5.40: Benzocarbazole *a/(a+c)* ratios of oil families in the Sirte Basin, do not correlate with either maturity or source facies and probably reflect fractionation processes during secondary migration. Samples in the squares and circles represent oils from centre and west, and triangles represent oils from east Sirt Basin.

In contrast, the oil families 5, 7, 8 and well G274-51 in oil family 6 that may represent oils generated from Sirte Shale, Rachmat source rocks and/or Middle Nubian Shale source rock in the Agedabia Trough in the eastern part of the basin as well as the North Sea Oil have a high benzocarbazole ratio, suggesting relatively short distance migration. Therefore the crude oils from oil families 5, 7, 8 oils may have migrated vertically from the Sirte Shale, Rachmat and/or Middle Nubian Shale source rocks to nearby reservoirs throughout the faults joints in the Agedabia Trough. Oils from families 1B, 2, and 3 oils may have migrated vertically from the source rock kitchen in the Marada Trough, to accumulate in traps in Dor Mansour, Kotla, Raiah, Raguba, Zelten oilfields throughout the faults system in Beda Platform and Kotla Graben. Family 1A oils that accumulated in the Hakim, Fidda, and Sabah oilfields may have migrated both vertically and laterally from the source kitchen rocks in the north Zellah Trough at the Gedari depression. In this case, the distance of migration for both lateral and vertical, is relatively short. Meanwhile, for the Mabruk oilfield in the Family 1A oils in the Dor El Abid Through, the migrations were lateral, and maybe of moderate

to long distance from the Gedari depression in the north of the Zellah Trough to the Mabruk and Dahra reservoirs in the Al Dahra Al Hofrah oilfields. Oil reservoir in the Aswad and Zellah oilfields (Family 4 oils) in the Zellah Trough maybe have migrated laterally, because they showed low benzocarbazole ratios, which may indicate that moderate to slightly long distance migration had occurred.

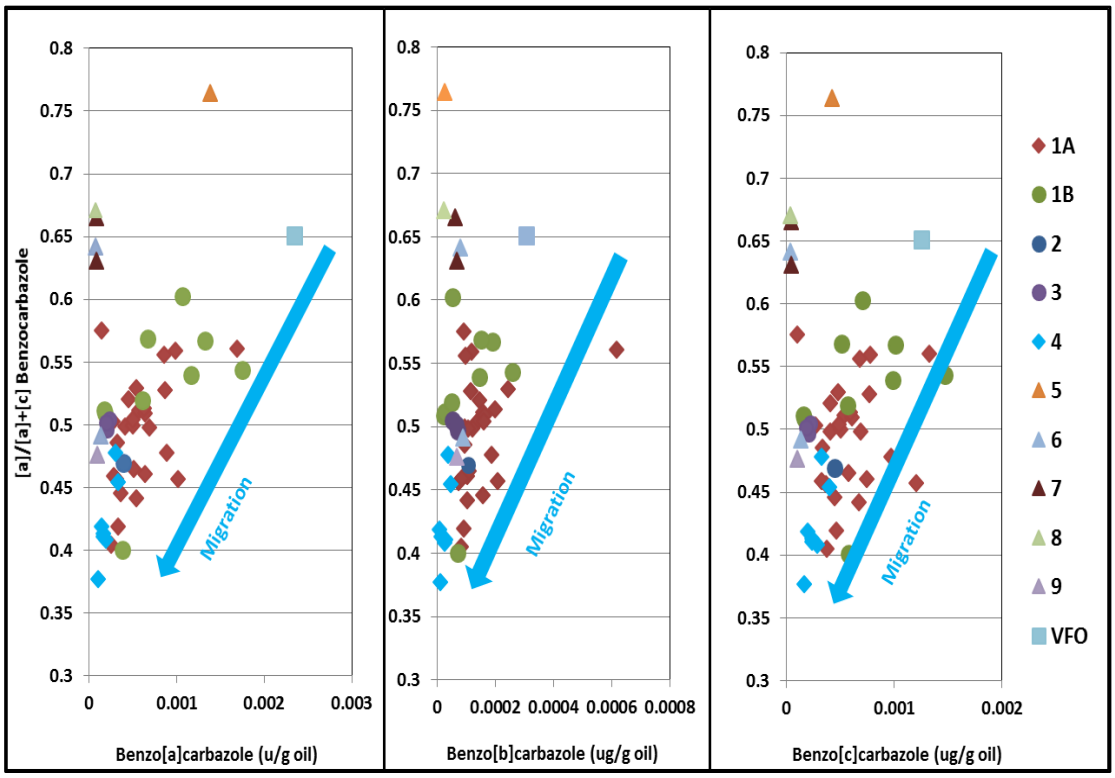

Figure 5.41: Benzocarbazole *a/(a+c)* ratios relative to benzocarbazole concentrations in oil families in the Sirte Basin, show decreasing benzocarbazole ratio with increasing fractionation processes during secondary migration. Samples in the squares and circles represent oils from centre and west, and triangles represent oils from east Sirt Basin.

Table 5-4a: Concentrations and proportions of the carbazoles, methylcarbazoles, dimethylcarbazoles, and benzocarbazoles and their ratios (together with some saturated hydrocarbon maturity and source parameters) in oil families in the Sirt Basin. CA-Carbazole; MCA-Methylcarbazole; DMCA-Dimethylcarbazoles; BNC-Benzocarbazole.

Location	Oil Families	Oil Filed	Well	Benzocarbazole concentratioins (µg/g oil)			BNC Ratio	BNC	Σ AC	Σ BNC	CA	MCA	DMCA	C_{29} Sterane	C_{27} Hopane	Iso-alkanes
			Name	a	b	c	a/(a+c)	b/(a+b+c)	µg/g oil	µg/g oil	%	%	%	ββ/(αβ+αα	Ts/Tm	Pr/Ph
West Sirt Basin	1A	West Mabruk	A31-17	0.0005	0.0002	0.0005	0.5294	0.1922	0.0119	0.0013	4.06	17.04	78.90	0.5537	0.87	1.51
			A29-17	0.0004	0.0002	0.0004	0.4457	0.1631	0.0153	0.0010	3.03	17.56	79.40	0.5043	1.21	1.52
			A86-17	0.0003	0.0001	0.0003	0.5031	0.2025	0.0114	0.0007	2.96	12.13	84.91	0.5710	1.27	1.52
			A44-17	0.0002	0.0001	0.0002	0.5030	0.2137	0.0113	0.0006	2.65	14.71	82.64	0.4991	1.29	1.52
			A66-17	0.0004	0.0001	0.0004	0.4986	0.1307	0.0174	0.0009	3.18	17.80	79.02	0.5331	1.24	1.51
			A15-17	0.0003	0.0001	0.0004	0.4567	0.0985	0.0140	0.0008	3.28	16.75	79.97	0.5273	1.32	1.52
			M1-17	0.0003	0.0001	0.0004	0.4049	0.1147	0.0066	0.0007	3.94	17.22	78.84	0.5275	1.33	1.50
			A46-17	0.0003	0.0001	0.0003	0.4857	0.1267	0.0104	0.0008	3.48	19.80	76.73	0.5028	1.32	1.55
			A82-17	0.0006	0.0001	0.0007	0.4608	0.0703	0.0221	0.0015	4.35	20.15	75.49	0.5588	1.32	1.55
			A94-17	0.0003	0.0001	0.0005	0.4195	0.1043	0.0142	0.0009	4.67	21.85	73.49	0.5328	1.34	1.50
			A39-17	0.0005	0.0001	0.0007	0.4419	0.0796	0.0206	0.0013	4.37	20.31	75.33	0.5119	1.31	1.52
			A27-17	0.0003	0.0001	0.0003	0.4591	0.1236	0.0094	0.0007	5.13	20.46	74.41	0.5248	1.39	1.49
			A38-17	0.0005	0.0001	0.0006	0.4652	0.0925	0.0166	0.0012	4.95	20.34	74.71	0.5345	1.33	1.52
		East Mabruk	A84-17	0.0006	0.0002	0.0005	0.5114	0.1250	0.0223	0.0013	4.31	21.14	74.55	0.5222	1.30	1.52
			A101-17	0.0004	0.0001	0.0004	0.5206	0.1459	0.0169	0.0010	3.47	18.08	78.45	0.5151	1.17	1.51
			A103-17	0.0005	0.0001	0.0005	0.4997	0.0854	0.0183	0.0011	3.53	18.91	77.56	0.5338	1.41	1.52
			A58-17	0.0006	0.0002	0.0006	0.5092	0.1162	0.0269	0.0014	4.07	18.55	77.37	0.5182	1.30	1.52
			A3-17	0.0006	0.0002	0.0006	0.5135	0.1418	0.0260	0.0014	4.36	18.72	76.92	0.5125	1.54	1.50
			A7-17	0.0005	0.0002	0.0005	0.5042	0.1416	0.0201	0.0011	4.56	21.99	73.45	0.5103	1.42	1.52
			A97-17	0.0001	0.0001	0.0001	0.5752	0.2706	0.0020	0.0003	4.44	10.50	85.06	0.6051	2.19	1.46
		Hakim	A1-NC74A	0.0010	0.0001	0.0008	0.5594	0.0630	0.0359	0.0019	6.10	21.40	72.50	0.5374	1.36	1.41
			A2-NC74A	0.0007	0.0001	0.0007	0.4984	0.0724	0.0225	0.0015	7.54	20.79	71.67	0.4764	0.99	1.43
		Fidda	B1-NC74A	0.0009	0.0002	0.0010	0.4779	0.0917	0.0265	0.0020	7.06	20.79	72.15	0.5223	1.20	1.33
			B2-NC74A	0.0010	0.0002	0.0012	0.4572	0.0864	0.0277	0.0024	6.66	20.72	72.62	0.5137	0.99	1.32
		Beda	B1-47	0.0009	0.0001	0.0008	0.5278	0.0664	0.0324	0.0017	1.84	13.58	84.58	0.5370	1.21	1.49
			B1-47	0.0009	0.0001	0.0007	0.5562	0.0602	0.0321	0.0016	1.82	13.79	84.39	0.5158	1.41	1.51
Centre Basin		East Meghile	J3-6	0.0017	0.0006	0.0013	0.5605	0.1698	0.0394	0.0036	6.11	16.58	77.31	0.5453	0.63	1.59

Table. 5.4b Concentrations and proportions of the carbazoles, methylcarbazoles, dimethylcarbazoles, and benzocarbazoles and their ratios (together with some saturated hydrocarbon maturity and source parameters) in oil families in the Sirt Basin. CA-Carbazole; MCA-Methylcarbazole; DMCA-Dimethylcarbazoles; BNC-Benzocarbazole.

Location	Oil Families	Oil Filed	Well	Benzocarbazole concentratioins (µg/g oil)			BNC Ratio	BNC	Σ AC	Σ BNC	CA	MCA	DMCA	C_{29} Sterane	C_{27} Hopane	Iso-alkanes
			Name	a	b	c	a/(a+c)	b/(a+b+c)	µg/g oil	µg/g oil	%	%	%	ββ/(αββ+ααα	Ts/Tm	Pr/Ph
Centre Sirt Basin	1B	Nasser	C98-6	0.0012	0.0001	0.0010	0.5396	0.0630	0.0432	0.0023	4.47	19.72	75.81	0.5693	1.67	1.60
			C98-6	0.0013	0.0002	0.0010	0.5672	0.0753	0.0425	0.0025	4.72	20.12	75.16	0.5290	2.17	1.59
		Raiah	DD12-6	0.0007	0.0002	0.0005	0.5686	0.1145	0.0234	0.0013	3.07	12.12	84.81	0.5175	1.05	1.50
		South Jebel	4B1-6	0.0018	0.0003	0.0015	0.5437	0.0748	0.0642	0.0035	2.52	17.86	79.62	0.5960	2.11	1.52
		Ragoba	E9-20	0.0002	0.0000	0.0002	0.5091	0.0609	0.0058	0.0004	3.64	18.31	78.05	0.5190	0.98	1.73
			E82-20	0.0002	0.0000	0.0002	0.5116	0.0768	0.0058	0.0004	3.12	18.56	78.33	0.5200	1.01	1.71
		West Meghil	4J2-6	0.0006	0.0001	0.0006	0.5194	0.0414	0.0235	0.0012	9.30	24.05	66.65	0.5560	1.67	1.80
		Zelten	4G1-6	0.0011	0.0001	0.0007	0.6026	0.0301	0.0767	0.0018	2.27	14.93	82.81	0.5476	1.50	1.53
West Basin		Sabah	G3-NC74F	0.0004	0.0001	0.0006	0.4008	0.0703	0.0156	0.0010	3.66	18.26	78.08	0.5154	1.10	1.50
Centre Basin	2	Kotla	C46-47	0.0004	0.0001	0.0004	0.4695	0.1143	0.0153	0.0009	2.90	15.98	81.12	0.4445	0.59	1.27
	3	Dor Mansour	Z3-47	0.0002	0.0001	0.0002	0.4968	0.1487	0.0063	0.0005	1.11	9.63	89.25	0.5362	0.71	1.26
			Z5-47	0.0002	0.0001	0.0002	0.5047	0.1066	0.0093	0.0005	1.44	10.62	87.94	0.5432	0.71	1.28
			GG1-47	0.0002	0.0001	0.0002	0.5017	0.1501	0.0105	0.0004	2.31	12.18	85.51	0.5560	0.77	1.36
West Sirt Basin	4	Aswad	B18-NC74B	0.0002	0.0000	0.0002	0.4133	0.0357	0.0066	0.0004	6.97	22.24	70.80	0.4719	0.26	1.30
			B18-NC74B	0.0002	0.0000	0.0003	0.4083	0.0534	0.0072	0.0005	6.36	20.50	73.13	0.4966	0.26	1.28
		Safsaf	C1-NC74B	0.0003	0.0000	0.0003	0.4779	0.0591	0.0138	0.0007	9.86	24.46	65.68	0.5490	0.57	1.52
		Safsaf South	D6-NC74B	0.0003	0.0000	0.0004	0.4545	0.0611	0.0171	0.0008	9.20	24.09	66.71	0.5140	0.58	1.54
		Zella	A5-NC74B	0.0001	0.0000	0.0002	0.4191	0.0253	0.0078	0.0004	5.39	19.47	75.14	0.4594	0.53	1.41
			A5-NC74B	0.0002	0.0000	0.0002	0.4109	0.0672	0.0072	0.0004	5.71	19.95	74.34	0.4187	0.52	1.43
			A28-NC74B	0.0001	0.0000	0.0002	0.3769	0.0466	0.0061	0.0003	5.31	20.51	74.17	0.4352	0.57	1.46
East Sirt Basin	5	As Sarah	B42-96	0.0014	0.0000	0.0004	0.7642	0.0150	0.0143	0.0018	1.96	16.79	81.25	0.6578	1.11	2.03
	6	Augla Nafora	G31-51	0.0001	0.0001	0.0000	0.6418	0.4273	0.0028	0.0002	4.12	13.20	82.68	0.5116	0.91	1.88
			G274-51	0.0001	0.0001	0.0001	0.4915	0.2446	0.0039	0.0004	6.67	19.35	73.98	0.5100	1.03	1.85
	7	NC125	N1-125	0.0001	0.0001	0.0000	0.6657	0.3293	0.0021	0.0002	3.41	10.19	86.40	0.6818	1.93	1.92
			A1-125	0.0001	0.0001	0.0000	0.6311	0.3471	0.0017	0.0002	5.32	20.82	73.86	0.6938	1.73	2.05
	8	Tuamma	C7-97	0.0001	0.0000	0.0000	0.6709	0.1811	0.0009	0.0001	8.16	23.78	68.06	0.6600	1.53	1.89
	9	Nakhla	G7-97	0.0001	0.0001	0.0001	0.4764	0.2546	0.0008	0.0003	6.97	11.78	81.25	0.6749	2.89	2.00
Nort Sea Oil	VFO		VFO	0.0023	0.0003	0.0013	0.6510	0.0755	0.0390	0.0036	7.32	25.13	67.56	0.6084	3.03	1.38

5.8 Light Hydrocarbons

Seven crude oil samples with high aromatic hydrocarbon contents that are thought to be affected by the secondary process of the evaporative fractionation (can increase light hydrocarbons) were selected for analysing using gas chromatography, as listed in Table 5.5. However, systematic changes in abundance and distribution of light hydrocarbon occur with increasing temperature and depth (Thompson, 1987).

Figure 5.42 is comprised of histograms showing the abundances of light hydrocarbons for the seven representative oils. It was found that butane, 2-methylbutane, pentane, propane, 2-methylpropane, 2-methylpentane and methylcyclohexane had the highest abundance, while those of normal alkanes, including *n*-hexane, *n*-heptane and *n*-octane were extremely low in the A28-NC74B, A15-17, A46-17, and B1-47 wells. In the 4J2-6 and A1-NC125 samples, 2-methylbutane, 2-methylpentane, methylcyclohexane, *n*-heptane and *n*-octane were in the highest abundances. The well B2-NC74B oil shows the highest abundances in the 1-trans,3-dimethyl cyclohexane, 1-cis,3-dimethylcyclohane, propane and 2-methylpropane components. Table 5.5 shows the abundance of light hydrocarbons quantified in the Sirt Basin oils.

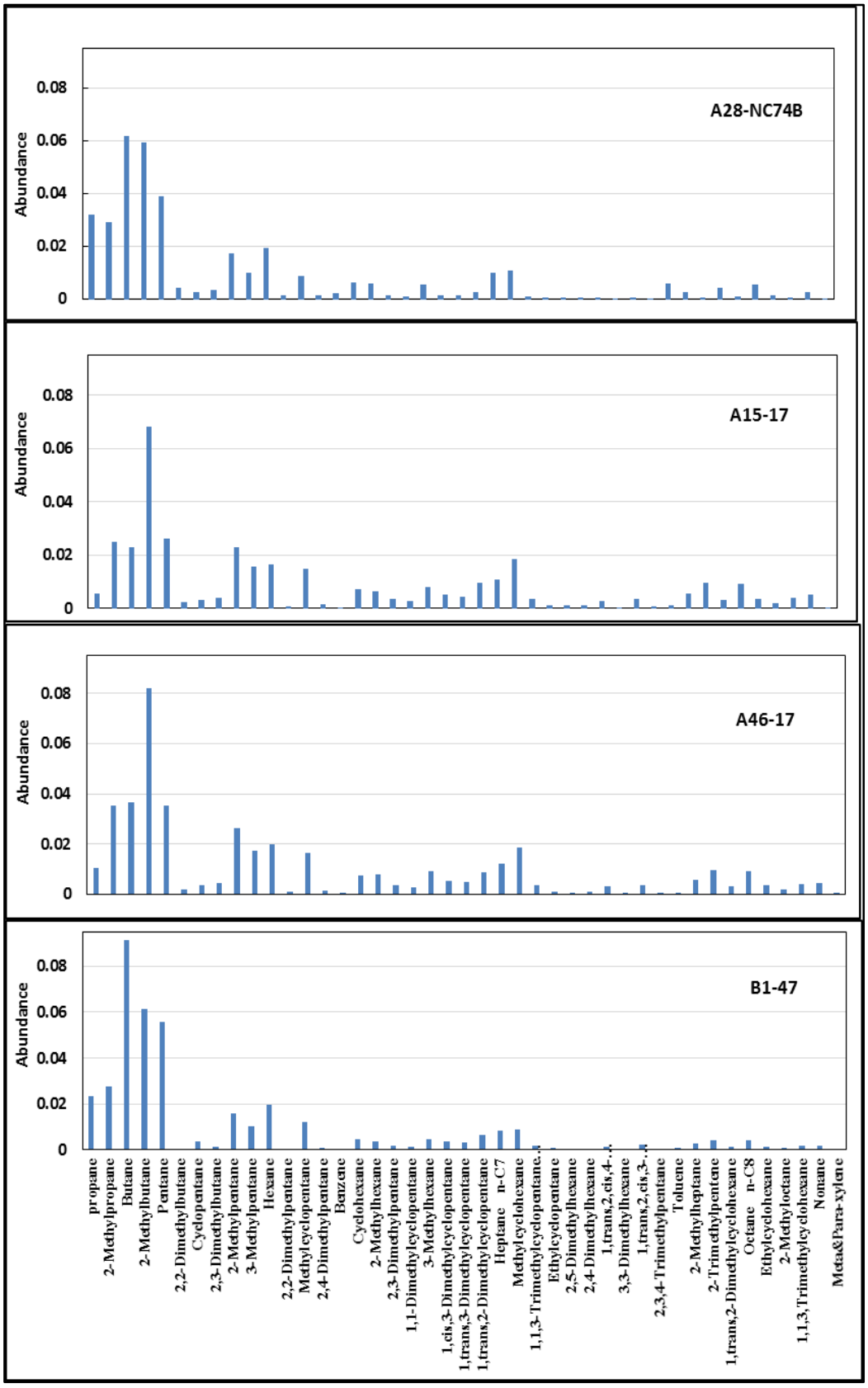

Figure 5.42: Abundances (mg/g oil) of individual light hydrocarbons in the studied oils.

Table 5-5: Concentration (mg/g oil) of the individual light hydrocarbons in the studied oils.

Oilfiled Name	West Mabruk		Zellah	Hakim	Beda	West Meghil	NC 125
Well Name	A15-17	A46-17	A28-NC74B	B2-NC74A	B1-47	4J-6	A1-125
light Hydrocarbons Compounds	mg/g oil	mg/g oil	mg/g oil	mg/g oil	mg/g oil	mg/g oil	mg/g oil
Propane	1.74	2.74	9.14	1.75	6.24	2.37	5.04
2-methyl propane	7.91	9.21	8.37	1.43	7.36	2.50	2.42
Butane	7.18	9.52	17.65	3.71	24.33	0.74	1.02
2-methylbutane	21.28	21.35	17.05	7.81	16.33	12.51	8.44
Pentane	8.21	9.26	11.17	7.61	14.82	2.25	2.34
2,2 dimethylbutane	0.69	0.53	1.25	0.58	0.12	1.45	3.44
cyclopentane	1.11	0.99	1.00	0.88	0.43	0.84	3.20
2-methylpentane	7.21	6.80	4.97	6.02	4.27	6.79	6.71
3-methylpentane	4.82	4.46	2.90	4.16	2.72	5.69	5.43
Hexane	5.14	5.16	5.49	8.81	5.22	3.20	5.53
Methylcyclopentane	4.64	4.17	2.49	5.62	3.18	5.53	1.83
2,4 dimethylpentane	0.50	0.30	0.40	0.64	0.11	1.02	1.56
Benzen	0.15	0.15	0.70	0.23	0.13	0.18	0.25
Cyclohexane	2.25	1.87	1.74	3.58	1.25	4.80	4.19
2-Methylhexane	1.99	1.87	1.73	3.53	0.95	3.50	5.18
2,3 dimethylpentane	1.12	0.85	0.41	0.92	0.38	2.48	2.24
1,1 dimethyl cyclopentane	0.86	0.66	0.30	1.25	0.39	2.17	1.44
3-mehylhexane	2.55	2.39	1.61	3.74	1.21	4.34	5.75
1,cis,3dimethylcyclopantane	1.63	1.38	0.46	2.25	0.94	2.38	0.95
1,trans,dimethylcyclopentane	1.42	1.27	0.41	1.88	0.84	2.02	0.80
1,trans,2 dimethyl cyclopentane	2.94	2.38	0.75	3.15	1.78	5.41	2.46
heptane	3.37	3.20	2.87	8.01	2.16	4.46	7.79
methylcyclohexane	5.84	4.77	3.15	11.22	2.33	11.32	10.00
2,5 dimethylheaxane	1.15	0.84	0.32	1.61	0.45	2.44	1.58
ethylcyclopentane	0.40	0.37	0.14	0.76	0.26	0.80	0.06
1,2,4-trimethylcyclopentane	0.84	0.69	0.18	1.26	0.43	1.90	0.58
Toluene	0.32	0.30	1.65	1.15	0.21	0.42	0.73
Octan n-C8	2.74	2.46	1.59	6.23	1.13	6.43	9.01
Meta&Para-xylene	0.01	0.03	0.11	0.20	0.02	0.06	0.03

Figure 5.43 shows a cross plot of the heptane values (H) versus isoheptane values (I) for the studied oils. It is clear from the figure that oil samples from these well 4J2-6 in oil family 1B, A15-17, B1-47, B2-NC74A and A46-17 in oil family 1A plot between the two curves, indicating highly aliphatic marine (Type II kerogen) source rocks. The A1-NC125 in oil family 7 and A28-NC74 in oil family 4 are plotted relatively close to the aromatic curve on this figure, suggesting slightly different marine (Type II-III kerogen) source.

Table 5-6: C6-C7 Thompson ratios describe light hydrocarbon distributions for studied wells.

Name	Oilfield Name	West Mabruk		Zellah	Hakim	West Meghil	Beda	NC 125	Property
	Ratio Well Name	A15-17	A46-17	A28-NC74B	B2-NC74A	4J-6	B1-47	A1-125	
A	Benzene/ n-Hexane	0.03	0.03	0.13	0.03	0.05	0.02	0.12	Aromaticity
B	Toluene/ Heptane	0.09	0.07	0.58	0.14	0.16	0.1	0.09	Aromaticity
X	Xylene (m & P)/n-Octane	0.003	0.013	0.415	0.032	0.009	0.02	0.003	Aromaticity
C	(n-Hexane +n-Heptane)/ (Cyclohexane +Methylcyclohexane)	1.06	1.24	1.7	1.13	0.47	2.04	0.95	Paraffinicity
I	Isoheptane value = (2-, 3-Methylhexane / 1c3-, 1t3-, 1t2-Dimethylcyclopentane)	0.76	0.9	2.08	0.95	0.84	0.61	2.55	Paraffinicity
F	n-Heptane/ Methylcyclohexane	0.58	0.67	0.91	0.71	0.37	0.92	0.79	Paraffinicity
H	Heptane value = (n-Heptane/ (Σ Cyclohexane trough Methylcyclohexane))*100	17	18	23	22	12	21	22	Paraffinicity
R	n-Heptane/ 2-Methylhexane	1.69	1.59	1.66	2.29	1.19	2.29	1.55	Paraffin branching
U	Cyclohexane/ Methylcyclopentane	0.48	0.45	0.71	0.66	0.90	0.39	2.07	Naphthene branching

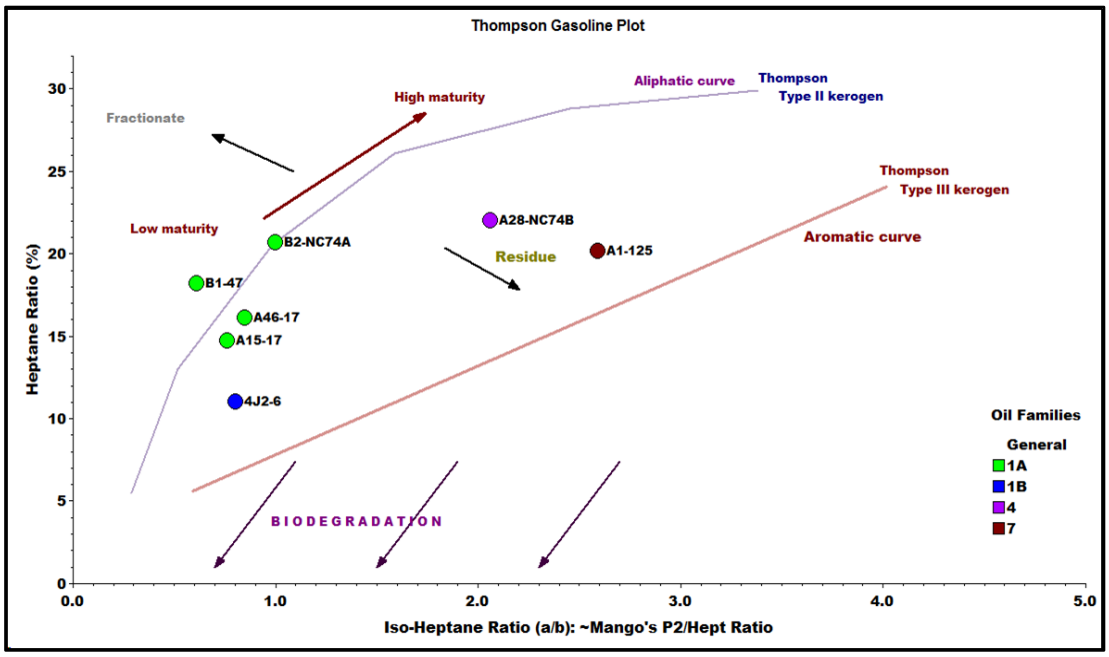

Figure 5.43: Cross plot of Heptane versus Isoheptane value for the Sirt Basin oils. H= n-C7/CH through to MCH) and Isoheptane (I=2MH+3MH)/1,3DMCP(cis+trans)+1-cis-2-DMCP).

According to Thompsons (Thompson 1983; 1987) the light hydrocarbon parameter ranges for different maturity levels, the studied oils fall in the range of normal oil for both ratios, except 4J2-6 well which appears to be low maturity or affected by biodegradation as shown in Figure 5.44. However, Thompsons (1983; 1987) have reported that non-biodegraded oils can yield heptane ratios as low as ~ 12. The normal values (18 to 22) for both ratios are probably because the oils are derived from normal paraffinic source rocks, which are likely to be marine shale source rocks.

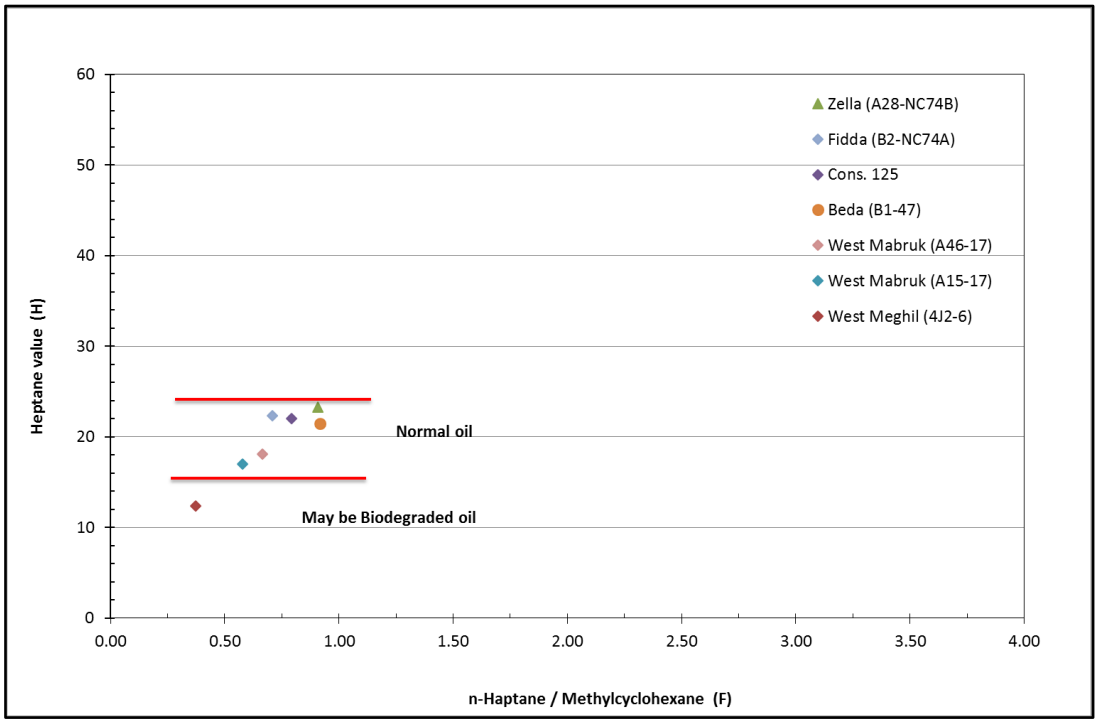

Figure 5.44: Cross plot of the Heptane value (H) and n-heptane/Methylcyclohexane (F) of the Sirt Basin oils. (After Thompson, 1987)

The temperature of a generation of the studied oils was calculated from [2,4-DMP/2,3-DMP] ratio using this equation $°C_{temp}$ = 140+15(ln[2,4-DMP/2,3-DMP]) as developed by Mango (1997). The studied oils appear to have been generated in a temperature range of 99 to 103 °C, which are equivalent to vitrinite reflectance values of 0.6 to 0.9%, and similar to those measured using aromatic hydrocarbons parameters that are mentioned earlier in this chapter. Although the (2,4-MDP/2,3-DMP) ratio has been described as an excellent maturity indicator (Mango, 1990; BeMent *et al.*, 1995), other studies proved that the ratio can be affected by other factors such as facies changes and reservoir alteration processes (Peters *et al.*, 2005b).

The cross plot of the aromaticity (B) versus paraffinicity (F) parameters for the selected Sirt Basin oils is shown in Figure 5.45. The oils represent the Upper Cretaceous source rocks, and show the remarkable original uniformity of composition for the wells A15-17, A46-17, A1-NC125, B1-47 and B2-NC74A, which have relatively high paraffinicity and low aromaticity. The samples from wells A28-NC74B and 4J2-6 exhibit a remarkably different original composition compared to the first five wells. The A28-NC74 well samples are characterized by high aromaticity and paraffinicity parameter values, which may reflect different organic inputs. The 4J2-6 well samples

are characterised by both low paraffinicity and aromaticity, again indicating different compositions and thus origins. It is clear from the figure that the studied oils are not enriched in light aromatic hydrocarbons, except A28-NC74B, which appears to be slightly enriched, which may indicate that this oil was affected by evaporation fractionation. Therefore, the maturity effect is probably a more favoured explanation for the variations seen in the light hydrocarbon parameters measured in the oils studied.

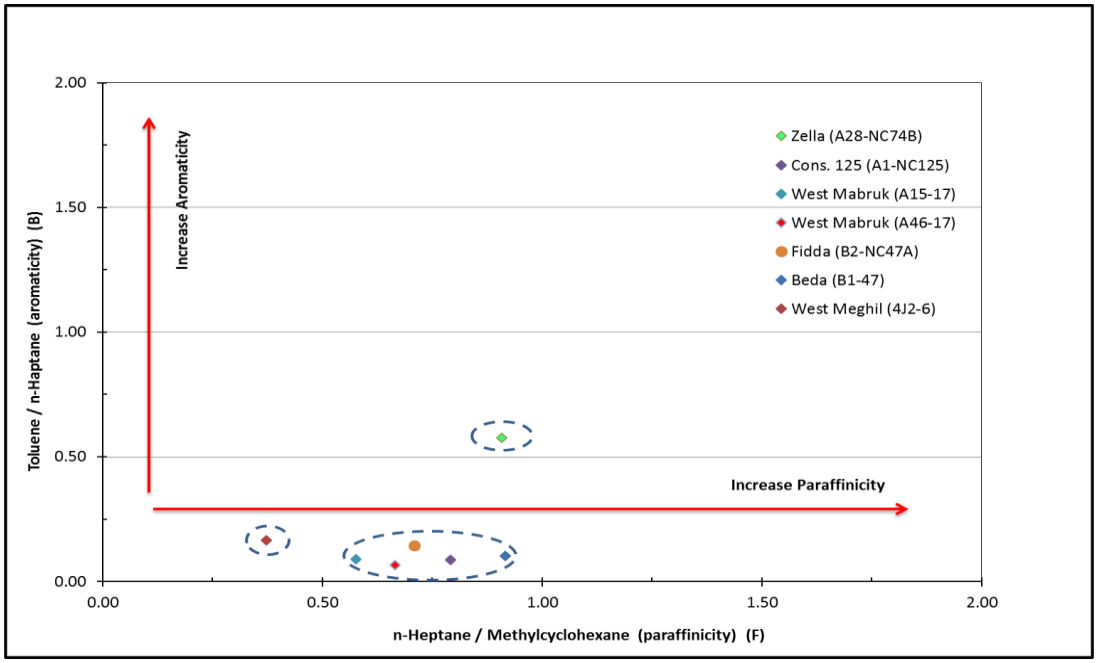

Figure 5.45: Cross plot of the Thompson (1987) Paraffinicity Index (F) and Aromaticity Index (B) for the Sirt Basin oils. B= Toluene/*n*-C7, F= *n*-C7/MCH.

5.9 Summary

The hydrocarbon composition of 51 crude oil samples from the Sirt Basin has been analysed and the results subjected to statistical data analysis. The data measured included the *n*-alkane composition, biomarkers, aromatic hydrocarbon distributions and compound specific stable carbon isotopic composition of saturated hydrocarbon fractions, in order to evaluate source organic facies, maturity, lithology and depositional environment for the Sirt Basin oils, followed by an attempt to link them genetically and to classify them in oil families. Based on this analysis, the crude oils discovered in the western, central and eastern regions of the Sirt Basin generally fall into ten genetic oil families.

The central and western Sirt Basin oils characterized by moderate to high API gravities ranging from 38º to 42º and they are not biodegraded. They have relatively high saturated hydrocarbon contents (38-69%), moderate to high aromatic hydrocarbons (24-55%), low to moderate resins (5-23%) and low asphaltenes (0.42-6%) contents with varying saturated hydrocarbon to aromatic hydrocarbon ratios (0.70-2.97). The crude oil samples from the eastern Sirt Basin display moderate to high API gravities ranging from 34º to 44º. They are also not biodegraded, have relatively higher saturated hydrocarbon contents (39-73%), moderate aromatic hydrocarbons (23-35%), and low resins and asphaltenes (2-18% and 1-3% respectively), with similar high saturated to aromatic hydrocarbon ratios.

The central and western Sirt Basin oils show similar *n*-alkane envelopes dominated by *n*-C_{11}-*n*-C_{18} and very low amounts of *n*-C_8-*n*-C_{11}, while eastern Sirt Basin oils show identical *n*-alkane envelopes dominated by *n*-C_{11}-*n*-C_{21} and very low amounts of *n*-C_8-*n*-C_{10}, but they contain relatively more abundant heavy *n*-alkanes (*n*-C_{23}+). Most of the crude oil samples show a weak odd over even predominance of long-chain *n*-alkanes indicated by carbon preference indices close to 1.0 unity.

The crude oil samples from the central and western Sirt Basin are characterised by low values of the pristane relative to the phytane, indicating that these oils arose within suboxic to anoxic conditions. Meanwhile, in the eastern basin the ratios were slightly higher, suggesting suboxic environments.

From the pristane/*n*-C_{17} and phytane/*n*-C_{18} ratios, it is concluded that all of the oils contain mixtures of marine and terrigenous organic matter deposited under suboxic to anoxic conditions. The east Sirt Basin oils are composed of mixed organic matter source input, in a depositional environment with suboxic conditions and are higher of maturity, whereas the oils from the central and western parts of the basin is characterised by moderate pristane/phytane ratios indicating suboxic to anoxic conditions in their source rock depositional environments and have lower levels of maturity. According to the pristane/*n*-C_{17} and phytane/*n*-C_{18} ratios, the crude oil samples in the Sirt Basin have been separated into nine oil families and two subfamilies. Subfamily 1A includes the Beda, Fidda, East Meghil, Hakim, and Mabruk oilfields. Subfamily 1B contains oils from the Nasser, Raiah, Raguba, Sabah, South Jebel, West

Meghil and Zelten oilfields. Family 2 includes the oils from the Kotla oilfield, family 3 from the Dor Mansour oilfield, and family 4 includes the oils from the Aswad, Safsaf and Zellah oilfields. Family 5 includes oil from the As Sarah oilfield, family 6 oils from the Augila Nafoora oilfield, and oil families 7, 8 and 9 contain oils from the NC125, Tuamma and Nakhla oilfields respectively.

The saturated biomarker data show that the oil samples collected from the As Sarah, Augila Nafoora, NC125 and Nakhla oilfields in oil families 5, 6, 7, 8 and 9 in the eastern part of the basin were generated from marine organic matter with major contributions from planktonic and/or benthic algae. The oil samples from the remaining oil families 1A, 1B, 2, and 3 show moderate to high amounts of steranes relative to hopanes and moderate C_{29} sterane relative percentages, suggesting that the oils were generated from source rock characterised by moderate to higher contributions from planktonic and/or benthic algae. Oil Families 4 are dominated by high levels of C_{29} sterane and low sterane relative hopane, which may suggest that these oils were probably derived from shale source rocks, characterized by high inputs of the land plant and/or cyanobacterial organic matter deposited in lacustrine to marine environments. Meanwhile, oil families 5, 7 and 9 have low sterane/hopane ratios and low C_{29} steranes, indicating that those oils were generated from marine organic matter with some contribution of land plants deposited in marine environments. Oil family 6 show low to moderate C_{29} sterane and this consistent with low sterane relative hopane ratios, suggesting that the oils were probably originated from shale source rocks, which more characterised of terrigenous and/or microbially reworked organic matter deposited in a marine environment. This might suggest that the oils were derived from three different sources, depositional environments and organic matter inputs. These variations in depositional environment may reflect the geographical distribution of source rocks within the Sirt Basin. Oil family 4 is located on the flanks of the western part of the basin and may be sourced from the Pre-Upper Cretaceous source rock or the Sirt Shale Formation, whereas oil families 1A, 1B, 2 and 3 in the western and central parts of the basin may have been produced from the Sirte Shale and Rachmat formations. Oil family 5 in the east part of the basin seems to have been generated from the Sirte Shale Formation, because it exhibits similar characteristics to those of oil families 1A, 1B, 2

and 3. Oil families 6 to 9 in the eastern part of the basin may be oils originating from the Sirte Shale and/or Pre-Upper Cretaceous Middle Nubian Shale Formation.

Crude oil samples from oil families 3 and 4 have significantly higher homohopane index ratios indicating a more reducing depositional environment for the source rock, and this conclusion is also obtained from the pristane/phytane ratios. Meanwhile the other oil families display, low to moderate homohopane index ratios, suggesting less reducing depositional environments for the source rocks and this is also reflected by the pristane/phytane ratios. The C_{29} αβ(H) hopane/C_{30} αβ(H) hopane ratios show that all of the oil families have ratios lower than 0.8, indicating that the oils were sourced from the clastic marine source rocks.

The high C_{26}/C_{25} tricyclic terpane and C_{31}/C_{30} αβ hopane ratios for Family 4 samples indicate that these oil families may have originated from lacustrine source rocks, while the low ratios for the rest of the oil family suggest that the oils were generated from marine and/or marine to lacustrine source rocks.

For most of the crude oil samples from all oil families, short chain C_{21} and C_{22} MAS compounds are present in greater abundance than long chain C_{27} to C_{29} MAS compounds. The distributions of long chain C_{27} to C_{29} monoaromatic steroids appear to be relatively high in oil families 1A, 1B, 2, 3, 4 and 6, while low in oil families 5, 7, 8 and 9. This may be due to the effects of maturity of long chain monoaromatic compounds or to changes in organic facies in these oil families. The distributions of the C_{27}, C_{28} and C_{29} monoaromatic steroids for oil families 1A, 1B, 2, 3, and 6 show a relatively higher abundance of C_{27} and C_{28} relative to C_{29}, suggesting marine source input. Family 5 oils show relatively higher abundances of C_{27} relative to C_{28} and C_{29}, suggesting a relatively high contribution of marine organic matter with some terrestrial material input, and deposited in a marine environment. The high abundance of C_{29} monoaromatic steroids in oil families 4, 7, 8 and 9 may reflect some contribution from both algal and terrestrial organic matter inputs deposited in a lacustrine to marine settings. The relatively high values of the monoaromatic steroid $C_{28}/(C_{28}+C_{29})$ ratios in oil families 1A, 1B, 2, 3, and 6 have indicated that these oils were generated from marine organic matter input, whereas oil samples from the Aswad and Zellah oilfields in the Family 4, the As Sarah oilfield in Family 5, and those from oil families 7 to 9,

have low ratios which may indicate that they were derived from non-marine shale deposits. However, the relatively high abundance of the C_{29} monoaromatic steroids may also reflect some contribution of algal and terrestrial organic matter inputs deposited in lacustrine and marine settings.

The aromatic hydrocarbon data show that the oil samples are characterised by a relatively high abundance of diaromatic and triaromatic hydrocarbons, including alkylated naphthalenes, phenanthrenes and dibenzothiophenes, with low levels of biphenyls, fluorenes, and monoaromatic and triaromatic steroids. This may indicate that the crude oils originated from clastic marine depositional environments with relatively high contributions of land plants and/or bacteria in marine and lacustrine source rocks. The distributions and relatively high abundances of the alkylnaphthalene compounds in the oil samples are probably related to their production from terpenoids derived from bacteria and land plants and also to maturity effects.

The trimethylnaphthalene ratios for oil families 1A, 1B, 2, 4 and 6 give relatively low TDE1 and TDE2 ratios, suggesting a marine source deposition environments with some contribution of angiosperm land plants. Oil family 3 is characterised by the highest TDE1 and low TDE2 ratios. The high abundance of 1,2,5-TMN in this Family may suggest that this component originated from a cyanobacterial hopanoid precursor. Oil families 5, 7, 8 and 9 are also characterised by relatively high TDE2 compared with other oil families and low TDE1 ratios, suggesting marine organic matter input with slightly higher contributions of angiosperm land plants. Furthermore, the 1,2,7-/1,3,7-trimethylnaphthalene ratios for all the oil families were low. This may indicate that the crude oils were derived from dysoxic to anoxic marine organic matter with some contribution of land plants deposited in a marine environment. Whereas the 1,2,5/1,3,6-trimethylnaphthalene ratios are higher in family 3 compared with other oil families, suggesting that this family may have higher contributions of angiosperm land plant input and the source rock was deposited in a marine environment with suboxic to anoxic conditions.

The abundance of 9-MP is higher than 1-MP in most oil families, reflecting the marine source precursors of these compounds with some isomers with land plant origins, particularly in Family 3 oil.

The concentrations of dibenzothiophenes in the crude oil samples from all oil families are very low and increase towards the central and western part of the basin. Oil family 1A represents the highest concentrations; oil families 1B, 2, 3 and 4 have moderate concentrations, while oil families 5 to 9 in the eastern part of the basin contain very low concentrations. The molecular marker data indicate that the origins of these crude oils are marine and lacustrine to marine siliciclastic source rocks, which is further indicated by the relationship between the dibenzothiophenes/phenanthrenes and the pristane/phytane ratios, which support the notion of marine suboxic to anoxic depositional environments.

The carbon isotopic signatures of the *n*-alkanes for oil families 1A, 1B, 2, 3 and 4 indicate that the oils are well-correlated and may have been generated from a similar source facies, while oil families 5 to 9 have slightly different source facies.

Principal component analysis (PCA) for the Sirt Basin oils shows that thermal maturity was the most significant parameter controlling the composition and distribution of biomarkers in the crude oil samples. In addition, the nature of source rocks, which are composed of clay-rich siliciclastic sediments, may have had an effect on the composition and distribution of biomarkers. The PCA separated the crude oil samples into eight groups. Group 1 consists of all samples from the Mabruk and Kotla oilfields; group 2 contains the samples from the Beda, Nasser, South Jebel, West Meghil and Zelten oilfields; group 3 the samples from the Dor Mansour, East Meghil, Fidda, Hakim and Raguba oilfields; group 4 samples from the Aswad, Augila Nafoora, Safsaf and Zellah oilfields; group 5 the As Sarah oilfield; group 6 the Tuamma oilfield; group 7 the NC125 oilfield; and group 8 represents the Nakhla oilfield.

Based upon saturated and aromatic hydrocarbon maturity-related biomarkers, the eastern Sirt Basin oils were generated at a higher level of thermal maturity than those of the central and western Sirt Basin.

The pyrrolic nitrogen compound fractionation distribution of the Sirt Basin oils suggests short migration for oil families 5, 7, and 8 in the eastern part of the Sirt Basin, while the data indicate that migration distance in the central and western parts of the

Sirt Basin for oil families 1A, 1B, 2, 3, 4, 6 and 9 are believed to be generally moderate or long.

The light hydrocarbons suggest that the oils were sourced from marine shale source rock, which is inferred from the relationship between heptane relative to isoheptane values. The thermal maturity was determined by several ratios and the results suggests normal maturity oils.

Chapter 6. Oil to Source Correlation

6.1 Oil-Source Rock Correlation

The aim of this chapter is to determine the likely main source rocks responsible for generating all of the petroleum so far discovered in the study area, by performing oil-source correlations. The correlation of a crude oil to its principal source rocks is a common application of petroleum geochemistry in the exploration sector. Curiale (1994) defined oil-source rock correlation as "a fundamental relationship, established between a crude oil and an oil-prone petroleum source rock, which is consistent with all known chemical, geochemical and geological information". Most correlation techniques use the molecular and isotopic comparison of components in crude oil with components extracted from a candidate source rock. Therefore, the distributions of biomarkers in source rocks and crude oils, and their ability to provide information on differences in type of organic matter inputs, depositional environments and thermal maturity, have been used to determine the genetic relationships between oils and source rocks in the Sirt Basin. Fifty-eight samples of crude oils and source rock samples from the Sirt Basin have been investigated in this study. The oil samples are from various carbonate and clastic reservoir rocks ranging in age from Cretaceous to Eocene at different intervals, with clastic reservoirs more common in the Cretaceous and carbonate rock reservoirs dominating in the Tertiary, while the source rock samples were from the Upper Cretaceous. Detailed organic geochemical characterizations of the samples were conducted in order to enable comprehensive oil to source correlation. All of the oil and source rock samples were analysed for their molecular composition, and 23 samples were selected for the compound specific stable carbon isotope analysis of *n*-alkanes. The samples analysed in this project include: fifty-one crude oil samples from the central, western and eastern parts of the Sirt Basin and forty-three source rock samples from the central and western parts of the basin. This was because source rock samples from the eastern part of the basin unfortunately were not available. Also due to their higher maturity levels, the crude oils from the eastern basin are excluded from the correlations. The saturated and aromatic hydrocarbon fractions of the samples were analysed by GC, GC-MS and GC-IRMS in order to investigate their geochemical characteristics.

6.2 Source Facies Characterisation and Comparison

Chapter five has provided evidence indicating that there are ten distinct families of oils in the study area of the Sirt Basin. They have been produced from both similar and dissimilar source rocks in the basin. The potential source rocks suggested for oil families 1A, 1B, 2, 3, 5 and 6 are from the Upper Cretaceous Sirte Shale Formation and to a less significant degree, the Rachmat Formation. The subdivision of the oil family 1 into two sub-families, 1A and 1B, was due to slight variations in source rock facies and some differences in the maturation levels of the oils, as family 1B was generated from deeper Sirte Shale source rocks in the central part of the Sirt Basin. Oils families 4, 7, 8 and 9 could have been generated either from potential source rock older than the Upper Cretaceous Sirte Shale and Rachmat Formations, which could be Upper Palaeozoic to Jurassic Middle Nubian Shale Formation.

Prior to considering the oil-source geochemical correlation, it is necessary to look at the regional distribution of the potential source rock across the study area in order to determine to what extent this distribution fits the occurrence of the different oil families. The distributions of the Upper Cretaceous, Sirte Shale and Rachmat formations and Middle Jurassic to Lower Cretaceous Nubian Shale Formation have been obtained from the literature, for instance, Barr and Weeger (1972); El-Alami *et al.* (1989); El-Alami (1996); Ben Ashour (2000); and Hallett (2002). The Sirte Shale and Rachmat Formations are widely distributed in the Sirt Basin and they reach the greatest thickness and depth in the trough regions and the lowest in the platforms as shown in the Figure 4.11. Meanwhile, the distribution of the Middle Nubian Shale potential source rocks is concentrated in the deep trough areas where it has the highest thickness, such as the Agedabia Trough in the eastern part of the Sirt Basin. However, although the Sirte Shale, Rachmat and Middle Nubian Formations are widely distributed in the Sirt Basin and they are thought to be the main potential source rocks in the eastern basin, the organic-rich shale is not found everywhere in the basin. This may due to a depleted supply of organic matter or variations in the depositional environment. The rifting process in the Upper Cretaceous occurred in the Cenomanian to Maastrichtian ages, during which the deposition of the Sirte Shale and Rachmat Formations occurred. This may be a primary cause of the maximum burial of these

formations in the trough areas as well as the overburdening of sediments deposited later on throughout geological time, where the latter may increase the level of thermal maturity sufficient to generate hydrocarbons. This is consistent with the presence of oil families 1A, 1B, 2, 3, 4 and 6 in the western and central part of the basin. The Middle Nubian Shale Formation is not present in the whole area, but is preserved in the east and southeast of the basin and may be considered along with the Sirte Shale Formation to have formed the principal source rock for oil families 5, 7, 8 and 9. Unfortunately, source rock samples from the Sirte Shale and Middle Nubian Shale Formations are not available from the eastern part of the Sirt Basin and therefore the correlation of these oils with a potential source rocks is not possible in this study.

According to the geochemical characteristics of the crude oil samples as analysed in Chapter five, it has been concluded that family 1A, 1B, 2, and 3 oils were generated from early to middle mature clastic clay-rich Upper Cretaceous marine source rocks, which are believed to be the Sirte Shale and Rachmat Formations. Oil samples from family 4 oils were established to have been derived from early to middle mature marine to lacustrine clastics interbedded with carbonate strata source rocks from the Upper Cretaceous or older, which are also thought to be from the Sirte Shale and Rachmat formations, or they could also be from the Etel Formation which is considered a local potential source rock in the Sirt Basin (El-Alami, 1996). Generally, the two potential source rocks, the Sirte Shale and Rachmat Formations have relatively similar kerogen source facies but with slight differences in thermal maturity level. The Rachmat Formation is deeper, and therefore more mature (Hamyani *et al.*, 1984; Gumati and Schamel, 1988; El-Alami *et al.*, 1989; Gumati *et al.*, 1996; Hallett and El Ghoul, 1996; Hallett, 2002; Burwood *et al.*, 2003). In this study, the available Rachmat Formation source rock samples are unfortunately not representative of all of the Upper Cretaceous sequences, which are rich in organic matter, but only two rock samples are present from the B1-NC74F borehole. Therefore, the subsequent oil-source rock correlations will mainly be based on a comparison of the Upper Cretaceous Sirte Shale rock samples with crude oils from oil families 1A, 1B, 2, 3 and 4. For the geochemical correlation between crude oils and source rock extracts, similarities in the chemical composition or characteristics of extracts and oils need to be established that indicate common points in the genetic features of the samples analysed. The main difficulty of geochemical

correlation is that most of the parameters utilized for correlation purposes are influenced by thermal maturity (Moldowan *et al.*, 1989; Peters and Moldowan, 1993; Curiale, 1994; Hunt, 1995; Peters, 2005b).

6.2.1 n-Alkanes and Isoprenoid Alkanes

The Pr/*n*-C_{17} versus Ph/*n*-C_{18} diagram shown in Figure 6.1 can provide information about the nature of the original organic matter and the stage of diagenesis in the petroleum system. Both Pr/*n*-C_{17} and Ph/*n*-C_{18} ratios decrease with increase maturity as a result of the increasing predominance of *n*-alkanes, and increase as a result of biodegradation due to the favoured loss of the *n*-alkanes *n*-C_{17} and *n*-C_{18}. The cross-plot shows a good correlation between the Sirte Shale source extracts from the 6A1-59, L1-16 and L1-17 wells and family 1A and 2 oil samples, as well as between Sirte Shale and Rachmat source extracts from the B1-NC74F, B2-NC74A, C2-16, FF14-6 and Z1-11 wells and family 1B, 3 and 4 oil samples. There is an overlap between oil families, which could be expected since the potentially associated source rock has similar characters. Whereas the difference which can be observed between the source rock extracts and oils that have lower isoprenoid values over *n*-alkanes may indicate that these samples are slightly more mature than the others. This is confirmed from the Rock-Eval analysis *Tmax*, spore colour index and vitrinite reflectance data. Therefore, it is clear that there is no huge difference caused by the source facies changes between the Sirte Shale and Rachmat source rock on the one hand and the oils in most oil families on the other.

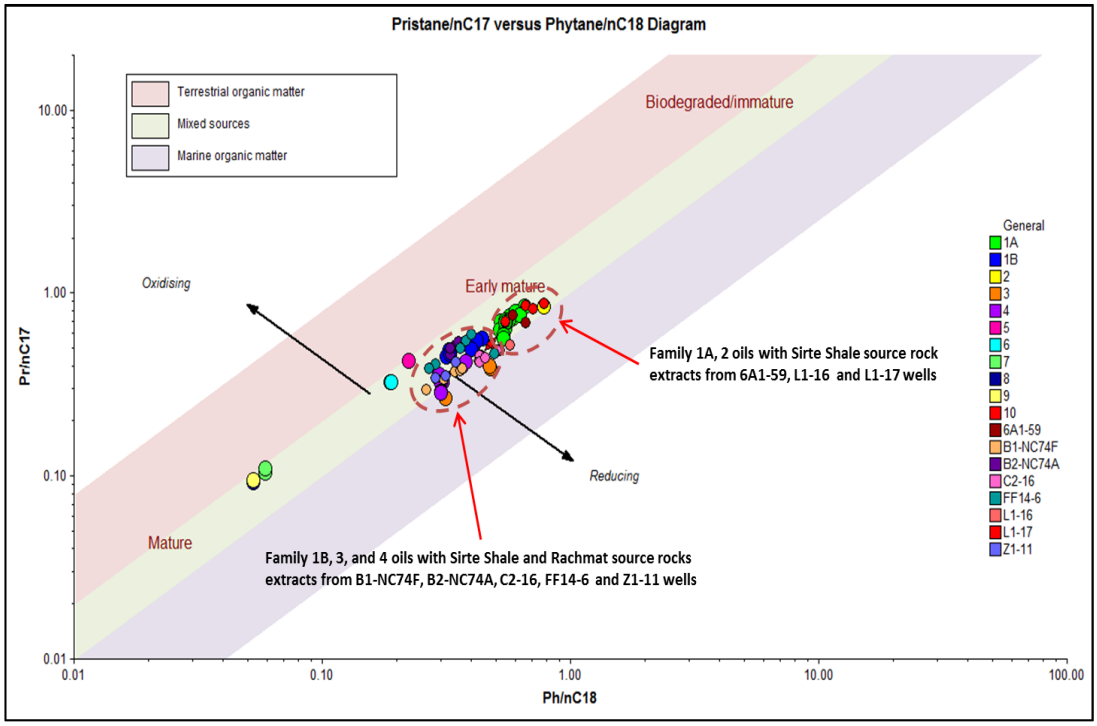

Figure 6.1: Cross plot of pristane/*n*-C_{17} versus phytane/*n*-C_{18} from Upper Cretaceous Sirte Shale and Rachmat Formation potential source rocks and oils; large circles represent oil samples and small circles represent source rocks extracts.

6.2.2 **Steranes and Terpanes**

Several organic facies biomarker parameters were selected in order to carry out oil-source rock correlation. The ternary diagrams showing the distribution of the C_{27}, C_{28} and C_{29} ααα and αββ steranes are presented in Figures 6.2 and 6.3. From these two diagrams the oil families and source rock extract samples can be separated into three groups. Both diagrams show the similarities between families 1A, 1B and 2 oils and the Sirte Shale source rock samples from wells 6A1-59, L1-16, and B2-NC74A at strata depth 9540 feet, C2-16 within the depth at 10260 feet, L1-17 at a depth of 6460 feet, and Z1-11 at the depth 8080 feet, indicating that the oils are likely to have been derived from Sirte Shale Formation. However, variations between oil families and source rock samples may reflect the lateral and vertical distributions of organic sediments in the Sirte Shale Formation within the Sirte Basin. Families 3 and 4 oils show similar characteristics to those of the Sirte Shale source rock samples from the B2-NC74A well at depths from 9570 to 9580 feet and the FF14-6 well at a depth of 12300 feet, also suggesting that the oils were generated from Sirte Shale source rocks. The remaining Sirte Shale and Rachmat source rock samples from the wells B1-NC74F, C2-16, FF14-

6, L1-17, and Z1-11 plot away from the oil families in Figures 6.2 and 6.3, suggesting lateral and vertical variations in the organic facies and depositional environments, as well as the influence of thermal maturity from one place to another in the Sirt Basin.

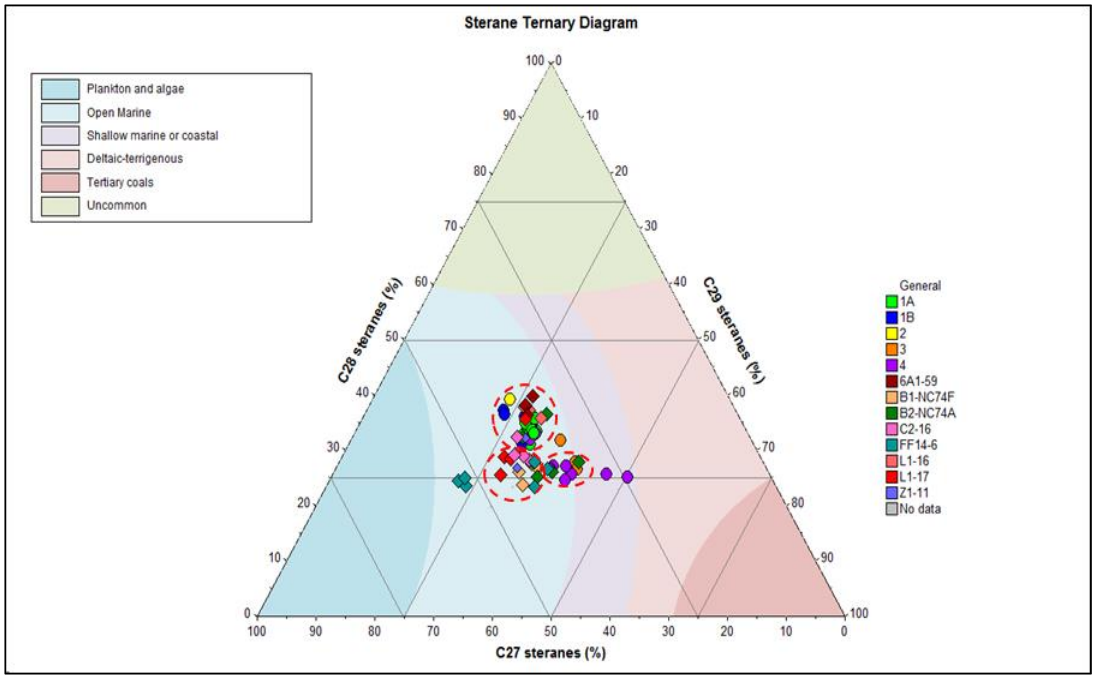

Figure 6.2: Ternary diagram of C_{27}, C_{28}, and C_{29} ααα steranes from Sirte Shale and Rachmat Formation potential source rocks and oils samples, circles represent oil samples while squares represent source rock extracts. Organic matter source interpretational overlays from pIGI software.

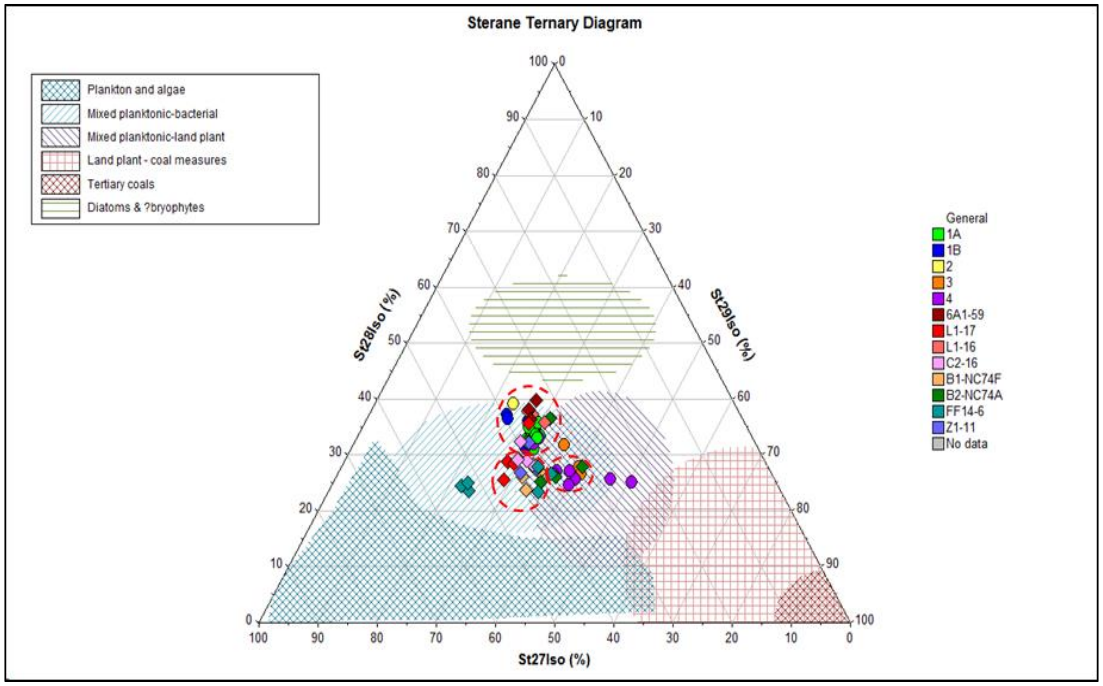

Figure 6.3: Ternary diagram of C_{27}, C_{28}, and C_{29} αββ steranes from Sirte Shale and Rachmat Formation potential source rocks and oils samples, circles represent oil samples while squares represent source rock extracts. Organic matter source interpretational overlays from pIGI software.

A ternary diagram showing the distribution of the C_{29}, C_{30} and C_{31} αβ hopanes is shown in Figure 6.4. From the diagram, the oil families and source rock extract samples are separated into three groups, which are slightly different compared to those based on the steranes. It is clear from the diagram that the majority of the crude oil samples and source rock extracts plot in the marine shale region, with a few samples plotting in the marine to lacustrine zone. The diagram shows similarities between the Aswad Field in family 4 oils and the Sirte Shale source rock samples from wells 6A1-59, L1-16, B1-NC74F, B2-NC74A at strata depths of 9520, 9570 and 9580 feet, and C2-16 within the depth at 10580 feet, indicating that the oils could be derived from the Sirte Shale Formation. The family 4 oils from the Safsaf, Safsaf South and Zellah oilfields showed similar characteristics to the Sirte Shale source rock samples from the FF14-6 well at depths from 11300, 11330 and 11615 feet and the L1-16 well at a depth of 7400 feet, suggesting that the oils may have been generated from Sirte Shale source rocks. Families 1A, 1B, 2 and 3 show similarities with the Sirte Shale and Rachmat source rock samples in the wells B2-NC74A, C2-16, FF14-6, L1-17, and Z1-11, suggesting that the oils were may have been generated from these source rocks. The differences

between the sterane and hopane ternary diagrams in separating the crude oil samples and source rock extracts may be related to differences in the origins of the sterane and hopane compounds, which may have been heterogeneously distributed in the source rock, though the oils represent an integration of the hydrocarbons generated from a wide area of the source rock.

The cross plot of the C_{29} Ts/Tm hopanes versus C_{35} S/C_{34} S homohopanes ratios in Figure 6.5 reveals that all of the oil families 1A, 1B and 3 are plotted close to the Sirt Shale source rock extracts from wells 6A1-59, B2-NC74A, B1-NC74F at a depth of 7190 feet, FF14-6 at a depth of 11320, 11615 and 11650 feet, and L1-16 at the depth of 7400 feet. The family 4 oils plot near to the Sirte Shale and Rachmat source rock extracts from B1-NC74F. The cross-plot also shows that the Sirte Shale source rock extracts from the C2-16, L1-16, L1-17 and Z1-11 wells plotted, well away from the crude oil samples, indicating that there is no close relationship with the oil families. But this may be due to lateral heterogeneities in the source rocks resulting from local changes in organic inputs and depositional environments (e.g. from suboxic to anoxic).

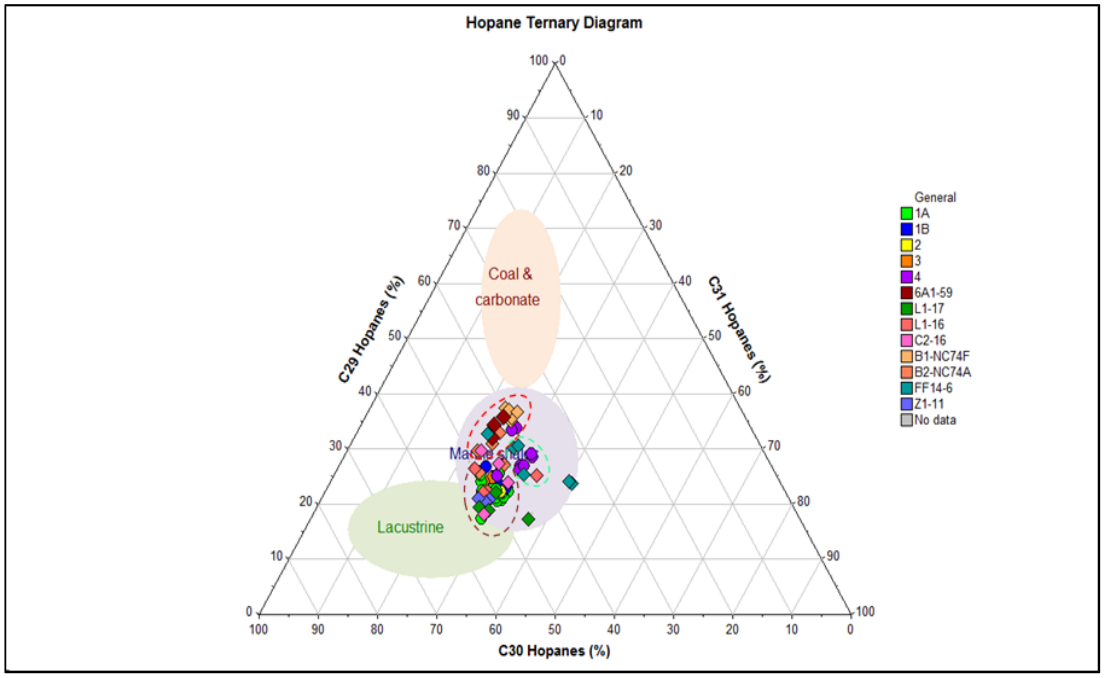

Figure 6.4: Ternary diagram C_{29}, C_{30}, and C_{31} αβ hopanes from potential source rocks Sirte Shale and Rachmat Formations and oils samples, circles represents oil samples while squares represent source rocks extracts. Organic matter source interpretational overlays from pIGI software.

Figure 6.6 is a cross-plot of the C_{27} Ts/Tm hopane versus C_{35} S/C_{34} S homohopane ratios, which shows that all of the oils from oil families 1A, 1B, 2 and 3 plot close to the Sirt Shale source rock extracts from wells 6A1-59, B2-NC74A, B1-NC74F at a depth of 7190 feet, FF14-6 at a depths of 11320, 11615 and 11650 feet, and L1-16 at the depth of 7400 feet. The family 4 oils plot close to the Sirte Shale and Rachmat source rock extracts from wells B1-NC74F, L1-16 at the depth of 7530 feet and L1-17 at a depth of 6060 feet. The cross-plot also shows that the Sirte Shale source rock extracts from the wells C2-16 and Z1-11 are plotting away from the crude oil samples, indicating that there is no close relation to the oil families. This may again be due to lateral heterogeneities in the source rocks resulting from local changes in organic inputs and depositional environments, as well as the influence of thermal maturity.

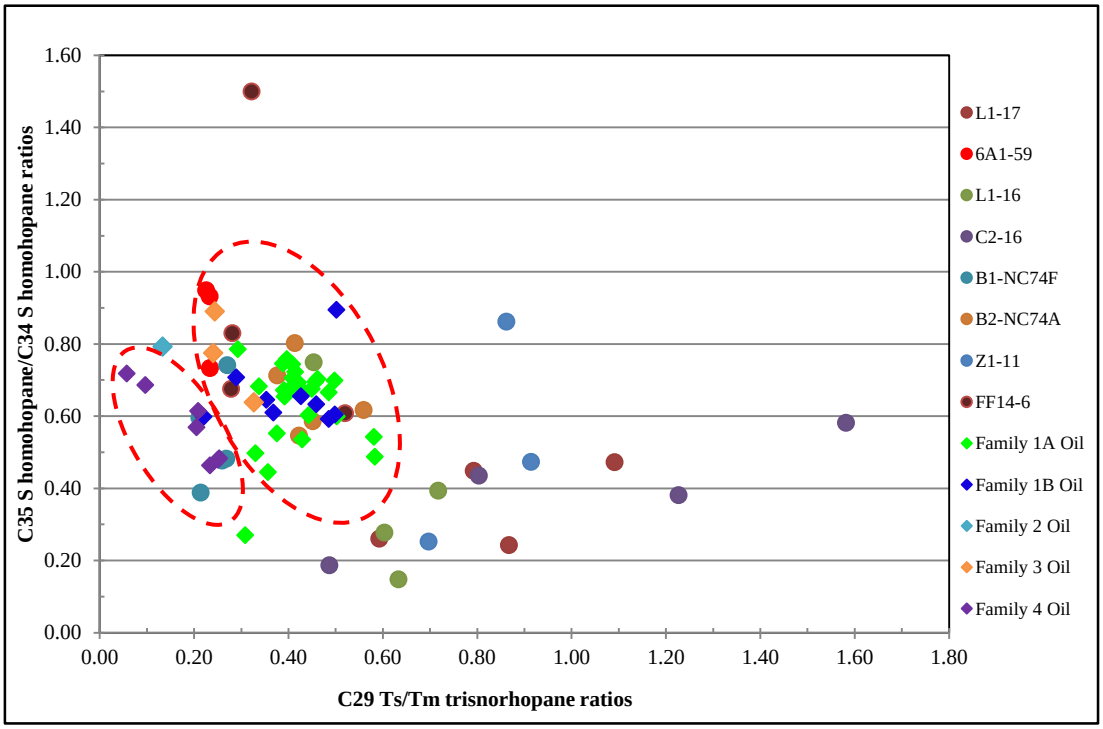

Figure 6.5: Cross plot of C_{29} Ts/Tm trisnorhopane versus C_{35} S/C_{34} S homohopane for the oils and Sirte Shale and Rachmat source rock extracts.

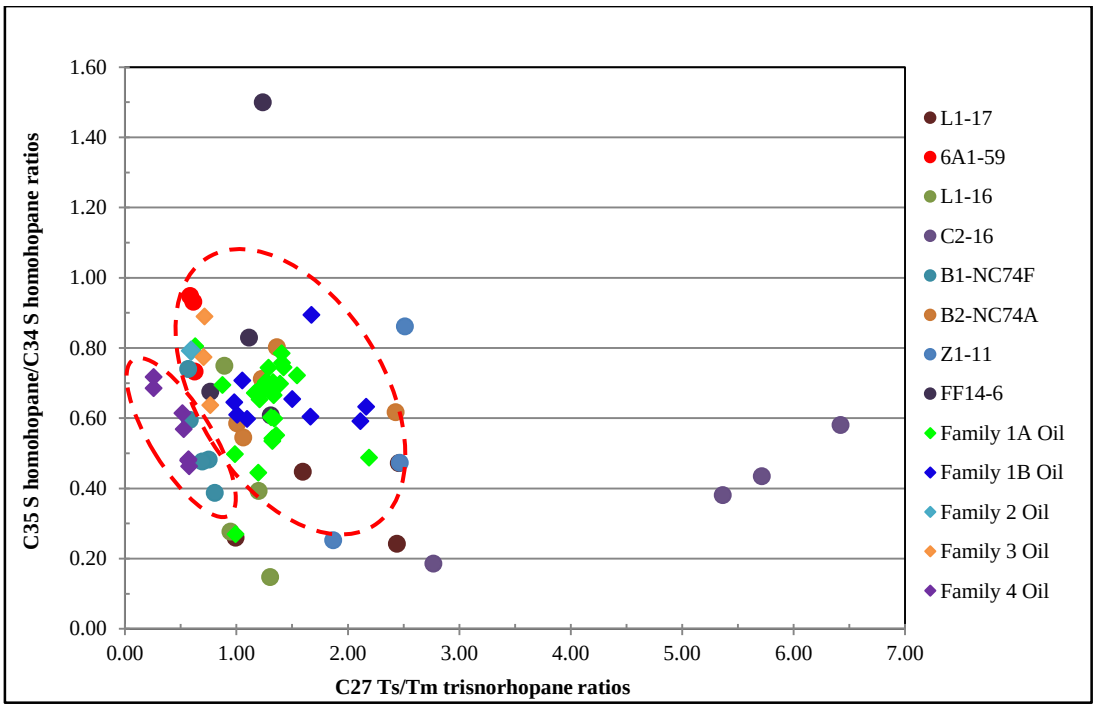

Figure 6.6: Cross plot of C_{27} Ts/Tm trisnorhopane versus C_{35} S/C_{34} S homohopane for the oils and Sirte Shale and Rachmat source rock extracts.

The cross-plot of the C_{29} norhopane/C_{30} αβ hopane versus the C_{31} R homohopane/C_{30} αβ hopane ratios is shown in Figure 6.7. The chart reveals that all of the crude oil samples from oil families 1A, 1B, and 3 plotted close to the Sirte Shale source rock extracts from wells L1-16, L1-17 and Z1-11. The family 4 oils plotted close to the Sirte Shale and Rachmat source rock extracts from wells 6A1-59, B1-NC74F, B2-NC74A, and FF14-6. The cross plot also shows that the family 2 oils from the Kotla oilfield in the central Sirt basin plotted away from the other oil families, but nearer to the FF14-6 extract samples at depths of 12290 and 12330 feet, where both have high C_{31} R homohopane/C_{30} αβ hopane ratios. The variations found amongst the crude oils and source rock extracts may be as a result of lateral and vertical changes in the kerogen facies, and depositional environments.

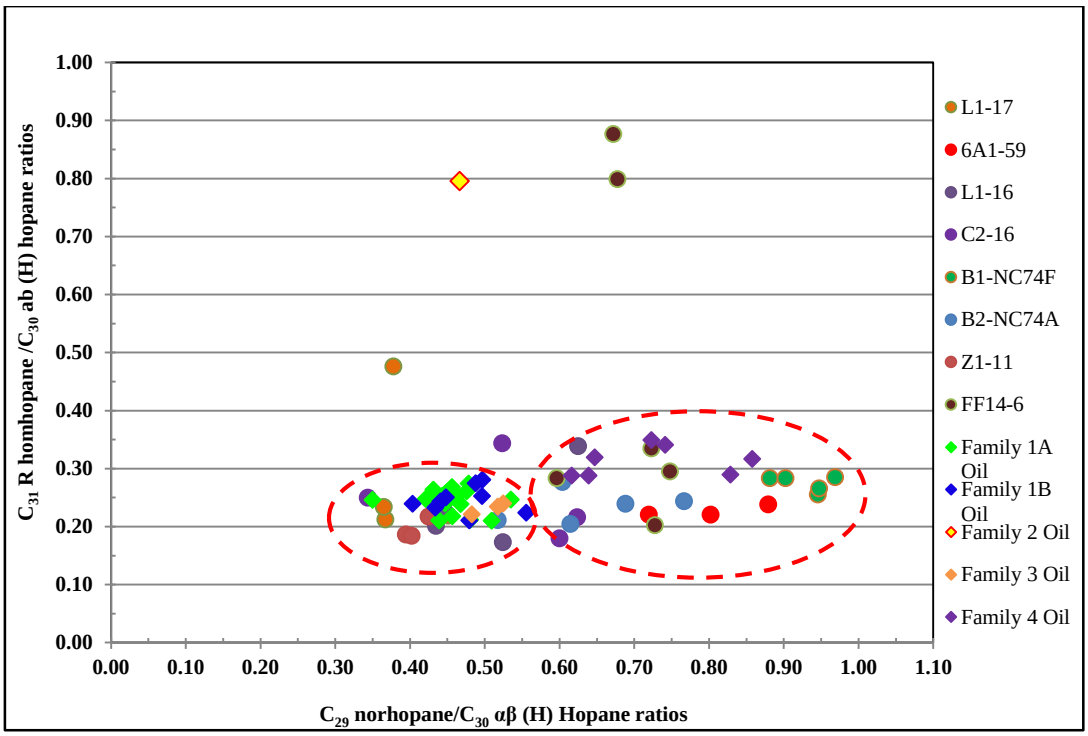

Figure 6.7: Cross plot of C_{29} norhopane/C30 αβ (H) hopane versus C_{31} S/C_{30} αβ (H) hopane from oil families and Sirte Shale and Rachmat source rock extracts in the Sirt Basin.

There is quite a good correlation between oil families 1A, 1B, and 2 and the Sirte Shale extracted from wells 6A1-59, B2-NC74A at the depths 9570 and 9610 feet, and the L1-16, L1-17 and Z1-11 well samples, and also between the Sirte Shale extracts from well B2-NC74A and the oil family 4 samples. The Sirte Shale and Rachmat source rock extracts from wells B1-NC74F and FF14-6 at depths of 11290, 11320 and 11615 feet show a good correlation with the oil family 1A oils at the Hakim oilfield in the A1-NC74A well. The chart also shows an overlap between oil families, which could be expected as their potentially associated source rocks are similar. However, a very large difference can be seen between the Sirte Shale source rock extracts in the [C_{20}+C_{21}]/[C_{20}-C_{28}] tricyclic terpanes ratios (Figure 6.8, Table 6.2 in Appendix III). Sirte Shale source rock extracts at wells B1-NC74F, C2-16 and FF14-6 have high values of C_{20}+C_{21} relative to the C_{20} to C_{28} tricyclic terpanes, which could give the impression of being slightly more mature than the rest of the Sirte Shale source extracts and crude oil samples, as shown in Figure 6.8.

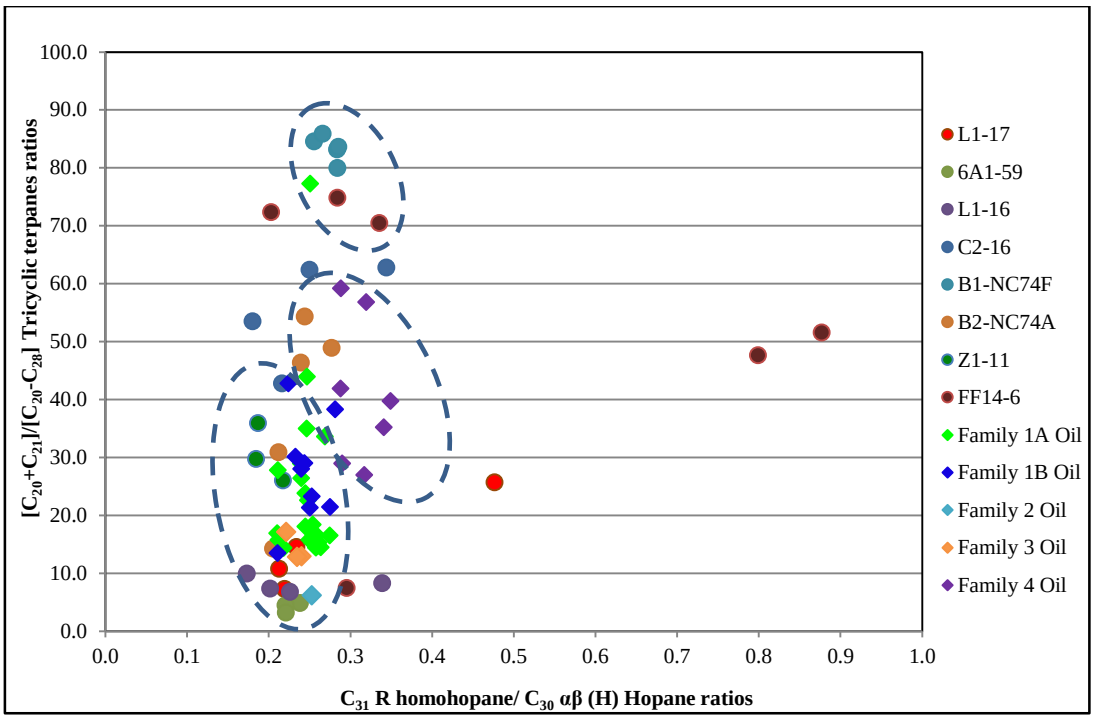

Figure 6.8: Cross plot of C_{31} S/C_{30} αβ hopane versus [C_{20}+C_{21}]/[C_{20}-C_{28}] tricyclic terpanes for oil families, Sirte Shale and Rachmat source rock extracts.

The major tricyclic terpanes appear to be more abundant in source rock and crude oil samples, while the tetracyclic terpanes are less abundant, similar to that observed by Aquino Neto *et al.* (1983). The C_{23} tricyclic terpane was predominant in the tricyclic group, followed by the C_{19}, C_{20}, and C_{24} compounds, respectively, in most of the study wells. This indicates that samples are characterized by moderate to high maturity, originated from microbial and/or an algal organic matter and was deposited in marine environments (e.g. Aquino Neto *et al.*, 1983; Farrimond *et al.*, 1999; Peters, 2005b). Figure 6.9 shows the C_{22}/C_{21} tricyclic terpane ratios versus the C_{24}/C_{23} tricyclic terpane ratios for the crude oil samples and source extracts. In general, the low C_{22}/C_{21} and C_{24}/C_{23} ratios suggest marine to lacustrine shale source rocks (e.g. Peters, 2005b). According to Yu *et al.* (2011), C_{21}/C_{23} tricyclic terpanes ratios <0.5 is in accordance with marine source rocks. The ratio in the samples ranges from 0.32 to 0.80, which indicate marine origin with little contributions of terrigenous organic matter. The Figure 6.9 plot shows no correlation between the Sirte Shale source rock extracts at wells 6A1-59, B1-NC74F, L1-16 and L1-17 with the oil families, while there is moderate to good correlation between the Sirte Shale source rock from wells B1-NC74F, B2-NC74A, C2-16, FF14-6, and oil families 1A, 1B, 2, 3 and 4. The plot shows

that the crude oil samples are plotted in the top right-hand corner, with higher values for both ratios and this may be as a result of their thermal maturity (e.g. Aquino Neto *et al.*, 1983; Neto *et al.*, 1986; Farrimond *et al.*, 1999; Peters *et al.*, 2005b). The relatively low abundance of the C_{24} tetracyclic terpane in most of the Sirte Shale and Rachmat source rock extracts and all oil families may suggest a low input of bacterial membranes deposited in siliciclastics marine environments (Peters, 2005b). For both oil families and source rock extracts the low ratios of C_{24}tetr/C_{23}tri (less than 0.41) and the absence of the C_{25} to C_{27} tetracyclic terpanes, suggest that the source rock extracts and oil families were derived from a marine clastic source associated with some contribution of terrestrial organic matter input (Peters, 2005b).

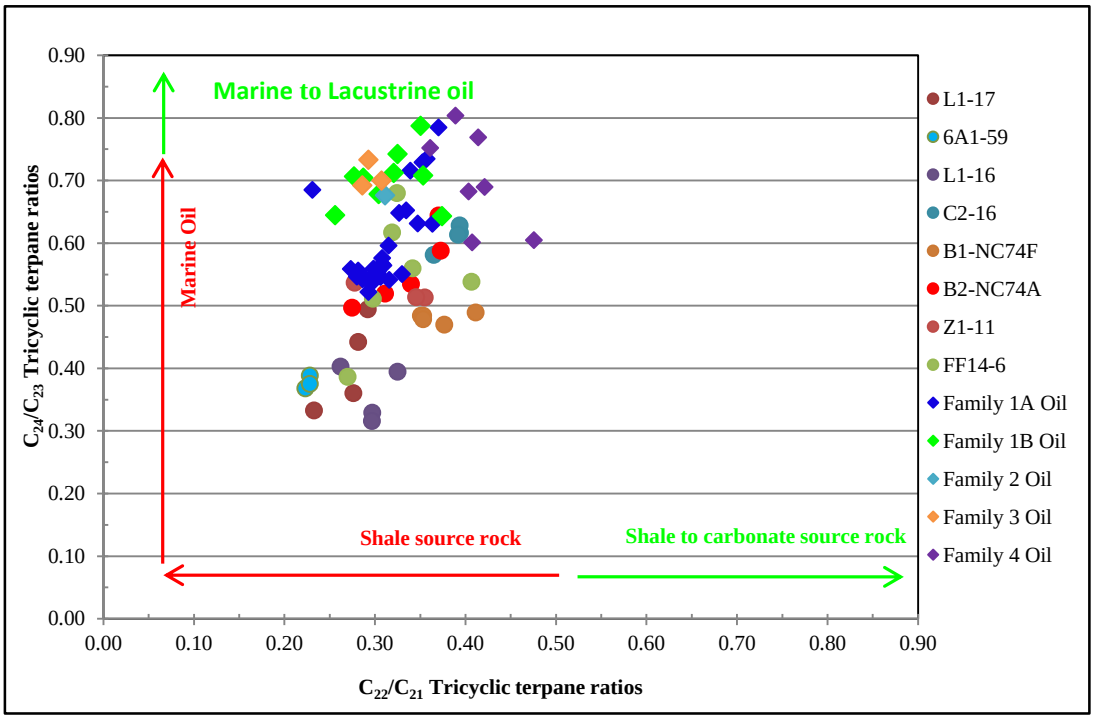

Figure 6.9: Cross plot of C_{22}/C_{21} tricyclic terpanes versus C_{24}/C_{23} tricyclic terpanes for oil families and Sirte Shale and Rachmat source rock extracts. Source interpretations trends are after (Peters et al., 2005b).

As shown in Figure 6.10, there is a good correlation between oil families 1A, 1B, 2 and 3 with the Sirte Shale and Rachmat source rock extracts from all study wells, indicating that the oils could have been generated from the Sirte Shale Formation. Family 4 oils show no close relationship to any of the source rock extracts from the Sirte Shale and Rachmat Formations, suggesting that those crude the oils were derived from another source rock. C_{26}/C_{25} tricyclic terpanes ratios >1.0 are typical of lacustrine deposit, but

an exception do occur. The high C_{26}/C_{25} tricyclic terpane values for family 4 oils suggest that these crude oils may have been generated from lacustrine source rocks (Schiefelbein *et al.*, 1999; Volk *et al.*, 2005; Peters, 2005b).

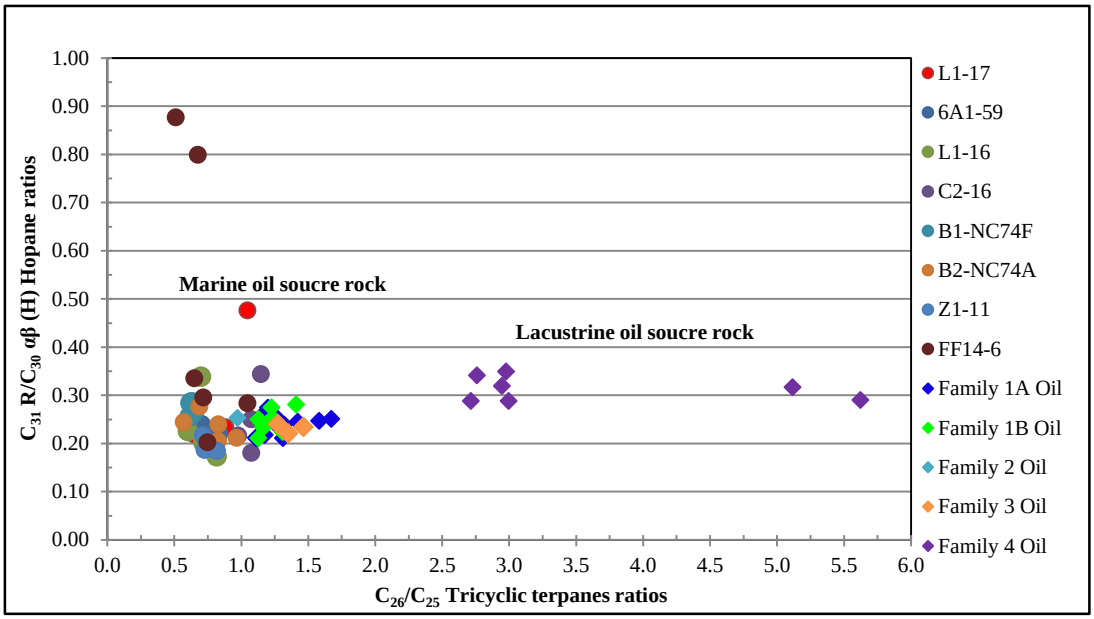

Figure 6.10: Cross plot of C_{26}/C_{25} tricyclic terpanes versus C_{31}/C_{30} αβ hopane ratios for oil families and, Sirte Shale and Rachmat source rock extracts in the Sirt Basin.

6.2.3 **Aromatic Compounds**

Figure 6.11 shows a cross-plot of the dibenzothiophene to phenanthrene ratio (DBT/P) versus Pr/Ph ratio of the various oil families and Sirt Basin source rock extracts. All of the oil families 1A, 1B, 2, 3 and 4 and Sirte Shale source rock extracts are shown to have similar source features, originating from marine to lacustrine shale source rocks, and their Pr/Ph ratios are in the range of 0.69 to 2.39, which suggests marine dysoxic to anoxic depositional environments. The Sirte Shale and Rachmat source rock extracts from wells B1-NC74F and B2-NC74A along with some intervals from the Sirte Shale Formation at wells FF14-6 and L1-16 are shown (Figure 6.11) to have originated from lacustrine, sulphate-poor lithological depositional environments and have low Pr/Ph ratios below 1.0 indicating anoxic depositional environments. Here, the differences in source rock characteristics indicate lateral and vertical variations in kerogen facies as well as changes in the depositional environments in the source rocks in the Sirt Basin.

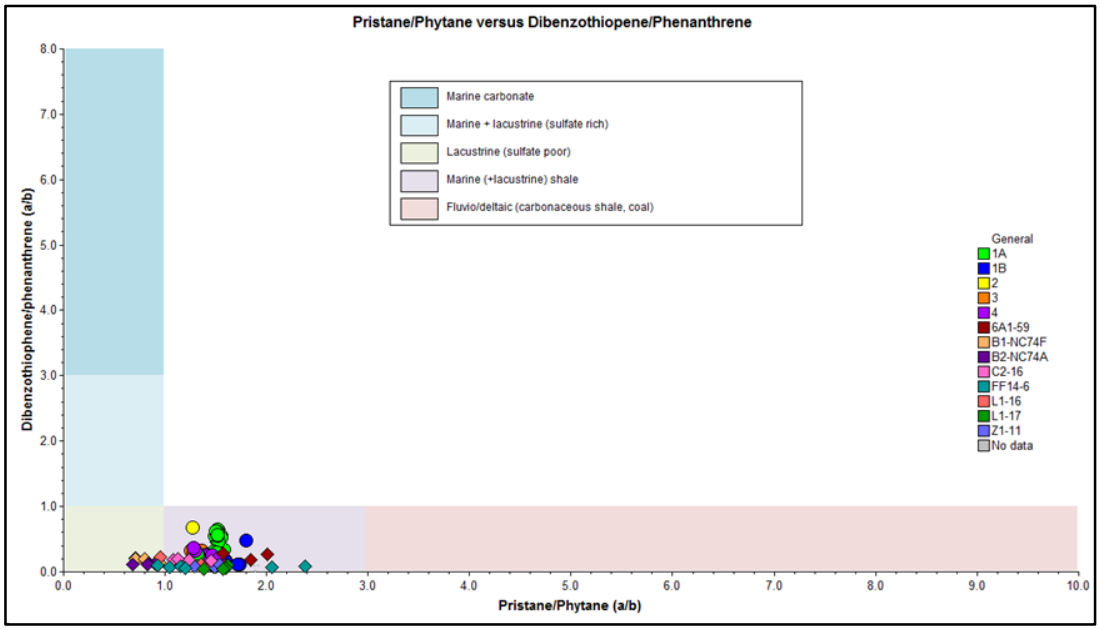

Figure 6.11: Cross plot of DBT/P versus Pr/Ph ratios from oil families and Sirte Shale and Rachmat source rock extracts in the Sirt Basin, circlers represent Family oils, and squares represent source rock samples. Depositional environment interpretational fields from pIGI software, after Hughes et al. (1995).

In alkylphenanthrenes compounds in sediments, a high abundance of the 9-MP component is closely related to a marine origin of the organic matter, whereas an abundance of 1-MP more related to terrestrial origin. and cross-plots of 1-MP/9-MP versus 1,7-DMP/(1,3-, 3,9, 2,10, 3,10-DMP) ratios have been successfully used for correlation studies of crude oils and source rocks from various geological ages (Alexander *et al.*, 1992b). Figure 6.12 shows a cross-plot of the 1-MP/9-MP versus 1,7-DMP/(1,3-, 3,9, 2,10, 3,10-DMP) ratios. It is clear from this figure that all the oil families 1A, 1B and 4 plot close to the Sirte Shale source rock extracts from the wells 6A1-59, B1-NC74F at depths 7050 and 7110 feet, B2-NC74A (9520'), and FF14-6 (11320'), indicating similarities between the crude oils and source rocks. The high relative abundance of 9-MP and 1,3-, 3,9-, 2,10- 3,10-DMP indicates that the crude oils and source rock extracts are from marine origins, whereas the slightly higher relative abundances of 1-MP and 1,3,7-DMP for the oil family 3 and Sirte Shale source rock extracts from the Z1-11 well (8140 feet) indicates that these crude oils and source rock have slightly higher contributions of terrigenous organic matter. This may reflect lateral and vertical variation in organic facies and depositional environments within the sedimentary sections of the Sirte Shale Formation in the Sirt Basin. Family 2 oils have

slight dissimilarities from other groups, but still have similar main characteristics of the oil families 1A, 1B and 4, while being completely different from the family 3 oils. This may reflect changes in organic facies within the Sirte Shale source rock in the Sirt Basin. The remaining Sirte Shale source rock extracts from B2-NC74A, C2-16, FF14-6, L1-16 and L1-17 wells show lower values for both ratios, indicating that these source rocks had marine origins (e.g. Alexander *et al.*, 1992b).

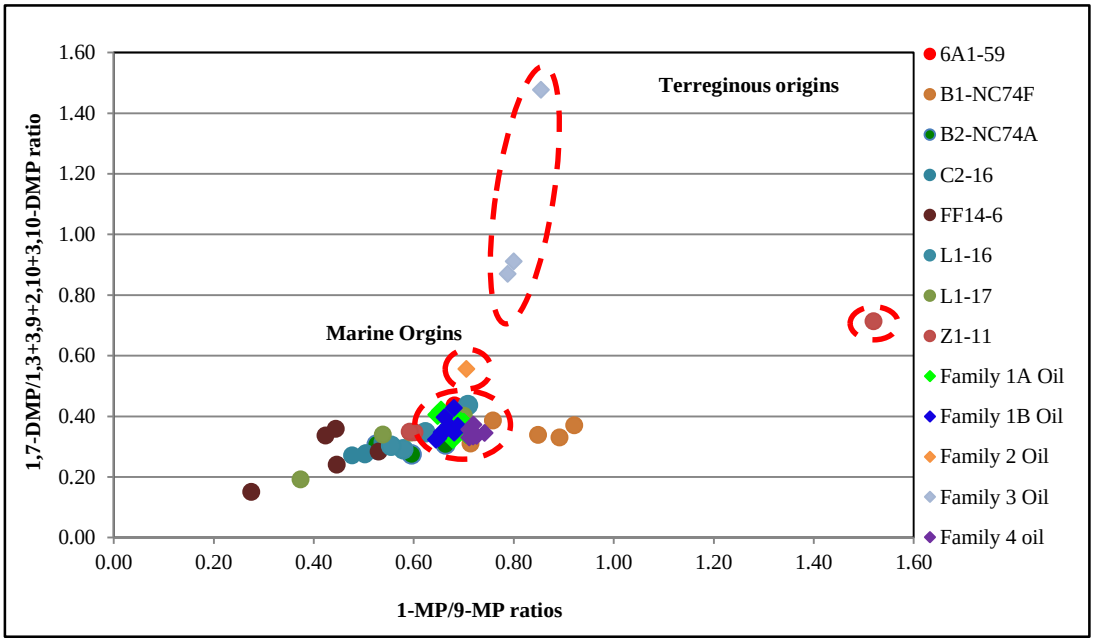

Figure 6.12: Cross plot of 1-MP/9-MP versus 1,7-DMP/(1,3-, 3,9, 2,10, 3,10-DMP) ratios from oil samples and source rock extracts in the Sirt Basin, circlers represent Sirt Shale and Rachmat source rock extracts samples, while squares represent oil families.

Figure 6.13 shows a cross-plot between the 1,2,5-TMN/1,2,7-TMN against 1,2,6-TMN/1,2,4-TMN ratios for the oil families and Sirte Shale and Rachmat source rock extracts. Strachan *et al.* (1988) suggested that the 1,2,7-TMN and 1,2,5-TMN compounds are angiosperm indicators, but non-angiosperm natural products could be also sources of 1,2,5-TMN. The extremely high abundance of 1,2,6-TMN relative to 1,2,4-TMN and of 1,2,5-TMN relative to 1,2,7-TMN in family 3 oils indicates different source precursors for these naphthalene isomers compared to the other oil families and source rock extracts. The high levels of these ratios indicate that these naphthalene isomers may have been sourced from different marine microbial origins or angiosperms. Oil Families 1A, 1B, 2 and 4 and Sirte Shale source extracts from the wells B1-NC74F at strata depths 7050, 7110 and 7190 feet, B2-NC74A well (9610

feet), and well Z1-11 (8140 feet) are located as close to each other on the diagram, indicating similar sources of the TMN. The Sirte Shale source rock extracts from wells 6A1-59, C2-16, FF14-6, L1-16 and L1-17 also plotted close to each other. These have a high abundance of 1,2,6-TMN relative to 1,2,4-TMN, and of 1,2,5-TMN relative to 1,2,7-TMN, indicating that their sources have similar characteristics and maybe originated from different marine microbes or angiosperms compared to those in the oil families. The remaining source rocks extracts from the wells B1-NC74A, B2-NC74A, L1-17 and Z1-11 have lower levels of 1,2,6-TMN relative to 1,2,4-TMN, suggesting that these source rocks were generated from different marine bacteria or angiosperms. Nevertheless, both the oil families and source rock extracts cluster at different places in the chart, indicating some variations in source inputs.

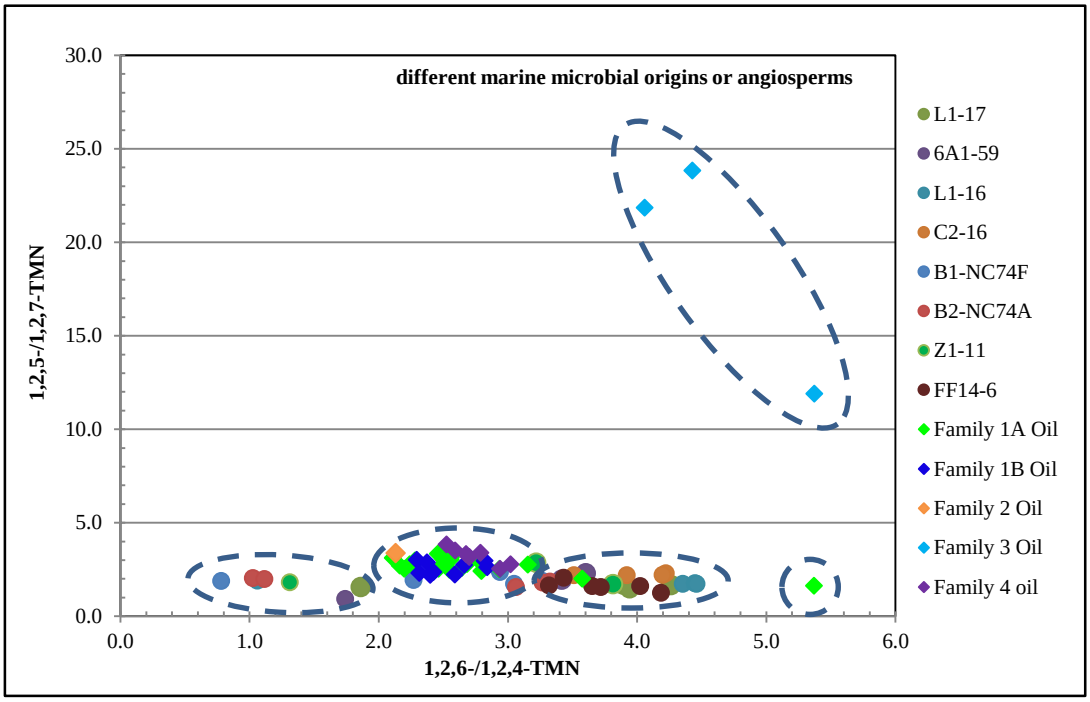

Figure 6.13: Crossplot of 1,2,6-TMN/1,2,4-TMN versus 1,2,5-TMN/1,2,7-TMN ratios from oil samples and source rock extracts in the Sirt Basin, circler represent Sirt Shale and Rachmat source rock extracts and square represent oil families.

The monoaromatic and triaromatic steroids are considered as very effective thermal maturity parameters for the oil generation window, but these compounds have also been reported as potentially source-dependent (Peters, 2005b). The monoaromatic steroids in the source rock extracts and oil samples analysed plot in the C_{27}-C_{28}-C_{29} ternary diagram in areas associated with terrigenous, marine, or lacustrine inputs, as

shown in Figure 6.14. The main application of this diagram is to achieve a correlation between oil and source rock, and it is considered more useful in helping to describe the depositional environment of source rock for petroleum. This diagram can provide supporting evidence for correlation between the crude oils and source rock extracts in the Sirt Basin. Oils generated from marine clastic shale generally contain less C_{29} MAS than non-marine. Typically, high levels of terrigenous organic matter are deposited in non-marine than in marine source rocks, and therefore, non-marine source rock thus has high C_{29} sterols. Generally, most of the marine oils or source rocks contain a higher proportion of C_{28} MAS than non-marine oils (Moldowan *et al.*, 1985). The distributions of the C_{27}, C_{28} and C_{29} monoaromatic steroids for oil families 1A, 1B, 2, 3 and the Safsaf oilfield in oil family 4 and Sirte Shale and Rachmat source rock extracts samples from the wells 6A1-59, B1-NC74F, B2-NC74A, C2-16, FF14-6, and Z1-11 are plotted close together in the diagram, showing a relatively higher abundance of C_{27} relative to the C_{28} and C_{29} and suggesting marine organic matter source inputs. The Aswad and Zellah oilfields within oil family 4 show relatively slightly higher abundance in C_{27} and C_{29} relative to C_{28}, suggesting a high contribution of marine algal organic matter with little terrestrial material input, and that the oils were deposited in marine to lacustrine environment.

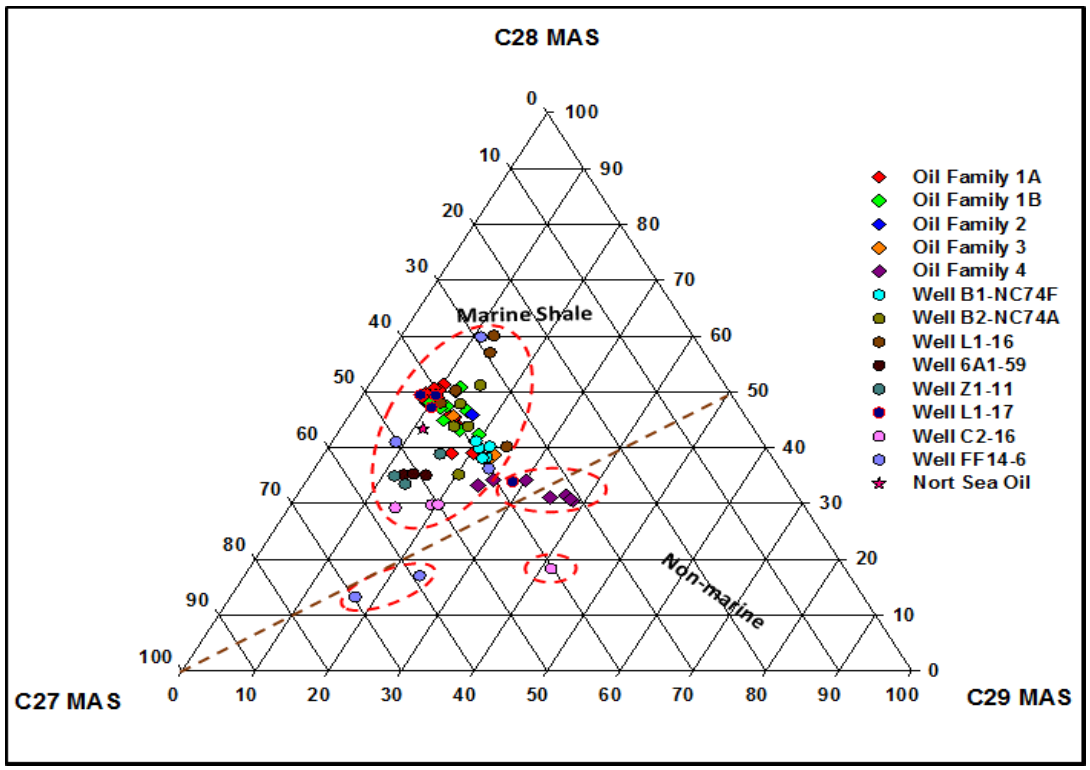

Figure 6.14: Ternary diagram C_{27}, C_{28}, and C_{29} monoaromatic steroids relative abundances showing marine and non-marine depositional settings of source rock and oils families in the Sirt Basin, circlers represent Sirt Shale and Rachmat source rock and squares represent oil families.

For both the oil families and Sirte Shale and Rachmat potential source rock extracts, the triaromatic steroids (TAS) show varying distributions of the short chain (C_{20} and C_{21} TAS) and long chain (C_{26} to C_{28} TAS) compounds in the Sirt Basin. In general, the short chain C_{20} and C_{21} compounds are present in higher abundance than long chain C_{26} to C_{28} compounds. Oil Families 1A, 1B, 2 and 3 and the Sirte Shale Formation from the wells 6A1-59, L1-16, L1-17, B2-NC74 at a depth 9570 feet, and FF14-6 at a depth 11320 feet, have higher abundances of the long chain relative to short chain TAS. However, the predominance of $C_{26}R$ + $C_{27}S$, and $C_{27}R$ TAS in the crude oils and source rock extracts may reflect similar source rock, as well as their marine origins. In oil family 4 and Sirte Shale and Rachmat source rocks from the wells B1-NC74F, B2-NC74A, C2-16, FF14-6 and Z1-11, there is a higher abundance of short chain TAS relative to long chain TAS. These also show similar levels of $C_{26}R$ +$C_{27}S$, and $C_{27}R$ TAS, suggesting that the crude oils and source extracts are derived from a mixture of marine and non-marine organic matter input at different levels of thermal maturity.

The ratios of the C_{26}/C_{28} S TAS and C_{27}/C_{28} R TAS can be used to distinguish between oil families and source rocks. Figure 6.15 displays the cross-plot of the C_{26}/C_{28} S TAS versus C_{27}/C_{28} R TAS ratios for oil families, Sirte Shale and Rachmat potential source rocks in the Sirt Basin. Oil Families 1A, 1B, and 2 and Sirte Shale source extracts from the wells L1-17 and Z1-11 plot close to each other in the diagram, indicating similar organic facies and marine depositional environments. The Sirte Shale source rock extracts from the sedimentary sections of the wells 6A1-59, C2-16, FF14-6, L1-16 and some intervals of the well L1-17 plot near to each other at the top-right corner of the diagram, suggesting similar organic matter inputs and deposition conditions for the source rocks, but the oil families 1A, 1B, and 2 plots further away, which may indicate variations in depositional environments. Oil families 3 and 4 plot close to the Sirte Shale and Rachmat source rocks from the B1-NC74F and B2-NC74A wells in the bottom left corner in the diagram, suggesting that these source rocks and oils were generated from similar organic facies deposited in a lacustrine to marine environments (e.g. Radke *et al.*, 1982a; Peters *et al.*, 2005a). The two source rock extracts from the FF14-6 well at depths of 12290 and 12330 feet plot in different places in the chart, indicating variations in source organic matter input and/or depositional environment.

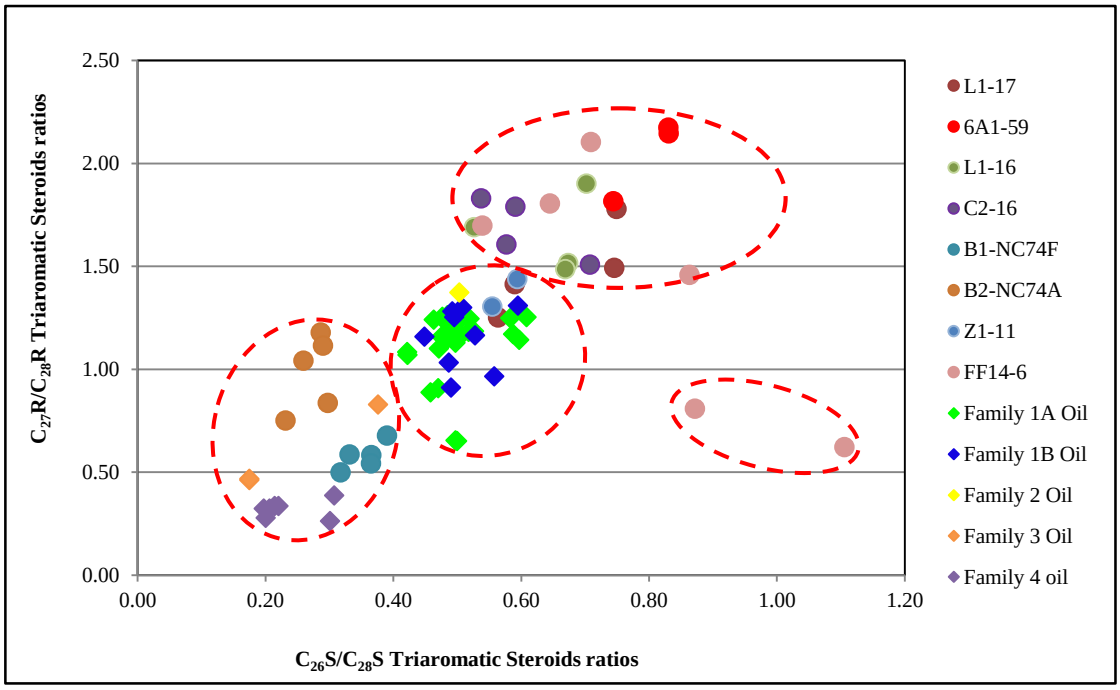

Figure 6.15: Cross plot of the $C_{26}S/C_{28}S$ triaromatic steroids versus $C_{27}R/C_{28}R$ triaromatic ratios from oils samples and source rocks in the Sirt Basin, circles represent Sirt Shale and Rachmat source rock and squares represent oil families.

6.3 *n*-Alkane Stable Carbon Isotopic Compositions

Compound-specific isotope analysis (CSIA) was performed to determine the stable carbon isotopic composition of the *n*-alkanes from the crude oils and source rocks in order to aid oil-to-source correlations for the Sirt Basin. The stable carbon isotopic compositions of *n*-C_{10} to *n*-C_{32} alkanes were measured using GC-IRMS for 13 crude oil and 10 potential source rock samples. The data for the carbon-specific isotopic analyses showing $\delta^{13}C$ values in the *n*-alkanes of the different oil groups are presented in Table 6.1. The $\delta^{13}C$ values of *n*-alkanes (*n*-C_{10} to *n*-C_{32}) are plotted in Figure 6.16, which shows that the values of the crude oil samples cover a broad range between -25.7 and -38.5‰ and that the Sirte Shale and Rachmat potential source rocks extracts also cover a very similar broad range between -26.5 and -38.3 ‰. The profile of $\delta^{13}C$ values of *n*-alkanes from family 1A and 1B oils and Sirte Shale source rock extracts from the wells 6A1-59, B1-NC74F, C2-16 and FF14-6 show a similar trend for most of the samples analysed, but slightly higher variations are observed in the $\delta^{13}C$ isotope values in *n*-C_{18}, which may be due to the co-elution of *n*-C_{18} with phytane component, where after *n*-C_{19}, the $\delta^{13}C$ isotope values are more similar (Figure 6.17). Also the profile of $\delta^{13}C$ values of *n*-alkanes from oil families 1A, 1B, 3, and 4 and samples from the 6A1-59 and C2-16 wells show a reduction in the $\delta^{13}C$ isotope values from *n*-C_{27} to *n*-C_{32}, which may be due to production of isotopically light carbon from the source rock kerogen. From the characteristics of the slope profile of the *n*-alkane carbon number versus $\delta^{13}C$ value plot, most of the oil families 1A, 1B, and 3 and the Sirte Shale and Rachmat source rock extracts from wells 6A1-59, B1-NC74F, C2-16 and FF14-6 appear with a nearly flat profile (Figure 6.17), which is generally characteristic of sources rich in marine organic matter input (Murray *et al.*, 1994). This flat profile may be produced by homogeneity in the distribution of $\delta^{13}C$ *n*-alkanes as a result of the derivation from a homogeneous marine kerogen. This similarity in the isotope profiles of oil families 1A, 1B, and 3 and the Sirte Shale and Rachmat source rocks may thus reflect their origin from a marine organic source facies, which has also been inferred from the molecular biomarker analyses (Section 6.2.1.2). Oil family 4 and the Sirte Shale source rock extracts from well B2-NC74A seem to be slightly different isotopically from other oil families, containing the heaviest $\delta^{13}C$ isotopic compositions among oil families 1A, 1B and 3 and Sirte Shale source rock (Figure 6.18). This may

be due to production of the *n*-alkanes from kerogens characterised by marine organic matter with moderate to high contributions from algae organic matter, as well as the effects of increased thermal maturity (e.g. Murray *et al.*, 1994). The Sirte Shale source rock extract from the L1-16 well showed reduced in $\delta^{13}C$ values in *n*-C_{18} compare to other studied wells, which may be as a result of very low to no co-elution with the phytane peak. Oil families 1A and 1B and the Sirte Shale source rock from wells C2-16 and FF14-6 have the isotopically lightest (most negative values) $\delta^{13}C$ values (Figure 6.19), and this may be consistent with a marine source or that source rock produced ^{12}C more than ^{13}C (e.g. Bjorøy *et al.*, 1994; Murray *et al.*, 1994). Thus, the *n*-alkane isotopes of the crude oils and source rock extracts are controlled by source and depositional environment as well as thermal maturity, which was also indicated in previous analyses of hydrocarbon distributions. The data for the carbon-specific isotopic analyses showing $\delta^{13}C$ values in the *n*-alkanes of the different oil groups are presented in Table 6.1.

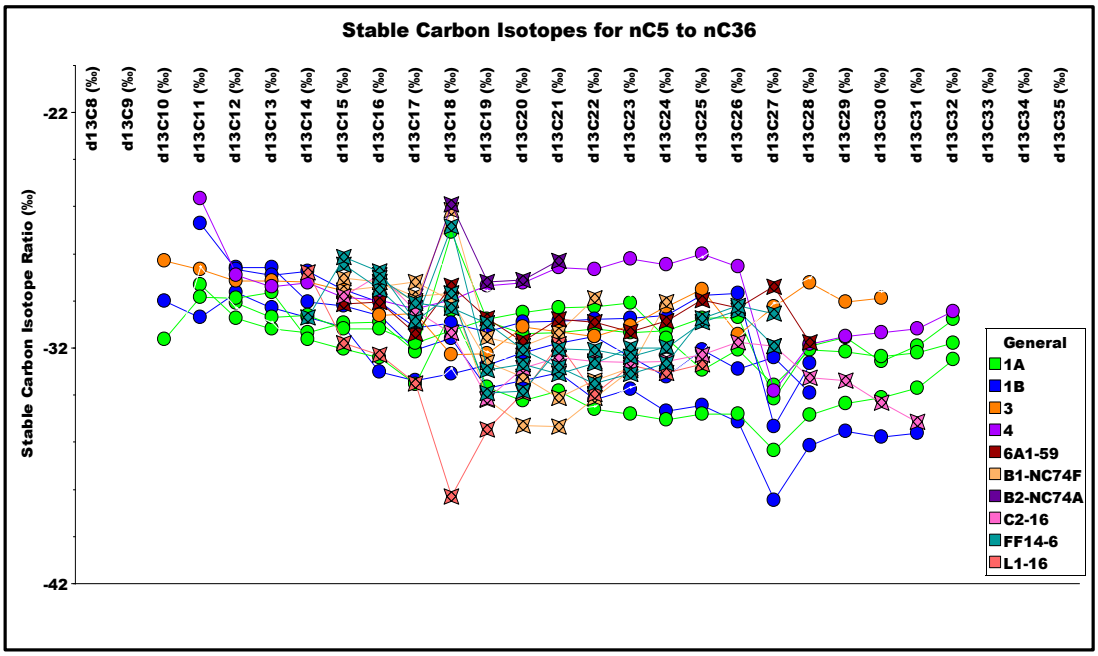

Figure 6.16: Stable carbon isotope plot of *n*-alkanes from the oils families and Sirte Shale and Rachmat source rocks extracts.

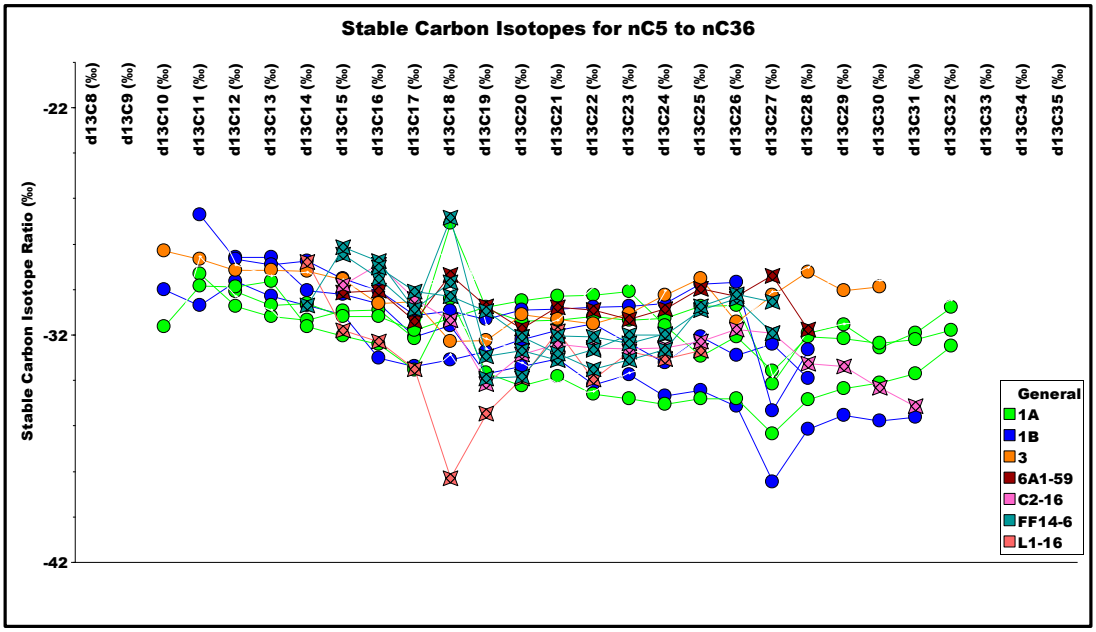

Figure 6.17: Stable carbon isotope plot of *n*-alkanes from the oils families and Sirte Shale and Rachmat source rocks extracts.

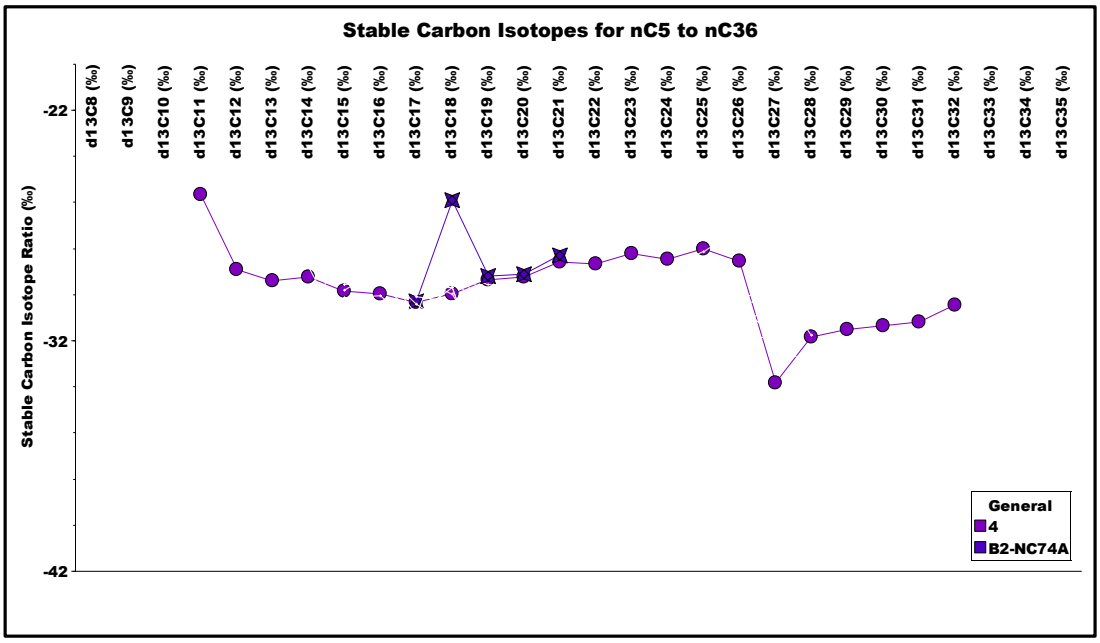

Figure 6.18: Stable carbon isotope plot of *n*-alkanes from the oils families and Sirte Shale and Rachmat source rocks extracts.

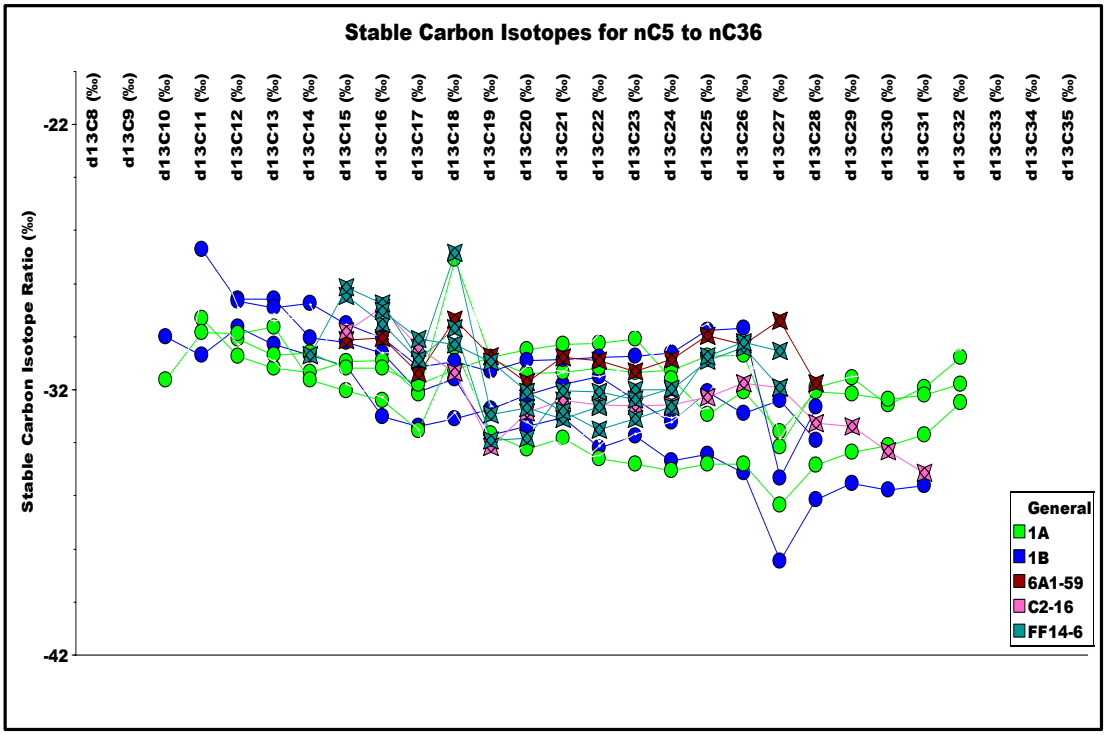

Figure 6.19: Stable carbon isotope plot of *n*-alkanes from the oils families and Sirte Shale and Rachmat source rocks extracts.

Table 6-1: $\delta^{13}C$ values for *n*-alkanes from the oil families and Sirte Shale and Rachmat source rock extracts.

Oil Field	West Mabruk		East Mabruk	Safsaf	South Jebel	West Meghil	Ragoba	Dor Mansour	6A1-59	B1-NC74F	B1-NC74F	B1-NC74F	B2-NC74A	C2-16	FF14-6	FF14-6	FF14-6	L1-16
Well	A31-17	A38-17	A58-17	C1-NC74B	4B1-6	4J2-6	E82-20	Z5-47	7250	7050	7190	7940	9570	9800	11290-310	11650	11320	7530
Location		West Sirt Basin				Central Sirt Basin							West Sirt Basin					
Groups		1A		4		1B		3	Sirte Shale source rok			Rachmat		Sirte Shale source rok				
n-C_{10}			-31.7			-30.0		-28.3										
n-C_{11}	-29.3		-29.9	-25.7		-30.7	-26.7	-28.7										
n-C_{12}	-30.8	-30.1	-29.9	-28.9	-28.6	-29.7	-28.7	-29.2										
n-C_{13}	-31.2	-30.7	-29.7	-29.4	-28.6	-30.3	-28.9	-29.2										-30.2
n-C_{14}	-31.4	-30.6	-31.7	-29.3	-30.1	-30.7	-28.8	-29.2	-28.8								-30.7	-30.1
n-C_{15}	-31.0	-31.2	-32.1	-29.9	-30.2	-31.1	-29.5	-29.6	-31.8	-29.6		-29.1		-29.8	-28.5		-28.2	-31.4
n-C_{16}	-30.9	-31.2	-32.4	-30.0	-30.6	-33.0	-30.1	-30.6	-32.3	-29.4	-29.2	-29.2		-28.9	-29.5	-29.1	-28.8	-29.4
n-C_{17}	-32.2	-31.8	-33.6	-30.4	-32.1	-33.4	-31.2	-30.6	-33.5	-29.2	-29.8	-30.0	-30.3	-30.4	-30.9	-30.1	-30.9	-30.8
n-C_{18}	-27.1	-31.3	-30.4	-30.0	-31.6	-33.1	-31.0	-32.3	-38.3	-30.0	-29.7	-26.2	-25.9	-31.4	-26.9	-30.3	-29.7	-31.7
n-C_{19}	-30.9	-30.8	-33.7	-29.4	-33.7	-32.8	-31.3	-32.3	-35.5	-32.6	-34.2	-31.6	-29.2	-34.2	-33.0	-31.0	-33.9	-30.8
n-C_{20}	-31.4	-30.5	-34.3	-29.3	-33.4	-32.2	-30.9	-31.1	-33.9	-33.2	-35.3	-31.9	-29.1	-32.9	-32.7	-32.1	-33.9	-30.9
n-C_{21}	-31.4	-30.3	-33.9	-28.6	-33.1	-31.8	-30.9	-31.3	-31.9	-34.1	-35.4	-31.4	-28.3	-32.4	-33.1	-32.8	-32.1	-31.3
n-C_{22}	-31.2	-30.3	-34.6	-28.7	-34.2	-31.5	-30.8	-31.5	-34.0	-33.4	-34.1	-29.9		-32.6	-32.7	-33.5	-32.1	-30.9
n-C_{23}	-31.4	-30.1	-34.8	-28.2	-33.8	-32.4	-30.8	-31.1	-32.8	-32.9	-33.0			-32.6	-32.0	-33.1	-32.4	-30.0
n-C_{24}	-31.3	-31.6	-35.1	-28.5	-34.7	-33.2	-30.6	-30.3	-33.1	-30.1				-32.6	-32.0	-32.7	-32.0	-30.3
n-C_{25}	-30.8	-33.0	-34.8	-28.0	-34.5	-32.1	-29.8	-29.5	-32.7					-32.3	-30.9	-30.8		-29.4
n-C_{26}	-30.7	-32.1	-34.8	-28.6	-35.2	-32.9	-29.7	-31.5						-31.8	-30.4	-30.2		-31.8
n-C_{27}	-34.2	-33.6	-36.4	-33.9	-38.5	-32.4	-35.4	-30.3						-31.9	-31.9	-30.6		
n-C_{28}	-31.9	-32.1	-34.9	-31.9	-36.2	-33.9	-32.7	-29.3						-33.3				
n-C_{29}	-31.6	-32.2	-34.4	-31.5	-35.6			-30.1						-33.4				
n-C_{30}	-32.6	-32.4	-34.1	-31.4	-35.8			-29.9						-34.3				
n-C_{31}	-31.9	-32.2	-33.7	-31.2	-35.6									-35.2				
n-C_{32}	-30.8	-31.8	-32.5	-30.5														

6.4 Principal Component Analysis

The data are composed of 10 variables, which include biomarker ratios and two maturity ratios, for the 46 crude oil samples from four oil families and 34 source rocks extracts from the Sirte Shale and Rachmat Formations in the western and central part of the Sirt Basin. The crude oils and source rock extracts samples were analysed using PCA to determine the major sources of variation within the sterane, diasterane, hopane and diahopane distributions, and the variables used in this analysis are listed in Table 6.2. The first three principal components obtained represent 34.0%, 27.5%, and 14.7% respectively of the variance within the data set. This type of variance analysis allows the relationships between samples to be studied in simple two-dimensional score plots of PC1 versus PC2. This includes the effects of all the original variables, which are source facies, molecular biomarker ratios and maturity, which together represent the bulk of the variance in the data of about 76.2%. PC1 explains 34.0% of the variance of the data set and is characterised by the moderately high loading for the source facies parameters C_{29}Ts/C_{29} H, C_{27}%, C_{28}% and sterane/hopane ratio with two maturity parameters C_{29} ααα S/(S+R) and C_{29} sterane αββ/(αββ+ααα). This may indicate that source facies along with maturity are the most significant factors controlling the composition and distribution of biomarkers in the Sirt Basin oils and source rock extracts. PC2 captures 27.5% of the variance and is characterised by moderately high loadings of biomarker parameters influenced by organic facies, the C_{27} Ts/Tm, C_{29}Ts/C_{29} H, C_{30} diahopane/C_{30} αβ hopane and ΣC_{27} diasterane/ΣC_{27} steranes, suggesting that source facies is the most important factor controlling the composition and distribution of biomarkers in the Sirt Basin crude oils and source rock extracts. PC3 captures 14.7% of the variance and is characterised by high loadings of C_{29}% sterane and moderate loading of C_{27}% source parameters, and is therefore considered to be primarily dependent on source organic matter type. In general, the rearranged sterane and terpane biomarker parameters such as C_{27} Ts/Tm, C_{29}Ts/C_{29} H, C_{30} diahopane/C_{30} αβ hopane, ΣC_{27} diasteranes/ΣC_{27} steranes ratios can be used to estimate the lithology and depositional environments of the source rock from their corresponding crude oils. Rubinstein *et al.* (1975); Sieskind *et al.* (1979) and reported that the diasteranes have no direct biological precursor and they are developed by a basic rearrangement of steroid molecules, which is catalysed by clay minerals and

occurs during the early diagenesis phase under mild thermal situations and thus they are typically more abundant in clastic source rocks (Peters, 2005b). In this study, relatively high proportions of C_{27} to C_{29} diasteranes (βα and αβ) are present in some crude oil samples and source extracts. This indicates that they are derived from clay-rich source rocks. While clay catalysis is thought to be the main factor in forming diasteranes, these compounds have also been found to increase in abundance compared to other sterane isomers with increasing thermal maturity (Requejo *et al.*, 1997).

Table 6-2: Correlation matrix of the bulk geochemical data and biomarker parameters used in the principle component analysis (PC1, PC2 and PC3) for oil families and Sirte Shale and Rachmat source rocks extracts in Sirt Basin.

Variables Parameters	C_{27} Ts/Tm	C_{30}dia/C_{30} H	C_{29}Ts/C_{29} H	C_{29} S/(S+R)	C_{29} abb/ (abb+aaa)	Σ C27 dia/ Σ C_{27} Sterane	C_{27}%	C_{28}%	C_{29}%	Sterane/ hopane	Percentage of variance explained (%)
C_{27} Ts/Tm	1.000										
C_{30}dia/C_{30} H	0.874	1.000									
C_{29}Ts/C_{29} H	0.840	0.709	1.000								
C_{29} S/(S+R)	0.031	0.043	-0.012	1.000							
C_{29} αββ/(αββ+ααα)	0.013	0.062	-0.096	0.804	1.000						
Σ C_{27} dia/Σ C_{27} Steran	-0.213	-0.288	-0.324	-0.199	-0.011	1.000					
C_{27}%	-0.092	0.044	-0.127	0.486	0.459	-0.533	1.000				
C_{28}%	0.083	-0.063	0.388	-0.579	-0.679	-0.930	-0.537	1.000			
C_{29}%	0.104	0.124	0.081	0.016	-0.076	-0.211	-0.447	-0.009	1.000		
Sterane/hopane	0.395	0.412	0.281	-0.619	-0.471	0.179	-0.265	0.466	-0.359	1.000	
PC1	0.271	0.223	0.300	-0.406	0.361	0.032	-0.334	0.413	0.038	0.416	34.00
PC2	0.482	0.497	0.430	0.288	0.253	-0.325	0.235	-0.158	0.054	0.003	27.50
PC3	-0.007	0.035	-0.064	-0.085	0.034	0.105	0.415	-0.046	-0.786	0.427	14.70

Figure 6.20 shows the PC1 versus PC2 plots for the oil families 1A, 1B, 2, 3 and 4 and the Sirte Shale and Rachmat source rock extracts. The cross-plot separates the oil families and source rock extracts into six groups. Group 1 consists of oil families 1A and 1B and Sirte Shale source rock extracts from well B2-NC74A at depths of 9570 and 9610 feet and well FF14-6 at depths of 11615 and 11650 feet; group 2 comprises samples from oil families 2, 3 and 4; group 3 contains Sirte Shale and Rachmat source rock extracts from boreholes B1-NC74F, and B2-NC74A at depths of 9520 and 9580 feet, and FF14-6 at depths of 12290 and 12330 feet; group 4 includes Sirte Shale source extracts from wells L1-17, Z1-11 and C2-16 at a depth of 10580 feet; group 5 contains the Sirte Shale source rock extracts from the wells 6A1-59, L1-16 and L1-17 at a depth of 6060 feet; and finally group 6 comprises Sirte Shale source rock extracts from the C2-16 well. The diagram shows a slight convergence between oil family 4 and the Sirte Shale and Rachmat source rocks from the B1-NC74F and B2-NC74A wells, which suggests that the crude oils may have been generated from similar source rocks. Oil families 1A and 1B may be generated from the Sirte Shale source rock close to the L1-17, L1-16 wells. However, the Sirte Shale source rock from the C2-16 well plotted far away from the other samples, indicating different organic facies in this Sirte Shale source rock. Alternatively, slightly higher thermal maturity, as indicated by the Rock-Eval T*max*, spore colour index, and vitrinite reflectance data and the biomarker maturity parameters, may have had an effect on these correlations.

Figure 6.21 shows the loadings of the different variables of the three principal components, where large loadings (either negative or positive) indicate a significant influence of each variable on that principal component. It is generally agreed that loadings can be considered high when values are more than 0.6, moderately high when above 0.3, and low when less than 0.3 (e.g. Kline, 1994; Jolliffe, 2002). A low loading suggests that there is little or no correlation between the variables and the PCs (Jolliffe, 2002).

The first principal component PC1 explains 34.0% of the total variance in the data, and moderately high loadings (0.3-0.6) are found in the parameters C_{29}Ts/C_{29} hopane, C_{27}%, C_{28}% sterane, sterane/hopane ratio and C_{29} ααS/ααS+ααR sterane, C_{29} αββ/αββ+ααα sterane. Organic facies parameters appear to be more dominant than

maturity in controlling the distributions of biomarkers in the crude oil samples and source rock extracts in the Sirt Basin.

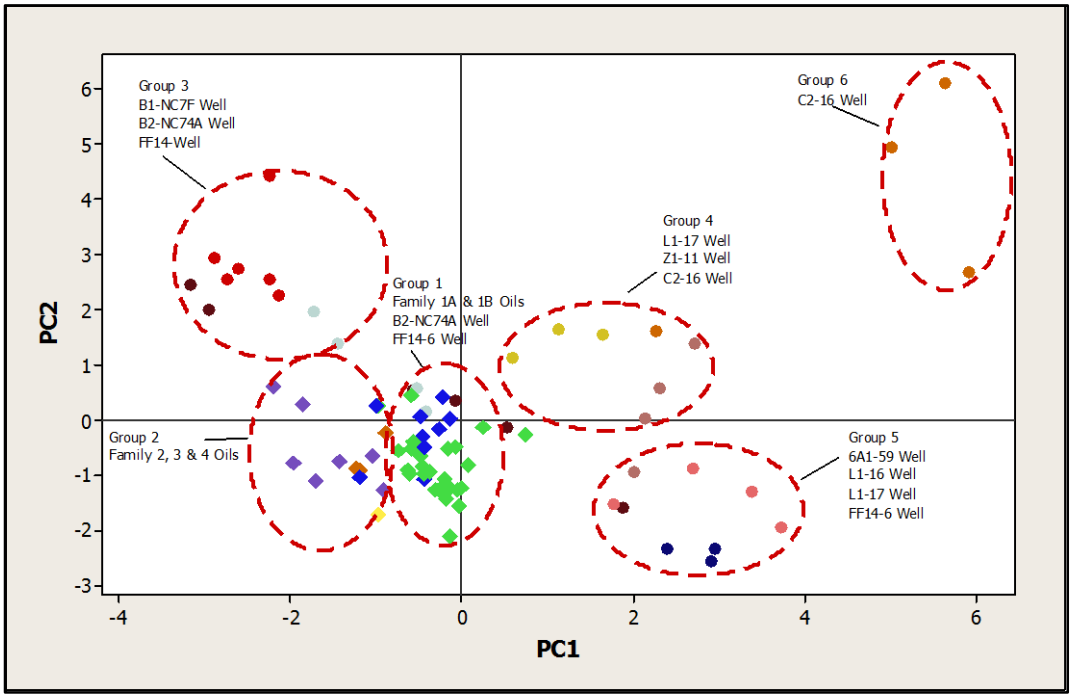

Figure 6.20: Cross plot of PC1 versus PC2 for the oil families and source rock extracts. The second principal component PC2 explains 27.5% of the total variance in the data. Moderately high loadings are observed for C_{27} Ts/Tm hopane, ΣC_{27} diasterane/Σ C_{27} sterane, C_{30} diahopane/ $C_{30}\alpha\beta$ hopane, and C_{29}Ts/C_{29} hopane. Consequently, it could be considered that organic facies appear to have more effect on PC2 than maturity, and this may impact on the distributions of biomarkers in source rock extracts and crude oils in the Sirt Basin.

The third principal component is less important than the first and second, representing 14.7% of the total variance in the data set. A moderately high loading is recorded for the C_{27}%, C_{29}% sterane and sterane/hopane ratio parameters. Therefore, it could be considered that source facies has more impact than maturity on the PC3. It is clear that from the analysis of the data set that PC3 is controlled by changes in organic facies in the Sirte Shale and Rachmat source rock extracts and oil families.

The combination of PC1 and PC2 and PC1 with PC3 account 61.5% and 48.7% respectively of the total data set variables, showing nearly similar effects of source

organic facies and maturity on the concentration and distribution of biomarkers in the source rock extracts and crude oils from the Sirt Basin.

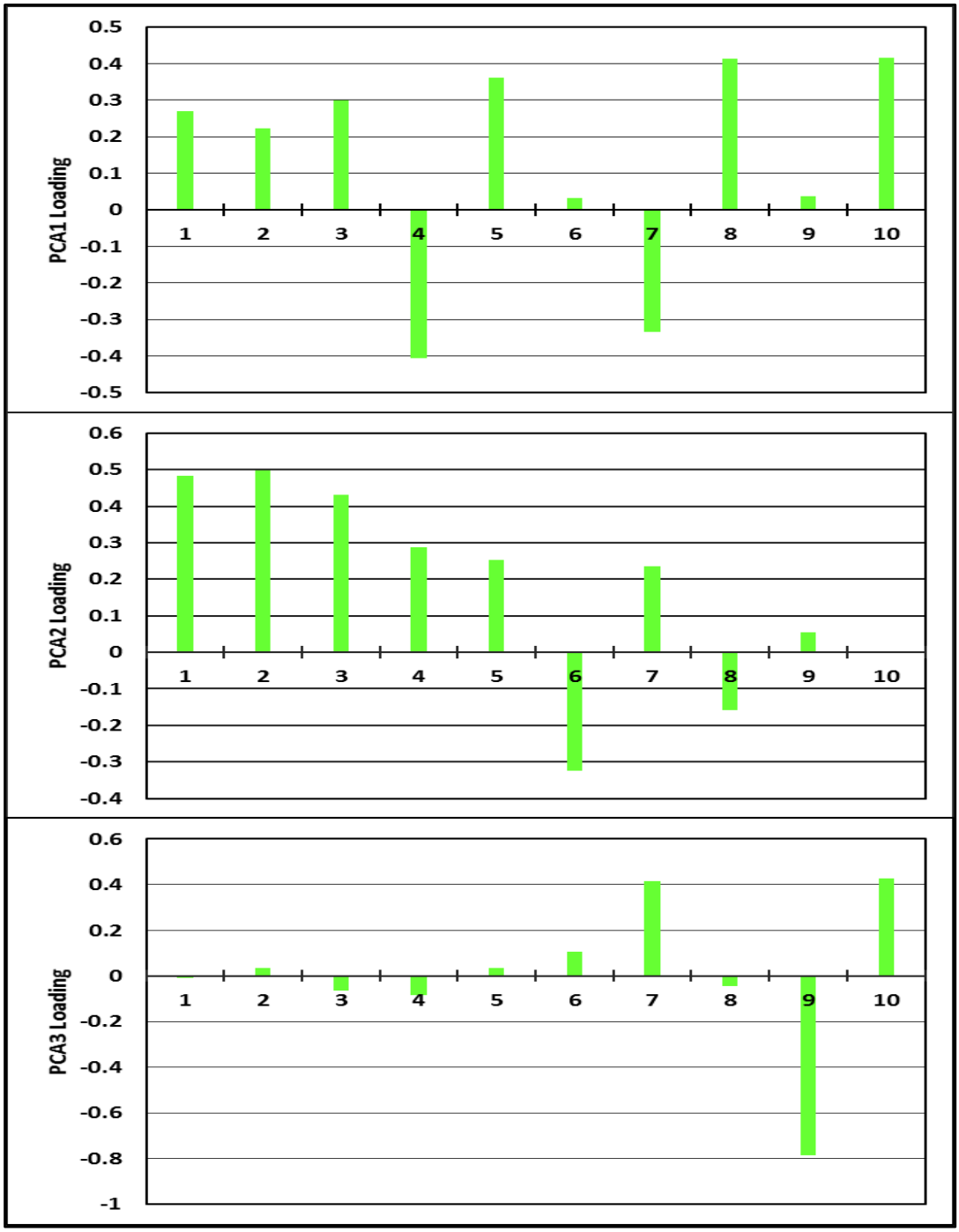

Figure 6.21: Loadings plots showing the composition of the first three PCs, which scored 35%, 28% and 15% of total variance in the data analysis set, respectively. The data listed in Table 6.2.

It is obvious from the analysis that the oil families 1A, 1B, 2, 3 and 4 in groups 1 and 2 are dominated by high ΣC_{27} diasteranes/ΣC_{27} steranes and a moderate abundance of

C_{27}% sterane, while they have lower Ts/Tm hopanes, C_{29}Ts/C_{29} H hopane, and sterane/hopane ratios, suggesting that these groups are from source rocks that had high clay contents and were deposited in suboxic to anoxic marine environments, characterised by moderate input from eukaryote and prokaryote organisms.

The Sirte Shale and Rachmat source rock extracts in group 3 showed high values for the C_{27}% steranes, while they were low in the C_{28}% and C_{29}% steranes, indicating high algal input with small contributions from terrestrial and/or cyanobacterial organic matter, and may have been deposited under suboxic to anoxic conditions in marine to lacustrine environments. Groups 4 and 6 contain Sirte Shale source rock extracts that have high steranes/hopanes, C_{29}%, C_{27} Ts/Tm hopane, C_{29}Ts/C_{29} hopane and C_{30} diahopane/ C_{30} αβ hopane and low ΣC_{27} diasteranes/ΣC_{27} sterane ratios relative to the other groups. This indicates that these groups have higher contributions of eukaryote organisms relative to prokaryote, and were deposited in the suboxic marine environments (e.g. Moldowan *et al.*, 1986; Moldowan *et al.*, 1989). Whereas group 5 is dominated by C_{28}%, ΣC_{27} diasteranes/ΣC_{27} steranes and sterane/hopane ratio, indicating that this group has high contributions of organic matter from diatoms (plankton and algae), eukaryotic organisms and prokaryotic bacteria and was deposited in suboxic to anoxic clay-rich marine conditions (e.g. Peters *et al.*, 1986; Peters and Moldowan, 1993; Peters *et al.*, 2005a).

6.5 Thermal Maturity

The evaluation of the thermal maturity of the source rocks and crude oils in the Sirt Basin has been previously discussed in sections 4.5 and 5.3.4. The maturity data showed that both the Sirte Shale and Rachmat Upper Cretaceous source rocks and the crude oils in the oil families 1A, 1B, 2, 3 and 4 had nearly the same levels of thermal maturity, when calibrated against the North Sea Oil (VFO) standard sample with known equivalent vitrinite reflectance and biomarker and aromatic maturity values.

6.5.1 Steranes and Terpanes

Oil families 1A and 1B in the western Sirt Basin appear to be the most mature oils compared to the oil families 2, 3 and 4. The Sirte Shale and Rachmat source rocks from

the 6A1-59 and B1-NC74F wells exhibits the lowest maturity compared to the C2-16, FF14-6, L1-17 and Z1-11 well samples, which are the most mature in the basin.

The biomarker maturity ratios of C_{27} Ts/(Ts+Tm), C_{29}Ts/(C_{29}Ts + C_{29} 17αβ(H) hopane), and C_{23} tricyclic terpane/(C_{23} tricyclic terpane + C_{30} 17 αβ (H) hopane) shown in Figures 6.22 and 6.23 display good correlations between the oil families 1A and 1B and with the Sirte Shale source rock samples from the B2-NC74A, L1-16 wells, and also with some sections in the L1-17 well. This observation supports the suggestion that these oils were mostly produced from the Upper Cretaceous Sirte Shale source rock, which has moderate maturity. Oil Families 2, 3 and 4 show good correlations with the Sirte Shale source rock samples from the 6A1-59 and B1-NC74F well that have the lowest maturity among the wells studied. The Sirte Shale source rock samples from wells C2-16, L1-17 and Z1-11 exhibit the highest maturity amongst the crude oils and source rock samples in the basin. However, the Sirte Shale source rocks extracts from the C2-16 well reveal different features compared to the Upper Cretaceous samples from another source rocks and oil families. As previously mentioned, that C_{27} Ts/(Ts+Tm), C_{29}Ts/(C_{29}Ts + C_{29} 17aβ(H) hopane), and C_{23} tricyclic terpane/(C_{23} tricyclic terpane + C_{30} 17 αβ (H) hopane) ratios applied in the Figures 6.22 and 6.23 are strongly affected by source facies. However, in the subsequent context, will observe that the maturity parameters that based on the triaromatic steroid hydrocarbons and the aromatic hydrocarbons obtained from methylphenanthrene and methylnaphthalenes such as MPI-1, and DNR values revealed a similar range of maturity for most the crude oils in the oil families 1A, 1B, 2, 3 and 4. But these maturity parameters showed slight differences in level of thermal maturity among the source rock extracts samples, and this may be due to variations in burial depth. Therefore, the close similarities shown by these ratios between the Sirte Shale source rock from the B2-NC74A, L1-16 wells, and some sections in the L1-17 well and oil families 1A and 1B, which is seen in the diagrams below, is considered as strong evidence for a genetic relationship between the crude oils from these families and the Sirte Shale source rock.

6.5.2 **Aromatic Compounds**

The aromatic hydrocarbon ratios based on the distribution of alkylnaphthalene and alkylphenanthrene compounds are widely used as thermal maturity indicators (e.g.

Radke and Welte, 1981; Alexander *et al.*, 1984; Alexander *et al.*, 1985; Radke *et al.*, 1986; Radke, 1988; Alexander *et al.*, 1992b; Radke *et al.*, 1994). Trimethylnaphthalene (TMN) maturity parameters are used in this project to evaluate and compare maturities between source rocks and crude oil samples. The cross-plot of the 2,3,6-TMN/(1,4,6-TMN+1,3,5-TMN) and 1,3,7-TMN-2,3,6-TMN/(1,3,5-TMN+1,4,6-TMN+1,3,6-TMN) ratios for the Sirte Shale and Rachmat source rock extracts and oil families are shown in Figure 6.24. The diagram shows that oil families 1A, 1B, 2, 3 and 4 have the highest maturity and there is moderate to good correlation with Sirte Shale and Rachmat source rocks extracts from the stratigraphic beds of the 6A1-59, B1-NC74F, B2-NC74A, C2-16, FF14-6, L1-17, Z1-11 wells. The alkylnaphthalene based maturity parameters reveal that the Sirte Shale source rock from the L1-16 well shows the lowest maturity compared with the other source rocks.

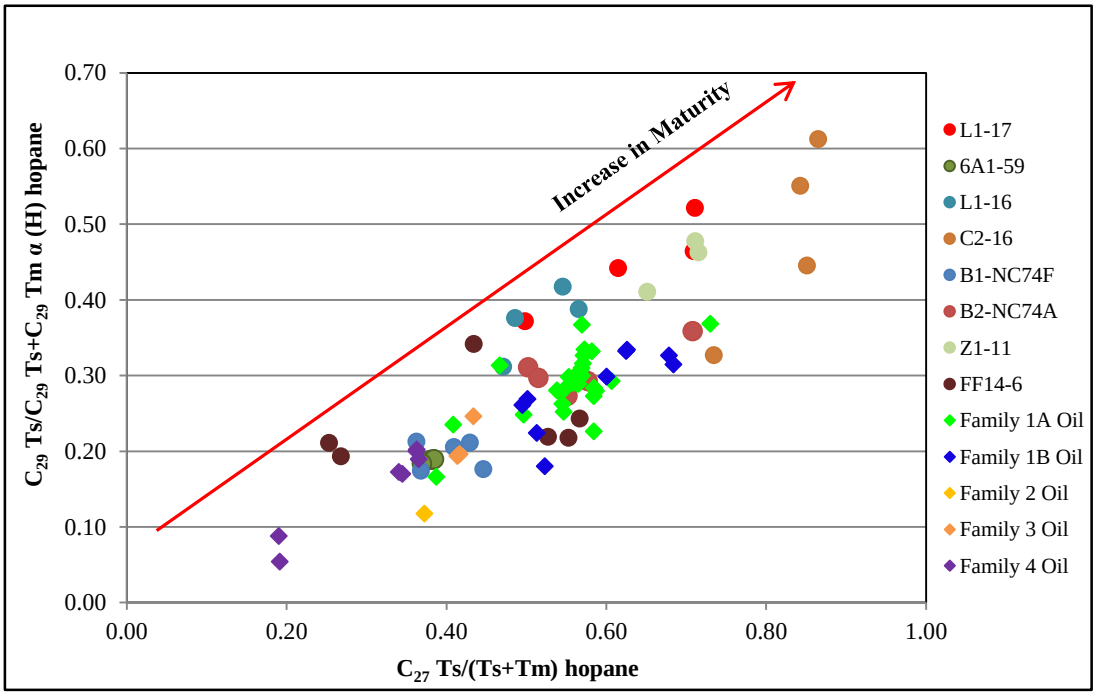

Figure 6.22: Cross plot of the maturity parameters C_{27}Ts/(Ts+Tm) versus C_{29}Ts/(C_{29}Ts + C_{29} 17 α(H) hopane) from source rocks and oil families in the Sirt Basin, circles represent source rocks, while squares represent oil families.

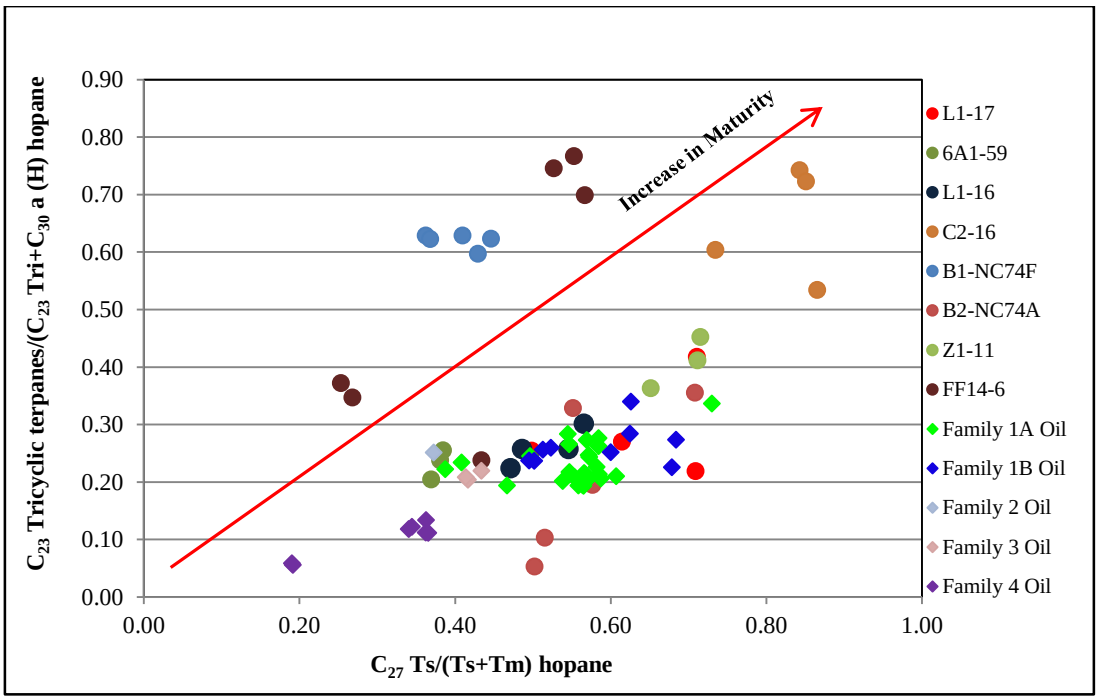

Figure 6.23: Cross plot of the maturity parameters C_{27}Ts/(Ts+Tm) versus C_{23} tricyclic terpanes/C_{23} tricyclic terpanes + C_{30} 17 α(H) hopane) from source rocks and oil families in the Sirt Basin, circles represent source rock, while square represent oil families.

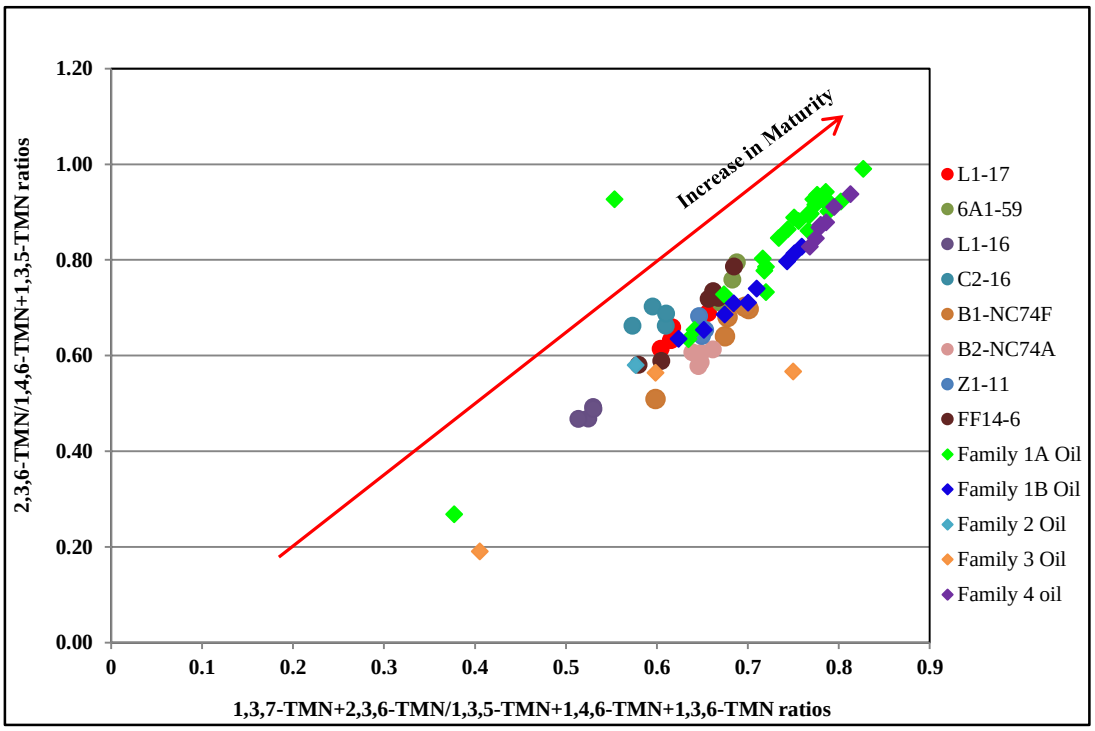

Figure 6.24: Cross plot of the alkylnaphthalenes maturity parameters 2,3,6-TMN/(1,4,6-TMN+1,3,5-TMN) versus 1,3,7-TMN-2,3,6-TMN/(1,3,5-TMN+1,4,6-TMN+1,3,6-TMN) from source rocks and oil families in the Sirt Basin, circles represent source rock, while square represent oil families.

Figure 6.25 shows the cross-plot of the methylphenanthrene index (MPI-1) versus the dimethylphenanthrene ratios for the oil families and the Upper Cretaceous Sirte Shale and Rachmat source rocks in the western and central part of the Sirt Basin. The diagram show that the Sirte Shale and Rachmat source rocks from the sedimentary sections of the wells B1-NC74F, B2-NC74A, C2-16, FF14-6, and Z1-11 have the highest maturity compared with the oil families 2 and 3, while the Sirte Shale source rocks from wells 6A1-59, L1-16 and L1-17 have the lowest maturity. Oil families 1A, 1B and 4 have a moderate thermal maturity.

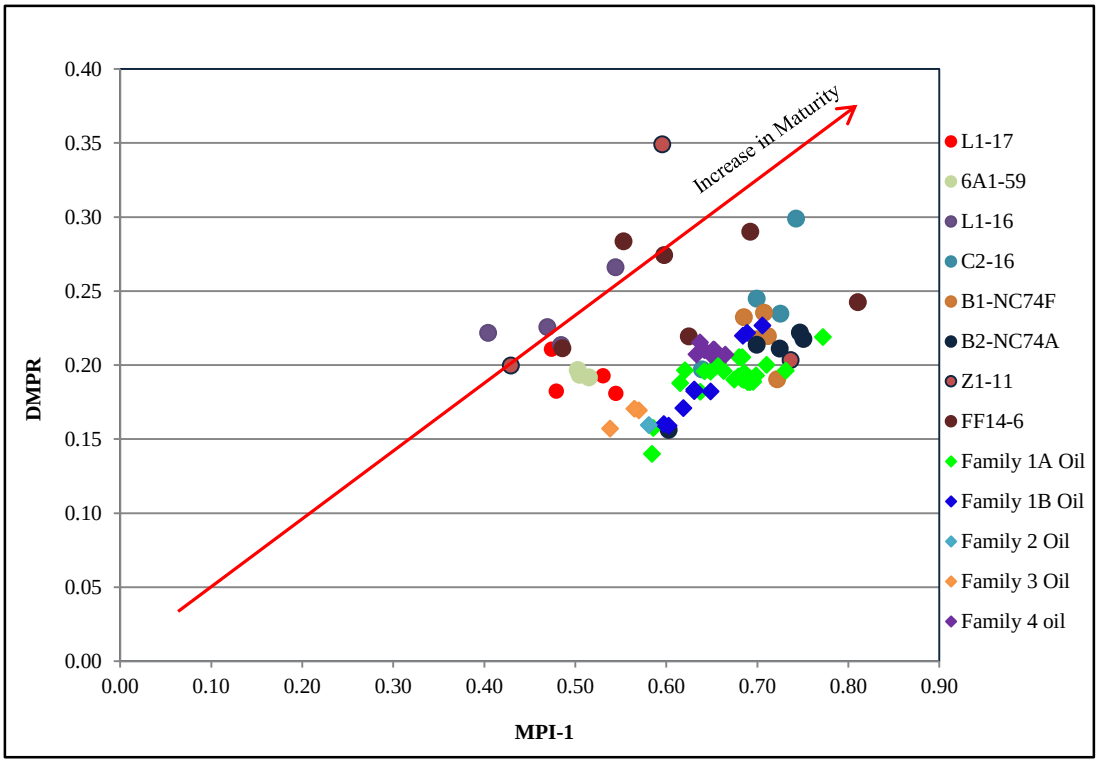

Figure 6.25: Cross plot of the Methylphenanthrene Index (MPI-1) versus dimethylphenanthrene ratios from source rocks and oil families in the Sirt Basin, circles represent source rock, while squares represent oil families.

6.6 Compare with previous Geochemical Studies

Comparing with previous geochemical studies that have been carried out in the Sirte Basin, for instance, El-Alami et al. (1989), Burwood *et al.* (2003) and Sikander (2008), this advanced geochemical study was provided new challenge for studying the main source rocks that have been generated hydrocarbon and correlate oils to oil and oil to source rocks in order to better understand the petroleum system in the basin.

El-Alami *et al.* (1989) demonstrated that the Upper Cretaceous marine Sirte Shale is the main hydrocarbon source rock in the Sirt Basin. In addition, El-Alami observed in 1996 that the variously coloured Lower Cretaceous Nubian Shale is one possible source rock in the eastern Sirt Basin at Hameimat Trough, but that geochemical analyses have indicated that it has only poor to fair source potential for hydrocarbon generation, while the Cenomanian-Turonian Etel Formation is considered to have oil source rock potential with an accumulation thickness of over 6000 feet in the depocentre of the Hameimat Trough. El-Alami *et al.* (1989) reported that gas chromatography and mass fragmantography data showed a relative abundance of steranes and rearrange steranes within the Sirt Shale, and this matches the present oil geochemical results section 5.2.1.2), but that in the depocentre of the basin, triterpanes are relatively more dominant. This is also supported by carbon isotope data of the bulk of the Sirte shale kerogen, which falls in to broad a group with values of around -29‰. These isotopic values, indicating of a terrestrial influence on the content accumulation organic matter.

The carbon isotopes data of the Sirte Shale kerogen showed that slightly heavier, positive values, suggesting significant algal influence in the constitution of the kerogen (Sofer *et al.*, 1986; Hoefs, 1987; Sofer *et al.*, 1991). In addition, the petrographic microscopic data of the Sirte Shale source rock show that the organic matter is comprised of amorphous, phytoclasts, and that algal fractions increase towards the depocentre of the trough regions, which is consistent with the above indications and also with the geochemical data in the present study (see section 4.5).

The aliphatic and aromatic hydrocarbon fraction isotopic data of the Sirte Shale and Rachmat formations showed that the upper Cretaceous source rock is characterized by terrestrial material input in organic matter deposited under marine reducing environments (El-Alami *et al.*, 1989; El-Alami, 1996). Hence, the isotopic data of the Sirte Shale and Rachmat formations show variations in the carbon isotope fractions and this may be associated with changes in the proportion of algal material input, which increases towards the depocentre of the trough regions. While, the lower Cretaceous

Nubian and Etel Evaporites Formations in the southeast part of the Sirt Basin characterized by heavy isotopic values (-23 to -26‰) (El-Alami, 1996). These oils showed heavier isotopic fractions, which may indicates that the oils has been originated from an algal source with some significant contribution from terrestrial component and were probably deposited in lagoon/lacustrine environments. This is also similar to isotope data that obtained from this geochemical analysis (see section 6.3).

Sikander (2008) reported that the Sirte Shale and Rachmat formations contain highly radioactive and organic-rich beds containing Type II kerogen, with some mixed Type III-II kerogen, in the Hameimat Trough in the eastern part of the Sirt Basin. The upper part of the Sirte Shale shows a TOC of over 2% by weight and S2 in excess of 13 mg/g. The Rachmat and Sirte Shale source rocks are comprised of Type II oil-prone kerogen, with high to very high HI values and excellent potential for generating oil in the Al Farigh Trough. In this Trough, the Mid-Nubian Shale is highly radioactive and it is considered to be organic-rich, with TOC values around 1%, with S2 values lying between 5 and 9 mg/g (Sikander, 2008). The Mid-Nubian Shale has TOC values between 5 and 6% by weight and of S2 in excess of 15 mg/g and high to very high HI values, with a mixture of Type I and II oil-prone kerogens, suggesting an exceptionally rich source rock in the Hameimat Trough (El-Alami, 1996; Burwood *et al.*, 2003; Sikander, 2008).

Burwood *et al.* (2003) classified eight families and subfamilies of crude oils in the eastern part of the Sirt Basin based on their geochemical biomarker signatures and carbon isotopes. They also provided evidence in East Sirt oils for the existence of mixed-charge oils deriving from a hybrid petroleum system and that the As Sarah crude oils and deeper reservoired Augila-Nafoora oils are characterized by high waxiness. The As Sarah oil is characterized isotopically by being relatively highly depleted ^{13}C in mid-range Augila-Nafoora, whereas at Tuamma it is relatively enriched with ^{13}C this agrees well with the results obtained from biomarker and carbon isotopic data in this present study (see section 5.4). The relationship between the ααα C_{29} vs sterane/hopane

ratios and αααC_{29} vs. *n*-C_{27}/*n*-C_{17} ratios (see section 5.2.1.1 and 5.2.1.2) suggests that the As Sarah oil was deposited in a more lacustrine setting, and a strong correlation has also been confirmed between lacustrine deposition conditions and wax content (Burwood *et al.*, 2003). Also the high C_{26}/C_{25} tricyclic terpane ratio (see sections 5.2.1.1 and 5.2.1.2) provides corroboration of the lacustrine source provenance of the As Sarah oil.

The stable carbon isotopes in whole oils, saturated and aromatic fractions in the Rachmat Formation, Upper Cretaceous marine Type II source rock, showed depletion in their isotopic values at -28‰, while, the Sirte Shale Formation is characterized by a isotopic value of -29‰ (Burwood *et al.*, 2003). The lower and earlier maturity Rachmat Formation shows a more ^{13}C enriched signature (-28‰) than the stratigraphically higher Sirte Shale Formation with a mean $\delta^{13}C$ value of -29‰ (see section 4.10), and although only a narrow isotopic contrast, this observation has proven invaluable in differentiating between marine sourced oils (Burwood *et al.*, 2003).

The $\delta^{13}C$ values of the Augila-Nafoora oil in the central Agedabia Trough indicates a marine source provenance and these are noteworthy in being the most sulphur-rich fluids of the eastern Sirt area, and are attributed to a predominantly Rachmat Formation provenance and constitute the Rachmat-Gialo petroleum system (Burwood *et al.*, 2003). El-Alami (1996) considered that the waxy crude oils of the Abu Attifel oils in the Hameimat Trough were sourced in the Cenomanian-Turonian, whereas Burwood et al. (2003) suggested a different, non-marine source rock for the Abu Attifel oils based on a highly enriched ^{13}C isotopic signature and a low sterane/hopane ratio.

Burwood *et al.* (2003) concluded that the strata in Agedabia Trough drop steeply to the north, driving the entire section down into the gas window. This is demonstrated by the presence of gas discovered at the Sahl and Assoumoud oil fields on the north flank of the Sirt Basin, and this also agrees with maturity data from this present study (see sections 4.4, 4.9, and 5.5). A small quantity of oil was generated in the Wadayat

Trough, in which Sirte Shale source rock, with its oil and gas-prone Type II kerogen, passed the oil window and has entered the gas window, which was confirmed by the maturity analyses of wells FF14-6 and C2-16 in the Wadayat and Maradah Troughs in the central part of the Sirt Basin (see sections 4.9, 5.5 and 6.5). Hence, the main type hydrocarbon generation expected to be in these troughs is dry gas at a high level of maturity.

6.7 Summary

Oil-source correlations have revealed that all of the crude oils from oil Families 1A, 1B and 2, including the oils from the Beda, Hakim, Kotla, Meghil, Mabruk, Nasser, Raiah, Raguba, and Zelten oilfields, show similar source facies features to the Sirte Shale source rocks from their stratigraphic bed units from the wells 6A1-59, C2-16, FF14-6, L1-16, L1-17 and the Z1-11 well in the western and central part of the Sirt Basin. Oil Family 3, covering only the Dor Mansour oilfield in the central part of the Sirt Basin, has similar source facies parameters to the Sirt Shale source rocks from their sedimentary sections from wells B2-NC74A and FF14-6. Oil family 4, which is consists of the Aswad, Safsaf and Zellah oilfields located in the west part of the basin, has similar biomarker features to those of the Sirte Shale and Rachmat source rocks from the B1-NC74F and FF14-6 wells. However, the crude oil samples of oil family 4 are thought to have been yielded from early to middle mature marine to lacustrine clastics interbedded with carbonate strata source rocks of Upper Cretaceous or older ages. These are also thought to be from the Sirte Shale and Rachmat formations, or they could be from the Etel Formation, which is considered also to be a local potential source rock in the Sirt Basin.

The Sirte shale source rock strata have provided a major contribution to the generation of these oils, as the biomarker and aromatic hydrocarbon parameters and specific carbon isotopic analysis of *n*-alkanes, together with principal component analysis, have shown.

The $\delta^{13}C$ isotopic value versus *n*-alkane carbon number slope profiles show that most of the oil families 1A, 1B, and 3 and Sirte Shale and Rachmat source rock strata from

the wells 6A1-59, B1-NC74F, C2-16 and FF14-6 have a nearly flat profile, which is generally associated with the $\delta^{13}C$ characteristics of sources rich in marine organic matter input. Oil family 4 and Sirte Shale source rock extracts from well B2-NC74A are slightly different isotopically from other oil families, as they contain the heaviest $\delta^{13}C$ isotopic values. This may be due to the production of the isotopically relatively heavy *n*-alkanes from source rock characterised by marine organic matter with high contribution from algal organic matter. Oil families 1A and 1B and Sirte Shale source rocks from wells C2-16 and FF14-6 have similar characteristics and appear as the isotopically lightest (with most negative) $\delta^{13}C$ isotopic values, and this may be consistent with a marine source or that source rock produced ^{12}C more than ^{13}C, suggesting a slightly higher contribution of the terrigenous organic matter inputs in a marine setting. It is clear that the isotopic compositions of the *n*-alkanes of most of the crude oils and source rock extracts analysed, are controlled by their organic matter sources and depositional environments as well as their thermal maturities, which were indicated by previous analyses of their saturated and aromatic hydrocarbon distributions.

Principal component analysis separated the oil families and source rock extracts into six groups. Group 1 consists of oil families 1A, 1B and Sirte Shale source rocks from well B2-NC74A at depths of 9570 and 9610 feet and FF14-6 at depths of 11615 and 11650 feet; group 2 comprises samples from oil families 2, 3 and 4; group 3 contains Sirte Shale and Rachmat source rocks from boreholes B1-NC74F and B2-NC74A at depths of 9520 and 9580 feet, and FF14-6 at depths of 12290 and 12330 feet; group 4 includes Sirte Shale source rocks from the wells L1-17, Z1-11 and C2-16 at a depth of 10580 feet; group 5 contains the Sirte Shale Source rock strata from the wells 6A1-59, L1-16 and L1-17 at a depth of 6060 feet; and group 6 comprises of Sirte Shale source rock extracts from the C2-16 well. The statistical results show a similarity between oil family 4 and the Sirte Shale and Rachmat source rocks strata from the B1-NC74F and B2-NC74A wells, suggesting that the crude oils may have been generated from similar source rocks. Oil families 1A and 1B may have been generated from Sirte Shale source rock strata close to the wells L1-17 and L1-16. Whereas the data shows that the Sirte Shale source rock strata from well C2-16 is associated with a different organic facies and depositional environment compared to the other Sirte Shale source rock strata and

oil families, and this may be related to the influence of maturity since this source is more mature.

It is shown from the statistical analysis that oil families 1A, 1B, 2, 3 and 4 in groups 1 and 2 are dominated by the high ΣC_{27} diasterane/ΣC_{27} sterane ratios and moderate abundances of C_{27} steranes (as a percentage of total $C_{27\text{-}29}$ steranes) while they have lower Ts/Tm hopane, C_{29}Ts/C_{29} H hopane, and high sterane/hopane ratios, suggesting that these groups originated from source rock with high clay content that was deposited in a suboxic to anoxic marine environment, characterised by a moderate input of eukaryotic and prokaryote organisms.

The Sirte Shale and Rachmat source rock strata in group 3 showed relatively high abundances of the C_{27}% sterane, while being low in the C_{28}% and C_{29}% steranes, indicating the high eukaryote input (Algae) with low contribution of terrestrial organic matter, and may have been deposited in a suboxic to anoxic marine environment. Groups 4 and 6 contain Sirte Shale source rocks that have high sterane/hopane ratios, C_{27} Ts/Tm hopane, C_{29}Ts/C_{29} hopane and C_{30} diahopane/C_{30} αβ hopane and low ΣC_{27} diasteranes/ΣC_{27} steranes relative to the other groups. This indicates that these groups have higher contributions of eukaryote organisms relative to prokaryotes and were deposited in a suboxic marine environment. In group 5, steranes are dominated by C_{28} and are low C_{27} components with moderate to high sterane/hopane ratio. This indicates that this group have had higher contributions of diatomic (plankton and algae) eukaryotic organisms and prokaryotic bacteria and it was deposited in a suboxic to anoxic clay-rich marine environment.

The maturity marker data showed that oil families 1A, 1B with along the Sirte Shale and Rachmat source rocks from the wells B2-NC74A, C2-16, FF14-6 and Z1-11 are more mature than the oil families 2, 3 and 4 along with the Sirte Shale stratigraphic beds from the wells 6A1-59, L1-16 and L1-17. This reflects the fact that most of the oils were generated from source rocks situated in the deep troughs where they reached sufficient maturity, particularly in the northeast and southwest parts of the study area.

Chapter 7. Sirt Basin Petroleum System

7.1 Introduction

The analysis of petroleum systems has become an increasingly significant discipline in assessing the petroleum potential in any basin area. The main components in the petroleum system analysis are source rocks, reservoirs, traps, seals, migration and timing of the hydrocarbon generation (Magoon and Dow, 1994). A knowledge of all these components is often necessary for an exploration programme to be successful. "A petroleum system is defined as a natural system that encompasses pod of active source rock and all related oil and gas, which includes all of the geologic elements and processes that essentially if a hydrocarbon accumulation is to exist" (Magoon and Dow, 1994). The essential elements are an effective source rock, reservoir, seal and overburden rock, while the processes involved trap formation and generation, migration and accumulation of petroleum. Magoon and Dow (1994) reported that these elements and processes have to occur in a specific order for the organic matter in a source rock to be converted into petroleum and then to be accumulated and preserved in reservoirs. Furthermore, if any of those elements or processes occurs out of the require sequence or is missing, a prospect loses their capability. Hantschel and Kauerauf (2009) defined basin modelling as the dynamic modelling of geological processes in a sedimentary basin over geological time. Therefore, the modelling of any sedimentary basin essentially needs information that is required to rebuild history of the basin. This involves the reconstruction of the basin's history, beginning from the deposition of the oldest strata forward through sequence deposition until the present day. Therefore, the model is developed based on input data which is simulated over several time steps, and the characteristics of the geological processes are calculated and updated at each time step (Waples, 1980; Welte and Yalcin, 1988; Magoon and Dow, 1994; Waples, 1998; Schiefelbein *et al.*, 1999; Hantschel and Kauerauf, 2009). The main geological processes considered in basin modelling are deposition, compaction, heat flow, hydrocarbon generation, expulsion and migration (Waples, 1980; Tissot and Welte, 1984; Magoon and Dow, 1994; Hunt, 1995).

A petroleum source rock is defined as a rock unit containing sufficient organic matter of suitable chemical composition to biogenically or thermally generate and expel

petroleum (Magoon and Dow, 1994). Meanwhile a pod active source rock is defined as a contiguous volume of source rock that is generating and expelling petroleum at the critical moment, and this is the provenance for a series of genetically related petroleum shows, seeps, and accumulation in a petroleum system, where a pod of mature source rock may be active, inactive or spent (Magoon and Dow, 1994).

Model construction consists of essential input data; the most important being stratigraphic formation tops and age in order to define a subsidence history. Lithology is used to attribute thermal characteristics, such as heat conductivity and capacity of the sedimentary section, and present temperature to characterize the present-day heat regime. The maturity model is calibrated against measured maturity. The geochemical characteristics of the source rock units such as organic richness, kerogen type and maturity (*%Ro*) are entered into the model, allowing volumes of generating and expelled hydrocarbons to be calculated and the timing of these processes to be estimated. Type II and Type II-III kerogen were used for source rocks.

One dimensional (1D) basin modelling (time-temperature index) has been found to be a valid method for measuring the level of thermal maturity of the source rock. It provides a simple graphical display of the history of the hydrocarbon generation in an area by reconstructing the burial rate and thermal gradient (Waples, 1980; Magoon and Dow, 1994; Waples, 1998; Hantschel and Kauerauf, 2009). Furthermore, the level of maturation in basin modelling can also be used to determine the timing and duration of hydrocarbon generation in any area (Christian H., 1993; Magoon and Dow, 1994; Waples, 1998; Al-Hajeri *et al.*, 2009). The main aim of basin modelling is to accurately predict the depth and time of oil and gas generation from a recognized source rock.

The Genesis 5.1 basin modelling software used in this work was developed by ZetaWare as part of its Interactive Petroleum System Tool. This was used to analyse burial history and hydrocarbon generation in the present study. The software suite handles the entire 1D model, with solver elements for temperature and pressure coupling, amongst other variables involved in hydrocarbon generation. A 1-D simulation can be performed in a matter of minutes, depending on the computing parameters involved.

The main aim of this chapter is to determine the burial and the hydrocarbon generation history of source rocks in the Sirt Basin through the modelling of subsidence history and thermal maturity, and to predict the migration pathways from the source rock to reservoirs.

7.2 Kinetic Modelling of the Petroleum Source Rock

The KinEx method is a fast source rock maturation modelling for predicting the expulsion of hydrocarbon products and gas oil ratio (GOR) from source rocks. Basin analysis uses kinetic model to predict the volume of hydrocarbon generation within potential source rocks from kerogen (Pepper and Corvi, 1995). However, bulk kinetic models are not able to predict hydrocarbon compositions, but only describe the bulk generation of hydrocarbon from organic matter by primary cracking.

Pepper and Corvi (1995) described five kerogen kinetic organic facies (A, B, C, D/E and F) and from them, in this study the source rock kinetic software employed to predict the generation state of source rocks, and their retained and expelled products with inter-bedded organic facies.

The basis of this model was built on two principles which govern the kinetic model for petroleum generation, first order kinetics and the Arrhenius Law. First order kinetics assume that the rate in which the concentration of kerogen degrades with time is closely related to the concentration of kerogen, based on the equation $dc/dt = -kc$. There k is the reaction rate constant which is assumed to be governed by the Arrhenius Law as expressed in the equation $k = Ae- E/RT$, where A is the frequency factors in (m/s), E is the activation energy (J/mol), R is the universal gas constant (8.31441 J mol^{-1} K^{-1}) and T is the absolute temperature in degrees Kelvin. Kerogen degradation involves a chain of reactions taking place simultaneously. Hence, a single reaction is unable to fully explain the rate of kerogen degradation by substitution in a series of equations $dci/dt = -kici$, where the subscript i represent the "ith" component within the reaction system. Therefore, the equation is changed to become ki = Ae-Ei/RT.

At the generation stage, the KinEx modelling shows oil to be generated at low thermal maturity, indicating that kerogen degradation occurs at low temperatures in the sedimentary basin over geologic time experiencing a heating rate of 2ºC per million

years. However, the first order kinetic equation can explain this phenomenon, because the rate constant (*k*) is not equal to zero in all situations, until the temperature declines to absolute zero (-273 ºC), hence the value of -E/RT is often small. Generally, the amounts of oil (in mg extract g^{-1} TOC) within source rock have low values at low depths of burial or temperatures, but there is then a rapid increase beyond a certain threshold in conjunction with kerogen degradation. The Kinex thermal model displays the top and bottom of the oil window at 120ºC and 160ºC respectively, and gas generation begins at 175ºC and end at 220ºC. However, with increased thermal maturity, the progressive increase in activation energy leads to a quickening of degradation and a breakdown of the stronger C-C bonds. The breakdown of high molecular compounds leads to the steady release of hydrocarbons as oil generation. The heating rate of the KinEx thermal model used was 2ºC/Ma, and any an increase or decrease by an order of magnitude of the heating rate would increase or decrease the oil or gas threshold by about 15ºC.

The level of retention and expulsion based on the KinEx thermal modelling shows (e.g. Figure 7.1a) that oil retention increases when approaching the oil window phase as well as within the oil window, until its peak is reached at 130ºC, where upon it begins to decrease due to expulsion. Oil is retained until the sorptive potential of kerogen is reached, and after that oil expulsion starts and migration becomes effective in liberating petroleum into sediment pore spaces. Oil expulsion finishes at 160ºC, indicating the end of oil generation.

The KinEx thermal model illustrates (e.g. Figure 7.1a and b) that gas expulsion commences at 175ºC at the same time as gas generation. This is because gas is lighter and more mobile relative to oil, and the gas also more easily diffuses in sedimentary rocks because it is characterised by low molecular weight.

This model uses simple distributions of different organic facies and kerogen types. A set of organic facies (A, B, C, D/E and F) is used for calibration and the calculation of the model for the source rocks (Pepper and Corvi, 1995). A Kinex model thermal history is used to assess the volume of petroleum expelled per area from the source rock kitchens. This kinetic modelling was applied to samples from eight wells in the Sirt Basin: 6A1-59, B1-NC74F, B2-NC74A, C2-16, FF14-6, L1-16, L1-17, and Z1-11.

The geochemical characteristics of the Kalash, Sirte Shale and Rachmat source rocks, such as initial total organic carbon (TOC°), initial hydrogen index (HI°), and thickness, are entered into the model, allowing the volumes of generated and expelled hydrocarbons to be calculated and the timing of these processes to be estimated, as listed in Table 7.1 and 7.2.

It is clear from previous chapters that the Kalash, Sirte Shale and Rachmat Formations are characterized by Type II and Type II-III marine organic matter containing, clay-rich source rock, indicating organic facies B.

Table 7-1: The initial hydrogen indices (HI°) and total organic carbon contents (TOC°) of the studied Upper Cretaceous source rocks.

Well Name Name	Formation Name	Depth Feet	Thickness Feet	Thickness Meter	TOC	HI	TOC°	HI°
6A1-59	Upper Kalash	7130-7170	40	12	3.42	564	5.81	542
	Lower Kalash	7180-7210	30	9	0.94	137	1.6	128
	Sirte Shale	7220-7280	60	18	2.71	448	4.61	401
B1-NC74F	Sirte Shale	6980-7200	220	67	2.31	208	3.92	212
	Rachmate	7930-8090	160	48	1.36	254	2.3	265
B2-NC74A	Upper Sirte Shale	9500-9570	60	20	0.71	149	1.21	118
	Lower Sirte Shale	9570-9740	160	53	1.34	154	2.29	135
C2-16	Upper Sirte Shale	9780-10580	800	262	1.25	97	2.13	127
	Lower Sirte Shale	10840-11020	180	56	1.06	77	1.8	97
FF14-6	Sirte Shale	11270-13050	1780	539	0.88	36	1.5	120
L1-16	Upper Sirte Shale	7400-7670	270	89	1.15	179	1.95	166
	Lower Sirte Shale	7700-8370	670	216	0.78	136	1.32	137
L1-17	Upper Sirte Shale	6060-6608	548	54	1.62	245	2.75	269
	Lower Sirte Shale	6640-7020	380	125	0.71	108	1.21	119
Z1-11	Sirte Shale	8050-8230	180	59	1.64	255	2.56	301

For well 6A1-59, the upper Kalash source rock is characterized by limestone interbedded with shaly limestone and it has a thickness around of 40 feet (12m). The shale unit has an average initial organic carbon content (TOC°) of 5.81% and an average initial hydrogen index (HI°) of 542 mg HC/g TOC. An initial Kinex thermal model using the kinetic parameters of organic facies B for this source rock is characterised by linear heating instructions starting at 0°C and ending at 300°C with 2°C/Ma as heating rate. The Kinex model demonstrates that an oil window for the amorphous organic matter could occur in the upper Kalash Formation starting at 115-160°C, with gas generation starting at 132°C. The kinetic model data from whole wells

studied are listed in Table 7.2 The model shows no expulsion of petroleum until temperatures are higher than 127ºC, as shown in Figure 7.1a. The kinetic thermal model suggests that the upper Kalash Formation will expel about 6,7645mmboe/km^2, mostly of oil with low amounts of gas as shown in Figure 7.1b.

The lower unit of the Kalash Formation is characterized by limestone with shaly intervals and has a thickness of 30 feet (9m). It has an average initial organic carbon of 0.94%, and an average initial hydrocarbon index of 128 mg HC/g TOC, suggesting that this organic matter is Type II-III, indicating kerogen organic facies B. The graph of the generation, expulsion and retention of the organic facies B for the lower Kalash Formation indicates that there no oil expulsion will occur, but from this kind of kerogen gas expulsion could commence at 150ºC, as shown in Figure 7.2.

The Sirte Shale Formation is characterized by dark grey to black shale. The KinEx model shows no expulsion of petroleum until more than 123ºC when the sorption potential of the kerogen is reached. The model shows a narrow window for oil expulsion subsequently followed by thermogenic gas expulsion. Based on the kinetic thermal model, the Sirte Shale Formation will expel about 5,87025mmboe/km^2, mostly of oil with a moderate amount of gas as shown in Figures 7.3a and b.

The B1-NC74F well is located in the southeast of the Zellah Trough (in the west Sabah oilfield) in the Sirt Basin. The KinEx model shows no expulsion of petroleum until temperature higher than 138ºC, when the sorption potential of the kerogen is reached. The model shows a narrow window for oil expulsion and then thermogenic gas expulsion. Based on the kinetic thermal model, the Sirte Shale Formation will expel about 10,2175mmboe/km^2, as shown in Figure 7.4a and b. It is obvious from the graph 7.4b that this source rock will produce low amounts of oil compared to huge amounts of gas.

In the B1-NC74F well, the Rachmat Formation in the southeast of the Zellah Trough is characterized by medium dark grey, dark grey to black shale interbedded with sandstone and limestone. The model shows a narrow window of oil expulsion followed by thermogenic gas expulsion. Based on the kinetic thermal model, the Rachmat Formation will expel about 5,52663mmboe/km^2, as shown in Figure 7.5a and b. It is

clear from the Figure 7.5b that this source rock will produce moderate amounts of oil relative to a rather high amount of gas.

Table 7-2: Summary of the kinetic modelling data from the studied wells.

Well Name	Location Sirt Basin	Formation Name	Thickness Feet	Kerogen Type	TOC° %	HI° mgHC/g TOC	Organic Facies	Oil commence Temperature °C	Gas commence Temperature °C	Oil expelled mmboe/Km^2	Gas expelled mmboe/km^2
6A1-59	West part	Upper Kalash	40	Type II	5.81	542	B	115	132	4,600	2,145
	Zellah Trough	Lower Kaalash	30	TypeII-III	0.94	128	B		150	***	0.198
		Sirte Shale	60	Type II	4.6	401	B	121	144	3,211	2.659
B1-NC74F	West part	Sirte Shale	220	Type II	3.9	212	B	135	141	2,000	8,218
	Zellah Trough	Rachmat	160	Type II	2.29	273	B	125	138	1,865	3,662
B2-NC74A	West part	Upper Sirte Shale	60	Type II-III	1.21	118	B		143	***	0.515
	Zellah Trough	Lower Sirte Shale	160	TypeII-III	2.29	136	B	125	141	***	2,722
C2-16	Central part	Upper Sirte Shale	800	Type II-III	2.14	127	B		144	***	12,891
	Marada Trough	Lower Sirte Shale	170	TypeII-III	1.8	97	B		148	***	1,671
FF14-6	Central part	Upper Sirte Shale	310	Type II	1.49	231	B	124	135	1,625	4,455
	Wadayat Trough	Middle Sirte Shale	50	Type II-III	1.38	195	B	132	146	3,850	25,727
		Lower Sirte Shale	130		3.03	104	B		143	***	2,103
L1-16	Central part	Upper Sirte Shale	270	Type II-III	1.95	166	B	125	141	0,175	5,199
	Nuflian High	Lower Sirte Shale	660	Type II-III	1.33	137	B			***	7,288
L1-17	West part	Upper Sirte Shale	550	Type II	2.75	269	B	124	137	8,185	16,241
	Dor Abid Trough	Lower Sirte Shale	380	Type II-III	1.21	119	B		145	***	3,252
Z1-11	West part Tagrifet Trough	Sirte Shale	180	Type II	2.56	301	B	123	145	3,185	4,421

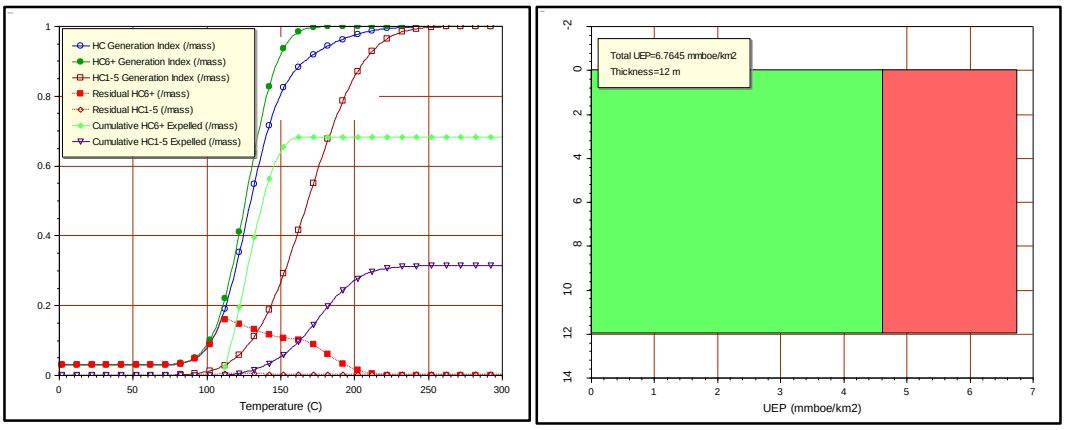

Figure 7.1 a) Chart of generation, expulsion and retention, and b) chart of petroleum expelled of the upper Kalash Formation.

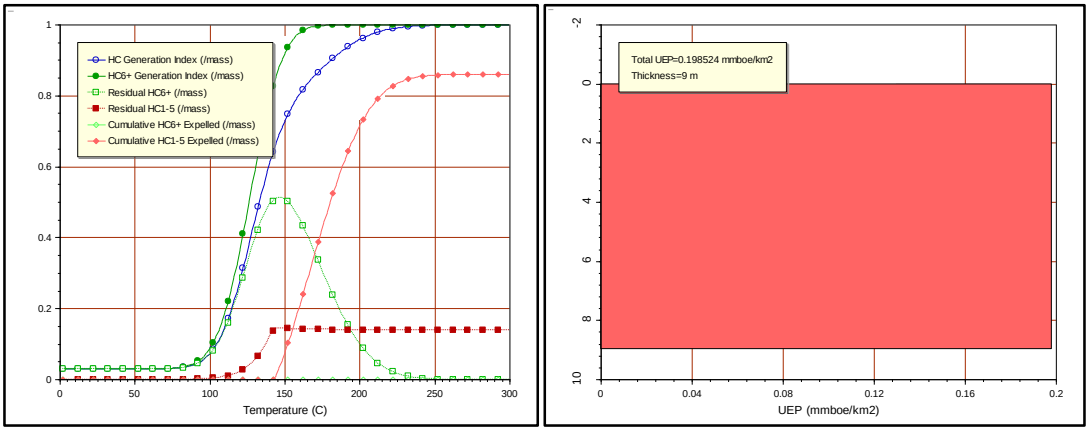

Figure 7.2 a) Chart of generation, expulsion and retention, and b) chart of petroleum expelled of the lower Kalash Formation.

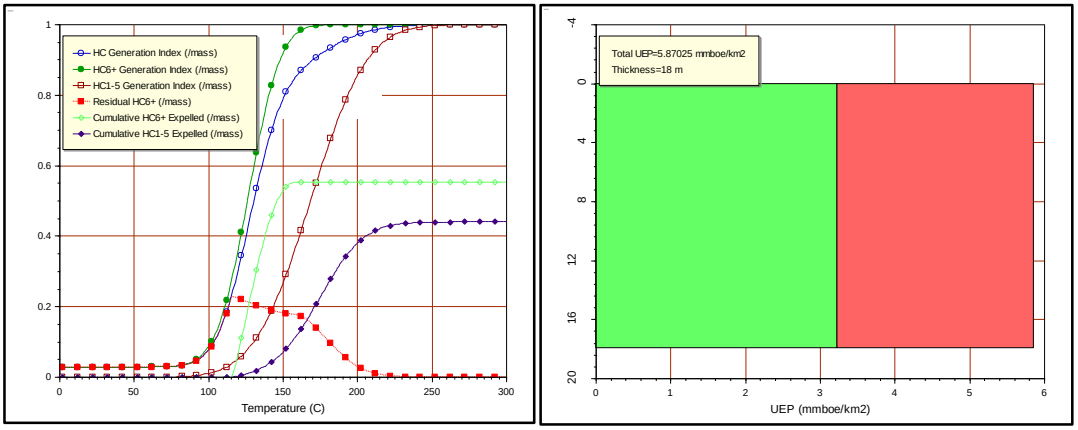

Figure 7.3: a) Chart of generation, expulsion and retention, and b) chart of petroleum expelled of the Sirte Shale Formation.

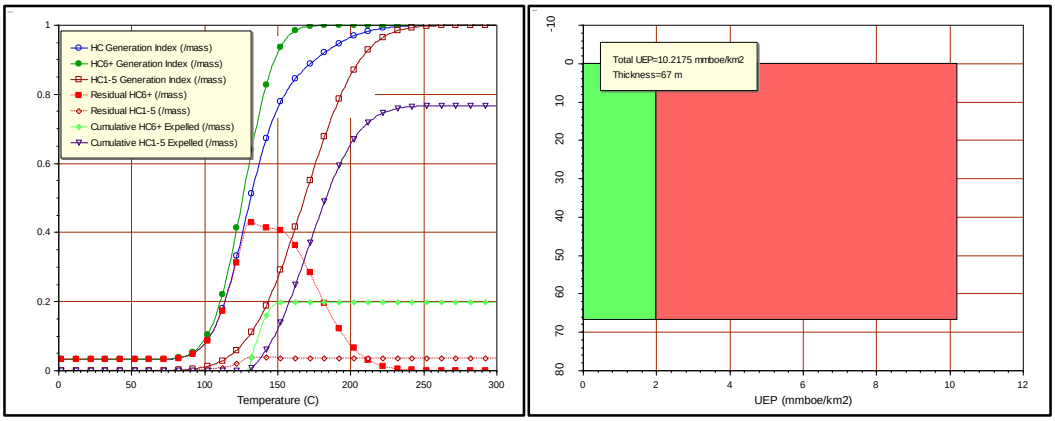

Figure 7.4: a) Chart of generation, expulsion and retention, and b) chart of petroleum expelled of the Sirte Shale Formation.

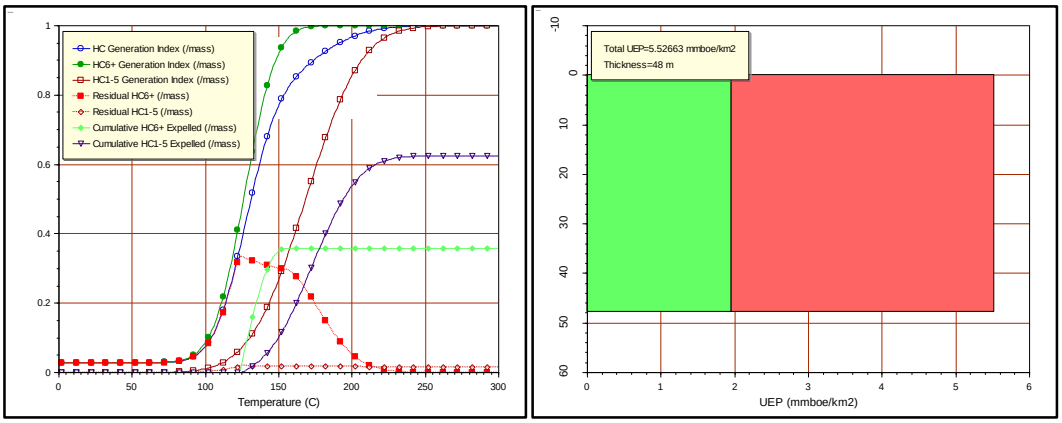

Figure 7.5: a) Graph of generation, expulsion and retention, and b) graph of petroleum expelled of the Rachmat Formation.

The B2-NC74A well is located in the Zellah Trough at the western edge of the Sirt Basin. The Sirte Shale was subdivided into two parts, upper and lower, based on their organic matter content and hydrocarbon potential. It is characterized by grey to dark grey shale interbedded with sandstone. The KinEx thermal model shows that no oil could be expelled from the upper Sirte Shale Formation, but very low amount of gas could be expelled and this may start at 143ºC, as shown in Figure 7.6a. Therefore, no oil source rock can be anticipated from the upper Sirte Shale Formation in this area. Meanwhile, the lower part of the Sirte Shale Formation consists of very dark grey to black shale The KinEx thermal model demonstrates that no oil could expel from the lower Sirte Shale Formation, but very low amounts of gas could be expelled and this may start at 141ºC, as shown in Figure 7.7a. Based on the kinetic thermal model, the lower Sirte Shale Formation will expel about 2,72253mmboe/km^2 of gas, as shown in

Figure 7.7b. Therefore, no oil source rock can be anticipated from the lower Sirte Shale Formation in this region, but it could be source of gas.

The C2-16 well is located in the Marada Trough in the central part of the Sirt Basin. The upper Sirte Shale Formation consists of dark grey and very dark to black shales with minor of sandstone and limestone. Based on the kinetic thermal model, the upper Sirte Shale Formation will expel about 12,8606mmboe/km^2 of gas as shown in Figure 7.8a and b. Therefore, there is no oil source rock to be anticipated from the Upper Sirte Shale Formation in this region, but it could be a gas source.

The lower Sirte Shale Formation consists of dark grey and very dark to black shales with minor of sandstone and limestone. Based on the kinetic thermal model, the lower Sirte Shale Formation will expel about 1,67141mmboe/km^2 of gas as shown in Figure 7.9a and b.

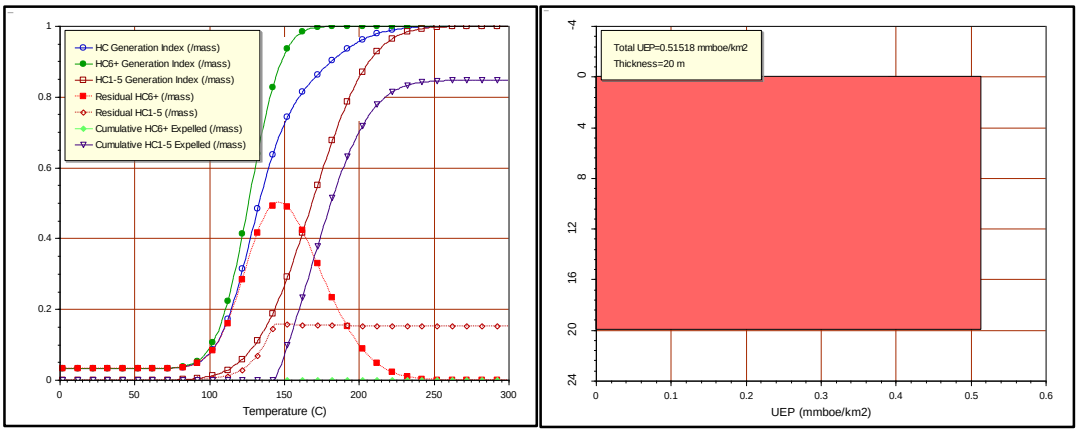

Figure 7.6: a) Graph of generation, expulsion and retention, and b) graph of petroleum expelled of the upper Sirte Shale Formation.

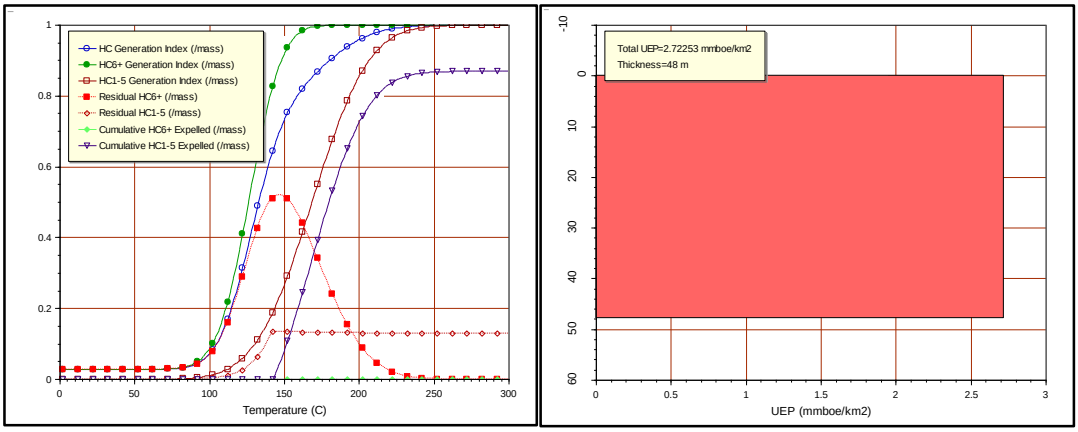

Figure 7.7: a) Graph of generation, expulsion and retention, and b) graph of petroleum expelled of the lower Sirte Shale Formation.

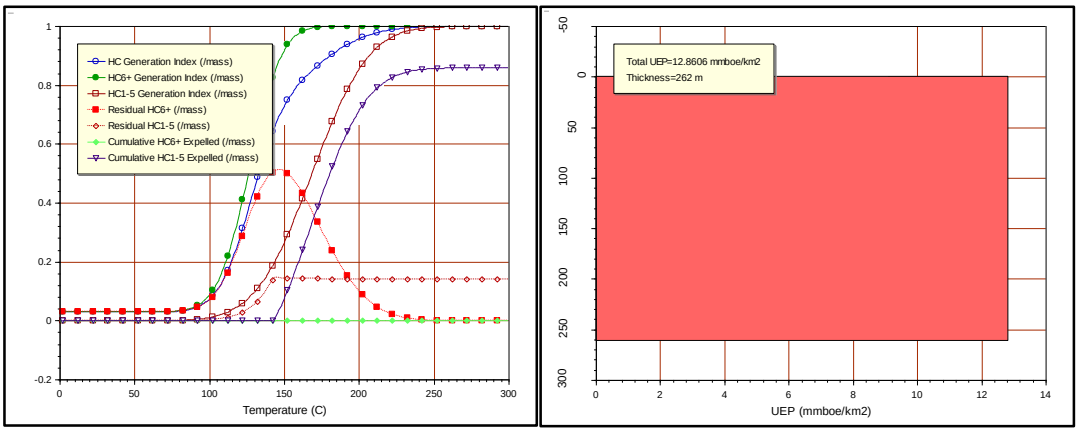

Figure 7.8: a) Graph of generation, expulsion and retention, and b) graph of petroleum expelled of the Upper Sirte Shale Formation.

The FF14-6 well is located in the Wadayat Trough at the centre of the Sirt Basin. The Sirte Shale Formation is subdivided into three units, upper, middle and lower, based on their initial values of TOC° and HI°. The upper Sirte Shale Formation is characterized by dark grey shale interbedded with limestone and sandstone. The KinEx model displays no expulsion of petroleum until reaching more than 135ºC when the sorption potential of the kerogen is reached. The model shows a narrow window for oil expulsion with thermogenic gas expulsion subsequently ensuing. Based on the kinetic thermal model, the upper Sirte Shale Formation will expel about 6,09778mmboe/km^2 as shown in Figure 7.10a and b, and it is clear from Figure 7.10b that this source rock will produce low amounts of oil and higher amounts of gas.

The middle Sirte Shale Formation is characterized by dark grey shale interbedded with limestone and sandstone. The KinEx model displays no expulsion of petroleum until reaching more than 139ºC when the sorption potential of the kerogen is reached. The model shows a narrow window for oil expulsion followed by the thermogenic gas expulsion. Based on the kinetic thermal model, the middle Sirte Shale Formation will expel about 0.759734mmboe/km^2, as shown in Figure 7.11a and b. It is obvious from the graph that this source rock will produce low amounts of oil relative to high amounts of gas.

Meanwhile the lower Sirte Shale Formation is characterized by dark grey shale interbedded with limestone and sandstone. Based on the kinetic thermal model, the lower Sirte Shale Formation will expel about 2,10292mmboe/km^2, as shown in Figure

7.12a and b, and from the graph that this source rock will produce only low amounts of gas.

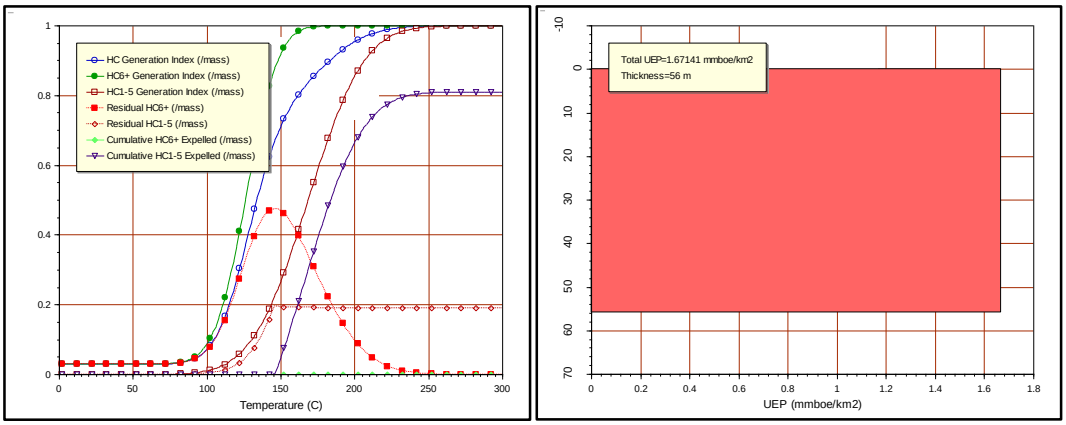

Figure 7.9: a) Graph of generation, expulsion and retention, and b) graph of petroleum expelled of the Lower Sirte Shale Formation.

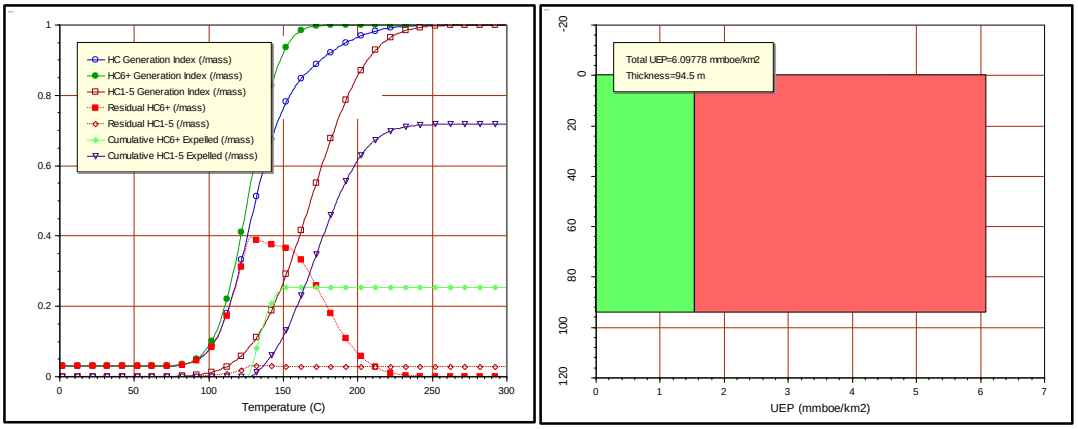

Figure 7.10: a) Graph of generation, expulsion and retention, and b) graph of petroleum expelled of the Upper Sirte Shale Formation.

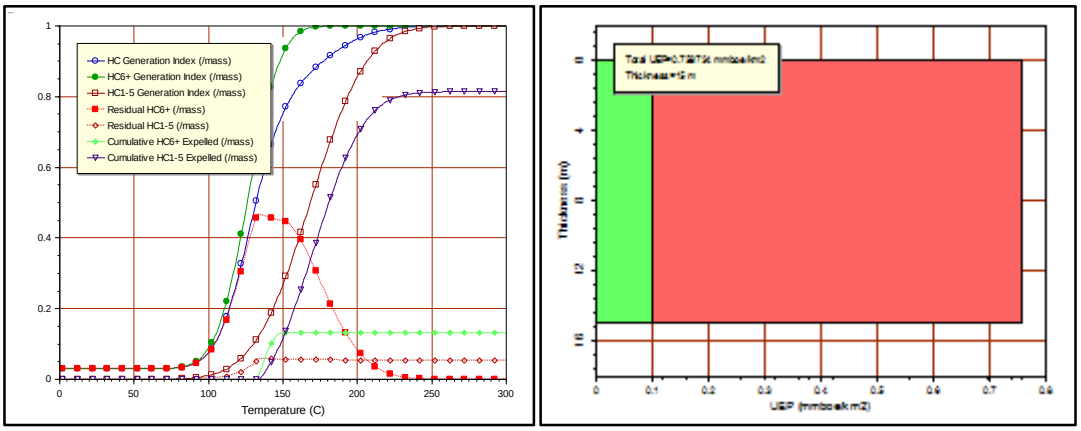

Figure 7.11: a) Graph of generation, expulsion and retention, and b) graph of petroleum expelled of the Middle Sirte Shale Formation.

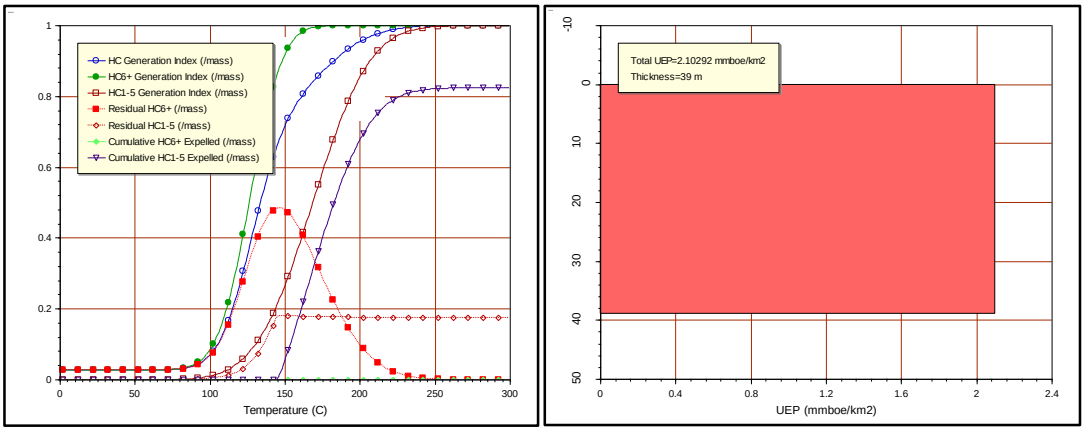

Figure 7.12: a) Graph of generation, expulsion and retention, and b) graph of petroleum expelled of the Lower Sirte Shale Formation.

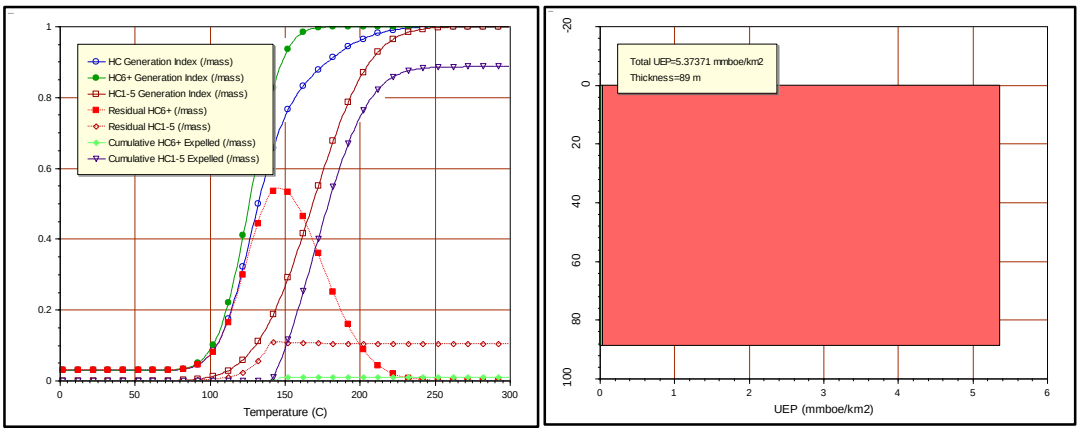

Figure 7.13: a) Graph of generation, expulsion and retention, and b) graph of petroleum expelled of the Upper Sirte Shale Formation.

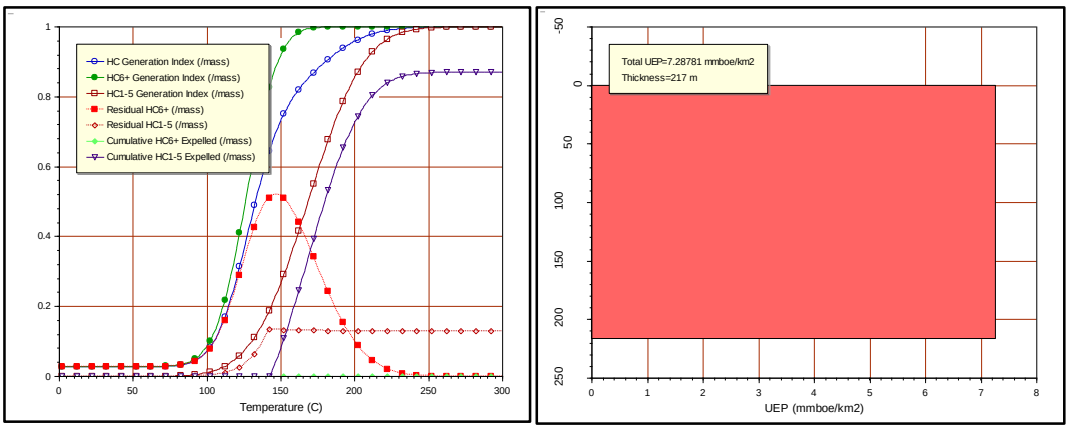

Figure 7.14: a) Graph of generation, expulsion and retention, and b) graph of petroleum expelled of the Lower Sirte Shale Formation.

The L1-16 well is located in the Nuflian High at the centre of the Sirt Basin. The Sirte Shale is subdivided into two units: upper and lower. The upper unit has a thickness of

about 270 feet and represents a medium dark grey to dark grey and black shale. The KinEx model displays very low expulsion of petroleum until reaching more than 141ºC. Based on the kinetic thermal model, the upper Sirte Shale Formation will expel about 5,37371mmboe/km^2, as shown in Figure 7.13a and b, and from the graph this source rock will produce very low amounts of oil relative to gas.

Meanwhile, the lower Sirte Shale Formation is characterized by medium dark grey shale interbedded with limestone and sandstone. Based on the kinetic thermal model, the lower Sirte Shale Formation will expel about 7,28781mmboe/km^2 of gas, as shown in Figure 7.14a and b.

The L1-17 well is situated in the Dor Al Abid Trough in the northwest part of the Sirt Basin. In this study well, the Sirte Shale Formation is subdivided into two upper and lower units. The upper unit consists of dark grey to black shale interbedded with limestone. The KinEx thermal model demonstrates an oil window for the upper Sirte Shale Formation starting at 124-151ºC and gas generation may commence at 137ºC and end at 244ºC, as shown in Figure 7.15a. The KinEx model shows no expulsion of petroleum until reaching more than 138ºC when the sorption potential of the kerogen is reached. The model shows a narrow window for oil expulsion subsequently followed by thermogenic gas expulsion. Based on the kinetic thermal model, the upper Sirte Shale Formation will expel about 24,4257mmboe/km^2, as shown in Figure 7.15b. From the graph this source rock will produce moderate amounts of oil compared to huge amounts of gas.

Whereas the lower Sirte Shale Formation consists of dark grey to medium dark grey shale interbedded with limestone. Based on the kinetic thermal model, the lower Sirte Shale Formation will expel about 3,225173mmboe/km^2 of gas, as shown in Figure 7.16a and b.

The Z1-11 is located in the Tagrifet Trough in the western part of the Sirt Basin. The Sirte Shale Formation is characterised by dark grey and dark brown to olive black shale. The KinEx model shows no expulsion of petroleum until reaching more than 135ºC when the sorption potential of the kerogen is reached. The model shows a narrow window for oil expulsion with subsequent thermogenic gas expulsion. Based on the kinetic thermal model, the Sirte Shale Formation will expel about 7,60565mmboe/km^2, as shown in Figure 7.17a and b. It is obvious from the graph that this source rock will produce moderate amounts of oil and gas.

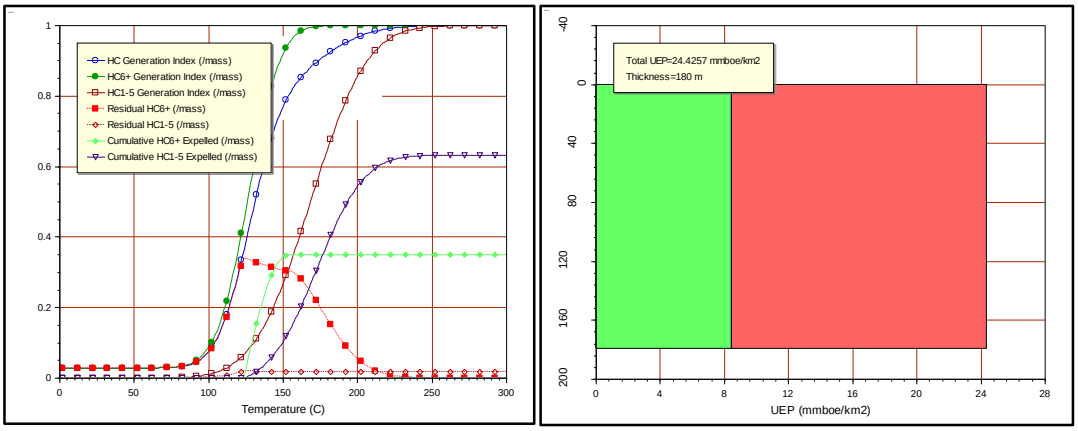

Figure 7.15: a) Graph of generation, expulsion and retention, and b) graph of petroleum expelled of the Upper Sirte Shale Formation.

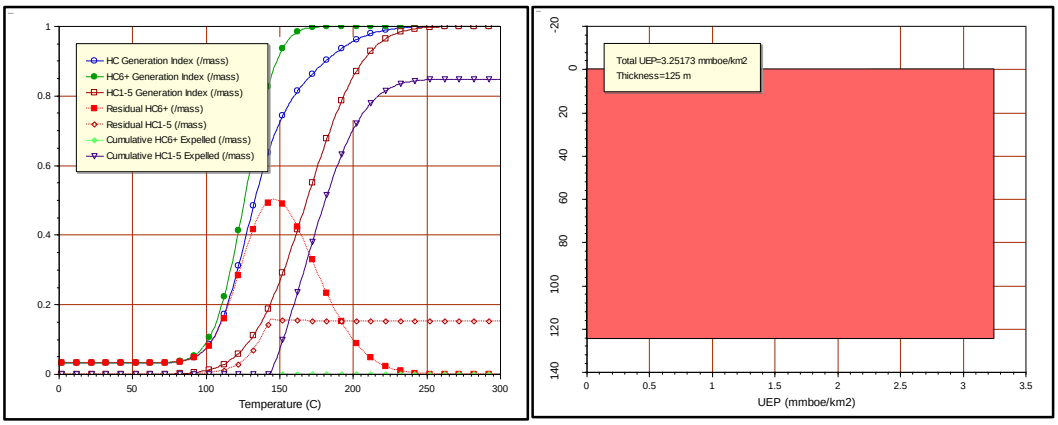

Figure 7.16: a) Graph of generation, expulsion and retention, and b) graph of petroleum expelled of the Lower Sirte Shale Formation.

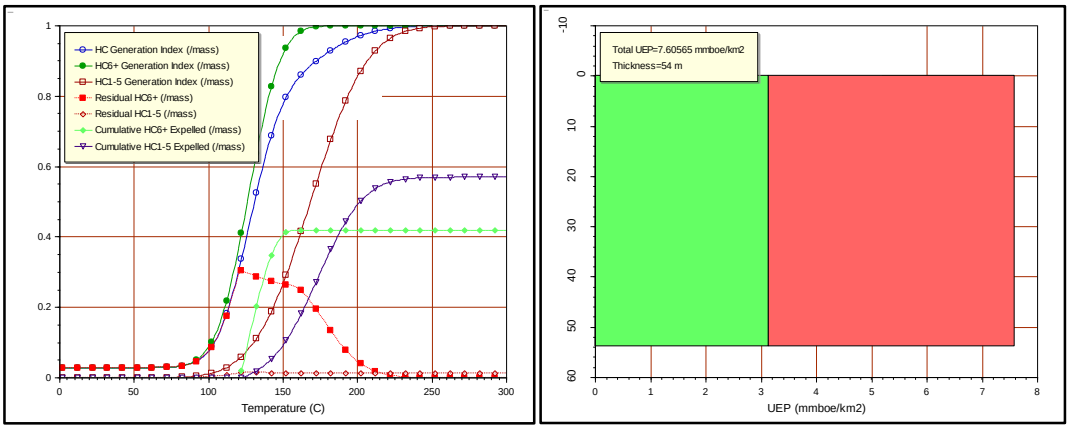

Figure 7.17: a) Graph of generation, expulsion and retention, and b) graph of petroleum expelled of the Sirte Shale Formation.

7.3 Petroleum System of the Sirt Basin

The petroleum system of the Sirt Basin province was evaluated based on the burial history, thermal maturity and timing of the generation of oil and/or gas. These elements were modelled for the main petroleum source rock units at eight boreholes situated in the Sirt Basin province. In the Sirt Basin the principal petroleum source rocks include the Upper Cretaceous Sirte Shale and Rachmat formations. In the present study, the Sirt Basin petroleum system is divided into three main areas in the western region centred on Zellah Trough, Dor Al Abdi Trough and Marada Trough. Location wells selected for burial history reconstructions include three in the deepest part of the basin (B1-NC74F, C2-16, and FF14-6); two of intermediate depth (L1-16 and Z1-11); and three at relatively shallow locations (6A1-59, B2-NC74A, and L1-17). 1D burial history, basin modelling was reconstructed from stratigraphy and lithology in the wells. Vitrinite reflectance (%*Ro*) was used to determine present day temperature and palaeotemperature. Stratigraphic data, such as depth, thickness, lithology and age were obtained from final or composite well logs, and geological reports were also used. From previous geological and geochemical studies it has observed that the Sirt Basin is characterized by multiple effective source rocks, established reservoir rocks and effective seals.

In the present study, the established petroleum system in the central and western part of the Sirt Basin is the Upper Cretaceous Petroleum System, which is comprised of the Upper Cretaceous Campanian and Maastrichtian marine shale source rocks; Lower and Upper Cretaceous; Palaeocene and Eocene sandstone; and carbonate as carrier beds and reservoirs. Therefore, the centre and western part of the Sirt Basin could be classified into two plays: the Upper Cretaceous and Palaeocene plays; and the Upper Cretaceous and Eocene plays.

The presence of these plays is mostly due to the combination of a regional Upper Cretaceous source rock with a structural geometry created later by the Upper Cretaceous and Palaeocene syn-rift system and the Eocene to Oligocene post-rift system and its subsequent subsidence. The Upper Cretaceous, Palaeocene and Eocene play represent the most fully explored and successful stratigraphic sequences, containing the majority of the resources discovered in the central and western part of the Sirt Basin (El-Alami *et al.*, 1989; El-Alami, 1996).

7.3.1 **1D Basin Modelling**

The one-dimensional basin model package of Genesis 5.1 software developed by ZetaWare as part of its Interactive Petroleum System Tool was used to model petroleum generation in the 6A1-59, B1-NC74F, B2-NC74A, C2-16, FF14-6, L1-16, L1-17, and Z1-11 wells. The Sirte Shale source rock is buried at different depths in these wells. The Kalash and Rachmat source rocks exist only in the 6A1-59 and B1-NC74F wells, respectively.

The basin model input and simulation data and results are presented below. The vitrinite reflectance value of 0.55 %*Ro* is taken for the initial oil generation, a value of 0.65 *%Ro* for the beginning of the oil window, a value of 0.95 *%Ro* for the peak of the oil window, and a value of 1.35 *%Ro* for the end of oil generation and the beginning of gas generation.

The 6A1-59 well is located in the area where the Kotla Graben and Zellah Troughs merge together to create an integrated fault system. Details of stratigraphic formation tops, age, and thickness of each unit accounted and the lithology are shown in Table 7.3. There is no significant nonconformity in the section above the source rocks. In order to match the thermal gradient defined by vitrinite reflectance values, the model requires a heat flow of 62.7 mW/m^2 at the base of the sedimentary section. In the model, the surface temperature 25ºC is taken as constant through time. The resulting calculated maturity gradient does not match the measured vitrinite reflectance gradient, either because it is too low or has shifted to lower maturity than that measured, as shown in Figure 7.18. The temperature model was 73ºC, which is not sufficient to crack the kerogen to hydrocarbons, as shown in Figure 7.18. The model does not show any hydrocarbon generation occurring due to the low maturity in the Kalash Formation, while little hydrocarbon generation for Sirte Shale source rocks is indicated by the low vitrinite reflectance values as shown in Figure 7.19.

Table 7-3: Time-stratigraphy in maturity model for source rock at wells 6A1-59, B1-NC74F and L1-17 in the Sirt Basin.

Well: 6A1-59

Age	Sub Age	Formation	Age (Ma)	Depth (ft)	Sub sea	Thickness	Ls %	Dolo%	Ss%	Sh%	Anhy%
Middle Eocene	Lutian	Gialo	49-36	165	805	970	80	0	10	10	0
Early Eocene	Ypresian	Gir	53-49	1115	-144	1638	5	10	0	0	85
Early Eocene	Ypresian	Facha	54-53	2753	-1782	304	0	100	0	0	0
Early Eocene	Thanetian	Kheir	55-54	3057	-2086	252	95	0	0	5	0
Upper Paleocene	Thanetian	Harash	56-55	3309	-2338	261	95	0	0	5	0
Late Paleocene	Thanetian	Zelten	57.9-56	3570	-2599	332	95	0	0	0	0
Late Paleocene	Selandian-Thanetian	Khalifa	58.5-57.9	3902	-2931	89	90	0	0	10	0
Late Paleocene	Thanetian	Dahra	59.9-58.5	3991	-3020	299	95	0	0	5	0
Late Paleocene	Selandian-Thanetian	Khalifa Shale	60.9-59.9	4290	-3319	336	50	0	0	50	0
Late Paleocene	Selandian	Upper Beda	61-60.9	4626	-3655	220	90	0	0	5	5
Late Paleocene	Selandian	Lower Beda	63-61	4846	-3875	747	85	15	0	0	0
Late Paleocene	Danian	Hagfa Shale	66.5-63	5593	-4622	957	5	0	0	95	0
Upper Cretaceous	Masstrichtian	Upper Kalash	68-66.5	6550	-5579	626	100	0	0	0	0
Upper Cretaceous	Masstrichtian	Lower Kalash	71.3-68	7176	-6309	44	5	0	5	90	0
Upper Cretaceous	Campanian	Lower Sirte Shale	89-83.5	7220	-6249	60	5	0	5	90	0
		TD		7280	-6329						

Well: B1-NC74F

Age	Sub Age	Formation	Ma	Depth (ft)	Subsea	Thickness	Ls %	Dolo %	Ss %	Sh %	Anhy %
Early Eocene	Ypresian	Gir	52.9-49	1489	-308		0	15	0	0	85
Early Eocene	Ypresian	Facha member	53.5-52.9	3828	-2647	2339	50	50	0	0	0
Late Paleocene	Thanetian	Kheir	54-53.5	4080	-2899	252	60	0	0	40	0
Late Paleocene	Thanetian	Harash	55.5-54	4450	-3269	370	40	0	0	60	0
Late Paleocene	Thanetian	Zelten (B)	56-55.5	4650	-3459	200	65	0	0	35	0
Late Paleocene	Thanetian	Zelten(C)	57.9-56	4902	-3721	252	100	0	0	0	0
Late Paleocene	Selandian-Thanetian	Khalifa	60.9-57.9	5207	-4026	305	65	0	0	35	0
Late Paleocene	Selandian	Beda	62-60.9	5714	-4533	507	60	0	0	40	0
Late Paleocene	Selandian	Beda (C)	63-62	5848	-4667	134	90	5	0	5	0
Early Paleocene	Danian	Hagfa	66.5-63	6801	-5620	953	0	0	0	100	0
Upper Cretaceous	Masstrichtian	Kalash	71.3-66.5	6858	-5677	57	40	0	0	60	0
Upper Cretaceous	Campanian	Sirte Shale	83.5-71.3	7018	-5837	160	10	0	0	90	0
Upper Cretaceous	Coniacian/Santonian	Rachmat	89-83.5	7554	-6373	536	10	0	0	90	0
Upper Cretaceous	Turonian	Etel	93.5-89	8154	-6973	600	0	5	0	75	20
Upper Cretaceous	Cenomain	Lidam	94-93.5	8565	-7384	411	0	100	0	0	0
Haitus		Nafisa	100-96								
Upper Cretaceous	Cenomain	Bahi	131-100	8987	-7806	422	0	0	65	35	0
		TD		10015	-8834	1028					

Well: L1-17

Age	Sub Age	Formation	Ma	Depth (ft)	Sub sea	Thickness	Ls %	Dolo %	Ss %	Sh %	Anhy %
		undifineted		152		216	25	0	30	45	0
Middle Eocene	Lutetian-Bartonian	Sheghega	49-36	368	534	1055	95	0	0	0	0
Early Eocene	Ypresion	Sitra	50-49	1423	-521	1711	15	30	0	5	50
Early Eocene	Ypresion	Amur	54-50	3134	-2285	181	100	0	0	0	0
Early Eocene	Ypresion	Ruaga	55-54	3315	-2466	375	100	0	0	0	0
Early Eocene	Ypresion	Heira	58-55	3690	-2841	177	10	0	0	90	0
Early Eocene	Ypresion	Mabruk	61.5-58	3867	-3018	649	90	0	0	10	0
Late Paleocene	Thanethian	Taleth	63.5-61.5	4516	-3667	80	60	0	0	40	0
Late Paleocene	Thanethian	Dahra	66.5-63.5	4596	-3747	1184	90	5	0	5	0
Upper Cretaceous-	Masstrichtian-Danian	Zmam	71.3-66.5	5780	-4031	251	100	0	0	0	0
Upper Cretaceous-	Santonian-Campania	Sirte	89-71.3	6031	-5182	963	10	0	0	90	0
Upper Cretaceous-	Turonian	Asad	93.5-89	6994	-6145	161	95	0	0	5	0
Upper Cretaceous-	Cenomanian-Turonia	Garian	96-93.5	7155	-6306	219	50	50	0	0	0
Upper Cretaceous-	Cenomanian-Turonia	Nefisa	98.9-96	7374	-6525	404	0	95	0	5	0
Cretaceous		Basal Cretaceous		7778	-6929	330	0	0	80	20	0
		TD		8108							

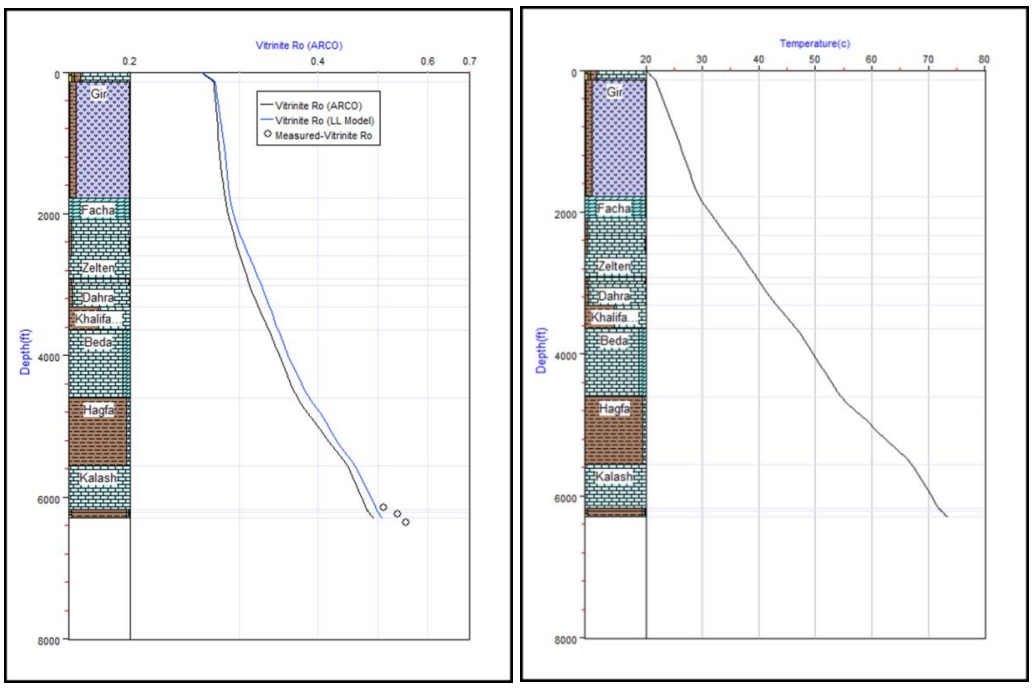

Figure 7.18: 1D Genesis software modelling of the vitrinite reflectance (*%Ro*) with temperature model versus depth for the Kalash and Sirte Shale source rocks in the Sirt Basin at 6A1-59 well.

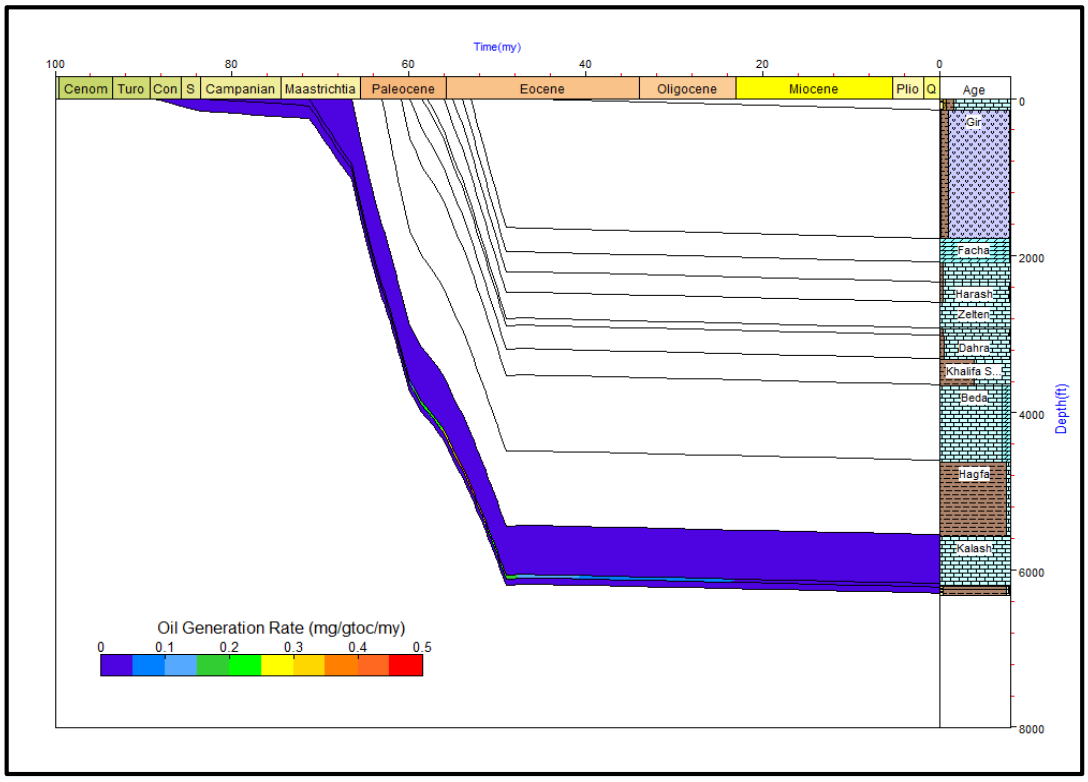

Figure 7.19: Burial history chart of the oil expels for the Kalash and Sirte Shale source rock in the Sirt Basin at 6A1-59 well.

The B1-NC74F well is located in the Zellah Trough, where the Sirte Shale and Rachmat source rocks are buried at between 7010 to 7200 feet and 7930 to 8090 feet, respectively. Details of stratigraphic formation tops, age, and thickness of each unit accounted and the lithology are expressed in Table 7.2. There is no significant nonconformity in the section above these source rocks. In order to match the thermal gradient defined by vitrinite reflectance values, the model requires a heat flow of 62.70mW/m^2 at the base of the sedimentary section. The surface temperature 25ºC is taken as constant through time. The resulting calculated maturity gradient matches the measured vitrinite reflectance, as shown in Figure 7.20. The temperatures modelled for both Sirte Shale and Rachmat source rocks were 67ºC and 76ºC respectively, which is not sufficient to fracture the kerogen to become hydrocarbon, as shown in Figure 7.20. Figure 7.21 shows burial history curves upon which temperature colour isograds are superimposed. This figure shows that the calculated temperature for the top of the Sirte Shale Formation reached 60ºC at a depth 3100 feet at approximately 55Ma in Palaeocene time, while the Rachmat Formation of the Upper Cretaceous age reached a temperature of 70ºC at a depth of 3754 feet at approximately 57Ma in the Palaeocene period. The model shows that the slight hydrocarbon generation occurred due to low maturity in both the Sirte Shale and Rachmat source rocks, as indicated by the low vitrinite reflectance values shown in Figure 7.22.

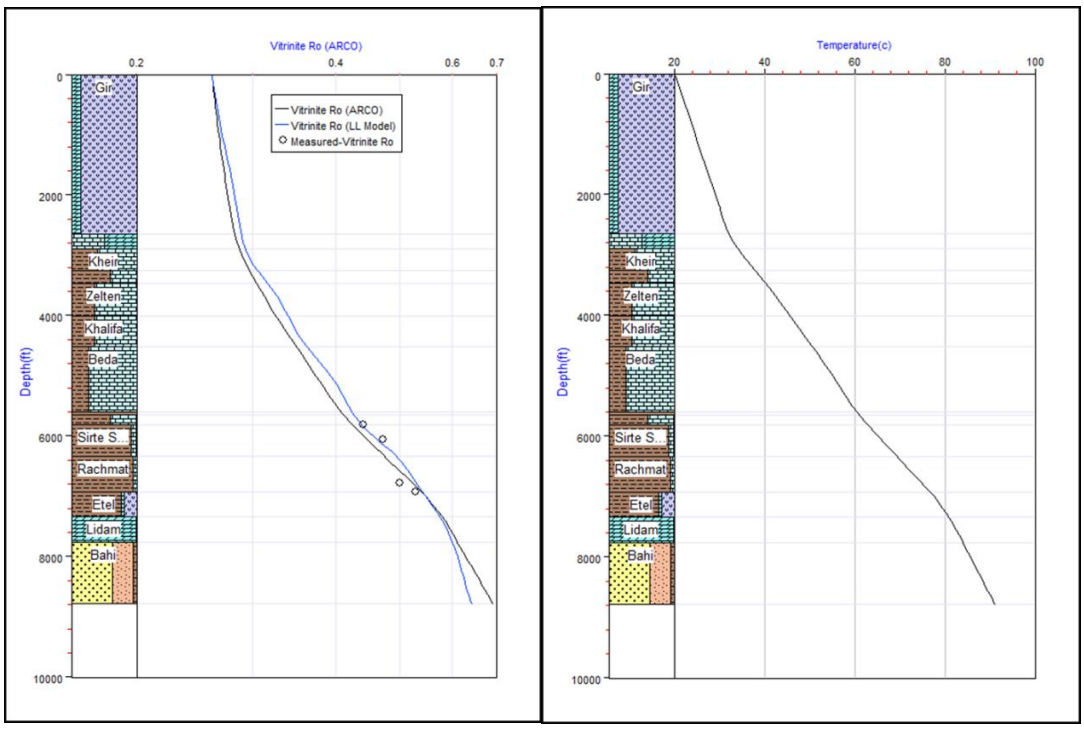

Figure 7.20: 1D Genesis software modelling of the vitrinite reflectance (*%Ro*) with temperature model versus depth for the Sirte Shale and Rachmat source rocks in the Sirt Basin at B1-NC74F well.

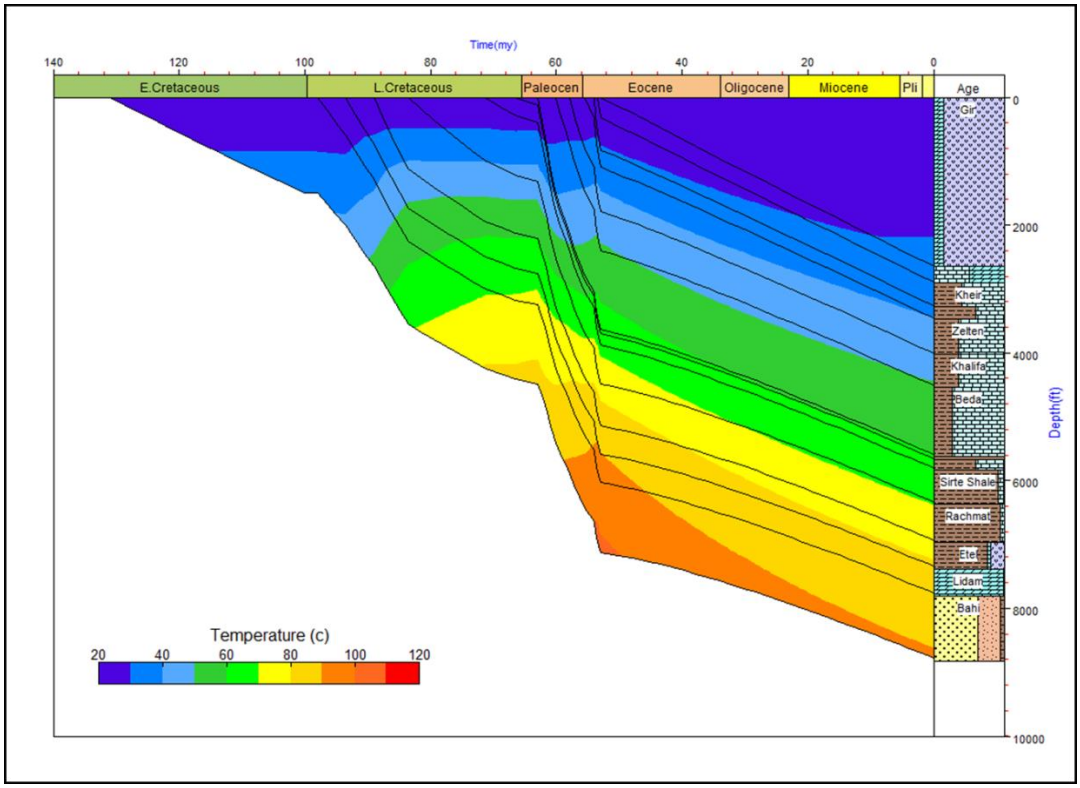

Figure 7.21: Burial history and temperature model for the Sirte Shale and Rachmat source rock in B1-NC74F well.

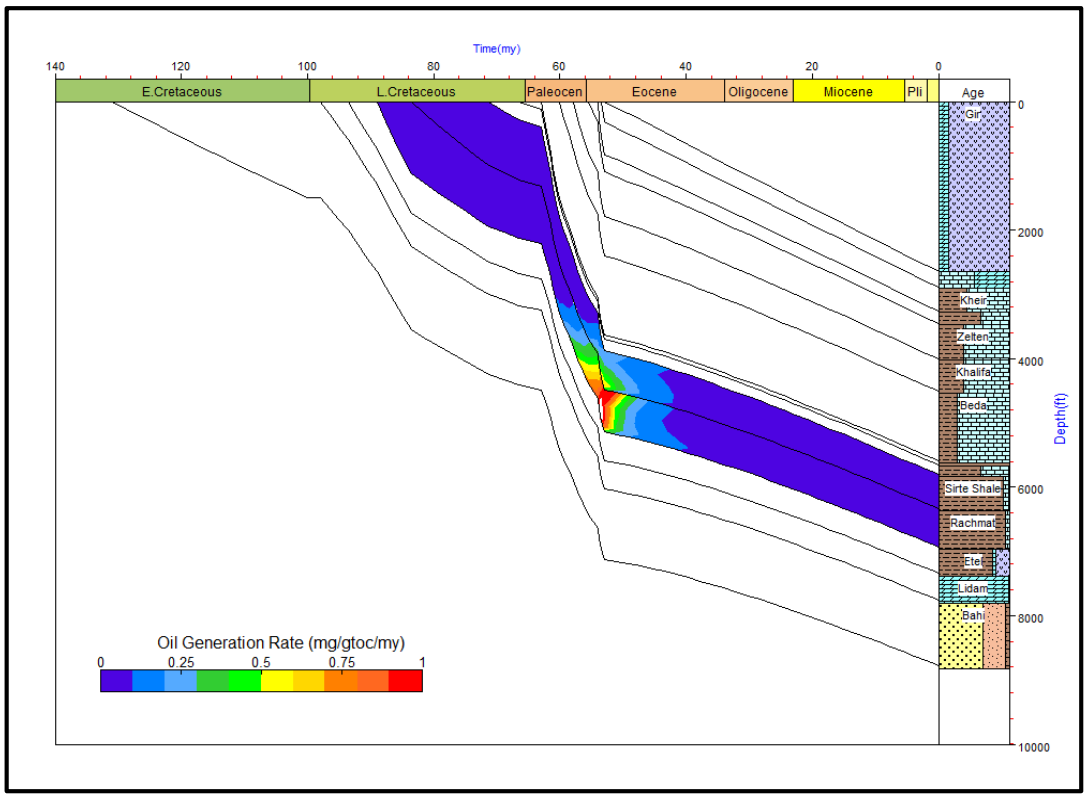

Figure 7.22: Burial history chart of the oil generation for the Sirte Shale and Rachmat source rocks in the Sirt Basin at B1-NC74F well.

The L1-17 well is situated in the Dor Al Abid Trough in the north-western part of the Sirt Basin. In this well the Sirte Shale source rock is at a depth between 6060 to 7020 feet. Details of stratigraphic formation tops, age, and thickness of each unit accounted and the lithology are shown in Table 7.2. There is no significant nonconformity in the sedimentary section above the Sirte Shale source rock, but there is some uplift and erosion or non-deposition from early Palaeocene times. The well was modelled with a present day heat flow value of 62.70mW/m^2. The well had continuous burial throughout its history with the deepest burial attained in the Upper Cretaceous period. The resulting calculated maturity gradient does not match with the measured vitrinite reflectance, as shown in Figure 7.23. The model temperature of the Sirte Shale source rocks was 78ºC, which is considered as sufficient temperature to fracture the kerogen to become hydrocarbon, as shown in Figure 7.23. Figure 7.24 show burial history curves where the temperature is overlaid in colour. This figure shows that the calculated temperature for the top of the Sirte Shale Formation reached a temperature of 60ºC at a depth 3133 feet at approximately 54Ma at the Palaeocene age. The model shows slight hydrocarbon generation occurring due to the low maturity of both the Sirte Shale and

Rachmat source rocks as indicated by low vitrinite reflectance values shown in Figure 7.25.

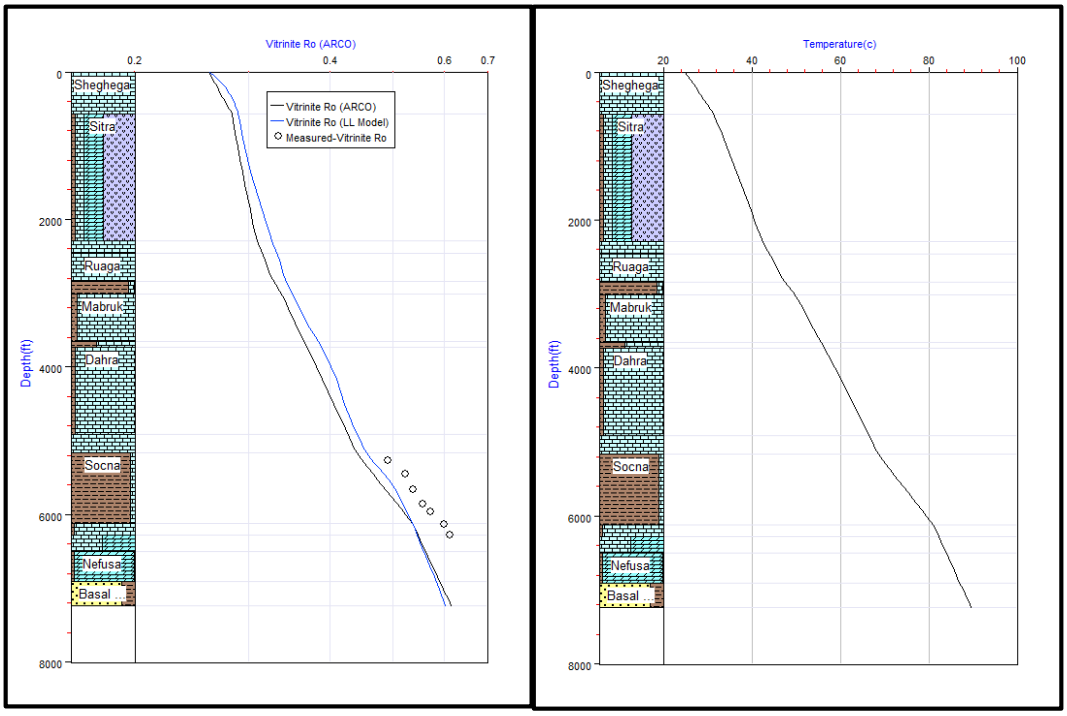

Figure 7.23: 1D Genesis software modelling of the vitrinite reflectance (*%Ro*) with temperature model versus depth for the Sirte Shale source rocks in the Sirt Basin at L1-17 well.

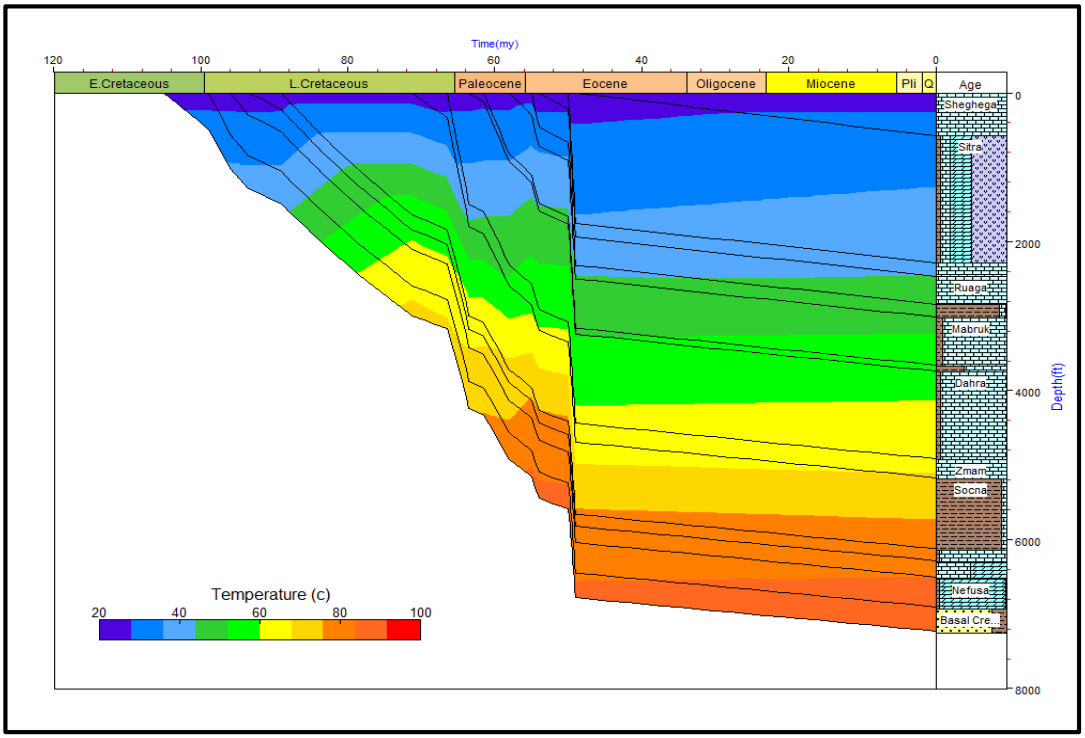

Figure 7.24: Burial history and temperature model for the Sirte Shale and Rachmat source rock in L1-17 well.

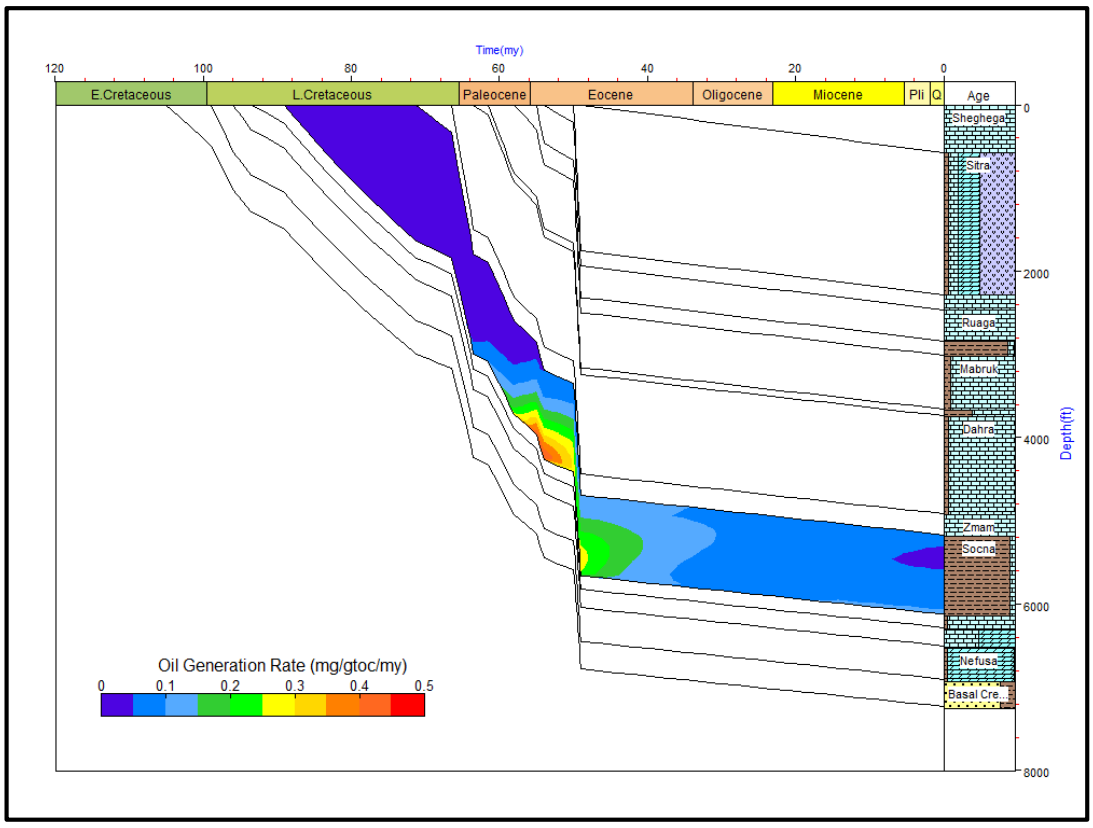

Figure 7.25: Burial history chart of the oil expels for the Sirte Shale and Rachmat source rocks in the Sirt Basin at L1-17 well.

The B2-NC74A well is located in the Zellah Trough at the western edge of the Sirt Basin. In this well the Sirte Shale source rocks are recognized at depths between 9500 to 9740 feet. Data for the stratigraphic formation tops, age, and thickness of each unit accounted and the lithology are given in Table 7.4. There is no significant nonconformity in the sedimentary section above the Sirte Shale source rock. The well was modelled with a present day heat flow value of 62.70mW/m^2. The well had continuous burial throughout its history with the deepest burial attained in the Upper Cretaceous. The resulting calculated maturity gradient does not match with the measured vitrinite reflectance, as shown in Figure 7.26. The model temperature of the Sirte Shale source rocks was 94ºC, which is a sufficient temperature to fracture the kerogen to become liquid hydrocarbon, as shown in Figure 7.26. Figure 7.27 show burial history curves which temperature are superimposed in colour. This figure shows that the calculated temperature for the top of the Sirte Shale Formation reached 80ºC at a depth of 7040 feet at approximately 40Ma in the Eocene period. Figure 7.28 shows the calculated vitrinite reflectance values superimposed in colour upon the burial

history plot. This figure shows the calculated vitrinite reflectance values for each formation compared with time (Ma) and depth (feet), where the Sirte Shale source rock reached early maturity at 8220 feet at approximately 13Ma in Eocene time. The model shows slight hydrocarbon generation occurring due to the low thickness of the Sirte Shale source rocks, as shown in Figure 7.29.

Table 7-4: Time-stratigraphy in maturity model for source rock at wells B2-NC74A and Z1-11 in the Sirt Basin.

Well: B2-NC74A

Age	Sub Age	Formation	Age Ma	Depth (ft)	Sub sea	Thickness	Ls %	Dolo %	Ss %	Sh %	Anhy	Salt
Middle Eocene	Bartonian	Bumaras	41.3-36	2422	-1404	805						
Middle Eocene	Lutetian	Gattar	49-41.3	3227	-2209	645						
Early Eocene	Ypresian	Gir	52-49	3872	-2854	680	0	10	0	0	90	0
Early Eocene	Ypresian	Salt	52.9-52	4552	-3534	1572	0	0	0	0	0	100
Early Eocene	Ypresian	Facha member	53.5-52.9	6124	-5106	302	10	90	0	0	0	0
Late Paleocene	Thanetian	Kheir	54-53.5	6426	-5408	226	60	0	0	40	0	0
Late Paleocene	Thanetian	Harash	55.5-54	6652	-5634	123	40	0	0	60	0	0
Late Paleocene	Thanetian	Zelten	57.9-55.5	6775	-5757	465	100	0	0	0	0	0
Late Paleocene	Thanetian	Dahra	60.9-57.9	7240	-6222	394	95	0	0	5	0	0
Late Paleocene	Selandian	Beda	63-60.9	7634	-6616	1150	95	0	0	0	0	0
Early Paleocene	Danian	Hagfa	66.5-63	8784	-7766	572	0	0	0	100	0	0
Upper Cretaceous	Mastrtchtian	Kalash	71.3-66.5	9356	-8338	304	90	0	0	10	0	0
Upper Cretaceous	Campanian	Sirte Shale	89-71.3	9660	-8642	80	0	0	0	100	0	0
		TD		9740								

Well: Z1-11

Age	Sub Age	Formation	Age Ma	Depth (ft)	Sub sea	Thickness	Ls %	Dolo %	Ss %	Sh %	Anhyd	Salt
Late Eocene			37-33.7	100		545	20	10	40	30	0	0
Middle Eocene	Bartonian	Bu mras	41.3-37	645	-205	885	30	35	5	30	0	0
Middle Eocene	Lutetian	Gattar	49-41.3	1530	-1086	886	50	0	0	50	0	0
Early Eocene	Ypresian	Gir	53.8-49	2416	-1972	2517	0	50	0	0	30	15
Late Paleocene	Thanetian	Kheir	55-53.8	4933	-4489	734	70	30	0	0	0	0
Haitus	Thanetian		57.9-55									
Late Paleocene	Danian --Sela	Dahra	58.5-57.9	5667	-5223	423	45	10	0	45	0	0
Paleocene	Danian --Sela	Mabruk	60.9-58.5	6090	-5636	1507	65	20	0	15	0	0
Haitus	Danian	Haitus	66.5-60.9									
Upper Cretaceous	Masstrichtian	Kalash	71.3-66.5	7597	-7163	468	90	0	0	10	0	0
Upper Cretaceous	Campanian	Sirte Shale	89.0-71.3	8065	-7621	179	0	0	0	100	0	0
		TD		8244								

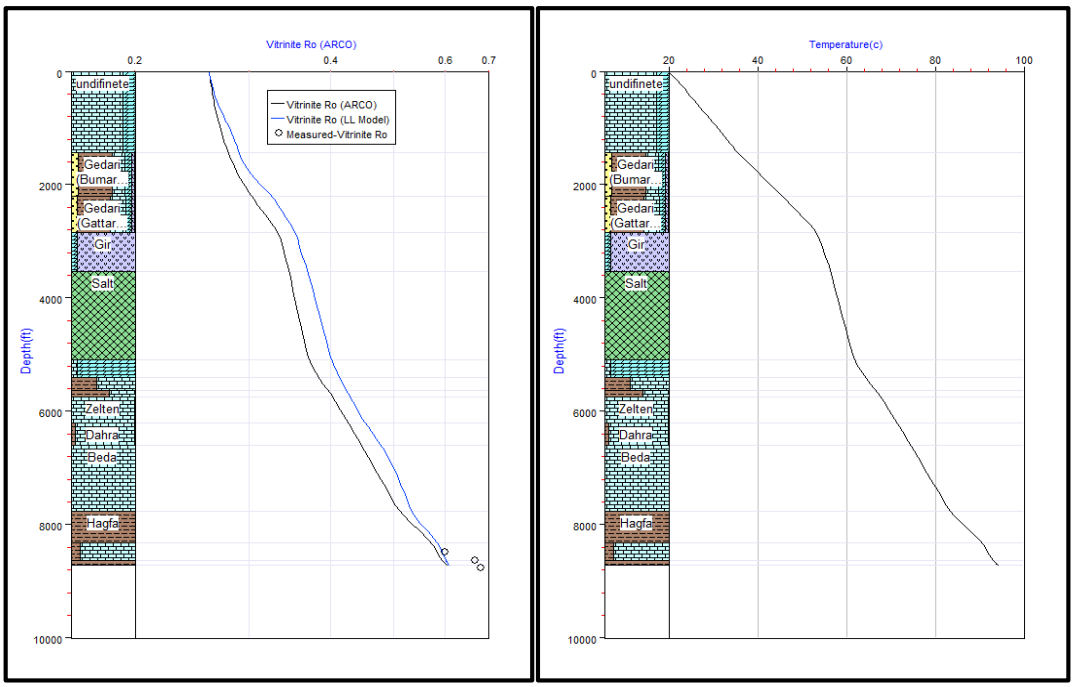

Figure 7.26: 1D Genesis software modelling of the vitrinite reflectance (*%Ro*) with temperature model versus depth for the Sirte Shale source rocks in the Sirt Basin at B2-NC74A well.

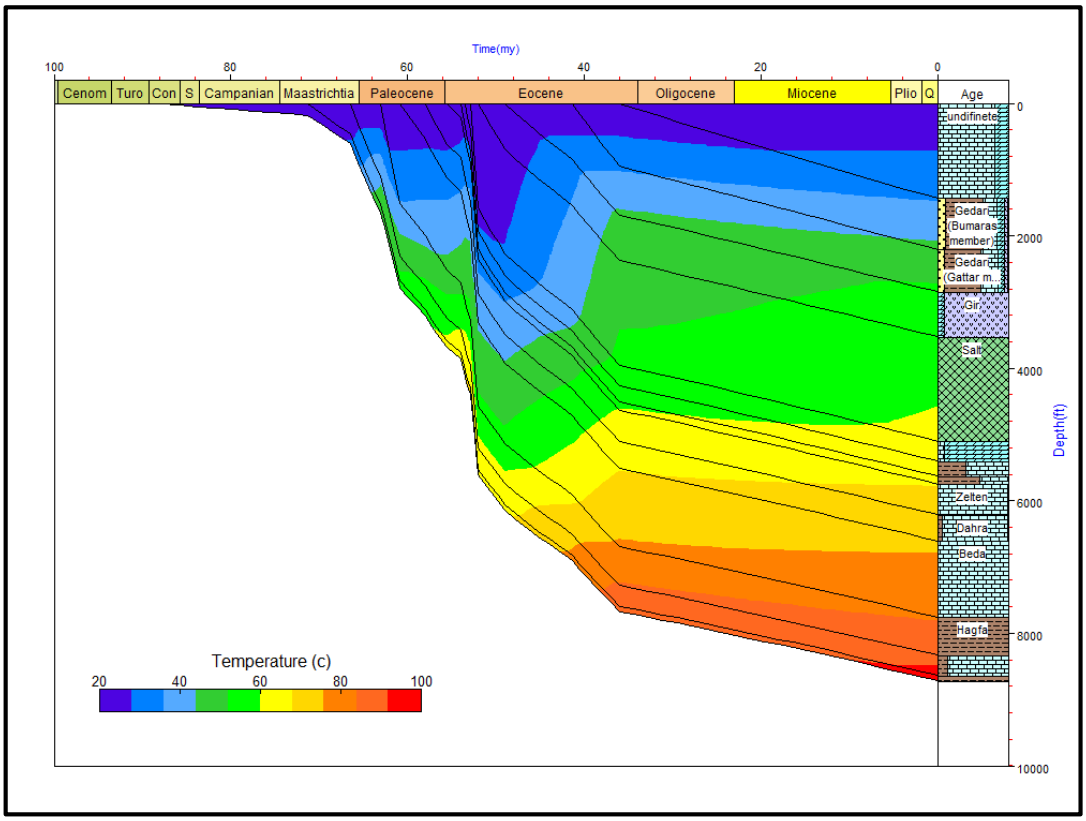

Figure 7.27: The Burial histories with temperature model for the Sirte Shale source rock in B2-NC74A well.

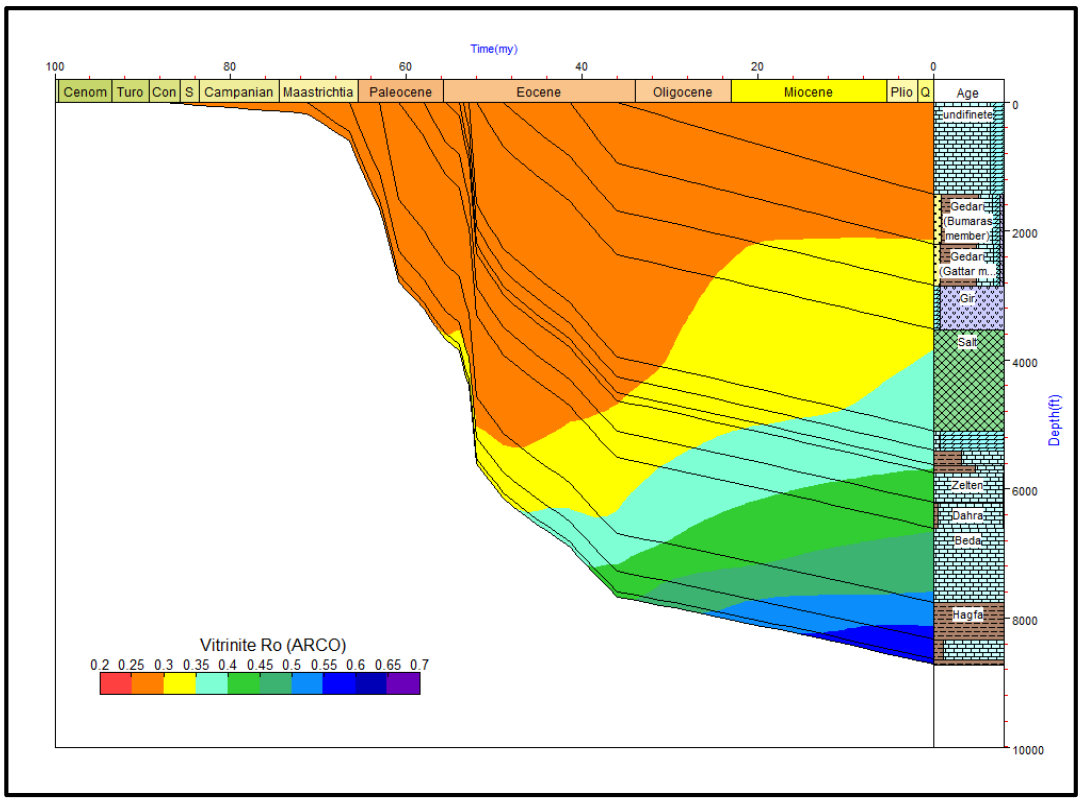

Figure 7.28: The Burial history with calculated vitrinite reflectance plot of the Sirte Shale source rock in the Dor Al Abad Trough in the Sirt Basin at B2-NC74A well.

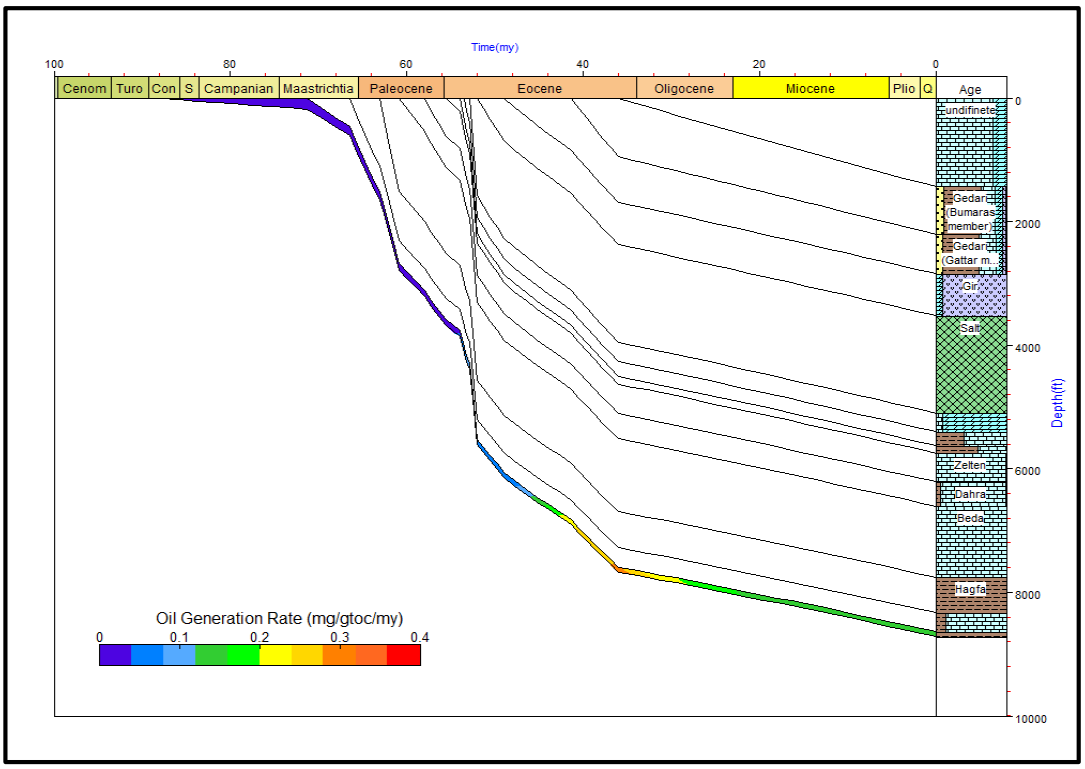

Figure 7.29: The Burial histories with hydrocarbon generation plot of the Sirte Shale source rock in the Dor Al Abad Trough in the Sirt Basin at B2-NC74A well.

The Z1-11 well is located in the Tagrifet Trough in the western part of the Sirt Basin. The Sirte Shale Formation here extends from 8050 to 8243 feet with a thickness of around 193 feet. Data for the stratigraphic formation tops, age, and thickness of each unit accounted and lithology are shown in Table 7.3. There is nonconformity in the sedimentary section above the Sirte Shale source rock, with uplift and erosion or non-deposition in the Danian and Thanetian in Palaeocene times. The well was modelled with a value of present day heat flow of 62.70mW/m^2. The well had continuous burial throughout its history, with the deepest burial occurring in the Upper Cretaceous period. The resulting calculated maturity gradient is a good match with the measured vitrinite reflectance as shown in Figure 7.30. The model temperature of the Sirte Shale source rocks was 95ºC, which is a sufficient temperature to fracture the kerogen to become liquid hydrocarbons as shown in Figure 7.30. Figure 7.31 shows burial history curves with temperature superimposed in colour. This figure shows that the calculated temperature for the top of the Sirte Shale Formation of the Upper Cretaceous age reaches 80ºC at a depth of 7394 feet at approximately 45Ma in Eocene time. Figure 7.32 shows calculated vitrinite reflectance values superimposed in colour upon the burial history plot. This figure shows that the calculated vitrinite reflectance values for the Sirte Shale source rock reached 0.55 *%Ro* at early maturity at 7506 feet at approximately 24Ma and in Eocene time. The model shows that hydrocarbon generation occurred with at a low bed thickness of the Sirte Shale source rocks within the Eocene to Oligocene ages, as shown in Figure 7.33.

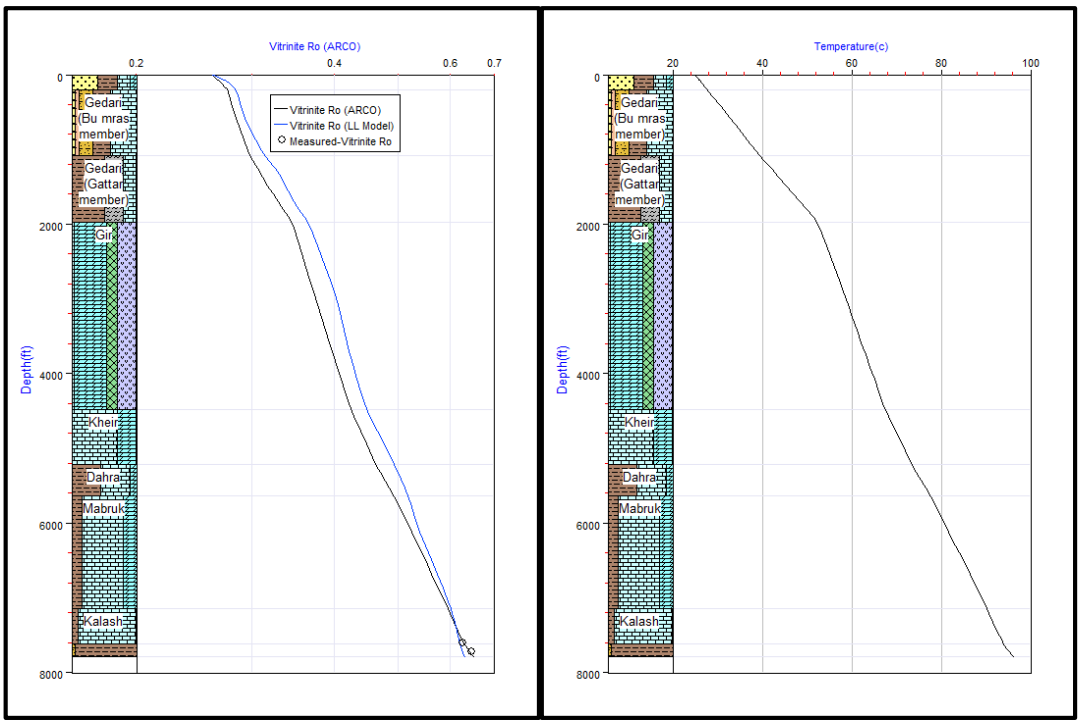

Figure 7.30: 1D Genesis software modelling of the vitrinite reflectance (%Ro) with temperature model versus depth for the Sirte Shale source rocks in the Sirt Basin at Z1-11well.

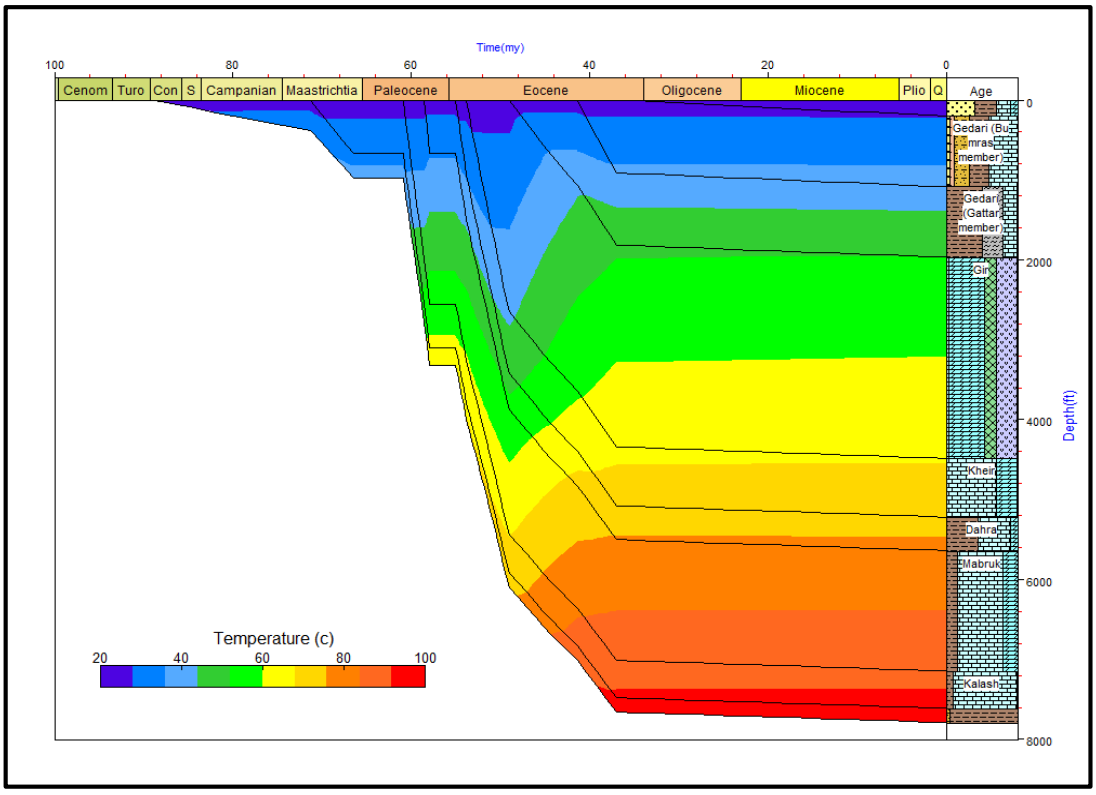

Figure 7.31: The Burial histories with temperature model of the Sirte Shale source rock in Z1-11well.

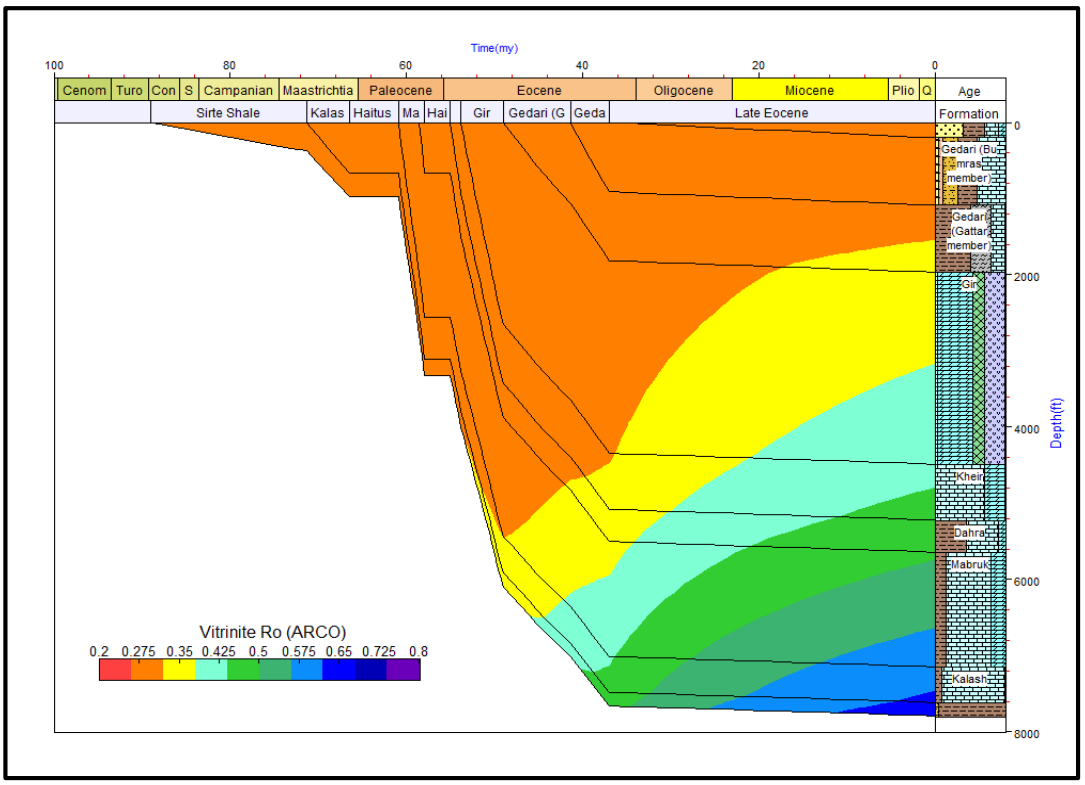

Figure 7.32: The Burial history with calculated vitrinite reflectance plot of the Sirte Shale source rock in the Tagrifet Trough in the Sirt Basin at Z1-11well.

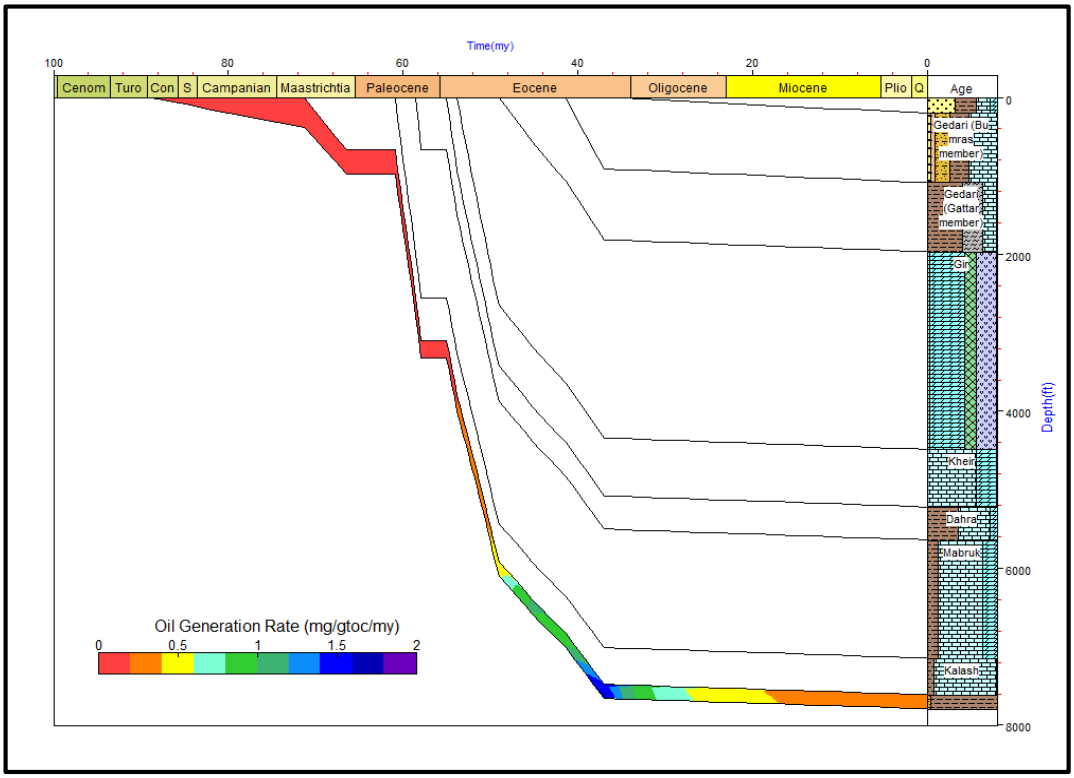

Figure 7.33: The Burial history with hydrocarbon generation plot of the Sirte Shale source rock in the Tagrifet Trough in the Sirt Basin at Z1-11well.

The C2-16 well is located in the Marada Trough in the central part of the Sirt Basin. The Sirte Shale Formation here has a thickness of around 1240 feet, and it extends from 9780 to 11020 feet. The stratigraphic tops, age, thickness of each unit accounted and lithology are shown in Table 7.4. There is nonconformity in the sedimentary section above the Sirte Shale source rock with uplift and erosion or non-deposition in the Seladndian and Thanetian in Late Palaeocene times and in the Ypresian in the Early Eocene time. The well was modelled with a value of present day heat flow of 62.73mW/m^2. The well had continuous burial throughout its history with the deepest burial attained in the Upper Cretaceous. The resulting calculated maturity gradient is a good match with the measured vitrinite reflectance, as shown in Figure 7.34. The model temperature of the Sirte Shale source rocks was 137ºC, which is a sufficient temperature to fracture the kerogen to become liquid and gas hydrocarbons, as shown in Figure 7.34. Figure 7.35 shows burial history curves on which temperature is superimposed in colour. This figure shows the calculated temperature for the top of the Sirte Shale Formation as reaching 90ºC (oil window) at a depth of 4000 feet of approximately 64Ma at the Early Palaeocene time, and a temperature 135ºC (beginning gas window) was reached at a depth of 9260 feet at approximately 6Ma in Miocene time. Figure 7.36 shows calculated vitrinite reflectance values superimposed in colour upon the burial history plot. This figure shows the calculated vitrinite reflectance values for the Sirte Shale source rock as reaching 0.65*%Ro* at middle maturity at 7106 feet at approximately 45Ma and in the Eocene time, and 0.90*%Ro* at the peak of oil generation at 9030 feet at approximately 13Ma and in Miocene time. The model shows that oil and gas hydrocarbon generation occurred in the Sirte Shale source rocks within the Palaeocene to Oligocene ages, as shown in Figure 7.37 and 7.38.

Table 7-5: Time-stratigraphy in maturity model for source rock at wells C2-16 and FF14-6 in the Sirt Basin.

Well: C2-16

Age	Sub Age	Formation	Age (Ma)	Depth (ft)	Sub sea	Thickness	Ls %	Dolo %	Ss %	Sh %	Anhy %
Miocene			20-15	290			100	0	0	0	0
Oligocene to Miocene		Muailah	23.8-20	723	-293	726	100	0	0	0	0
Oligocene		Etel	33.7-23.8	1449	-1019	575	50	0	0	50	0
Haitus 2			36-33.7								
Middle Eocene	Lutetian-Bartonian	Sheghega	49-36	2024	-1594	1812	100	0	0	0	0
Middle to Late Eocene		Domran	50-49	3836	-3406	1913	95	5	0	0	0
Early Eocene	Ypresion	Amur	54-49	5749	-5319	433	100	0	0	0	0
Early Eocene	Ypresion	Ruaga	58-54	6182	-5752	555	80	0	0	20	0
Early Eocene	Ypresion	Heira	58-55	6737	-6307	183	5	0	0	95	0
Early Eocene	Ypresion	Mabruk	61-58	6920	-6490	178	95	0	0	5	0
Haitus 1	Danian		64-61								
Early Paleocene	Danian	Dahra	66.5-64	7098	-6668	1969	5	0	0	95	0
Upper Cretaceous	Masstrichtian-Dani	Zmam	71.3-66.5	9067	-8637	804	100	0	0	0	0
Upper Cretaceous	Santonian-Campan	Sirte Shale	89-71.3	9871	-9441	1144	15	0	0	85	0
		TD		11015	-10585						

Well: FF14-6

Age	Sub Age	Formation	Age (Ma)	Depth (ft)	Sub sea	Thickness	Ls %	Dolo %	Ss %	Sh %	Anhy %
Miocene			20-18	996	-621	1268	40		35	15	0
Oligocene to Miocene		Muailah	23-20	2264	-1889	1760	0	0	80	5	0
Oligocene		Etel	33.7-23	4024	-3649	471	0	0	5	95	0
Middle Eocene	Lutetian-Bartonian	Sheghega	49-36	4495	-4120	1796	95	0	0	5	0
Early Eocene	Ypresian	Domran	54-49	6291	-5916	1176	100	0	0	0	0
Paleocene to lower Eocene		Ruaga	55-54	7467	-7092	353	95	0	0	5	0
Paleocene to Early	Danian-Thanet	Heira	63-55	7820	-7445	2724	10	0	0	90	0
Upper Cretaceous	Masstrictian	Zmam	71.3-63	10544	-10169	677	100	0	0	0	0
Upper Cretaceous		Sirte Shale	83.5-71.3	11221	-10846	1866	15	0	5	80	0
Upper Cretaceous		Bahi	98.9-98	13087	-12712	139	0	0	95	5	0
Cambro-Ordovacian				13226	-12851	214					
		TD		13440	-13065						

Well: L1-16

Age	Sub Age	Formation	Age Ma	Depth (ft)	Sub sea	Thickness	Ls %	Dolo %	Ss %	Sh %	Anhy %
Oligocene			33.7-23.8	315	331 sea l	1319					
Middle Eocene	Lutetian-Bartonian	Sheghga	49-36	1634	-1293	1762	100	0	0	0	0
Early Eocene	Ypresian	Domran	54-49	3396	-3065	1729	85	10	0	5	0
Early Eocene	Danian-Thantet	Ruaga	55-54	5125	-4794	739	10	90	0	0	0
Early Eocene	Danian-Thantet	Heira	66.5-55	5864	-5533	901	20	0	40	40	0
Upper Cretaceous-	Masstrichtian-Dani	Zamam	71.3-66.5	6765	-6434	643	20	70	0	10	0
Upper Cretaceous	Santonian-Campan	Sirte Shale	89-71.3	7408	-7077	874	10	0	10	80	0
Cambro-Ordovician			405	8282	-7951	333	0	0	100	0	0
		TD		8615	-8284						

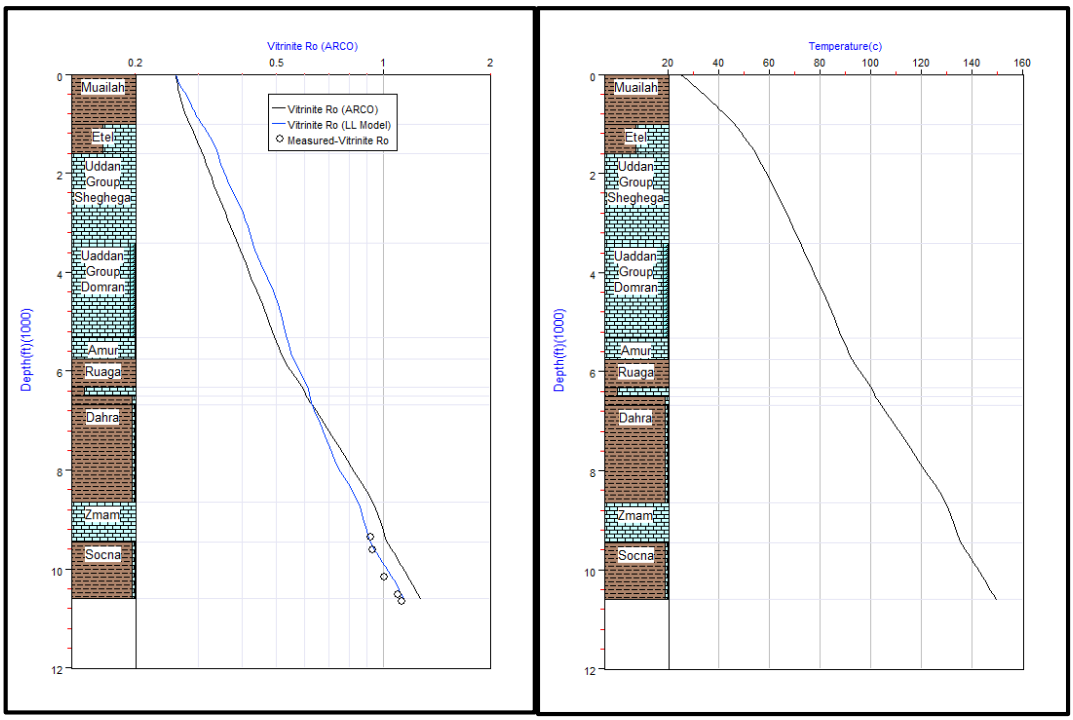

Figure 7.34: 1D Genesis software modelling of the vitrinite reflectance (%Ro) with temperature model versus depth for the Sirte Shale source rocks in the Sirt Basin at C2-16 well.

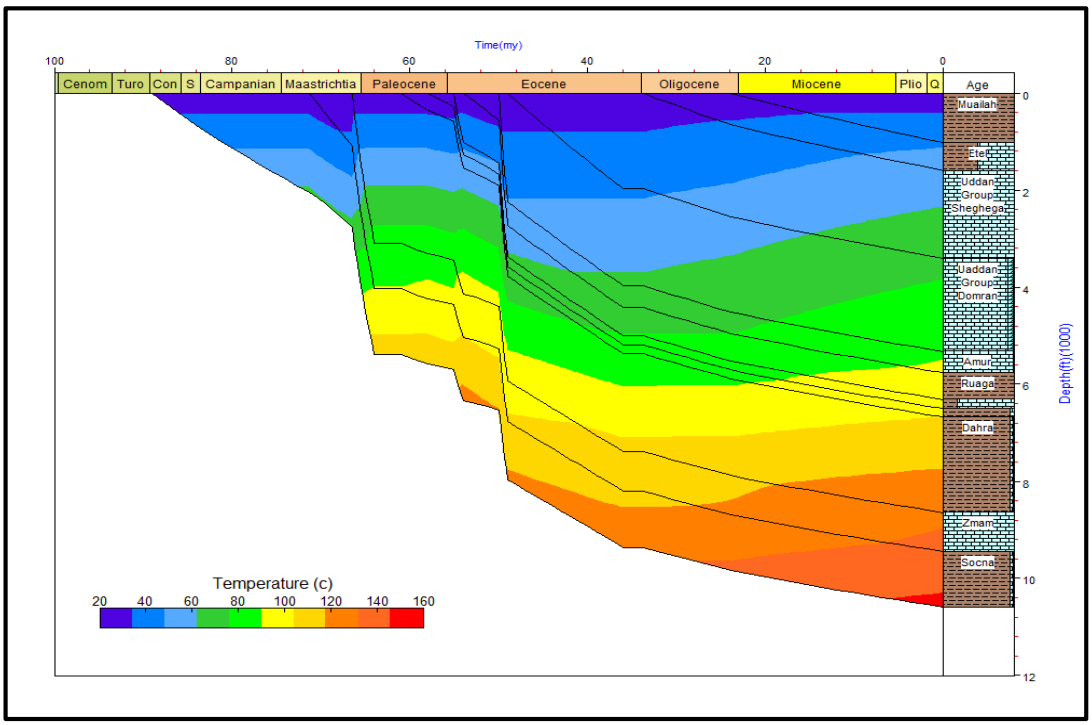

Figure 7.35: The Burial histories with temperature model for the Sirte Shale source rock in C2-16 well.

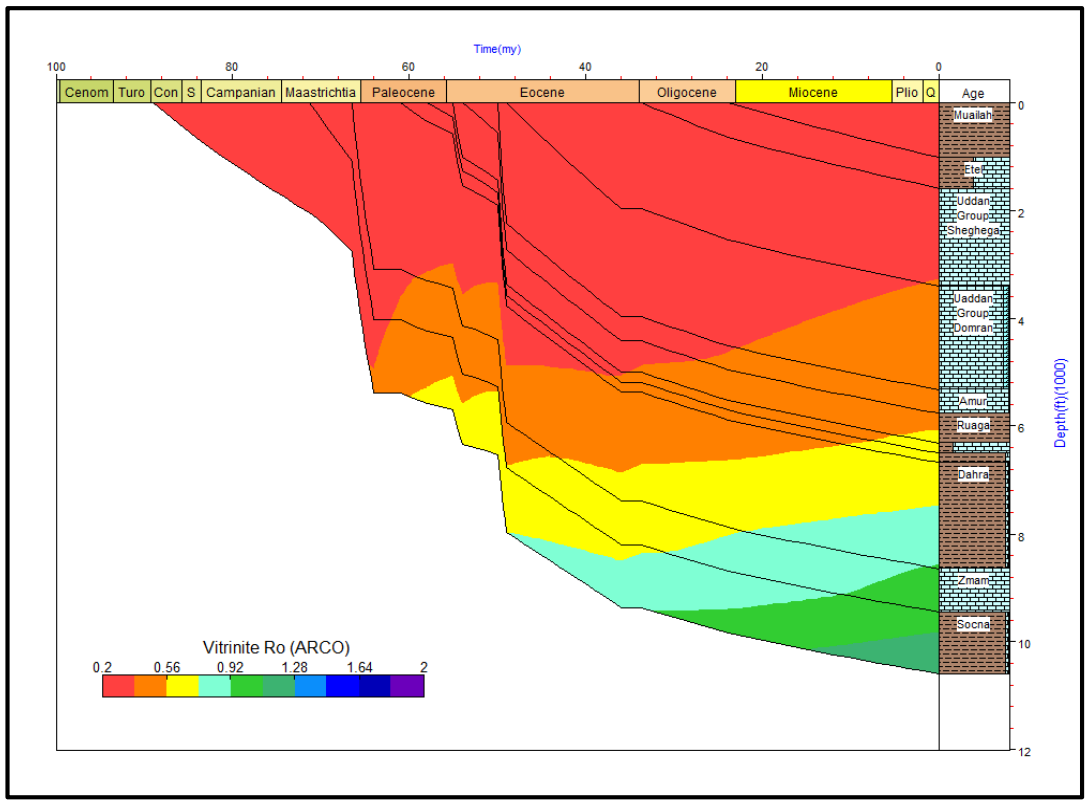

Figure 7.36: The Burial history with calculated vitrinite reflectance plot of the Sirte Shale source rock in the Marada Trough in the Sirt Basin at C2-16 well.

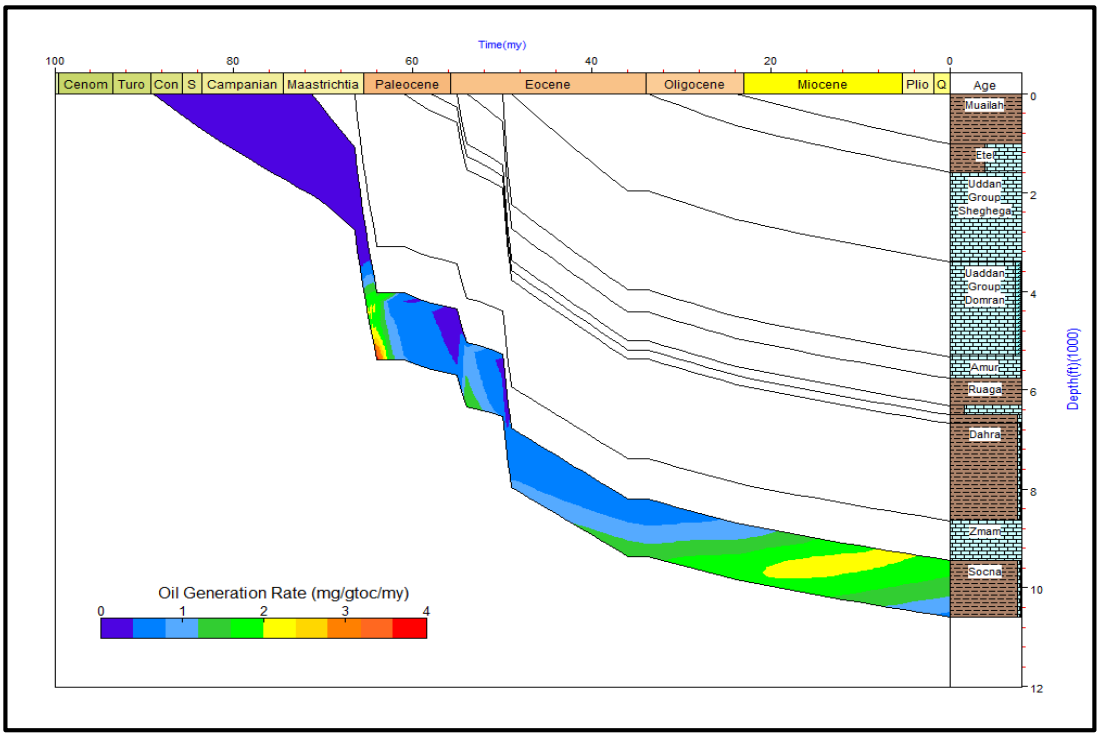

Figure 7.37: The Burial histories with oil generation plot for the Sirte Shale source rock in the Marada Trough in the Sirt Basin at C2-16 well.

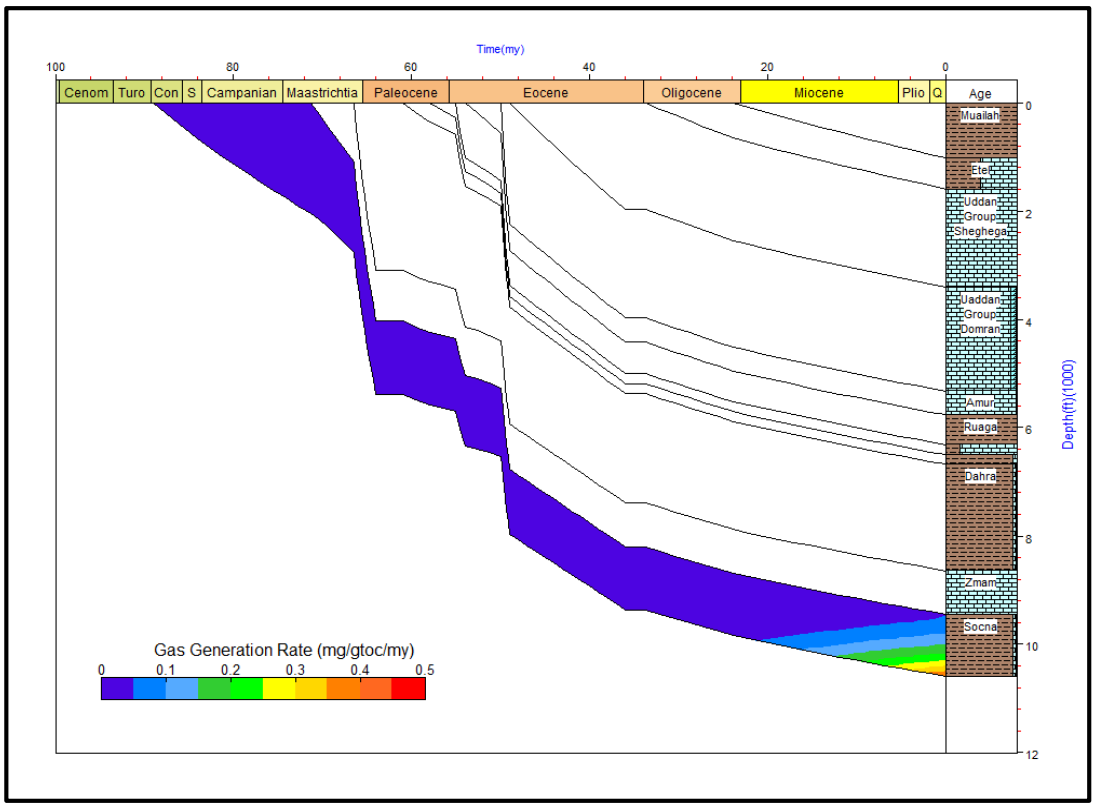

Figure 7.38: The Burial histories with gas generation plot for the Sirte Shale source rock in the Marada Trough in the Sirt Basin at C2-16 well.

The FF14-6 well is located in the Wadayat Trough in the central part of the Sirt Basin. The Sirte Shale Formation here has a thickness of around 1817 feet, and it extends from 11270 to 13087 feet. Data for stratigraphic formation tops, age, thickness of each unit accounted and lithology are expressed in Table 7.3. There is no nonconformity in the sedimentary section above the Sirte Shale source rock. The well was modelled with a value of present day heat flow of 62.71mW/m^2. The well had continuous burial throughout its history with the deepest burial in the Upper Cretaceous. The resulting calculated maturity gradient matches with the measured vitrinite reflectance, as shown in Figure 7.39. The model temperature of the Sirte Shale source rocks was 140ºC, which is sufficient to fracture the kerogen to become gaseous hydrocarbons, as shown in Figure 7.39. Figure 7.40 show burial history curves with temperature superimposed in colour. This figure shows that the calculated temperature for the top of the Sirte Shale Formation is reached at 90ºC (oil window) at a depth of 4125 feet of approximately 58Ma in the Early Palaeocene, and at 135ºC (beginning of gas window) at a depth of 9990 feet of approximately 12Ma in the Miocene. Figure 7.41 shows the calculated vitrinite reflectance values superimposed in colour upon the burial history

plot. This figure shows that the calculated vitrinite reflectance values for the Sirte Shale source rock reached 0.65*%Ro* at middle maturity at depth 7385 feet at approximately 37Ma and in the Eocene, and 0.90*%Ro* at the peak of oil generation at depth 9560 feet at approximately 19Ma in the Miocene. The model shows oil and gas hydrocarbon generation occurred in the Sirte Shale source rocks within the Palaeocene to Oligocene ages, as shown in Figure 7.42 and 7.43.

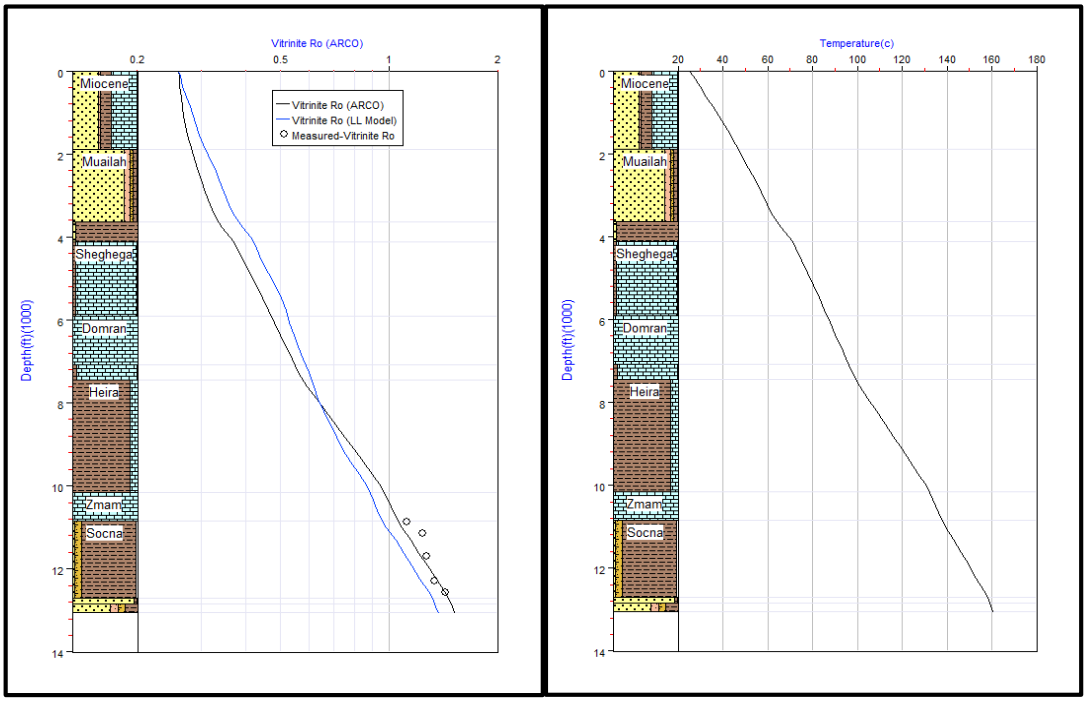

Figure 7.39: 1D Genesis software modelling of the vitrinite reflectance (%Ro) with temperature model versus depth for the Sirte Shale source rocks in the Sirt Basin at FF14-6 well.

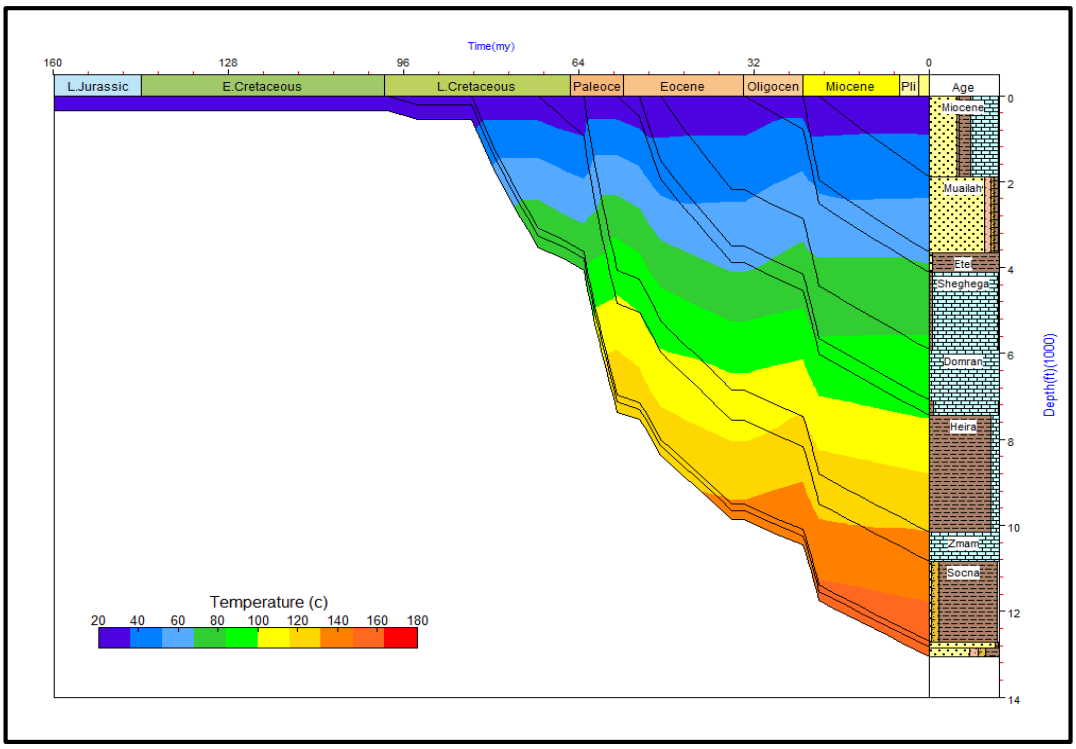

Figure 7.40: The Burial histories with temperature model for the Sirte Shale source rock in FF14-6 well.

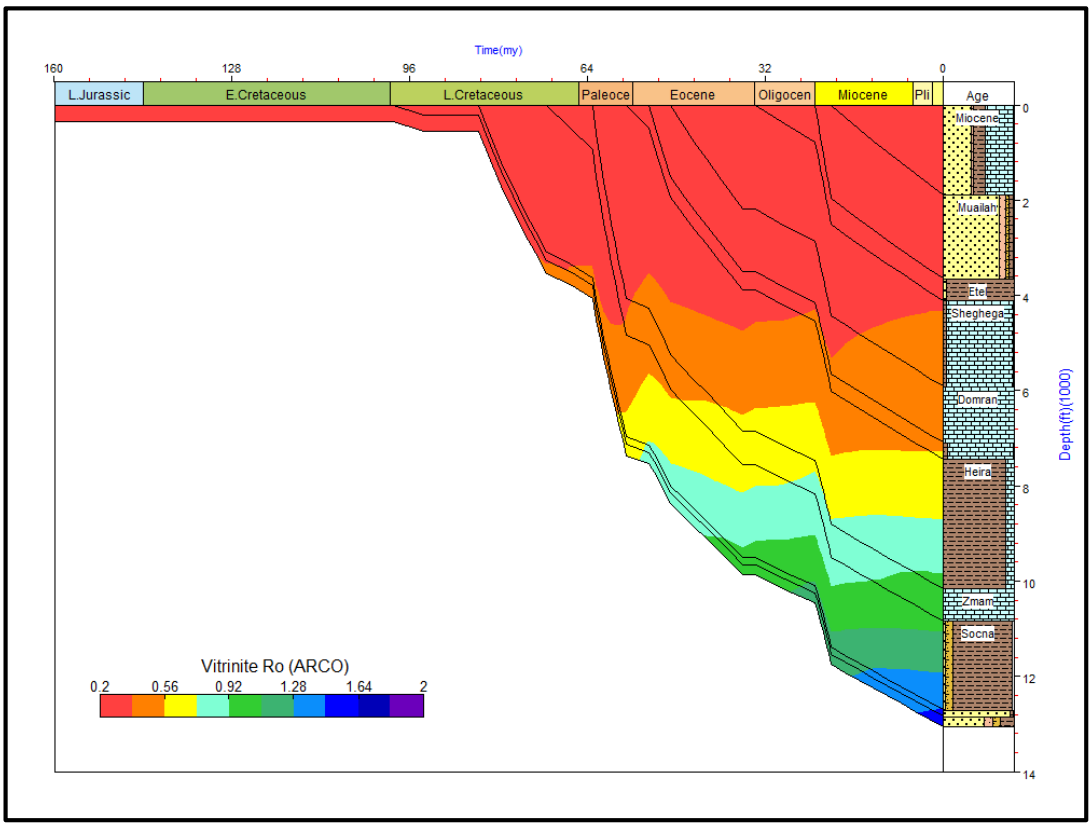

Figure 7.41: The Burial histories with calculated vitrinite reflectance plot for the Sirte Shale source rock in the Wadayat Trough in the Sirt Basin at FF14-6 well.

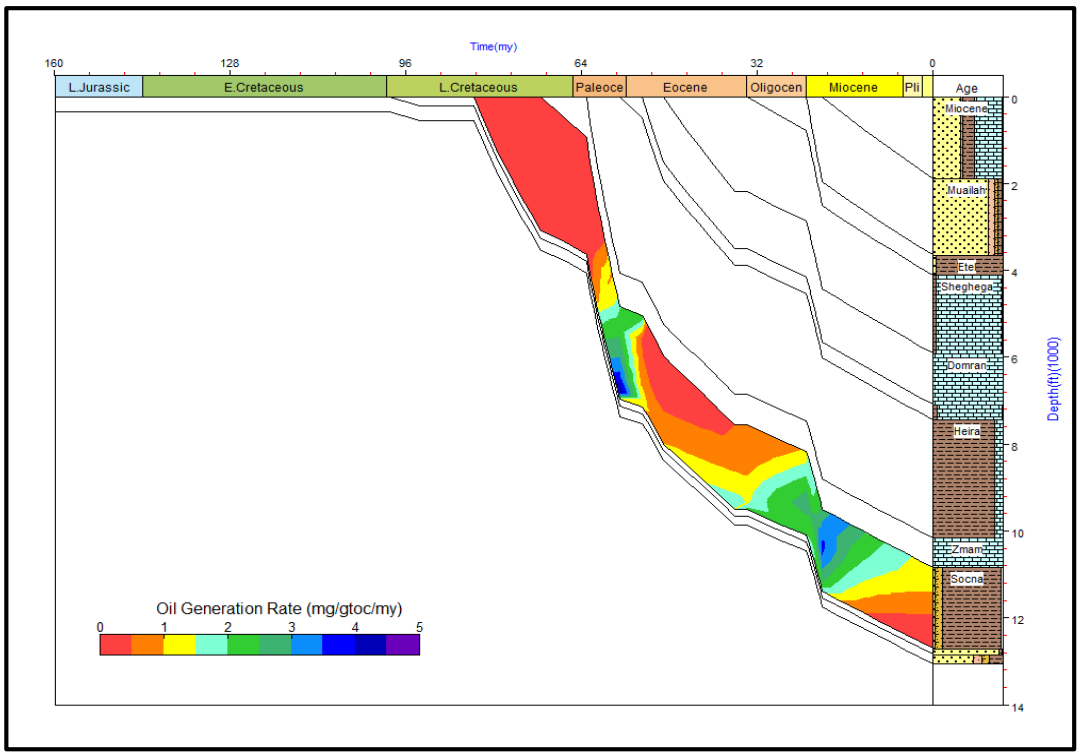

Figure 7.42: The Burial histories with oil generation plot for the Sirte Shale source rock in the Wadayat Trough in the Sirt Basin at FF14-6 well.

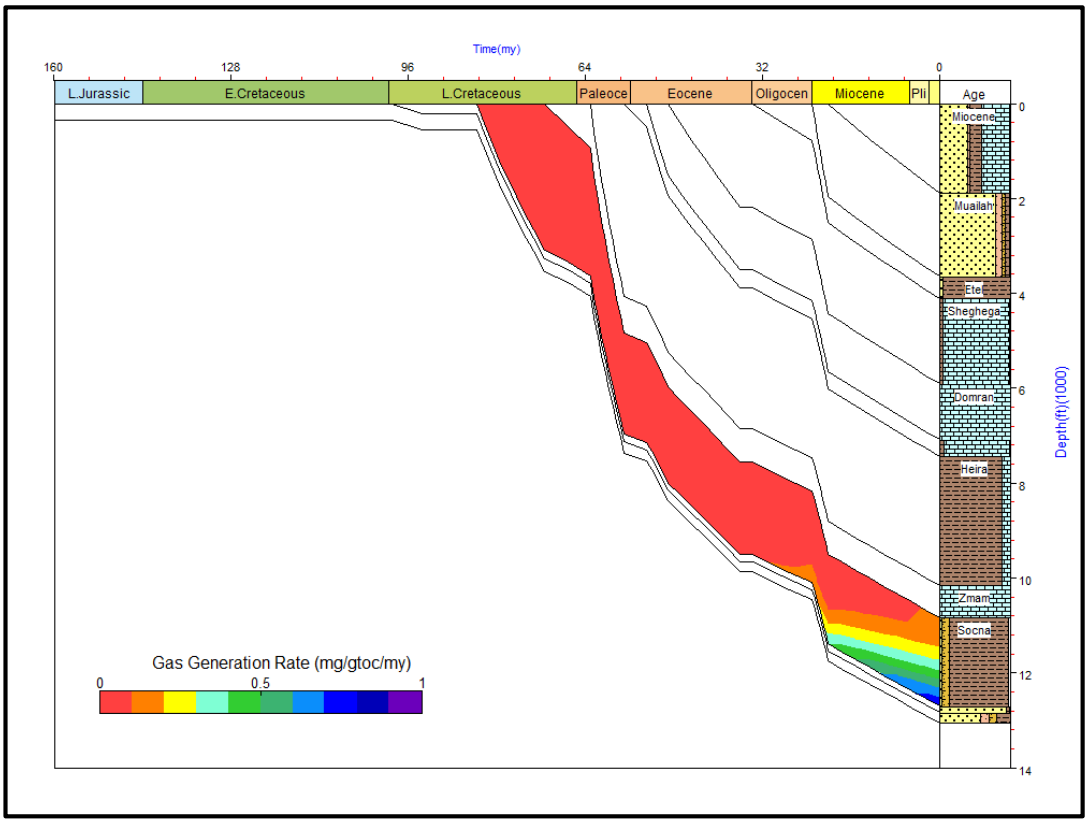

Figure 7.43: The Burial history with gas generation plot of the Sirte Shale source rock in the Wadayat Trough in the Sirt Basin at FF14-6 well.

The L1-16 well is located in the Nuflian High at the centre of the Sirt Basin. The Sirte Shale Formation here has a thickness of around of 960 feet, which extends from 7400 to 8360 feet. Data for stratigraphic formation tops, age, and thickness of each unit accounted for and lithology are shown in Table 7.3. There is nonconformity in the sedimentary section above and below the Sirte Shale source rock with uplift and erosion or non-deposition in Late Eocene times and between the Lower Cretaceous and Upper Cretaceous ages during the syn-rift phase I. The well was modelled with a present day heat flow value of 63mW/m^2. The well had continuous burial throughout its history, with the deepest burial attained in Cambro-Ordovician times. The resulting calculated maturity gradient is a good match with the measured vitrinite reflectance as shown in Figure 7. 44. The model temperature of the Sirte Shale source rocks was 85ºC, which is sufficient to fracture the kerogen to become liquid hydrocarbons, as shown in Figure 7.44. Figure 7.45 show burial history curves with temperature overlaid in colour. This figure shows that the calculated temperature for the top of the Sirte Shale Formation in the Upper Cretaceous age reached 80ºC at a depth of 5680 feet at approximately 40Ma in the Eocene. Figure 7.46 shows the calculated vitrinite reflectance values superimposed in colour upon the burial history plot. This figure shows that the calculated vitrinite reflectance values for the Sirte Shale source rock reached 0.55*%Ro* at early maturity at 6895 feet at approximately 6Ma and in the Miocene. The model shows that little hydrocarbon generation occurred in the Sirte Shale source rocks within the Miocene age, as shown in Figure 7.47.

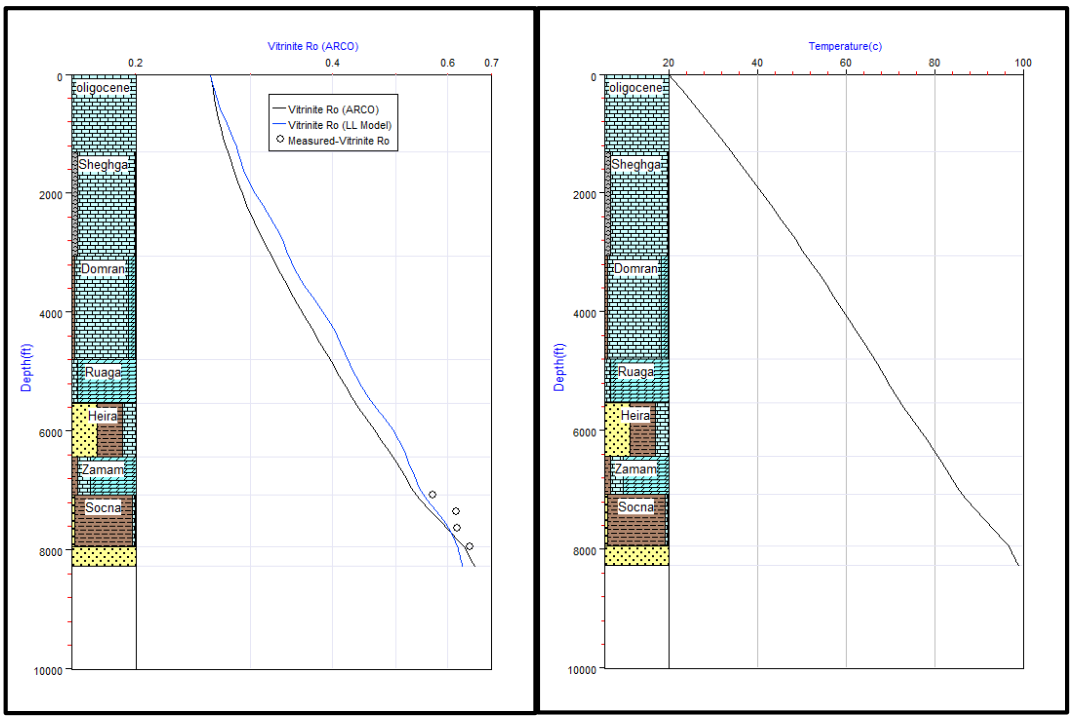

Figure 7.44: 1D Genesis software modelling of the vitrinite reflectance (*%Ro*) with temperature model versus depth for the Sirte Shale source rocks in the Sirt Basin at L1-16 well.

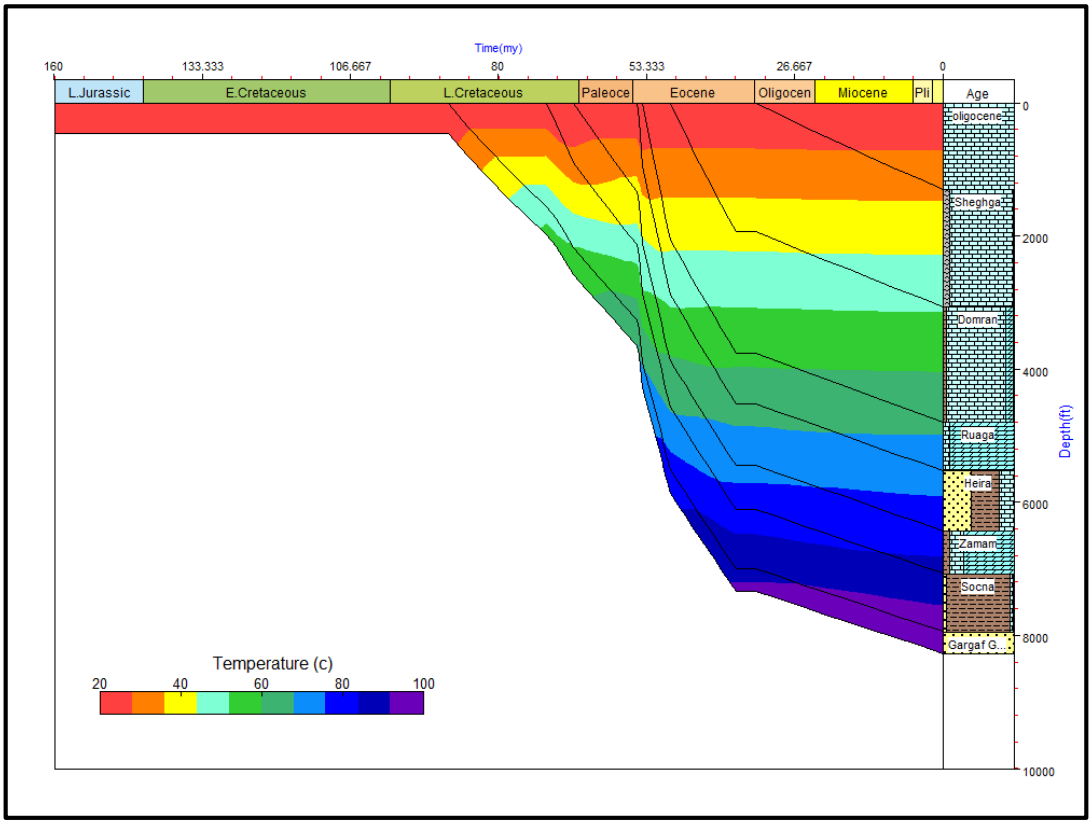

Figure 7.45: The Burial histories with temperature model for the Sirte Shale source rock in L1-16 well.

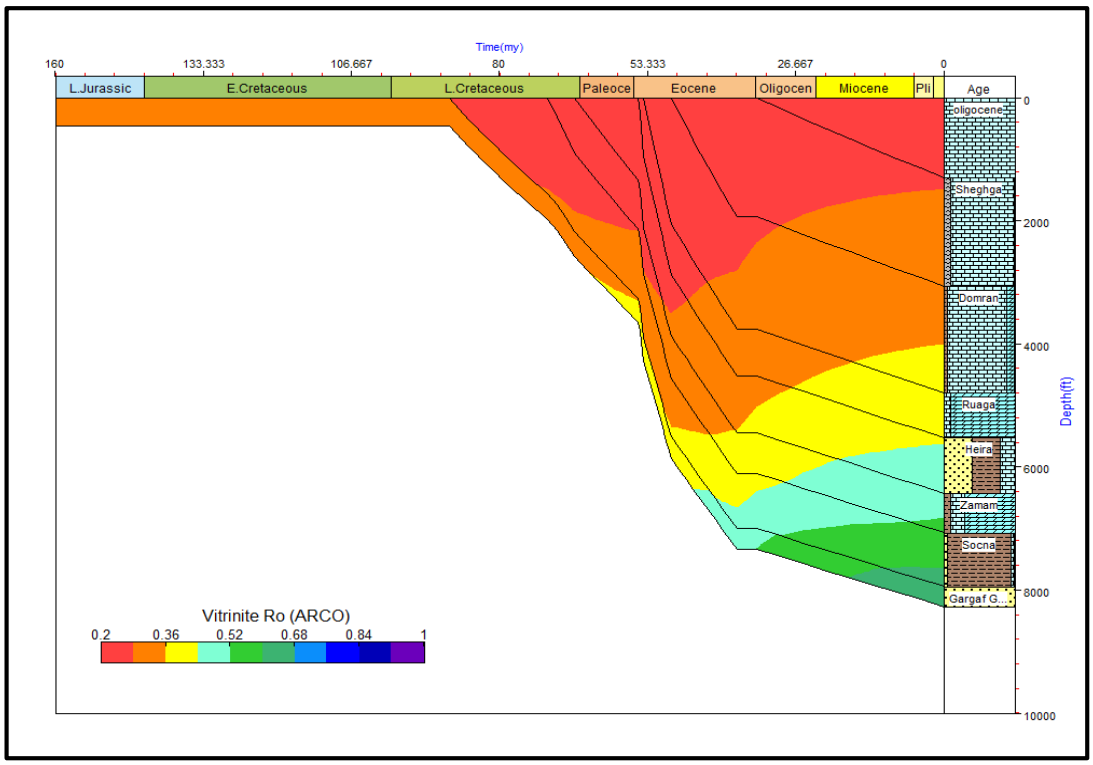

Figure 7.46: The Burial history with calculated vitrinite reflectance plot of the Sirte Shale source rock in the Nuflian high in the central Sirt Basin at L1-16 well.

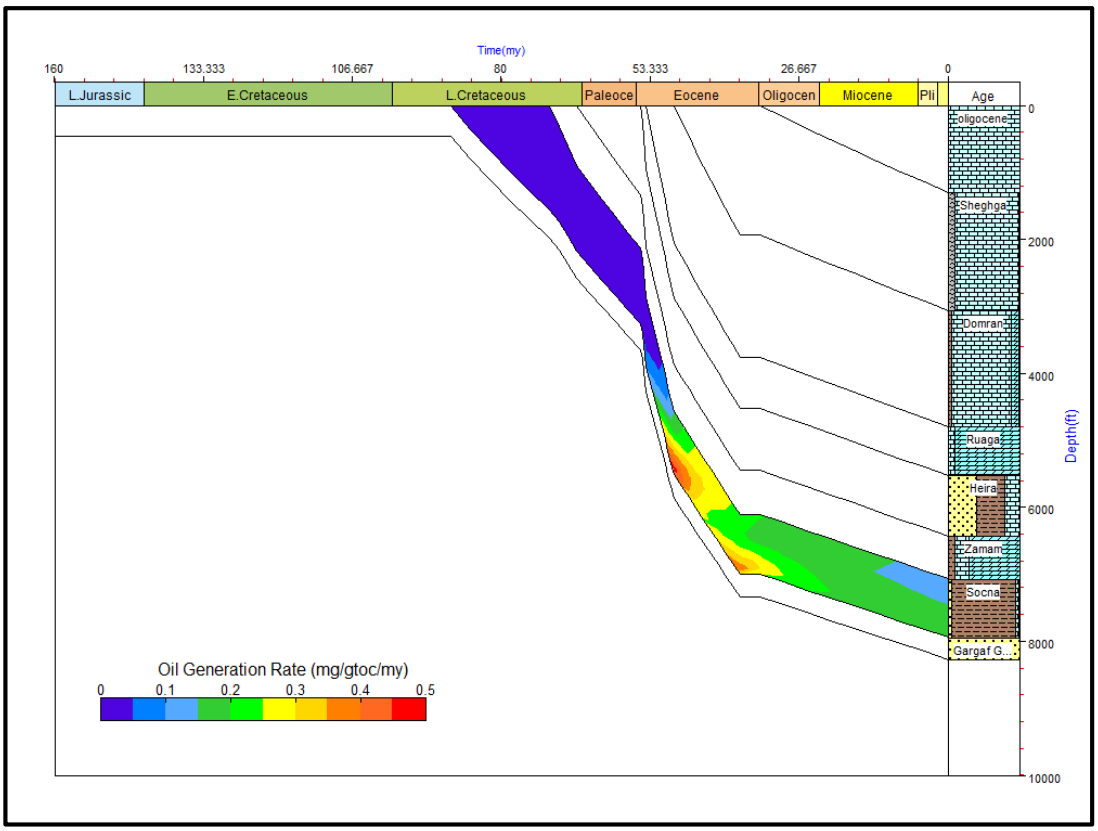

Figure 7.47: The Burial histories with oil generation plot for the Sirte Shale source rock in the Nuflian high in the central Sirt Basin at L1-16 well.

7.3.2 Petroleum Source Rock

In the present study, the Sirt Basin contains two main source rock stratigraphic intervals thought to be responsible for most of the commercial oil and gas found in the basin with some contribution from other local source rocks. These source rocks occur in the study area, and include the Upper Cretaceous sedimentary section of the Kalash, Sirte Shale and Rachmat formations, which are oil to gas prone.

7.3.2.1 Kalash Formation

The Kalash Formation is considered to be a local source rock in the study area, but has low thermal maturities make it incapable to generate significant amounts of hydrocarbons. Age determination for this formation is Maastrichtian (Barr and Weeger, 1972). It is characterized by Type II to Type II-III kerogens and is rated as having fair to good source rock potential. The source potential of the shale within the Kalash Formation is directly related to organic facies changes, which vary vertically and sometimes laterally. The environment of deposition in the Kalash Formation was suboxic to anoxic marine condition.

7.3.2.2 Sirte Shale Formation

The Sirte Shale Formation is thought to be the principal hydrocarbon source rock in the study area. It is widely distributed throughout the Sirt Basin, particularly in the Grabens region. The Sirte Shale organic matter consists mostly of Type II and Type II-III marine kerogens and it is rated as a good to very good oil generating source rock with some gas at higher maturity levels. It has been preserved in a suboxic to anoxic marine environment. The Sirte Shale is also considered as a significant source rock for gas generation, especially in the northeast Marada Trough at the centre of the basin.

7.3.2.3 Rachmat Formation

In this study, the Rachmat Formation is only penetrated in well B1-NC74F at the southeast of the Zellah Trough. It is recognized as from the Santonian to Coniacian Age. It has good source rock potential for hydrocarbon generation. The Rachmat Formation has Type II-III to Type II kerogen, and it was deposited in suboxic to anoxic marine condition.

7.3.3 Thermal Maturity of Source Rocks

In this study, maturation evaluations for the main Upper Cretaceous source rock, Sirte Shale and Rachmat formation as well as the Kalash Formation was based on vitrinite reflectance measurements. Vitrinite measurements taken for the eight wells covering the interval between 6060 to 13050 feet in the central and western Sirt Basin range between 0.51 and 1.50*%Ro*. The vitrinite reflectance values from the eight boreholes indicate that thermal maturity increases with depth. These values show that the Kalash Formation (Maastrichtian period) is immature to early mature (0.51*%Ro*), and the source rock horizon for the Sirte Shale Formation (Campanian to Maastrichtian periods) is early to middle, and late mature, ranging from 0.51 to 1.50*%Ro*. The vitrinite reflectance measurement for the Rachmat Formation (Santonian to Coniacian age) is in the early to middle mature stage. Consequently, the Upper Cretaceous source rocks from the Zellah Trough and Dor Al Abid Trough in the western part of the Sirt Basin are in the early to middle mature stages, whereas further northeast at wells situated in the Marada Trough and in the Wadayat Trough, the organic sediments are in the middle to late mature stage. Thermal maturity stages of the potential source rock vary both vertically and laterally, from being shallower at marginal areas to the deeper in central parts of the troughs, and therefore different crude oils will be generated at different temperatures and over time.

7.3.4 Reservoir Rocks

Generally, the Sirt Basin petroleum system is produced from several reservoir units that extend from the Precambrian to Oligocene periods. The hydrocarbon distributions in the Sirt Basin have been strongly controlled by major tectonic elements. The complex tectonic and sedimentary history of the Sirt Basin has created a multitude of reservoir units and conditions that favoured hydrocarbon generation, migration, and accumulation (Hamyani *et al.*, 1984; Gumati and Kanes, 1985; El-Alami *et al.*, 1989; Gumati *et al.*, 1996; Ben Ashour, 2000; Burwood *et al.*, 2003; Abadi *et al.*, 2008). These oil reservoirs are mostly composed of Mesozoic clastic rocks and Tertiary carbonate rocks. Gumati *et al.* (1996) showed that the major reservoir units in the Sirt Basin are situated in the fracture basement of the Precambrian rocks and also in Cambro-Ordovician sandstone of the Gargaf Group in the Amal, Augila and Nafoora

oilfields in the eastern part of the Sirt Basin. Whereas in the Sarir, Amal, Augila, and Abutfill oilfields, the lower Cretaceous Nubian Formation is considered the main reservoir unit which produces hydrocarbons in the eastern part of the Sirt Basin. Generally in the Sirt Basin, Cambro-Ordovician sandstone, Lower Cretaceous and Upper Jurassic clastic rocks, carbonate rocks of the Upper Cretaceous and Palaeocene reefs represent the main reservoir units such as in the Hofra, Bahi, Lidam, Kalash, Beda, Satal, Zelten, Dahra, and Mabruk formations in the central and western Sirt Basin (Gumati *et al.*, 1996; Ben Ashour, 2000; Hallett, 2002; Abadi *et al.*, 2008). These reservoir units have potentially moderate to large thickness, accompanied with structures Horst blocks that maybe juxtaposed to the Sirte Shale source rock, making them potential exploration drilling objects (Goudarzi, 1980; Hamyani *et al.*, 1984; El-Alami *et al.*, 1989; Gumati *et al.*, 1996; Hallett and El Ghoul, 1996; Roohi, 1996; Roohi, 1996b; Hallett, 2002; Abadi *et al.*, 2008). However, in the study area, the Cambro-Ordovician and Cretaceous reservoirs are considered insignificant because no commercial oil has been found. This may be due to lack of an effective channel between the source rock and reservoirs beneath the Sirte Shale source rock. Only the Kalash Limestone has established a variable reservoir in platform areas where nearshore facies are developed. Rocks from the Palaeocene and Eocene periods represent the major reservoir units in the study area.

7.3.4.1 Hofra Sandstone Formation

The Hofra Sandstone Formation from the Cambro-Ordovician age is comprised of clean quartz sandstone with trace amounts of shale, siltstone, conglomerate and a thin interbedding of volcanic rocks. It has a thickness of 1105m, which increases to around 1369m towards the northwest (Barr and Weeger, 1972; Hallett, 2002). It is characterized by the presence of secondary fracture porosity and produces oil in the Belhedan, Ora, Raguba and Samah oilfields. It could be equivalent to the Amal Formation in the eastern part of the Sirt Basin (Hallett, 2002; Aboglila, 2011).

7.3.4.2 Bahi Sandstone Formation

The Bahi Sandstone Formation of the Cenomanian, Upper Cretaceous age consists of interbedded sandstone, siltstone, conglomerate and shale. It is characterized by a

predominance of sandstone (Barr and Weeger, 1972; Hallett, 2002; Abadi *et al.*, 2008). It has varied thicknesses ranging from a few metres to a maximum of about 122 metres (Barr and Weeger, 1972). It has varying porosity between 12 to 28% associated with a permeability of about 150md. It is an oil producing reservoir unit in the Bahi oilfield, but in the study area has only been recorded as having oil show in some wells.

7.3.4.3 Lidam Formation

The Lidam Formation of the Cenomanian, Upper Cretaceous age is comprised of dolomite with sandstone. The formation represents the first distinctive marine deposit overlying the basement rocks, and Palaeozoic strata (Barr and Weeger, 1972). It usually overlies the Bahi Sandstone Formation in the western part of the Sirt Basin. It has a variable thickness ranging between a few metres to 20 metres, and a porosity ranging from 10 to 20%. The only significant oil show has been observed from several wells in the Bahi oilfield.

7.3.4.4 Kalash Limestone Formation

The Kalash Limestone Formation of the Maastrichtian, Upper Cretaceous age is comprised of limestone, dolomite and shale with sandstone (Barr and Weeger, 1972). The Kalash Formation is widespread in the Sirt Basin and has varying thickness mostly between 100 to 200 feet (30 to 60 metres) in the study area, but could have greater thickness in the deepest part of the basin of up to 1500 feet (600m), particularly in the Agedabia Trough in the eastern Sirt Basin (Abadi *et al.*, 2008). It has a porosity range between 15 to 25%. Some oil show has been recorded in wells in the Bahi oilfield.

7.3.4.5 Satal Carbonate Formation

The Satal Formation carbonate rocks of the Maastrichtian–Danian age occur on the subsurface of the western Sirt Basin. It is restricted in the area distribution to the Al Beda and Dahra-Hofra Platforms. The Satal Formation is subdivided into two members (Barr and Weeger, 1972). The Lower member of the Upper Cretaceous age consists mainly of limestone with thin dolomite and shale. The upper member of the Palaeocene age consists of dolomite, anhydrite and shale beds. Contact with the underlain Sirte Shale Formation is often conformable, but unconformable with the Hofra Formation of

Cambro-Ordovician age. The upper contact is sharp, but seems to be conformable with the Thalith Member of the Beda Formation of the Middle Palaeocene age (Barr and Weeger, 1972). The Satal Formation is considered one of the principal oil reservoir units in the western Sirt Basin. It has produced oil only in the Al Dahra-Al Hofra Platform, and in the Ali, Arbab and Almas oilfields. The Upper Satal Formation has a thickness of about 130 metres with an excellent porosity of 20% to 30% and good permeability.

7.3.4.6 Beda Formation

The Beda Formation Seladndian of the Palaeocene age is widely distributed in the western Sirt Basin. The formation consists of various interbedded limestones with calcareous shale and dolomite. However, the Beda Formation becomes shalier in the northwest of the basin. It is subdivided into two members, the upper Rabia Shale Member and the lower Thalith Member (Barr and Weeger, 1972). The Thalith member is dominated by argillaceous limestone with minor amounts of shale or chalky marl. It is about 90 feet (35m) thick. The lower contact is conformable with the Hagfa Shale or Satal Formation, where upper contact is conformable with the Rabia Shale Member. The Rabia Shale Member is predominantly composed of shale and mudstone with minor amounts of interbedded limestone. It has a thickness of about 180 feet (70m). It is conformable with both the underlain Thalith Member and overlain Dahra Formation. In the study area, the Thalith member of the Beda Formation is found to be oil-bearing in most oilfields, for the most part; those south of the Waddan Uplift where the Beda is productive in the structural trap.

In the Zellah Trough, the Beda Formation reaches a maximum thickness of 1650 feet (500m) with an average of 592 feet (180m) in the platform (Bezan *et al.*, 1996).

On the other hand, Bezan *et al.* (1996) subdivided the Beda Formation into two members, the lower Beda Farrud Member and upper Beda Ora Member in the Dahra field, and the Zellah Trough in the western Sirt Basin. The Farrud Member consists of skeletal oolitic calcarenite limestone transient to dolomite. It has excellent reservoir characteristics, and is oil-producing in several oilfields such as the Ghani field. It has a thickness of about 150 feet (45m). The Farrud Member was deposited in a shallow marine environment. Porosity in this member ranges as high as 35% (Bezan *et al.*,

1996). The Ora Member of the Upper Beda Formation comprises mainly of dolomite. The member has varying thickness, ranging from 30 to 333 feet (12 to 100m) in the Beda Platform and Kotla Graben respectively. This member is oil-producing for several oilfields in the Beda Platform. At the Wadi oilfield, the Lower Beda carbonate Formation is found to be restricted between two deeper shale sections. This carbonate unit has been found to contain oil at the Wadi and Zaqqut oilfields.

7.3.4.7 Dahra Formation

The Dahra Formation, Thanetian period of the Palaeocene age, is widespread in the western Sirt Basin. The formation is composed of limestone and dolomite with thin interbedded shale (Barr and Weeger, 1972; Hallett, 2002; Abadi *et al.*, 2008). However, in the direction of the south-western part of the Sirt Basin, the lower part changes to shale. The Dahra Formation has recorded thicknesses reaching up to 333 feet (100m). The lower boundary is conformable with the Rabia Shale Member of the Beda Formation and the upper contact is conformable with the Khalifa Formation. The Dahra Formation forms the main reservoir unit in the Dahra-Hofra oilfields. The formation has a porosity ranging between 15 and 25% in limestone sections and represents a good to very good reservoir (El-Alami *et al.*, 1989; Gumati *et al.*, 1996; Mansour and Magairyah, 1996; Roohi, 1996; Roohi, 1996b; Hallett, 2002). In the study area, the Dahra Formation produces oil in most of the oilfields. These oilfields are situated along the western part of the Dahra-Hofra Platform, which is a prominent tectonic structural feature of the area. Most of these oilfields are predominantly with structure traps. Within the Mabruk, Facha, Tagrifet, Qsur, Dahra, Aswad, and Safsaf oilfields, the Dahra Formation is considered the main reservoir, and has a fair reservoir quality (Roohi, 1996b; Hallett, 2002) .

7.3.4.8 Zelten Formation

The Thanetian Zelten Formation of the Late Palaeocene age is well distributed in the the Sirt Basin. It consists of limestone with some dolomite (Barr and Weeger, 1972; Roohi, 1996). It conformably overlies the Khalifa Formation or Lower Sabil Carbonate, and the conformable overlain Harash Formation (Barr and Weeger, 1972). The Formation has various variation in thickness recorded in the Zellah and Marada

Troughs at about 460 feet (140m), and at over 500 feet (150m) in the Agedabia Trough. It has a porosity reaching up to 40% in the Nasser oilfield. The formation forms the reservoir rock unit for the Nasser oilfield situated on the Zelten Platform. In the study area, the Zelten Formation is considered to be a non-commercial oil-producing rock because has relatively poor reservoir quality and also due to the lack of an adequate seal with the upper Harash Formation. The absence of a seal may represent the main reason for the Zelten Formation not being a significant reservoir in the study area.

7.3.4.9 Harash Formation

The Harash Formation of the Thanetian of the Late Palaeocene age is comprised of chalky, argillaceous limestone with minor interbedded shale. It is conformably overlain by the Kheir Formation and the Facha Dolomite Member of the Gir Formation, and also conformable with the underlain Khalifa Formation. It has thicknesses varying between 75 and 100 feet (23-30m), and is recognized as of poor reservoir quality (Barr and Weeger, 1972; Hallett, 2002). In the Dahra oilfield, traces of oil show are observed from several wells in the highest structural locations.

7.3.4.10 Facha Dolomite Member (Gir Formation)

The Facha Member of the Gir Formation of the Eocene age is confined to the western Sirt Basin and consists mainly of massive dolomite with minor amounts of anhydrite (Barr and Weeger, 1972). It is conformable with the overlain Hun Evaporite Member. It was deposited in an open marine environment and has a thickness range between 300 to 500 feet (100-150m). The porous dolomite of the Facha Member is a significant oil reservoir unit (20 to 25%) in the Zellah Trough. Elag (1996) studied the Facha dolomite Member from several wells and observed that its upper part is considered the best reservoir unit in the Zellah Trough. The Facha Member represents the main reservoir unit in many oilfields in the study area, such as the Ghani, Fidda, and Hakim oilfields. The Hun Evaporite Member represents the seal for this reservoir.

7.3.4.11 Hun Evaporite (Gir Formation)

The Hun Evaporite Member of the Gir Formation of the Eocene age consists of interbedded anhydrite and dolomite with minor amounts of shale. Its thickness varies

from 1625 to 3500 feet (490 to 1060m) in the Zellah Trough (Barr and Weeger, 1972). It represents the middle member of the Gir Formation having conformable contact boundaries with the upper Member Mesdar Limestone and the lower Facha Dolomite Member. It has a porosity range between 25 to 28%. Oil has been found in the dolomite reservoir unit from the bottom to around the middle of the Hun Member.

7.3.5 Seal Rock

In the Zellah Trough two major seals exist in the Palaeocene and Eocene sequences. The Rabia Member of the Beda Formation and Khalifa Formation represent the main Palaeocene seals (Barr and Weeger, 1972; Hamyani *et al.*, 1984; Gumati and Kanes, 1985; Hallett, 2002; Abadi *et al.*, 2008). The Khalifa Formation of the Lower Palaeocene period consists of lower shale unit sequences of about 335 feet (100m) and an upper argillaceous limestone unit of around 190 feet (60m). The Rabia Member of the Beda Formation of the Middle Palaeocene period contains shale and mudstone with minor limestone interbedded, and has a thickness of about 230 feet (69m). Both are widespread in the western and central Sirt Basin. The Rabia Member and Khalifa Shale unit represent the main seal for most of the Palaeocene reservoir in the central and western part of the Sirt Basin, particularly for the Dahra, Beda, and Satal formations (Parsons *et al.*, 1980; Hamyani *et al.*, 1984; Gumati and Kanes, 1985; Hallett, 2002; Burwood *et al.*, 2003).

The Hun Evaporite Member of the Gir Formation of the Eocene period forms the main seal for the Facha and Hun dolomite reservoirs. The evaporite section has a thickness over 1950 feet (600m) in the Zellah Trough (El-Alami *et al.*, 1989; Hallett, 2002; Abadi *et al.*, 2008).

7.3.6 Overburden Rocks

The very thick Upper Cretaceous-Tertiary marine sediments are associated with many source rocks in the troughs in the region and relate to many reservoir rocks in the platforms which provide excellent conditions for hydrocarbon generation and accumulation in the Sirt Basin (Gumati and Kanes, 1985; Gumati and Schamel, 1988; Gumati *et al.*, 1996; Roohi, 1996; Roohi, 1996b; Hallett, 2002). The northeast-southeast-trending Horst and Graben structures formed in the Sirt Basin from the Late

Cretaceous to the end of the Palaeocene periods in the central and western part of the Sirt Basin (Ahlbrandt, 2001). The overburden was largely deposited during pre-rift and early syn-rift deposition and is comprised of clastic rocks during the Cambro-Ordovician and Upper Jurassic-Lower Cretaceous stages, while later syn-rift deposition was dominated by carbonate and clastic sediments during the Upper Cretaceous-Palaeocene stage. The overburden was largely deposited during post-rift sedimentation during the Oligocene-Miocene stage and comprised of clastics and carbonate rocks.

7.3.7 **Traps**

Traps in the Sirt Basin are structural traps formed during Eocene tectonics. In the study area, typical structure traps range from normal to complex faults and fold structures sometimes associated with wrench faults (Gumati and Kanes, 1985; Gumati and Schamel, 1988; Abadi *et al.*, 2008). The faults are considered the main reason for the trapping mechanism in several reservoir units, as shown in the trends in the structural map of the Sirt Basin. In addition, several types of stratigraphic trap are present in the central and western part of the Sirt Basin (Parsons *et al.*, 1980; Gumati and Kanes, 1985; Baird *et al.*, 1996; Gumati *et al.*, 1996; Roohi, 1996; Roohi, 1996b). They are characterized by lithological facies changes from carbonate to argillaceous carbonate to shale in the Dahra and Beda reservoir units. The Satal carbonate bank of the Lower Palaeocene age represents a major reservoir in many oilfields in the western Sirt Basin. Hallett (2002) reported that the Dahra and Hofra oilfields are much bigger than the other oilfields located in the Al Dahra-Al Hofra Platform, because they have a rollover or fold component to them.

However, structural traps are predominant in the Zellah Trough and almost all are related to the Eocene tectonic structure that created faults in the western part of the Sirt Basin (Parsons *et al.*, 1980; El-Alami *et al.*, 1989; Roohi, 1996; Schröter, 1996; Roohi, 1996b; Hallett, 2002; Abadi *et al.*, 2008). Schröter (1996) observed that the Ghani and Adh Dhib oilfields are situated on the Ar Ramlah Syncline in the centre of the Zellah Trough and most fault closures are on the western margin of tilted fault blocks, while the Hakim and Fidda oilfields are located on the Ma Amir Graben. The Mabruk and Facha oilfields are located on the up-dip side of the depocenter of the Dor Al Abdi Trough, and this is associated with a north-westerly trending anticlines fault. Most of

the Zellah field group is composed of larger anticline structures (Roohi, 1996; Schröter, 1996). In the area of the narrow Subbasin joining the Abu Tumayam Trough to the Zellah Trough in the Sabah oilfield an anticline fault is at shallower depth (Roohi, 1996; Schröter, 1996). In addition, Knyth *et al.* (1996) reported that there are combination of drag folds and wrench faults in the southern part of the Zellah Trough; they create spectacular flower structures, which may form traps for several small oil pools. Parsons *et al.* (1980) reported that more than 80% of the oil discovered in the Sirt Basin is found in structural traps.

7.3.8 **Timing of Oil Generation**

Figure 7.19 shows the history of petroleum generating in the 6A1-59 well in the Zellah Trough. The figures show that the Kalash and Sirte Shale source rock are in the immature to early mature stage, and therefore no hydrocarbon generation can be anticipated from these source rocks.

As shown in Figure 7.22 for well B1-NC74F in the Zellah Trough, the Sirte Shale source rock was immature until the present day; therefore, no hydrocarbon generation can be anticipated from the Sirte shale Formation. The shale interval in the Rachmat source rock reached the onset of oil generation at approximately 20Ma at Miocene time, but has not reached its peak of oil generation until the present day due to low maturity.

Figure 7.25 shows the oil generation history of the well L1-17 in the Dor Al Abid Trough. The figure shows that the Sirte Shale source rock was generally immature until the late Oligocene at 28.5Ma. The onset of oil generation in the Sirte Shale occurred at around 12Ma in the Miocene, but has not reached the peak of oil generation until the present day due to low maturity.

Figure 7.29 shows the oil generation history of the well B2-NC74A in the Zellah Trough. The Sirte Shale source rock was immature until Oligocene times at approximately 33Ma, and the onset of oil generation started at around 22Ma in the Miocene, but has not reached the peak of oil generation until the present day due to low maturity.

As shown in Figure 7.33 for well Z1-11 in the Tagrifet Trough, the Sirte Shale source rock was immature until the Eocene at 38Ma since which time it has generated little oil, but it has not reached the peak of oil generation due to lower maturity.

Figures 7.37 and 7.38, shows the petroleum generation history of the well C2-16 in the Marada Trough. The Sirte Shale source rock was generally immature until the Early Eocene at around 58Ma, from which time it has generated hydrocarbons. The onset of oil generation occurred at about 53Ma, and the peak of oil generation started at approximately 20Ma in the Early Miocene. The source rock became mature for gas generation at approximately 2Ma in the Pliocene and has generated oil and gas up till the present day.

As shown in Figures 7.42 and 7.43 for the FF14-6 well in Wadayat Trough, the Sirte Shale source rock was generally immature until the Palaeocene to Early Eocene at about 59Ma. The onset of oil generation in the Sirte Shale began at about 52Ma in the Eocene. The source rock became mature for oil generation about 35Ma with peak oil generation beginning approximately at 19Ma in the Miocene, and it became mature for gas generation at about 9Ma in the Miocene until the present day.

Figure 7.47 shows the petroleum generation history of well L1-16 in the Nuflian High in the central Sirt Basin. The Sirte Shale source rock was generally immature until the Middle Miocene time at around 13Ma, from which time it has generated little hydrocarbons. The onset of oil generation occurred at about 8Ma, the peak of oil generation has not been reached due to lower maturity.

At present day, the Sirte Shale in deeper parts of the Marada Trough and the Wadayat Trough area in the central Sirt Basin is generating oil to condensate to gas, while the Dor Al Abid and Tagrifet troughs generate a little oil. In the Zellah and Dor Al Abid troughs and Nuflian High, at the study wells 6A1-59, B1-NC74F, B2-NC74A, L1-16, and L1-17 is generating a little to moderate oil.

7.3.9 **Migration**

In general, most of the hydrocarbon migration in the Sirt Basin occurred when the Upper Cretaceous organic-rich rocks entered the oil window during the late Oligocene and Miocene times (Parsons *et al.*, 1980; El-Alami *et al.*, 1989; El-Alami, 1996; Hallett and El Ghoul, 1996; Roohi, 1996; Roohi, 1996b; Ben Ashour, 2000; Hallett, 2002). It is recognized that major oil accumulations in the Sirt Basin occurred on platform regions near to the oil generative depressions and this may suggest generally short lateral distances of oil migration as shown in Figure 7.48. This may be attributed to low

permeability to impermeability within carbonate facies variations that represent the carrier beds (Thomas, 1995). Hallett (2002) provided evidence that, during the eastward tilting of the basin, oil migrated from source rock to traps in the western Sirt Basin mainly from the northeast to southwest trends. Most of the hydrocarbons found in the platforms are thought to have migrated from neighbouring troughs. However, migration of the platforms was achieved by flowage up fault channels on the eastern boundary fault of the platforms and into the porous carrier bed (Roohi, 1996b; Hallett, 2002). After that westward migration occurred, but this was after trap formation was established and much of the hydrocarbons migrated to the extent of the western margin of the platform (Roohi, 1996b; Hallett, 2002). The north-central area consists of several gas fields which are thought to have migrated from the deepest gas source kitchen in the Marada and Agedabia troughs (El-Alami *et al.*, 1989; Roohi, 1996b; Hallett, 2002). Harding (1984) established that the Sirt Basin is dominated by with a petroleum system vertical migration, but lateral migration could also be found. Price (1980) demonstrated that the Upper Cretaceous source rock is responsible for charging most of the multiple reservoir units beside the faulty region closest to the Horsts and Grabens. Guiraud and Bosworth (1997) established the significance of the right-lateral wrench fault system of the Santonian age, and pointed out that the periodic rejuvenation of these fault systems in the Sirt Basin was particularly important in the vertical migration of hydrocarbons. Pratsch (1991) reported that the Sirt Basin was an example of lateral migration and vertically stacked hydrocarbon systems isolated from each other.

On the other hand El-Alami *et al.* (1989) suggested that all oils in the western part of the Sirt Basin have been charged from mature, rich source rock in the northwest of the Zellah Trough and Kotla Graben. They also demonstrated that most of the significant oil accumulations have migrated from the source rock kitchen from the east to the west. These oils have been trapped in the neighbouring Horst after a short distance of vertical migration in an up-faults throughout the porous carrier beds. Roohi (1996b) has established that the present structural configuration of the Sirt Basin, accompanied by the mature potential source rock in the Agedabia and Marada troughs, is considered to be the main sites of major hydrocarbon generation for the accumulations found in the Beda and Al Dahra-Al Hofra Platforms in the western Sirt Basin, and these show a mainly W-SW trend of hydrocarbon migration. Roohi (1996b) reported that, in the eastern Sirt Basin, the peak of oil generation occurred mainly during the Oligocene-

Miocene age when the burial depth of the source rocks was at 4000 metres or more deeper. Therefore, hydrocarbon generation, migration and accumulation occurred mainly after the huge post Eocene subsidence, when the present structural configuration of the basin was established. At that time, the source rock in the Zellah Trough in the west of the basin was still marginally mature.

El-Alami *et al.* (1989) suggested that the Dahra oilfield over the Al Dahra-Al Hofra Platform could have been charged from the adjacent western depression by the vertical migration through the Gedair fault. Meanwhile the oilfields situated to the west of the depression, such as the Hakim and Zellah oilfields could have been charged from oil moving vertically and laterally to the reservoirs, and therefore the migration distances for both vertical and lateral components is relatively short. This contrasts with the Mabruk oilfield, which may charge from a slightly longer lateral migration distance from the western depression to the north. It is still thought that most of the oil discovered enclose to the Al Dahra-Al Hofra Platform is charged from the western depression. In the study area, some geochemical evidence suggests that hydrocarbons have both vertical and lateral components, over relatively short distances.

El-Alami *et al.* (1989) reported that the Dahra-Hofra oil field was sourced from Sirte Shale kitchen source rock in the Zellah Trough, by migrating up the platform bounding fault. But Roohi (1996) and Hallett (2002) argued that from the substantial Neogene subsidence history of the area and the situation of the Dahra-Hofra oilfields adjacent to the early mature source kitchen, it is difficult to see how these large fields could have been charged from the Zellah Trough. Therefore, the generating capacity of the immature to early mature source kitchen in the Zellah Trough was probably insufficient to fill the giant oilfields in the Al Dahra-Al Hofra Platform. But this study has established that the geochemical evidence from carbazole and benzocarbazole data indicate a short migration distance, which is contrary to the suggestion by Roohi (1996b) that the Dahra-Hofra Oilfield was charged over long migration distances from the Marada and Agedabia troughs. The current study has observed that Mabruk oilfield in the northwest part of the basin was charged from the Sirte Shale source rock at the north of the Zellah Trough and/or from Dor Al Abid Trough, suggesting short to moderate distance of migration. Meanwhile the hydrocarbons in the Aswad, Zellah, Hakim, Safsaf, Fidda and Sabah oilfields in the southwest part of the basin were thought to be charged from the Sirte Shale source rock or maybe older source rocks in

the Zellah Trough that perhaps have migrated laterally, which may indicate moderate distances of migration. The Nasser, Raiah, South Jebel, Raguba, west Meghil, Zelten, Kotla, Dor Mansur in the central part of the basin were charged from the Sirte Shale and Rachmat source rocks at the Marada Trough and Kotla Graben, suggesting relatively short distance vertical migration. In contrast to the Augila Nafoora, Tuamma, As Sarah, Nakhla oilfields and NC125 that generated oils from Sirte Shale, Rachmat source rocks and/or Middle Nubian Shale source rocks in the Agedabia Trough in the eastern part of the basin, suggesting relatively short distance migration. Therefore, the hydrocarbons that accumulated in those oilfields were migrated vertically from the source rocks to near reservoirs throughout the faults joints in the Agedabia Trough.

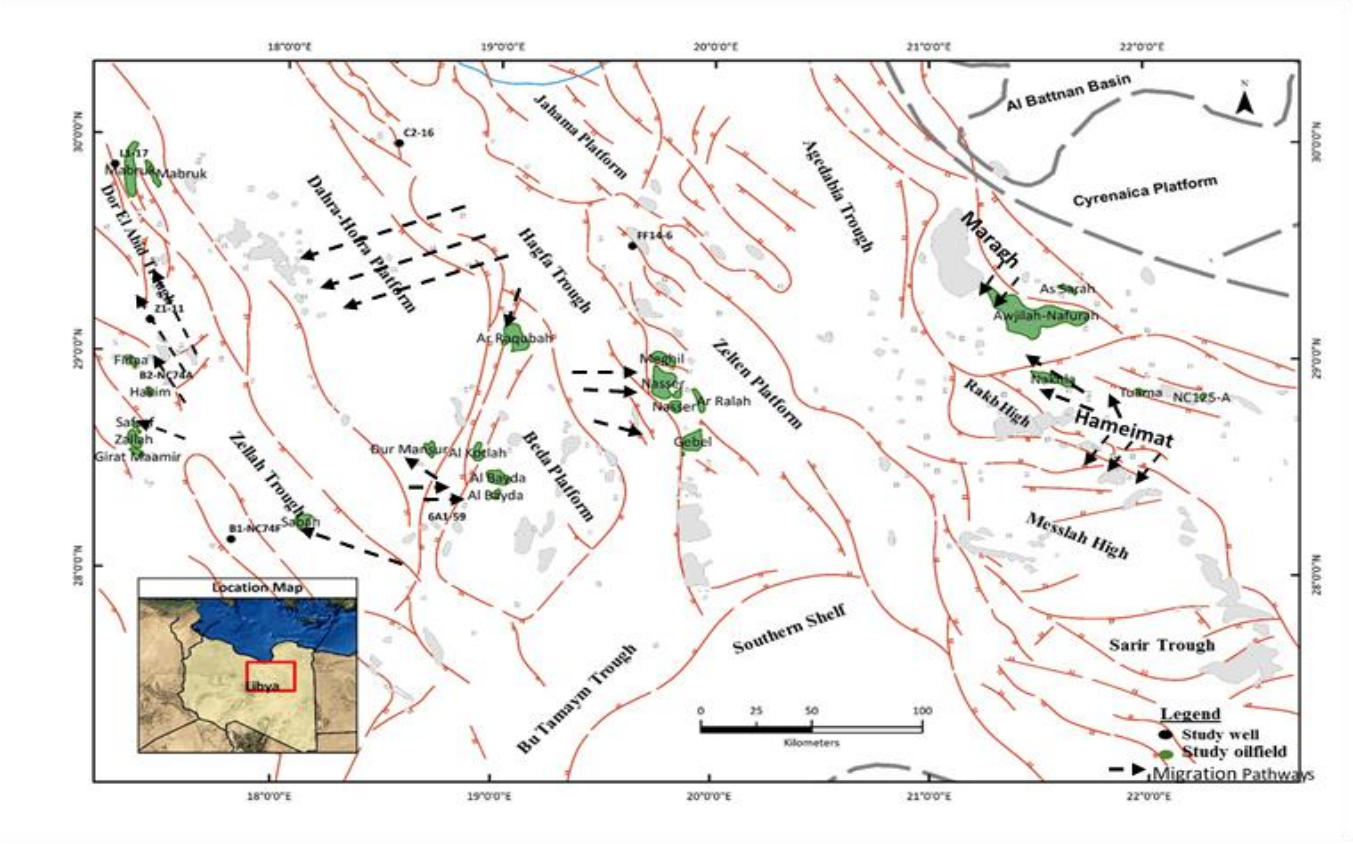

Figure 7.48: Migration map showing the hydrocarbon migration pathways from the oil source kitchen to platforms in the Sirt Basin, Modified after El Alami 1989; Rohi, 1996; Skinder, 2008).

7.4 Mass Balance Calculations

Rough mass balance assessments were performed using the present-day Rock-Eval data (TOC, S2 and HI) to give estimates of the original potential of the source rock prior to any petroleum generation, the rock density and the thickness of the source rocks. These data were used to calculate the volume of hydrocarbons that might have been produced from about 1km^2 volume of source rock for the 6A1-59, B1-NC74F, B2-NC74A, C2-16, FF14-6, L1-16, L1-17, and Z1-11 wells within the Sirt Basin. The difference between the present and original yields gives the approximate mass of hydrocarbons generated. It is also used to estimate the volume of oil produced and expelled from the source rock, and to estimate the amount of producible oil reserves. The original TOC was determined using the equation TOC (current) x 1.2 (allowance for a 20% reduction in TOC with maturation). The source rock density was estimated from:

% Organic matter = TOC (current) x 1.4

Source rock density kg/ m^3 = (((% OM/ 100) x 1200)) + ((% mineral/ 100) x 2700))

The percentages of expulsion efficiency and gas fraction of hydrocarbon were calculated by using the formula of Pepper and Corvi (1995).

The calculated yields of hydrocarbons for the Kalash, Sirte Shale and Rachmat source rocks in the wells studied for about 1km^2 are summarized in Tables 7.1 and 7.2 in Appendix IV. In well 6A1-59, the oil potential for the Upper Kalash Formation source rock (12m) at the present-day HI is calculated to be about 6 x 10^8 kg (oil expelled, 2 x 10^6 bbl) was possible. This calculation demonstrates that the source rock has already generated 49% of the oil and the other 51%, which may represent either gas or oil has not yet been expelled. The high expulsion efficiency of 59% may be due to the high HI, reflecting good kerogen quality.

While the Lower Kalash Formation source rock (9m) at the present day HI is calculated to contain about 3 x 10^7 kg (oil expelled, 1 x 10^5 bbl). This calculation demonstrates that the source rock has already generated 54% of oil and the rest (46%) may be either gas or oil and has not yet been expelled due to lower maturity. The low value of expulsion efficiency of 8% may be due to low hydrocarbon generation within the source rock because it does not have enough organic matter input and also has not reached sufficient maturity.

The Sirte Shale source rock in the 6A1-59 well has a thickness about of 18m, and the present day HI is calculated to be about 5 x 10^8kg (oil expelled, 2 x 10^6 bbl). This calculation demonstrates that the source rock has already generated 50% of its oil and the rest may be either gas or oil, but has not yet been expelled due to lower maturity. The high expulsion efficiency of 45% may be due to the high HI, reflecting good kerogen quality.

In well B1-NC74F the oil potential of the Sirte Shale source rock (67m) at the present-day HI is calculated to be about 7 x 10^8 kg (oil expelled, 3 x 10^6 bbl). The calculation shows that the source rock has already generated 52% of its hydrocarbons and remained may be either gas or oil but is not able to be expelled. The low value of expulsion efficiency of 17% may be due to low levels of hydrocarbons generated within the source rock because has not reached sufficient maturity.

The Rachmat source rock in well B1-NC74F has a thickness about of 48m, and oil generating potential at the present day HI is calculated to be about 4 x 10^8 kg (oil expelled, 1 x 10^6 bbl). The calculation shows that the source rock has already generated 51% of its oil and the remainder may represent either gas or oil but cannot be expelled. The moderate value of expulsion efficiency of 24% may be due to moderate levels of hydrocarbons generated within the source rock.

In well B2-NC74A, the oil potential for the Upper Sirte Shale source rock (20m) at the present-day HI is calculated to be about 5 x 10^7 kg (oil expelled, 2 x 10^5 bbl). The calculation shows that the source rock has already generated 54% of hydrocarbons and the remaining gas or oil is not able to be expelled. The low value of expulsion efficiency of 6% may be due to low levels of hydrocarbons generated within the source rock because it does not have enough organic matter input as well as not having reached sufficient maturity. The Lower Sirte Shale has a thickness of about 48m, and the oil generating potential at the present day HI is calculated to be 2 x 10^8 kg (oil expelled, 1 x 10^8 bbl). The calculation shows that the source rock has already generated 54% of its oil and the remaining gas or oil has not been able to be expelled. The low value of expulsion efficiency of 7% may be due to all hydrocarbons within the source rock having been generated or because this source has weak generating potential.

In well C2-16, the oil potential for the Upper Sirte Shale source rock (262 meter) at the present-day HI is calculated to be about 8 x 10^8 kg (oil expelled, 3 x 10^6 bbl). The calculation shows that the source rock has already generated 54% of its oil and the

remaining gas or oil cannot be expelled. The low expulsion efficiency of 7% may be due to all hydrocarbons within the source rock having been generated and it has become a spent source rock, or this source may have only weak generating potential. The Lower Sirte Shale has a thickness of about 56m, and oil generating potential at the present day HI is calculated to be 1 x 10^8 kg (oil expelled, 5 x 10^5 bbl). The calculation shows that the source rock has already generated 55% of oil and the remainder may be which gas or oil is not able to be expelled. The low value of expulsion efficiency of 3% may be due to all hydrocarbons within the source rock having been generated and it has become spent, or that this source has weak generating potential.

In well FF14-6, the oil potential for the Upper Sirte Shale source rock (94m) at the present-day HI is calculated to be about 1 x 10^8 kg (oil expelled, 5 x 10^5 bbl). The source rock has already generated 52% of its oil and the remaining gas or oil cannot be expelled. The moderate value of expulsion efficiency of 19% may be due to all its hydrocarbons having been generated and has become a spent source rock or the source has weak generating potential. The Middle Sirte Shale has a thickness of about 15m, and oil generating potential at the present day HI is calculated to be 1 x 10^7 kg (oil expelled, 6 x 10^4 bbl). The source rock has already generated 53% of its hydrocarbons and the rest of the gas or oil cannot be expelled. From the low value of expulsion efficiency of 15% the source rock may be spent or this source may have weak generating potential. The Lower Sirte Shale has a thickness of about 39m, and the oil generating potential at the present day HI is calculated to be 1 x 10^8 kg (oil expelled, 5 x 10^5 bbl). 55% of the source rock oil has already been generated and the other gas or oil cannot be expelled. The low value of expulsion efficiency of 4% may be because source rock is spent or this source may have weak generating potential.

In well L1-16 the oil potential for the Upper Sirte Shale source rock (89m) at the present-day HI is calculated to be about 4 x 10^8 kg (oil expelled, 2 x 10^6 bbl). The source rock has already generated 53% of hydrocarbons and the remaining gas or oil is not able to be expelled. The low expulsion efficiency of 11% may indicate that all hydrocarbons have been generated or that this source has weak generating potential. The Lower Sirte Shale has a thickness of about 217m, and the oil generating potential at present day HI is calculated to be 6 x 10^8 kg (oil expelled, 2 x 10^8 bbl). 54% of its oil has already been generated and the remaining gas or oil cannot be expelled. The low

expulsion efficiency of 8% may suggest that all hydrocarbons within the source rock have been generated or that this source has weak generating potential.

In well L1-17, the oil generating potential for the upper Sirte Shale source rock (180m) at the present-day HI is calculated to be about 1 x 10^9 kg (oil expelled, 8 x 10^6 bbl). The calculation shows that the source rock has already generated 52% of its oil and the remaining hydrocarbons cannot be expelled. The moderate value of expulsion efficiency of 21% may be due to only a moderate hydrocarbon generation within the source rock. The lower Sirte Shale source rock has a thickness of about 125m, and oil generating potential at the present day HI is calculated to be about 2 x 10^8 kg (oil expelled, 1 x 10^6 bbl). Thus, the source rock has already generated 54% of its oil and the remaining gas or oil is not able to be expelled. The low expulsion efficiency of 6% may mean the source rock is spent or that this source has weak generating potential.

In well Z1-11, the oil potential of the Sirte Shale source rock (54m) at the present-day HI is calculated to be about 6 x 10^8 kg (oil expelled, 2 x 10^6 bbl). The source rock has already generated 51% of its hydrocarbons and the remains may be not be able to be expelled. The moderate value expulsion efficiency of 28% may suggest a spent source rock or this source may have only low to moderate generating potential.

The comparison of the mass balance equation results for the Sirte shale source rock in the eight localities suggests that the Sirte Shale in wells 6A1-59, C2-16, FF14-6, L1-16, L1-17, and Z1-11 is a more effective source rock than that in well B1-NC74F and B2- NC74A. Also, the comparison of the expulsion efficiency and gas fraction results suggests that Sirte Shale Formation in wells 6A1-59, B1-NC74, FF14-6, L1-17, Z1-11, and L1-16 has a higher yield than that in wells B2-NC74, and C2-16,.

The relationship proposed by Cole (1994) was also applied to the Rachmat and Kalash formations which have similar lithofacies and organic characteristics, in order to estimate oil potential. The mass calculation demonstrated that the Rachmat Formation has already expelled 51% of its oil and what remains may not be able to be expelled. The Kalash Formation has expelled 49%, but still has significant remaining potential if its maturity is even higher.

7.5 Summary

Kinetic source rock maturation and expulsion modelling software have been used to estimate the petroleum generation from the organic-rich Kalash, Sirte Shale and Rachmat source rocks in the central and western Sirt Basin. For the 6A1-59 well, the Kinex model demonstrates that an oil window could occur for the upper Kalash Formation, and the formation may well expel hydrocarbon, which is mostly oil with low amounts of gas. Whereas for the lower Kalash Formation, the kinetic maturation model demonstrated that no oil expulsion could occur, but with such a kerogen type, gas expulsion may occur. Meanwhile, for the Sirte Shale Formation an oil window may occur.

In the B1-NC74F well, the kinetic thermal model demonstrates that an oil window for the Sirte Shale Formation and Rachmat formations may occur and it is suggested that these formations will expel oil.

For well B2-NC74A, the kinetic thermal model demonstrates that no oil could be expelled from the Sirte Shale Formation, but very low amounts of gas could be expelled.

For C2-16 well, the kinetic model demonstrates that no oil could be expelled from the Sirte Shale Formation, but low to moderate amounts of gas could be expelled.

In the FF14-6 well, the kinetic thermal model demonstrates that an oil window for the upper Sirte Shale Formation may occur with gas. In the comparison of the middle Sirte Shale Formation, the model demonstrates an oil window in the middle unit with gas occured, suggesting that the middle formation will expel gas with low amounts of oil. Meanwhile the model shows no oil expelled from the lower Sirte Shale Formation, but it could expel a little amount of gas.

In the L1-16 well, the kinetic thermal model demonstrates an oil window for the upper Sirte Shale Formation may occur and will be expelled some oil with gas. Meanwhile, the kinetic thermal model illustrates that no oil could be expelled from the lower Sirte Shale Formation, but low to moderate amounts of gas could be expelled.

In the L1-17 well, the kinetic thermal model demonstrates an oil window for the upper Sirte Shale Formation with gas, suggesting that the formation will expel amount of oil compared to huge amounts of gas. The model indicates that no oil could be expelled from the lower Sirte Shale Formation, but that it may expel low amounts of gas.

For the Z1-11 well, the kinetic thermal model demonstrates an oil window for the Sirte Shale Formation may occur and it is suggested that the Formation will expel about moderate amount of gas.

The hydrocarbon generation 1D basin model results suggest that the hydrocarbon potential is lower in the Zellah and Dor Al Abid Troughs in the western part of the study area, due to lower maturity. Meanwhile the hydrocarbon potential is moderate to high in the Tagrifet and Marada Troughs and the Wadayat Trough in the central and northeast parts of the study area. The timing of oil generation for the main Sirte Shale and Rachmat source rocks ranges from the Eocene to a more recent, based on burial depth in different parts of the study area. In the deeper parts, oil generation occurred from the Early to Late Miocene based on the modelling of the FF14-6 and C2-16 wells. The 1D model assumes that hydrocarbon movement is predominantly vertical, and so the lateral migration of oil is not considered. As a result of tectonic activity during the rift-system in the Oligocene to Miocene times, the vertical and lateral migration of oil and gas may have significantly affected the accumulation of hydrocarbons in the study area. Therefore, the most promising areas are those where traps were formed before the Eocene age and situated on an oil migration pathway from the mature source kitchen.

Most recently published studies suggest that the petroleum in the Sirt Basin was sourced from the Upper Cretaceous source rock of the Sirte Shale and Rachmat formations. The reservoirs range from the Cambro-Ordovician and Cretaceous to Eocene ages. Sandstone reservoirs predominate in the Cambro-Ordovician and Cretaceous, while carbonate reservoirs are the main reservoir units in the Tertiary age.

Structural traps, which are mainly fault-controlled, are a major reason of the trapping mechanism for many of the reservoirs in the Sirt Basin. In the study area, the structural traps are comprised of simple normal faults to more complex faults and fold structures associated with wrench faults. At the Zellah Trough, structural traps predominate and are mainly related to an Eocene deformation of the heavily faulted in the western side of the basin. Additionally, several types of stratigraphic traps are also present in the study area. They are characterized by facies changes from argillaceous carbonate to sands and shales, for instance in the Beda and Dahra reservoirs.

Anhydrite and shales of the Upper Cretaceous and Tertiary times form the principal seals in the Sirt Basin.

Migration of the generated and expelled oil and gas from the Upper Cretaceous Sirte Shale and Rachmat Formations to the reservoir of the Upper Cretaceous-Tertiary petroleum system occurred along both vertical and lateral pathways along the faults in the Oligocene to Miocene times. But, in general, the Sirt Basin is considered to be one of the best examples of the vertical component.

In the study wells, the Rough mass balance calculation demonstrated that there are significant amounts of oil may have expelled from the Sirte Shale source rock and are estimated to be between 5×10^5 to 2×10^8 bbl, while from the Rachmat source rocks is estimated to be 1×10^6 bbl. But for the Kalash source rock, the oil that may have expel is estimated to be 2×10^6 bbl.

Chapter 8. Conclusions and Future work

8.1 Introduction

The main aims of this study were to attempt to distinguish the oil families and establish the Upper Cretaceous source rocks responsible for generating and expelling the oils in the western and central Libyan Sirt Basin study area. The purpose of this was to gain a better understanding of the distribution of the petroleum in this area and evaluate the petroleum source rock potential and petroleum systems in the Sirt Basin. Towards these aims, a number of objectives were considered:

- Determination of the genetically distinct oil families in the basin.
- Utilisation of the geochemical characteristics of the oil families to deduce their source facies, thermal maturity level and degree of preservation.
- Determination of the most likely source units in each part of the study area by comparing the oil families and their inferred source facies with regional stratigraphy and available source rock data.
- Correlation of each oil family to specific stratigraphic units.
- Predication of oil properties at different maturity levels.
- Estimation of migration directions by comparing oil family compositions with the locations of known oil kitchens within the study area.
- Determination of the time of hydrocarbon generation within each source kitchen.

A total of 51 crude oils and 269 ditches cutting rock samples from the Sirt Basin were collected from the Upper Cretaceous Kalash, Sirt Shale and Rachmat Formations in the Sirt Basin, and were analysed geochemically. The crude oil samples were attributed to different reservoir horizons from the Lower Cretaceous to Miocene periods. The rock samples were selected from eight different boreholes distributed throughout the western and central parts of the Sirt Basin. In addition to the source rock samples, 51 crude oil samples were also taken from 24 selected oilfields in the Basin.

To achieve the objectives of this study, bulk geochemical parameters including TOC analysis and Rock-Eval type pyrolysis (S1, S2, HI, PI, and T*max*) were recorded for all rock samples taken from the Upper Cretaceous source rocks. On the basis of these bulk

screening results (especially TOC and hydrogen indices) about seventy nine samples were selected for microscopic analysis involving standard non-oxidative palynological procedures. Samples were analyzed and counted under transmitted white light and then examined using blue light fluorescence and incident light (Tyson, 1995). The level of thermal maturity was also determined using spore colour indices and vitrinite reflectance measurements. Whole crude oil and selected shale rock samples were analysed using several geochemical techniques, including the solvent extraction of hydrocarbons, and thin layer chromatography with flame ionization detection (TLC-FID). The solvent extracts were fractionated into hydrocarbons and polar fractions using a solid phase extraction (SPE) method and the hydrocarbon fractions were further fractionated into saturated and aromatic hydrocarbons using silver nitrate impregnated silica SPE. Non-hydrocarbon fractions were separated into carbazoles and phenol fractions using SPE. All hydrocarbon fractions were analysed using gas chromatography (GC), gas chromatography-mass spectrometry (GC-MS) and some by gas chromatography-isotopic ratio mass spectrometry (GC-IRMS). Data collected from these analyses were then interpreted using a combination of conventional (cross-plot type) and statistical techniques (principal component analysis), as well as providing input data for the construction of thermal history and hydrocarbon generation models (i.e. 1D thermal modelling analysis) for the basin.

8.2 Geochemical Evaluation of the Upper Cretaceous Source Rocks in the Sirt Basin

The dark grey, brown, and black shale of the Kalash Formation are in the early mature stage and have total organic carbon values in the range of 3.04 to 3.81 wt% with an average of 3.42 wt%, which represents good source rock potential. It has Type II kerogen and is dominated by yellow to orange fluorescent amorphous marine organic matter. The Upper Cretaceous Sirt Shale Formation consists of mainly dark grey to black shales and carbonates; it is believed to be the main source rock across the study area. The Sirte Shale source rock samples analysed in this study exhibited fair to good to extremely rich organic matter content represented by TOC content in the 0.50 to 6.73 wt% range, with a mean value of 1.41 wt%. The medium-dark grey to brown and black shale of the Sirte Shale Formation is in the early or middle to late mature stage, and has fair to excellent source rock potential. Its Type II to II-III kerogen is dominated by

yellow orange, dull orange to brown fluorescent amorphous organic matter, which is sometimes non-fluorescent at higher levels of maturity, and with minor contributions of phytoclast material. It is likely to have produced significant amounts of hydrocarbons, particularly oil and some gas. The dark grey to black shale of the Rachmat Formation is in the middle mature stage, and has a TOC content ranging between 1.05 to 1.90 wt% with an average of 1.36 wt%, which is rated as having good source rock potential. Its Type II kerogen is dominated by yellow-orange to dull orange fluorescent amorphous organic matter with a minor contribution of terrestrial organic matter.

The Upper Cretaceous Sirte Shale and Rachmat source rocks strata are early mature or middle to late mature and have measured vitrinite reflectance ranges from 0.51 to 1.50 *%Ro*. This maturity interval indicates that the Upper Cretaceous source rock strata from the Zellah Trough and Dor Al Abid Trough in the western part of the Sirt Basin are in the early to middle mature stages, whereas those further northeast at wells C2-16 in the Maradah Trough and FF14-6 in the Wadayat Trough were found to be at higher maturity, and are in the main oil window or are over-mature, at the onset of the condensate to gas window.

8.3 Molecular Biomarker Characteristics of the Source Rocks

Normal alkane distributions of most of the source rock samples investigated had a dominance of short over long chain hydrocarbons, indicating non-waxy source rocks and crude oils generated from marine and marine to lacustrine Type II to Type II-III kerogen deposited in suboxic to anoxic environments.

The Upper Cretaceous source rock intervals across the study area could be separated into two main groups with regard to sterane and triterpane distributions. Group I contained samples from wells 6A1-59, L1-16 and L1-17 and most of these samples have moderate to high TOC contents and petroleum yield (S1+S2). This group is characterised by the occurrence of low abundances of hopane relative to regular steranes. Also the regular sterane to regular sterane+ C_{29} to C_{30} 17α(H) hopane ratios are greater than 0.90. This suggests higher input from eukaryotic (algal) versus prokaryotic organic matter, but this may also be due to the better preservation of steroid compounds in a highly anoxic depositional environment. There is a low abundance of

extended tricyclic terpanes from C_{29} to C_{30}, and no detectable extended C_{32} to C_{35} tricyclic terpanes. The C_{24} tetracyclic/C_{26} tricyclic (S+R) ratio was in the range 0.38 to 1.80, showing moderate to the high abundance of the C_{24} tetracyclic terpanes compared to the C_{26} tricyclic terpanes, with high C_{29} αβ relative to C_{29} Ts and C_{30} α(H) diahopane, and also showing high C_{30} α(H) hopane relative to C_{30} α(H) diahopane and high pentacyclic terpanes relative to tricyclic terpanes. The abundance of diasteranes relative to regular steranes in the Upper Cretaceous source rock samples was found to be lower in the Sirte Shale source rock in Group I samples than the Sirte Shale and Rachmat source rock samples in Group II due to their lower maturity.

Group II consists of samples from wells B1-NC74F, B2-NC74A, C2-16, FF14-6, and Z1-11. Most of these samples have low to moderate to slightly high TOC content and petroleum yield, and are characterized by high levels of tricyclic terpanes relative to pentacyclic terpanes. This group is also characterised by the occurrence of low to moderate abundance of hopane relative to regular steranes, and with regular sterane/regular sterane+C_{29} to C_{30} 17α(H) hopane ratios ranging from 0.30 to 2.60, which may suggest low to moderate to high input from eukaryotic (algae and land plants) rather than prokaryotic organisms. It may also be due to moderate to better preservation of steroid compounds in suboxic to anoxic depositional environment. There is a low abundance of extended tricyclic terpanes from C_{29} to C_{30}, and no detectable extended C_{32} to C_{35} tricyclic terpanes. The C_{24} tetracyclic/C_{26} tricyclic (S+R) ratios are in the range of 0.30 to 2.79, showing moderate to the high abundance of the C_{24} tetracyclic terpanes compared with the C_{26} tricyclic terpanes S and R, with high C_{29} αβ relative to C_{29} Ts and C_{30} α(H) diahopane. There are also high levels of C_{30} α(H) hopane relative to C_{30} α(H) diahopane. In addition, Group II has a similar slightly high relative abundance of Ts over Tm, and moderate to high abundances of diasteranes relative to regular steranes. Within the steranes, C_{27} βα diasterane S+R and C_{29} βα S are more abundant.

The C_{35}α/C_{34}α ratios of all of the rock extract samples had values below 0.80, consistent with the organic matter being derived from a marine shale source. Levels of homohopane C_{31} to C_{35} terpanes showed a predominance of C_{31} over other homologous series, and this may suggest a moderate to high marine reducing clastic facies of the

source rocks. For well B1-NC74F, the chromatograms showed a relatively high abundance of the C_{34} terpane and this may reflect a difference in bacterial input.

8.4 Aromatic Hydrocarbons

For most of the study wells, the short chain C_{21} and C_{22} monoaromatic steroid compounds were present in greater abundances than the long chain C_{27} to C_{29} compounds. This may reflect the fact that a short chain is more resistant to maturity. The distributions of long chain C_{27} to C_{29} monoaromatic steroids appear to be moderate to high in the wells 6A1-59, B1-NC74F, B2-NC74A, L1-16 and L1-17 at the western part of the basin, relative to the other wells C2-16, FF14-6, and Z1-11 situated in the central part of the basin. This may be due to the effects of maturity of long chain monoaromatic compounds or to changes in organic facies. Most of the samples are dominated by $C_{29}\beta$ and $C_{28}\alpha$ (S and R), and $C_{28}\beta$ S monoaromatic steroid hydrocarbons, which can be attributed to marine sourced organic matter input.

The triaromatic steroids (TAS) are present with different distributions in the source rock samples, where long chain compounds are relatively more abundant than short chain compounds. This may reflect the fact that all of the source rock samples have originated from similar organic matter input, but with different depositional environments and levels of thermal maturity.

The Sirte Shale and Rachmat source rock strata are characterized by a relatively high abundance of triaromatic compounds, including phenanthrene and dibenzothiophene; with low levels of fluorene and a relatively low abundance of diaromatic hydrocarbons, (e.g. biphenyl and naphthalene). This may indicate that the sediments were derived from clastic marine depositional environments with some contribution of land plant input in the apparently more lacustrine-influenced source rocks.

According to the DBT/P relative to the Pr/Ph ratios, most of the source rock strata from the Sirte Shale and Rachmat Formations are assumed to have originated from marine to lacustrine shale source rocks and their Pr/Ph ratios lay within the range 0.73 to 2.39, supporting the notion of marine suboxic to anoxic depositional environments.

8.5 Principal Components Analysis

The main objective of the statistical analysis was to reduce the dimensionality of the data to a few important components that best explain the variation in the data set. Principal component analysis and most of the organic facies parameters applied in this study clearly separate the source rocks into three major groups. Group A consists of all source rock samples of well 6A1-59; group B samples from wells B2-NC74A (9570 and 9610 feet), FF14-6 (11320 feet), L1-16 (7400, 750, and 7640 feet), and L1-17 (6060, 6300, and 6460 feet); and group C comprises samples from wells B1-NC74A (7050, 7110, 7190, and 8080 feet), B2-NC74F (9520, 9540, and 9580 feet), C2-16 (9800, 10260, 10380, 10580 feet), FF14-6 (11290, 11650, 12290, and 12330 feet), L1-16 (7850 feet), L1-17 (6600 feet), and Z1-11 (8080, 8140, 8200 feet).

The Sirte shale source rock samples in groups A and B are dominated by the abundance of TOC, hydrocarbon potential, steranes, diasteranes, and hopanes while they have relatively low abundances of tricyclic terpanes, suggesting that both groups have a moderate to high input of eukaryotes relative to prokaryotic organisms. This may be as a result of a better preservation of steroid and hopanoid compounds in suboxic to anoxic marine environments. The abundance of diasterane compounds may be due to clay-rich lithology and/or higher maturity. Both groups are less affected by maturity than the rocks in group C.

The Sirte Shale and Rachmat source rocks from group C showed moderate TOC and petroleum potential compared with the other two groups. Group C samples also had less tricyclic terpanes, tetracyclic terpanes, steranes, diasteranes, hopanes, and diahopanes relative to groups A and B. The difference in biomarker distribution in the Sirte Shale and Rachmat source rocks in group C may be due to the effects of dilution, which appears to lead to slightly higher mineral carbon content relative to total organic carbon. Alternatively, the changes in depositional environment may have led to moderate preservation in organic matter within suboxic conditions, or it might be that the organic matter exhibited higher thermal maturity due to overburdened sediments.

8.6 Carbon Isotopic Composition of the Source Rock

The similarity in the $\delta^{13}C$ isotope profiles of most of the Sirte Shale and Rachmat source rock samples analysed may reflect the origin of organic source facies rich in marine organic matter which has been inferred from the molecular biomarker analyses. The Sirte source rock samples from L1-16 seem to be completely different isotopically from the other source rock samples, as represented the lightest $\delta^{13}C$ values; this may be consistent with marine sources containing relatively high terrigenous contributions. The Sirte Shale source rock from the well B2-NC74A showed higher values of $\delta^{13}C$, which suggests a marine sources with moderate to higher contribution of algal organic matter. It is clear from the isotopic composition of the source rock extracts that each group is most probably controlled by source and deposition environment, as well as maturity.

8.7 Oil to Oil Correlations

The oil samples are attributed to several reservoir horizons from the Lower Cretaceous to Miocene times. The crude oils studied showed different geochemical signatures representing either differences in their origins, depositional environments or maturation in the source rocks. In the western and central parts of the Sirt Basin, the *n*-alkane distribution of all the oils investigated had a predominance of short-chain relative to long-chain hydrocarbons consistent with a non-waxy crude oils generated from marine Type II to Type II-III kerogen deposited in suboxic to anoxic conditions. In the eastern part of the basin all of the crude oils studied also had a dominance of short-chain *n*-alkane compared to long-chain hydrocarbons, but with relatively less abundance of heavy *n*-alkanes, which indicates a mixture of marine and terrigenous organic matter inputs. Most of the crude oil samples show a slight odd over even predominance of long-chain *n*-alkanes indicated by carbon preference indices up to 1.12. The crude oil samples from the Aswad, Beda, Dor Mansour, Hakim, Fidda, Safsaf, and Sabah oilfields and the three wells of the Mabruk oilfield in the central and western Sirt Basin are considered to be lighter oils than the other oils in the study area. Most of the crude oils in the Sirt Basin have siliciclastic-source signatures as shown by biomarkers, except for the crude oil samples from the Aswad, Safsaf and Zellah oilfields that exhibited a combination of siliciclastic and carbonate in their source signatures. The

thermal maturity level of the oil samples studied ranged from early to middle mature in the central and western part of the basin, and middle to late mature in the eastern part of the basin as revealed by various biomarker-related parameters and diamondoids. According to *n*-alkane to isoprenoid alkane ratios and biomarker facies related parameters, the crude oil samples in the Sirt Basin have been separated into nine oil families and two subfamilies. Family 1A includes the Beda, Fidda, Hakim, East Meghil and Mabruk oilfields. Family 1B contains the oils from the Nasser, Raiah, Raguba, Sabah, South Jebel, West Meghil and Zelten oilfields. Family 2 includes only the oil from the Kotla oilfield. Family 3 comprises the oils from the Dor Mansour oilfield, and Family 4 includes the oils from the Aswad, Safsaf and Zellah oilfields. Family 5 comprises oils from the As Sarah oilfield. Family 6 contains oil from the Augila Nafoora oilfield, while Families 7, 8 and 9 contain the oils from the NC125, Tuamma and Nakhla oilfields, respectively. The very high ratios of the *n*-alkane relative to isoprenoid alkane in the oil families 7, 8 and 9 indicate that the oil samples had been exposed to higher levels of thermal maturity.

The saturated hydrocarbon biomarker data show that the oil samples collected from the As Sarah, NC125 and Nakhla fields in oil families 5, 7 and 9 in the eastern part of the basin were generated from marine organic matter with major contributions from planktonic and/or benthic algae. However, the oil samples from the remaining families 1A, 1B, 2, 3, 4, 6 and 8 were generated from source rocks characterised by moderate to high contributions from eukaryotic organisms as opposed to prokaryotic organisms. Oil families 3 and 4 have significantly higher homohopane index ratios, indicating a more reducing depositional environment for the source rock, and this conclusion is also obtained from the pristane/phytane ratios. Meanwhile the other oil families show low to moderate homohopane index ratios, suggesting less reducing depositional environments for the source rocks, and this is also reflected in the pristane/phytane ratios.

Sterane and hopane based maturity parameters were found to be affected by source lithology, but can still be used to assess the maturity of crude oils. Hopane maturity parameters such as C_{27} Ts/(Ts+Tm), and C_{32} homohopane 22S/(22S+22R) isomerization ratio and sterane based maturity ααα 20S/(20S+20R) and αββ/(αββ+ααα)

C_{29} sterane ratios, for the oil families 1A, 1B, 2, 3, 4 and 6 showed similar thermal maturity, but they have not reached full maturity with respect to the equilibrium stage. Meanwhile, oil families 5, 7, 8 and 9 have a similar levels of thermal maturity and these oils have reached their equilibrium phase.

Age diagnostic biomarkers (C_{28}/C_{29} sterane) indicated that oil families 1A, 1B, 2 and 3 were Upper Cretaceous oils in the Mesozoic time; while the oils from the Aswad, Safsaf and Zellah oilfields in oil families 4 and 8 oil (Tuamma oilfield) and 9 (Nakhla oilfield) have ratios in the range of 0.36 to 0.60, suggesting that these oils may have been derived from the Upper Palaeozoic to Lower Cretaceous periods.

Most of the oil are characterized by a predominance of C_{27} and C_{29} diasteranes relative to regular steranes, indicating the clay-rich- nature of the source rock. The relative abundance of C_{27}, C_{28} and C_{29} sterane showed that the oil families 1A, 1B, 2, 5, 6, 7 and 8 originated from mixed plankton and bacteria in an open marine region, while oil families 3, 4, and 9 are derived from mixed plankton, bacteria and land plants in open to shallow marine regions.

The aromatic hydrocarbon data show that all of the oil families are characterised by a relatively high abundance of diaromatic and triaromatic hydrocarbons, including naphthalene, phenanthrene and dibenzothiophene, with low levels of biphenyl, fluorene, and monoaromatic and triaromatic steroids. This may indicate that the crude oils originated from clastic marine depositional environments with relatively high contributions of land plants and/or bacteria in marine source rocks. The relatively higher abundances of the alkylnaphthalene compounds in the oil samples could be related to their production from terpenoids derived from microbacteria and land plants. The high abundance of 9-MP relative to 1-MP in most oil families reflected the marine source precursors of these compounds with some isomers with land plant origins, particularly in family 3 oil.

The carbon isotopic signatures of the *n*-alkanes for oil families 1A, 1B, 2, 3 and 4 show good correlations and may indicate that these oils have been generated from a similar source facies, while oil families 5 to 9 have slightly different source facies which may

be due either to variations in depositional environments or the effects of maturity in the source rocks.

8.8 Oil to Source Correlation

Oil-source rock correlations confirmed that oil families 1A, 1B, 2 and 3 were generated from the Upper Cretaceous Sirte Shale and Rachmat formations, while oil family 4 may have been generated from the Sirte Shale or an older source rock. The variation between crude oils and source rocks samples may also reflect lateral and vertical variations in the organic facies and depositional environments as well as the influence of thermal maturity from one place to another in the Sirt Basin.

The low abundance of C_{24} tetracyclic terpanes in most of the Sirte Shale and Rachmat source rock extracts and all oil families may suggest a moderate input of algae, land plants or microbes. The low (less than 0.41) C_{24}tetr/C_{23}tri ratios and the absence of the C_{25} to C_{27} tetracyclic terpanes suggest that the source rock extracts and oil families were derived from a marine clastic source associated with some contribution of terrestrial organic matter input. The high C_{26}/C_{25} tricyclic terpane values for family 4 oils suggest that these crude oils were generated from the lacustrine source rock.

The aromatic hydrocarbon data showed that all of the oil families 1A, 1B, 2, 3 and 4 and Sirte Shale source rock extracts are shown to have similar source features, originating from marine to lacustrine shale source rocks, and their Pr/Ph ratios are in the range of 1.0 to 2.39 which suggests a marine dysoxic to anoxic depositional environment. The Sirte Shale and Rachmat source rock extracts from wells B1-NC74F and B2-NC74A, along with some strata intervals from the Sirte Shale Formation at wells FF14-6 and L1-16, are indicated to have originated from lacustrine sulphate-poor lithology source rock and they have low Pr/Ph ratios below 1.0 indicating anoxic depositional environments. Here, the differences in source rock characteristics indicate lateral and vertical variations in kerogen facies input, as well as changes in the depositional environments in the source rock within the Sirt Basin.

The similarity in the isotope profiles of oil families 1A, 1B, and 3 and the Sirte Shale and Rachmat source rocks strata may reflect the origins from organic source facies richer in the marine organic matter. Family 4 oils and Sirte Shale source rock extracts

from well B2-NC74A seem to be slightly different isotopically from the other oil families, as they contain the heaviest $\delta^{13}C$ isotope values. This may be due to the production of the *n*-alkanes from source rocks characterised by lacustrine to marine organic matter with high contributions from algal organic matter. Family 1A and 1B oils and Sirte Shale and Rachmat source rocks from the wells C2-16 and FF14-6 have similar characteristics and appear as the isotopically light, and this may be consistent with a marine source but with relatively high contributions of terrigenous organic matter.

Principal component analysis separated the oil families and source rock extracts into six groups. Group 1 consists of oil families 1A, 1B and Sirte Shale source rock strata from wells B2-NC74A at depths of 9570 and 9610 feet and FF14-6 at depths of 11615 and 11650 feet; group 2 comprises samples from oil families 2, 3 and 4; group 3 contains Sirte Shale and Rachmat source rock strata from the boreholes B1-NC74F and B2-NC74A at depths of 9520 and 9580 feet, and FF14-6 at depths of 12290 and 12330 feet; group 4 includes Sirte Shale source strata from the wells L1-17, Z1-11 and C2-16 at a depth of 10580 feet; group 5 contains the Sirte Shale Source rock strata from the wells 6A1-59, L1-16 and L1-17 at the depth of 6060 feet; and group 6 comprises of Sirte Shale source rock extracts from the C2-16 well.

The maturity trends in the source-related oils showed that the oil families 1A and 1B along with the Sirte Shale and Rachmat source rock strata from the wells B2-NC74A, C2-16, FF14-6 and Z1-11, are more mature than the oil families 2, 3 and 4 along with the Sirte Shale stratigraphic beds from the wells 6A1-59, L1-16 and L1-17.

8.9 Sirt Basin Petroleum System

For the 6A1-59, B1-NC74F, L1-16, L1-17 and Z1-11 boreholes, the kinetic thermal model demonstrates that an oil window may have occurred and could expel moderate amounts of oil with huge amounts of gas from the Sirt Shale and Rachmat formations in the central and western parts of the Sirt Basin, while for B2-NC74A there is no oil could be expelled. The kinetic model for the C2-16 and FF14-6 wells demonstrates that the Sirte Shale source rock in the central part of the basin could have expelled moderate oil with huge amounts of gases at the present time.

The hydrocarbon generation 1D basin model indicated that the hydrocarbon potential is lower in the Zellah and Dor Al Abid Troughs in the western part of the study area, due to lower maturity. Meanwhile the hydrocarbon potential is moderate to high in the Tagrifet, Marada and Wadayat Troughs in the central and northeast part of the study area. The timing of oil generation for the main Sirte Shale and Rachmat source rocks ranges from the Eocene to a more recent, based on burial depth in different parts of the study area. As a result of tectonic activity during the rift-system in the Oligocene to Miocene times, the lateral and vertical migration of oil and gas may have significantly affected the accumulation of hydrocarbons in the study area. Therefore, the most promising areas are those where traps were formed before the Eocene age and are situated on an oil migration pathway from the mature source kitchen. In the Sirt Basin the reservoir rocks range from the Cambro-Ordovician and Cretaceous to Eocene times. Sandstone reservoirs predominate in the Cambro-Ordovician and Cretaceous, while carbonate reservoirs are the main reservoir units in the Tertiary age. Structural traps which are mainly fault-controlled are a major cause of the trapping mechanism for many of the reservoirs in the basin. The structural traps are comprised of simple normal faults to more complex faults and fold structures associated with wrench faults. In the Zellah Trough, structural traps predominate and are mainly related to the Eocene deformation of the heavily faulted in the western side of the basin, and several types of stratigraphic traps are also present. In the Sirt Basin, anhydrite and shales of the Upper Cretaceous and Tertiary ages form the principal seals. Migration of the generated and expelled oil and gas from the Upper Cretaceous Sirte Shale and Rachmat source rocks to the reservoir of the Upper Cretaceous-Tertiary petroleum system occurred along both vertical and lateral pathways along the faults in the Oligocene to Miocene periods.

Rough Mass balance calculations demonstrate that the Sirte Shale and Rachmat formations have generated and expelled moderate to large quantities of hydrocarbons.

Geochemical evaluation of the Upper Cretaceous source rocks shows that Sirte Shale and Rachmat formations contain oil-prone to oil-gas-prone kerogen in the study area. This may have important implications for ongoing petroleum exploration activities in the Sirt Basin.

8.10 Implication and Challenge of the Study

Although relationships among crude oils are readily addressed using biomarkers, oil-source rock correlations are more difficult, partly because few thermally mature source-rock extracts are available. Active source rock is buried deeply and generally occurs far from up dip, shallower sites of petroleum accumulation. Also, drilling is costly and normally ends when reservoir objectives are reached at these shallower depths. Unfortunately, the source of trapped petroleum is commonly unknown, and only oil samples are available for study. For this reason, the use of biomarkers to predict the characteristics of the source rock is a critical technology. Although biomarkers are already powerful tools, further research is needed to improve the systematic understanding of source inputs and sedimentology controls on biomarker composition. Therefore, current understanding of the effects of depositional and diagenetic processes on geochemical parameters is limited but still useful. The results of these studies may help to explain the controls in the organic facies development. The application of geochemical parameters is mostly related to organic matter input and depositional environment as well as maturity and generally depends on non-systematic, empirical evidence and also to limited support from other geological data. For instance, applied triangular plots of tricyclic and pentacyclic terpanes can be used to distinguish between the three source-rock organic matter inputs. Therefore, more systematic, statistical studies may improve the usefulness of these geochemical parameters. In addition, principal component analysis allows the identification of biomarker parameters that were most useful in discriminating between the samples according to environment or relative thermal maturity. So, if petroleum geochemists are able to determine the source rock for crude oil, then probable migration pathways or types of petroleum to be expected can be used to develop new petroleum plays.

The Sirt Basin crude oils vary in quality from light to slightly heavy and have similar geochemical signatures, indicating that they originate from similar sources in the western part of the Sirt Basin. Meanwhile, crude oils in the eastern part of the Sirt basin

vary in quality from light to heavy and have different geochemical signatures representing differences in either their origins, depositional environments or maturation. Two potential source rocks that have the same characteristics were identified in the study area, and these were the Upper Cretaceous, Sirte Shale and Rachmat formations, in addition to the Triassic-Lower Cretaceous, Middle Nubian Shale Formation in the east Sirt Basin. Only a few studies have been performed to assess the differences and similarities among crude oils in the study areas, such as El-Alami *et al.* (1989); El-Alami (1996); Burwood *et al.* (2003) and Sikander (2008). Additionally, few publication analyse the suspected sources of hydrocarbons existing in the Sirt Basin. Existing studies principally utilize petroleum geochemistry, biomarkers and carbon isotopes, basin modelling and statistical analyses to investigate and distinguish between the main chemical features and characteristics of the Sirt Basin crude oils. Therefore, the main contributions of the present research can be summarized in the following points:

1- Classifying the Sirt Basin oils into ten genetic families based on molecular biomarker and isotopic analysis.

2- Distinguishing and characterising the main source rock responsible for generating all the hydrocarbons so far discovered in the Sirt Basin, and linking them to oil families in order to determine the genetic relationships between oil families and the Upper Cretaceous source rocks.

3- Identifying the modification processes that may have affected the generation, migration and accumulation of hydrocarbons in the study area (such as the preservation and maturation of organic matter and biodegradation)

4- Estimating migration pathways, which may lead to assess the exploration activity programme to find new prospective areas in the study area.

5- Adding new geochemical knowledge to the Libyan oil industrial database that may help to solve a lot of problems that are related to the geoscience, and also to improve exploration activity in Libya.

6- This study may also help to reduce the risks in exploration activity in the Sirt Basin.

Nearly all agree that the Upper Cretaceous Sirte Shale, Rachmat formations, and Triassic-Lower Cretaceous, Middle Nubian Shale Formation represent the main potential hydrocarbon source rocks in the Sirt Basin. However, now the oils within Sirt Basin are classified into groups and families, this may help to recognize the main source producing specific crude oils. Thus, these source rocks are linked to the oil families in order to determine the genetic relationships between oil families and the Upper Cretaceous source rocks, and to differentiate between the two Upper Cretaceous, Sirte Shale and Rachmat source rocks and Triassic-Lower Cretaceous, Middle Nubian Shale source rock and their related crude oils. The oil mixing potential between different sources in the crude oils can then be assessed and quantified. Defining the migration pathways depends on the availability of geological and geochemical data. All studies have integrated geochemical and geological data to better understand the chemical variation of crude oils and to show the significant role of its very complicated tectonic setting in controlling the migration pathways, and consequently, the distribution of oil families in the Sirt Basin. All studies illustrate that there are variations between crude oils and source rocks and this may reflect lateral and vertical variations in the organic facies and depositional environments, as well as the influence of thermal maturity from one place to another in the Sirt Basin. That the biomarker and aromatic hydrocarbon data show that Sirte Shale source rocks have similar source features, originating from marine to lacustrine depositional environments and suggesting marine dysoxic to anoxic depositional environments, is now a consensus among all researchers.

Petroleum geochemistry researchers should work as research teams and use high-end analytical techniques such as gas chromatography-mass spectrometry and compound-specific light-stable isotope mass spectrometry to better understand the petroleum systems of basins by providing good geochemical and geological study, such as oil-

source and oil-oil correlation, to establish the principal source rock and the origins of oils within basins.

One major critical question and challenge that faced in this research concerned how to discover new prospective areas that contain oils and gases in the study area. Attempts were made to apply numerous petroleum geochemical techniques to correlate petroleum compounds found in reservoirs to find new pools of petroleum and to assess potential migration pathways. Further advanced research should consider larger sample sets of ancient sediment and rock samples to provide more insights into the origins and sources of oils and gases in the study area. Analysis of reservoir core samples from the Sirt Basin is needed for more oil-oil and oil-source correlation investigations. In addition, bulk carbon isotope analyses should be conducted for both aliphatic and aromatic hydrocarbon fractions, as well as hydrogen isotopes in order to better understand and interpret the depositional environment of the source rocks. 2D and 3D basin modelling analysis combined with seismic interpretation and geochemical data may enable us to better understand the tectonic features of this basin and to identify delineate the migration pathway and hydrocarbon accumulation.

8.11 Future Work

This study has provided results largely achieving the initial aims, however, several areas demand further attention.

- All the samples analyzed in this study came from ditch cuttings and it would be beneficial to apply the geochemical parameters to core samples for the same intervals. This may help give a clearer picture of the thermal maturity and depositional environment throughout the Upper Cretaceous sequence.

- It would be beneficial to apply bulk carbon isotope analyses for both saturated and aromatic hydrocarbon fractions as well as hydrogen isotopes in order to interpret the deposition environment and thermal maturity and to allow correlations between source rock and oil to be conducted.

- It would beneficial to have crude oil samples from the Dahra and Hofrah oilfields in the western part of the Sirt Basin to conduct oil-source correlation with oil families 1A and 1B, in order to complete the whole picture of correlations using biomarkers and carbon isotopic analysis.

- The complex structural and stratigraphic framework of the trough regions in the basin needs to be better understood by obtaining more geological and geophysical information to define more fully the migration pathways of petroleum in the basin.

- The analysis of reservoir core samples is needed from the Sirt Basin for more oil-oil and oil-source correlation investigations, particularly in the western part of the basin.

- With geochemical analysis, it will be beneficial to apply 2D and 3D basin modelling analysis combined with sequence stratigraphy and seismic interpretation in order to better understand the tectonic features of the basin as well as to identify the delineate migration pathway and hydrocarbon accumulations in the Sirt Basin.

Chapter 9. References

Abadi, A.M., van Wees, J.-D., van Dijk, P.M. and Cloetingh, S.A.P.L. (2008) 'Tectonics and subsidence evolution of the Sirt Basin, Libya', *AAPG bulletin*, 92(8), pp. 993-1027.

Aboglila, S., Grice K., Trinajstic, K., Dawson, D., Williford, K.H. (2011) 'Use of biomarker distributions and compound specific isotopes of carbon and hydrogen to delineate hydrocarbon characteristics in the East Sirte Basin ', *Organic Geochemistry*, 26, pp. 1694-1705.

Ahlbrandt, T.S. (2001) *The Sirte Basin Province of Libya: Sirte-Zelten Total Petroleum System*. US Department of the Interior, US Geological Survey.

Al-Hajeri, M.M., Al Saeed, M., Derks, J., Fuchs, T., Hantschel, T., Kauerauf, A., Neumaier, M., Schenk, O., Swientek, O. and Tessen, N. (2009) 'Basin and petroleum system modeling', *Oilfield Review*, 21(2), pp. 14-29.

Alexander, R., Kagi, R. and Sheppard, P. (1984) '1, 8-Dimethylnaphthalene as an indicator of petroleum maturity', *Nature*, 308, pp. 442-443.

Alexander, R., Kagi, R.I., Rowland, S.J., Sheppard, P.N. and Chirila, T.V. (1985) 'The effects of thermal maturity on distributions of dimethylnaphthalenes and trimethylnaphthalenes in some ancient sediments and petroleums', *Geochimica et Cosmochimica Acta*, 49(2), pp. 385-395.

Alexander, R., Larcher, A.V., Kagi, R.I. and Price, P.L. (1992b) *An oil-source correlation study using age-specific plant derived aromatic biomarker. In Biological Markers in Sediments and Petroleum. (eds J. M. Moldowan, P. Albrecht and R. P. Philip), Prentice Hall, Englewood Cliffs, pp.201-221.*

Alsharhan, A.S. (2003) 'Petroleum geology and potential hydrocarbon plays in the Gulf of Suez rift basin, Egypt', *AAPG bulletin*, 87(1), pp. 143-180.

Anketell, J.M. (1996) 'Structural history of the Sirt basin and its relationship to the Sabrata basin and Cyrenaica platform, northern Libya', *The Geology of the Sirt basin*, 3, pp. 57-89.

Aquino Neto, F.R., Trendel, J.m., Restle, A., Connan, J. and Albercht, P.A. (1983) *Occurrence and formation tricyclic and tetracyclic terpanes in sediments and petroleum. In: Advance in Organic Geochemistry 1981* (eds M. Biory, rt al), Wiley, Chichester.

Askri, H.A., A. Belmecheri, B. Benrabah, A. Boudjema, K. Boumendjel, M. Daoudi, M. Drid, T. Ghalem, A. M. Docca, H. Ghandriche, A. Ghomari, N. Guellati, M. Khennous, R. Lounici, H. Naili, D. Takherist, M. Terkmani (1995) 'Geology of Algeria', *Well Evaluation Conference Algeria*. Algaria. Schlumbrger, pp. 1-93.

Baird, W.D., Aburawi, R.M. and Bailey, J.N. (1996) *Geohistory and Petroleum in the Central Sirt Basin. In: the Geology of the Sirt Basin. In: the Geology of the Sirt Basin* (*eds* M. J. Salam, M. T. Busrewil, A. A. Misallati, M. A. Sola), Elsevier, Amsterdam, III, pp 3-56.

Baldridge, W.S., Eyal, Y., Bartov, Y., Steinitz, G. and Eyal, M. (1991) 'Miocene magmatism of Sinai related to the opening of the Red Sea', *Tectonophysics*, 197(2), pp. 181-201.

Baric, G., Spanic, D. and Maricic, M. (1996) *Geochemical characterization of source rocks in the NC-157 block (Zaltan Platform), Sirt Basin*. (3 vols). Elsevier, Amsterdam: M. J. Salam, A. S. El-Hawat and A. M Sbeta).

Barr, F.T. and Weeger, A.A. (1972) *Stratigraphic Nomenclature of the Sirt Basin*. Tripoli, Libya, p 279: Libyan Petroleum Exploration Society.

Bastow, T.P., Alexander, R., Sosrowidjojo, I.B. and Kagi, R.I. (1998) 'Pentamethylnaphthalenes and related compounds in sedimentary organic matter', *Organic geochemistry*, 28(9-10), pp. 585-595.

Bayoumi, A.I.a.L., H. I., (1989) 'Modes of Structure evolution of the Abu Gharadig Basin, Western Desert of Egypt, as deduced from seismic data', *African Earth Society*, 9, pp. 273-287.

Belazi, H.S. (1989) 'The geology of the Nafoora oilfields, Sirt Basin, Libya', *Petroleum Geology*, 12, pp. 353-366.

BeMent, W.O., Levey, R.A. and Mango, F.D. (1995) *The temperature of oil generation as defined with C7 chemistry maturity parameter (2,4-DMP / 2,3-DMP ratio)*. Spain: AIGOA, Don Ostia-San Sebastian.

Ben Ashour, A.M. (2000) 'Estimated generation time and migration trends pf upper cretaceous source rocks, Sirt Basin', *Petroleum Research Journal*, 12, pp. 25-38.

Bendoraitis, J.G. (1974) *Hydrocarbons of biogenic origin in petroleum: Aromatic triterpanes and bicyclic sesquiterpenes*.

Bennett, B. and Larter, S.R. (2000) 'Quantitative separation of aliphatic and aromatic hydrocarbons using silver ion-silica solid-phase extraction', *Analytical Chemistry*, 72(5), pp. 1039-1044.

Bezan, M.A., Belhaj, F. and Hammuda, K. (1996) *The Beda Formation in the Sirt Basin. In: The Geology of the Sirt Basin*. (*eds* M. J. Salem, M. T. Busrewil, A. A. Misallati and M. A. Sola), Elsevier, Amsterdam, II, pp 135-152.: .

Bigge, M.A. and Farrimond, P. (1998) 'Biodegradation of seep oils in the Wessex Basin—a complication for correlation', *Geological Society, London, Special Publications*, 133(1), pp. 373-386.

Bishop, W.F. (1988) 'Petroleum geology of east-central Tunisia', *AAPG Bulletin*, 72(9), pp. 1033-1058.

Bissada, K.K. (1982) 'Geochemical constraints on petroleum generation and migration – a review.', *Proc 2nd ASCOPE Conference*. Manila, Oct, 1981. pp. 69-87.

Bjorøy, M., Hall, K., Gillyon, P. and Jumeau, J. (1991) 'Carbon isotope variations in n-alkanes and isoprenoids of whole oils', *Chemical Geology*, 93(1), pp. 13-20.

Bjorøy, M., Hall, P.B., Hustad, E. and Williams, J.A. (1992) 'Variation in stable carbon isotope ratios of individual hydrocarbons as a function of artificial maturity', *Organic geochemistry*, 19(1), pp. 89-105.

Bjorøy, M., Hall, P.B. and Moe, R.P. (1994) 'Stable carbon isotope variation of *n*-alkanes in Central Graben oils.', *Organic Geochemistry*, 22(3), pp. 355-381.

Boon, J.J., Hine, S.H. and Burlingame, A.L. (1983) *Organic geochemical studies of Slar Lake laminated cyanobacterial mats*. New York: John Wiley and Sons.

Bordovskiy, O.K. (1965) 'Sources of organic matter in marine basins', *Marine Geology*, 3(1), pp. 5-31.

Bowler, B.F.J., Larter, S.R., Clegg, H., Wilkes, H., Horsfield, B. and Li, M. (1997) 'Dimethylcarbazoles in crude oils: Comment on "Liquid chromatographic separation schemes for pyrrole and pyridine nitrogen aromatic heterocycle fractions from crude oils suitable for rapid characterization of geochemical samples"', *Analytical chemistry*, 69(15), pp. 3128-3129.

Breger, I.A. (1960) 'Diagenesis of metabolites and a discussion of the origin of petroleum hydrocarbons', *Geochimica et Cosmochimica Acta*, 19(4), pp. 297-308.

Budzinski, H., Garrigues, P., Connan, J., Devillers, J., Domine, D., Radke, M. and Oudins, J.L. (1995) 'Alkylated phenanthrene distributions as maturity and origin indicators in crude oils and rock extracts', *Geochimica et Cosmochimica Acta*, 59(10), pp. 2043-2056.

Burwood, R., Redfern, J. and Cope, M.J. (2003) 'Geochemical evaluation of East Sirte Basin (Libya) petroleum systems and oil provenance', *Geological Society, London, Special Publications*, 207(1), pp. 203-240.

Busson, G. (1998) 'Sedimentary dynamics of the epicontinental platform: Middle Cretaceous of the Algero–Tunisian Sahara. Dynamics and Methods of Study of Sedimentary Basins'. Oxford and IBH Publishing and Editions Technip, Paris.

Cahen, L., Snelling, N.J., Delhal, J. and Vail, J.R. (1984) 'The geochronology of Africa'. Clarendon Press, Oxford.

Carr, I.D. (2003) 'A sequence stratigraphic synthesis of the North African Mesozoic', *Journal of Petroleum Geology*, pp. 133-152.

Cassani, F., Gallango, O., Talukdar, S., Vallejos, C. and Ehrmann, U. (1988) 'Methylphenanthrene maturity index of marine source rock extracts and crude oils from the Maracaibo Basin', *Organic Geochemistry*, 13(1), pp. 73-80.

Chakhmakhchev, A., Suzuki, M. and Takayama, K. (1997) 'Distribution of alkylated dibenzothiophenes in petroleum as a tool for maturity assessments', *Organic Geochemistry*, 26(7), pp. 483-489.

Chen, J., Fu, J., Sheng, G., Liu, D. and Zhang, J. (1996) 'Diamondoid hydrocarbon ratios: novel maturity indices for highly mature crude oils', *Organic Geochemistry*, 25(3), pp. 179-190.

Christian H. (1993) 'Basin modelling techniques an overview', *Basin Modelling Advance and Applications. Norwegian Petroleum Society (NPF)*, (3).

Clark, J.P. and Philp, R.P. (1989) 'Geochemical characterization of evaporite and carbonate depositional environments and correlation of associated crude oils in the Black Creek Basin, Alberta', *Bulletin of Canadian Petroleum Geology*, 37(4), pp. 401-416.

Clayton, C. (1991) 'Carbon isotope fractionation during natural gas generation from kerogen', *Marine and Petroleum Geology*, 8(2), pp. 232-240.

Clayton, C.J. and Bjorøy, M. (1994) 'Effect of maturity on 13C12C ratios of individual compounds in North Sea oils', *Organic Geochemistry*, 21(6), pp. 737-750.

Clegg, H., Wilkes, H. and Horsfield, B. (1997) 'Carbazole distributions in carbonate and clastic source rocks', *Geochimica et Cosmochimica Acta*, 61(24), pp. 5335-5345.

Cole, G.A. (1994) 'Graptolite-chitinozoan reflectance and its relationship to other geochemical maturity indicators in the Silurian Qusaiba Shale, Saudi Arabia', *Energy & fuels*, 8(6), pp. 1443-1459.

Collins, A. (1990) 'The 1-10 Spore Colour Index (SCI) scale: a universally applicable colour maturation scale, based on graded picked palynomorphs ', *International Symposium on Organic Petrology*. mededelingen rijks geologische dienst. pp. 40-47.

Connan, J., Bouroullec, J., Dessort, D. and Albrecht, P. (1986) 'The microbial input in carbonate-anhydrite facies of a sabkha palaeoenvironment from Guatemala: a molecular approach', *Organic Geochemistry*, 10(1), pp. 29-50.

Connan, J. and Dessort, D. (1987) 'Novel family of hexacyclic hopanoid alkanes (C 32 and C 35 occurring in sediments and oils from anoxic paleoenvironments', *Organic Geochemistry*, 11(2), pp. 103-113.

Cornford, C., Christie, O., Endresen, U., Jensen, P. and Myhr, M.-B. (1988) 'Source rock and seep oil maturity in Dorset, southern England', *Organic geochemistry*, 13(1), pp. 399-409.

Cornford, C., Gardner, P. and Burgess, C. (1998) 'Geochemical truths in large data sets. I: Geochemical screening data', *Organic Geochemistry*, 29(1), pp. 519-530.

Creaney, S. and Passey, Q.R. (1993) 'Recurring patterns of total organic carbon and source rock quality within a sequence stratigraphic framework', *AAPG Bulletin*, 77(3), pp. 386-401.

Curiale, J.A. (1992) *Molecular maturity parameters within a single oil family: a case study from the Sverdrup Basin. In: Biological Markers in Sediments and Petroleum*. Moldowan J. M., Albracht P., Philp R. P. edn. Prentice-Hall, Englewood Cliffs, New Jersey, pp 295-300

Curiale, J.A. (1994) *Correlation of oils and source rocks-a conceptual and historical perspective*. New York, USA, pp 251-265.

Cushman, J.A.a.P., F. L. (1974) 'Bulimina and related foraminifear Genero', *U. S. Geology Survy Prof. Pap*, 210, p. 170.

Dahl, J.E., Moldowan, J.M., Peters, K.E., Claypool, G.E., Rooney, M.A., Michael, G.E., Mello, M.R. and Kohnen, M.L. (1999) 'Diamondoid hydrocarbons as indicators of natural oil cracking', *Nature*, 399(6731), pp. 54-57.

Dahl, J.E.P., Moldowan, J.M., Teerman, S.C., McCaffrey, M.A., Sundararaman, P. and Stelting, C.E. (1994) 'Source rock quality determination from oil biomarkers I: a new geochemical technique', *AAPG bulletin*, 78(10), pp. 1507-1526.

Dawson, D., Grice, K., Alexander, R. and Edwards, D. (2007) 'The effect of source and maturity on the stable isotopic compositions of individual hydrocarbons in sediments and crude oils from the Vulcan Sub-basin, Timor Sea, Northern Australia', *Organic Geochemistry*, 38(7), pp. 1015-1038.

De Grande, S.M.B., Aquino Neto, F.R. and Mello, M.R. (1993) 'Extended tricyclic terpanes in sediments and petroleums', *Organic geochemistry*, 20(7), pp. 1039-1047.

Demaison, G. (1984) 'The generative basin concept'.

Demaison, G.J.a.M., G. T. (1980) 'Anoxic environments and oil pressure bed genesis', *AAPG bulletin*, 64, pp. 1179-1209.

Didyk, B.M., Simoneit, B.R.T., Brassell, S.C.t. and Eglinton, G. (1978) 'Organic geochemical indicators of palaeoenvironmental conditions of sedimentation', *Nature*, 272(5650), pp. 216-222.

Dolson, J.C., Shann, M.V., Matbouly, S., Harwood, C., Rashed, R. and Hammouda, H. (2001) 'AAPG Memoir 74, Chapter 23: The Petroleum Potential of Egypt'.

Dow, W.G. (1977) 'Kerogen studies and geological interpretations', *Journal of Geochemical Exploration*, 7, pp. 79-99.

Ekweozor, C.M. and Strausz, O.P. (1981) 'Tricyclic terpanes in the Athabasca oil sands: their geochemistry', *Advances in Organic Geochemistry*, pp. 746-766.

El-Alami, M. (1996) *Habitat of oil Abu Attifel area, Sirt Basin, Libya. In the Geology of the Sirt Basin. In: The Geology of the Sirt Basin.* (*eds* M. J. Salam, M. T. Busrewil, A. A. Misallati, M. A. Sola), Elsevier, Amsterdam, II, pp 337-347.

El-Alami, M., Rahouma, S. and Butt, A. (1989) 'Hydrocarbon habitat in the Sirt Basin, northern Libya', *Petroleum Research Centre Journal*, , v. 5, pp. 17-28.

El-Bakai, M.T. (1996) 'Diagenesis and diagenetic history of the Lidam Formation in NW Sirt Basin', *The geology of Sirt Basin, II, Amsterdam, Elsevier*, pp. 83-98.

El-Gayar, M.S. (2005) 'Aromatic Steroids in Medeatern Crude Oils: Identification and Geochemical Application', *Petroleum Science and Technology* 23(7-8), pp. 971-990.

El Ghoul, A. (1996) *An approach to locate subtle Waha structural traps on the Zaltan Platform: grology and geophysics. In: The Geology of Sirt Basin*. (*eds* M.J. Salem, M.T. Busrewil, A.A Misallati and M.J Sola), Elsevier, Amsterdam, III, pp 137-154

Elag, M.O. (1996) *Sedimentological study of the Facha Member in the southwest Sirt Basin, Libya. In: The Geology of Sirt Basin.* (*eds* M. J. Salam, A. S. El-Hawat and A. M Sbeta), Elsevier, Amsterdam, II, pp 99-114.

Espitalie, J., Madec, M., Tissot, B., Mennig, J.J. and Leplat, P. (1977) 'Source rock characterization method for petroleum exploration', *Offshore Technology Conference*.

Fairhead, J.D. (1988) 'Mesozoic plate tectonic reconstruction of the central South Atlantic Ocean: The role of the West and Central Africa rift system', *Tectonophysics*, 155, pp. 181-191.

Fan, P., Philp, R.P., Li, Z., Yu, X. and Ying, G. (1991) 'Biomarker distributions in crude oils and source rocks from different sedimentary environments', *Chemical geology*, 93(1), pp. 61-78.

Farrimond, P., Bevan, J.C. and Bishop, A.N. (1999) 'Tricyclic terpane maturity parameters: response to heating by an igneous intrusion', *Organic Geochemistry*, 30(8), pp. 1011-1019.

Forster, P.G., Alexander, R. and Kagi, R.I. (1989) 'Identification and analysis of tetramethylnaphthalenes in petroleum', *Journal of Chromatography A*, 483, pp. 384-389.

Fowler, M.G. and Douglas, A.G. (1984) 'Distribution and structure of hydrocarbons in four organic-rich Ordovician rocks', *Organic Geochemistry*, 6, pp. 105-114.

Freeman, K.H., Hayes, J.M., Trendel, J.-M. and Albrecht, P. (1990) 'Evidence from carbon isotope measurements for diverse origins of sedimentary hydrocarbons', *Nature*, 343(6255), pp. 254-256.

Gaaya, A. and Ghenima, R. (1998) *60th EAGE Conference & Exhibition*.

Garrigues, P. and Ewald, M. (1983) 'Natural occurrence of 4-methyl-phenanthrene in petroleums and recent marine sediments: A new sensitive method to identify and quantify isomers in a series of alkyl—PAH: High resolution spectrofluorimetry at 15 K in n-alkane (Shpolskii effect)', *Organic geochemistry*, 5(2), pp. 53-56.

Gealey, W.K. (1988) 'Plate tectonic evolution of the Mediterranean-Middle East region', *Tectonophysics*, 155(1), pp. 285-306.

Goudarzi, G.H. (1980) *Structure – Libya. In: The Geology of Libya.* (*eds* M. J. Salem, M. T. Busrewil), Academic Press, London, III, pp 879-892.

Grantham, P.J. and Wakefield, L.L. (1988) 'Variations in the sterane carbon number distributions of marine source rock derived crude oils through geological time', *Organic Geochemistry*, 12(1), pp. 61-73.

Greenwood, P.F. and George, S.C. (1999) 'Mass spectral characteristics of C19 and C20 tricyclic terpanes detected in Latrobe tasmanite oil shale', *European Mass Spectrometry*, 5(3), pp. 221-230.

Gregory, W.A. and Hart, G.F. (1992) 'Towards a predictive model for the palynologic response to sea-level changes', *Palaios*, pp. 3-33.

Guiaud, R., Bellion, Y., Benkhelil, J., and Moreau, C., (1987) 'Post-Hercynian tectonics in Northern and Western Africa', *Geology*, 22, pp. 443-466.

Guiraud, R. (1998) 'Mesozoic rifting and basin inversion along the northern African Tethyan margin: an overview', *Geological Society, London, Special Publications*, 132(1), pp. 217-229.

Guiraud, R., Bellion, Y., (1995) *Late Carboniferous to Recent geodynamic evolution of West Gondwanian cratonic Tethyan margins.* . New York: Planum.

Guiraud, R., Binks, R.M., Fairhead, J.D. and Wilson, M. (1992) 'Chronology and geodynamic setting of Cretaceous-Cenozoic rifting in West and Central Africa', *Tectonophysics*, 213(1), pp. 227-234.

Guiraud, R. and Bosworth, W. (1997) 'Senonian basin inversion and rejuvenation of rifting in Africa and Arabia: synthesis and implications to plate-scale tectonics', *Tectonophysics*, 282(1), pp. 39-82.

Guiraud, R. and Bosworth, W. (1999) 'Phanerozoic geodynamic evolution of northeastern Africa and the northwestern Arabian platform', *Tectonophysics*, 315(1), pp. 73-104.

Guiraud, R.a.M., J, C. (1992) 'Early Cretaceous rifts of Western and Central Africa: an overview.', *Tectonophysics*, 213, pp. 153-168.

Gumati, Y.D. and Kanes, W.H. (1985) 'Early Tertiary subsidence and sedimentary facies--northern Sirte Basin, Libya', *AAPG Bulletin*, 69(1), pp. 39-52.

Gumati, Y.D., Kanes, W.H. and Schamel, S. (1996) 'An evaluation of the hydrocarbon potential of the sedimentary basins of Libya', *Journal of Petroleum Geology*, 19(1), pp. 95-112.

Gumati, Y.D. and Schamel, S. (1988) 'Thermal maturation history of the Sirte Basin, Libya', *Journal of Petroleum Geology*, 11(2), pp. 205-218.

Gürgey, K. (2003) 'Correlation, alteration, and origin of hydrocarbons in the GCA, Bahar, and Gum Adasi fields, western South Caspian Basin: geochemical and multivariate statistical assessments', *Marine and petroleum geology*, 20(10), pp. 1119-1139.

Hallam, A. and Bradshaw, M.J. (1979) 'Bituminous shales and oolitic ironstones as indicators of transgressions and regressions', *Journal of the Geological Society*, 136(2), pp. 157-164.

Hallett, D. (2002) *Petroleum Geology of Libya*. (*eds* Don Hallett), Elsevier, Amsterdam, I, p 503.

Hallett, D. and El Ghoul, A. (1996) *Oil and gas potential of deep troughs area in the Sirt Basin, Libya. In: The Geology of Sirt Basin.* (*eds* M. J. Salem, A. S. El-Hawat, and A. M. Sbeta), Elsevier, Amsterdam, II, 455-484.

Hamyani, E.A., Amr, I.A., Riani, M.A., El-Ghull, A.B. and Rahoma, S.A. (1984) 'Source and habitat of oil in Libyan basins', *Seminar on Source and Habitat of Petroleum in the Arab Countries*. Kuwait, October 1984. OAPEC, Kuwait, pp. 125-148.

Hantschel, T. and Kauerauf, A.I. (2009) *Fundamentals of basin and petroleum systems modeling*. Springer Dordrecht Heidelberg London New York: Springer Science & Business Media.

Haq, B.U., Hardenbol, J. and Vail, P.R. (1987) 'Chronology of fluctuating sea levels since the Triassic', *Science*, 235(4793), pp. 1156-1167.

Hardenbol, J. (1998) 'Mesozoic and Cenozoic sequence chronostratigraphic framework of European basins'.

Harding, T.P. (1984) 'Graben hydrocarbon occurrences and structural style', *AAPG Bulletin*, 68(3), pp. 333-362.

Hase, A. and Hites, R.A. (1976) 'On the origin of polycyclic aromatic hydrocarbons in recent sediments: biosynthesis by anaerobic bacteria', *Geochimica et Cosmochimica Acta*, 40(9), pp. 1141-1143.

Hayes, J.M. (1993) 'Factors controlling 13C contents of sedimentary organic compounds: Principles and evidence', *Marine Geology*, 113(1), pp. 111-125.

Hayes, J.M., Freeman, K.H., Popp, B.N. and Hoham, C.H. (1990) 'Compound-specific isotopic analyses: a novel tool for reconstruction of ancient biogeochemical processes', *Organic Geochemistry*, 16(4), pp. 1115-1128.

Hayes, J.M., Takigiku, R., Ocampo, R., Callot, H.J. and Albrecht, P. (1987) 'Isotopic compositions and probable origins of organic molecules in the Eocene Messel shale', *Nature*, 329, pp. 48-51.

Haynes, J.R. (1981) *Foraminifera*. Wiley Online Library.

Hays, J.D. and Pitman, W.C. (1973) 'Lithospheric plate motion, sea level changes and climatic and ecological consequences', *Nature*, 246(5427), pp. 18-22.

Hermanrud, C. (1993) 'Basin modelling: Advances and applications : Basin modelling techniques-an overview', *Norsk petroleumsforening. The Norwegian Petroleum Society's Conference*. Stavanger, Norway, 13-15 March 1991. Elsevier, p. 675.

Hirsch, F., Flexer, A., Rosenfeld, A. and Yellin - Dror, A. (1995) 'Palinspastic and crustal setting of the eastern Mediterranean', *Journal of Petroleum Geology*, 18(2), pp. 149-170.

Hoefs, J. (1987) *Stable isotope geochemistry*. (*eds* Hoefs, Jochen), Springer, New York, New York, p 241.

Holba, A.G., Tegelaar, E., Ellis, L., Singletary, M.S. and Albrecht, P. (2000) 'Tetracyclic polyprenoids: Indicators of freshwater (lacustrine) algal input', *Geology*, 28(3), pp. 251-254.

Huang, D., Jinchao, L. and Dajiang, Z. (1990) 'Maturation sequence of continental crude oils in hydrocarbon basins in China and its significance', *Organic Geochemistry*, 16(1), pp. 521-529.

Huc, A.Y. (1988) 'Aspects of depositional processes of organic matter in sedimentary basins', *Organic Geochemistry*, 13(1), pp. 263-272.

Hughes, W.B., Holba, A.G. and Dzou, L.I.P. (1995) 'The ratios of dibenzothiophene to phenanthrene and pristane to phytane as indicators of depositional environment and lithology of petroleum source rocks', *Geochimica et Cosmochimica Acta*, 59(17), pp. 3581-3598.

Hughes, W.B., Holba, A.G., Miller, D.E. and Richardson, J.S. (1985) 'Geochemistry of greater Ekofisk crude oils', in *Petroleum Geochemistry in Exploration of the Norwegian Shelf*. Springer, pp. 75-92.

Hunt, M.J. (1995) *Petroleum Geochemistry and Geology. (eds Hunt, M. J.), W. H. Freeman and Company, New York, USA, p 743*

Hussler, G., Chappe, B., Wehrung, P. and Albrecht, P. (1981) 'C27—C29 ring A monoaromatic steroids in Cretaceous black shales'.

Ishiwatari, R. and Fukushima, K. (1979) 'Generation of unsaturated and aromatic hydrocarbons by thermal alteration of young kerogen', *Geochimica et Cosmochimica Acta*, 43(8), pp. 1343-1349.

Issler, D.R. and Snowdon, L.R. (1990) 'Hydrocarbon generation kinetics and thermal modelling, Beaufort-Mackenzie Basin', *Bulletin of Canadian Petroleum Geology*, 38(1), pp. 1-16.

Janssen, M.E., Stephenson, R.A. and Cloetingh, S. (1995) 'Temporal and spatial correlations between changes in plate motions and the evolution of rifted basins in Africa', *Geological Society of America Bulletin*, 107(11), pp. 1317-1332.

Jinggui, L., Philp, P., Zifang, M., Wenhui, L., Jianjing, Z., Guojun, C., Mei, L. and Zhaoyun, W. (2005) 'Aromatic compounds in crude oils and source rocks and their application to oil–source rock correlations in the Tarim basin, NW China', *Journal of Asian Earth Sciences*, 25(2), pp. 251-268.

Jolliffe, I.T. (2002) *Principal Component Analysis. Springer-Verlag New York, USA, II, p 478*.

Karlsen, D.A. and Larter, S.R. (1991) 'Analysis of petroleum fractions by TLC-FID: applications to petroleum reservoir description', *Organic Geochemistry*, 17(5), pp. 603-617.

Killops, S.D. and Killops, V.J. (2009) *Introduction to organic geochemistry*. (*eds* Killops, Stephen D., Killops, Vanessa J.), John Wiley & Sons, p 408.

Kline, P. (1994) *An Easy Guide to Factor Analysis*. (eds Kline, P), Routledge, Psycholgy Press, p 194.

Klitgord, K.D.a.S., H. (1986) 'Kinematics of the central Atlantic. '. pp. 351-378 DNAG-GSA.

Knyth, J., Brydle, G. and Greenwood, D. (1996) *Tectonic history and structural development of the Kaf-Themar trend of the western Sirt Basin*. 1 edn. Amsterdam: Elsevier.

Kruge, M.A. (1986) 'Biomarker geochemistry of the Miocene Monterey Formation, west San Joaquin Basin, California: implications for petroleum generation', *Organic geochemistry*, 10(1), pp. 517-530.

Laflamme, R.E. and Hites, R.A. (1979) 'Tetra-and pentacyclic, naturally-occurring, aromatic hydrocarbons in recent sediments', *Geochimica et Cosmochimica Acta*, 43(10), pp. 1687-1691.

Langford, F.F. and Blanc-Valleron, M.M. (1990) 'Interpreting Rock-Eval Pyrolysis Data Using Graphs of Pyrolizable Hydrocarbons vs. Total Organic Carbon (1)', *AAPG Bulletin*, 74(6), pp. 799-804.

Larter, S., Huang, H., Adams, J., Bennett, B. and Snowdon, L.R. (2012) 'A practical biodegradation scale for use in reservoir geochemical studies of biodegraded oils', *Organic Geochemistry*, 45, pp. 66-76.

Larter, S.R. and Aplin, A.C. (1995) 'Reservoir geochemistry: methods, applications and opportunities', *Geological Society, London, Special Publications*, 86(1), pp. 5-32.

Larter, S.R., Bowler, B.F.J., Li, M., Chen, M., Brincat, D., Bennett, B., Noke, K., Donohoe, P., Simmons, D. and Kohnen, M. (1996) 'Molecular indicators of secondary oil migration distances', *Nature*, 383(6601), pp. 593-597.

Le Pichon, X., Bergerat, F. and Roulet, M.-J. (1988) 'Plate kinematics and tectonics leading to the Alpine belt formation; a new analysis', *Geological Society of America Special Papers*, 218, pp. 111-132.

Lewan, M.D., Spiro, B., Illich, H., Raiswell, R., Mackenzie, A.S., Durand, B., Manning, D.A.C., Comet, P.A., Berner, R.A. and De Leeuw, J.W. (1985) 'Evaluation of petroleum generation by hydrous pyrolysis experimentation [and discussion]', *Philosophical Transactions of the Royal Society of London. Series A, Mathematical and Physical Sciences*, 315(1531), pp. 123-134.

Li, M., Fowler, M.G., Obermajer, M., Stasiuk, L.D. and Snowdon, L.R. (1999) 'Geochemical characterisation of Middle Devonian oils in NW Alberta, Canada: possible source and maturity effect on pyrrolic nitrogen compounds', *Organic Geochemistry*, 30(9), pp. 1039-1057.

Li, M. and Larter, S.R. (1993) 'Interactions of organic species in crude oils with minerals, water and organic network: implications for petroleum geochemistry'. American Chemical Society.

Li, M., Larter, S.R., Frolov, Y.B. and Bjoroy, M. (1994) 'Adsorptive interaction between nitrogen compounds and organic and/or mineral phases in subsurface rocks. Models for compositional fractionation of pyrrolic nitrogen compounds in petroleum during petroleum migration', *Journal of high resolution chromatography*, 17(4), pp. 230-236.

Li, M., Larter, S.R., Stoddart, D. and Bjorøy, M. (1992) 'Practical liquid chromatographic separation schemes for pyrrolic and pyridinic nitrogen aromatic heterocycle fraction from crude oils suitable for rapid characterisation of geochemical samples.', *Analytical Chemistry*, 64, pp. 1337-1344.

Li, M., Larter, S.R., Stoddart, D. and Bjorøy, M. (1995b) 'Fractionation of pyrrolic nitrogen compounds in petroleum during migration: derivation of migration-related geochemical parameters', *Geological Society, London, Special Publications*, 86(1), pp. 103-123.

Li, M., Yao, H., Stasiuk, L.D., Fowler, M.G. and Larter, S.R. (1997) 'Effect of maturity and petroleum expulsion on pyrrolic nitrogen compound yields and distributions in Duvernay Formation petroleum source rocks in central Alberta, Canada', *Organic Geochemistry*, 26(11), pp. 731-744.

Luening, S., Marzouk, A.M. and Kuss, J. (1998) 'The Paleocene of central East Sinai, Egypt;" sequence stratigraphy" in monotonous hemipelagites', *The Journal of Foraminiferal Research*, 28(1), pp. 19-39.

Luning, S. (2003) 'Campanian-Maastrichtian organic-rich strata in North Africa: Distribution and depositional model ', *Petroleum Geology*.

Lüning, S., Kuss, J., Bachmann, M., Marzouk, A.M. and Morsi, A.M. (1998) 'Sedimentary response to basin inversion: Mid cretaceous-early tertiary pre-to syndeformational deposition at the Areif El Naqa anticline (Sinai, Egypt)', *Facies*, 38(1), pp. 103-136.

Mackenzie, A.S. (1984) *Application of biological markers in petroleum chemistry. In: Advances in Petroleum Geochemistry* (*eds* J. Brooks, D. H. Welte), Academic Press, London, pp 115-214.

Mackenzie, A.S., Hoffmann, C.F. and Maxwell, J.R. (1981) 'Molecular parameters of maturation in the Toarcian shales, Paris Basin, France—III. Changes in aromatic steroid hydrocarbons', *Geochimica et Cosmochimica Acta*, 45(8), pp. 1345-1355.

Mackenzie, A.S. and McKenzie, D. (1983) 'Isomerization and aromatization of hydrocarbons in sedimentary basins formed by extension', *Geological Magazine*, 120(05), pp. 417-470.

Mackenzie, A.S., Patience, R.L., Maxwell, J.R., Vandenbroucke, M. and Durand, B. (1980) 'Molecular parameters of maturation in the Toarcian shales, Paris Basin, France—I. Changes in the configurations of acyclic isoprenoid alkanes, steranes and triterpanes', *Geochimica et Cosmochimica Acta*, 44(11), pp. 1709-1721.

Magoon, L.B. and Dow, W.G. (1994) 'The petroleum system', *The petroleum system—From source to trap: AAPG Memoir*, 60, pp. 3-24.

Mango, F.D. (1990) 'The origin of light cycloalkanes in petroleum', *Geochimica et Cosmochimica Acta*, 54(1), pp. 23-27.

Mango, F.D. (1997) 'The light hydrocarbons in petroleum: a critical review', *Organic Geochemistry*, 26(7), pp. 417-440.

Mansour, T.A. and Magairyah, I.A. (1996) *Petroleum geology and stratigraphy of the south eastern part of the Sirt Basin. In: the Geology of the Sirt Basin. (eds M. J. Salam, M. T. Busrewil, A. A. Misallati, M. A. Sola), Elsevier, Amsterdam, II, pp 485-528*

Marshall, J.E.A., Brown, J.F. and Hindmarsh, S. (1985) 'Hydrocarbon source rock potential of the Devonian rocks of the Orcadian Basin', *Scottish Journal of Geology*, 21(3), pp. 301-320.

Matthews, D.E. and Hayes, J.M. (1978) 'Isotope-ratio-monitoring gas chromatography-mass spectrometry', *Analytical Chemistry*, 50(11), pp. 1465-1473.

McKirdy, D.M. and Aldridge, A.K. (1981) 'A Geochemical Comparison of sorne crude oils from Pre-Ordovician carbonate rocks', *Advances in organic geochemistry*, pp. 99-107.

McKirdy, D.M., Kantsler, A.J., Emmett, J.K. and Aldridge, A.K. (1984) *Hydrocarbon genesis and organic facies in Cambrian carbonates of the eastern Officer Basin, South Australia, In: Petroleum Geochemistry and Source Rock Potential of Carbonate Rocks*. Memori, SG 18, AAPG, New York, USA.

Meglen, R.R. (1992) 'Examining large databases: a chemometric approach using principal component analysis', *Marine Chemistry*, 39(1), pp. 217-237.

Mello, M.R., Gaglianone, P.C., Brassell, S.C. and Maxwell, J.R. (1988a) 'Geochemical and biological marker assessment of depositional environments using Brazilian offshore oils', *Marine and Petroleum Geology*, 5(3), pp. 205-223.

Mello, M.R., Telnaes, N., Gaglianone, P.C., Chicarelli, M.I., Brassell, S.C. and Maxwell, J.R. (1988b) 'Organic geochemical characterisation of depositional palaeoenvironments of source rocks and oils in Brazilian marginal basins', *Organic Geochemistry*, 13(1), pp. 31-45.

Moldowan, J.M. and Fago, F.J. (1986) 'Structure and significance of a novel rearranged monoaromatic steroid hydrocarbon in petroleum', *Geochimica et Cosmochimica Acta*, 50(3), pp. 343-351.

Moldowan, J.M., Fago, F.J., Huizinga, B.J. and Jacobson, S.R. (1991) '3.7) Analysis of oleanane and its occurrence in Upper Cretaceous rocks', *Organic Geochemistry: Advances and Applications in the Natural Environment*, 15, p. 195.

Moldowan, J.M., Lee, C.Y., Sundararaman, P., Salvatori, T., Alajbeg, A., Gjukic, B. and Demaison, G.J. (1989) 'Source correlation and maturity assessment of select oils and rocks from the Central Adriatic Basin (Italy and Yugoslavia)', *Preprints-American Chemical Society. Division of Petroleum Chemistry*, 34(1), pp. 112-121.

Moldowan, J.M., Lee, C.Y., Sundararaman, P., Salvatori, T., Alajbeg, A. and Gjukic, D. (1992) 'N.-E. AND WATT, DS, 1992. Source correlation and maturity assessment of select oils and rocks from the Central Adriatic basin (Italy and Yugoslavia)', *Biological Markers in Sediments and Petroleum. Prentice Hall (Englewood Cliffs)*, pp. 370-401.

Moldowan, J.M., Seifert, W.K. and Gallegos, E.J. (1983) 'Identification of an extended series of tricyclic terpanes in petroleum', *Geochimica et Cosmochimica Acta*, 47(8), pp. 1531-1534.

Moldowan, J.M., Seifert, W.K. and Gallegos, E.J. (1985) 'Relationship between petroleum composition and depositional environment of petroleum source rocks', *AAPG bulletin*, 69(8), pp. 1255-1268.

Moldowan, J.M., Sundararaman, P. and Schoell, M. (1986) 'Sensitivity of biomarker properties to depositional environment and/or source input in the Lower Toarcian of SW-Germany', *Organic Geochemistry*, 10(4), pp. 915-926.

Moustafa, A.R. and Khalil, M.H. (1990) 'Structural characteristics and tectonic evolution of north Sinai fold belts', *The geology of Egypt*, pp. 381-389.

Murray, A.P., Summons, R.E., Boreham, C.J. and Dowling, L.M. (1994) 'Biomarker and *n*-alkane isotope profiles for Tertiary oils: relationship to source rock depositional setting', *Organic Geochemistry*, 22(3), pp. 521-IN6.

Neto, F.R., Cardoso, J.N., Rodrigues, R. and Trindade, L.A.F. (1986) 'Evolution of tricyclic alkanes in the Espirito Santo Basin, Brazil', *Geochimica et Cosmochimica Acta*, 50(9), pp. 2069-2072.

Noble, R.A., Alexander, R., Kagi, R.I. and Nox, J.K. (1986) 'Identification of some diterpenoid hydrocarbons in petroleum', *Organic Geochemistry*, 10(4), pp. 825-829.

Orr, W.L. (1986) 'Kerogen/asphaltene/sulfur relationships in sulfur-rich Monterey oils', *Organic Geochemistry*, 10(1), pp. 499-516.

Ourisson, G., Albrecht, P. and Rohmer, M. (1979) 'The hopanoids: palaeochemistry and biochemistry of a group of natural products', *Pure and Applied Chemistry*, 51(4), pp. 709-729.

Ourisson, G., Albrecht, P. and Rohmer, M. (1982) 'Predictive microbial biochemistry—from molecular fossils to procaryotic membranes', *Trends in Biochemical Sciences*, 7(7), pp. 236-239.

Parfitt, M.A. and Farrimond, P. (1998) 'The Mupe Bay oil seep: a detailed organic geochemical study of a controversial outcrop', *Geological Society, London, Special Publications*, 133(1), pp. 387-397.

Parsons, M.G., Zagaar, A.M. and Curry, J.J. (1980) *Hydrocarbon occurrences in the Sirte basin, Libya*. Facts and Principles of World Petroleum Occurrence , AAPG, Memoir 6, CSPG Special Publications, pp 723-732

Pasley, M.A., Gregory, W.A. and Hart, G.F. (1991) 'Organic matter variations in transgressive and regressive shales', *Organic geochemistry*, 17(4), pp. 483-509.

Pepper, A.S. and Corvi, P.J. (1995) 'Simple kinetic models of petroleum formation. Part I: oil and gas generation from kerogen', *Marine and Petroleum Geology*, 12(3), pp. 291-319.

Peters, K., Walters, C. C., and Moldowan, J. M. (2005b) *The biomarker guide. Vol. 2, Biomarkers and isotopes in petroleum systems and Earth history*. 2nd ed. / K.E. Peters, C.C. Walters, J.M. Moldowan.. edn. Cambridge, UK

Peters, K.E. (1986) 'Guidelines for evaluating petroleum source rock using programmed pyrolysis', *AAPG Bulletin*, 70(3), pp. 318-329.

Peters, K.E. and Cassa, M.R. (1994) *Applied source rock geochemistry*. (eds Magoon, L. B and W. G. Dow), AAPG, New York, USA. pp 93-117.

Peters, K.E. and Moldowan, J.M. (1991) 'Effects of source, thermal maturity, and biodegradation on the distribution and isomerization of homohopanes in petroleum', *Organic geochemistry*, 17(1), pp. 47-61.

Peters, K.E. and Moldowan, J.M. (1993) *The biomarker guide: interpreting molecular fossils in petroleum and ancient sediments*. (*eds* Peters, Kenneth E. Moldowan, J. Michael), Prentice Hall Englewood Cliffs, NJ, p 363.

Peters, K.E., Moldowan, J.M., Driscole, A.R. and Demaison, G.J. (1989) 'Origin of Beatrice oil by co-sourcing from Devonian and Middle Jurassic source rocks, inner Moray Firth, United Kingdom', *AAPG Bulletin*, 73(4), pp. 454-471.

Peters, K.E., Moldowan, J.M., Schoell, M. and Hempkins, W.B. (1986) 'Petroleum isotopic and biomarker composition related to source rock organic matter and depositional environment', *Organic Geochemistry*, 10(1), pp. 17-27.

Peters, K.E., Walters, C.C. and Moldowan, J.M. (2005a) *The Biomarker guide, biomarkers and isotopes in petroleum exploration and earth history, vol 1–2*. New York: Cambridge University Press.

Philip, J., M. Floquet (2000a) *Atlas Peri-Tethys, Palaeogeographic maps*. In: Dercourt, J. edn. Paris: CCGM/CGMW.

Philip, J., M. Floquet (2000b) *Atlas Peri-Tethys, Palaeogeographic maps*. Paris: CCGM/CGMW.

Philp, R.P. (1985) 'Biological markers in fossil fuel production', *Mass Spectrometry Reviews*, 4(1), pp. 1-54.

Pratsch, J.C. (1991) 'Vertical hydrocarbon migration: a major exploration parameter', *Journal of Petroleum Geology*, 14(3), pp. 429-444.

Price, L.C. (1980) 'Utilization and documentation of vertical oil migration in deep basins', *Journal of Petroleum Geology*, 2(4), pp. 353-387.

Püttmann, W. and Villar, H. (1987) 'Occurrence and geochemical significance of 1, 2, 5, 6-tetramethylnaphthalene', *Geochimica et Cosmochimica Acta*, 51(11), pp. 3023-3029.

Radke, M. (1987) 'Organic geochemistry of aromatic hydrocarbons', *Advances in Petroleum Geochemistry, Academic Press, New York*, pp. 141-207.

Radke, M. (1988) 'Application of aromatic compounds as maturity indicators in source rocks and crude oils', *Marine and Petroleum Geology*, 5(3), pp. 224-236.

Radke, M., Leythaeuser, D. and Teichmüller, M. (1984) 'Relationship between rank and composition of aromatic hydrocarbons for coals of different origins', *Organic Geochemistry*, 6, pp. 423-430.

Radke, M., Rullkötter, J. and Vriend, S.P. (1994) 'Distribution of naphthalenes in crude oils from the Java Sea: source and maturation effects', *Geochimica et Cosmochimica Acta*, 58(17), pp. 3675-3689.

Radke, M. and Welte, D.H. (1981) 'The methylphenanthrene index (MPI): a maturity parameter based on aromatic hydrocarbons', *Advances in organic geochemistry*, 1983, pp. 504-512.

Radke, M., Welte, D.H. and Willsch, H. (1982a) 'Geochemical study on a well in the Western Canada Basin: relation of the aromatic distribution pattern to maturity of organic matter', *Geochimica et Cosmochimica Acta*, 46(1), pp. 1-10.

Radke, M., Welte, D.H. and Willsch, H. (1986) 'Maturity parameters based on aromatic hydrocarbons: influence of the organic matter type', *Organic Geochemistry*, 10(1), pp. 51-63.

Radke, M. and Willsch, H. (1991) 'Occurrence and thermal evolution of methylated benzo- and dibenzothiophenes in petroleum source rocks of western Germany', *Advances and Applications in Energy and the Natural Environment 15th Meeting of European Association of Organic Geochemists*. Manchester University Press, UK. pp. 480-484.

Requejo, A.G., Hieshima, G.B., Hsu, C.S., McDonald, T.J. and Sassen, R. (1997) 'Short-chain (C 21 and C 22) diasteranes in petroleum and source rocks as indicators of maturity and depositional environment', *Geochimica et cosmochimica acta*, 61(13), pp. 2653-2667.

Requejo, A.G., Sassen, R., McDonald, T., Denoux, G., Kennicutt Ii, M.C. and Brooks, J.M. (1996) 'Polynuclear aromatic hydrocarbons (PAH) as indicators of the source and maturity of marine crude oils', *Organic Geochemistry*, 24(10), pp. 1017-1033.

Riolo, J., Hussler, G., Albrecht, P. and Connan, J. (1986) 'Distribution of aromatic steroids in geological samples: their evaluation as geochemical parameters', *Organic Geochemistry*, 10(4), pp. 981-990.

Robison, V.D. (1995) 'Source rock characterization of the late cretaceous brown limestone of Egypt', in *Petroleum source rocks*. Springer, pp. 265-281.

Roohi, M. (1996) *A geological view of source-reservoir relationships in the western Sirt Basin. In: The geology of Sirt Basin.* (*eds* Salem, M.J., El-Hawat, A.S., Sbeta, A.M), Elsevier, Amsterdam, II, pp 323-336.

Roohi, M. (1996b) *Geological history and hydrocarbon migration pattern of the central Az Zahrah-Al Hufrah Platform. In: The geology of Sirt Basin.* . (*eds* Salem, M.J., El-Hawat, A.S., Sbeta, A.M.), Elsevier, Amsterdam, II, pp 435-454.

Rubinstein, I., Sieskind, O. and Albrecht, P. (1975) 'Rearranged sterenes in a shale: occurrence and simulated formation', *Journal of the Chemical Society, Perkin Transactions 1*, (19), pp. 1833-1836.

Rullkötter, J., Spiro, B. and Nissenbaum, A. (1985) 'Biological marker characteristics of oils and asphalts from carbonate source rocks in a rapidly subsiding graben, Dead Sea, Israel', *Geochimica et Cosmochimica Acta*, 49(6), pp. 1357-1370.

Savostin, L.A., Sibuet, J.-C., Zonenshain, L.P., Le Pichon, X. and Roulet, M.-J. (1986) 'Kinematic evolution of the Tethys belt from the Atlantic Ocean to the Pamirs since the Triassic', *Tectonophysics*, 123(1), pp. 1-35.

Schandelmeier, H.R.O. (1997) *Paleogeographic-Paleotectonic Atlas of North-Eastern Africa, Arabia and Adjacent Areas*. Balkema, Rotterdam.

Schiefelbein, C.F., Zumberge, J.E., Cameron, N.R. and Brown, S.W. (1999) 'Petroleum systems in the South Atlantic margins', *Geological Society, London, Special Publications*, 153(1), pp. 169-179.

Schlanger, S.O., and Jenkys, H. C. (1976) 'Creetaceous oceanic anoxic events: causes and consequences', *Geologie en Mijnbouw*, 55, pp. 179-184.

Schlanger, S.O., Jenkyns, H.C. and Premoli-Silva, I. (1981) 'Volcanism and vertical tectonics in the Pacific Basin related to global Cretaceous transgressions', *Earth and Planetary Science Letters*, 52(2), pp. 435-449.

Schoell, M., Hwang, R.J., Carlson, R.M.K. and Welton, J.E. (1994) 'Carbon isotopic composition of individual biomarkers in gilsonites (Utah)', *Organic Geochemistry*, 21(6), pp. 673-683.

Schröter, T. (1996) *Tectonic and sedimentary development of the central Zallah Trough (west Sirt Basin, Libya). In: The geology of Sirt Basin.* (*eds* M.J. Salem, M.T. Busrewil, A.A. Midallati, M.J. Sola), Elsevier, Amsterdam, III, pp 123-136.

Schwab, V.F. and Spangenberg, J.E. (2007) 'Molecular and isotopic characterization of biomarkers in the Frick Swiss Jura sediments: A palaeoenvironmental reconstruction on the northern Tethys margin', *Organic geochemistry*, 38(3), pp. 419-439.

Seifert, W.K. and J. M. Moldowan. (1981) 'Application of biological markers in combination with stable carbon isotopes to source rock/oil correlation, Prudhoe Bay, Alaska', *American Association of Petroleum Geologists Bulletin*, 65, pp. 990-1.

Seifert, W.K., Michael Moldowan, J. and Demaison, G.J. (1984) 'Source correlation of biodegraded oils', *Organic Geochemistry*, 6, pp. 633-643.

Seifert, W.K. and Moldowan, J. (1978) 'Applications of steranes, terpanes and monoaromatics to the maturation, migration and source of crude oils', *Geochimica et Cosmochimica Acta*, 42(1), pp. 77-95.

Seifert, W.K. and Moldowan, J.M. (1980) 'The effect of thermal stress on source-rock quality as measured by hopane stereochemistry', *Physics and Chemistry of the Earth*, 12, pp. 229-237.

Seifert, W.K. and Moldowan, J.M. (1986) *Use of biological markers in petroleum exploration. In: Methods in Geochemistry and Geophysics.* (eds R. B. Johns), Elsevier, Amsterdam, v. 24, pp 261-291.

Sghair, A.M.A. and El-Almi, M.A. (1996) *Depositional environment and diagenetic history of the Maragh Formation, NE Sirt Basin, Libya. In: The Geology of the Sirt Basin.* (eds M.J. Salm, M.T. Busrewil, A.A. Misallati, M.A. Sola), Elsevier, Amsterdam, II, pp 263-271.

Sieskind, O., Joly, G. and Albrecht, P. (1979) 'Simulation of the geochemical transformations of sterols: superacid effect of clay minerals', *Geochimica et Cosmochimica Acta*, 43(10), pp. 1675-1679.

Sikander, H., Basou, A. Wafa, F. and Rhouma, M. (2008) *Hydrocarbon potential and volumetric considerations for Cretaceous source rocks. In: The Geology of the East Libya,The geology of Libya, Earth Scince Society of Libya, (eds. Mustfa. J. Salem Elsveir Amstrdam) ,II, p. 393*

Silliman, J.E., Li, M., Yao, H. and Hwang, R. (2002) 'Molecular distributions and geochemical implications of pyrrolic nitrogen compounds in the Permian Phosphoria Formation derived oils of Wyoming', *Organic geochemistry*, 33(5), pp. 527-544.

Sliter, W.V. (1989) 'Aptian anoxia in the Pacific Basin', *Geology*, 17(10), pp. 909-912.

Sofer, Z., Bjoroy, M. and Hustad, E. (1991) '3.12) Isotopic composition of individual w-alkanes in oils', *Organic Geochemistry: Advances and Applications in the Natural Environment*, 15, p. 207.

Sofer, Z., Zumberge, J.E. and Lay, V. (1986) 'Stable carbon isotopes and biomarkers as tools in understanding genetic relationship, maturation, biodegradation, and migration of crude oils in the Northern Peruvian Oriente (Maranon) Basin', *Organic geochemistry*, 10(1), pp. 377-389.

Strachan, M.G., Alexander, R. and Kagi, R.I. (1986) 'Trimethylnaphthalenes as depositional environmental indicators.', *192nd Annual American Chemical Society Meeting*. Anaheim CA.

Strachan, M.G., Alexander, R. and Kagi, R.I. (1988) 'Trimethylnaphthalenes in crude oils and sediments: effects of source and maturity', *Geochimica et Cosmochimica Acta*, 52(5), pp. 1255-1264.

Subroto, E.A., Alexander, R. and Kagi, R.I. (1991) '30-Norhopanes: their occurrence in sediments and crude oils', *Chemical Geology*, 93(1), pp. 179-192.

Suess, E. (1904) *The face of the Earth*. Рипол Классик.

Taylor, G.H., Teichmuller, M., Davis, A., Diessel, C.F.K., Littke, R. and Robert, P. (1998) *Organic Petrology*. Gebrüder Borntraeger, Berlin, p 704.

Ten Haven, H.L., De Leeuw, J.W., Damsté, J.S.S., Schenck, P.A., Palmer, S.E. and Zumberge, J.E. (1988) 'Application of biological markers in the recognition of palaeohypersaline environments', *Geological Society, London, Special Publications*, 40(1), pp. 123-130.

Thompson, K.F.M. (1987) 'Fractionated aromatic petroleums and the generation of gas-condensates', *Organic Geochemistry*, 11(6), pp. 573-590.

Tissot, B.P. and Welte, D.H. (1984) *Petroleum Formation and occurrence*. 2 edn (I vols). Springer-Verlag, New York, USA, 699p.

Tyson, R.V. (1995) *Sedimentary organic matter; Organic facies and palynofacies*. London: Chapman & Hall, London, p 615.

Tyson, R.V. and Pearson, T.H. (1991) 'Modern and ancient continental shelf anoxia: an overview', *Geological Society, London, Special Publications*, 58(1), pp. 1-24.

Van Der Meer, F. and Cloetingh, S. (1993) 'Intraplate stresses and the subsidence history of the Sirte Basin (Libya)', *Tectonophysics*, 226(1), pp. 37-58.

Van Krevelen, D.W. (1993) *Coal-Typology, Physics, Chemistry, Constitution* Elsevier, Amsterdam, p 979.

Volk, H., George, S.C., Middleton, H. and Schofield, S. (2005) 'Geochemical comparison of fluid inclusion and present-day oil accumulations in the Papuan Foreland–evidence for previously unrecognised petroleum source rocks', *Organic Geochemistry*, 36(1), pp. 29-51.

Volkman, J. (2003) 'Sterols in microorganisms', *Applied microbiology and Biotechnology*, 60(5), pp. 495-506.

Volkman, J.K., Alexander, R., Kagi, R.I., Noble, R.A. and Woodhouse, C.W. (1983) 'A geochemical reconstruction of oil generation in the Barrow Sub-basin of Western Australia', *Geochimica et Cosmochimica Acta*, 47(12), pp. 2091-2105.

Volkman, J.K., Allen, D.I., Stevenson, P.L. and Burton, H.R. (1986) 'Bacterial and algal hydrocarbons in sediments from a saline Antarctic lake, Ace Lake', *Organic Geochemistry*, 10(4), pp. 671-681.

Volkman, J.K., Gllan, F.T., Johns, R.B. and Eglinton, G. (1981) 'Sources of neutral lipids in a temperate intertidal sediment', *Geochimica et Cosmochimica Acta*, 45(10), pp. 1817-1828.

Waples, D.W. (1980) 'Time and temperature in petroleum formation: application of Lopatin's method to petroleum exploration', *AAPG Bulletin*, 64(6), pp. 916-926.

Waples, D.W. (1985) *Geochemistry in petroleum exploration*. International Human Resources Development Corporation, Boston, MA, USA.

Waples, D.W. (1998) 'Basin modelling: how well have we done?', *Geological Society, London, Special Publications*, 141(1), pp. 1-14.

Waples, D.W. and Machihara, T. (1990) 'Application of sterane and triterpane biomarkers in petroleum exploration', *Bulletin of Canadian Petroleum Geology*, 38(3), pp. 357-380.

Welte, D.H. and Yalcin, M.N. (1988) 'Basin modelling—a new comprehensive method in petroleum geology', *Organic Geochemistry*, 13(1), pp. 141-151.

Wignall, P.B. (1994) *Black shales*. Clarendon Press Oxford.

Wignall, P.B. and Hallam, A. (1991) 'Biofacies, stratigraphic distribution and depositional models of British onshore Jurassic black shales', *Geological Society, London, Special Publications*, 58(1), pp. 291-309.

Wignall, P.B. and Maynard, J.R. (1993) 'The Sequence Stratigraphy of Transgressive Black Shales: Chapter 4'.

Williams, J.J. (1972) *Augila Field, Libya: Depositional Environment and Diagenesis of Sedimentary Reservoir and Description of Igneous Reservoir: Case Histories*. AAPG, M16, 623-632.

Wilson, M., Guiraud, R., Moreau, C. and Bellion, Y.-C. (1998) 'Late Permian to Recent magmatic activity on the African-Arabian margin of Tethys', *Geological Society, London, Special Publications*, 132(1), pp. 231-263.

Wilson, P.A. and Norris, R.D. (2001) 'Warm tropical ocean surface and global anoxia during the mid-Cretaceous period', *Nature*, 412(6845), pp. 425-429.

Wingert, W.S. (1992) 'GC-MS analysis of diamondoid hydrocarbons in Smackover petroleums', *Fuel*, 71(1), pp. 37-43.

Yamamoto, M., Taguchi, K. and Sasaki, K. (1991) 'Basic nitrogen compounds in bitumen and crude oils', *Chemical geology*, 93(1), pp. 193-206.

Yu, Q., Wen, Z. and Tang, Y. (2011) 'Geochemical characteristics of Ordovician crude oils in the northwest of the Tahe oil field, Tarim Basin', *Chinese Journal of Geochemistry*, 30(1), pp. 93-98.

Zhang, C., Zhang, Y., Zhang, M., Zhao, H. and Cai, C. (2008) 'Carbazole distributions in rocks from non-marine depositional environments', *Organic Geochemistry*, 39(7), pp. 868-878.

Zhang, S.C., Hanson, A.D., Moldowan, J.M., Graham, S.A., Liang, D.G., Chang, E. and Fago, F. (2000) 'Paleozoic oil–source rock correlations in the Tarim basin, NW China', *Organic Geochemistry*, 31(4), pp. 273-286.

Ziegler, P.A. (1988) 'Evolution of the Arctic-North Atlantic and western Tethys'. p. 198 43.

Ziegler, P.A. (ed.) (1990) *Geological Atlas of Western and Central Europe*. Shell International and Geological Society Soc. of London edn. London.

Ziegler, P.A., Cloetingh, S., Guiraud, R. and Stamphli, G. M. (2001) 'Peri-Tethyan platforms: Constraints on dynamics of rifiting and basin inversion. In: Pre-Tethys Memoir 6: Pre-Tethyan Rift/Wrench Basins and Passive Margin', *(eds P.A. Ziegler, W. Cavazza, A. H. F. Robertson and S. Crasquin-Soleau. Mem. Mus. nath. Hist. Nat.)*, 186, pp. 9-49.

Appendices

Appendix I: Table 4.1 Total organic carbon and Rock-Eval pyrolysis data for the Upper Cretaceous source rocks in the Sirt Basin.

Well Name	Age	Formation Name	Depth feet	TOC wt%	S1 mgHC/g rock	S2	HI mg HC/g TOC	PI	T max ºC	S1+S2 mgHC/g rock	S1/TOC	HIº mg HC/g TOC	TOCº wt%
6A1-59	Upper Cretaceous	Kalash	7130	3.05	1.30	15.97	524	0.08	433	17.27	0.43	489	5.18
			7140	3.81	1.44	21.38	561	0.06	434	22.82	0.38	542	6.48
			7150	3.76	1.55	22.42	596	0.06	437	23.97	0.41	636	6.39
			7160	3.19	1.25	18.13	568	0.06	432	19.38	0.39	511	5.43
			7170	3.28	1.06	18.79	572	0.05	433	19.85	0.32	534	5.58
			7180	1.23	0.14	2.75	224	0.05	439	2.89	0.11	254	2.09
			7190	0.85	0.04	0.94	110	0.04	430	0.98	0.05	92	1.45
			7200	0.87	0.09	0.98	113	0.08	432	1.07	0.10	102	1.48
			7207	0.82	0.07	0.68	83	0.09	430	0.75	0.09	69	1.40
			7210	0.94	0.11	1.45	154	0.07	429	1.56	0.12	123	1.60
		Sirte Shale	7220	2.50	0.49	9.82	393	0.05	434	10.31	0.20	380	4.25
			7230	2.08	0.52	8.33	400	0.06	429	8.85	0.25	320	3.54
			7240	2.76	0.82	12.59	457	0.06	432	13.41	0.30	411	4.69
			7250	3.88	1.79	22.08	569	0.07	432	23.87	0.46	512	6.59
			7260	3.01	1.15	15.16	504	0.07	432	16.31	0.38	454	5.11
			7270	1.98	0.39	6.69	338	0.06	432	7.08	0.20	304	3.36
			7280	2.77	0.99	13.11	473	0.07	432	14.10	0.36	425	4.72
B1-NC74F	Upper Creteacous	Sirte Shale	6980-90	0.71	0.73	1.32	185	0.36	433	2.05	1.02	173	1.21
			7000-10	0.51	0.61	0.99	193	0.38	433	1.6	1.19	180	0.87
			7010-20	1.51	1.62	2.34	155	0.41	430	3.96	1.08	130	2.56
			7010-20	1.51	1.74	2.25	149	0.44	429	3.99	1.16	120	2.56
			7020-30	1.45	2.29	1.95	134	0.54	437	4.24	1.58	143	2.47
			7030-40	1.11	2.27	2.47	223	0.48	430	4.74	2.05	186	1.88
			7040-50	1.64	2.28	2.91	177	0.44	433	5.19	1.39	166	2.79
			7050-60	1.66	3.02	3.72	223	0.45	435	6.74	1.81	223	2.83
			7050-60	1.66	3.12	3.84	231	0.45	433	6.96	1.87	215	2.83
			7060-70	1.79	2.01	4.39	245	0.31	435	6.4	1.12	245	3.05

TOC: Total organic Carbon content, wt%; S1: Free hydrocarbons, mg/g rock; S2: Potential hydrocarbon, mg HC/g rock; HI: Hydrogen Index, mg HC/g TOC; PI: Production Index, (S1/S1+S2); Tmax ºC: Temperature Pyrolysis; HIº: Initial Hydrogen Index; TOCº: Initial Total Organic Carbon

Appendix I: Cont. Table 4.1 Total organic carbon and Rock-Eval pyrolysis data for the Upper Cretaceous source rocks in the Sirt Basin.

Well Name	Age	Formation Name	Depth feet	TOC wt%	S1 mgHC/g rock	S2	HI mg HC/g TOC	PI	T max ºC	S1+S2 mgHC/g rock	S1/TOC	HI° mg HC/g TOC	TOC° wt%
B1-NC74F	Upper Creteacous	Sirte Shale	7070-80	1.56	1.91	2.92	187	0.4	431	4.83	1.23	162	2.65
			7080-90	1.81	2.12	2.89	160	0.42	433	5.01	1.17	149	3.07
			7090-100	1.68	2.85	3.9	233	0.42	428	6.75	1.70	178	2.85
			7110-120	1.83	5.27	8.31	455	0.39	441	13.58	2.89	546	3.10
			7110-120	1.83	5.34	8.11	444	0.4	436	13.45	2.92	459	3.10
			7120-130	4.04	4.45	8.96	222	0.33	443	13.41	1.10	281	6.86
			7130-140	3.88	2.11	4.88	126	0.3	433	6.99	0.54	117	6.59
			7130-140	3.88	2.04	4.84	125	0.3	438	6.88	0.53	137	6.59
			7140-150	1.95	2.76	3.88	199	0.42	435	6.64	1.42	199	3.31
			7140-150	1.95	2.57	3.77	194	0.41	442	6.34	1.32	239	3.31
			7150-160	1.78	1.87	3.72	209	0.33	440	5.59	1.05	244	3.02
			7160-70	1.68	1.18	2.93	174	0.3	433	4.11	0.70	163	2.86
			7170-180	1.47	2.08	3.67	250	0.36	439	5.75	1.41	283	2.50
			7170-180	1.47	2	3.39	231	0.37	436	5.39	1.36	238	2.50
			7180-190	1.74	1.05	3.33	191	0.24	439	4.38	0.60	216	2.97
			7190-200	1.70	1.68	3.18	187	0.35	441	4.86	0.99	224	2.90
			7200-210	6.73	7.55	8.44	125	0.47	430	15.99	1.12	104	11.44
			7200-10	6.73	7.89	10.1	150	0.44	436	17.98	1.17	155	11.44
		Rachmat	7930-40	1.38	1.78	3.15	228	0.36	435	4.93	1.29	228	2.35
			7930-40	1.38	1.83	3.32	240	0.35	434	5.15	1.32	232	2.35
			7940-50	1.05	1.69	3.03	287	0.36	437	4.72	1.60	306	1.79
			7940-50	1.05	1.09	2.59	246	0.3	437	3.68	1.03	262	1.79
			7950-60	1.22	1.19	2.79	228	0.31	435	3.98	0.97	228	2.08
			7960-70	1.24	1.45	2.91	235	0.33	433	4.36	1.17	219	2.11
			7960-70	1.24	1.44	2.92	236	0.33	435	4.36	1.16	236	2.11
			7970-80	1.31	1.7	3.21	245	0.35	431	4.91	1.30	212	2.23
			7980-90	1.51	2.23	4.12	274	0.35	442	6.35	1.48	337	2.56
			7990-8000	1.49	2.03	3.62	243	0.36	437	5.65	1.36	259	2.54
			7990-8000	1.49	2.42	5.75	385	0.3	437	8.17	1.62	411	2.54
			7990-8000	1.49	2.42	5.74	385	0.3	441	8.16	1.62	461	2.54

Appendix I: Cont. Table 4.1 Total organic carbon and Rock-Eval pyrolysis data for the Upper Cretaceous source rocks in the Sirt Basin.

Well Name	Age	Formation Name	Depth feet	TOC wt%	S1 mgHC/g rock	S2	HI mg HC/g TOC	PI	T max ºC	S1+S2 mgHC/g rock	S1/TOC	HI* mg HC/g TOC	TOC* wt%
B1-NC74F	Upper Cretacous	Rachmat	8020-30	1.90	2.05	3.68	194	0.36	431	5.73	1.08	168	3.23
			8020-30	1.90	1.95	3.75	197	0.34	437	5.7	1.03	211	3.23
			8070-80	1.35	1.83	3.51	260	0.34	436	5.34	1.35	268	2.30
			8080-90	1.15	1.44	2.64	230	0.35	435	4.08	1.26	230	1.95
			8090-100	1.20	1.41	2.68	223	0.35	435	4.09	1.17	223	2.04
			8090-100	1.20	1.38	3.01	250	0.32	437	4.39	1.15	267	2.04
			8090-100	1.20	1.28	3.01	250	0.3	439	4.29	1.07	284	2.04
B2-NC74A	Upper Cretaceous	Sirte Shale	9500-10	0.70	0.61	1.03	147	0.37	428	1.64	0.87	113	1.19
			9510-20	0.58	0.33	0.82	141	0.29	429	1.15	0.57	112	0.99
			9520-30	0.71	0.58	1.11	157	0.35	425	1.69	0.82	104	1.20
			9530-40	0.67	0.51	1.17	175	0.32	430	1.68	0.76	146	1.14
			9540-50	0.81	0.58	1.04	129	0.36	426	1.62	0.72	90	1.37
			9550-60	0.80	0.52	1.21	151	0.36	433	1.73	0.65	141	1.36
			9560-70	0.71	0.40	1.00	141	0.29	431	1.40	0.56	122	1.20
			9570-80	1.09	0.82	1.67	154	0.33	428	2.49	0.75	118	1.85
			9580-90	1.41	0.79	1.68	119	0.32	429	2.47	0.56	95	2.40
			9590-600	1.36	0.32	1.07	79	0.23	436	1.39	0.24	81	2.31
			9600-610	0.84	0.50	1.20	143	0.29	431	1.70	0.60	124	1.42
			9610-20	0.79	0.34	1.16	147	0.23	433	1.50	0.43	137	1.34
			9680-90	1.46	1.33	2.51	172	0.35	429	3.84	0.91	138	2.48
			9690-700	1.24	0.74	1.83	147	0.29	431	2.57	0.60	128	2.11
			9700-710	1.39	1.18	2.33	167	0.34	430	3.51	0.85	139	2.37
			9710-720	1.58	1.72	2.96	187	0.37	431	4.68	1.09	162	2.69
			9720-730	1.72	1.56	3.23	188	0.33	432	4.79	0.91	169	2.92
			9730-740	1.62	1.80	2.86	176	0.31	436	4.66	1.11	182	2.76
			9730-740	1.62	1.42	2.70	166	0.34	433	4.12	0.87	155	2.76

Appendix I: Cont. Table 4.1 Total organic carbon and Rock-Eval pyrolysis data for the Upper Cretaceous source rocks in the Sirt Basin.

Well Name	Age	Formation Name	Depth feet	TOC wt%	S1 mgHC/g rock	S2	HI mg HC/g TOC	PI	T max ºC	S1+S2 mgHC/g rock	S1/TOC	HI₀ mg HC/g TOC	TOC₀ wt%
C2-16	Upper Cretaceous	Sirte Shale	9780-90	1.61	0.62	2.28	142	0.21	445	2.9	0.39	189	2.73
			9800-05	1.61	0.58	2.56	159	0.18	439	3.14	0.36	180	2.74
			9826-30	1.43	0.39	1.36	95	0.22	444	1.75	0.27	124	2.43
			9840-50	1.41	0.24	0.97	69	0.2	447	1.21	0.17	97	2.39
			9860-70	1.39	0.48	1.75	126	0.22	445	2.23	0.35	168	2.36
			9880-90	1.31	0.35	1.38	105	0.2	447	1.73	0.27	147	2.23
			9900-10	1.03	0.28	1.02	99	0.22	446	1.3	0.27	135	1.75
			9920-30	0.98	0.26	0.95	97	0.22	441	1.21	0.26	116	1.67
			9940-50	0.98	0.15	1.19	121	0.11	442	1.34	0.15	149	1.67
			9960-70	1.06	0.12	0.61	57	0.17	443	0.73	0.11	73	1.81
			9980-90	1.12	0.21	0.86	77	0.2	445	1.07	0.19	102	1.90
			10000-10	1.16	0.38	1.22	105	0.24	446	1.6	0.33	143	1.98
			10010-20	1.19	0.31	1.28	108	0.2	448	1.59	0.26	155	2.02
			10020-30	1.04	0.19	0.8	77	0.19	444	0.99	0.18	100	1.77
			10040-50	1.09	0.11	0.91	84	0.11	443	1.02	0.10	106	1.85
			10060-70	1.14	0.19	1.12	98	0.15	447	1.31	0.17	138	1.93
			10090-100	1.08	0.1	0.76	71	0.12	440	0.86	0.09	82	1.83
			10110-20	1.08	0.23	1.08	100	0.18	445	1.31	0.21	133	1.84
			10130-40	0.82	0.13	0.57	69	0.19	440	0.7	0.16	81	1.40
			10150-60	0.97	0.1	0.63	65	0.14	441	0.73	0.10	78	1.64
			10180-90	1.37	0.27	1.11	81	0.2	442	1.38	0.20	100	2.33
			10200-10	1.47	0.44	1.73	117	0.2	444	2.17	0.30	153	2.51
			10220-30	1.57	0.45	1.63	104	0.22	443	2.08	0.29	131	2.67
			10240-50	1.31	0.25	1.08	82	0.19	447	1.33	0.19	115	2.23
			10260-70	1.58	0.65	2.22	141	0.23	439	2.87	0.41	160	2.68
			10280-90	1.11	0.3	1.13	102	0.21	449	1.43	0.27	149	1.89

Appendix I: Cont. Table 4.1 Total organic carbon and Rock-Eval pyrolysis data for the Upper Cretaceous source rocks in the Sirt Basin.

Well Name	Age	Formation Name	Depth feet	TOC wt%	S1 mgHC/g rock	S2	HI mg HC/g TOC	PI	T max ºC	S1+S2 mgHC/g rock	S1/TOC	HI° mg HC/g TOC	TOC° wt%
C2-16	Upper Cretaceous	Sirte Shale	10300-10	1.24	0.21	0.94	76	0.18	444	1.15	0.17	99	2.11
			10320-30	0.98	0.22	1	102	0.18	446	1.22	0.22	139	1.67
			10340-50	1.14	0.24	1.17	103	0.17	447	1.41	0.21	144	1.93
			10360-70	1.44	0.37	1.54	107	0.19	445	1.91	0.26	143	2.44
			10380-90	1.76	0.45	1.89	107	0.19	446	2.34	0.26	147	2.99
			10400-10	1.17	0.26	1.13	96	0.19	446	1.39	0.22	131	2.00
			10420-30	1.30	0.36	1.37	106	0.21	442	1.73	0.28	130	2.20
			10440-50	1.66	0.4	1.23	74	0.25	442	1.63	0.24	92	2.81
			10460-70	1.27	0.4	1.36	107	0.23	446	1.76	0.31	146	2.17
			10480-90	1.52	0.54	1.64	108	0.25	450	2.18	0.35	162	2.59
			10500-10	1.33	0.44	1.59	120	0.22	444	2.03	0.33	156	2.25
			10520-30	0.97	0.09	0.37	38	0.2	443	0.46	0.09	48	1.65
			10540-50	1.34	0.27	0.9	67	0.23	445	1.17	0.20	90	2.27
			10550-60	1.21	0.2	0.83	69	0.2	438	1.03	0.17	76	2.05
			10560-70	1.23	0.28	1.47	120	0.16	443	1.75	0.23	151	2.09
			10580-90	1.35	0.44	1.66	123	0.21	443	2.1	0.33	156	2.29
			10600-10	0.89	0.17	0.85	95	0.17	445	1.02	0.19	127	1.52
			10620-30	0.90	0.13	0.68	75	0.16	445	0.81	0.14	100	1.53
			10640-50	0.88	0.12	0.59	67	0.17	442	0.71	0.14	83	1.49
			10660-70	0.79	0.1	0.72	91	0.12	441	0.82	0.13	109	1.35
			10680-90	0.90	0.08	0.6	67	0.12	437	0.68	0.09	71	1.53
			10700-10	0.97	0.16	0.75	77	0.18	444	0.91	0.16	101	1.65
			10720-30	0.96	0.15	0.58	61	0.21	441	0.73	0.16	73	1.63
			10740-50	0.83	0.08	0.28	34	0.22	435	0.36	0.10	34	1.42
			10760-70	0.79	0.13	0.37	47	0.26	438	0.5	0.16	52	1.34
			10780-90	0.98	0.1	0.35	36	0.23	441	0.45	0.10	43	1.66
			10800-10	0.99	0.2	0.92	93	0.18	441	1.12	0.20	112	1.68

Appendix I: Cont. Table 4.1 Total organic carbon and Rock-Eval pyrolysis data for the Upper Cretaceous source rocks in the Sirt Basin.

Well Name	Age	Formation Name	Depth feet	TOC wt%	S1 mgHC/g rock	S2	HI mg HC/g TOC	PI	T max ºC	S1+S2 mgHC/g rock	S1/TOC	HI- mg HC/g TOC	TOC- wt%
C2-16	Upper Cretaceous	Sirte Shale	10820-30	0.92	0.21	0.69	75	0.23	438	0.9	0.23	82	1.57
			10840-50	1.03	0.23	1.06	103	0.18	441	1.29	0.22	124	1.75
			10860-70	0.92	0.18	0.67	73	0.21	445	0.85	0.20	97	1.56
			10880-90	1.04	0.21	0.82	79	0.21	443	1.03	0.20	100	1.76
			10900-10	0.99	0.33	0.86	87	0.28	447	1.19	0.33	121	1.69
			10920-30	1.06	0.32	0.86	81	0.27	441	1.18	0.30	98	1.80
			10940-50	1.03	0.09	0.51	50	0.15	444	0.6	0.09	64	1.75
			10960-70	1.09	0.25	0.83	76	0.23	442	1.08	0.23	94	1.86
			10980-90	1.12	0.16	0.73	65	0.18	441	0.89	0.14	78	1.90
			11000-10	1.15	0.25	0.8	70	0.24	444	1.05	0.22	91	1.95
			11010-20	1.17	0.45	1	86	0.31	441	1.45	0.39	103	1.98
FF14-6	Upper Cretaceous	Sirte Shale	11270	1.01	0.27	1.05	104	0.20	532	1.32	0.27	442	1.71
			11330	0.99	0.17	0.65	66	0.21	519	0.82	0.17	251	1.67
			11360	1.03	0.18	0.53	51	0.25	544	0.71	0.17	238	1.75
			11400	0.97	0.13	0.35	36	0.27	542	0.48	0.13	165	1.65
			11420	0.87	0.22	0.6	69	0.27	506	0.82	0.25	232	1.48
			11440	0.97	0.22	0.53	55	0.29	545	0.75	0.23	256	1.64
			11470	0.72	0.14	0.32	44	0.30	549	0.46	0.19	213	1.22
			11490	1.01	0.16	0.47	46	0.25	532	0.63	0.16	197	1.72
			11510	0.89	0.17	0.56	63	0.23	513	0.73	0.19	228	1.51
			11550	0.66	0.13	0.27	41	0.33	495	0.4	0.20	124	1.11
			11580	0.53	0.05	0.24	45	0.17	535	0.29	0.09	195	0.91
			11590	0.46	0.04	0.08	17	0.33	522	0.12	0.09	67	0.79
			11615	0.60	0.08	0.09	15	0.47	521	0.17	0.13	58	1.02
			11628	0.78	0.1	0.39	50	0.20	514	0.49	0.13	181	1.33
			11630	0.58	0.11	0.07	12	0.61	436	0.18	0.19	13	0.98
			11680	0.80	0.09	0.13	16	0.41	497	0.22	0.11	50	1.35

Appendix I: Cont. Table 4.1 Total organic carbon and Rock-Eval pyrolysis data for the Upper Cretaceous source rocks in the Sirt Basin.

Well Name	Age	Formation Name	Depth feet	TOC wt%	S1 mgHC/g rock	S2	HI mg HC/g TOC	PI	T max ºC	S1+S2 mgHC/g rock	S1/TOC	HI- mg HC/g TOC	TOC- wt%
FF14-6	Upper Cretaceous	Sirte Shale	11720	0.78	0.08	0.63	80	0.11	533	0.71	0.10	343	1.33
			11750	0.74	0.36	0.25	34	0.59	526	0.61	0.48	136	1.26
			11770	0.91	0.09	0.23	25	0.28	532	0.32	0.10	107	1.54
			11800	1.34	0.05	0.3	22	0.14	435	0.35	0.04	22	2.27
			11810	0.76	0.04	0.07	9	0.36	517	0.11	0.05	34	1.29
			11814	0.81	0.03	0.01	1	0.75	515	0.04	0.04	5	1.38
			11830	1.07	0.09	0.18	17	0.33	504	0.27	0.08	55	1.82
			11880	0.73	0.1	0.19	26	0.34	418	0.29	0.14	11	1.23
			11920	0.96	0.1	0.03	3	0.77	478	0.13	0.10	8	1.64
			11950	0.59	0.09	0.26	44	0.26	436	0.35	0.15	45	1.01
			12000	0.74	0.05	0.01	1	0.83	421	0.06	0.07	1	1.26
			12050	0.62	0.08	0.15	24	0.35	545	0.23	0.13	113	1.05
			12070	0.61	0.22	0.68	111	0.24	486	0.9	0.36	300	1.04
			12100	0.69	0.12	0.36	53	0.25	515	0.48	0.18	193	1.17
			12140	0.68	0.07	0.16	24	0.30	512	0.23	0.10	84	1.15
			12170	0.58	0.28	0.78	134	0.26	511	1.06	0.48	473	0.99
			12210	3.44	0.27	2.05	60	0.12	434	2.32	0.08	58	5.84
			12250	0.74	0.18	0.44	60	0.29	520	0.62	0.24	229	1.25
			12270	0.52	0.07	0.55	11	0.56	503	0.125	0.13	34	0.89
			12300	2.02	0.22	1.11	55	0.17	449	1.33	0.11	81	3.43
			12340	2.20	0.25	1.77	80	0.12	449	2.02	0.11	118	3.74
			12380	0.75	0.12	0.04	5	0.75	513	0.16	0.16	19	1.28
			12410	0.36	0.1	0.1	28	0.50	501	0.2	0.28	89	0.61
			12440	0.74	0.06	0.07	9	0.46	487	0.13	0.08	26	1.26
			12500	0.59	0.15	0.09	15	0.63	510	0.24	0.25	53	1.01
			12560	0.52	0	0.02	4	0.00	479	0.02	0.00	9	0.89
			12650	0.66	0.12	0.26	39	0.32	454	0.38	0.18	64	1.12

Appendix I: Cont. Table 4.1 Total organic carbon and Rock-Eval pyrolysis data for the Upper Cretaceous source rocks in the Sirt Basin.

Well Name	Age	Formation Name	Depth feet	TOC wt%	S1 mgHC/g rock	S2	HI mg HC/g TOC	PI	T max ºC	S1+S2 mgHC/g rock	S1/TOC	HI◦ mg HC/g TOC	TOC◦ wt%
FF14-6	Upper Creta	Sirte Shale	12680	0.46	0.02	0.01	2	0.67	425	0.03	0.04	1	0.78
			12710	0.71	0.07	0.01	1	0.88	486	0.08	0.10	4	1.20
			12870	0.40	0.02	0.02	5	0.50	523	0.04	0.05	20	0.67
			13050	1.77	0.03	0.02	1	0.60	541	0.05	0.02	5	3.01
L1-16	Upper Cretaceous	Sirte Shale	7400-10	1.10	0.19	2.96	270	0.06	436	3.15	0.17	279	1.86
			7440-50	1.04	0.17	1.57	151	0.10	432	1.74	0.16	135	1.77
			7470-80	1.06	0.18	1.55	147	0.10	433	1.73	0.17	137	1.80
			7490-500	0.95	0.13	1.26	133	0.09	432	1.39	0.14	120	1.61
			7510-20	1.03	0.17	1.65	161	0.09	432	1.82	0.17	145	1.75
			7530-40	1.34	0.22	2.52	188	0.08	432	2.74	0.16	169	2.28
			7530-40d	1.34	0.25	2.49	186	0.09	430	2.74	0.19	155	2.28
			7550-60	1.03	0.19	1.77	171	0.10	432	1.96	0.18	154	1.76
			7570-80	1.04	0.17	1.77	170	0.09	434	1.94	0.16	164	1.77
			7590-600	1.25	0.23	2.38	190	0.09	434	2.61	0.18	183	2.13
			7610-20	1.22	0.22	2.18	178	0.09	433	2.4	0.18	167	2.08
			7610-20d	1.22	0.22	2.12	173	0.09	430	2.34	0.18	145	2.08
			7630-40	1.04	0.21	1.51	145	0.12	435	1.72	0.20	145	1.76
			7640-50	1.22	0.21	2.58	211	0.08	433	2.79	0.17	197	2.07
			7650-60	1.30	0.25	2.51	193	0.09	431	2.76	0.19	167	2.21
			7670-80	1.19	0.22	2.35	197	0.09	434	2.57	0.18	191	2.02
			7700-10	0.98	0.14	1.49	152	0.09	433	1.63	0.14	142	1.67
			7720-30	0.88	0.2	1.39	158	0.13	435	1.59	0.23	158	1.49
			7750-60	0.80	0.15	1.13	142	0.12	434	1.28	0.19	137	1.36
			7770-80	0.74	0.08	0.78	106	0.09	433	0.86	0.11	99	1.25
			7790-800	0.72	0.1	0.78	109	0.11	431	0.88	0.14	94	1.22
			7820-30	0.68	0.07	0.61	90	0.10	434	0.68	0.10	87	1.16

Appendix I: Cont. Table 4.1 Total organic carbon and Rock-Eval pyrolysis data for the Upper Cretaceous source rocks in the Sirt Basin.

Well Name	Age	Formation Name	Depth feet	TOC wt%	S1 mgHC/g rock	S2	HI mg HC/g TOC	PI	T max ºC	S1+S2 mgHC/g rock	S1/TOC	HI° mg HC/g TOC	TOC° wt%
L1-16	Upper Cretaceous	Sirte Shale	7850-60	1.08	0.14	1.55	144	0.08	434	1.69	0.13	139	1.83
			7890-900	0.92	0.09	1.11	121	0.08	433	1.2	0.10	112	1.57
			7920-30	0.62	0.07	0.62	101	0.10	433	0.69	0.11	94	1.05
			7940-50	0.59	0.14	0.77	131	0.15	431	0.91	0.24	113	1.00
			7980-90	0.50	0.09	0.57	114	0.14	433	0.66	0.18	106	0.85
			8060-70	0.78	0.14	2	255	0.07	444	2.14	0.18	332	1.33
			8260-70	0.88	0.3	1.47	168	0.17	438	1.77	0.34	184	1.49
			8360-70	0.78	0.22	0.98	126	0.18	434	1.2	0.28	121	1.33
L1-17	Upper Cretaceous	Sirte Shale	6060-70	2.00	0.27	6.77	339	0.04	439	7.04	0.14	384	3.39
			6100-10	1.91	0.44	6.86	359	0.06	436	7.3	0.23	371	3.25
			6120-30	1.74	0.18	4.89	282	0.04	439	5.07	0.10	319	2.95
			6150-60	1.20	0.22	3.06	254	0.07	435	3.28	0.18	254	2.05
			6170-80	1.61	0.37	4.55	282	0.08	437	4.92	0.23	301	2.74
			6200-10	1.46	0.23	4.24	291	0.05	434	4.47	0.16	282	2.47
			6240-50	1.02	0.13	1.71	168	0.07	437	1.84	0.13	179	1.73
			6260-70	0.99	0.08	1.04	105	0.07	431	1.12	0.08	91	1.68
			6290-300	1.53	0.2	3.47	227	0.05	438	3.67	0.13	249	2.60
			6300-10	1.94	0.23	5.76	296	0.04	438	5.99	0.12	326	3.31
			6340-50	1.75	0.28	4.69	268	0.06	438	4.97	0.16	295	2.97
			6350-60	1.14	0.17	2.26	198	0.07	435	2.43	0.15	198	1.94
			6370-80	1.53	0.31	3.7	243	0.08	436	4.01	0.20	251	2.59
			6390-400	1.36	0.1	2.48	182	0.04	441	2.58	0.07	219	2.31
			6420-30	1.42	0.19	3.06	216	0.06	436	3.25	0.13	223	2.41
			6440-50	2.11	0.28	6.37	302	0.04	440	6.65	0.13	352	3.59
			6460-70	2.41	0.47	6.79	282	0.06	439	7.26	0.19	319	4.10
			6480-90	2.02	0.41	6.4	316	0.06	441	6.81	0.20	379	3.44

Appendix I: Cont. Table 4.1 Total organic carbon and Rock-Eval pyrolysis data for the Upper Cretaceous source rocks in the Sirt Basin.

Well Name	Age	Formation Name	Depth feet	TOC wt%	S1 mgHC/g rock	S2	HI mg HC/g TOC	PI	T max ºC	S1+S2 mgHC/g rock	S1/TOC	HI◦ mg HC/g TOC	TOC◦ wt%
L1-17	Upper Crettaceous	Sirte Shale	6500-10	1.99	0.42	5.81	291	0.07	443	6.23	0.21	369	3.39
			6540-50	1.47	0.29	3.36	228	0.08	439	3.65	0.20	258	2.51
			6580-90	1.23	0.23	2	163	0.10	441	2.23	0.19	195	2.09
			6600-08	2.04	0.19	2.86	140	0.06	438	3.05	0.09	154	3.47
			6608-10	1.34	0.18	2.65	197	0.06	438	2.83	0.13	217	2.28
			6640-50	0.84	0.07	1.22	146	0.05	440	1.29	0.08	170	1.42
			6700-10	0.56	0.03	0.51	91	0.06	438	0.54	0.05	100	0.95
			6720-30	0.53	0.08	0.82	154	0.09	442	0.9	0.15	189	0.91
			6760-70	0.50	0.01	0.27	54	0.04	436	0.28	0.02	56	0.85
			6810-20	0.73	0.06	0.81	111	0.07	436	0.87	0.08	115	1.24
			6870-80	0.60	0.1	0.59	99	0.14	429	0.69	0.17	79	1.01
			6900-10	0.69	0.03	0.7	102	0.04	441	0.73	0.04	122	1.17
			6940-50	0.85	0.04	1.03	121	0.04	438	1.07	0.05	134	1.44
			6970-80	0.87	0.05	1.16	134	0.04	436	1.21	0.06	138	1.47
			7000-10	0.73	0.05	0.68	93	0.07	438	0.73	0.07	103	1.24
			7010-20	0.85	0.06	0.76	90	0.07	440	0.82	0.07	105	1.44
			7020-30	0.85	0.08	0.82	97	0.09	442	0.9	0.09	120	1.44
Z1-11	Upper Cretaceous	Sirte Shale	8018-50	0.51	0.05	0.3	59	0.15	442	0.35	0.10	72	0.87
			8050-80	1.34	0.29	2.72	203	0.1	442	3.01	0.22	250	2.28
			8080-110	1.65	0.43	5.06	308	0.08	438	5.49	0.26	338	2.80
			8110-40	1.62	0.3	3.91	242	0.07	440	4.21	0.19	282	2.75
			8140-70	1.97	0.41	6.13	310	0.06	437	6.54	0.21	331	3.36
			8170-200	1.80	0.41	4.87	270	0.08	441	5.28	0.23	325	3.06
			8200-30	1.49	0.74	3.75	251	0.16	440	4.49	0.50	293	2.54
			8230-43	1.65	0.54	3.31	201	0.14	448	3.85	0.33	288	2.80

Appendix I: Cont. Table 4.2 Summary of maturity parameters measurements and kerogen compositions for the Upper Cretaceous source rock in the Sirt Basin.

Well Name	Age	Formation Name	Depth Feet	Maturity					Kerogen Type %					Fluorescence Scale
				T max ºC	PI	SCI	CSI	Ro%	Amorphous AMO	Palynomorphs Spore	Palynomorphs Dinocyts	Phytoclasts Vitrinite	Phytoclasts Interinte	FS
6A1-59	**Upper Cretaceous**	**Kalash**	7140	434	0.06	3.5-4.0	2.0-2.5	0.51	90	5	3	2	0	5
			7170	433	0.05	3.5-4.0	2.0-2.5	0.51	90	5	3	1	1	5
			7180	439	0.05	4.0	2.5	0.53	90	5	3	1	1	4
			7200	432	0.08	4.0	2.5	0.54	85	5	5	2	0	4
			7210	429	0.07	4.0-4.5	3.0-3.5	0.54	80	5	10	5	0	4
		Sirte Shale	7220	434	0.05	4.0-4.5	3.0-3.5	0.54	90	5	4	1	0	4
			7240	432	0.06	4.0-4.5	3.5	0.54	92	3	4	1	0	5
			7260	432	0.07	4.0-4.5	3.5	0.55	95	3	2	0	0	5
			7280	432	0.07	4.5-5.0	3.5-4.0	0.55	95	3	1	1	0	5
C2-16	**Upper Cretaceous**	**Sirte Shale**	9780	445	0.21	6.5-7.0	4.5-5.0	0.74	95	0	3	2	0	4
			9840	447	0.2	7.0	5.5	0.74	98	0	2	0	0	4
			9900	446	0.22	7.0-7.5	5.5	0.75	95	0	5	0	0	4
			10010	448	0.2	7.5	5.5-6.0	0.75	95	0	5	0	0	4
			10150	447	0.14	7.5	6.0-6.5	0.77	98	0	2	0	0	3
			10480	441	0.25	7.5-8.0		0.77	100	0	0	0	0	4
			10600	450	0.17	8.0	6.0-6.5	0.79	90	0	5	5	0	3
			10700	445	0.18	8.0	6-6.5	0.95	95	0	5	0	0	4
			10800	444	0.18	8.0	6-6.5	0.95	95	0	5	0	0	3
			10900	447	0.28	8.0-8.5	6.5	1.1	95	0	5	0	0	3
			10960	442	0.23	8.0-8.5	6.5	1.24	95	0	5	0	0	3
			11000	444	0.24	8.5	6.5-7.0	1.3	90	0	5	5	0	3

Tmax- Pyrolysis temperature PI-Production Index SCI-Spore Colour Index CSI-Dinocyts Colour Index Ro-Vitrinite reflectance

Appendix I: Cont. Table 4.2 Summary of maturity parameters measurements and kerogen compositions for the Upper Cretaceous source rock in the Sirt Basin.

Well Name	Age	Formation Name	Depth Feet	Maturity					Kerogen Type %					Fluorescence Scale
				T max ºC	PI	SCI	CSI	Ro%	Amorphous AMO	Palynomorphs Spore	Palynomorphs Dinocyts	Phytoclasts Vitrinite	Phytoclasts Interinte	FS
FF14-6	**Upper Cretaceous**	**Sirte Shale**	11250	389	0.35	7.5-8.0	6.0-6.5	0.95	90	0	5	5	0	3
			11330	519	0.21	7.5-8.0	6.0-6.5	0.95	90	0	5	5	0	3
			11470	549	0.30	8.0	6.5	0.99	90	0	7	3	0	3
			11510	513	0.23	8.0	6.5	1	95	0	3	2	0	3
			11650	395	0.33	7.5-8.0	6.0-6.5	1.1	95	0	3	2	0	3
			11950	436	0.33	8.0	6.5	1.1	95	0	3	2	0	3
			12070	486	0.24	8.0	6.5	1.15	95	0	5	0	0	3
			12170	511	0.26	8.0-8.5	6.5-7.0	1.2	80	0	10	10	0	4
			12270	503	0.56	8.0-8.5	6.5-7.0	1.2	85	0	5	10	0	3
			12340	449	0.12	8.0-8.5	6.5-7.0	1.25	85	0	5	10	0	3
			12650	454	0.32	8.5		1.4	85	0	0	15	0	3
			12870	523	0.50	8.5-9.0		1.5	60	0	0	40	0	3
L1-16	**Upper Cretaceous**	**Sirte Shale**	7400	436	0.06	4.0-4.5	3.5-4.0	0.57	90	0	7	3	0	4
			7470	433	0.10	4	3.5-4.0	0.59	85	0	10	5	0	3
			7590	434	0.09	4.5-5.0	3.5-4.0	0.63	90	0	5	5	0	3
			7640	433	0.08	5.0-5.5	3.5-4.0	0.64	95	0	3	2	0	4
			7700	433	0.09	5.5	4.0	0.64	90	0	5	5	0	4.0
			7750	434	0.12	5.5	3.5-4.0	0.65	90	0	5	5	0	4
			7850	434	0.08	5.5-6.0	4.0	0.66	80	0	10	5	5	4
			7940	431	0.15	5.5-6.0	4.0-4.5	0.67	85	0	10	5	0	4
			8060	444	0.07	5.5-6.0	4.0	0.69	90	0	8	2	0	5
			8260	438	0.17	6.0	4.0-4.5	0.7	90	0	8	2	0	4

Appendix I: Cont. Table 4.2 Summary of maturity parameters measurements and kerogen compositions for the Upper Cretaceous source rock in the Sirt Basin.

Well Name	Age	Formation Name	Depth Feet	Maturity					Kerogen Type %					Fluorescence Scale
				T max	PI	SCI	CSI	Ro%	Amorphous	Palynomorphs		Phytoclasts		
				ºC					AMO	Spore	Dinocyts	Vitrinite	Interinte	FS
L1-17	**Upper Cretaceous**	**Sirte Shale**	6120	439	0.04	3.5-4.0	2.5	0.50	80	5	10	5	0	5
			6170	437	0.08	3.5-4.0	2.5	0.51	82	5	10	5	0	5
			6260	431	0.07	3.5-4.0	2.5-3.0	0.53	90	5	5	0	0	4
			6300	438	0.04	4.0	3.0	0.53	85	5	8	2	0	5
			6350	435	0.07	4.0	3.0	0.54	85	5	8	2	0	4
			6440	440	0.04	4.0-4.5	3.5	0.55	85	5	10	0	0	5
			6600	443	0.06	4.0-4.5	3.5	0.56	85	5	7	3	0	4
			6700	438	0.06	4.0-4.5	3.5-4.0	0.58	75	5	15	5	0	4
			6810	436	0.07	4.5	3.5-4.0	0.6	85	5	3	2	0	4
			6970	436	0.04	4.5	3.5-4.0	0.63	85	5	10	5	0	4
			7000	438	0.07	4.5	3.5-4.0	0.65	75	5	10	10	0	4
			7020	442	0.09	5.0	3.5-4.0	0.65	85	5	5	5	0	4
Z1-11	**Upper C**	**Sirte Sha**	8050	438	0.10	5.0-5.5	3.5-4.0	0.63	90	5	3	2	0	4
			8110	437	0.07	5.5-6.0	4	0.66	90	5	3	2	0	4
			8170	440	0.08	6	4.5	0.67	90	5	3	2	0	5

Appendix I: Cont. Table 4.2 Summary of maturity parameters measurements and kerogen compositions for the Upper Cretaceous source rock in the Sirt Basin.

Well Name	Age	Formation Name	Depth Feet	Maturity					Kerogen Type %					Fluorescence Scale
				T max ºC	PI	SCI	CSI	Ro%	Amorphous	Palynomorphs		Phytoclasts		
									AMO	Spore	Dinocyts	Vitrinite	Interinte	FS
B1-NC74F	**Upper Cretaceous**	**Sirte Shale**	7000	433	0.38			0.56						
			7040	433	0.44			0.56						
			7060	435	0.31			0.57						
			7090	428	0.42			0.57						
			7120	443	0.33			0.58						
			7150	440	0.33			0.59						
			7180	439	0.24			0.59						
			7200	436	0.44			0.59						
			7930	434	0.35			0.62						
			7960	435	0.33			0.62						
			7990	441	0.3			0.63						
			8060	436	0.34			0.65						
B2-NC74A	**Upper Cretaceous**	**Sirte Shale**	9500	434	0.37			0.60						
			9540	437	0.36			0.63						
			9560	435	0.29			0.63						
			9690	438	0.29			0.67						
			9710	434	0.37			0.68						
			9730	438	0.31			0.69						

Appendix I: Table 4.3. Summary separations of the aliphatic, aromatic, resin and asphaltenes (SARA) data for crude oil of the Sirt Basin.

Location	Oi Field	Well	Depth	Hydrocarbons and non-Hydrocarbons Compounds				Saturated/
		Name	Feet	Saturated %	Aromatic %	NSO %	Asphaltenes %	Aromatic
Western Sirt Basin	West Waha	6A1-59	7150	59.07	15.62	1.22	24.10	3.78
			7170	59.66	14.91	1.52	23.91	4.00
			7250	54.82	15.34	2.45	27.39	3.57
	West Sabah	B1-NC74F	7050	53.16	6.77	8.57	31.50	7.86
			7110	44.61	6.18	9.30	39.91	7.22
			7190	41.60	5.08	12.93	40.39	8.19
			7940	24.48	1.90	23.04	50.58	12.89
			8080	20.78	1.34	24.20	53.68	15.52
	Fidda	B2-NC74A	9520	53.69	3.56	16.28	26.47	15.08
			9540	49.61	3.92	14.98	31.49	12.64
			9570	47.75	3.83	13.04	35.39	12.48
			9580	49.49	2.21	16.57	31.73	22.38
			9610	36.64	0.83	22.57	39.96	44.23
Central Sirt Basin	South-East Bazuzi	C2-16	9800	67.04	6.02	6.02	20.92	11.13
			10260	73.27	6.56	4.22	15.95	11.17
			10380	68.33	8.20	5.11	18.36	8.33
			10580	71.65	6.12	4.81	17.42	11.70
	Attahadi	FF14-6	11290-310	70.89	5.76	4.13	19.21	12.31
			11320-340	70.01	6.13	3.84	20.01	11.42
			11615	59.73	1.95	6.23	32.10	30.69
			11650	74.58	4.23	5.24	15.95	17.63
			12290	54.65	11.78	5.42	28.15	4.64
			12330	49.36	8.07	6.81	35.76	6.11

Appendix I: Cont. Table 4.3. Summary separations of the aliphatic, aromatic, resin and asphaltenes (SARA) data for crude oil of the Sirt Basin.

Location	Oi Field	Well	Depth	Hydrocarbons and non-Hydrocarbons Compounds				Saturated/
		Name	Feet	Saturated %	Aromatic %	NSO %	Asphaltenes %	Aromatic
Western Sirt Basin	Nuflian High	L1-16	7400	46.86	7.33	13.41	32.39	6.39
			7530	38.26	8.97	15.35	37.42	4.27
			7640	39.07	9.69	14.06	37.18	4.03
			7850	36.77	8.23	15.92	39.07	4.47
	West Mabruk	L1-17	6060	47.24	11.62	10.48	30.66	4.06
			6300	43.66	16.36	9.75	30.23	2.67
			6460	46.07	19.07	2.33	32.53	2.42
			6600	39.49	12.05	11.98	36.47	3.28
	North Ghani Zenad	Z1-11	8080	38.38	5.01	16.33	40.27	7.66
			8140	49.32	10.23	4.19	36.25	4.82
			8200	43.76	7.62	10.57	38.04	5.74

Appendix I: Table 4.4. Summary of the *n*-alkane and isoprenoid ratios for selected source rock samples from the Sirt Basin.

Location	Oi Field	Well Name	Depth Feet	Pr/Ph	Pr/(Pr+Ph)	Pr/nC17	Ph/nC18	(C27+C29+C31)/(C15+C17+C19)	nC17/nC25	nC17/nC27	CPI 1	OER	C13+C14+C15/C25+C26+C27	nC15-nC19 *n*-alkanes	n-C27-nC31/ *n*-alkanes
Western Sirt Basin	West Waha	6A1-59	7150	2.02	0.67	0.76	1.18	0.09	8.25	12.19	0.93	0.63	4.27	0.66	0.06
			7170	1.85	0.65	0.69	1.00	0.07	9.55	14.62	1.07	0.81	4.24	0.68	0.04
			7250	1.57	0.61	0.69	1.03	0.09	8.67	12.87	1.10	0.79	3.15	0.70	0.05
	West Sabah	B1-NC74F	7050	0.73	0.42	0.34	0.23	0.01	27.13	105.86	1.32	0.97	5.87	0.65	0.00
			7110	0.71	0.41	0.37	0.24	0.01	22.97	86.72	1.30	0.82	7.69	0.63	0.00
			7190	0.71	0.41	0.30	0.19	0.01	17.82	64.59	1.24	0.77	3.19	0.60	0.00
			7940	0.95	0.49	0.38	0.34	0.00	30.84	172.28	1.09	0.69	16.68	0.67	0.00
			8080	0.80	0.44	0.39	0.29	0.01	24.51	102.07	1.27	0.81	6.70	0.64	0.00
	Fidda	B2-NC74A	9520	0.90	0.47	0.46	0.29	0.01	40.72	109.30	1.11	0.99	1.37	0.76	0.01
			9540	0.84	0.46	0.51	0.30	0.01	45.34	82.55	1.02	0.89	1.82	0.75	0.01
			9570	0.83	0.45	0.52	0.29	0.02	23.54	47.40	1.06	0.83	1.09	0.71	0.01
			9580	0.83	0.45	0.50	0.27	0.01	52.99	107.25	0.98	0.96	1.85	0.74	0.00
			9610	0.69	0.41	0.54	0.24	0.21	2.93	3.63	1.02	0.90	0.14	0.52	0.10
Central Sirt Basin	South-East Bazuzi	C2-16	9800	1.08	0.52	0.48	0.55	0.22	4.01	5.50	1.05	1.04	0.53	0.51	0.09
			10260	1.24	0.55	0.45	0.53	0.28	2.96	4.20	1.00	0.99	0.41	0.44	0.11
			10380	1.46	0.59	0.42	0.63	0.13	7.16	10.17	1.04	0.98	1.08	0.62	0.07
			10580	1.13	0.53	0.44	0.51	0.16	5.19	7.52	0.99	0.93	0.77	0.54	0.08
	Attahadi	FF14-6	11290-310	1.05	0.51	0.55	0.40	0.07	2.79	7.61	1.18	0.81	0.84	0.44	0.03
			11650	1.20	0.54	0.50	0.43	0.05	4.32	11.91	1.16	0.78	1.82	0.51	0.02
			11320-340	0.93	0.48	0.47	0.46	0.04	18.91	31.51	0.98	0.85	2.93	0.73	0.03
			11615-30	1.16	0.54	0.60	0.46	0.10	1.72	4.84	1.17	0.79	0.56	0.35	0.03
			12290-310	2.06	0.67	0.41	0.59	0.07	4.29	11.00	1.10	0.97	3.82	0.40	0.02
			12330-350	2.39	0.70	0.39	0.64	0.06	6.40	13.39	1.04	0.99	5.18	0.46	0.02

Pr: Pristane; Ph: Phytane; OER: Odd to Evan Ratio, 2*(C29)/(C28+C30);
CPI 1: Carbon Preference Index, 0.5* (C25+C27+C29+C31)+(C25+C27+C29+C31+C33))/((C24+C26+C28+C30+C32)+(C26+C28+C30+C32+C34))

Appendix I: Cont. Table 4.4. Summary of the n-alkane and isoprenoid ratios for selected source rock samples from the Sirt Basin.

Location	Oi Field	Well Name	Depth Feet	Pr/Ph	Pr/(Pr+Ph)	Pr/nC17	Ph/nC18	(C27+C29+C31)/ (C15+C17+C19)	nC17/ nC25	nC17/ nC27	CPI 1	OER	C13+C14+C15/ C25+C26+C27	nC15-nC19 *n*-alkanes	n-C27-nC31/ *n*-alkanes
Western Sirt Basin	Nuflian High	L1-16	7400	0.96	0.49	0.49	0.50	0.02	25.90	53.86	1.10	0.82	5.28	0.77	0.01
			7530	1.46	0.59	0.46	0.64	0.02	21.02	39.18	1.36	1.38	14.59	0.75	0.01
			7640	1.35	0.57	0.52	0.77	0.05	9.11	17.03	1.22	1.12	9.40	0.66	0.03
			7850	1.60	0.61	0.43	0.68	0.09	7.92	14.15	1.19	1.15	3.45	0.61	0.04
	West Mabruk	L1-17	6060	1.62	0.62	0.86	1.06	0.15	4.68	6.25	1.15	1.02	3.02	0.55	0.07
			6300	1.38	0.58	0.88	1.08	0.13	4.45	7.28	1.19	1.32	4.14	0.53	0.05
			6460	1.60	0.62	0.82	1.13	0.11	4.83	8.48	1.19	1.16	4.47	0.55	0.05
			6600	1.57	0.61	0.70	0.86	0.12	4.01	7.10	1.29	1.36	4.27	0.51	0.05
	North Ghani Zenad	Z1-11	8080	1.49	0.60	0.42	0.51	0.04	31.00	38.56	1.29	1.51	5.96	0.74	0.02
			8140	1.29	0.56	0.35	0.40	0.02	33.99	52.75	1.20	1.29	9.89	0.73	0.01
			8200	1.53	0.61	0.34	0.44	0.02	59.97	84.32	1.27	1.29	10.18	0.78	0.01

Appendix I: Table 4.5 Sterane biomarker ratios of the Upper Cretaceous source rocks of the Sirt Basin.

Location	Oi Field	Well Name	Depth Feet	Sterane ααα 20R						Total Streanse	Total Hopane	Sterane/ Hopane	Reg. Sterar α(H) Hopar	Σ C_{30}/ C_{29} Steran	DC_{27} βαS/ C_{27} αααR	ΣDC_{27}/ ΣDC_{29}	A	B	C	D	E	F
				C_{27} %	C_{28} %	C_{29} %	C_{27}/C_{28}	C_{27}/C_{29}	C_{28}/C_{29}													
Western Sirt Basin	West	6A1-59	7150	37	39	24	0.949	1.535	1.618	1.199	0.678	1.769	2.503	0.190	0.190	0.869	0.265	1.807	1.230	0.313	0.265	0.298
			7170	36	39	25	0.908	1.438	1.584	0.913	0.579	1.575	2.210	0.201	0.242	0.894	0.295	1.599	1.561	0.231	0.264	0.271
	Waha		7250	36	37	27	0.994	1.346	1.354	0.787	0.551	1.427	1.953	0.236	0.276	0.981	0.290	1.443	1.344	0.223	0.267	0.299
	West	B1-NC74F	7050	62	16	22	3.895	2.871	0.737	0.015	0.026	0.578	0.835	0.116	0.869	1.036	0.579	0.654	0.894	0.004	0.493	0.568
			7110	66	15	19	4.467	3.560	0.797	0.012	0.020	0.598	0.872	0.056	0.930	1.099	0.666	0.940	0.888	0.003	0.540	0.587
	Sabah		7190	66	13	21	4.965	3.223	0.649	0.013	0.019	0.694	1.042	0.050	0.818	1.137	0.624	0.853	1.273	0.003	0.427	0.553
			7940	72	14	14	5.145	4.987	0.969	0.006	0.008	0.758	1.123	0.099	0.695	1.107	0.675	1.122	0.759	0.001	0.492	0.556
			8080	65	16	19	3.996	3.491	0.873	0.009	0.014	0.662	0.969	0.094	0.845	1.163	0.645	0.945	0.942	0.002	0.511	0.592
			9520	51	22	26	2.295	1.973	0.860	0.040	0.154	0.257	0.365	0.135	0.864	0.921	0.544	0.907	1.217	0.012	0.545	0.524
			9540	64	16	19	3.913	3.368	0.861	0.025	0.060	0.416	0.568	0.116	0.894	1.057	0.646	0.996	1.268	0.007	0.703	0.551
	Fidda	B2-NC74A	9570	33	23	45	1.432	0.732	0.511	0.117	0.518	0.225	0.316	0.109	1.183	0.698	0.459	0.796	0.802	0.048	0.441	0.442
			9580	53	15	31	3.492	1.694	0.485	0.039	0.134	0.292	0.421	0.110	0.933	1.036	0.507	1.016	0.822	0.013	0.469	0.431
			9610	34	29	37	1.171	0.925	0.790	0.172	0.373	0.462	0.614	0.098	1.266	0.691	0.541	0.637	1.163	0.061	0.460	0.552
Western Sirt Basin			7400	35	34	31	1.011	1.110	1.098	0.227	0.311	0.731	1.669	0.190	0.873	1.158	0.421	1.281	0.904	0.069	0.366	0.270
	Nuflian High	L1-16	7530	35	40	26	0.872	1.359	1.559	0.245	0.156	1.566	2.598	0.184	0.919	1.276	0.480	1.087	1.461	0.061	0.276	0.266
			7640	32	40	28	0.818	1.167	1.426	0.236	0.199	1.185	2.025	0.219	1.512	1.363	0.556	1.196	2.084	0.063	0.314	0.308
			7850	34	37	29	0.922	1.199	1.301	0.108	0.103	1.050	1.403	0.102	1.628	1.367	0.552	0.920	0.535	0.032	0.325	0.358
			6060	38	35	27	1.103	1.427	1.294	0.292	0.298	0.980	1.250	0.183	1.842	1.590	0.583	1.287	1.043	0.073	0.371	0.317
	West Mabruk	L1-17	6300	34	36	30	0.965	1.134	1.175	0.175	0.192	0.911	1.175	0.221	4.068	1.456	0.739	1.121	1.512	0.038	0.433	0.380
			6460	30	37	33	0.803	0.921	1.146	0.160	0.228	0.700	0.898	0.212	3.465	1.261	0.682	0.894	1.256	0.043	0.430	0.453
			6600	32	27	41	1.181	0.792	0.670	0.048	0.069	0.695	0.902	0.108	5.651	1.302	0.763	1.120	1.908	0.012	0.383	0.437
	North		8080	42	27	30	1.533	1.389	0.906	0.041	0.096	0.425	0.555	0.131	0.268	0.530	0.640	0.932	0.959	0.012	0.458	0.434
	Ghani	Z1-11	8140	34	35	31	0.992	1.122	1.131	0.048	0.091	0.526	0.702	0.201	3.547	1.164	0.754	1.000	1.027	0.013	0.505	0.473
	Zenad		8200	39	26	35	1.477	1.105	0.748	0.002	0.005	0.498	0.689	0.215	3.667	1.350	0.657	0.847	0.955	0.001	0.445	0.483

C: Sterane; DC: Diasterane; A: DC_{29} βα20R/[DC_{29} βα20R+ C_{29} ααα 20R]; B: [Σ DC_{27} to DC_{29} βα (20S+20R)]/[Σ C_{27} to C_{29} αββ(20S+20R)]; C: C_{28}αββ20S/C_{29}αββ20S; D: C_{29}ααα (S+R) +C_{29} αββ (S+R) E: C_{29} ααα [20S/(20S+20R)] Sterane; F: C_{29} [αββ/(αββ+ααα)] Sterane. Regular sterane C_{27} to C_{29} ααα (S+R) + C_{27} to C_{29} αββ (S+R)/ C_{29} to C_{33} αβ(H) hopane, From C_{31} to C_{33} α(H) Homohopane (S+R).

Appendix I: Cont. Table 4.5 Sterane biomarker ratios of the Upper Cretaceous source rocks of the Sirt Basin.

Location	Oi Field	Well Name	Depth Feet	Sterane ααα 20R C_{27} %	C_{28} %	C_{29} %	C_{27}/C_{28}	C_{27}/C_{29}	C_{28}/C_{29}	Total Streanse	Total Hopane	Sterane/ Hopane	Reg. Sterar α(H) Hopar	Σ C_{30}/ C_{29} Steran	DC_{27} βαS/ C_{27} ααR	ΣDC$_{27}$/ ΣDC$_{29}$	A	B	C	D	E	F
Central Sirt Basin	South-East Bazuzi	C2-16	9800	35	29	36	1.235	0.976	0.791	0.083	0.059	1.390	1.669	0.192	4.567	1.323	0.726	0.901	1.095	0.024	0.506	0.545
			10260	44	22	34	1.945	1.278	0.657	0.049	0.022	2.179	2.598	0.208	4.693	1.409	0.772	1.019	1.448	0.012	0.517	0.513
			10380	34	23	43	1.462	0.785	0.537	0.036	0.020	1.815	2.025	0.189	3.239	1.338	0.605	0.951	1.326	0.011	0.312	0.350
			10580	39	26	35	1.496	1.133	0.757	0.027	0.025	1.084	1.403	0.200	3.754	1.461	0.713	1.067	2.052	0.007	0.405	0.432
	Attahadi	FF14-6	11290	50	23	27	2.131	1.821	0.854	0.029	0.040	0.727	1.008	0.249	3.689	1.898	0.725	0.988	1.205	0.006	0.442	0.437
			11320	36	34	30	1.047	1.191	1.137	0.368	0.498	0.740	0.968	0.124	1.016	1.178	0.462	1.342	0.723	0.106	0.347	0.270
			11615	48	21	31	2.327	1.566	0.673	0.115	0.114	1.006	1.485	0.151	3.406	2.087	0.610	1.034	1.176	0.023	0.357	0.357
			11650	46	24	30	1.875	1.548	0.826	0.042	0.046	0.921	1.279	0.123	3.374	1.700	0.654	0.923	1.294	0.009	0.414	0.448
			12290	49	19	32	2.589	1.559	0.602	0.011	0.058	0.187	0.242	0.087	2.559	1.541	0.588	0.817	0.394	0.004	0.617	0.542
			12330	65	9	26	7.391	2.500	0.338	0.005	0.021	0.240	0.302	0.118	1.612	1.965	0.443	0.748	0.949	0.002	0.443	0.580
UK	North Sea	VFO		29	26	44	1.1	0.65	0.59	1.186	10.95	0.108	1.060	0.411	2.981	0.785	0.62	1.085	0.825	0.432	0.463	0.501

Appendix I: Table 4.6 Hopane biomarker ratios of the Upper Cretaceous source rocks of the Sirt Basin.

Location	Oi Field	Well Name	Depth Feet	C_{27} Ts/ (TS+Tm)	$C_{30}\beta\alpha$/ $C_{30}\alpha\beta$	C_{35} αβ (S+R)/ ΣC_{31}-$C_{35}\alpha\beta$ (S+R)*100	C_{29} αβ/ C_{30} αβ	C_{35} αβ/ $C_{34}\alpha\beta$	C_{31} αβ/ C_{30} αβ	C_{29}Ts/ C_{29}Ts+C_{29}Tm	C_{30}-dih/ C_{30}dih+$C_{30}\alpha\beta$	C_{30}Mor/ C_{30}Mor+$C_{30}\alpha\beta$	C_{27} Tm/Ts	C_{27} Ts/Tm	C_{32} αβ22S/ 22S+22R	Streane/ ıe+ C_{29}+C_{30} 17αβ h
Western Sirt Basin	West Waha	6A1-59	7150	0.38	0.17	9.00	0.88	0.81	0.24	0.19	0.04	0.15	1.63	0.62	0.57	0.40
			7170	0.38	0.17	7.13	0.80	0.72	0.22	0.19	0.04	0.14	1.60	0.63	0.57	0.36
			7250	0.37	0.16	8.04	0.72	0.80	0.22	0.18	0.03	0.14	1.71	0.59	0.59	0.37
	West Sabah	B1-NC74F	7050	0.43	0.10	7.79	0.88	0.52	0.28	0.21	0.13	0.09	1.33	0.75	0.55	0.19
			7110	0.41	0.11	9.06	0.90	0.66	0.28	0.21	0.09	0.10	1.44	0.69	0.57	0.19
			7190	0.36	0.07	8.23	0.95	0.72	0.26	0.21	0.11	0.07	1.76	0.57	0.62	0.19
			7940	0.45	0.13	3.78	0.95	0.34	0.27	0.18	0.08	0.11	1.24	0.81	0.59	0.17
			8080	0.37	0.11	10.29	0.97	0.69	0.29	0.17	0.08	0.10	1.72	0.58	0.63	0.20
	Fidda	B2-NC74A	9520	0.58	0.15	7.72	0.69	0.81	0.24	0.29	0.07	0.13	0.73	1.36	0.58	0.10
			9540	0.71	0.12	6.44	0.60	0.59	0.28	0.36	0.12	0.11	0.41	2.43	0.56	0.16
			9570	0.50	0.17	4.50	0.61	0.59	0.21	0.31	0.07	0.15	0.99	1.01	0.56	0.11
			9580	0.55	0.13	4.93	0.77	0.56	0.24	0.27	0.06	0.11	0.81	1.23	0.61	0.12
			9610	0.52	0.13	6.00	0.52	0.61	0.21	0.30	0.06	0.11	0.94	1.06	0.59	0.19
Central Sirt Basin	South-East Bazuzi	C2-16	9800	0.87	0.23	2.64	0.34	0.41	0.25	0.61	0.33	0.19	0.16	6.42	0.61	0.30
			10260	0.84	0.33	2.63	0.52	0.35	0.34	0.55	0.49	0.25	0.19	5.37	0.60	0.34
			10380	0.85	0.30	3.53	0.60	0.52	0.18	0.45	0.39	0.23	0.17	5.72	0.64	0.33
			10580	0.73	0.20	2.10	0.62	0.22	0.22	0.33	0.28	0.17	0.36	2.77	0.68	0.24
	Attahadi	FF14-6	11290	0.55	0.10	1.66	0.72	0.70	0.34	0.22	0.04	0.09	0.81	1.24	0.61	0.18
			11320	0.43	0.12	4.60	0.60	0.71	0.28	0.34	0.06	0.11	1.30	0.77	0.60	0.27
			11615	0.57	0.05	3.04	0.73	1.29	0.20	0.24	0.04	0.05	0.76	1.31	0.62	0.22
			11650	0.53	0.10	4.68	0.75	0.83	0.30	0.22	0.06	0.09	0.90	1.11	0.64	0.23
			12290	0.25	0.21	0.00	0.67	0.00	0.88	0.21	0.08	0.17	2.95	0.34	0.73	0.10
			12330	0.27	0.28	0.00	0.68	0.00	0.80	0.19	0.12	0.22	2.73	0.37	0.61	0.10
Western Sirt Basin	Nuflian High	L1-16	7400	0.47	0.14	6.52	0.62	0.72	0.34	0.31	0.06	0.12	1.12	0.89	0.58	0.29
			7530	0.49	0.18	4.09	0.45	0.34	0.23	0.38	0.07	0.15	1.06	0.95	0.61	0.37
			7640	0.55	0.21	5.12	0.43	0.39	0.20	0.42	0.12	0.17	0.83	1.20	0.63	0.32
			7850	0.57	0.19	1.57	0.52	0.19	0.17	0.39	0.12	0.16	0.77	1.30	0.64	0.30
	West Mabruk	L1-17	6060	0.50	0.17	2.31	0.45	0.30	0.22	0.37	0.07	0.15	1.01	0.99	0.63	0.28
			6300	0.61	0.15	4.20	0.37	0.53	0.21	0.44	0.10	0.13	0.63	1.60	0.63	0.23
			6460	0.71	0.15	2.75	0.37	0.30	0.23	0.46	0.13	0.13	0.41	2.44	0.61	0.23
			6600	0.71	0.11	3.06	0.38	0.50	0.48	0.52	0.22	0.10	0.41	2.46	0.67	0.19
	North Ghani Zenad	Z1-11	8080	0.65	0.15	2.60	0.42	0.25	0.22	0.41	0.11	0.13	0.54	1.87	0.59	0.16
			8140	0.71	0.15	2.95	0.39	0.43	0.19	0.48	0.16	0.13	0.41	2.47	0.64	0.17
			8200	0.72	0.13	1.99	0.40	0.75	0.18	0.46	0.14	0.11	0.40	2.51	0.64	0.16

Appendix I: Table 4.7 Tricyclic terpane biomarker ratios of the Upper Cretaceous source rocks of the Sirt Basin.

Location	Oi Field	Well Name	Depth Feet	C_{23}/C_{24}	C_{23}/C_{21}	C_{22}/C_{21}	C_{24}/C_{23}	$(C_{19}+C_{20})/C_{23}$	$C_{23}/C_{23}+C_{30}\,\alpha\beta$ Hop	C_{24} Tetr/ Tri C_{26} (S+R)	C_{19}/C_{21}	C_{21}/C_{23}	C_{26}/C_{25}	C_{24}Tetr/ C_{23} Tri	$(C_{20}+C_{21})/[C_{20}+C_{21}+$ C26+C27+C28]	$C_{28}+C_{29}/$ $C_{28}+C_{29}+$Ts	$C_{19}/$ $(C_{19}+C_{23})$	C_{24}Tet/ C_{24}Tetr+C_{23}Tri	C_{23}Tri/ $C_{30}\,\alpha\beta$ hop	C_{24}Tetr/ $C_{30}\,\alpha\beta$ hop	C_{26}A/ C_{26}A+C_{26}B
Western Sirt Basin	West Waha	6A1-59	7150	2.57	2.21	0.23	0.39	0.39	0.24	1.03	0.17	0.45	0.70	0.23	4.91	0.52	0.07	0.16	0.31	0.06	0.47
			7170	2.72	2.28	0.22	0.37	0.39	0.26	0.93	0.21	0.44	0.83	0.22	4.48	0.57	0.08	0.13	0.34	0.05	0.47
			7250	2.66	2.46	0.23	0.38	0.36	0.20	0.93	0.15	0.41	0.75	0.23	3.26	0.58	0.06	0.14	0.26	0.04	0.51
	West Sabah	B1-NC74F	7050	2.07	1.17	0.35	0.48	1.35	0.60	3.14	0.68	0.85	0.64	0.35	83.22	0.57	0.37	0.25	1.49	0.49	0.36
			7110	2.13	1.29	0.38	0.47	1.25	0.63	3.13	0.72	0.78	0.62	0.38	80.02	0.58	0.36	0.27	1.70	0.63	0.47
			7190	2.04	1.16	0.41	0.49	1.16	0.63	3.12	0.54	0.86	0.61	0.41	84.59	0.57	0.32	0.29	1.70	0.70	0.46
			7940	2.06	1.21	0.35	0.48	1.20	0.62	3.06	0.60	0.83	0.65	0.35	85.93	0.71	0.33	0.26	1.66	0.57	0.44
			8080	2.09	1.12	0.35	0.48	1.14	0.62	2.94	0.56	0.89	0.63	0.35	83.68	0.64	0.33	0.28	1.65	0.65	0.46
	Fidda	B2-NC74A	9520	1.92	0.99	0.31	0.52	1.67	0.20	2.05	0.66	1.01	0.83	0.31	46.40	0.30	0.40	0.35	0.24	0.13	0.46
			9540	2.01	0.85	0.27	0.50	1.86	0.36	2.64	0.68	1.18	0.69	0.27	48.97	0.38	0.44	0.27	0.55	0.21	0.42
			9570	1.70	1.41	0.37	0.59	0.93	0.05	1.35	0.49	0.71	0.83	0.37	14.28	0.28	0.26	0.44	0.06	0.04	0.47
			9580	1.87	1.39	0.34	0.54	1.01	0.33	3.25	0.51	0.72	0.57	0.34	54.36	0.31	0.27	0.31	0.49	0.22	0.44
			9610	1.55	2.14	0.37	0.64	0.51	0.10	0.87	0.38	0.47	0.97	0.37	30.94	0.55	0.15	0.32	0.12	0.05	0.50
Central Sirt Basin	South-East Bazuzi	C2-16	9800	1.62	1.42	0.39	0.62	0.95	0.53	1.13	0.58	0.70	1.07	0.39	62.45	0.68	0.29	0.21	1.15	0.31	0.50
			10260	1.59	1.34	0.39	0.63	1.15	0.74	1.03	0.68	0.75	1.15	0.39	62.85	0.85	0.34	0.14	2.88	0.47	0.49
			10380	1.63	1.24	0.39	0.61	1.39	0.72	1.28	0.79	0.80	1.08	0.39	53.51	0.82	0.39	0.16	2.61	0.51	0.51
			10580	1.72	1.11	0.37	0.58	1.62	0.60	1.46	0.82	0.90	0.98	0.37	42.81	0.81	0.42	0.16	1.53	0.28	0.52
	Attahadi	FF14-6	11290	1.79	1.76	0.34	0.56	0.88	0.77	2.16	0.19	0.57	0.65	0.34	70.50	0.80	0.10	0.12	3.30	0.43	0.51
			11320	2.59	1.36	0.27	0.39	0.89	0.24	1.37	0.49	0.74	1.05	0.27	74.85	0.23	0.27	0.24	0.31	0.10	0.45
			11615	1.47	1.64	0.32	0.68	0.34	0.70	1.72	0.14	0.61	0.75	0.32	72.38	0.78	0.08	0.13	2.32	0.34	0.50
			11650	1.62	1.63	0.32	0.62	0.36	0.75	1.91	0.15	0.61	0.72	0.32	7.50	0.81	0.08	0.13	2.93	0.42	0.51
			12290	1.96	1.30	0.30	0.51	1.64	0.37	2.96	0.87	0.77	0.51	0.30	51.58	0.50	0.40	0.33	0.59	0.29	0.37
			12330	1.86	1.28	0.41	0.54	1.29	0.35	2.20	1.03	0.78	0.68	0.41	47.71	0.50	0.45	0.38	0.53	0.32	0.35
Western Sirt Basin	Nuflian High	L1-16	7400	2.48	1.30	0.26	0.40	0.94	0.22	2.03	0.54	0.77	0.70	0.26	8.32	0.29	0.29	0.26	0.29	0.10	0.35
			7530	3.04	1.60	0.30	0.33	0.84	0.26	1.57	0.63	0.63	0.60	0.30	6.84	0.40	0.28	0.22	0.35	0.10	0.37
			7640	3.17	1.76	0.30	0.32	0.54	0.26	1.07	0.39	0.57	0.72	0.30	7.39	0.43	0.18	0.18	0.35	0.08	0.48
			7850	2.53	1.64	0.33	0.39	0.82	0.30	1.27	0.60	0.61	0.82	0.33	9.99	0.45	0.27	0.30	0.43	0.19	0.38
	West Mabruk	L1-17	6060	3.00	1.87	0.23	0.33	0.32	0.25	1.32	0.20	0.53	0.65	0.23	7.35	0.37	0.10	0.16	0.34	0.06	0.50
			6300	2.77	2.04	0.28	0.36	0.26	0.27	1.01	0.13	0.49	0.73	0.28	10.79	0.51	0.06	0.13	0.37	0.06	0.47
			6460	2.26	1.66	0.28	0.44	0.39	0.22	1.15	0.21	0.60	0.88	0.28	14.55	0.43	0.11	0.16	0.28	0.05	0.46
			6600	2.02	1.65	0.29	0.49	0.86	0.42	1.28	0.24	0.61	1.05	0.29	25.71	0.44	0.13	0.20	0.72	0.18	0.46
	North Ghani Zenad	Z1-11	8080	1.95	1.24	0.36	0.51	1.01	0.36	1.63	0.50	0.81	0.71	0.36	26.05	0.50	0.29	0.19	0.57	0.13	0.49
			8140	1.86	1.32	0.28	0.54	0.72	0.41	1.61	0.35	0.76	0.73	0.28	35.97	0.56	0.21	0.18	0.70	0.15	0.51
			8200	1.95	1.45	0.35	0.51	0.72	0.45	1.75	0.42	0.69	0.82	0.35	29.77	0.51	0.22	0.19	0.83	0.20	0.53

Appendix I: Table 4.8 Aromatic hydrocarbons percentage of the Upper Cretaceous source rock samples from the Sirt Basin.

Location	Oi Field	Well Name	Depth Feet	Naphthalene N %	Phenanthrene P %	Fluorene F %	Biphenyl Bp%	Dibenzothiophene DBT%	Triaromatic Steroids C20 %	C21 %	Monoaromatic Steroid % C21-5β %	C22-5β
Western Sirt Basin	West Waha	6A1-59	7150	5.55	58.02	1.77	8.32	15.45	5.60	3.20	0.44	1.64
			7170	2.72	47.81	1.22	5.29	8.91	31.16	1.72	0.46	0.70
			7250	3.77	62.15	1.95	7.13	17.28	3.90	2.24	0.49	1.09
	West Sabah	B1-NC74F	7050	0.53	80.49	0.54	0.48	14.10	1.60	0.62	0.88	0.75
			7110	0.53	78.13	0.61	0.50	16.03	1.77	0.67	0.93	0.85
			7190	0.59	78.29	0.57	0.65	15.41	1.95	0.74	1.13	0.67
			7940	2.57	76.24	2.22	1.73	10.24	3.65	1.35	0.52	1.47
			8080	4.93	69.27	1.29	3.14	13.92	3.44	1.37	0.81	1.84
	Fidda	B2-NC74A	9520	2.60	82.15	1.71	1.53	10.84	0.34	0.12	0.52	0.20
			9540	2.86	81.24	2.57	1.83	10.11	0.41	0.15	0.58	0.24
			9570	3.73	79.31	2.99	2.38	10.20	0.52	0.30	0.38	0.19
			9580	2.03	83.70	2.00	1.51	9.65	0.40	0.15	0.31	0.27
			9610	5.02	77.61	2.74	2.73	8.49	1.13	0.96	0.88	0.44
Central Sirt Basin	South-East Bazuzi	C2-16	9800	3.77	74.57	2.31	2.35	13.81	1.65	0.94	0.46	0.14
			10260	3.39	77.30	1.15	2.00	13.95	0.96	0.39	0.82	0.03
			10380	3.78	77.85	1.44	2.57	13.01	0.64	0.24	0.41	0.05
			10580	3.59	75.95	2.19	2.38	14.52	0.51	0.16	0.65	0.04
	Attahadi	FF14-6	11290	7.41	72.32	2.90	5.81	5.58	2.38	1.27	2.02	0.31
			11320	6.07	79.70	1.66	5.65	5.08	0.94	0.43	0.40	0.08
			11615	4.72	79.06	2.47	3.67	7.91	0.64	0.43	0.79	0.32
			11650	4.35	82.33	1.24	4.26	4.06	1.11	0.62	1.92	0.09
			12290	8.14	68.85	1.98	16.06	4.32	0.19	0.11	0.33	0.02
			12330	9.61	65.34	2.82	16.31	5.26	0.14	0.11	0.36	0.04
Western Sirt Basin	Nuflian High	L1-16	7400	3.81	72.32	2.31	3.39	16.31	0.61	0.40	0.58	0.27
			7530	5.80	75.97	1.91	4.58	8.18	1.99	0.88	0.22	0.48
			7640	5.59	73.67	2.26	5.11	7.98	3.12	1.36	0.47	0.44
			7850	8.29	72.98	2.30	6.78	6.47	1.95	0.78	0.23	0.22
	West Mabruk	L1-17	6060	5.03	71.78	3.21	3.70	6.85	5.28	2.75	0.43	0.98
			6300	5.56	78.43	1.67	3.11	3.25	4.67	1.98	0.75	0.58
			6460	4.40	76.14	2.09	3.46	4.25	6.14	2.47	0.40	0.65
			6600	7.95	76.22	2.61	3.83	3.55	2.88	0.71	2.09	0.16
	North Ghani Zenad	Z1-11	8080	6.32	77.99	3.23	3.46	5.57	1.86	1.32	0.09	0.16
			8140	2.23	83.22	1.63	1.77	7.41	2.22	1.25	0.12	0.15
			8200	5.73	75.64	3.93	3.96	8.90	0.93	0.57	0.20	0.13

Appendix I: Cont. Table 4.8 Aromatic hydrocarbons ratios of the Upper Cretaceous source rock samples from the Sirt Basin.

Location	Oi Field	Well Name	Depth Feet	MNR	DMNR	TED1	TED2	A	B	DMPR	MPI1	Rc%	DBT/P	1-MP/9-MP	C
Western Sirt Basin	West Waha	6A1-59	7150	1.06	3.89	3.31	0.40	0.20	0.29	0.19	0.51	0.70	0.27	0.67	0.40
			7170	1.05	4.16	3.36	0.50	0.26	0.32	0.20	0.50	0.70	0.19	0.68	0.40
			7250	0.96	4.01	3.35	2.10	0.52	0.29	0.19	0.52	0.71	0.28	0.68	0.44
	West Sabah	B1-NC74F	7050	1.05	3.16	3.18	0.72	0.35	0.48	0.24	0.71	0.82	0.05	0.71	0.31
			7110	0.97	3.34	3.32	0.48	0.24	0.41	0.19	0.72	0.83	0.18	0.76	0.39
			7190	0.94	3.18	3.49	0.66	0.34	0.40	0.23	0.69	0.81	0.21	0.85	0.34
			7940	1.17	3.94	2.85	1.94	0.34	0.45	0.22	0.70	0.82	0.20	0.92	0.37
			8080	1.75	5.00	3.62	0.58	0.32	0.40	0.22	0.71	0.83	0.13	0.89	0.33
	Fidda	B2-NC74A	9520	1.33	3.76	3.78	1.81	0.38	0.52	0.16	0.60	0.76	0.20	0.66	0.31
			9540	1.12	3.13	3.14	1.41	0.33	0.47	0.21	0.70	0.82	0.13	0.53	0.29
			9570	1.32	3.60	3.43	0.55	0.34	0.45	0.21	0.72	0.83	0.12	0.53	0.31
			9580	1.33	3.66	3.47	0.59	0.37	0.47	0.22	0.75	0.85	0.13	0.68	0.35
			9610	1.26	3.51	2.50	0.52	0.31	0.34	0.22	0.75	0.85	0.12	0.60	0.27
	Nuflian High	L1-16	7400	1.24	3.39	4.35	2.16	0.36	0.40	0.27	0.54	0.73	0.23	0.58	0.29
			7530	1.24	2.89	4.76	0.63	0.32	0.31	0.23	0.47	0.68	0.11	0.62	0.35
			7640	1.26	2.82	4.76	0.60	0.32	0.32	0.21	0.48	0.69	0.11	0.71	0.44
			7850	1.29	2.88	4.93	0.64	0.31	0.30	0.22	0.40	0.64	0.09	0.55	0.30
	West Mabruk	L1-17	6060	1.13	3.54	3.55	0.54	0.42	0.43	0.18	0.48	0.69	0.10	0.59	0.35
			6300	0.95	3.50	3.30	0.56	0.44	0.40	0.21	0.47	0.68	0.04	0.70	0.40
			6460	0.94	3.20	3.62	0.51	0.36	0.35	0.18	0.54	0.73	0.06	0.54	0.34
			6600	1.03	3.62	3.92	1.35	0.32	0.32	0.19	0.53	0.72	0.05	0.37	0.19
	North Ghani Zenad	Z1-11	8080	1.08	3.68	3.65	0.56	0.31	0.32	0.20	0.74	0.84	0.11	0.60	0.35
			8140	1.16	3.68	5.11	0.55	0.27	0.51	0.20	0.43	0.66	0.07	1.52	0.71
			8200	1.12	3.44	3.70	1.56	0.31	0.37	0.35	0.60	0.76	0.09	0.59	0.35

Appendix I: Cont. Table 4.8 Aromatic hydrocarbons ratios of the Upper Cretaceous source rock samples from the Sirt Basin.

Location	Oi Field	Well Name	Depth Feet	MNR	DMNR	TED1	TED2	A	B	DMPR	MPI1	Rc%	DBT/P	1-MP/9-MP	C
Central Sirt Basin	South-East Bazuzi	C2-16	9800	1.25	3.64	4.19	0.54	0.31	0.39	0.20	0.64	0.78	0.19	0.50	0.27
			10260	1.29	3.66	5.22	0.54	0.31	0.35	0.30	0.74	0.85	0.18	0.54	0.32
			10380	1.37	3.87	4.81	0.52	0.31	0.35	0.24	0.70	0.82	0.17	0.50	0.28
			10580	1.29	3.50	4.43	0.52	0.31	0.37	0.23	0.73	0.84	0.19	0.48	0.27
	Attahadi	FF14-6	11290	1.34	5.05	3.00	0.57	0.26	0.20	0.21	0.49	0.69	0.12	0.45	0.24
			11320	1.27	3.50	3.80	0.54	0.32	0.38	0.24	0.81	0.89	0.08	0.67	0.39
			11615	1.33	4.89	3.30	0.56	0.27	0.27	0.22	0.62	0.77	0.06	0.28	0.15
			11650	1.42	4.28	3.58	0.55	0.27	0.27	0.28	0.55	0.73	0.10	0.53	0.28
			12290	1.60	5.43	3.33	0.61	0.31	0.31	0.29	0.69	0.82	0.06	0.42	0.34
			12330	1.37	5.06	3.37	0.58	0.29	0.27	0.27	0.60	0.76	0.08	0.44	0.36

MNR: Methylnaphthalene ratio, 2-MN/1-MN; DMNR: Dimethylnaphthalene ratio, 2,6-DMN+2,7-DMN/1,5-DMN; TED1: 1,2,5-TMN/1,2,4-TMN; TED2: 1,2,7-TMN/1,2,6-TMN; A: 1,2,7-TMN/1,3,7-TMN; B: 1,2,5/1,3,6-TMN; C: 1,7DMP/1,3+3,9+2,10+3,10-DMP; Rc%: (0.60*MPI 1)+0.4; MPI1: 1.5[(2-MP+3-MP)/(P+1-MP+9-MP)]; TMN: Trimethylnaphthalenes; MP: Methylphenanthrene; DMP: Dimethylphenanthrene; DBT: Dibenzothiophene; P: Phenanthrene.

Appendix I: Cont. Table 4.8 Monoaromatic and triaromatic ratios of the Upper Cretaceous source rock samples from the Sirt Basin.

Oi Field	Well Name	Depth Feet	$(C_{21}+C_{22})/[C_{21}+C_{22}+C_{27}+C_{28}+C_{29})$	$C_{27}/(C_{27}-C_{29})$	$C_{28}/(C_{27}-C_{29})$	$C_{29}/(C_{27}-C_{29})$	$C_{28}/(C_{28}+C_{29})$	$C_{20}TAS/C_{21}TAS$	$C_{20}/(C_{20}+C_{28}(S+R)$	$(C_{20}+C_{21})/[C_{20}+C_{21}+C_{26}+C_{27}+C_{28}]$	$C_{26}S/C_{28}S$ TAS	$C_{27}R/C_{28}R$ TAS
West	6A1-59	7150	3.41	28.36	40.51	31.13	0.57	1.75	12.24	4.91	0.83	2.17
		7170	3.59	28.39	40.36	31.25	0.56	1.84	11.45	4.48	0.83	2.15
Waha		7250	2.74	27.30	40.41	32.29	0.56	1.75	7.60	3.26	0.74	1.82
West	B1-NC74F	7050	39.60	17.37	43.09	39.54	0.52	2.58	90.50	83.22	0.39	7.03
		7110	38.29	17.45	43.38	39.17	0.53	2.65	85.41	80.02	0.37	0.58
Sabah		7190	44.30	17.30	43.66	39.03	0.53	2.65	88.53	84.59	0.33	0.59
		7940	29.62	17.02	43.26	39.73	0.52	2.71	89.68	85.93	0.36	0.54
		8080	31.36	16.78	43.51	39.71	0.52	2.51	87.05	83.68	0.32	0.50
	B2-NC74A	9520	61.17	17.58	44.76	37.66	0.54	2.72	57.32	46.40	0.30	0.84
		9540	53.29	19.02	45.10	35.88	0.56	2.68	62.28	48.97	0.29	1.18
Fidda		9570	20.98	18.08	43.25	38.67	0.53	1.72	17.35	14.28	0.23	0.75
		9580	44.85	14.27	47.48	38.25	0.55	2.74	65.06	54.36	0.26	1.04
		9610	31.25	15.96	47.12	36.92	0.56	1.17	37.56	30.94	0.29	1.11
South-	C2-16	9800	37.15	29.08	37.54	33.37	0.53	1.75	76.65	62.45	0.71	1.51
East		10260	55.56	30.38	30.07	39.56	0.43	2.49	78.68	62.85	0.58	1.61
Bazuzi		10380	37.72	30.72	37.76	31.52	0.54	2.69	73.23	53.51	0.59	1.79
		10580	60.37	29.89	37.17	32.93	0.53	3.12	64.25	42.81	0.54	1.83
	FF14-6	11290	79.56	28.06	41.12	30.81	0.57	1.78	83.70	70.50	0.64	1.81
		11320	54.15	31.92	36.56	31.52	0.54	2.20	87.88	74.85	0.86	1.46
Attahadi		11615	68.71	30.05	41.18	28.77	0.59	1.87	86.20	72.38	0.71	2.10
		11650	9.91	11.66	50.74	37.60	0.57	1.47	14.42	7.50	0.54	1.70
		12290	39.62	42.11	27.93	29.96	0.48	1.72	63.75	51.58	1.11	0.62
		12330	47.06	33.28	31.77	34.95	0.48	1.32	55.25	47.71	0.87	0.81
	L1-16	7400	8.50	11.16	50.17	38.67	0.56	1.50	15.87	8.32	0.53	1.69
Nuflian		7530	5.69	18.22	47.26	34.52	0.58	2.26	21.79	6.84	0.71	12.36
High		7640	7.36	19.28	46.35	34.37	0.57	2.30	16.13	7.39	0.67	1.52
		7850	7.21	17.27	44.09	38.64	0.53	2.50	21.56	9.99	0.67	1.49
	L1-17	6060	5.56	20.93	46.42	32.66	0.59	1.92	16.51	7.35	0.75	1.78
West		6300	8.00	21.63	45.36	33.00	0.58	2.35	23.04	10.79	0.75	1.49
Mabruk		6460	8.86	20.28	45.96	33.76	0.58	2.49	27.21	14.55	0.56	1.25
		6600	40.00	19.18	41.43	39.39	0.51	4.08	46.60	25.71	0.59	1.41
North	Z1-11	8080	14.02	22.18	42.61	35.21	0.55	1.41	38.26	26.05	0.55	1.30
Ghani		8140	14.51	23.12	41.52	35.37	0.54	1.78	53.11	35.97	0.59	1.44
Zenad		8200	25.87	29.73	39.21	31.06	0.56	1.62	42.64	29.77	0.49	1.26

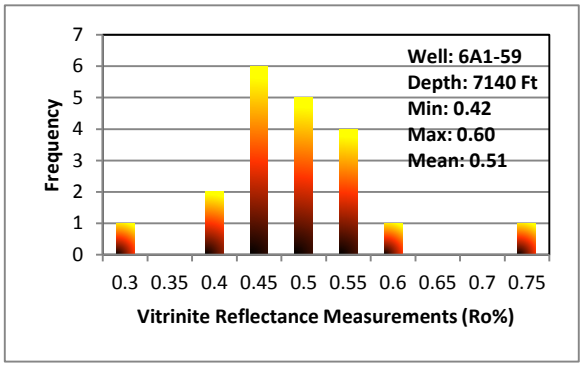

0.42 0.44 0.45 0.46 0.47 0.48 0.49 0.50 0.51 0.52 0.53 0.54 0.57 0.59 0.60 0.75

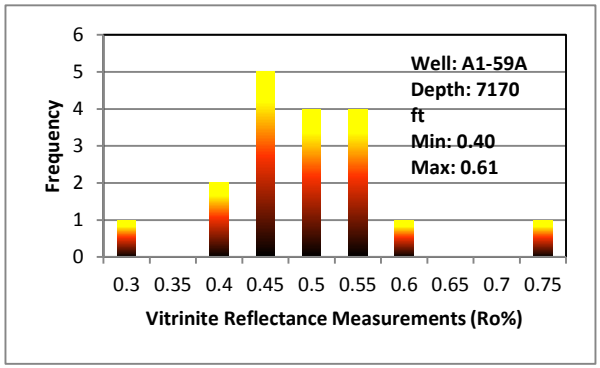

0.44 0.44 0.45 0.46 0.47 0.48 0.49 0.50 0.52 0.53 0.54 0.55 0.56 0.58 0.59 0.60 0.76

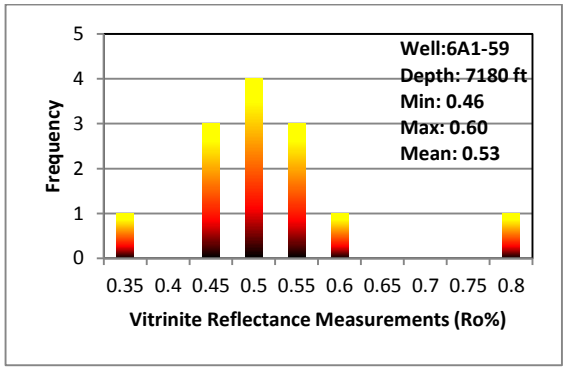

0.46 0.47 0.48 0.50 0.51 0.53 0.54 0.56 0.57 0.59 0.56 0.56 0.57 0.59 0.60 0.81

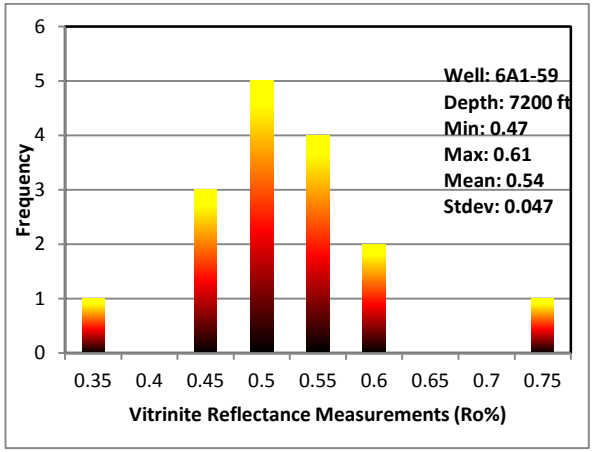

0.47 0.48 0.49 0.50 0.51 0.52 0.53 0.54 0.55 0.57 0.58 0.60 0.61

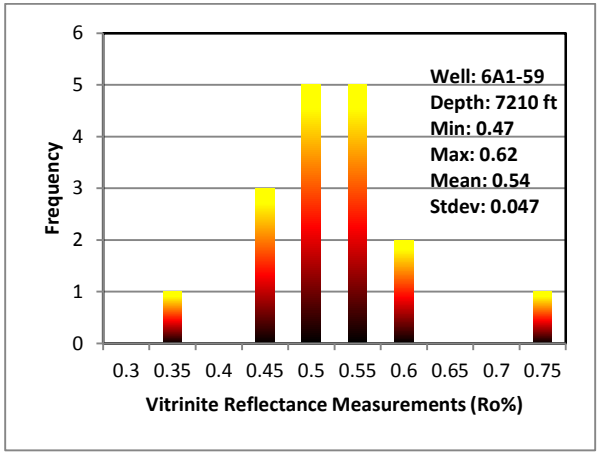

0.46 0.48 0.49 0.50 0.51 0.52 0.53 0.53 0.55 0.56 0.58 0.58 0.59 0.60 0.61

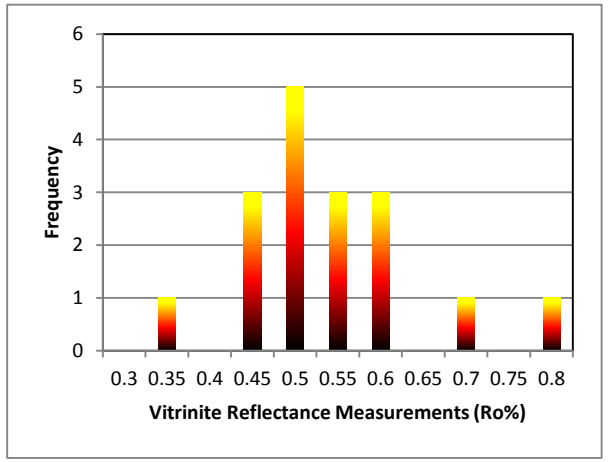

0.46 0.48 0.49 0.50 0.51 0.52 0.53 0.54 0.55 0.56 0.58 0.59 0.59 0.60 0.62

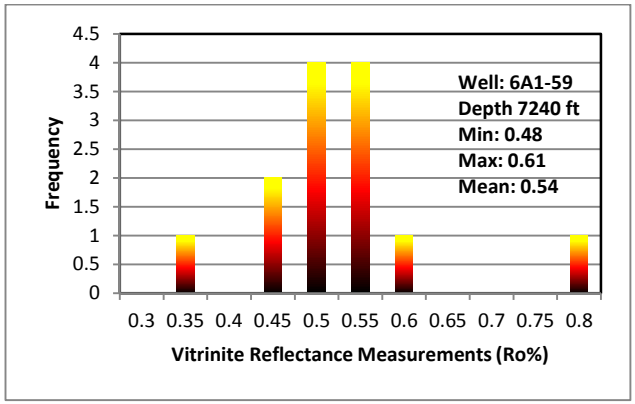

0.48 0.49 0.50 0.52 0.53 0.54 0.55 0.57 0.58 0.59 0.61

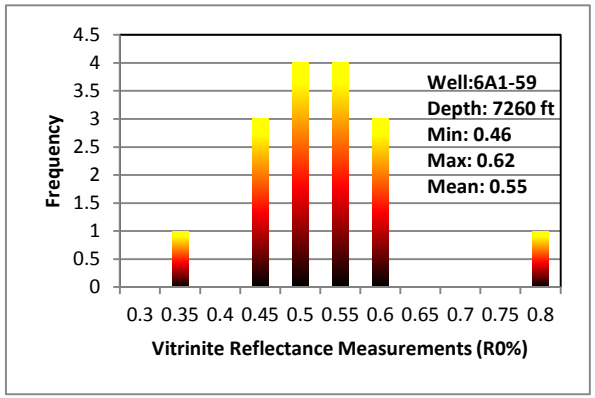

0.46 0.48 0.48 0.50 0.51 0.52 0.53 0.55 0.56 0.57 0.58 0.60 0.61 0.62

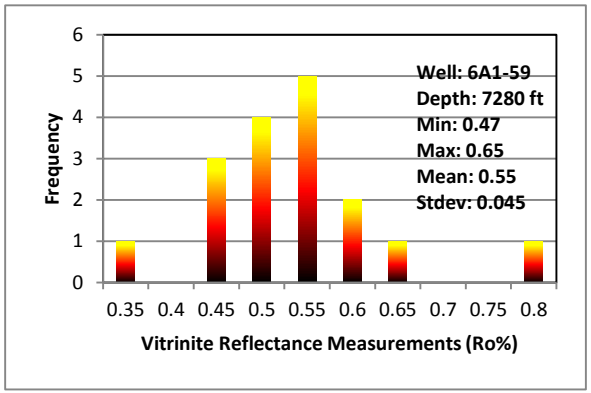

0.47 0.48 0.50 0.51 0.52 0.53 0.55 0.56 0.58 0.58 0.59 0.61 0.61 0.63 0.65

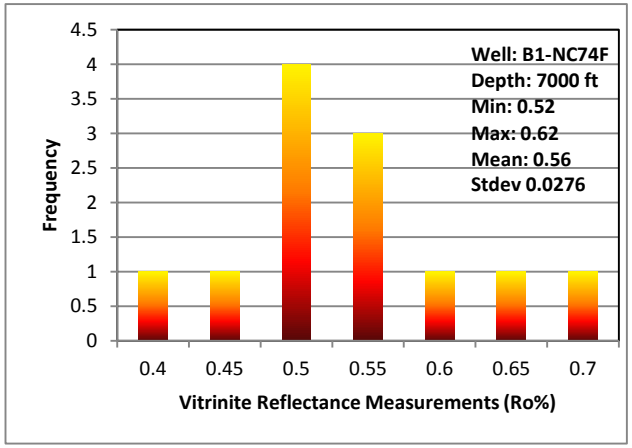

0.40 0.45 0.52 0.52 0.53 0.54 0.55 0.57 0.59 0.60 0.65 0.70

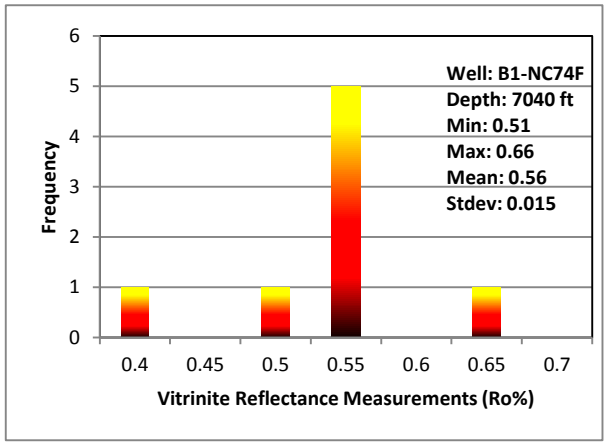

0.40 0.51 0.55 0.56 0.57 0.58 0.59 0.65

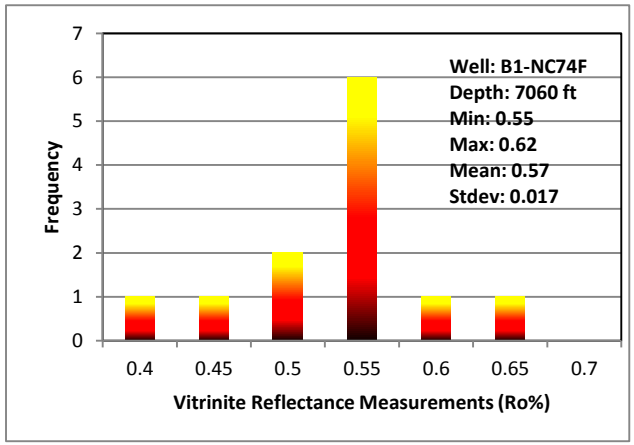

0.40 0.45 0.53 0.54 0.55 0.56 0.56 0.57 0.58 0.59 0.61 0.62

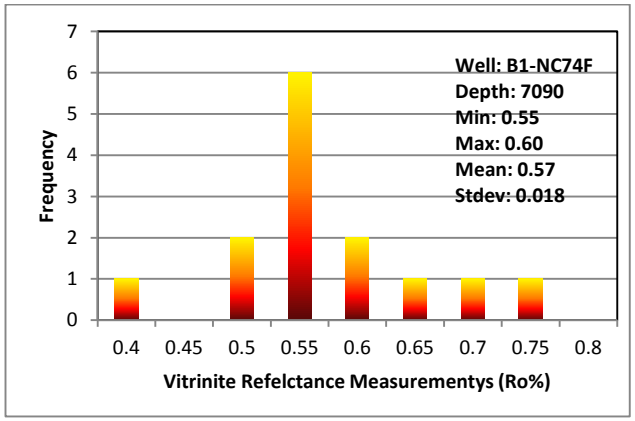

0.40 0.53 0.54 0.55 0.56 0.57 0.58 0.59 0.59 0.60 0.60 0.70 0.75

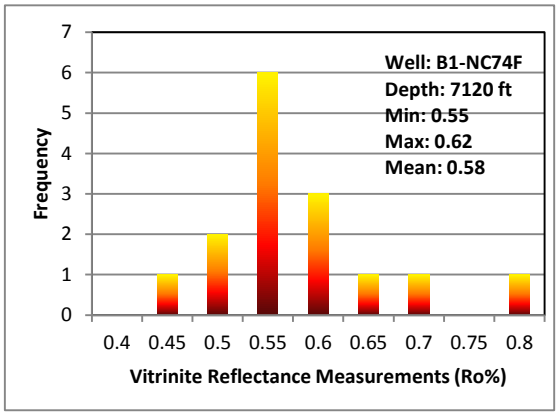

0.45 0.52 0.53 0.55 0.56 0.57 0.58 0.59 0.59 0.60 0.61 0.62 0.65 0.70 0.81

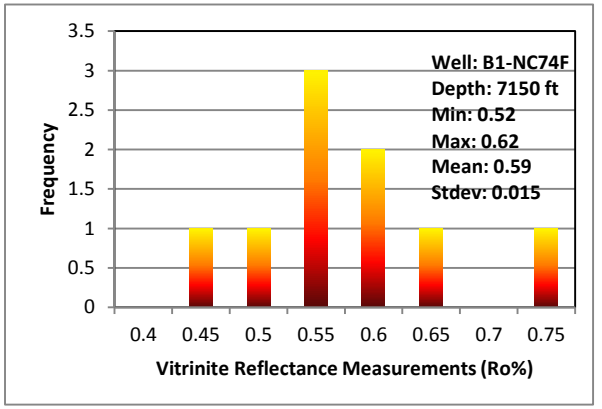

0.46 0.52 0.55 0.56 0.59 0.61 0.62 0.66 0.75

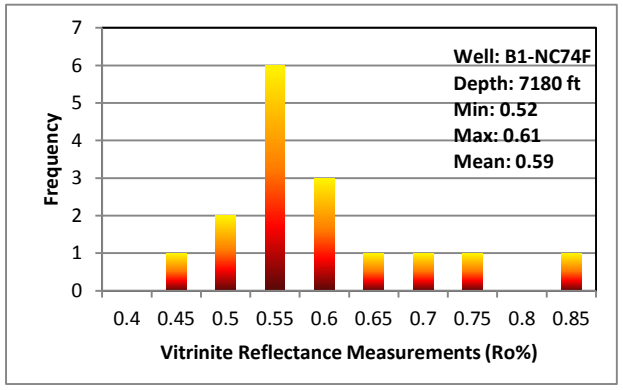

0.45 0.50 0.51 0.52 0.55 0.56 0.57 0.58 0.58 0.59 0.60 0.61 0.61 0.66 0.71 0.75 0.85

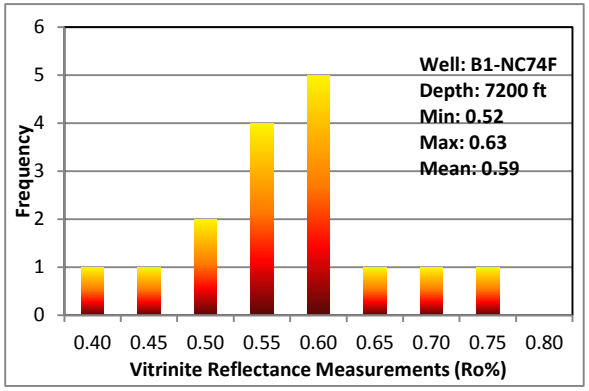

0.40 0.45 0.51 0.52 0.55 0.56 0.58 0.59 0.60 0.61 0.62 0.63 0.63 0.66 0.72 0.76

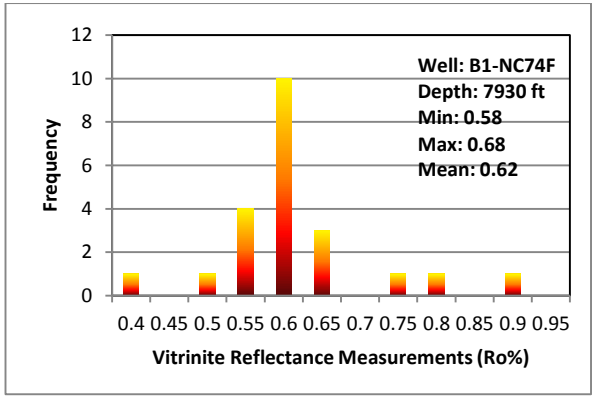

0.40 0.50 0.55 0.56 0.58 0.59 0.60 0.61 0.62 0.62 0.63 0.64 0.64 0.64 0.64 0.64 0.67 0.68 0.75 0.92 0.91

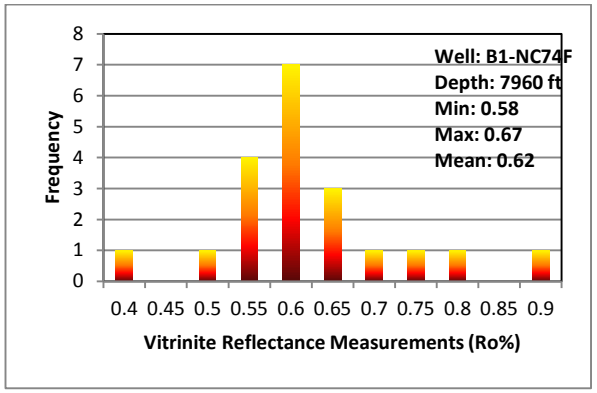

0.40 0.53 0.58 0.58 0.59 0.59 0.60 0.60 0.61 0.62 0.62 0.63
0.64 0.65 0.66 0.67 0.73 0.77 0.82 0.91

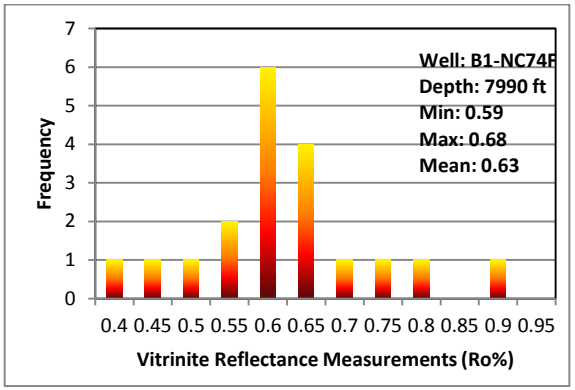

0.40 0.45 0.51 0.59 0.59 0.60 0.61 0.62 0.63 0.63 0.64
0.65 0.66 0.68 0.68 0.73 0.76 0.83 0.93

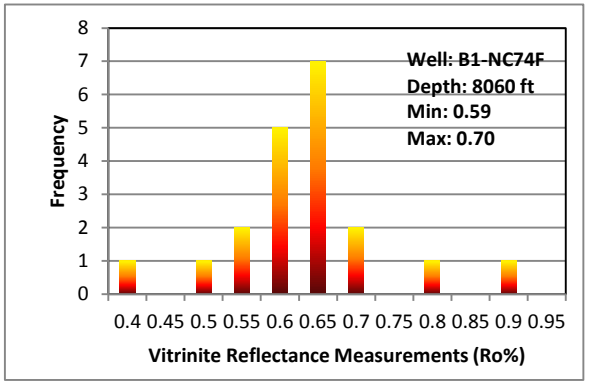

0.41 0.53 0.59 0.59 0.60 0.61 0.62 0.63 0.64 0.65 0.66
0.67 0.68 0.69 0.69 0.69 0.70 0.70 0.83 0.92

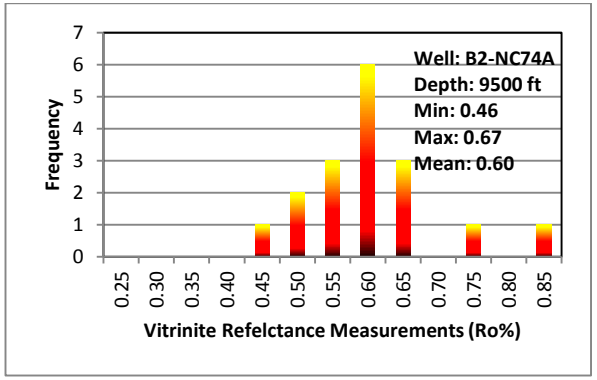

0.46 0.50 0.52 0.55 0.55 0.56 0.60 0.61 0.62 0.63 0.64
0.64 0.65 0.66 0.67

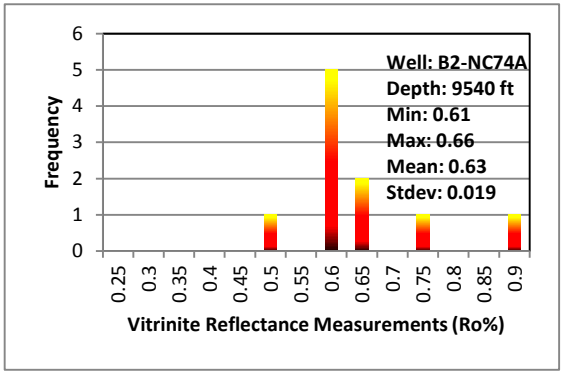

0.40 0.61 0.62 0.63 0.64 0.65 0.66

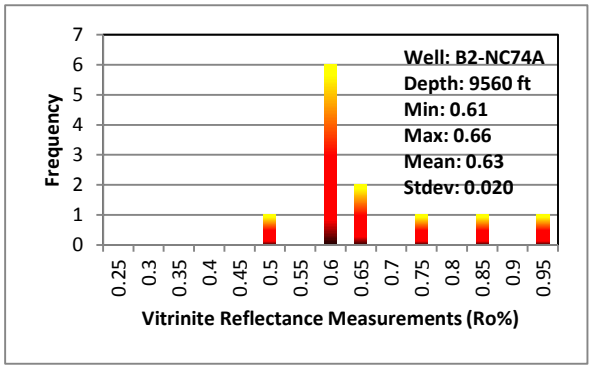

0.61 0.61 0.62 0.62 0.63 0.64 0.65 0.66

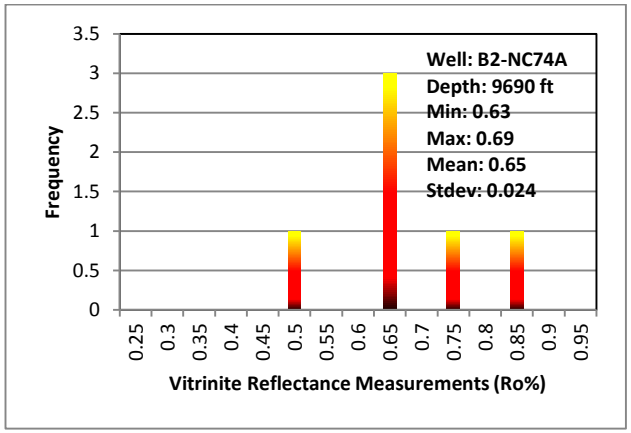

0.63 0.64 0.65 0.67 0.69 0.75 0.86

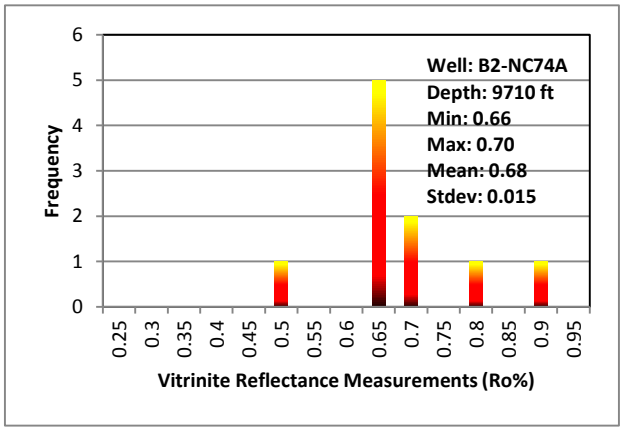

0.66 0.67 0.68 0.69 0.69 0.70 0.70 0.80 0.91

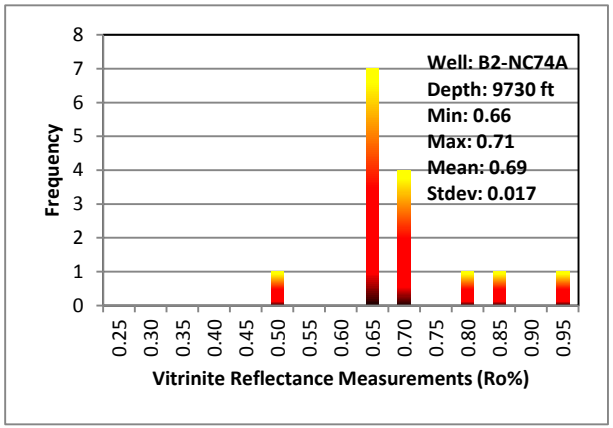

0.66 0.67 0.67 0.68 0.69 0.69 0.69 0.70 0.70 0.71 0.71

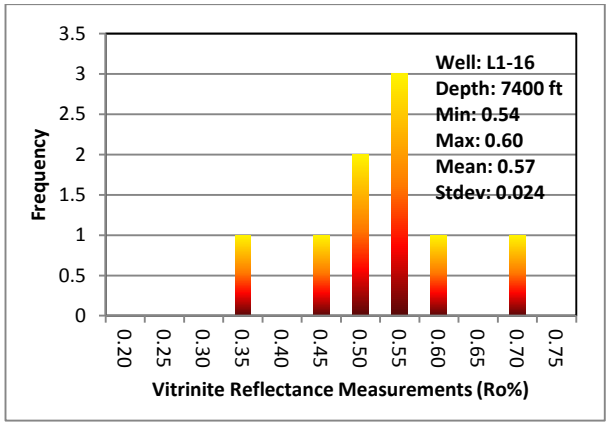

0.35 0.54 0.54 0.57 0.58 0.59 0.60

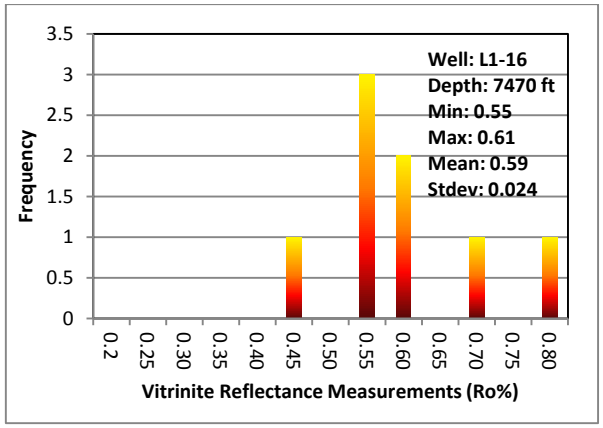

0.45 0.55 0.56 0.57 0.60 0.60 0.60 0.61 0.61 0.61

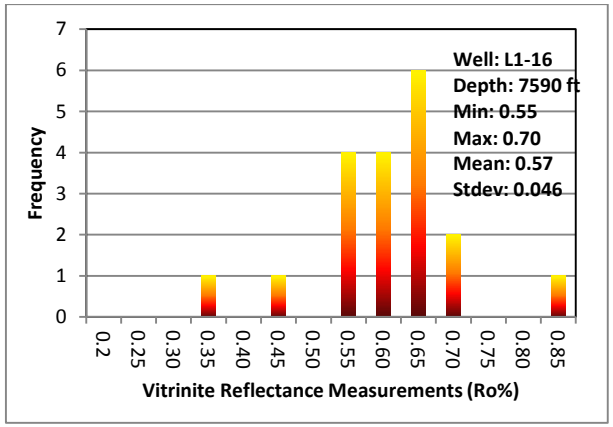

0.55 0.56 0.57 0.58 0.60 0.62 0.62 0.63 0.65 0.65 0.65 0.66 0.67 0.70 0.70

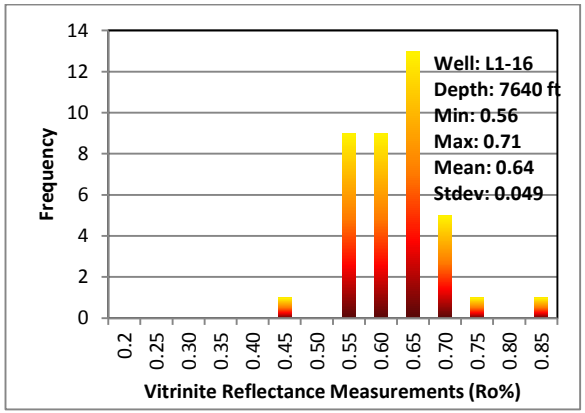

0.45 0.56 0.56 0.56 0.57 0.57 0.58 0.58 0.59 0.60 0.61
0.62 0.62 0.63 0.63 0.63 0.63 0.64 0.65 0.65 0.66 0.66 0.67
0.67 0.67 0.68 0.68 0.68 0.69 0.70 0.70 0.71 0.71

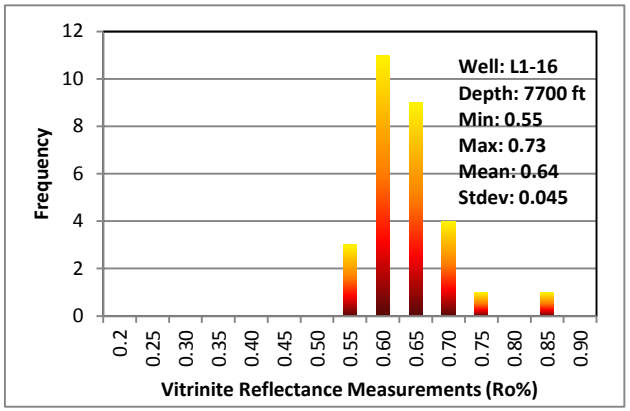

0.55 0.57 0.58 0.59 0.60 0.61 0.62 0.62 0.63 0.63 0.63 0.64
0.64 0.64 0.65 0.65 0.66 0.66 0.67 0.68 0.69 0.70 0.71 0.72 0.73

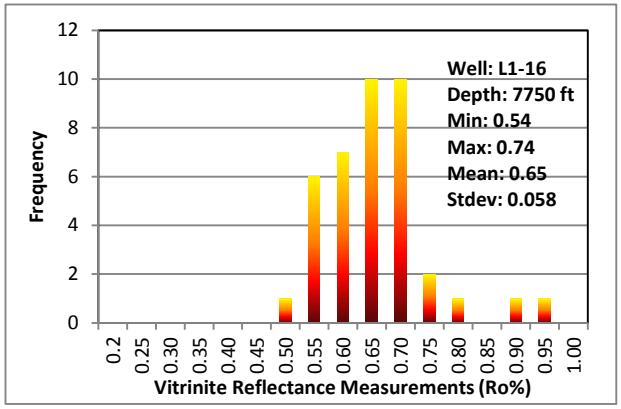

0.50 0.54 0.55 0.56 0.57 0.57 0.58 0.59 0.60 0.61 0.61
0.61 0.62 0.63 0.63 0.63 0.65 0.65 0.65 0.65 0.65 0.65 0.66 0.66
0.66 0.66 0.66 0.67 0.69 0.70 0.71 0.71 0.71 0.71 0.72
0.72 0.73 0.74

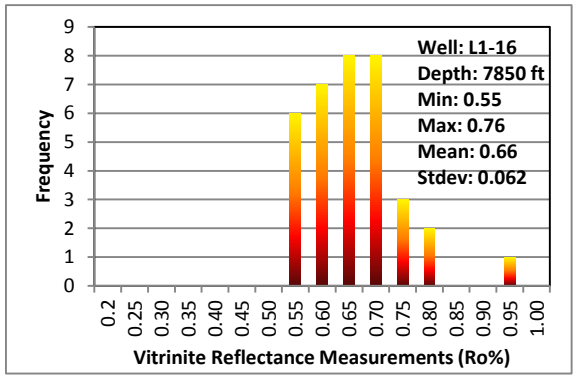

0.55 0.56 0.56 0.57 0.58 0.59 0.60 0.62 0.62 0.64 0.64
0.66 0.67 0.67 0.68 0.69 0.69 0.70 0.70 0.69
0.71 0.73 0.73 0.74 0.75 0.76 0.76

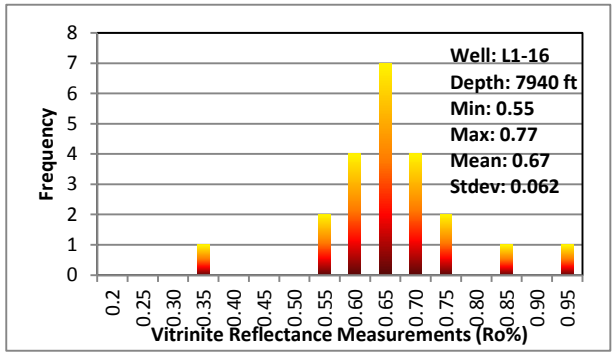

0.55 0.56 0.60 0.61 0.62 0.63 0.65 0.66 0.67 0.68 0.68 0.69
0.70 0.72 0.73 0.74 0.75 0.77

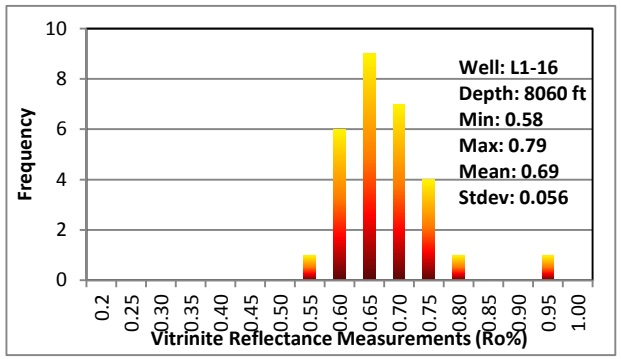

0.58 0.60 0.61 0.62 0.63 0.64 0.64 0.65 0.66 0.67 0.67 0.64 0.64 0.65
0.67 0.68 0.69 0.69 0.70 0.71 0.71 0.72 0.72 0.73 0.74 0.76
0.79 0.79 0.79

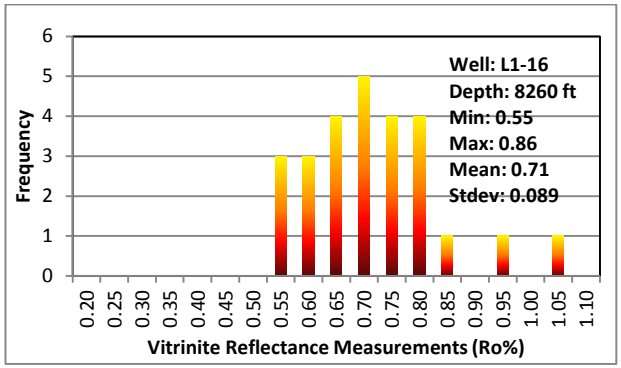

0.55 0.56 0.58 0.61 0.62 0.64 0.65 0.65 0.66
0.67 0.69 0.70 0.71 0.72 0.73 0.74 0.75 0.76
0.78 0.79 0.80 0.81 0.82 0.84 0.86 0.95 1.05

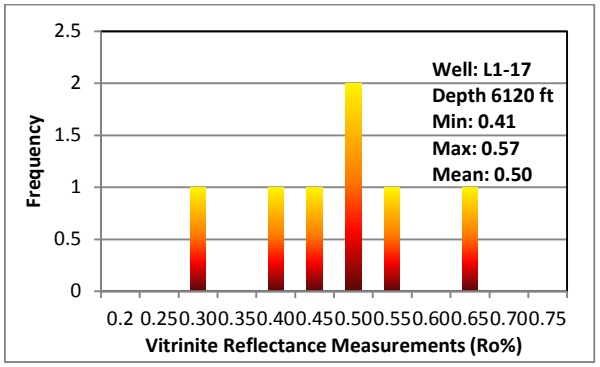

0.41 0.47 0.52 0.54 0.57 0.65

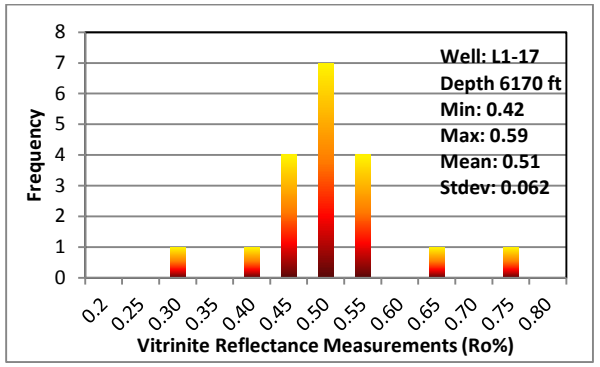

0.42 0.45 0.46 0.46 0.47 0.50 0.50 0.51 0.52
0.53 0.54 0.54 0.55 0.56 0.57 0.59

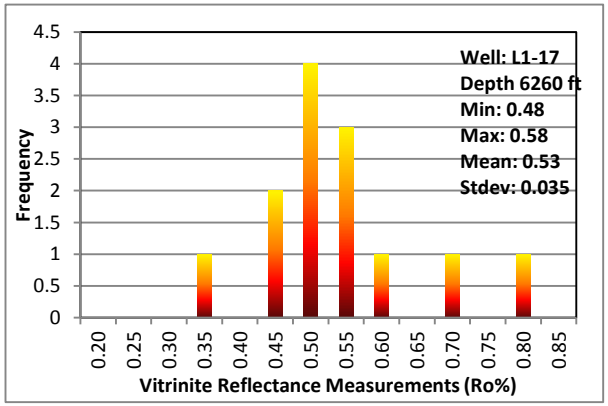

0.35 0.48 0.48 0.50 0.51 0.52 0.53 0.55 0.57 0.58

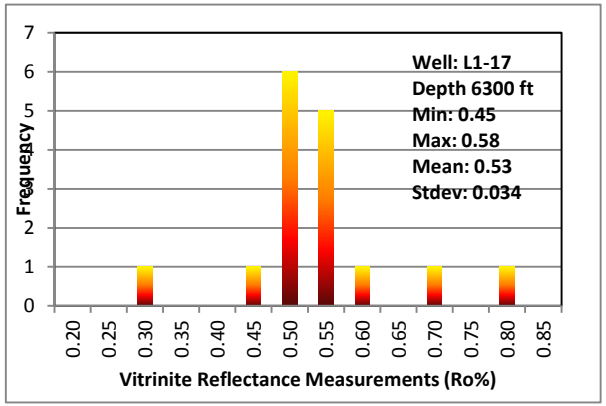

0.45 0.50 0.51 0.52 0.53 0.54 0.55 0.55 0.56 0.57 0.58

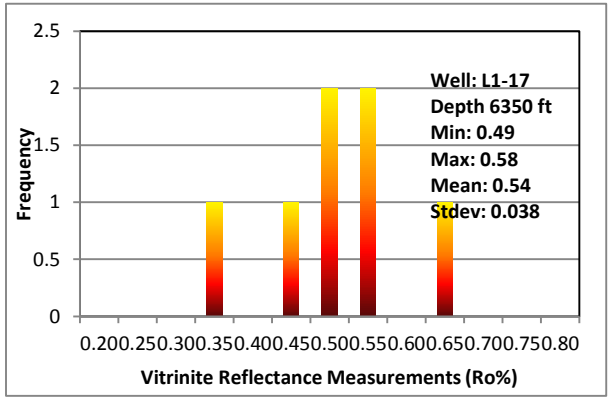

0.35 0.49 0.53 0.54 0.55 0.58 0.65

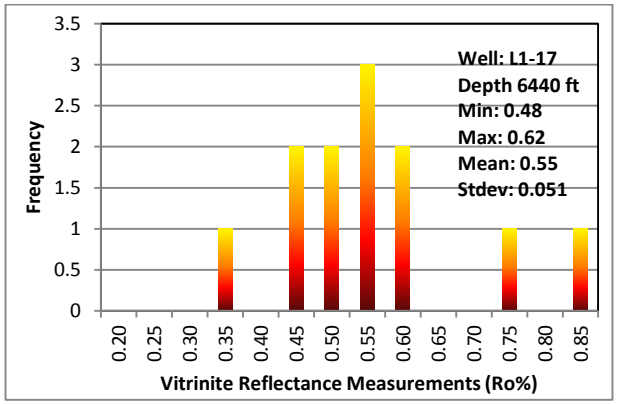

0.35 0.48 0.49 0.51 0.52 0.55 0.56 0.58 0.61 0.62

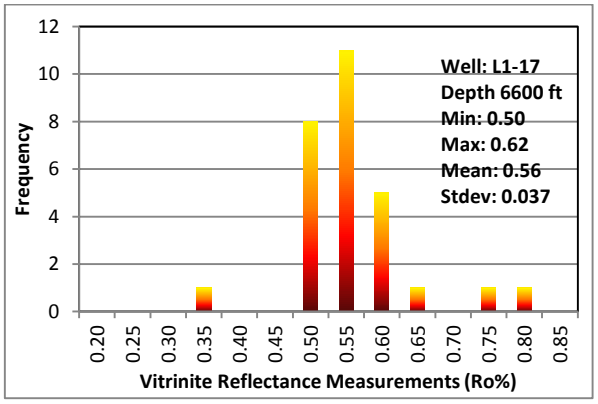

0.36 0.50 0.51 0.52 0.52 0.53 0.53 0.53 0.54 0.55 0.55 0.56 0.56 0.57 0.58 0.59 0.60 0.60 0.60 0.61 0.62

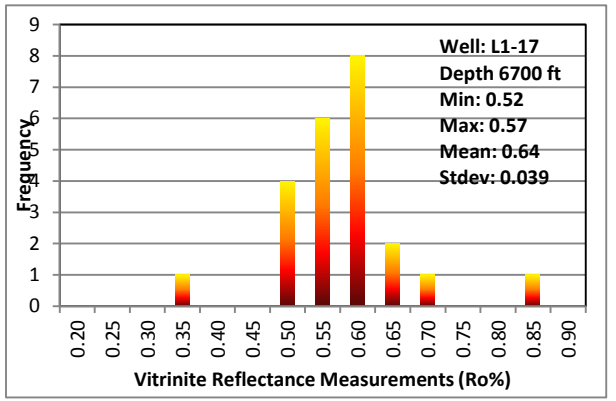

0.36 0.52 0.53 0.54 0.54 0.55 0.57 0.58 0.59 0.60 0.60 0.61 0.62 0.62 0.63 0.64

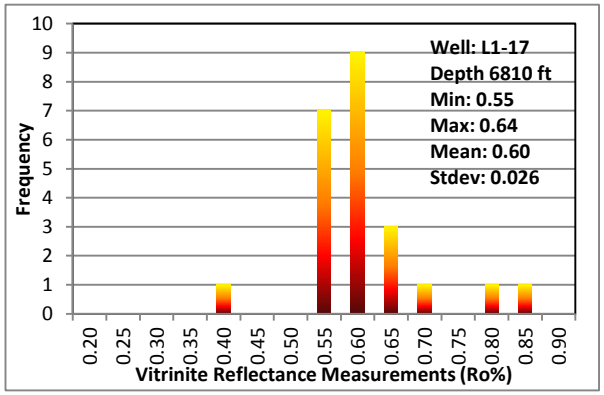

0.41 0.55 0.56 0.57 0.57 0.58 0.59 0.59 0.60 0.60 0.61 0.61 0.62 0.62 0.63 0.63 0.64 0.69 0.71 0.81 0.86

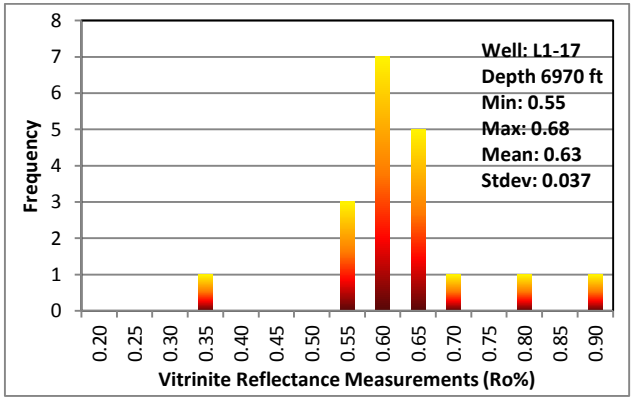

0.37 0.55 0.57 0.59 0.60 0.61 0.61 0.62 0.63 0.64 0.64 0.65 0.66 0.66 0.67 0.68 0.73 0.81 0.86

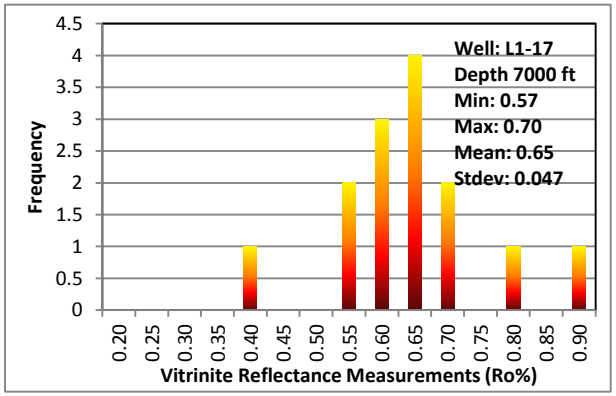

0.42 0.57 0.58 0.61 0.62 0.64 0.65 0.67 0.69 0.69 0.70 0.70 0.83 0.92

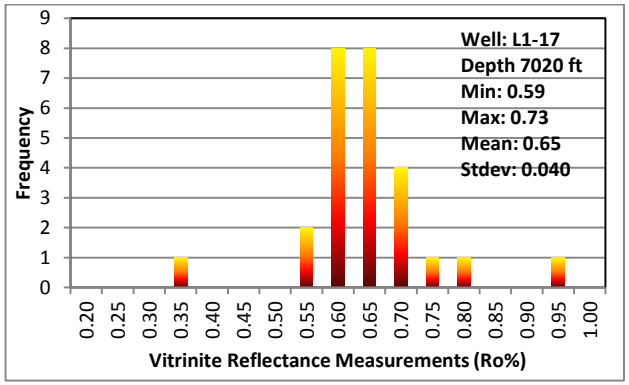

0.35 0.59 0.59 0.60 0.61 0.62 0.62 0.63 0.63 0.64 0.64 0.65 0.65 0.65 0.66 0.67 0.68 0.69 0.70 0.71 0.72 0.73 0.77 0.82 0.96

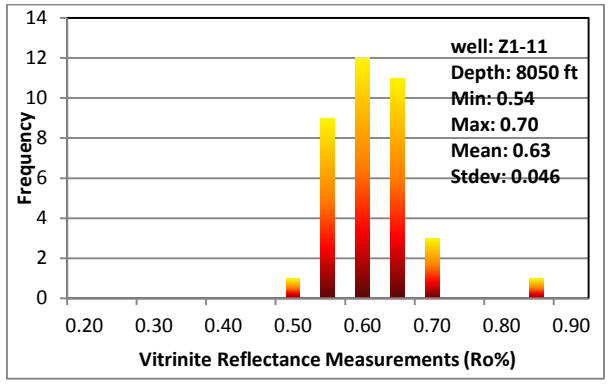

0.54 0.55 0.57 0.57 0.58 0.58 0.58 0.58 0.58 0.59 0.60 0.60 0.61 0.61 0.63 0.63 0.64 0.64 0.64 0.64 0.64 0.64 0.65 0.65 0.65 0.66 0.67 0.67 0.67 0.68 0.68 0.69 0.69 0.70 0.70 0.70

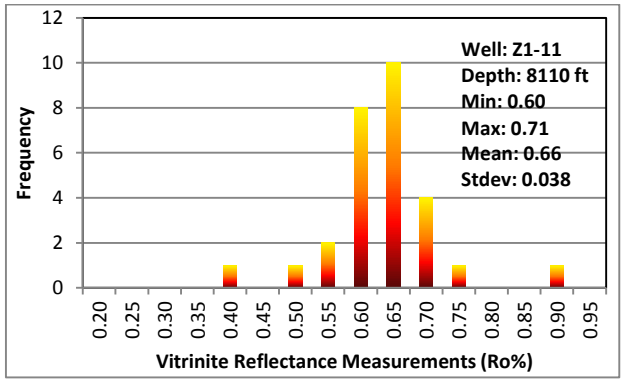

0.42 0.51 0.55 0.60 0.60 0.60 0.61 0.62 0.63 0.64 0.64 0.64 0.65 0.65 0.66 0.66 0.67 0.68 0.69 0.69 0.69 0.69 0.70 0.71 0.71 0.71 0.77 0.91

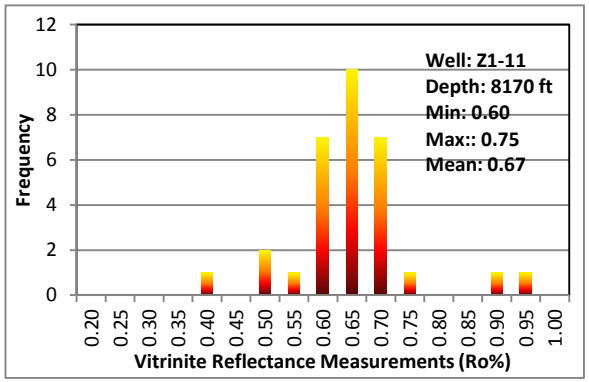

0.41 0.52 0.55 0.60 0.60 0.60 0.61 0.62 0.63 0.64 0.65 0.65 0.66 0.66 0.67 0.68 0.69 0.69 0.69 0.69 0.70 0.71 0.72 0.73 0.74 0.74 0.74 0.75 0.91 0.95

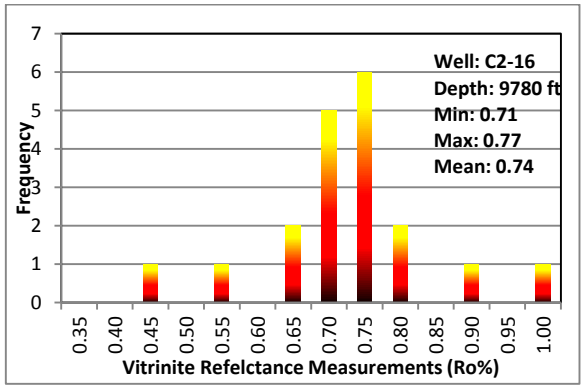

0.46 0.56 0.65 0.65 0.70 0.70 0.71 0.73 0.73 0.75 0.75 0.76 0.76 0.77 0.77 0.84 0.84 0.92 1.01

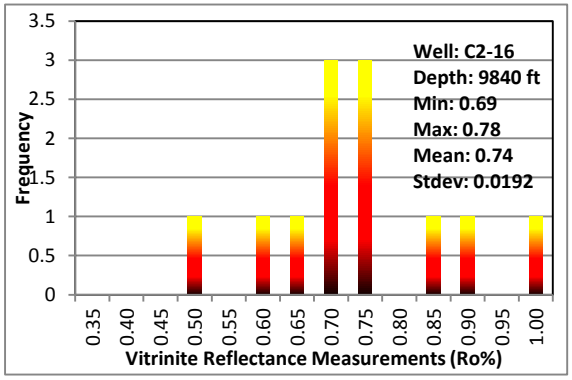

0.51 0.62 0.65 0.69 0.70 0.73 0.74 0.75 0.76 0.78 0.85 0.93 1.02

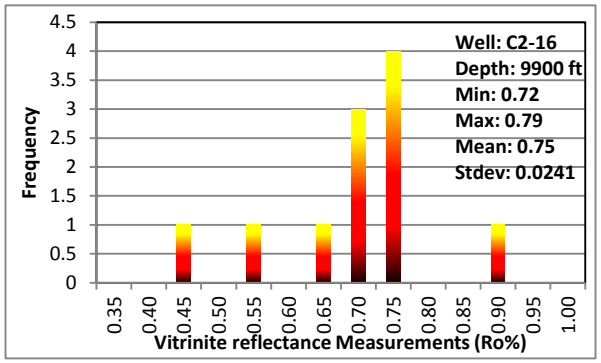

0.46 0.55 0.65 0.72 0.73 0.74 0.75 0.76 0.77 0.79 0.91

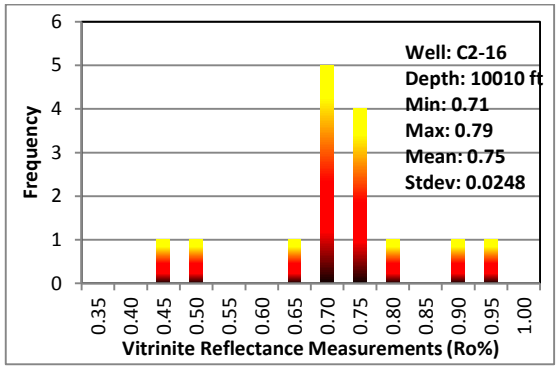

0.46 0.53 0.66 0.71 0.72 0.73 0.74 0.74 0.75 0.76 0.77
0.79 0.83 0.91 0.96

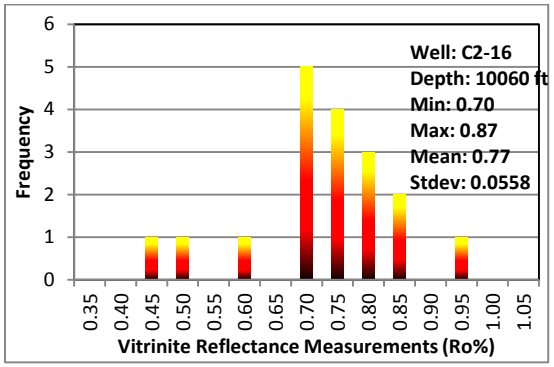

0.47 0.54 0.62 0.70 0.71 0.71 0.71 0.72 0.75 0.76 0.77 0.78
0.80 0.81 0.82 0.85 0.87 0.96

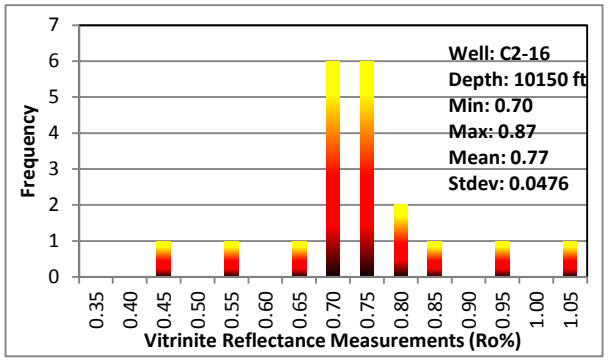

0.46 0.56 0.65 0.70 0.71 0.72 0.73 0.74 0.74 0.75 0.76 0.77
0.78 0.78 0.79 0.81 0.84 0.87 0.96 1.05

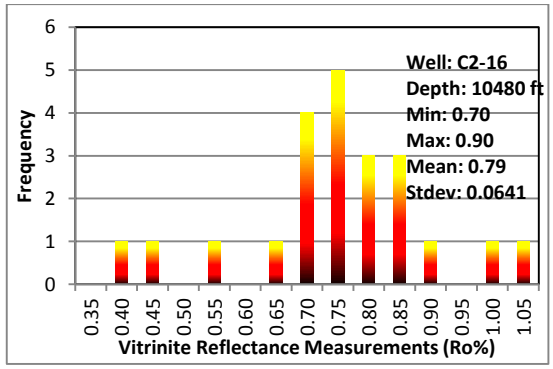

0.43 0.46 0.56 0.66 0.70 0.70 0.71 0.73 0.75 0.76 0.76 0.77
0.79 0.80 0.81 0.83 0.85 0.86 0.88 0.90 1.02 1.05

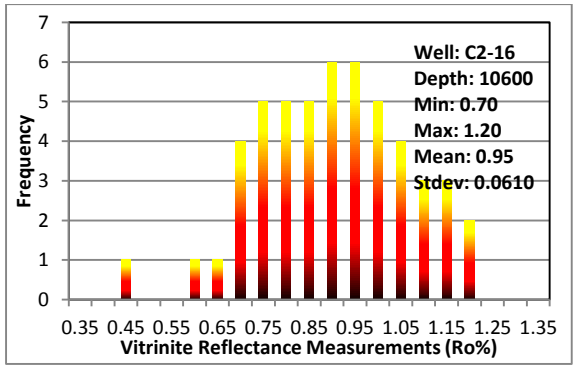

0.47 0.62 0.66 0.70 0.70 0.71 0.72 0.74 0.75 0.75 0.76 0.77 0.78 0.80
0.80 0.80 0.82 0.83 0.85 0.85 0.85 0.86 0.87 0.90 0.91 0.91 0.92 0.92
0.93 0.94 0.96 0.96 0.98 0.99 1.00 1.00 1.01 1.03 1.04 1.06 1.07 1.08
1.09 1.10 1.11 1.12 1.13 1.14 1.15 1.16 1.17 1.18 1.19 1.20 1.20

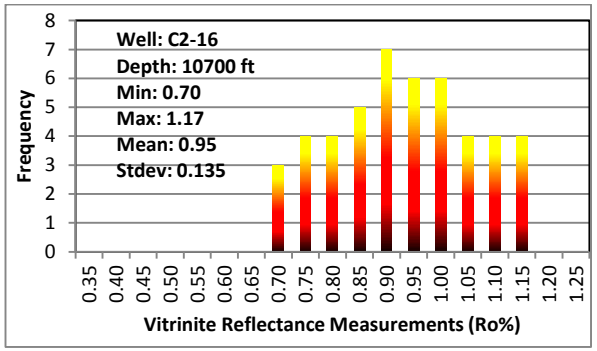

0.70 0.72 0.73 0.75 0.76 0.77 0.77 0.78 0.80 0.80 0.81 0.82 0.85 0.85 0.85 0.87 0.88 0.90 0.91 0.92 0.93 0.94 0.94 0.96 0.97 0.98 0.98 0.99 1.00 1.01 1.02 1.03 1.05 1.05 1.05 1.06 1.06 1.07 1.08 1.10 1.11 1.13 1.13 1.14 1.15 1.15 1.15 1.15 1.17

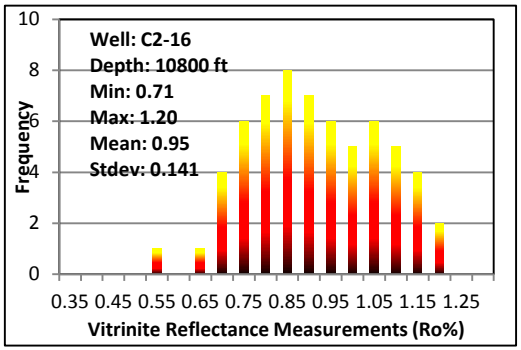

0.55 0.65 0.71 0.72 0.73 0.74 0.75 0.76 0.77 0.78 0.79 0.80 0.80 0.80 0.82 0.83 0.84 0.84 0.85 0.86 0.86 0.87 0.87 0.88 0.89 0.89 0.90 0.92 0.93 0.94 0.94 0.95 0.96 0.97 0.98 0.99 0.99 1.00 1.01 1.02 1.03 1.04 1.05 1.06 1.07 1.08 1.08 1.09 1.10 1.10 1.12 1.14 1.14 1.16 1.17 1.18 1.19 1.20 1.20

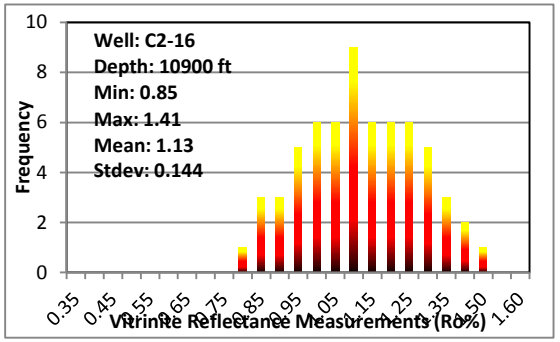

0.80 0.85 0.86 0.88 0.90 0.91 0.93 0.95 0.95 0.96 0.97 0.99 1.00 1.00 1.01 1.03 1.04 1.05 1.06 1.07 1.08 1.09 1.10 1.10 1.10 1.11 1.12 1.13 1.13 1.14 1.14 1.15 1.16 1.16 1.16 1.17 1.18 1.19 1.20 1.21 1.22 1.23 1.24 1.25 1.26 1.27 1.27 1.28 1.28 1.30 1.32 1.31 1.32 1.33 1.35 1.37 1.40 1.41 1.51

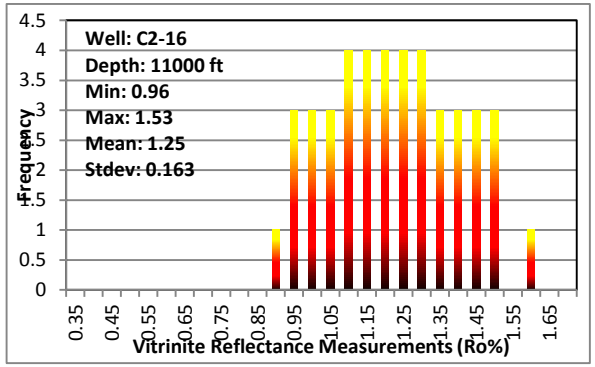

0.96 0.98 0.99 1.00 1.03 1.04 1.05 1.08 1.09 1.10 1.12 1.13
1.14 1.14 1.15 1.16 1.17 1.18 1.20 1.21 1.23 1.24 1.26 1.27
1.28 1.29 1.30 1.33 1.34 1.34 1.37 1.38 1.39 1.42 1.41 1.43
1.44 1.45 1.47 1.49 1.50 1.51 1.53 1.61

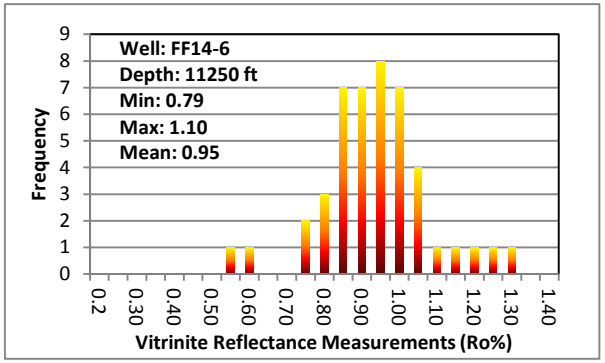

0.79 0.79 0.80 0.83 0.85 0.86 0.87 0.87 0.87 0.88 0.89
0.90 0.90 0.91 0.94 0.94 0.95 0.95 0.96 0.98 0.98 0.98
0.99 0.99 0.99 1.01 1.02 1.03 1.05 1.09 1.09 1.09 1.10

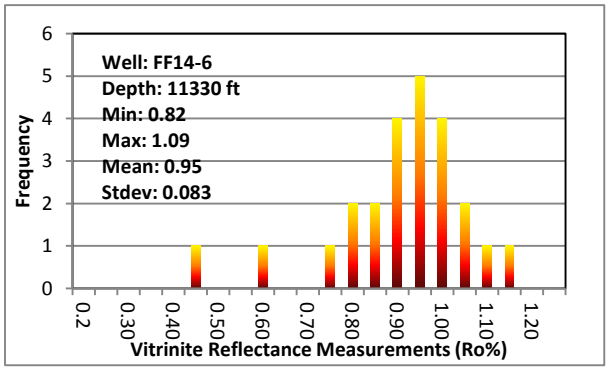

0.82 0.82 0.86 0.86 0.90 0.91 0.93 0.94 0.95 0.97 0.98 1.02
1.03 1.05 1.07 1.09

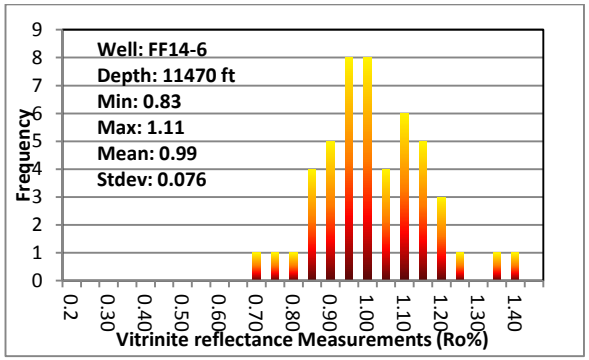

0.83 0.86 0.87 0.89 0.89 0.92 0.94 0.94 0.94 0.95 0.96 0.97
0.97 0.98 1.00 1.00 1.00 1.01 1.02 1.03 1.03 1.05 1.05 1.07
1.08 1.08 1.08 1.10 1.11 1.11

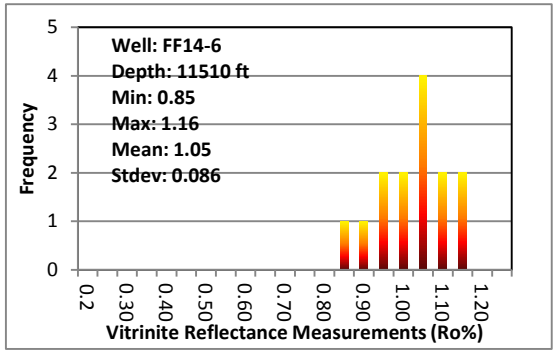

0.85 0.92 0.94 0.96 0.99 1.02 1.04 1.05 1.07 1.08 1.09
1.12 1.13 1.15 1.15 1.16

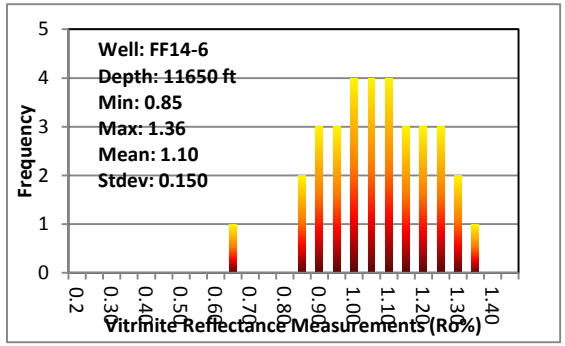

0.85 0.88 0.90 0.91 0.93 0.95 0.96 0.99 1.00 1.00 1.01 1.02
1.05 1.05 1.05 1.09 1.10 1.12 1.13 1.14 1.17 1.18 1.19 1.22
1.23 1.24 1.26 1.27 1.29 1.32 1.34 1.36

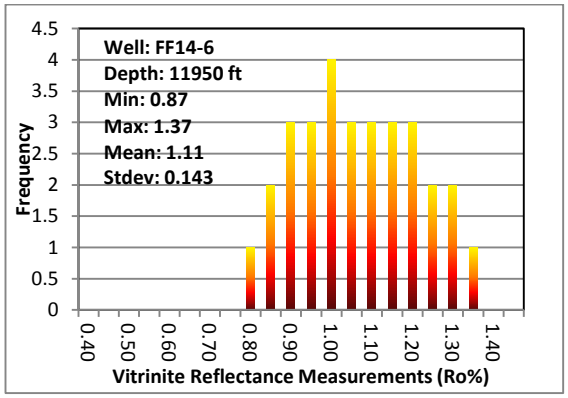

0.87 0.88 0.90 0.93 0.94 0.96 0.97 0.99 1.00 1.02 1.03 1.04
1.06 1.06 1.07 1.10 1.12 1.13 1.16 1.17 1.19 1.20 1.22 1.23
1.25 1.26 1.28 1.31 1.33 1.36

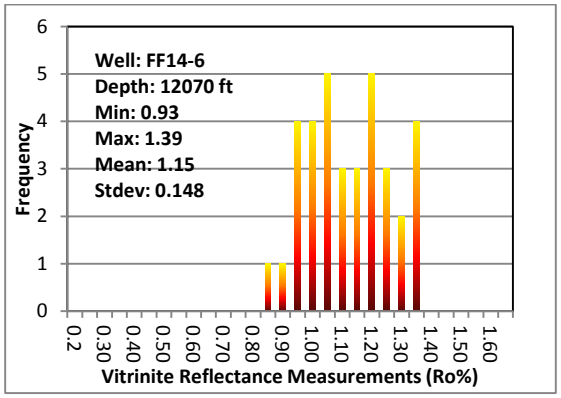

0.93 0.95 0.95 0.96 0.97 1.00 1.00 1.01 1.02 1.05 1.05
1.05 1.06 1.07 1.12 1.13 1.14 1.16 1.17 1.19 1.22 1.23
1.23 1.24 1.24 1.28 1.28 1.29 1.31 1.33 1.35 1.36 1.39

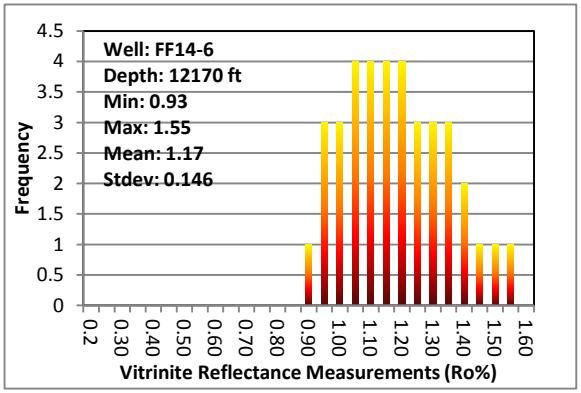

0.93 0.95 0.97 0.99 1.00 1.01 1.03 1.05 1.06 1.07 1.08 1.10
1.11 1.13 1.15 1.15 1.16 1.17 1.19 1.20 1.22 1.23 1.24 1.25
1.26 1.28 1.31 1.32 1.34 1.38 1.39 1.42 1.43 1.48 1.51 1.55

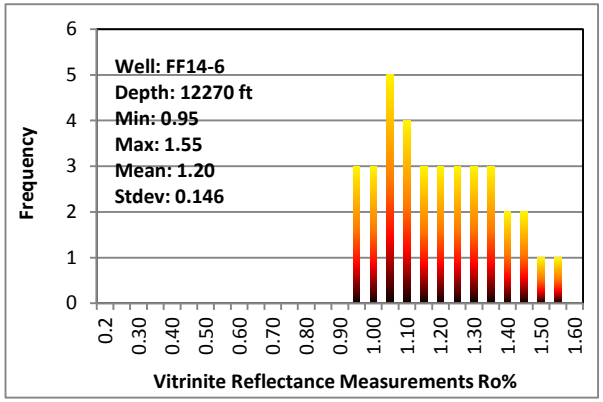

0.95 0.96 0.97 1.00 1.01 1.02 1.05 1.06 1.07 1.08 1.09 1.10
1.11 1.12 1.13 1.15 1.16 1.19 1.20 1.22 1.23 1.25 1.26 1.28
1.31 1.32 1.33 1.35 1.36 1.38 1.41 1.42 1.46 1.49 1.51 1.55

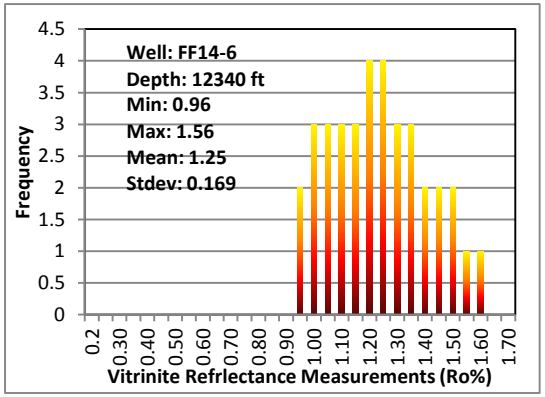

0.96 0.98 1.00 1.01 1.03 1.05 1.07 1.09 1.10 1.11 1.12
1.15 1.17 1.19 1.22 1.23 1.24 1.24 1.26 1.27 1.28 1.29
1.29 1.29 1.32 1.33 1.34 1.35 1.38 1.39 1.41 1.42 1.46

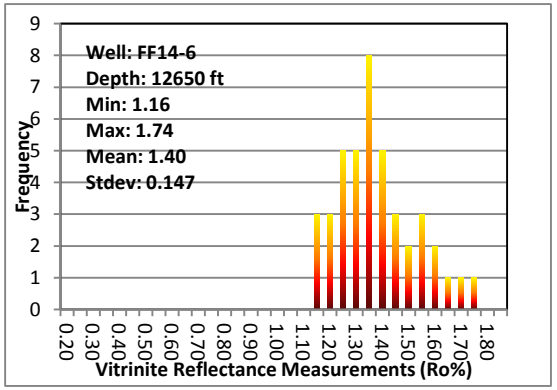

1.16 1.17 1.19 1.20 1.23 1.25 1.25 1.26 1.28 1.29 1.31 1.31
1.32 1.33 1.34 1.35 1.36 1.36 1.38 1.38 1.39 1.39 1.41 1.42
1.42 1.44 1.44 1.46 1.48 1.49 1.51 1.52 1.55 1.58 1.59 1.61
1.64 1.67 1.70 1.74

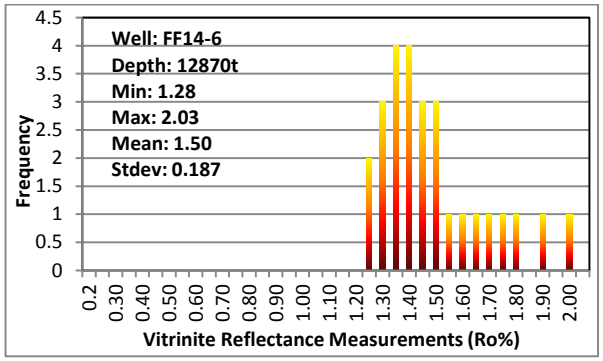

1.28 1.29 1.31 1.32 1.33 1.35 1.36 1.38 1.39 1.40 1.41 1.42 1.43
1.45 1.48 1.49 1.51 1.51 1.54 1.58 1.60 1.67 1.71 1.75 1.81 1.92 2.03

Appendix II Table 5.1: Steranes biomarker concentrations (µg/mg oil) of the oil families in the Sirt Basin.

Location	Family	Oil Filed	Well Name	C_{21}	C_{22}	DC_{27} βα20S	DC_{27} βα20R	DC_{27} αβ20S	DC_{27} αβ20R	DC_{28}S βα24S+R	DC_{28}R βα24S+R	C_{27} ααα20S	DC_{28} αβ20S	C_{27} αββ20R	DC_{29} βα20S	C_{27} αββ20S	DC_{28} αβ20R	C_{27} ααα20R	DC_{29} βα20R
West Sirt Basin	1A	West Mabruk	A31-17	2.60	1.53	5.61	2.84	1.36	1.59	4.54	3.21	2.23	2.23	3.44	5.39	5.43	5.43	4.52	3.91
			A29-17	4.42	2.65	8.72	4.91	2.12	2.41	7.68	5.27	3.12	3.12	4.48	7.50	6.33	6.33	6.15	6.61
			A86-17	2.87	1.76	6.02	3.38	1.49	1.88	6.05	3.63	2.08	2.08	3.96	6.01	5.63	5.63	4.98	3.81
			A44-17	2.92	1.62	5.75	3.11	1.46	1.72	5.20	2.77	2.05	2.05	3.18	4.88	4.37	4.37	4.97	3.74
			A66-17	2.94	1.63	5.78	3.03	1.50	1.76	5.48	3.56	2.00	2.00	3.05	5.00	4.08	4.08	4.38	3.51
			A15-17	2.90	1.83	6.21	3.32	1.60	1.81	5.19	3.64	2.02	2.02	4.17	5.71	4.78	4.78	4.72	4.00
			M1-17	3.28	1.91	6.14	3.34	1.65	1.70	5.58	3.61	2.02	2.02	4.03	5.65	4.83	4.83	4.83	4.27
			A46-17	3.39	2.05	6.95	3.89	1.68	2.03	6.09	4.33	2.48	2.48	3.52	5.39	4.98	4.98	4.81	5.61
			A82-17	1.45	1.13	4.75	2.76	1.61	1.57	5.42	4.07	1.49	1.49	1.90	3.82	3.65	3.65	1.77	3.21
			A94-17	2.01	1.24	5.17	2.61	1.45	1.50	4.74	3.30	1.62	1.62	2.33	4.08	3.17	3.17	2.53	3.87
			A39-17	2.68	1.65	6.33	3.36	1.54	1.89	5.76	3.89	2.04	2.04	2.53	4.77	4.21	4.21	3.33	4.62
			A27-17	1.67	1.40	5.76	2.95	1.54	1.71	5.50	3.70	1.88	1.88	2.92	5.21	5.04	5.04	3.08	4.69
			A38-17	1.75	1.27	5.25	3.10	1.72	1.63	6.27	3.76	1.94	1.94	2.66	4.77	4.82	4.82	2.74	4.05
		East Mabruk	A84-17	2.82	1.50	5.59	3.00	1.52	1.61	5.37	3.36	1.89	1.89	2.78	4.78	3.85	3.85	3.57	4.02
			A101-17	2.83	1.60	5.86	3.16	1.54	1.50	4.68	3.31	1.99	1.99	2.82	4.87	4.02	4.02	3.83	4.17
			A103-17	2.90	1.56	5.56	3.27	1.70	1.89	6.30	3.94	2.43	2.43	3.73	5.85	6.03	6.03	4.05	4.64
			A58-17	3.08	1.74	6.30	3.43	1.76	1.90	5.42	3.96	2.33	2.33	3.67	6.01	4.94	4.94	4.26	4.70
			A3-17	3.13	1.72	6.30	3.39	1.73	1.76	5.19	3.88	2.19	2.19	3.26	5.33	4.28	4.28	3.88	4.59
			A7-17	2.79	1.52	5.59	3.08	1.59	1.59	5.23	3.30	2.03	2.03	2.77	5.10	4.03	4.03	3.73	4.04
			A97-17	1.85	1.33	4.97	2.47	1.00	1.16	5.30	3.11	1.35	1.35	3.55	3.55	2.56	2.56	1.49	3.24
		Hakim	A1-NC74A	1.25	0.66	1.58	0.72	0.36	0.39	1.36	1.08	0.40	0.40	0.67	1.29	1.14	1.14	0.63	0.93
			A2-NC74A	0.87	0.45	1.07	0.46	0.25	0.29	1.10	0.57	0.33	0.33	0.68	0.91	0.96	0.96	0.76	0.71
		Fidda	B1-NC74A	2.25	1.33	3.47	1.61	0.81	0.89	3.72	2.45	1.07	1.07	1.60	2.79	2.50	2.50	2.07	2.91
			B2-NC74A	2.29	1.33	3.59	1.83	0.83	1.01	3.36	2.24	1.13	1.13	1.41	2.81	2.65	2.65	1.80	2.68
		Beda	B1-47	3.03	1.83	3.35	1.81	0.81	0.97	2.66	1.95	1.28	1.28	2.12	3.23	2.99	2.99	3.43	2.12
			B1-47	3.21	1.74	3.35	1.67	0.84	0.98	3.04	2.27	1.39	1.39	2.21	3.17	2.94	2.94	4.21	1.76
Centre		E. Meghile	J3-6	2.94	1.74	4.87	2.28	1.13	1.26	3.45	2.38	1.50	1.50	2.78	4.10	3.51	3.51	3.80	3.28

DC: diasterane; C: sterane

Appendix II Cont. Table 5.1: Steranes biomarker concentrations (µg/mg oil) of the oil families in the Sirt Basin.

Location	Family	Oil Filed	Well Name	C_{21}	C_{22}	DC_{27} βα20S	DC_{27} βα20R	DC_{27} αβ20S	DC_{27} αβ20R	DC_{28}S βα24S+R	DC_{28}R βα24S+R	C_{27} ααα20S	DC_{28} αβ20S	C_{27} αββ20R	DC_{29} βα20S	C_{27} αββ20S	DC_{28} αβ20R	C_{27} ααα20R	DC_{29} βα20R
Centre Sirt Basin	1B	Nasser	C98-6	2.81	1.61	4.51	2.78	1.19	1.24	3.38	2.26	1.16	1.16	3.26	3.55	2.96	2.96	2.56	2.66
			C98-6	2.81	1.61	4.56	2.16	1.08	1.28	1.99	2.39	1.31	1.31	2.04	3.58	2.95	2.95	2.54	2.52
		Raiah	DD12-6	2.44	1.88	3.47	1.83	0.90	1.04	3.07	1.59	1.39	1.39	2.33	3.46	3.22	3.22	3.87	2.56
		S. Jebel	4B1-6	4.15	2.43	5.17	2.61	1.20	1.35	4.02	2.57	1.50	1.50	2.36	4.44	4.08	4.08	2.57	4.07
		Zelten	4G1-6	2.45	1.65	4.81	2.46	1.17	1.39	3.69	2.57	1.38	1.38	2.67	4.11	3.38	3.38	3.13	2.98
		Ragoba	E9-20	1.74	0.94	2.43	1.10	0.53	0.68	2.14	1.70	0.73	0.73	1.10	1.87	1.54	1.54	1.62	1.33
			E82-20	1.79	0.89	2.49	1.15	0.56	0.67	1.98	1.34	0.82	0.82	1.01	1.80	1.65	1.65	1.35	1.82
		Sabah	G3-NC74F	2.34	1.23	2.81	1.42	0.70	0.72	2.78	1.78	1.18	1.18	1.17	2.36	2.10	2.10	1.90	2.11
W. Basin		W. Meghil	4J2-6	2.37	1.26	3.15	1.52	0.68	0.84	2.34	1.68	0.79	0.79	1.50	2.34	1.86	1.86	1.79	1.84
Centre Sirt B	2	Kotla	C46-47	3.31	2.12	3.37	1.91	0.91	1.30	2.70	2.26	1.87	1.87	4.84	4.67	4.45	4.45	8.60	2.66
	3	Dor	Z3-47	2.85	1.53	3.60	1.77	0.86	0.94	2.48	2.08	1.60	1.60	3.16	5.89	4.21	4.21	3.98	4.05
		Mansour	Z5-47	2.76	1.58	3.72	1.78	0.85	0.98	2.51	2.01	1.42	1.42	3.01	5.82	3.64	3.64	3.44	3.63
			GG1-47	1.88	1.09	2.80	1.25	0.66	0.68	1.95	1.34	0.88	0.88	1.84	3.62	2.48	2.48	2.32	2.55
West Sirt Basin	4	Aswad	B18-NC74E	2.04	1.44	1.61	0.79	0.45	0.47	1.34	0.90	0.77	0.77	1.40	2.28	1.42	1.42	2.26	1.39
			B18-NC74E	1.99	1.36	1.46	0.87	0.45	0.41	1.26	0.79	0.69	0.69	1.52	2.42	1.51	1.51	2.08	1.28
		Safsaf South	D6-NC74B	1.11	0.50	1.23	0.57	0.30	0.29	0.90	0.60	0.33	0.33	0.61	1.33	0.83	0.83	0.78	0.86
		Zella	A5-NC74B	1.55	0.77	2.12	1.00	0.58	0.65	1.56	1.11	0.61	0.61	1.15	2.16	1.07	1.07	1.59	1.49
			A5-NC74B	1.58	0.75	2.08	1.01	0.56	0.54	1.48	1.10	0.62	0.62	1.05	2.06	1.03	1.03	1.20	1.63
			A28-NC74E	1.16	0.61	1.55	0.73	0.45	0.43	1.09	0.80	0.43	0.43	0.78	1.48	0.69	0.69	0.86	1.18
		Safsaf	C1-NC74B	0.82	0.42	1.00	0.46	0.16	0.18	1.04	1.07	0.32	0.32	0.91	0.91	0.44	0.44	0.44	0.69
East Sirt Basin	5	As Sarah	B42-96	0.01	0.01	0.30	0.12	0.02	0.09	0.24	0.17	0.12	0.12	0.17	0.17	0.08	0.08	0.15	0.17
	6	Augla	G31-51	0.80	0.47	1.43	0.58	0.40	0.53	1.12	0.80	0.45	0.45	0.68	1.14	0.90	0.90	0.98	1.09
		Nafoora	G274-51	0.85	0.46	1.06	0.48	0.28	0.26	0.98	0.77	0.40	0.40	0.63	1.00	0.77	0.77	0.98	0.89
	7	NC125	N1-125	0.01	0.00	0.15	0.05	0.04	0.04	0.08	0.06	0.09	0.09	0.10	0.10	0.05	0.05	0.12	0.06
			A1-125	0.01	0.00	0.13	0.04	0.03	0.04	0.07	0.07	0.07	0.07	0.08	0.08	0.06	0.06	0.13	0.07
	8	Tuamma	C7-97	0.00	0.00	0.01	0.00	0.00	0.00	0.00	0.00	0.00	0.00	0.01	0.00	0.00	0.00	0.01	0.00
	9	Nakhla	G7-97	0.01	0.00	0.17	0.04	0.03	0.03	0.06	0.06	0.06	0.06	0.12	0.12	0.07	0.07	0.09	0.08
North Sea Oil		VFO		1.30	0.88	3.46	1.73	0.79	0.87	2.18	1.56	0.80	0.80	0.68	2.53	1.31	1.31	0.72	2.10

Appendix II Cont. Table 5.1: Steranes biomarker concentrations (µg/mg oil) of the oil families in the Sirt Basin.

Location	Family	Oil Filed	Well Name	DC_{30} βα20S	C_{28} ααα20S	C_{28} αββ20R	DC_{29} αβ20S	C_{28} αββ20S	DC_{30} βα20R	DC_{29} αβ20R	C_{28} ααα20R	C_{29} ααα20S	C_{29} αββ20R	C_{29} αββ20S	C_{29} ααα20R	C_{30} αββ20R	C_{30} αββ20S	C30 ααα20R
West Sirt Basin	1A	West Mabruk	A31-17	1.02	0.67	4.33	4.33	3.85	2.04	2.04	3.40	3.61	4.31	2.53	3.47	1.47	0.69	0.96
			A29-17	0.93	1.69	6.22	6.22	5.28	1.89	1.89	5.35	4.45	5.52	3.05	5.42	2.36	0.93	1.45
			A86-17	0.66	1.76	4.30	4.30	3.78	1.43	1.43	4.00	4.20	5.13	2.74	3.85	1.82	0.74	0.97
			A44-17	0.66	1.33	4.42	4.42	3.80	1.41	1.41	3.67	3.29	3.79	3.13	3.80	1.58	0.68	0.90
			A66-17	0.60	1.07	3.91	3.91	3.42	1.34	1.34	3.35	3.51	3.86	3.01	3.38	1.54	0.63	0.96
			A15-17	0.77	0.60	4.21	4.21	3.79	1.42	1.42	3.56	3.30	4.27	2.37	3.83	2.43	0.61	0.92
			M1-17	0.66	0.97	3.95	3.95	3.84	1.47	1.47	3.80	3.29	4.34	2.28	3.88	1.60	0.75	1.04
			A46-17	0.70	0.77	4.79	4.79	4.23	1.54	1.54	4.48	4.13	4.37	3.67	4.33	1.73	0.77	0.97
			A82-17	0.38	0.65	1.96	1.96	1.80	0.74	0.74	1.46	1.28	1.77	1.37	1.39	0.75	0.27	0.37
			A94-17	0.73	0.94	2.96	2.96	2.62	1.61	1.61	1.99	1.99	2.40	2.31	2.11	0.85	0.62	0.64
			A39-17	0.62	0.88	3.82	3.82	3.32	1.34	1.34	3.03	2.83	3.39	2.61	3.23	1.05	0.92	0.99
			A27-17	0.86	1.09	3.57	3.57	3.18	1.97	1.97	2.60	2.61	2.93	2.29	2.65	1.31	0.46	0.71
			A38-17	0.74	0.93	2.99	2.99	2.61	1.44	1.44	1.87	1.84	2.25	1.66	1.96	1.01	0.41	0.60
		East Mabruk	A84-17	0.53	1.21	2.58	2.58	2.57	1.22	1.22	3.02	2.73	3.34	2.48	3.05	2.08	0.39	0.79
			A101-17	0.60	1.31	2.56	2.56	2.79	1.17	1.17	3.21	2.97	3.63	3.25	3.41	1.30	0.90	0.89
			A103-17	1.12	1.00	3.96	3.96	4.15	1.89	1.89	3.05	3.38	3.70	2.77	3.23	1.52	0.44	0.78
			A58-17	0.80	0.97	4.37	4.37	3.87	1.40	1.40	3.61	3.24	4.12	2.23	3.84	1.81	0.72	0.98
			A3-17	0.65	0.66	2.65	2.65	2.94	1.24	1.24	3.28	2.91	3.64	3.32	3.46	1.75	0.63	0.82
			A7-17	0.70	0.28	2.61	2.61	2.43	1.31	1.31	3.08	2.68	3.43	2.41	3.29	1.30	0.86	0.80
			A97-17	0.32	1.20	1.38	1.16	1.61	0.68	0.68	1.28	0.94	1.58	1.02	1.29	0.94	0.09	0.35
		Hakim	A1-NC74A	0.11	0.24	0.66	0.66	0.73	0.32	0.32	0.49	0.54	0.63	0.44	0.54	0.25	0.06	0.14
			A2-NC74A	0.15	0.21	0.57	0.57	0.61	0.38	0.38	0.44	0.49	0.50	0.40	0.55	0.23	0.09	0.14
		Fidda	B1-NC74A	0.55	0.36	2.51	2.51	2.31	1.06	1.06	1.59	1.66	1.88	2.00	1.72	0.87	0.36	0.41
			B2-NC74A	0.33	0.32	2.41	2.41	2.33	0.81	0.81	1.79	1.79	2.12	1.70	2.01	0.97	0.37	0.53
		Beda	B1-47	0.41	0.28	3.11	3.11	2.83	1.08	1.08	2.82	2.82	3.52	2.09	3.04	1.82	0.46	0.85
			B1-47	0.41	0.33	3.07	3.07	2.78	0.98	0.98	2.84	2.73	3.11	2.46	2.92	1.28	0.52	0.88
Centre		E. Meghile	J3-6	0.59	0.43	3.31	3.31	3.12	1.20	1.20	3.04	3.97	4.44	2.78	3.70	1.36	0.77	0.93

Appendix II Cont. Table 5.1: Steranes biomarker concentrations (µg/mg oil) of the oil families in the Sirt Basin.

Location	Family	Oil Filed	Well Name	DC_{30} βα20S	C_{28} ααα20S	C_{28} αββ20R	DC_{29} αβ20S	C_{28} αββ20S	DC_{30} βα20R	DC_{29} αβ20R	C_{28} ααα20R	C_{29} ααα20S	C_{29} αββ20R	C_{29} αββ20S	C_{29} ααα20R	C_{30} αββ20R	C_{30} αββ20S	C30 ααα20R
Centre Sirt Basin	1B	Nasser	C98-6	0.43	0.52	2.29	2.29	2.20	0.95	0.95	1.60	1.79	2.44	1.29	1.85	1.43	0.36	0.39
			C98-6	0.45	0.52	2.22	2.22	2.18	0.81	0.81	1.73	1.88	2.18	1.60	1.94	0.99	0.48	0.58
		Raiah	DD12-6	0.43	1.35	3.25	3.25	3.07	1.20	1.20	3.26	3.04	3.82	2.05	3.56	2.14	0.57	1.00
		S. Jebel	4B1-6	0.60	0.48	3.65	3.65	3.50	2.27	2.27	2.38	2.86	3.86	2.35	2.61	2.17	0.53	0.87
		Zelten	4G1-6	0.67	0.70	2.56	2.56	2.63	1.09	1.09	2.27	2.34	3.07	1.70	2.54	1.82	0.50	0.75
		Ragoba	E9-20	0.25	0.30	1.38	1.38	1.26	0.52	0.52	0.98	1.19	1.25	0.86	1.15	0.59	0.24	0.32
			E82-20	0.25	0.20	1.50	1.50	1.41	0.58	0.58	1.22	1.21	1.35	1.02	1.24	0.57	0.24	0.34
		Sabah	G3-NC74F	0.28	0.30	2.07	2.07	2.03	0.90	0.90	1.40	1.48	1.87	1.01	1.75	1.01	0.16	0.37
W. Basin		W. Meghil	4J2-6	0.24	0.33	1.48	1.48	1.54	0.65	0.65	1.26	1.36	1.78	0.87	1.42	0.76	0.28	0.33
Centre Sirt B	2	Kotla	C46-47	0.83	2.07	5.29	5.29	4.54	0.99	0.99	4.78	3.99	3.71	3.50	4.64	2.15	1.14	1.80
	3	Dor	Z3-47	0.88	1.58	3.33	3.33	3.70	2.71	2.71	3.01	5.05	5.43	2.90	4.70	1.37	0.46	0.78
		Mansour	Z5-47	0.57	1.06	2.58	2.58	2.90	1.63	1.63	2.79	4.90	5.36	2.74	4.51	1.11	0.58	0.80
			GG1-47	0.42	0.80	1.87	1.87	2.02	1.67	1.67	1.69	1.97	2.62	1.34	2.09	0.71	0.32	0.47
West Sirt Basin	4	Aswad	B18-NC74B	0.42	0.45	1.89	1.89	1.48	2.41	2.41	1.45	2.87	3.16	2.90	3.54	0.68	0.42	0.42
			B18-NC74B	0.35	0.17	1.14	1.14	0.75	0.47	0.47	1.31	3.02	3.19	2.65	3.24	0.61	0.41	0.33
		Safsaf South	D6-NC74B	0.19	0.31	0.51	0.51	0.57	0.57	0.57	0.37	0.90	0.82	0.71	0.77	0.18	0.09	0.07
		Zella	A5-NC74B	0.26	0.53	0.87	0.87	0.96	0.92	0.92	0.84	1.40	1.57	0.67	1.85	0.34	0.30	0.23
			A5-NC74B	0.22	0.50	0.78	0.78	0.89	1.07	1.07	0.85	1.38	1.37	0.82	1.91	0.38	0.12	0.29
			A28-NC74B	0.12	0.38	0.56	0.56	0.67	0.77	0.77	0.59	1.02	0.91	0.67	1.18	0.20	0.16	0.19
		Safsaf	C1-NC74B	0.07	0.31	0.26	0.24	0.28	0.31	0.31	0.34	0.64	0.69	0.36	0.56	0.14	0.06	0.07
East Sirt Basin	5	As Sarah	B42-96	0.03	0.11	0.06	0.06	0.06	0.05	0.05	0.06	0.16	0.11	0.05	0.06	0.13	0.04	0.02
	6	Augla	G31-51	0.14	0.74	0.79	0.79	0.85	0.31	0.31	0.89	1.18	0.94	0.65	0.90	0.45	0.12	0.17
		Nafoora	G274-51	0.14	0.87	0.84	0.84	0.90	0.63	0.63	0.94	1.05	0.86	0.59	0.95	0.47	0.12	0.12
	7	NC125	N1-125	0.08	0.08	0.02	0.02	0.02	0.01	0.01	0.03	0.10	0.03	0.03	0.01	0.06	0.05	0.06
			A1-125	0.06	0.07	0.02	0.01	0.02	0.01	0.01	0.01	0.07	0.04	0.02	0.02	0.05	0.04	0.06
	8	Tuamma	C7-97	0.00	0.00	0.00	0.00	0.00	0.00	0.00	0.00	0.00	0.01	0.00	0.00	0.00	0.00	0.00
	9	Nakhla	G7-97	0.10	0.09	0.01	0.02	0.03	0.05	0.05	0.01	0.10	0.07	0.05	0.04	0.09	0.09	0.04
North Sea Oil		VFO		0.23	0.68	0.84	0.84	1.09	1.01	1.01	0.62	0.78	1.18	0.59	0.76	0.56	0.09	0.20

Appendix II Cont. Table 5.1: Hopane biomarker concentrations (µg/mg oil) of the oil families in the Sirt Basin.

Location	Family	Oil Filed	Well Name	C_{27}Ts	C_{27}Tm	C_{28}-αββ-bnh	C_{29}-nor25h	C_{29}Tm	C_{29}Ts	C_{30}dh	C_{29}-norMor	C_{30}αβ	C_{30}-Mor	C_{31} αβS	C_{31} αβR
West Sirt Basin	1A	West Mabruk	A31-17	3.12	3.57	0.98	0.31	7.99	3.65	1.22	0.67	18.51	1.99	6.74	4.88
			A29-17	4.94	4.09	1.56	0.46	13.07	5.13	1.91	0.98	27.46	2.68	10.23	7.17
			A86-17	3.51	2.77	1.04	0.36	9.12	3.73	1.29	0.71	20.28	1.94	7.20	5.23
			A44-17	3.42	2.66	1.02	0.31	8.96	3.66	1.30	0.75	19.60	1.91	7.01	5.10
			A66-17	3.23	2.61	0.99	0.33	8.10	3.45	1.29	0.61	17.79	1.77	6.58	4.50
			A15-17	3.53	2.67	1.54	0.31	8.93	4.02	1.27	0.63	20.15	2.06	7.17	5.11
			M1-17	4.15	3.12	1.13	0.44	9.38	4.33	1.52	0.65	20.90	2.02	7.27	5.12
			A46-17	3.87	2.93	1.01	0.22	9.72	4.17	1.44	0.70	21.28	2.03	7.25	4.64
			A82-17	1.92	1.45	0.54	0.14	3.39	1.97	1.31	0.39	7.43	0.98	2.75	2.00
			A94-17	2.34	1.74	0.59	0.16	4.74	2.38	1.19	0.49	11.27	1.22	4.02	2.80
			A39-17	3.24	2.47	0.94	0.29	7.45	3.30	1.41	0.73	16.69	1.74	6.07	4.24
			A27-17	2.54	1.82	1.11	0.21	5.84	2.90	1.47	0.59	13.06	1.41	4.40	3.13
			A38-17	2.36	1.77	0.63	0.18	4.52	2.19	1.20	0.48	10.43	1.07	3.64	2.55
		East Mabruk	A84-17	3.01	2.31	1.00	0.21	7.51	3.15	1.26	0.50	16.28	1.86	6.07	4.11
			A101-17	3.22	2.76	0.96	0.23	8.15	3.18	1.27	0.53	17.92	1.71	6.52	4.57
			A103-17	3.09	2.19	0.98	0.15	7.83	3.10	1.42	0.59	16.37	1.66	6.28	4.49
			A58-17	3.82	2.94	1.09	0.29	9.18	3.73	1.67	0.79	20.48	2.15	7.76	5.28
			A3-17	3.38	2.19	0.98	0.33	8.47	3.51	1.64	0.62	18.30	1.82	6.80	4.66
			A7-17	3.26	2.29	0.98	0.21	7.86	3.05	1.32	0.45	17.20	1.92	6.16	4.41
			A97-17	2.36	1.08	0.75	0.30	2.39	1.39	1.10	0.42	7.31	0.93	2.26	1.64
		Hakim	A1-NC74A	1.15	0.84	0.33	0.26	2.14	0.80	0.46	0.20	4.71	0.54	1.58	1.18
			A2-NC74A	0.83	0.83	0.33	0.17	2.45	0.76	0.31	0.26	4.59	0.49	1.55	1.13
		Fidda	B1-NC74A	2.32	1.94	1.11	0.41	5.17	1.84	0.68	0.49	11.78	1.00	3.58	2.49
			B2-NC74A	2.64	2.68	0.91	0.39	6.79	2.24	0.77	0.41	14.51	1.10	5.09	3.47
		Beda	B1-47	2.57	2.13	1.63	0.63	7.54	2.54	0.88	0.66	15.68	1.51	4.55	3.32
			B1-47	2.64	1.87	1.63	0.59	7.80	2.28	0.88	0.82	15.32	1.47	4.34	3.22
Centre		E.Meghile	J3-6	3.13	4.95	1.66	0.64	11.85	2.37	1.29	0.88	21.57	2.23	7.34	5.40

Bnh: bisnorhopane; nor25h: trisnorhopane; Dh: diahopane; norMor: nor-Mortane; Mor: Mortane;

Appendix II Cont. Table 5.1: Hopane biomarker concentrations (µg/mg oil) of the oil families in the Sirt Basin.

Location	Family	Oil Filed	Well Name	C_{27}Ts	C_{27}Tm	C_{28}-αββ-bnh	C_{29}-nor25h	C_{29}Tm	C_{29}Ts	C_{30}dh	C_{29}-norMor	C_{30}αβ	C_{30}-Mor	C_{31} αβS	C_{31} αβR
Centre Sirt Basin	1B	Nasser	C98-6	2.67	1.60	0.80	0.46	4.98	2.48	1.25	0.44	11.48	1.18	3.58	2.67
			C98-6	2.83	1.31	0.71	0.29	5.06	2.32	1.23	0.34	11.49	1.29	3.73	2.80
		Raiah	DD12-6	2.69	2.56	1.30	0.64	8.54	2.47	0.83	1.02	17.82	1.75	5.21	3.76
		South Jebel	4B1-6	4.00	1.89	1.27	0.66	7.17	3.48	1.52	0.71	17.76	1.76	5.54	4.26
		Zelten	4G1-6	3.06	2.04	1.30	0.50	6.68	2.85	1.28	0.62	14.92	1.67	4.89	3.74
		Ragoba	E9-20	1.51	1.54	0.40	0.33	3.77	1.33	0.51	0.32	7.59	0.78	2.63	1.92
			E82-20	1.72	1.71	0.47	0.30	3.94	1.45	0.55	0.34	8.08	0.84	2.95	2.22
		Sabah	G3-NC74F	2.37	2.16	1.04	0.59	6.35	1.40	0.74	0.64	11.43	1.26	3.30	2.56
West		W. Meghil	4J2-6	2.15	1.28	0.55	0.53	3.42	1.72	0.76	0.29	6.88	0.60	2.53	1.93
Centre	2	Kotla	C46-47	2.53	4.26	1.13	0.20	11.59	1.55	0.92	1.70	24.85	2.68	9.01	6.29
	3	Dor Mansour	Z3-47	5.01	7.00	1.37	0.80	13.69	3.34	1.33	1.35	26.08	2.63	8.47	6.26
			Z5-47	4.96	7.03	1.57	0.84	13.16	3.17	1.18	1.31	25.45	2.53	8.26	5.97
			GG1-47	2.34	3.05	0.60	0.50	6.09	1.99	1.10	0.49	12.62	1.35	3.77	2.79
West Sirt Basin	4	Aswad	B18-NC74B	2.62	10.14	0.31	0.23	27.36	1.57	0.92	1.98	31.89	2.78	11.15	10.11
			B18-NC74B	2.43	9.40	0.21	0.21	24.88	2.40	0.54	1.90	30.03	2.45	10.50	8.71
		Safsaf South	D6-NC74B	1.68	2.92	0.35	0.14	6.40	1.50	0.46	0.35	9.89	0.85	4.21	3.16
		Zella	A5-NC74B	2.57	4.89	0.50	0.23	11.71	2.40	0.62	0.94	16.20	1.62	7.37	5.66
			A5-NC74B	2.57	4.98	0.34	0.24	12.07	2.52	0.69	1.04	16.28	1.53	7.41	5.55
			A28-NC74B	1.69	2.96	0.22	0.15	5.85	1.49	0.52	0.53	9.49	0.89	4.08	2.74
		Safsaf	C1-NC74B	1.39	2.44	0.26	0.17	5.25	1.32	0.38	0.50	8.22	0.64	3.57	2.37
East Sirt Basin	5	As Sarah	B42-96	1.00	0.90	0.06	0.03	0.14	0.12	0.17	0.04	0.32	0.07	0.08	0.07
	6	Augla	G31-51	2.57	2.83	0.72	0.45	7.01	2.69	2.39	0.85	12.38	1.86	3.03	2.32
		Nafoora	G274-51	2.76	2.68	0.72	0.53	7.31	4.34	2.80	1.24	13.38	2.37	3.25	2.44
	7	NC125	N1-125	0.83	0.43	0.04	0.02	0.08	0.11	0.14	0.01	0.12	0.06	0.04	0.02
			A1-125	0.79	0.46	0.03	0.01	0.05	0.08	0.11	0.01	0.09	0.04	0.02	0.02
	8	Tuamma	C7-97	0.17	0.11	0.02	0.01	0.02	0.02	0.04	0.01	0.02	0.02	0.01	0.01
	9	Nakhla	G7-97	1.02	0.35	0.03	0.02	0.11	0.11	0.09	0.01	0.15	0.05	0.04	0.03
North Sea Oil		VFO		1.26	0.41	0.31	0.24	1.20	0.89	0.83	0.28	2.91	0.38	1.28	1.12

Appendix II Cont. Table 5.1: Hopane biomarker and methydiamantane concentrations (µg/mg oil) of the oil families in the Sirt Basin.

Location	Family	Oil Filed	Well Name	C_{32} αβS	C_{32} αβR	C_{33} αβS	C_{33} αβR	C_{34} αβS	C_{34} αβR	C_{35} αβS	C_{35} αβR	4-mdiam	1-mdiam	3-mdiam	diam
West Sirt Basin	1A	West Mabruk	A31-17	5.09	3.35	3.72	2.61	2.71	1.65	1.89	1.00	0.17	0.07	0.05	0.16
			A29-17	7.34	5.05	5.72	3.77	3.94	2.34	2.57	1.55	0.27	0.10	0.08	0.24
			A86-17	5.66	3.69	4.04	2.98	2.90	1.77	2.04	1.16	0.17	0.07	0.05	0.15
			A44-17	5.62	3.61	4.02	2.73	2.86	1.74	2.13	1.43	0.17	0.07	0.05	0.15
			A66-17	5.05	3.19	3.58	2.55	2.61	1.54	1.77	0.85	0.17	0.07	0.05	0.15
			A15-17	5.48	3.51	4.13	2.82	2.79	1.59	1.89	0.90	0.20	0.08	0.06	0.18
			M1-17	5.70	3.79	3.90	2.64	2.92	1.65	2.05	1.09	0.25	0.10	0.08	0.21
			A46-17	5.58	3.51	4.26	2.88	2.75	1.58	1.47	0.66	0.18	0.07	0.05	0.16
			A82-17	2.35	1.57	1.41	1.03	1.32	0.70	0.72	0.49	0.20	0.09	0.07	0.19
			A94-17	3.13	2.12	2.32	1.53	1.72	0.91	1.03	0.70	0.18	0.08	0.06	0.17
			A39-17	4.70	3.11	3.72	2.19	2.51	1.48	1.51	0.95	0.19	0.08	0.06	0.17
			A27-17	3.55	2.36	2.68	1.76	2.02	1.13	1.41	0.99	0.20	0.09	0.06	0.19
			A38-17	3.01	2.12	2.27	1.51	1.51	0.98	1.00	0.74	0.19	0.08	0.06	0.17
		East Mabruk	A84-17	4.63	3.07	3.56	2.37	2.53	1.47	1.75	1.08	0.14	0.06	0.04	0.13
			A101-17	5.20	3.35	3.99	2.74	2.71	1.61	1.82	1.07	0.15	0.06	0.05	0.14
			A103-17	4.81	3.02	3.29	2.30	2.63	1.44	1.99	0.96	0.15	0.06	0.05	0.13
			A58-17	6.02	3.95	4.29	3.10	3.16	2.02	2.15	1.22	0.15	0.06	0.05	0.14
			A3-17	5.25	3.49	3.68	2.74	2.74	1.63	1.98	1.09	0.15	0.06	0.05	0.13
			A7-17	4.98	3.27	3.52	2.48	2.47	1.50	1.84	1.29	0.14	0.06	0.04	0.12
			A97-17	1.84	1.28	1.48	0.98	0.96	0.60	0.47	0.29	0.30	0.18	0.10	0.28
		Hakim	A1-NC74A	1.31	0.93	0.75	0.51	0.80	0.44	0.44	0.15	0.08	0.05	0.04	0.07
			A2-NC74A	1.47	1.07	0.96	0.69	2.00	1.25	0.54	0.36	0.03	0.02	0.02	0.03
		Fidda	B1-NC74A	2.98	1.94	2.34	1.47	2.32	1.29	1.03	0.81	0.04	0.03	0.02	0.04
			B2-NC74A	4.55	2.88	3.39	2.05	4.41	2.59	2.19	1.34	0.05	0.03	0.02	0.04
		Beda	B1-47	3.33	2.34	2.53	1.66	1.66	1.02	1.13	0.84	0.02	0.01	0.01	0.02
			B1-47	3.22	2.27	2.50	1.65	1.65	1.01	1.30	0.60	0.02	0.01	0.01	0.02
Centre		E.Meghile	J3-6	5.38	3.81	3.85	2.60	2.62	1.55	2.11	1.18	0.05	0.03	0.03	0.04

Appendix II Cont. Table 5.1: Hopane biomarker and methydiamantane concentrations (µg/mg oil) of the oil families in the Sirt Basin.

Location	Family	Oil Filed	Well Name	C_{32} αβS	C_{32} αβR	C_{33} αβS	C_{33} αβR	C_{34} αβS	C_{34} αβR	C_{35} αβS	C_{35} αβR	4-mdiam	1-mdiam	3-mdiam	diam
Centre Sirt Basin	1B	Nasser	C98-6	2.92	2.06	2.02	1.54	1.46	0.80	0.88	0.38	0.03	0.02	0.02	0.02
			C98-6	3.15	2.11	2.45	1.73	1.50	0.82	0.95	0.53	0.02	0.02	0.02	0.02
		Raiah	DD12-6	3.68	2.70	2.81	2.00	1.93	1.23	1.37	0.97	0.02	0.01	0.01	0.02
		South Jebel	4B1-6	4.94	3.47	3.95	2.78	2.19	1.35	1.30	0.58	0.01	0.01	0.01	0.01
		Zelten	4G1-6	4.16	2.85	3.22	2.12	2.00	1.22	1.31	1.00	0.02	0.02	0.02	0.02
		Ragoba	E9-20	2.01	1.29	1.19	0.91	0.89	0.52	0.57	0.43	0.03	0.03	0.03	0.03
			E82-20	2.10	1.48	1.43	1.00	0.93	0.66	0.57	0.38	0.03	0.03	0.03	0.03
		Sabah	G3-NC74F	2.43	1.81	1.77	1.23	1.40	0.95	0.84	0.32	0.05	0.03	0.03	0.05
West		West Meghi	4J2-6	2.09	1.49	1.28	1.17	0.92	0.63	0.82	0.39	0.06	0.04	0.03	0.06
Centre	2	Kotla	C46-47	5.83	4.05	4.58	3.17	3.11	2.01	2.47	1.61	0.01	0.01	0.00	0.01
	3	Dor	Z3-47	7.78	5.57	4.54	2.97	3.98	2.37	3.54	1.76	0.15	0.08	0.04	0.15
		Mansour	Z5-47	7.53	5.33	4.32	2.91	3.75	2.25	2.90	1.73	0.15	0.08	0.04	0.15
			GG1-47	2.94	2.10	1.94	1.33	1.59	0.88	1.01	0.67	0.20	0.10	0.06	0.18
West Sirt Basin	4	Aswad	B18-NC74B	12.89	8.34	6.15	3.95	11.01	7.00	7.90	4.78	0.12	0.08	0.06	0.10
			B18-NC74B	11.95	7.61	5.65	3.65	10.55	6.22	7.23	4.38	0.11	0.08	0.06	0.11
		Safsaf South	D6-NC74B	3.89	2.62	2.46	1.52	4.28	2.65	1.98	1.13	0.15	0.10	0.08	0.14
		Zella	A5-NC74B	6.62	4.65	4.38	2.81	7.47	4.87	4.25	2.56	0.16	0.11	0.09	0.15
			A5-NC74B	6.81	4.56	4.41	3.03	7.67	4.86	4.72	2.66	0.16	0.10	0.08	0.14
			A28-NC74B	3.74	2.81	2.49	1.67	4.48	2.85	2.16	1.12	0.21	0.14	0.11	0.19
		Safsaf	C1-NC74B	3.22	2.18	2.09	1.42	3.74	2.27	1.79	1.06	0.12	0.07	0.06	0.10
East Sirt Basin	5	As Sarah	B42-96	0.08	0.05	0.04	0.03	0.03	0.01	0.02	0.02	0.09	0.07	0.07	0.05
	6	Augla	G31-51	2.29	1.60	1.48	1.03	1.03	0.47	0.42	0.24	0.01	0.01	0.01	0.01
		Nafoora	G274-51	2.50	1.72	1.48	1.06	1.05	0.58	0.48	0.31	0.01	0.01	0.01	0.01
	7	NC125	N1-125	0.03	0.02	0.02	0.01	0.01	0.01	0.00	0.00	0.04	0.03	0.03	0.03
			A1-125	0.02	0.01	0.01	0.01	0.01	0.00	0.01	0.00	0.03	0.03	0.02	0.02
	8	Tuamma	C7-97	0.01	0.01	0.01	0.01	0.01	0.00	0.00	0.00	0.05	0.04	0.03	0.03
	9	Nakhla	G7-97	0.04	0.03	0.02	0.01	0.02	0.01	0.01	0.01	0.37	0.26	0.21	0.31
North Sea Oil		VFO		1.19	0.90	0.87	0.60	0.59	0.48	0.62	0.52	0.01	0.01	0.01	0.01

Appendix II Cont. Table 5.1: Tricyclic and tetracyclic terpanes biomarker concentrations (µg/mg oil) of the oil families in the Sirt Basin.

Location	Family	Oil Filed	Well Name	C_{19} Tri	C_{20} Tri	C_{21} Tri	C_{22} Tri	C_{23} Tri	C_{24} Tri	C_{25} Tri A	C_{25} Tri B	C_{24} tetr	C_{26} Tri A	C_{26} Tri B	C_{28} Tri A	C_{28} Tri B	C_{29} Tri A	C_{29} Tri B	C_{30} Tri A	C_{30} Tri B
West Sirt Basin	1A	West Mabruk	A31-17	0.03	0.07	0.15	0.04	0.30	0.16	0.10	0.09	0.01	0.14	0.08	0.10	0.10	0.08	0.08	0.05	0.04
			A29-17	0.06	0.11	0.27	0.08	0.53	0.29	0.20	0.11	0.01	0.23	0.13	0.17	0.16	0.14	0.14	0.07	0.05
			A86-17	0.03	0.07	0.17	0.05	0.33	0.18	0.12	0.08	0.01	0.16	0.09	0.12	0.12	0.09	0.09	0.06	0.04
			A44-17	0.02	0.07	0.17	0.05	0.33	0.18	0.12	0.08	0.01	0.15	0.09	0.11	0.11	0.08	0.08	0.06	0.04
			A66-17	0.03	0.07	0.17	0.05	0.31	0.17	0.12	0.07	0.01	0.14	0.08	0.11	0.11	0.08	0.08	0.06	0.03
			A15-17	0.04	0.09	0.19	0.05	0.36	0.20	0.12	0.10	0.01	0.17	0.10	0.11	0.12	0.08	0.08	0.06	0.04
			M1-17	0.04	0.09	0.20	0.06	0.37	0.22	0.11	0.09	0.01	0.19	0.10	0.11	0.11	0.09	0.09	0.07	0.05
			A46-17	0.03	0.09	0.20	0.06	0.39	0.21	0.13	0.09	0.01	0.17	0.10	0.13	0.13	0.10	0.10	0.07	0.05
			A82-17	0.03	0.05	0.13	0.04	0.19	0.13	0.04	0.08	0.01	0.09	0.05	0.07	0.08	0.07	0.07	0.04	0.02
			A94-17	0.02	0.05	0.13	0.04	0.26	0.14	0.08	0.05	0.01	0.11	0.06	0.09	0.09	0.07	0.07	0.05	0.02
			A39-17	0.03	0.07	0.17	0.05	0.32	0.18	0.11	0.08	0.01	0.15	0.08	0.11	0.11	0.09	0.09	0.07	0.03
			A27-17	0.02	0.05	0.13	0.04	0.26	0.14	0.09	0.06	0.01	0.12	0.07	0.10	0.10	0.07	0.07	0.05	0.02
			A38-17	0.02	0.05	0.14	0.04	0.24	0.14	0.08	0.05	0.01	0.11	0.06	0.08	0.07	0.07	0.07	0.05	0.02
		East Mabruk	A84-17	0.02	0.07	0.16	0.05	0.30	0.17	0.12	0.06	0.01	0.14	0.08	0.10	0.10	0.08	0.08	0.06	0.03
			A101-17	0.03	0.07	0.16	0.05	0.31	0.17	0.13	0.06	0.01	0.15	0.08	0.11	0.11	0.08	0.08	0.06	0.03
			A103-17	0.02	0.07	0.16	0.05	0.30	0.17	0.13	0.06	0.01	0.14	0.09	0.10	0.10	0.08	0.08	0.04	0.04
			A58-17	0.03	0.07	0.18	0.05	0.33	0.19	0.14	0.07	0.01	0.16	0.09	0.12	0.12	0.10	0.10	0.06	0.03
			A3-17	0.03	0.08	0.17	0.06	0.33	0.18	0.14	0.06	0.01	0.15	0.08	0.11	0.11	0.09	0.09	0.05	0.05
			A7-17	0.03	0.07	0.17	0.05	0.31	0.17	0.08	0.10	0.01	0.15	0.08	0.10	0.11	0.08	0.08	0.05	0.04
			A97-17	0.03	0.07	0.14	0.05	0.25	0.16	0.07	0.08	0.01	0.11	0.08	0.09	0.10	0.09	0.09	0.04	0.02
		Hakim	A1-NC74A	0.03	0.04	0.08	0.03	0.12	0.10	0.04	0.03	0.00	0.07	0.04	0.04	0.04	0.03	0.03	0.02	0.01
			A2-NC74A	0.01	0.03	0.06	0.02	0.10	0.07	0.03	0.02	0.00	0.06	0.03	0.03	0.03	0.03	0.03	0.01	0.01
		Fidda	B1-NC74A	0.02	0.07	0.15	0.05	0.33	0.21	0.11	0.07	0.01	0.15	0.10	0.12	0.12	0.10	0.10	0.04	0.02
			B2-NC74A	0.02	0.07	0.15	0.05	0.33	0.21	0.12	0.08	0.01	0.16	0.10	0.12	0.12	0.10	0.10	0.04	0.02
		Beda	B1-47	0.02	0.10	0.19	0.06	0.39	0.28	0.15	0.12	0.01	0.18	0.13	0.15	0.15	0.12	0.12	0.04	0.03
			B1-47	0.02	0.11	0.19	0.07	0.38	0.28	0.17	0.10	0.01	0.17	0.12	0.15	0.14	0.12	0.12	0.03	0.03
Centre		E. Meghile	J3-6	0.05	0.16	0.26	0.06	0.40	0.27	0.14	0.11	0.02	0.19	0.11	0.11	0.11	0.10	0.10	0.05	0.04

Tri: tricyclic terpane; tetr: tetracyclic terpane.

Appendix II Cont. Table 5.1: Tricyclic and tetracyclic terpanes biomarker concentrations (µg/mg oil) of the oil families in the Sirt Basin.

Location	Family	Oil Filed	Well Name	C_{19} Tri	C_{20} Tri	C_{21} Tri	C_{22} Tri	C_{23} Tri	C_{24} Tri	C_{25} Tri A	C_{25} Tri B	C_{24} tetr	C_{26} Tri A	C_{26} Tri B	C_{28} Tri A	C_{28} Tri B	C_{29} Tri A	C_{29} Tri B	C_{30} Tri A	C_{30} Tri B
Centre Sirt Basin	1B	Nasser	C98-6	0.04	0.10	0.20	0.06	0.31	0.22	0.10	0.09	0.01	0.14	0.09	0.10	0.10	0.09	0.09	0.05	0.04
			C98-6	0.04	0.10	0.19	0.06	0.30	0.21	0.12	0.08	0.01	0.14	0.09	0.10	0.10	0.09	0.09	0.04	0.03
		Raiah	DD12-6	0.03	0.12	0.16	0.06	0.41	0.29	0.17	0.11	0.02	0.18	0.13	0.15	0.16	0.15	0.15	0.04	0.02
		South Jebel	4B1-6	0.04	0.10	0.20	0.07	0.36	0.28	0.13	0.12	0.02	0.18	0.12	0.13	0.14	0.12	0.12	0.07	0.05
		Zelten	4G1-6	0.04	0.09	0.21	0.07	0.34	0.25	0.13	0.10	0.01	0.16	0.10	0.10	0.11	0.10	0.10	0.05	0.04
		Ragoba	E9-20	0.03	0.06	0.10	0.03	0.16	0.11	0.06	0.03	0.01	0.07	0.04	0.05	0.04	0.04	0.04	0.02	0.02
			E82-20	0.03	0.06	0.11	0.03	0.17	0.11	0.06	0.04	0.01	0.08	0.04	0.05	0.05	0.04	0.04	0.03	0.02
		Sabah	G3-NC74F	0.03	0.08	0.14	0.05	0.27	0.18	0.09	0.08	0.01	0.14	0.08	0.10	0.09	0.07	0.07	0.03	0.03
West		W. Meghil	4J2-6	0.04	0.08	0.17	0.05	0.25	0.17	0.07	0.06	0.01	0.12	0.07	0.07	0.07	0.06	0.06	0.03	0.03
Centre	2	Kotla	C46-47	0.02	0.18	0.28	0.09	0.56	0.38	0.24	0.16	0.02	0.23	0.16	0.19	0.19	0.18	0.18	0.02	0.02
	3	Dor Mansour	Z3-47	0.09	0.17	0.23	0.07	0.45	0.33	0.19	0.13	0.01	0.29	0.12	0.16	0.16	0.14	0.14	0.05	0.04
			Z5-47	0.09	0.18	0.24	0.07	0.46	0.32	0.18	0.12	0.02	0.32	0.13	0.17	0.16	0.13	0.13	0.05	0.04
			GG1-47	0.10	0.10	0.13	0.04	0.24	0.17	0.09	0.07	0.01	0.15	0.07	0.08	0.08	0.07	0.07	0.03	0.03
West Sirt Basin	4	Aswad	B18-NC74B	0.04	0.05	0.06	0.03	0.13	0.08	0.03	0.02	0.01	0.24	0.02	0.03	0.02	0.02	0.02	0.03	0.02
			B18-NC74B	0.04	0.05	0.06	0.03	0.13	0.08	0.03	0.02	0.01	0.24	0.02	0.03	0.03	0.02	0.02	0.03	0.02
		Safsaf South	D6-NC74B	0.05	0.04	0.05	0.02	0.09	0.07	0.03	0.02	0.01	0.11	0.02	0.03	0.02	0.02	0.02	0.02	0.01
		Zella	A5-NC74B	0.04	0.05	0.08	0.03	0.16	0.11	0.04	0.03	0.01	0.18	0.04	0.05	0.04	0.03	0.03	0.03	0.02
			A5-NC74B	0.04	0.05	0.08	0.03	0.15	0.10	0.04	0.03	0.00	0.16	0.03	0.04	0.04	0.03	0.03	0.03	0.03
			A28-NC74B	0.04	0.04	0.06	0.02	0.10	0.08	0.03	0.02	0.00	0.11	0.03	0.03	0.03	0.02	0.02	0.01	0.01
		Safsaf	C1-NC74B	0.03	0.04	0.05	0.02	0.07	0.06	0.02	0.02	0.00	0.09	0.02	0.02	0.02	0.02	0.02	0.01	0.01
East Sirt Basin	5	As Sarah	B42-96	0.04	0.08	0.17	0.04	0.15	0.11	0.03	0.03	0.01	0.09	0.05	0.04	0.04	0.04	0.04	0.06	0.02
	6	Augla	G31-51	0.04	0.11	0.20	0.05	0.22	0.14	0.05	0.06	0.01	0.14	0.08	0.06	0.06	0.05	0.05	0.09	0.02
		Nafoora	G274-51	0.05	0.12	0.22	0.05	0.25	0.16	0.06	0.06	0.01	0.13	0.07	0.06	0.06	0.05	0.05	0.10	0.02
	7	NC125	N1-125	0.05	0.08	0.13	0.03	0.08	0.06	0.02	0.02	0.00	0.05	0.03	0.02	0.02	0.02	0.02	0.04	0.01
			A1-125	0.05	0.08	0.12	0.02	0.09	0.06	0.02	0.01	0.01	0.05	0.04	0.02	0.02	0.02	0.02	0.03	0.01
	8	Tuamma	C7-97	0.03	0.03	0.05	0.01	0.04	0.03	0.01	0.01	0.01	0.02	0.01	0.01	0.01	0.01	0.01	0.01	0.01
	9	Nakhla	G7-97	0.04	0.08	0.14	0.03	0.10	0.07	0.02	0.02	0.01	0.06	0.03	0.03	0.03	0.02	0.02	0.04	0.01
North Sea Oil		VFO		0.04	0.04	0.06	0.02	0.06	0.06	0.03	0.02	0.00	0.06	0.02	0.02	0.02	0.02	0.02	0.04	0.01

Appendix II Table 5.2: Source facies biomarker ratios of the oil families in the Sirt basin.

Location	Oil Famiy	Oil Filed	Well Name	C27 ααα R%	C28 ααα R%	C29 ααα R%	A	B	C	D	E	F	G	H	I	J	K	L	M	N
West Sirt Basin	1A	West Mabruk	A31-17	40	30	30	1.22	0.22	0.98	0.54	0.37	0.34	0.43	0.47	0.26	0.66	9	0.04	1.70	1.19
			A29-17	36	32	32	1.13	0.26	0.99	0.68	0.26	0.31	0.48	0.55	0.26	0.66	8	0.04	1.82	1.18
			A86-17	39	31	30	1.27	0.22	1.04	0.56	0.27	0.35	0.45	0.56	0.26	0.69	9	0.05	1.75	1.24
			A44-17	40	29	31	1.17	0.23	0.96	0.61	0.27	0.33	0.46	0.56	0.26	0.77	10	0.05	1.61	1.19
			A66-17	39	30	30	1.20	0.23	0.99	0.65	0.28	0.35	0.46	0.55	0.25	0.63	8	0.05	1.73	1.20
			A15-17	39	29	32	1.16	0.29	0.93	0.61	0.27	0.32	0.44	0.57	0.25	0.63	8	0.05	1.64	1.22
			M1-17	39	30	31	1.09	0.25	0.98	0.60	0.27	0.31	0.45	0.57	0.24	0.69	9	0.03	1.42	1.42
			A46-17	35	33	32	1.19	0.21	1.04	0.69	0.26	0.35	0.46	0.57	0.22	0.49	6	0.05	1.66	1.18
			A82-17	38	31	30	1.35	0.24	1.04	0.85	0.35	0.35	0.46	0.57	0.27	0.60	8	0.04	2.16	1.21
			A94-17	38	30	32	1.29	0.24	0.94	0.81	0.43	0.35	0.42	0.57	0.25	0.66	9	0.03	1.91	1.27
			A39-17	35	32	34	1.15	0.25	0.94	0.80	0.29	0.33	0.45	0.57	0.25	0.62	8	0.05	1.72	1.20
			A27-17	37	31	32	1.39	0.24	0.98	0.67	0.43	0.36	0.45	0.58	0.24	0.76	10	0.04	1.97	1.26
			A38-17	42	28	30	1.42	0.26	0.96	0.69	0.42	0.34	0.43	0.57	0.24	0.70	9	0.06	1.80	1.29
		East Mabruk	A84-17	37	31	32	1.13	0.28	0.99	0.71	0.28	0.33	0.46	0.57	0.25	0.71	9	0.04	1.78	1.17
			A101-17	37	31	33	1.10	0.23	0.94	0.71	0.25	0.34	0.45	0.54	0.25	0.67	9	0.04	1.72	1.17
			A103-17	39	30	31	1.36	0.21	0.95	0.54	0.37	0.35	0.48	0.59	0.27	0.72	9	0.04	1.72	1.20
			A58-17	36	31	33	1.12	0.26	0.94	0.64	0.27	0.31	0.45	0.57	0.26	0.65	9	0.03	1.65	1.21
			A3-17	37	31	33	1.11	0.24	0.95	0.71	0.26	0.33	0.46	0.61	0.25	0.70	9	0.04	1.78	1.14
			A7-17	37	30	33	1.06	0.25	0.94	0.69	0.28	0.32	0.46	0.59	0.26	0.79	10	0.05	1.71	1.25
			A97-17	34	38	28	1.99	0.20	0.99	0.81	0.35	0.33	0.35	0.73	0.25	0.49	6	0.05	2.39	1.27
		Hakim	A1-NC74A	38	29	33	0.78	0.21	0.90	0.81	0.37	0.24	0.46	0.58	0.25	0.48	7	0.03	1.68	1.67
			A2-NC74A	44	25	32	0.74	0.23	0.79	0.56	0.41	0.22	0.53	0.41	0.25	0.28	8	0.05	1.91	1.58
		Fidda	B1-NC74A	38	30	32	0.99	0.23	0.92	0.70	0.38	0.30	0.44	0.55	0.21	0.51	9	0.03	2.56	1.31
			B2-NC74A	32	32	36	0.81	0.25	0.89	0.78	0.29	0.26	0.47	0.50	0.24	0.51	11	0.03	2.36	1.32
		Beda	B1-47	32	33	34	1.10	0.27	0.93	0.52	0.26	0.33	0.48	0.55	0.21	0.74	9	0.05	3.10	1.11
			B1-47	42	29	29	1.13	0.24	0.97	0.47	0.25	0.33	0.51	0.58	0.21	0.71	9	0.04	2.85	1.12
tre Sirt B		E. Meghil	J3-6	36	29	35	0.90	0.21	0.82	0.62	0.24	0.31	0.55	0.39	0.25	0.79	9	0.05	2.09	1.21

A: Regular Sterane/regular sterane+ regular hopane; B: C_{30} ααα 20R/C_{29} ααα 20R; C: C_{28}/C_{29} Sterane; D: C_{27} diasterane/C_{27}αββ-Sterane+C_{27}; E: C_{29} diasterane 20R/C_{29} diasterane 20R+C_{29} ααα 20R; F: C_{29} ααα 20(S+R)+C_{29} αββ 20(S+R)/ C_{29} ααα 20(S+R)+C_{29} αββ 20(S+R)+C_{29} αβ(H)-hopane+C_{30} αβ(H)-hopane; G:C_{29} αβ(H)-hopane/C_{30} αβ(H)-hopane; H: C_{27} Ts/(Ts+Tm); I: C_{31} R αβ(H)-homohopane/ C_{30} αβ(H)-hopane; J: C_{35} αβ (H)-homohopane/ C_{34} αβ (H)-homohopane; K: Homohopane index=C_{35} αβ (S+R)-homohopane/C_{31} – C_{35} αβ (S+R)-homohopane; L: C_{24} Tetracyclic/ C_{26} Tricyclic terpanes; M: C_{28}+C_{29} tricyclic terpane/ C_{29} Ts; N: C_{26}/C_{25} Tricyclic terpanes.

Appendix II Cont. Table 5.2: Source facies biomarker ratios of the oil families in the Sirt basin.

Location	Oil Famiy	Oil Filed	Well Name	C27 ααα R%	C28 ααα R%	C29 αααR%	A	B	C	D	E	F	G	H	I	J	K	L	M	N
Centre Sirt Basin	1B	Nasser	C98-6	43	27	31	1.12	0.30	0.87	0.73	0.34	0.31	0.43	0.62	0.23	0.56	7	0.05	2.03	1.16
			C98-6	41	28	31	1.09	0.27	0.89	0.76	0.30	0.31	0.44	0.68	0.24	0.64	7	0.04	1.99	1.15
		Raiah	DD12-6	36	30	33	1.11	0.30	0.91	0.49	0.25	0.32	0.48	0.51	0.21	0.74	9	0.06	3.34	1.13
		S. Jebel	4B1-6	34	31	35	1.04	0.31	0.91	0.74	0.46	0.32	0.40	0.68	0.24	0.53	6	0.05	1.81	1.18
		Ragoba	E9-20	39	29	31	0.92	0.26	0.85	0.69	0.31	0.28	0.45	0.60	0.25	0.72	9	0.09	1.64	1.23
			E82-20	43	26	33	0.90	0.24	0.98	0.71	0.32	0.29	0.50	0.50	0.28	0.71	8	0.07	1.48	1.23
		W. Megh	4J2-6	35	32	32	1.12	0.25	0.89	0.76	0.31	0.34	0.49	0.50	0.28	0.60	7	0.08	1.68	1.41
		Zelten	4G1-6	38	28	32	1.06	0.32	0.90	0.67	0.30	0.31	0.56	0.52	0.25	0.49	7	0.04	2.02	1.13
st Sirt Ba		Sabah	G3-NC74F	40	28	35	0.83	0.25	0.80	0.79	0.34	0.26	0.50	0.63	0.22	0.79	9	0.06	2.10	1.31
Centre Sirt	2	Kotla	C46-47	48	27	26	1.28	0.32	1.03	0.27	0.18	0.30	0.47	0.37	0.25	0.80	10	0.04	4.40	0.97
	3	Dor	Z3-47	34	26	40	0.82	0.14	0.64	0.41	0.37	0.31	0.52	0.42	0.24	0.84	11	0.03	1.78	1.27
		Mansour	Z5-47	32	26	42	0.76	0.14	0.62	0.48	0.27	0.31	0.52	0.41	0.23	0.77	10	0.04	1.74	1.46
			GG1-47	38	28	34	0.90	0.19	0.81	0.54	0.44	0.30	0.48	0.43	0.22	0.68	9	0.05	1.85	1.35
West Sirt Basin	4	Aswad	B18-NC74B	31	20	49	0.34	0.12	0.41	0.41	0.41	0.17	0.86	0.19	0.32	0.70	15	0.02	0.48	5.12
			B18-NC74B	31	20	49	0.33	0.11	0.40	0.40	0.13	0.18	0.83	0.19	0.29	0.69	15	0.02	0.50	5.62
		Safsaf	C1-NC74B	41	19	42	0.31	0.12	0.60	0.71	0.35	0.14	0.65	0.37	0.29	0.45	11	0.04	0.81	3.00
		S. Safsaf	D6-NC74B	37	20	40	0.35	0.11	0.47	0.71	0.42	0.16	0.72	0.34	0.32	0.55	13	0.04	0.82	2.95
		Zella	A5-NC74B	30	22	43	0.37	0.14	0.45	0.79	0.33	0.16	0.74	0.34	0.35	0.59	14	0.03	0.83	2.98
			A5-NC74B	33	22	48	0.34	0.14	0.45	0.82	0.36	0.16	0.62	0.36	0.34	0.45	12	0.02	0.80	2.76
			A28-NC74B	33	25	45	0.43	0.16	0.50	0.69	0.40	0.20	0.64	0.36	0.29	0.48	12	0.03	0.89	2.71
East Sirt Basin	5	As Sarah	B42-96	57	22	28	0.56	0.51	1.03	0.80	0.45	0.45	0.42	0.64	0.22	0.85	8	0.05	1.51	2.21
	6	Augla	G31-51	39	27	32	0.39	0.20	0.99	0.67	0.26	0.16	0.57	0.48	0.19	0.44	5	0.04	1.32	2.14
		Nafoora	G274-51	39	32	33	0.34	0.21	0.99	0.56	0.40	0.14	0.55	0.51	0.18	0.48	5	0.04	1.20	1.66
	7	NC125	N1-125	75	17	14	0.54	1.04	2.08	0.56	0.46	0.45	0.62	0.68	0.17	0.25	3	0.05	1.29	2.05
			A1-125	80	9	11	0.51	0.90	0.76	0.52	0.32	0.52	0.56	0.68	0.16	0.53	8	0.06	1.13	2.52
	8	Tuamma	C7-97	73	6	23	0.12	0.52	0.36	0.51	0.43	0.24	0.59	0.70	0.38	0.71	9	0.25	1.65	1.45
	9	Nakhla	G7-97	70	6	25	0.23	0.82	0.40	0.64	0.58	0.51	0.76	0.74	0.24	0.49	7	0.08	1.11	2.22
Nort Sea Oil			VFO	34	30	36	0.86	0.26	0.82	1.47	0.57	0.45	0.41	0.75	0.39	1.06	14	0.03	0.94	1.56

Appendixes II Table 5.3 Aromatic hydrocarbon concentration (µg/mg oil) of the oil families in the Sirt Basin.

Location	Family	Oil Filed	Well Name	N	ΣMN	ΣDMN	ΣTMN	ΣEN	P	ΣMP	ΣDMP	ΣDBTH	ΣMBDT	ΣDMBDT	ΣBp	Σ MBp	ΣMDBp	F	ΣMF	ΣMAS	ΣTAS
West Sirt Basin	1A	West Mabruk	A31-17	0.0026	0.0099	0.0173	0.0149	0.0013	0.0013	0.0032	0.0041	0.0008	0.0012	0.0009	0.0002	0.0004	0.0007	0.0005	0.0013	0.0007	0.0023
			A29-17	0.0053	0.0175	0.0283	0.0316	0.0021	0.0021	0.0051	0.0066	0.0013	0.0020	0.0016	0.0003	0.0007	0.0011	0.0008	0.0020	0.0010	0.0035
			A86-17	0.0032	0.0113	0.0192	0.0161	0.0014	0.0014	0.0033	0.0043	0.0008	0.0011	0.0009	0.0002	0.0005	0.0008	0.0006	0.0014	0.0007	0.0026
			A44-17	0.0028	0.0103	0.0179	0.0156	0.0013	0.0014	0.0033	0.0043	0.0009	0.0013	0.0011	0.0002	0.0004	0.0013	0.0005	0.0013	0.0007	0.0022
			A66-17	0.0034	0.0115	0.0192	0.0160	0.0014	0.0015	0.0038	0.0049	0.0009	0.0014	0.0012	0.0002	0.0005	0.0008	0.0006	0.0014	0.0007	0.0023
			A15-17	0.0033	0.0113	0.0188	0.0157	0.0014	0.0014	0.0035	0.0046	0.0009	0.0014	0.0013	0.0002	0.0004	0.0008	0.0005	0.0013	0.0007	0.0022
			M1-17	0.0011	0.0054	0.0150	0.0158	0.0010	0.0021	0.0044	0.0066	0.0007	0.0009	0.0009	0.0002	0.0005	0.0010	0.0006	0.0015	0.0008	0.0020
			A46-17	0.0043	0.0134	0.0219	0.0191	0.0017	0.0018	0.0039	0.0049	0.0010	0.0016	0.0013	0.0002	0.0006	0.0010	0.0006	0.0016	0.0008	0.0024
			A82-17	0.0069	0.0240	0.0425	0.0367	0.0028	0.0028	0.0077	0.0103	0.0014	0.0024	0.0016	0.0006	0.0013	0.0019	0.0011	0.0029	0.0003	0.0011
			A94-17	0.0054	0.0158	0.0257	0.0222	0.0018	0.0021	0.0046	0.0061	0.0010	0.0015	0.0011	0.0004	0.0008	0.0012	0.0007	0.0018	0.0004	0.0014
			A39-17	0.0062	0.0208	0.0280	0.0265	0.0023	0.0026	0.0059	0.0073	0.0014	0.0024	0.0018	0.0005	0.0011	0.0015	0.0010	0.0024	0.0006	0.0023
			A27-17	0.0056	0.0165	0.0263	0.0229	0.0020	0.0017	0.0045	0.0060	0.0009	0.0014	0.0010	0.0003	0.0007	0.0011	0.0007	0.0017	0.0005	0.0017
			A38-17	0.0062	0.0209	0.0358	0.0314	0.0024	0.0029	0.0070	0.0085	0.0014	0.0018	0.0010	0.0005	0.0013	0.0018	0.0011	0.0027	0.0005	0.0016
		East Mabruk	A84-17	0.0046	0.0159	0.0263	0.0209	0.0018	0.0020	0.0048	0.0058	0.0011	0.0013	0.0010	0.0003	0.0007	0.0011	0.0008	0.0018	0.0007	0.0022
			A101-17	0.0038	0.0132	0.0222	0.0181	0.0016	0.0016	0.0040	0.0051	0.0010	0.0015	0.0011	0.0003	0.0006	0.0009	0.0007	0.0016	0.0006	0.0021
			A103-17	0.0046	0.0149	0.0237	0.0216	0.0017	0.0017	0.0041	0.0051	0.0010	0.0014	0.0011	0.0003	0.0007	0.0010	0.0007	0.0016	0.0006	0.0021
			A58-17	0.0043	0.0177	0.0303	0.0241	0.0020	0.0022	0.0055	0.0066	0.0013	0.0019	0.0013	0.0004	0.0009	0.0012	0.0009	0.0022	0.0007	0.0026
			A3-17	0.0046	0.0171	0.0294	0.0225	0.0020	0.0021	0.0054	0.0067	0.0013	0.0021	0.0016	0.0004	0.0008	0.0012	0.0009	0.0021	0.0008	0.0025
			A7-17	0.0037	0.0124	0.0199	0.0156	0.0014	0.0015	0.0036	0.0045	0.0008	0.0011	0.0008	0.0003	0.0006	0.0008	0.0006	0.0014	0.0006	0.0023
			A97-17	0.0008	0.0037	0.0144	0.0181	0.0007	0.0015	0.0047	0.0074	0.0002	0.0002	0.0002	0.0004	0.0012	0.0021	0.0003	0.0013	0.0003	0.0007
		Hakim	A1-NC74A	0.0177	0.0494	0.0629	0.0365	0.0030	0.0040	0.0093	0.0101	0.0005	0.0008	0.0005	0.0021	0.0036	0.0036	0.0017	0.0036	0.0001	0.0005
			A2-NC74A	0.0081	0.0201	0.0256	0.0154	0.0014	0.0017	0.0039	0.0042	0.0003	0.0004	0.0002	0.0007	0.0015	0.0017	0.0006	0.0015	0.0001	0.0003
		Fidda	B1-NC74A	0.0106	0.0273	0.0370	0.0258	0.0023	0.0033	0.0071	0.0079	0.0009	0.0013	0.0008	0.0007	0.0016	0.0021	0.0010	0.0026	0.0003	0.0007
			B2-NC74A	0.0110	0.0309	0.0433	0.0293	0.0027	0.0031	0.0075	0.0087	0.0009	0.0013	0.0010	0.0008	0.0018	0.0022	0.0011	0.0027	0.0004	0.0008
Centre Sirt		Beda	B1-47	0.0045	0.0142	0.0228	0.0174	0.0012	0.0016	0.0040	0.0053	0.0005	0.0008	0.0005	0.0004	0.0007	0.0008	0.0005	0.0013	0.0003	0.0010
			B1-47	0.0055	0.0173	0.0282	0.0216	0.0015	0.0020	0.0051	0.0060	0.0006	0.0010	0.0006	0.0005	0.0008	0.0009	0.0006	0.0016	0.0004	0.0010
		East Meghile	J3-6	0.0011	0.0059	0.0156	0.0152	0.0009	0.0025	0.0058	0.0070	0.0008	0.0016	0.0014	0.0003	0.0007	0.0011	0.0004	0.0010	0.0003	0.0012

N: Naphthalene; P: Phenanthrene; F: Fluorene; Bp: Benzothiophene; DBT: Dibenzothiophene; C21-5MAS: C21 Monoaromatic Steroids; C20 TAS: C20 Triaromatic Steroids; C21 TAS: C21 Triaromatic Steroids; C22-5bMAS: C22 Monoaromatic Steroids.

Appendixes II Cont. Table 5.3 Aromatic hydrocarbon concentration (µg/mg oil) of the oil families in the Sirt Basin.

Group	Oil Filed	Well Name	N	ΣMN	ΣDMN	ΣTMN	ΣEN	P	ΣMP	ΣDMP	ΣDBTH	ΣMBDT	ΣDMBDT	ΣBp	Σ MBp	ΣMDBp	F	ΣMF	ΣMAS	ΣTAS
1B	Nasser	C98-6	0.0046	0.0200	0.0378	0.0277	0.0017	0.0035	0.0086	0.0098	0.0006	0.0011	0.0007	0.0012	0.0020	0.0023	0.0010	0.0026	0.0002	0.0006
		C98-6	0.0043	0.0182	0.0342	0.0253	0.0016	0.0033	0.0082	0.0101	0.0006	0.0008	0.0006	0.0010	0.0018	0.0021	0.0009	0.0025	0.0003	0.0009
	Raiah	DD12-6	0.0025	0.0100	0.0188	0.0153	0.0010	0.0014	0.0036	0.0046	0.0004	0.0009	0.0009	0.0003	0.0006	0.0007	0.0004	0.0011	0.0004	0.0012
	South Jebel	4B1-6	0.0016	0.0150	0.0363	0.0298	0.0015	0.0035	0.0089	0.0101	0.0005	0.0011	0.0008	0.0006	0.0014	0.0016	0.0009	0.0024	0.0004	0.0010
	Ragoba	E9-20	0.0088	0.0234	0.0329	0.0195	0.0014	0.0027	0.0060	0.0064	0.0003	0.0004	0.0003	0.0017	0.0032	0.0036	0.0005	0.0018	0.0001	0.0005
		E82-20	0.0071	0.0197	0.0276	0.0164	0.0012	0.0023	0.0054	0.0059	0.0003	0.0004	0.0003	0.0014	0.0027	0.0029	0.0004	0.0014	0.0001	0.0005
	West Meghil	4J2-6	0.0020	0.0101	0.0197	0.0144	0.0013	0.0017	0.0039	0.0058	0.0008	0.0008	0.0006	0.0005	0.0008	0.0014	0.0006	0.0014	0.0002	0.0004
	Zelten	4G1-6	0.0038	0.0198	0.0376	0.0288	0.0018	0.0037	0.0089	0.0099	0.0008	0.0012	0.0010	0.0009	0.0017	0.0019	0.0010	0.0024	0.0003	0.0011
	Sabah	G3-NC74F	0.0147	0.0320	0.0388	0.0249	0.0026	0.0027	0.0063	0.0070	0.0005	0.0007	0.0004	0.0008	0.0018	0.0022	0.0011	0.0024	0.0002	0.0006
2	Kotla	C46-47	0.0032	0.0089	0.0129	0.0107	0.0010	0.0008	0.0019	0.0024	0.0006	0.0012	0.0010	0.0001	0.0002	0.0003	0.0003	0.0007	0.0006	0.0024
3	Dor Mansour	Z3-47	0.0040	0.0056	0.0129	0.0165	0.0006	0.0012	0.0029	0.0047	0.0004	0.0007	0.0008	0.0005	0.0005	0.0007	0.0000	0.0007	0.0004	0.0013
		Z5-47	0.0036	0.0058	0.0141	0.0200	0.0006	0.0014	0.0032	0.0050	0.0004	0.0006	0.0006	0.0005	0.0005	0.0007	0.0002	0.0007	0.0004	0.0014
		GG1-47	0.0104	0.0323	0.0678	0.0671	0.0021	0.0025	0.0063	0.0100	0.0008	0.0012	0.0008	0.0014	0.0021	0.0020	0.0008	0.0019	0.0002	0.0006
4	Aswad	B18-NC74B	0.0156	0.0331	0.0373	0.0231	0.0028	0.0026	0.0052	0.0059	0.0008	0.0014	0.0008	0.0017	0.0036	0.0038	0.0009	0.0021	0.0008	0.0008
		B18-NC74B	0.0197	0.0399	0.0440	0.0259	0.0033	0.0023	0.0051	0.0056	0.0008	0.0013	0.0007	0.0020	0.0040	0.0042	0.0009	0.0022	0.0006	0.0007
	Safsaf	C1-NC74B	0.0203	0.0502	0.0580	0.0322	0.0034	0.0032	0.0066	0.0069	0.0006	0.0007	0.0004	0.0028	0.0044	0.0042	0.0015	0.0030	0.0002	0.0005
	Safsaf South	D6-NC74B	0.0209	0.0500	0.0586	0.0339	0.0034	0.0037	0.0075	0.0077	0.0008	0.0013	0.0009	0.0027	0.0047	0.0044	0.0015	0.0034	0.0002	0.0006
	Zella	A5-NC74B	0.0267	0.0607	0.0691	0.0417	0.0047	0.0043	0.0087	0.0092	0.0011	0.0018	0.0011	0.0028	0.0055	0.0057	0.0017	0.0040	0.0005	0.0008
		A5-NC74B	0.0264	0.0593	0.0663	0.0396	0.0046	0.0041	0.0086	0.0093	0.0011	0.0015	0.0008	0.0026	0.0051	0.0053	0.0016	0.0020	0.0006	0.0009
		A28-NC74B	0.0217	0.0448	0.0487	0.0291	0.0033	0.0030	0.0060	0.0063	0.0007	0.0011	0.0005	0.0019	0.0038	0.0040	0.0012	0.0027	0.0003	0.0005
5	As Sarah	B42-96	0.0048	0.0166	0.0303	0.0217	0.0010	0.0062	0.0110	0.0108	0.0001	0.0001	0.0001	0.0005	0.0007	0.0010	0.0004	0.0015	0.0000	0.0000
6	Augla Nafora	G31-51	0.0013	0.0039	0.0071	0.0067	0.0003	0.0015	0.0028	0.0028	0.0001	0.0001	0.0001	0.0005	0.0006	0.0007	0.0001	0.0003	0.0001	0.0003
		G274-51	0.0011	0.0030	0.0066	0.0072	0.0003	0.0018	0.0033	0.0033	0.0002	0.0001	0.0001	0.0004	0.0006	0.0008	0.0001	0.0003	0.0001	0.0003
7	NC125	N1-125	0.0025	0.0061	0.0096	0.0059	0.0005	0.0033	0.0049	0.0038	0.0003	0.0003	0.0003	0.0017	0.0019	0.0019	0.0002	0.0008	0.0004	0.0010
		A1-125	0.0012	0.0039	0.0077	0.0057	0.0004	0.0032	0.0049	0.0038	0.0001	0.0001	0.0000	0.0011	0.0015	0.0018	0.0002	0.0007	0.0000	0.0000
8	Tuamma	C7-97	0.0056	0.0082	0.0098	0.0043	0.0005	0.0032	0.0045	0.0033	0.0000	0.0000	0.0000	0.0020	0.0016	0.0016	0.0004	0.0010	0.0000	0.0000
9	Nakhla	G7-97	0.0026	0.0046	0.0053	0.0037	0.0003	0.0014	0.0020	0.0015	0.0001	0.0000	0.0000	0.0024	0.0014	0.0012	0.0001	0.0003	0.0000	0.0000
	North sea Oil	VFO	0.0211	0.0560	0.0629	0.0313	0.0036	0.0079	0.0160	0.0141	0.0009	0.0015	0.0013	0.0055	0.0078	0.0056	0.0029	0.0052	0.0002	0.0004

Appendix II Table 5.4: Aromatic hydrocarbon source facies ratios of the oil families in the Sirt Basin.

Location	Group	Oil Filed	Well Name	1,2,5-TMN/ 1,3,6-TMN	1,2,7-TMN/ 1,3,7-TMN	1,2,6TMN/ 1,2,4-TMN	1,2,5-TMN/ 1,2,7-TMN	TED1	TED2	1-MP/ 9-MP	1,7-DMP/1,3+3,9+ 2,10+3,1-DMP	Pr/Ph	DBT/P
West Sirt Basin	1A	West Mabruk	A31-17	0.33	0.19	2.16	2.72	2.22	0.38	0.70	0.38	1.51	0.63
			A29-17	0.33	0.18	2.24	2.78	2.19	0.35	0.70	0.38	1.52	0.63
			A86-17	0.33	0.18	2.28	2.82	2.23	0.35	0.67	0.37	1.52	0.60
			A44-17	0.33	0.17	2.28	2.95	2.21	0.33	0.68	0.38	1.52	0.64
			A66-17	0.32	0.15	2.46	3.35	2.18	0.26	0.69	0.38	1.51	0.62
			A15-17	0.32	0.17	2.28	2.99	2.18	0.32	0.69	0.38	1.52	0.65
			M1-17	0.33	0.15	2.11	3.12	2.10	0.32	0.70	0.34	1.50	0.32
			A46-17	0.34	0.21	2.20	2.54	2.21	0.40	0.69	0.38	1.55	0.55
			A82-17	0.24	0.14	2.79	2.42	2.29	0.34	0.71	0.36	1.55	0.51
			A94-17	0.28	0.16	2.64	2.57	2.28	0.34	0.69	0.37	1.50	0.47
			A39-17	0.29	0.15	2.68	2.79	2.42	0.32	0.70	0.37	1.52	0.55
			A27-17	0.30	0.15	2.69	2.87	2.30	0.30	0.69	0.37	1.49	0.54
			A38-17	0.29	0.15	2.81	2.74	2.34	0.30	0.70	0.37	1.52	0.46
		East Mabruk	A84-17	0.30	0.15	2.54	3.05	2.26	0.29	0.68	0.37	1.52	0.55
			A101-17	0.31	0.15	2.50	3.06	2.19	0.29	0.70	0.37	1.51	0.62
			A103-17	0.18	0.14	2.51	3.33	2.19	0.26	0.70	0.36	1.52	0.60
			A58-17	0.30	0.14	2.54	3.21	2.19	0.27	0.69	0.37	1.52	0.61
			A3-17	0.15	0.14	5.37	1.63	2.29	0.26	0.68	0.37	1.50	0.62
			A7-17	0.31	0.15	2.56	3.03	2.29	0.29	0.69	0.37	1.52	0.57
			A97-17	0.13	0.09	3.58	2.00	1.94	0.27	0.67	0.34	1.46	0.14
		Hakim	A1-NC74A	0.18	0.09	3.16	2.76	2.37	0.27	0.68	0.33	1.41	0.11
			A2-NC74A	0.21	0.10	2.78	2.99	2.34	0.28	0.70	0.36	1.43	0.18
		Fidda	B1-NC74A	0.26	0.15	2.93	2.52	2.66	0.36	0.68	0.37	1.33	0.26
			B2-NC74A	0.25	0.15	2.55	2.48	2.26	0.36	0.69	0.37	1.32	0.28
		Beda	B1-47	0.27	0.14	2.56	3.15	2.33	0.29	0.65	0.42	1.49	0.30
			B1-47	0.27	0.17	2.46	2.54	2.34	0.37	0.65	0.41	1.51	0.30
ntre Sirt Ba		East Meghile	J3-6	0.29	0.14	2.51	3.29	2.38	0.29	0.68	0.40	1.59	0.33

TMN: Trimethylnaphthalene; MP: Methylphenanthrene; DMP: Dimethylphenanthrene; Pr: pristane; Ph: Phytane; DBT: Dibenzothiophene; P: phenanthrene; TDE-1: 1,2,5-TMN/1,2,4-TMN; TDE-2: 1,2,7-TMN/1,2,6-TMN.

Appendix II Cont. Table 5.4: Aromatic hydrocarbon source facies ratios of the oil families in the Sirt Basin.

Location	Group	Oil Filed	Well Name	1,2,5-TMN/ 1,3,6-TMN	1,2,7-TMN/ 1,3,7-TMN	1,2,6TMN/ 1,2,4-TMN	1,2,5-TMN/ 1,2,7-TMN	TED1	TED2	1-MP/ 9-MP	1,7-DMP/1,3+3,9+ 2,10+3,1-DMP	Pr/Ph	DBT/P
Centre Sirt Basin	1B	Nasser	C98-6	0.19	0.11	2.84	2.63	2.20	0.29	0.66	0.35	1.60	0.17
			C98-6	0.19	0.13	2.59	2.23	2.19	0.38	0.66	0.40	1.59	0.17
		Raiah	DD12-6	0.27	0.15	2.37	2.89	2.28	0.33	0.68	0.43	1.50	0.31
		South Jebel	4B1-6	0.23	0.12	2.82	2.96	2.37	0.28	0.67	0.37	1.52	0.15
		Zelten	4G1-6	0.24	0.13	2.66	2.74	2.29	0.31	0.69	0.37	1.53	0.22
		Ragoba	E9-20	0.15	0.09	2.42	2.36	1.87	0.33	0.65	0.33	1.73	0.11
			E82-20	0.16	0.10	2.40	2.21	1.99	0.38	0.65	0.34	1.71	0.11
		Sabah	G3-NC74F	0.28	0.18	2.31	2.32	2.46	0.46	0.68	0.35	1.50	0.17
est Sirt Bas		West Meghil	4J2-6	0.21	0.10	2.29	3.02	2.08	0.30	0.64	0.32	1.80	0.48
Centre Sirt B	2	Kotla	C46-47	0.45	0.23	2.13	3.38	2.43	0.34	0.71	0.56	1.27	0.68
	3	Dor Mansour	Z3-47	4.11	0.18	4.06	21.85	20.76	0.23	0.79	0.87	1.26	0.32
			Z5-47	2.94	0.19	4.43	23.83	24.92	0.24	0.80	0.91	1.28	0.28
			GG1-47	3.04	0.35	5.37	11.90	29.44	0.46	0.85	1.48	1.36	0.33
West Sirt Basin	4	Aswad	318-NC74B	0.35	0.14	2.59	3.51	3.08	0.34	0.72	0.37	1.30	0.33
			318-NC74B	0.33	0.12	2.52	3.84	2.98	0.31	0.71	0.36	1.28	0.36
		Safsaf South	D6-NC74B	0.23	0.11	3.02	2.78	2.77	0.33	0.72	0.33	1.54	0.21
		Zella	A5-NC74B	0.30	0.12	2.79	3.40	2.81	0.30	0.74	0.35	1.41	0.27
			A5-NC74B	0.30	0.13	2.68	3.32	2.80	0.31	0.72	0.34	1.43	0.26
			A28-NC74E	0.29	0.13	2.70	3.18	2.77	0.32	0.73	0.34	1.46	0.25
		Safsaf	C1-NC74B	0.23	0.13	2.94	2.55	2.79	0.37	0.71	0.33	1.52	0.17
East Sirt Basin	5	As Sarah	B42-96	0.08	0.20	8.87	0.56	3.33	0.67	0.60	0.41	2.03	0.02
	6	Augla Nafora	G31-51	0.54	0.12	3.60	6.51	4.99	0.21	0.51	0.39	1.88	0.09
			G274-51	0.56	0.13	3.41	6.48	4.63	0.21	0.54	0.41	1.85	0.08
	7	NC125	N1-125	0.16	0.19	5.46	1.32	3.73	0.52	0.65	0.36	1.92	0.09
			A1-125	0.18	0.23	4.27	1.19	3.31	0.65	0.69	0.40	2.05	0.02
	8	Tuamma	C7-97	0.06	0.16	6.96	0.59	3.57	0.87	0.70	0.37	1.89	0.01
	9	Nakhla	G7-97	0.67	0.40	3.81	2.21	5.40	0.64	0.67	0.41	2.00	0.04
North Sea Oil		VFO		0.21	0.39	2.85	0.70	2.68	1.34	0.73	0.36	1.38	0.12

Appendix II Table 5.5: Maturity biomarker ratios of the oil families in the Sirt Basin.

Location	Family	Oil Filed	Well Name	C29 ααα [20S/ (20S+20R)]	C29 [αββ/ (αββ+ααα)]	Ts/ (TS+Tm)	C32 22S/ (22S+22R)	C30-Mort βα/ C30αβ	C29 αβ(H)/ /C30 αβ(H)	C30-diah/ C30-diah+C30αβ	C30-Mor/ C30-Mor+C30αβ	C_{20}-C_{30} Tri/C_{20}-C_{30}Tri+ C_{27}-C_{35} hopane	C_{23}/ C_{23}+C_{30} Hopane
West Sirt Basin	1A	West Mabruk	A31-17	0.51	0.55	0.47	0.60	0.11	0.43	0.06	0.10	0.02	0.19
			A29-17	0.45	0.50	0.55	0.59	0.10	0.48	0.07	0.09	0.03	0.22
			A86-17	0.52	0.57	0.56	0.61	0.10	0.45	0.06	0.09	0.02	0.19
			A44-17	0.46	0.50	0.56	0.61	0.10	0.46	0.06	0.09	0.02	0.20
			A66-17	0.51	0.53	0.55	0.61	0.10	0.46	0.07	0.09	0.02	0.21
			A15-17	0.46	0.53	0.57	0.61	0.10	0.44	0.06	0.09	0.02	0.20
			M1-17	0.46	0.53	0.57	0.60	0.10	0.45	0.07	0.09	0.02	0.21
			A46-17	0.49	0.50	0.57	0.61	0.10	0.46	0.06	0.09	0.03	0.21
			A82-17	0.48	0.56	0.57	0.60	0.13	0.46	0.15	0.12	0.04	0.27
			A94-17	0.49	0.53	0.57	0.60	0.11	0.42	0.10	0.10	0.03	0.24
			A39-17	0.47	0.51	0.57	0.60	0.10	0.45	0.08	0.09	0.03	0.21
			A27-17	0.50	0.52	0.58	0.60	0.11	0.45	0.10	0.10	0.03	0.23
			A38-17	0.48	0.53	0.57	0.59	0.10	0.43	0.10	0.09	0.03	0.25
		East Mabruk	A84-17	0.47	0.52	0.57	0.60	0.11	0.46	0.07	0.10	0.02	0.22
			A101-17	0.47	0.52	0.54	0.61	0.10	0.45	0.07	0.09	0.02	0.20
			A103-17	0.51	0.53	0.59	0.61	0.10	0.48	0.08	0.09	0.02	0.21
			A58-17	0.46	0.52	0.57	0.60	0.11	0.45	0.08	0.10	0.02	0.19
			A3-17	0.46	0.51	0.61	0.60	0.10	0.46	0.08	0.09	0.02	0.21
			A7-17	0.45	0.51	0.59	0.60	0.11	0.46	0.07	0.10	0.02	0.21
			A97-17	0.56	0.61	0.73	0.59	0.13	0.35	0.14	0.11	0.05	0.34
		Hakim	A1-NC74A	0.50	0.54	0.58	0.58	0.11	0.46	0.09	0.10	0.04	0.28
			A2-NC74A	0.47	0.48	0.41	0.58	0.11	0.53	0.06	0.10	0.03	0.23
		Fidda	B1-NC74A	0.49	0.52	0.55	0.61	0.08	0.44	0.05	0.08	0.04	0.28
			B2-NC74A	0.47	0.51	0.50	0.61	0.08	0.47	0.05	0.07	0.03	0.25
		Beda	B1-47	0.50	0.54	0.55	0.59	0.10	0.48	0.05	0.09	0.04	0.27
			B1-47	0.48	0.52	0.58	0.59	0.10	0.51	0.05	0.09	0.04	0.26
Centre Sirt Basi		East Meghile	J3-6	0.52	0.55	0.39	0.59	0.10	0.55	0.06	0.09	0.03	0.22

Appendix II Cont. Table 5.5: Maturity biomarker ratios of the oil families in the Sirt Basin.

Location	Family	Oil Filed	Well Name	C29 ααα [20S/ (20S+20R)]	C29 [αββ/ (αββ+ααα)]	Ts/ (TS+Tm)	C32 22S/ (22S+22R)	C30-Mort βα/ C30αβ	C29 αβ(H)/ C30 αβ(H)	C30-diah/ C30-diah+C30αβ	C30-Mor/ C30-Mor+C30αβ	C20-C30 Tri/ C20-C30Tri + C27-C□23+C30 Hopane	C23/
Centre Sirt Basin	1B	Nasser	C98-6	0.49	0.57	0.62	0.59	0.10	0.43	0.10	0.09	0.04	0.28
			C98-6	0.49	0.53	0.68	0.60	0.11	0.44	0.10	0.10	0.04	0.27
		Raiah	DD12-6	0.46	0.52	0.51	0.58	0.10	0.48	0.04	0.09	0.04	0.26
		South Jebel	4B1-6	0.52	0.60	0.68	0.59	0.10	0.40	0.08	0.09	0.03	0.23
		Ragoba	E9-20	0.51	0.52	0.50	0.61	0.10	0.50	0.06	0.09	0.03	0.24
			E82-20	0.49	0.52	0.50	0.59	0.10	0.49	0.06	0.09	0.03	0.24
		West Meghil	4J2-6	0.49	0.56	0.63	0.58	0.09	0.50	0.10	0.08	0.05	0.34
		Zelten	4G1-6	0.48	0.55	0.60	0.59	0.11	0.45	0.08	0.10	0.03	0.25
West Sirt Basin		Sabah	G3-NC74F	0.46	0.52	0.52	0.57	0.11	0.56	0.06	0.10	0.04	0.26
Centre Sirt Bas	2	Kotla	C46-47	0.46	0.44	0.37	0.59	0.11	0.47	0.04	0.10	0.03	0.25
	3	Dor Mansour	Z3-47	0.52	0.54	0.42	0.58	0.10	0.52	0.05	0.09	0.03	0.20
			Z5-47	0.52	0.54	0.41	0.59	0.10	0.52	0.04	0.09	0.03	0.21
			GG1-47	0.49	0.56	0.43	0.58	0.11	0.48	0.08	0.10	0.03	0.22
West Sirt Basin	4	Aswad	B18-NC74B	0.45	0.47	0.19	0.61	0.09	0.86	0.03	0.08	0.01	0.06
			B18-NC74B	0.48	0.50	0.19	0.61	0.08	0.83	0.02	0.08	0.01	0.06
		Safsaf	C1-NC74B	0.53	0.55	0.36	0.60	0.08	0.64	0.04	0.07	0.01	0.11
		Safsaf South	D6-NC74B	0.54	0.51	0.37	0.60	0.09	0.65	0.04	0.08	0.01	0.11
		Zella	A5-NC74B	0.43	0.46	0.34	0.59	0.10	0.72	0.04	0.09	0.01	0.12
			A5-NC74B	0.42	0.42	0.34	0.60	0.09	0.74	0.04	0.09	0.01	0.12
			A28-NC74B	0.46	0.44	0.36	0.57	0.09	0.62	0.05	0.09	0.01	0.13
East Sirt Basin	5	As Sarah	B42-96	0.75	0.66	0.64	0.63	0.22	0.42	0.35	0.18	0.26	0.33
	6	Augla Nafora	G31-51	0.57	0.51	0.48	0.59	0.15	0.57	0.16	0.13	0.03	0.21
			G274-51	0.56	0.51	0.51	0.59	0.18	0.55	0.17	0.15	0.03	0.21
	7	NC125	N1-125	0.88	0.68	0.68	0.57	0.51	0.62	0.53	0.34	0.27	0.55
			A1-125	0.81	0.69	0.68	0.62	0.45	0.56	0.54	0.31	0.28	0.56
	8	Tuamma	C7-97	0.54	0.66	0.70	0.48	0.56	0.59	0.64	0.52	0.41	0.68
	9	Nakhla	G7-97	0.74	0.67	0.74	0.60	0.31	0.76	0.39	0.24	0.26	0.49
UK	VFO	North Sea Oil	VFO	0.51	0.61	0.75	0.53	0.12	0.43	0.22	0.12	0.03	0.24

Appendix II Table 5.6: Aromatic hydrocarbon maturity ratios of the oil families in the Sirt Basin.

Location	Group	Oil Field	Well Name	MA(I)/ MA(I+II)	TA(I)/ TA(I+II)	MPI 1	Rc%	MNR	DMNR	TMNR	MDI	MDIA/DIA
West Sirt Basin	1A	West Mabruk	A31-17	13.97	14.52	0.68	0.81	1.27	5.19	0.85	59	1.88
			A29-17	13.69	15.32	0.68	0.81	1.31	5.39	0.27	59	1.89
			A86-17	12.20	14.48	0.69	0.81	1.29	5.27	0.88	59	1.91
			A44-17	13.92	14.81	0.69	0.81	1.25	5.09	0.86	58	1.89
			A66-17	13.81	15.35	0.70	0.82	1.31	5.17	0.93	59	1.92
			A15-17	14.26	15.71	0.70	0.82	1.30	5.29	0.89	59	1.85
			M1-17	17.46	18.11	0.62	0.77	1.26	4.68	0.73	59	2.03
			A46-17	13.93	14.40	0.65	0.79	1.29	5.23	0.80	59	1.90
			A82-17	20.72	33.66	0.71	0.83	1.35	5.97	0.92	55	1.90
			A94-17	15.40	22.63	0.65	0.79	1.33	5.59	0.90	57	1.83
			A39-17	12.92	18.46	0.68	1.04	1.37	5.71	0.93	58	1.92
			A27-17	14.27	26.44	0.73	0.84	1.33	5.60	0.89	58	1.83
			A38-17	18.39	23.87	0.68	0.81	1.34	5.50	0.90	57	1.90
		East Mabruk	A84-17	14.98	17.36	0.68	0.81	1.30	5.19	0.92	59	1.88
			A101-17	15.03	16.15	0.69	0.81	1.32	5.28	0.94	58	1.90
			A103-17	15.16	16.56	0.67	0.80	1.32	5.29	0.93	58	1.92
			A58-17	15.31	16.75	0.69	0.82	1.33	5.25	0.94	58	1.91
			A3-17	15.21	16.43	0.69	0.81	1.26	5.02	0.90	59	1.92
			A7-17	12.30	16.14	0.70	0.82	1.32	5.26	0.92	58	1.94
			A97-17	28.13	35.02	0.77	0.86	1.52	7.28	0.99	52	2.09
		Hakim	A1-NC74A	45.29	77.29	0.66	0.80	1.45	6.05	0.91	46	2.53
			A2-NC74A	20.82	44.00	0.66	0.79	1.45	5.86	0.86	43	2.75
		Fidda	B1-NC74A	18.94	27.83	0.62	0.77	1.37	5.22	0.78	45	2.32
			B2-NC74A	16.83	29.02	0.64	0.78	1.39	5.42	0.79	47	2.27
		Beda	B1-47	17.19	15.79	0.58	0.75	1.24	3.87	0.65	49	2.30
ıtre Sirt Ba			B1-47	17.84	16.94	0.59	0.75	1.23	3.89	0.63	50	2.41
		East Meghile	J3-6	15.30	15.86	0.64	0.79	1.09	3.85	0.73	47	2.83

MPI-1: 1.5([2-MP]+[3-MP]/[P]+[1-MP]+[9-MP]; Rc%: (0.6*MPI-1)+0.4; MNR: 2-MN/1-MN, DNR: [2,6-DMN]+[2,7-DMN]/[1,5-DMN]; DMNR: [2,6-DMN+2,7-DMN]/[1,5-DMN]; TMNR: [2,3,6-TMN]/[1,3,5-TMN+1,4,6-TMN].

Appendix II Cont. Table 5.6: Aromatic hydrocarbon maturity ratios of the oil families in the Sirt Basin.

Location	Group	Oil Field	Well Name	MA(I)/ MA(I+II)	TA(I)/ TA(I+II)	MPI 1	RC%	MNR	DMNR	TMNR	MDI	MDIA/DIA
center Sirt Basin	1B	Nasser	C98-6	27.17	30.18	0.63	0.78	1.21	4.71	0.74	40	3.20
			C98-6	26.87	29.03	0.65	0.79	1.23	4.86	0.71	38	2.98
		Raiah	DD12-6	14.48	13.54	0.60	0.76	1.22	3.89	0.64	54	2.22
		South Jebel	4B1-6	27.65	28.04	0.60	0.76	1.08	3.70	0.65	27	3.21
		Ragoba	E9-20	25.46	23.33	0.71	0.82	1.51	6.67	0.83	35	3.33
			E82-20	21.08	21.48	0.69	0.81	1.47	6.35	0.81	33	3.31
		West Meghil	4J2-6	17.42	38.35	0.68	0.81	1.24	5.05	0.80	45	2.23
		Zelten	4G1-6	22.32	21.36	0.62	0.77	1.12	4.00	0.69	42	2.82
		Sabah	G3-NC74F	33.90	42.81	0.63	0.78	1.30	4.98	0.71	46	2.37
	2	Kotla	C46-47	6.11	6.21	0.58	0.75	1.14	3.32	0.58	53	2.16
	3	Dor Mansour	Z3-47	14.49	12.96	0.57	0.74	1.19	2.54	0.57	56	1.84
			Z5-47	15.30	12.88	0.56	0.74	1.20	2.33	0.56	56	1.84
			GG1-47	16.13	17.15	0.54	0.72	1.33	2.20	0.19	55	1.97
West Sirt Basin	4	Aswad	B18-NC74B	7.09	27.02	0.64	0.78	1.37	5.11	0.83	46	2.52
			B18-NC74B	7.44	28.99	0.66	0.80	1.34	5.22	0.84	44	2.41
		Safsaf	C1-NC74B	22.50	59.22	0.65	0.79	1.43	6.37	0.91	48	2.43
		Safsaf South	D6-NC74B	19.18	56.86	0.64	0.79	1.46	6.28	0.94	46	2.35
		Zella	A5-NC74B	14.90	39.79	0.65	0.79	1.39	5.47	0.88	46	2.41
			A5-NC74B	13.30	35.27	0.65	0.79	1.38	5.49	0.87	47	2.48
			A28-NC74B	15.19	41.90	0.63	0.78	1.37	5.57	0.87	46	2.46
East Sirt Basin	5	As Sarah	B42-96	41.51	85.68	0.72	0.83	2.39	16.13	1.40	37	4.35
	6	Augla Nafora	G31-51	12.84	17.37	0.41	0.65	1.13	4.40	0.69	42	3.57
			G274-51	15.23	16.24	0.42	0.65	0.96	3.76	0.69	39	3.69
	7	NC125	N1-125	69.46	60.32	0.49	0.70	1.21	5.83	0.90	41	3.52
			A1-125	61.29	85.57	0.49	0.69	0.96	4.75	0.78	40	3.41
	8	Tuamma	C7-97	55.26	70.67	0.65	0.79	1.74	11.03	1.19	40	3.73
	9	Nakhla	G7-97	49.02	81.87	0.27	0.56	0.93	2.86	0.55	44	2.77
Uk	N. Sea oil		VFO	31.08	47.33	0.59	0.75	1.25	4.39	0.64	29	3.46

Appendix III Table 6.1: Tricyclic and tetracyclic terpanes biomarker ratios of the Upper Cretaceous source rocks in the Sirt Basin.

Location	Group	Oil Field	Well Name	Depth Feet	A	C_{23}-Tri/ (C_{23}+C_{21}-Tri)	C_{21}-Tri/ C_{23}+C_{21}-Tri	C_{23}-Tri/ C_{24}-Tri	C_{23}-Tri/ C_{21}-Tri	C_{22}-Tri/ C_{21}-Tri	C_{24}-Tri/ C_{23}-Tri	C_{19}+C_{20}-Tri/ C_{23}-Tri	C_{23}-Tri/ -Tri+C30 αβ Hopa	C_{28}+C_{29}-Tri(S+R)/ TS	C_{24}-tetr/ C_{26}-Tri	C_{19}-Tri/ C_{21}-Tri	C_{21}-Tri/ C_{23}-Tri	C_{26}-Tri/ C_{25}-Tri	C_{24}-tetr/ C_{23}-Tri
west Sirt Basin	A	W. Mabruk	L1-17	6060	0.09	0.65	0.35	3.00	1.87	0.23	0.33	0.32	0.25	0.58	1.32	0.20	0.53	0.65	0.23
				6300	0.16	0.67	0.33	2.77	2.04	0.28	0.36	0.26	0.27	1.05	1.01	0.13	0.49	0.73	0.28
				6460	0.14	0.62	0.38	2.26	1.66	0.28	0.44	0.39	0.22	0.74	1.15	0.21	0.60	0.88	0.28
				6600	0.14	0.62	0.38	2.02	1.65	0.29	0.49	0.86	0.42	0.79	1.28	0.24	0.61	1.05	0.29
	B	Waha 59	6A1-59	7150	0.10	0.69	0.31	2.57	2.21	0.23	0.39	0.39	0.24	1.07	1.03	0.17	0.45	0.70	0.23
				7170	0.11	0.69	0.31	2.72	2.28	0.22	0.37	0.39	0.26	1.32	0.93	0.21	0.44	0.83	0.22
				7250	0.11	0.71	0.29	2.66	2.46	0.23	0.38	0.36	0.20	1.40	0.93	0.15	0.41	0.75	0.23
center Sirt basin	C	N. E. Atthadai	L1-16	7400	0.05	0.57	0.43	2.48	1.30	0.26	0.40	0.94	0.22	0.41	2.03	0.54	0.77	0.70	0.26
				7530	0.11	0.62	0.38	3.04	1.60	0.30	0.33	0.84	0.26	0.68	1.57	0.63	0.63	0.60	0.30
				7640	0.13	0.64	0.36	3.17	1.76	0.30	0.32	0.54	0.26	0.75	1.07	0.39	0.57	0.72	0.30
				7850	0.11	0.62	0.38	2.53	1.64	0.33	0.39	0.82	0.30	0.81	1.27	0.60	0.61	0.82	0.33
		S. E. Buzuzi	C2-16	9800	0.38	0.59	0.41	1.62	1.42	0.39	0.62	0.95	0.53	2.09	1.13	0.58	0.70	1.07	0.39
				10260	0.63	0.57	0.43	1.59	1.34	0.39	0.63	1.15	0.74	5.79	1.03	0.68	0.75	1.15	0.39
				10380	0.54	0.55	0.45	1.63	1.24	0.39	0.61	1.39	0.72	4.69	1.28	0.79	0.80	1.08	0.39
				10580	0.43	0.53	0.47	1.72	1.11	0.37	0.58	1.62	0.60	4.28	1.46	0.82	0.90	0.98	0.37
west Sirt Basin	1D	South east Fidda	B1-NC74F	7050	0.17	0.54	0.46	2.07	1.17	0.35	0.48	1.35	0.60	1.34	3.14	0.68	0.85	0.64	0.35
				7110	0.11	0.56	0.44	2.13	1.29	0.38	0.47	1.25	0.63	1.36	3.13	0.72	0.78	0.62	0.38
				7190	0.23	0.54	0.46	2.04	1.16	0.41	0.49	1.16	0.63	1.33	3.12	0.54	0.86	0.61	0.41
				7940	0.20	0.55	0.45	2.06	1.21	0.35	0.48	1.20	0.62	2.42	3.06	0.60	0.83	0.65	0.35
				8080	0.16	0.53	0.47	2.09	1.12	0.35	0.48	1.14	0.62	1.82	2.94	0.56	0.89	0.63	0.35
	2D	West Sabah	B2-NC74A	9520	0.05	0.50	0.50	1.92	0.99	0.31	0.52	1.67	0.20	0.43	2.05	0.66	1.01	0.83	0.31
				9540	0.18	0.46	0.54	2.01	0.85	0.27	0.50	1.86	0.36	0.61	2.64	0.68	1.18	0.69	0.27
				9570	0.01	0.58	0.42	1.70	1.41	0.37	0.59	0.93	0.05	0.38	1.35	0.49	0.71	0.83	0.37
				9580	0.30	0.58	0.42	1.87	1.39	0.34	0.54	1.01	0.33	0.44	3.25	0.51	0.72	0.57	0.34
				9610	0.02	0.68	0.32	1.55	2.14	0.37	0.64	0.51	0.10	1.21	0.87	0.38	0.47	0.97	0.37
	E	Ghani-Zen	Z1-11	8080	0.16	0.55	0.45	1.95	1.24	0.36	0.51	1.01	0.36	1.01	1.63	0.50	0.81	0.71	0.36
				8140	0.22	0.57	0.43	1.86	1.32	0.28	0.54	0.72	0.41	1.26	1.61	0.35	0.76	0.73	0.28
				8200	0.17	0.59	0.41	1.95	1.45	0.35	0.51	0.72	0.45	1.02	1.75	0.42	0.69	0.82	0.35
center Sirt basin	F	S. E. Atthadia	FF14-6	11290	0.30	0.64	0.36	1.79	1.76	0.34	0.56	0.88	0.77	3.89	2.16	0.19	0.57	0.65	0.34
				11320	0.05	0.58	0.42	2.59	1.36	0.27	0.39	0.89	0.24	0.30	1.37	0.49	0.74	1.05	0.27
				11615	0.32	0.62	0.38	1.47	1.64	0.32	0.68	0.34	0.70	3.58	1.72	0.14	0.61	0.75	0.32
				11650	0.32	0.62	0.38	1.62	1.63	0.32	0.62	0.36	0.75	4.37	1.91	0.15	0.61	0.72	0.32
				12290	0.10	0.57	0.43	1.96	1.30	0.30	0.51	1.64	0.37	0.99	2.96	0.87	0.77	0.51	0.30
				12330	0.09	0.56	0.44	1.86	1.28	0.41	0.54	1.29	0.35	0.99	2.20	1.03	0.78	0.68	0.41

A: Extended tricyclic terpane C_{28}+C_{29}-Tri (S+R)/(C_{28}+C_{29}-Tri (S+R)+C_{29} to C_{30} αβ(H)-hopane).

Appendix III Cont. Table 6.1: Tricyclic and tetracyclic terpanes biomarker ratios of the oil families in the Sirt Basin.

Location	Oil Family	Oil Field	Well Name	A	C_{23}-Tri/ (C_{23}+C_{21}-Tri	C_{21}-Tri/ (C_{23}+C_{21}-Tri	C_{23}-Tri/ C_{24}-Tri	C_{23}-Tri/ C_{21}-Tri	C_{22}-Tri/ C_{21}-Tri	C_{24}-Tri/ C_{23}-Tri	(C_{19}+C_{20}-Tri/ C_{23}-Tri	C_{23}-Tri/ (Tri+C30 αβ Hop	(C_{28}+C_{29}-Tri(S+R)/ TS	C_{24}-tetr/ C_{26}-Tri	C_{19}-Tri/ C_{21}-Tri	C_{21}-Tri/ C_{23}-Tri	C_{26}-Tri/ C_{25}-Tri	C_{24}-tetr/ C_{23}-Tri
West Sirt Basin	1A	West Mabruk	A31-17	0.01	0.66	0.34	1.84	1.94	0.29	0.54	0.32	0.19	1.70	0.04	0.17	0.51	1.19	0.03
			A29-17	0.01	0.66	0.34	1.83	1.91	0.28	0.55	0.33	0.22	1.82	0.04	0.21	0.52	1.18	0.03
			A86-17	0.01	0.65	0.35	1.85	1.89	0.29	0.54	0.30	0.19	1.75	0.05	0.15	0.53	1.24	0.04
			A44-17	0.01	0.66	0.34	1.77	1.95	0.31	0.56	0.30	0.20	1.61	0.05	0.15	0.51	1.19	0.04
			A66-17	0.01	0.65	0.35	1.80	1.84	0.30	0.55	0.31	0.21	1.73	0.05	0.15	0.54	1.20	0.04
			A15-17	0.01	0.66	0.34	1.79	1.92	0.27	0.56	0.36	0.20	1.64	0.05	0.20	0.52	1.22	0.04
			M1-17	0.01	0.66	0.34	1.73	1.90	0.31	0.58	0.34	0.21	1.42	0.03	0.20	0.52	1.42	0.03
			A46-17	0.01	0.66	0.34	1.91	1.94	0.29	0.52	0.30	0.21	1.66	0.05	0.16	0.52	1.18	0.03
			A82-17	0.02	0.61	0.39	1.53	1.55	0.33	0.65	0.41	0.27	2.16	0.04	0.21	0.65	1.21	0.03
			A94-17	0.02	0.66	0.34	1.85	1.91	0.32	0.54	0.30	0.24	1.91	0.03	0.18	0.52	1.27	0.02
			A39-17	0.01	0.65	0.35	1.77	1.86	0.31	0.57	0.31	0.21	1.72	0.05	0.16	0.54	1.20	0.03
			A27-17	0.02	0.67	0.33	1.84	2.00	0.29	0.54	0.29	0.23	1.97	0.04	0.16	0.50	1.26	0.03
			A38-17	0.02	0.63	0.37	1.68	1.74	0.32	0.60	0.32	0.25	1.80	0.06	0.17	0.58	1.29	0.04
		East Mabruk	A84-17	0.01	0.65	0.35	1.83	1.90	0.30	0.55	0.30	0.22	1.78	0.04	0.16	0.53	1.17	0.03
			A101-17	0.01	0.65	0.35	1.80	1.89	0.28	0.56	0.30	0.20	1.72	0.04	0.16	0.53	1.17	0.03
			A103-17	0.01	0.65	0.35	1.83	1.89	0.31	0.55	0.32	0.21	1.72	0.04	0.14	0.53	1.20	0.03
			A58-17	0.01	0.65	0.35	1.79	1.89	0.30	0.56	0.32	0.19	1.65	0.03	0.19	0.53	1.21	0.03
			A3-17	0.01	0.66	0.34	1.81	1.92	0.33	0.55	0.33	0.21	1.78	0.04	0.17	0.52	1.14	0.03
			A7-17	0.01	0.65	0.35	1.86	1.84	0.30	0.54	0.33	0.21	1.71	0.05	0.19	0.54	1.25	0.04
			A97-17	0.03	0.64	0.36	1.54	1.76	0.33	0.65	0.38	0.34	2.39	0.05	0.19	0.57	1.27	0.04
		Fidda	B1-NC74A	0.02	0.69	0.31	1.58	2.26	0.36	0.63	0.29	0.28	2.56	0.03	0.15	0.44	1.31	0.02
			B2-NC74A	0.02	0.69	0.31	1.58	2.18	0.35	0.63	0.29	0.25	2.36	0.03	0.16	0.46	1.32	0.03
		Hakim	A1-NC74A	0.02	0.60	0.40	1.27	1.49	0.37	0.78	0.58	0.28	1.68	0.03	0.33	0.67	1.67	0.03
			A2-NC74A	0.01	0.64	0.36	1.36	1.75	0.36	0.73	0.43	0.23	1.91	0.05	0.23	0.57	1.58	0.05
		Beda	B1-47	0.02	0.68	0.32	1.40	2.12	0.34	0.72	0.33	0.27	3.10	0.05	0.13	0.47	1.11	0.04
			B1-47	0.02	0.67	0.33	1.37	2.03	0.35	0.73	0.33	0.26	2.85	0.04	0.11	0.49	1.12	0.03
Center		E. Meghile	J3-6	0.01	0.60	0.40	1.46	1.52	0.23	0.69	0.51	0.22	2.09	0.05	0.18	0.66	1.21	0.04

A: Extended tricyclic terpane C_{28}+C_{29}-Tri (S+R)/(C_{28}+C_{29}-Tri (S+R)+C_{29} to C_{30} αβ(H)-hopane).

Appendix III Cont. Table 6.1: Tricyclic and tetracyclic terpanes biomarker ratios of the oil families in the Sirt Basin.

Location	Oil Family	Oil Field	Well Name	A	C_{23}-Tri/ (C_{23}+C_{21}-Tri	C_{21}-Tri/ (C_{23}+C_{21}-Tri	C_{23}-Tri/ C_{24}-Tri	C_{23}-Tri/ C_{21}-Tri	C_{22}-Tri/ C_{21}-Tri	C_{24}-Tri/ C_{23}-Tri	C_{19}+C_{20}-Tri/ C_{23}-Tri	C_{23}-Tri/ Tri+C30 αβ Hop	C_{28}+C_{29}-Tri(S+R)/ TS	C_{24}-tetr/ C_{26}-Tri	C_{19}-Tri/ C_{21}-Tri	C_{21}-Tri/ C_{23}-Tri	C_{26}-Tri/ C_{25}-Tri	C_{24}-tetr/ C_{23}-Tri
Center Sirt Basin	1B	Nasser	C98-6	0.02	0.61	0.39	1.42	1.58	0.29	0.70	0.45	0.28	2.03	0.05	0.20	0.63	1.16	0.04
			C98-6	0.02	0.61	0.39	1.40	1.57	0.32	0.71	0.45	0.27	1.99	0.04	0.20	0.64	1.15	0.03
		Raiah	DD12-6	0.02	0.71	0.29	1.41	2.49	0.35	0.71	0.35	0.26	3.34	0.06	0.16	0.40	1.13	0.05
		S. Jebel	4B1-6	0.02	0.64	0.36	1.27	1.79	0.35	0.79	0.41	0.23	1.81	0.05	0.20	0.56	1.18	0.04
		Ragoba	E9-20	0.01	0.60	0.40	1.47	1.53	0.30	0.68	0.55	0.24	1.64	0.09	0.27	0.66	1.23	0.06
			E82-20	0.01	0.60	0.40	1.55	1.53	0.26	0.65	0.54	0.24	1.48	0.07	0.29	0.66	1.23	0.05
		W. Meghil	4J2-6	0.02	0.60	0.40	1.42	1.48	0.28	0.71	0.51	0.34	1.68	0.08	0.25	0.67	1.41	0.06
		Zelten	4G1-6	0.02	0.62	0.38	1.35	1.65	0.32	0.74	0.38	0.25	2.02	0.04	0.19	0.61	1.13	0.03
West		Sabah	G3-NC74F	0.02	0.66	0.34	1.55	1.93	0.37	0.64	0.40	0.26	2.10	0.06	0.22	0.52	1.31	0.05
Center Sirt Ba	2	Kotla	C46-47	0.02	0.67	0.33	1.48	2.02	0.31	0.68	0.35	0.25	4.40	0.04	0.08	0.50	0.97	0.03
	3	Dor	Z3-47	0.01	0.66	0.34	1.36	1.94	0.29	0.73	0.58	0.20	1.78	0.03	0.40	0.52	1.27	0.03
		Mansour	Z5-47	0.01	0.66	0.34	1.44	1.93	0.29	0.69	0.58	0.21	1.74	0.04	0.39	0.52	1.46	0.04
			GG1-47	0.01	0.65	0.35	1.43	1.88	0.31	0.70	0.81	0.22	1.85	0.05	0.74	0.53	1.35	0.04
West Sirt Basin	4	Aswad	B18-NC74B	0.00	0.68	0.32	1.66	2.17	0.41	0.60	0.67	0.06	0.48	0.02	0.67	0.46	5.12	0.04
			B18-NC74B	0.00	0.68	0.32	1.65	2.13	0.48	0.61	0.64	0.06	0.50	0.02	0.58	0.47	5.62	0.04
		Safsaf	C1-NC74B	0.01	0.61	0.39	1.30	1.56	0.41	0.77	0.96	0.11	0.81	0.04	0.74	0.64	3.00	0.06
		afsaf Sout	D6-NC74B	0.01	0.61	0.39	1.33	1.60	0.36	0.75	1.00	0.11	0.82	0.04	0.82	0.63	2.95	0.06
		Zella	A5-NC74B	0.00	0.66	0.34	1.45	1.92	0.42	0.69	0.64	0.12	0.83	0.03	0.55	0.52	2.98	0.04
			A5-NC74B	0.00	0.65	0.35	1.46	1.89	0.40	0.68	0.62	0.12	0.80	0.02	0.52	0.53	2.76	0.03
			A28-NC74B	0.01	0.62	0.38	1.24	1.62	0.39	0.80	0.80	0.13	0.89	0.03	0.63	0.62	2.71	0.04
East Sirt Basin	5	As Sarah	B42-96	0.22	0.47	0.53	1.39	0.89	0.23	0.72	0.75	0.33	1.51	0.05	0.23	1.13	2.21	0.04
	6	Augla	G31-51	0.01	0.53	0.47	1.56	1.13	0.23	0.64	0.68	0.21	1.32	0.04	0.23	0.88	2.14	0.04
		Nafoora	G274-51	0.01	0.53	0.47	1.57	1.11	0.24	0.64	0.68	0.21	1.20	0.04	0.23	0.90	1.66	0.03
	7	NC125	N1-125	0.23	0.39	0.61	1.37	0.65	0.22	0.73	1.48	0.55	1.29	0.05	0.37	1.55	2.05	0.05
			A1-125	0.27	0.43	0.57	1.44	0.75	0.19	0.70	1.41	0.56	1.13	0.06	0.43	1.33	2.52	0.06
	8	Tuamma	C7-97	0.46	0.45	0.55	1.30	0.81	0.22	0.77	1.40	0.68	1.65	0.25	0.50	1.23	1.45	0.20
	9	Nakhla	G7-97	0.21	0.43	0.57	1.49	0.76	0.21	0.67	1.22	0.49	1.11	0.08	0.31	1.32	2.22	0.08
Nort Sea Oil			VFO	0.02	0.53	0.47	1.04	1.14	0.36	0.96	1.21	0.24	0.94	0.03	0.65	0.88	1.56	0.04

A: Extended tricyclic terpane C_{28}+C_{29}-Tri (S+R)/(C_{28}+C_{29}-Tri (S+R)+C_{29} to C_{30} αβ(H)-hopane).

Appendix IV: Table 7.1 Mass balance calculation of original oil potential for the Upper Cretaceous source rocks in studied wells.

Well Name	6A1-59			B1-NC74F		B2-NC74A		L1-17	
Formation Name	U. Kalash	L. Kalash	Sirte Shale	Sirte Shale	Rachmat	U. Sirte Shale	L. Sirte Shale	U. Sirte Shale	L. Sirte Shale
Calculated for an area of $1km^2$									
1 Tonne = 1000kg									
Shale density: assume 2335 kg/tonne (kg/tonne = g/cm^3 * 1000)									
Oil density: 784 kg/tonne	784	784	784	784	784	784	784	784	784
1 m^3 to barrels = x 6.3									
% Expulsion efficiency approx. = (0.0012 * HI) – 0.086	59%	0.078	0.452	0.167	0.242	0.056	0.077	0.208	0.057
% Gas fraction of HC approx. = -0.0803 * LN(HI) +0.71	49%	0.538	0.497	0.523	0.514	0.544	0.539	0.518	0.543
Source rock calculation sequence									
Area rock: m2 (m*m)	1,000,000	1,000,000	1,000,000	1,000,000	1,000,000	1,000,000	1,000,000	1,000,000	1,000,000
Volume rock: m3 (m*m*m)	12,000,000	9,000,000	18,000,000	67,000,000	48,000,000	20,000,000	48,000,000	180,000,000	125,000,000
Mass rock: tonne (m3*kg/t=kg=/1000=tonne)	31,536,000	24,120,000	47,574,000	177,885,000	128,256,000	53,700,000	128,256,000	479,880,000	335,625,000
Hydrocarbon mass generated (S2 = kg/tonne rock)(S2 x tonnes rock)	609,906,240	32,803,200	596,577,960	752,453,550	443,765,760	56,385,000	269,337,600	1,977,105,600	261,787,500
Oil mass generated (oil kg) (HC x(1- (%gas/100))	606,923,358	32,626,581	593,612,357	748,515,508	441,483,135	56,078,475	267,886,741	1,966,861,228	260,365,121
Oil mass expelled (kg) (Oil S2*expulsion efficiency)	296,829,395	17,566,847	295,086,113	391,743,165	227,088,391	30,485,822	144,304,379	1,019,129,073	141,465,113
Oil volume expelled (m3)	378,609	22,407	376,385	499,672	289,654	38,885	184,062	1,299,910	180,440
Barrels oil expelled (bbl)	2,385,236	141,162	2,371,228	3,147,936	1,824,817	244,975	1,159,589	8,189,430	1,136,773
Trapped (av. about 3%) (0.03)	71,557	4,235	71,137	94,438	54,745	7,349	34,788	245,683	34,103
Recoverable (av. about 45%) (0.45)	32,201	1,906	32,012	42,497	24,635	3,307	15,654	110,557	15,346
Formation Thikness	12	9	18	67	48	20	48	180	125
NB Density = mass/vol. (e.g. g/cm3)	48.67	53.55	49.46	52.06	51.17	54.07	53.58	51.55	54.04
thus m = d * v and v = m/d									
Source rock properties									
S2	19.34	1.36	12.54	4.23	3.46	1.05	2.1	4.12	0.78
TOC*	4.1	1.13	3.25	2.59	1.62	0.85	1.61	1.62	0.86
HI*	564	137	448	211	273	118	136	245	119
Ln HI*	2.75	2.14	2.65	2.32	2.44	2.07	2.13	2.39	2.08
Rock density	2628	2680	2643	2655	2672	2685	2672	2666	2685

Appendix IV: Cont. Table 7.1 Mass balance calculation of original oil potential for the Upper Cretaceous source rocks in studied wells.

Well Name	C2-16		Z1-11	FF14-6			L1-16	
Formation Name	U. Sirte Shale	L.Sirte Shale	Sirte Shale	U. Sirte Shale	M. Sirte Shale	L. Sirte Shale	U. Sirte Shale	L. Sirte Shale
Calculated for an area of 1km^2								
1 Tonne = 1000kg								
Shale density: assume 2335 kg/tonne (kg/tonne = g/cm^3 ´ 1000)								
Oil density: 784 kg/tonne	784	784	784	784	784	784	784	784
1 m^3 to barrels = x 6.3								
% Expulsion efficiency approx. = (0.0012 * HI) – 0.086	0.066	0.030	0.275	0.191	0.148	0.039	0.11	0.08
% Gas fraction of HC approx. = -0.0803 * LN(HI) +0.71	0.541	0.550	0.511	0.520	0.526	0.548	0.53	0.54
Source rock calculation sequence								
Area rock: m2 (m*m)	1,000,000	1,000,000	1,000,000	1,000,000	1,000,000	1,000,000	1,000,000.00	1,000,000.00
Volume rock: m3 (m*m*m)	262,000,000	56,000,000	54,000,000	94,000,000	15,000,000	39,000,000	89,000,000.00	217,000,000.00
Mass rock: tonne (m3*kg/t=kg=/1000=tonne)	700,588,000	149,968,000	143,910,000	252,108,000	40,245,000	103,857,000	238,164,000.00	582,428,000.00
Hydrocarbon mass generated (S2 = kg/tonne rock)(S2 x tonnes rock)	868,729,120	121,474,080	611,617,500	128,575,080	14,890,650	122,551,260	492,999,480.00	634,846,520.00
Oil mass generated (oil kg) (HC x(1- (%gas/100))	864,028,735	120,805,411	608,492,311	127,906,230	14,812,309	121,879,640	490,378,076.93	631,428,370.87
Oil mass expelled (kg) (Oil S2*expulsion efficiency)	467,495,328	66,498,816	310,921,992	66,537,071	7,792,907	66,793,970	260,746,440.14	339,974,508.58
Oil volume expelled (m3)	596,295	84,820	396,584	84,869	9,940	85,196	332,584.75	433,640.95
Barrels oil expelled (bbl)	3,756,659	534,365	2,498,480	534,673	62,622	536,737	2,095,283.89	2,731,938.02
Trapped (av. about 3%) (0.03)	112,700	16,031	74,954	16,040	1,879	16,102	62,858.52	81,958.14
Recoverable (av. about 45%) (0.45)	50,715	7,214	33,729	7,218	845	7,246	28,286.33	36,881.16
Formation Thikness	262	56	54	94	15	39	89	217
NB Density = mass/vol. (e.g. g/cm3)	53.81	54.74	50.84	51.75	52.33	54.50	52.89	53.55
thus m = d * v and v = m/d								
Source rock properties								
S2	1.24	0.81	4.25	0.51	0.37	1.18	2.07	1.09
TOC°	1.51	1.27	1.98	1.05	0.97	2.14	1.38	0.94
HI°	127	97	301	231	195	104	166	137
Ln HI°	2.10	1.99	2.48	2.36	2.29	2.02	2.22	2.14
Rock density	2674	2678	2665	2682	2683	2663	2676	2684